ARISTOTLE UNIVERSITY OF THESSALONIKI
SCHOOL OF ENGINEERING - DEPARTMENT OF CIVIL ENGINEERING
DIVISION OF GEOTECHNICAL ENGINEERING

STAVROULA D. FOTOPOULOU
Civil Engineer, Msc

SEISMIC VULNERABILITY OF REINFORCED CONCRETE BUILDINGS IN SLIDING SLOPES

DOCTORAL THESIS

THESSALONIKI 2012

STAVROULA D. FOTOPOULOU

SEISMIC VULNERABILITY OF REINFORCED CONCRETE BUILDINGS IN SLIDING SLOPES

DOCTORAL THESIS

Submitted to the Department of Civil Engineering,
Division of Geotechnical Engineering,
Laboratory of Soil Mechanics, Foundations & Geotechnical Earthquake Engineering

Date of defence: 23 November, 2012

Examining Committee:

Prof. K. Pitilakis, Supervisor
Prof. C. Anagnostopoulos, Member of the Advisory Committee
Prof. J. Corominas, Member of the Advisory Committee
Prof. T. Chatzigogos, Examiner
Assist. Prof. A. Anastasiadis, Examiner
Assoc. Prof. D. Raptakis, Examiner
Lecturer D. Pitilakis, Examiner

© Stavroula D. Fotopoulou
© AUTH

Seismic vulnerability of reinforced concrete buildings in sliding slopes
ISBN

'Acceptance of this Doctoral Thesis by the Department of Civil Engineering of Aristotle University Thessaloniki does not imply acceptance of the opinions of the author' (Law 5343/1932, article 202, par. 2)

To my dear family

ACKNOWLEDGEMENTS

First of all, I owe a warm thank to my supervisor, prof. Kyriazis Pitilakis, for his continuous scientific guidance and support through the course of this study. He encouraged me from my first steps while at the same time he entrusted me with large amounts of independence and initiative. I'm also grateful he offered me the opportunity to participate in large European research projects he was scientifically in charge of. This gave me the privilege to meet and collaborate with important researchers in the field of earthquake and landslide engineering.

I sincerely thank the members of my advisory committee prof. Christos Anagnostopoulos and prof. Jordi Corominas for their constructive and pointed comments, suggestions and guidance, which made this work possible and helped me improve it.

I would also like to thank my examiners Prof. T. Chatzigogos, Assist. Prof. A. Anastasiadis, Assoc. Prof. D. Raptakis and Lecturer D. Pitilakis for taking the time to review this thesis and for their valuable contributions to it.

The work described in this thesis was financially supported by the European research projects SafeLand (2009-2012) "Living with landslide risk in Europe: Assessment, effects of global change, and risk management strategies" and REAKT (2011-2013) "Strategies and tools of Real Time Earthquake Rick Reduction". This support is gratefully acknowledged. The additional one-year fund from AUTH Research committee is also greatly appreciated.

I would like to express my sincere gratitude to Dr. Alberto Callerio (Studio Geotecnico Italiano S.r.l.) and Prof. George Athanasopoulos (University of Partas, Civil Engineering Department), for providing me with valuable inputs for the case histories analysis and for their critical comments and suggestions on my work.

Special thanks go to my dear friends and colleagues at AUTH: Dr. Sevasti Tegou, Dr. Sotiris Argyroudis, Sotiria Karapetrou, Grigoris Tsinidis, Anna Karatzetzou, Kostas Trevlopoulos, Evi Riga, Dr. Jacopo Selva (now in INGV, Italy), Dr. Kalliopi Kakderi, Anastasia Argyroudi, Dr. Kostas Senetakis, Dr. Maria Manakou, Dimitra Manou, Achileas Pistolas and many others. This thesis would not have been completed if it weren't for their persistent support and help during the past four years.

Finally, I would like to deeply thank my parents, Dimitris and Maria, my sister, Lena, and my husband, Manolis, for their endless support, encouragement and love throughout my whole studies. This thesis is dedicated to them.

Stavroula D. Fotopoulou

Research is to see what everybody else has seen, and to think what nobody else has thought.

Albert Szent-Gyorgyi, 1893-1986, Hungarian Biochemist

Η απαισιοδοξία είναι θέμα διάθεσης. Η αισιοδοξία είναι θέμα θέλησης.

Émile Chartier (Alain), 1868-1951, Γάλλος φιλόσοφος

Η επιστήμη είναι οργανωμένη γνώση. Η σοφία είναι οργανωμένη ζωή.

Εμμάνουελ Καντ, 1724-1804, Γερμανός φιλόσοφος

SUMMARY

Seismically triggered landslides represent one of the most devastating collateral hazards associated with earthquakes, as they may result in significant direct and indirect losses to the population and built environment. Predicting the expected degree of damage to affected built structures subjected to earthquake-induced landslides is thus important for design, urban planning, and for seismic and landslide risk assessment and mitigation studies.

Stemming from the general lack of comprehensive methodologies to assess building vulnerability to slides as well as the inherent uncertainties associated with them, one of the most significant challenges of the present research is the proposition and quantification of a new analytical methodology to estimate the physical vulnerability of reinforced concrete (RC) frame buildings subjected to earthquake triggered slow-moving slides. According to the suggested method, the damage caused by a slow moving slide on a single building is attributed to the cumulative permanent (absolute or differential) displacement and it is concentrated within the unstable or moving area. A RC building located next to the crown of a potential unstable slope, is subjected to forced differential displacement and subsequently to structural distress and damage. In terms of numerical computations, a two-step uncoupled analysis is performed. In the first step, the differential permanent deformation demand at the building's foundation level is estimated using a dynamic non-linear finite difference slope-foundation model. To enhance the reliability of the dynamic analysis results, the computed permanent displacements at the slope area are compared with Newmark-type displacement methods. In the second step, the calculated differential permanent displacements are statically imposed at the building's nonlinear finite element model at the foundation level to assess the building's response to differing permanent seismic ground displacements. Structural limit states are defined in terms of threshold values of strains for the reinforced concrete structural components. Various sets of probabilistic fragility curves are proposed both in terms of peak ground acceleration (PGA) and permanent ground displacement (PGD) based on the suggested methodological framework, via an extensive parametric investigation and

sensitivity analysis of various slope geometries, soil properties and distances of the building with respect to the slope's crown. The slope inclination in conjunction with the slope soil material are proved to be the most influential features on the vulnerability of the building exposed to the seismically induced landslide. The slope height may also greatly influence the building's fragility for sand steep slope configurations. The developed curves might be used by scientists and practitioners for efficient implementation within a probabilistic risk assessment framework from site specific to local scales. To gain confidence on the proposed methodological framework and the respective fragility functions, representative fragility curves developed in this study are compared with literature ones and recorded building damages from real past events.

Traditionally, the structural vulnerability implicitly refers to the intact, as-built structure assuming an optimum plan of maintenance. However, structures deteriorate due to various time-dependent mechanisms after they are put into service, without always subjected to the necessary interventions during their lifetime. These issues are becoming even more crucial in presence of natural hazards striking the structure, such as landslides and/or earthquakes. To bridge this gap, the proposed approach is also extended to account for the evolution of building vulnerability over time by proposing time-dependent fragility curves for RC buildings exposed to the earthquake -induced landslide hazard. In particular, the progressive aging of typical RC buildings due to exposure to aggressive corrosive environment was investigated by including probabilistic models of corrosion deterioration of the RC elements within the vulnerability modeling framework. It is shown that the fragility of the structures may increase over time due to corrosion.

CONTENTS

CONTENTS ..... **i**
List of Figures ..... **v**
List of Tables ..... **xxv**

Chapter 1 ..... **1**
Introduction *1*
1.1 Motivation and objectives of the research *1*
1.2 Outline of the Thesis *3*
1.3 Evidence of originality of the Thesis *6*

Chapter 2 ..... **9**
Landslides triggered by earthquakes *9*
2.1 Introduction *9*
2.1.1 Worldwide destructive earthquake induced landslides 10
2.1.2 Experience from earthquake induced landslides in Greece 16
2.2 Landslide classification and mechanisms *20*
2.2.1 General classification of earthquake induced landslides 20
2.2.2 Parameters affecting seismic slope stability 24
2.3 Methods to assess earthquake induced landslide hazards *30*
2.3.1 Likelihood or probability of occurrence of a landslide 30
2.3.2 Factor of safety of a slope 31
2.3.3 Slope displacement along a slip surface 33
2.3.4 Discussion 37

Chapter 3 ..... **39**
Literature review on assessing building vulnerability to landslides *39*
3.1 Introduction *39*
3.2 Physical vulnerability to landslides *39*
3.2.1 Landslide intensity measures 42
3.2.2 Damage to structures impacted by slow moving slides 43
3.3 Quantification of physical vulnerability to slides *47*
3.3.1 Fragility functions 47
3.3.2 Review of quantitative methodologies to assess building vulnerability to slides . 55

Chapter 4 69
Vulnerability assessment methodology 69
4.1 Introduction 69
4.2 Conception and description of the method 69
4.3 Layout- Numerical example 74
4.3.1 Dynamic analysis of the slope 74
4.3.2 Non linear static analysis of the RC structures 90
4.4 Fragility functions 93
4.4.1 Definition of limit states 94
4.4.2 Construction of the fragility curves 96
4.4.3 Discussion 112

Chapter 5 115
Newmark- type displacement methods: Comparison with numerical results 115
5.1 Introduction 115
5.1.1 Analytical Newmark rigid block model 116
5.1.2 Rathje and Antonakos (2011) decoupled model 117
5.1.3 Bray and Travasarou (2007) coupled model 120
5.2 Comparison between the displacement-based methods and with the numerical approach 123
5.2.1 Literature review 123
5.2.2 Implementation of the selected displacement-based predictive models 125
5.2.3 Comparison of displacements estimated by displacement-based methods and dynamic analyses 134

Chapter 6 145
Fragility curves for low-rise RC buildings subjected to slow-moving slides 145
6.1 Introduction 145
6.2 General description of the parametric investigation 145
6.2.1 Derivation of fragility curves 149
6.2.2 Generalized fragility curves 167
6.3 Sensitivity analysis 170
6.3.1 Effect of water table 170
6.3.2 Effect of strain softening in slope soil material 171
6.3.3 Effect of foundation compliance 174
6.3.4 Effect of building geometry 175
6.3.5 Effect of building code design level 180

6.4 Conclusive remarks 181

Chapter 7 183

Validation of the proposed method 183

7.1 Introduction 183

7.2 Comparison of the developed fragility curves with literature curves 183

7.2.1 Comparison with empirical curves 184

7.2.2 Comparison with expert judgment curves 188

7.2.3 Comparison with numerically derived curves 193

7.2.4 Comparison with seismic fragility curves for horizontally layered soil media ... 196

7.3 Application to Kato Achaia slope- western Greece 204

7.3.1 Introduction 204

7.3.2 The Earthquake of 8 June 2008 in Achaia-Ilia, Greece 204

7.3.3 Slope non-linear dynamic analysis 206

7.3.4 Fragility analysis of the building 212

7.4 Application to buildings in Corniglio village- Italy 214

7.4.1 Introduction 214

7.4.2 Landslide movement and building damage data in Corniglio village 215

7.4.3 Comparison of the observed building damage with the damage predicted by the proposed and simulated fragility curves 225

7.5 Conclusive remarks 235

Chapter 8 237

Evolution of building vulnerability over time 237

8.1 Introduction 237

8.2 Environmental deterioration of RC structures 238

8.2.1 Corrosion of reinforcement 238

8.2.2 Carbonation-induced corrosion 240

8.2.3 Chloride-induced corrosion 246

8.3 Application to reference RC buildings 253

8.3.1 Numerical modeling of the buildings 253

8.3.2 Quantification of aging probabilistic parameters 254

8.3.3 Time-dependent fragility functions 259

8.4 Conclusions 280

Chapter 9 281

Conclusions-Limitations- Future work.....281
9.1 Summary of findings and contributions 281
9.2 Limitations and recommendations for future work.....286

References 289

Annex A.....309
Slope Configurations 309
A.1 Slope geometries used for the parametric analysis.....309

Annex B.....317
Fragility curves for "low-code" buildings 317
B.1 Proposed curves for "low-code" designed RC buildings.....317

Εκτενής Περίληψη 321
I.1 Εισαγωγή.....321
I.2 Μεθοδολογία αποτίμησης της τρωτότητας 322
I.3 Εμπειρικές μέθοδοι εκτίμησης των μόνιμων μετακινήσεων: Συγκρίσεις με τα αποτελέσματα των μη-γραμμικών, δυναμικών αναλύσεων 328
I.4 Καμπύλες τρωτότητας κτιρίων Ο/Σ σε κατολισθαίνοντα πρανή.....332
I.5 Αξιολόγηση της προτεινόμενης μεθόδου 338
I.6 Εξέλιξη της τρωτότητας των κατασκευών στο χρόνο 345
I.7 Συμπεράσματα.....349
I.8 Βιβλιογραφικές αναφορές.....350

LIST OF FIGURES

Figure 2.1. Non-shaking earthquake fatalities for all deadly earthquakes between September 1968 and June 2008, with deaths from the 2004 Sumatra event removed (source: Marano et al., 2010) 9

Figure 2.2. Las Colinas landslide in El Salvador 10

Figure 2.3. General view of the Higashi Takezawa landslide and the head scarp of past landslide (Sassa et al., 2005)..... 11

Figure 2.4. School building hit by the landslide mass (Sassa, 2005) 11

Figure 2.5. (a) Damage to houses as a result of ground deformation (b) Differential settlement of periphery road (c) Slope failure of valley fill (Ohtsuka et al., 2009) 12

Figure 2.6. Damage to the built environment as a result of the 1999 Chi-Chi Taiwan earthquake induced landslides 13

Figure 2.7. General view of the Jiufengershan landslide (Dong et al., 2007) 13

Figure 2.8. View to the source of the Hattian Bala rock avalanche (Dana Hill) from the high point of the dam crest (Dunning et al., 2007). 14

Figure 2.9. Oblique aerial view (a) and vertical air photo (b) of the Chengxi landslide in Beichuan (Yin et al., 2009) 15

Figure 2.10. Calitri landslide activation in 1980, producing damage: on the Francesco De Sanctis main street (a), on the Torre street (b), along the landslide scarp at the Giacomo Matteotti main street (c), on the Garibaldi main street (d) (Martino and Scarascia Mugnozza, 2005) 16

Figure 2.11. 3D perspective of a typical earthquake-induced landslide at Eratini Gulf (Bouckovalas et al.,1995)..... 17

Figure 2.12. Rockfalls in Agios Kyprianos (Fokaefs and Papadopoulos, 2007) 17

Figure 2.13. Rockfalls due to detachment and possible overturn at the Agios Nikitas (left); Cars were buried under landslides near the same area (right)..... 18

Figure 2.14. Plan (left) and side (right) view of the natural slope landslide at the main square of Mitata village (Karakostas et al., 2006)..... 19

Figure 2.15. Santomeri village: location of the detached rock block that toppled (left) - the rock block itself (volume 6 to 7 cubic meters) that caused severe structural damage at one of the houses of the village (right) (Margaris et al., 2008) 20

Figure 2.16. Classification of landslides (Modified after Varnes, 1978) 21

Figure 2.17. Relations between area affected by landslides and earthquake magnitude (Keefer, 2002) 26

Figure 2.18. Maximum epicentral distance as a function of the event magnitude for the three landslide categories (dashed line: disrupted landslides, dash-double-dot line: coherent landslides, dotted line: lateral spreads and flows) (Keefer, 1984) 27

Figure 2.19. Relation of landslide concentration to the distance from the fault rupture zone (a) and to the epicentral distance (b) for landslides in the southern Santa Cruz Mountains triggered by the 1989 Loma Prieta, California, earthquake (Keefer, 2002) ... 28

Figure 2.20. Pseudostatic slope stability analysis 32

Figure 2.21. Newmark Sliding-block analogy 34

Figure 2.22. Decoupled dynamic response/rigid sliding block analysis and fully coupled analysis (Bray, 2007) 35

Figure 3.1. Schematic overview of landslide damage types, related to different landslide types, elements at risk and the location of the exposed element in relation to the landslide (Van Westen et al., 2006) 41

Figure 3.2. Landslide intensity criteria (after Leone et al. 1996) 43

Figure 3.3. Typical shallow foundation systems - Types and layout 44

Figure 3.4. Building damage due to a deep sited landslide in Austria (Geological Survey of Austria) 45

Figure 3.5. (a) Structural damage caused by deep-seated slide at Monteverde on December 22, 1982. (b) Total damage caused by deep-seated slide at Valderchia on January 6, 1997. (c) Total damage caused by deep-seated slide at Nuvole di Morra on December 9, 2005. (d) Functional damage caused by deep-seated slide at Badia and Podere Cipresso (Orvieto) on December 6, 2004. Open arrows show location of damage, filled arrows show approximate direction of landslide movement (Galli and Guzzetti, 2007). 46

Figure 3.6. Classification of building damage mechanisms impact by slope instability triggered by the 2011 Great East Japan Earthquake (Japanese Geotechnical Society, 2011). 46

Figure 3.7. Building damage due to differential displacement in Sendai City, Japan following the 2011 Great East Japan Earthquake (Japanese Geotechnical Society, 2011). 47

Figure 3.8. Concept of fragility curve 49

Figure 3.9. HAZUS fragility curves derived for buildings for different damage states (NIBS, 2004) 50

Figure 3.10. Correlation of Damage level to Angular Distortion and Horizontal Extension Strain (after Boscardin and Cording, 1989) 53

Figure 3.11. Proportion of landslide damage (DL) as a function of landslide area (AL) for different elements at risk in the Umbria region, central Italy (Galli and Guzzetti, 2007). 57

Figure 3.12. Kinetic and kinematic intensity models (Uzielli et al., 2008) 61

Figure 3.13. Theoretical changing trend of Vulnerability with Intensity/Resistance (a) and Intensity (b) (Li et al., 2010) 62

Figure 3.14. Building vulnerability map in a region of northern Himalaya, India (Das et al., 2011)..... 64

Figure 3.15. Fragility curves obtained for a one bay-one storey encasing RC frame building, considering 4 damage limit states: Slight (LS1), Moderate (LS2), Extensive (LS3) and Complete (LS4) (Negulescu and Foerster, 2010) 65

Figure 4.1. Flowchart for the proposed framework of fragility analysis of RC buildings. 71

Figure 4.2. (a) Slope and foundation configuration used for the numerical modeling (b) and FLAC 2D dynamic model..... 75

Figure 4.3. Specification of FLAC Rayleigh damping parameters for the present study (ξ_{min}=3%, f_{min}=3.1 Hz)..... 78

Figure 4.4. Normalized average elastic response spectrum of the input motions in comparison with the corresponding elastic design spectrum for soil type A (rock) according to EC8 80

Figure 4.5. Absolute and differential horizontal and vertical displacement time histories at the closest edge of the assumed building from the slope' crest (i.e. 3.0 m) considering stiff and flexible foundations for the building and at the same location in the absence of any structure for two different input motions (cascia, pacoima) scaled at two PGA levels (0.3, 0.7 g) (sand slope). 84

Figure 4.6. Absolute and differential horizontal and vertical displacement time histories at the closest edge of the assumed building from the slope' crest (i.e. 3.0 m) considering stiff and flexible foundations for the building and at the same location in the absence of any structure for two different input motions (cascia, pacoima) scaled at two PGA levels (0.3, 0.7 g) (clay slope). 86

Figure 4.7. Regression of differential displacement vector for buildings with flexible (top) and stiff (bottom) foundation system on the maximum computed permanent ground displacement (sand slope). 87

Figure 4.8. Regression of differential displacement vector for buildings with flexible (top) and stiff (bottom) foundation system on the maximum computed permanent ground displacement (clay slope). 88

Figure 4.9. Maximum values of differential displacement vector for buildings with flexible (top) and stiff foundation (bottom) system (sand slope). 89

Figure 4.10. Maximum values of differential displacement vector for buildings with flexible (top) and stiff foundation (bottom) system (clay slope). 89

Figure 4.11. Discretisation in fibre modelling of a typical reinforced concrete cross-section (Seismosoft, Seismostruct 2011) 90

Figure 4.12. Single bay-single storey RC frame buildings with flexible (a) and stiff (b) foundation system and displacement loading pattern considered for the non-linear quasi-static analysis 91

Figure 4.13. Stress-strain models for concrete (a) and steel (b) material 92

Figure 4.14. Deformed shapes for buildings with flexible (b) and stiff (b) foundations. 93

Figure 4.15. Maximum recorded strain as a function of PGA (left) and PGD (right) for 1bay-1story RC frame buildings with stiff and flexible foundation system on top of a sand slope 96

Figure 4.16. Maximum recorded strain as a function of PGA (left) and PGD (right) for 1bay-1story RC frame buildings with stiff and flexible foundation system on top of a clay slope 96

Figure 4.17. PGA- $\ln(\varepsilon_s)$ (a) and ln(PGD)- $\ln(\varepsilon_s)$ (b) relationships for the building with flexible foundation system resting close to the crest of the sand slope. 99

Figure 4.18. Fragility curves for low rise-RC buildings with flexible foundation system on sand slope based on the regression analysis method 101

Figure 4.19. Fragility curves for low rise-RC buildings with flexible foundation system on clay slope based on the regression analysis method 102

Figure 4.20. Fragility curves for low rise-RC buildings with stiff foundation system on sand slope based on the regression analysis method 103

Figure 4.21. Fragility curves for low rise-RC buildings with stiff foundation system on clay slope based on the regression analysis method 104

Figure 4.22. Fragility curves for low rise-RC buildings with flexible foundation system on sand slope based on the Maximum likelihood method 107

Figure 4.23. Fragility curves for low rise-RC buildings with flexible foundation system on clay slope based on the Maximum likelihood method 108

Figure 4.24. Fragility curves for low rise-RC buildings with stiff foundation system on sand slope based on the Maximum likelihood method 109

Figure 4.25. Fragility curves for low rise-RC buildings with stiff foundation system on clay slope based on the Maximum likelihood method 110

Figure 4.26. Comparison of Fragility curves in terms of PGA (left) and PGD (right) developed based on the regression Analysis (RA) and the Maximum likelihood (ML) methods 112

Figure 5.1. (a) Newmark Sliding-block model (b) Newmark algorithm for seismically-induced permanent displacements (adapted from Wilson and Keefer, 1983). 116

Figure 5.2. Predicted values of sliding displacement as a function of T_s with k_y=0.05(a) and k_y=0.1 (b) for the (PGA, PGV) Rathje and Antonakos (2011) model..... 120

Figure 5.3. Generic seismic slope displacement problem of height H and initial stiffness Vs and (b) idealized nonlinear stick with one-way sliding used in Bray and Travasarou (2007)..... 121

Figure 5.4. Trends from the Bray and Travasarou (2007) model: (a) probability of negligible displacements and (b) median displacement estimate for a M_w = 7 strike-slip earthquake at a distance of 10 km, and (c) seismic displacement as a function of yield coefficient for several intensities of ground motion (M_w = 7.5) for a sliding block with T_s = 0.3 s (adopted from Bray, 2007) 123

Figure 5.5. Input acceleration time histories (before scaling) and Fourier spectra 126

Figure 5.6. Newmark displacement versus critical acceleration ratio k_y/k_{max} for different acceleration time histories (cascia, pacoima) scaled at different levels of PGA (PGA=0.3g, 0.7g)..... 127

Figure 5.7. Bray and Travasarou (2007) displacement versus critical acceleration ratio k_y/k_{max} considering a nearly rigid sliding mass (T_s=0.032 sec) for different acceleration time histories (cascia, pacoima) scaled at different levels of PGA (PGA=0.3g, 0.7g) ... 128

Figure 5.8. Rathje and Antonakos (2011) displacement versus critical acceleration ratio k_y/k_{max} considering a nearly rigid sliding mass (T_s=0.032 sec) for different acceleration time histories (cascia, pacoima) scaled at different levels of PGA (PGA=0.3g, 0.7g) ... 128

Figure 5.9. Comparison of the different predictive models for permanent slope displacement considering a nearly rigid sliding mass (T_s=0.032 sec) for a certain earthquake scenario (cascia scaled at 0.3g) 129

Figure 5.10. Comparison of the different predictive models for permanent slope displacement considering a nearly rigid sliding mass (T_s=0.032 sec) for a certain earthquake scenario (pacoima scaled at 0.3g) 129

Figure 5.11. Comparison of the different predictive models for permanent slope displacement considering a nearly rigid sliding mass (T_s=0.032 sec) for a certain earthquake scenario (cascia scaled at 0.7g) 130

Figure 5.12. Comparison of the different predictive models for permanent slope displacement considering a nearly rigid sliding mass (Ts=0.032 sec) for a certain earthquake scenario (pacoima scaled at 0.7g) 130

Figure 5.13. Bray and Travasarou (2007) displacement versus critical acceleration ratio k_y/k_{max} considering a deformable sliding mass (T_s=0.16 sec) for different acceleration time histories (cascia, pacoima) scaled at different levels of PGA (PGA=0.3g, 0.7g) ... 131

Figure 5.14. Rathje and Antonakos (2011) displacement versus critical acceleration ratio k_y/k_{max} considering a deformable sliding mass (T_s=0.16 sec) for different acceleration time histories (cascia, pacoima) scales at different levels of PGA (PGA=0.3g, 0.7g) ... 131

Figure 5.15. Comparison of the different predictive models for permanent slope displacement considering a deformable sliding mass (T_s=0.16 sec) for a certain earthquake scenario (cascia scaled at 0.3g) 132

Figure 5.16. Comparison of the different predictive models for permanent slope displacement considering a deformable sliding mass (T_s=0.16 sec) for a certain earthquake scenario (pacoima scaled at 0.3g) 132

Figure 5.17. Comparison of the different predictive models for permanent slope displacement considering a deformable sliding mass (T_s=0.16 sec) for a certain earthquake scenario (cascia scaled at 0.7g) 133

Figure 5.18. Comparison of the different predictive models for permanent slope displacement considering a deformable sliding mass (T_s=0.16 sec) for a certain earthquake scenario (Pacoima scaled at 0.7g) 133

Figure 5.19. Slope configuration used for the numerical modeling..... 134

Figure 5.20. Error (%) of the predictive models in the median displacement estimation compared to the corresponding FLAC displacement calculation for rock outcropping accelerograms scaled at PGA=0.7g- sand slope (T_s=0.032sec) 137

Figure 5.21. Average error (%) of the predictive models in the median displacement estimation compared to the corresponding FLAC displacement calculation for rock outcropping accelerograms scaled at PGA=0.7g- sand slope (T_s=0.032sec) 137

Figure 5.22. Dispersion of the error (%) of the predictive models in the median displacement estimation in relation to the corresponding FLAC results for rock outcropping accelerograms scaled at PGA=0.7g- sand slope (T_s=0.032sec) 138

Figure 5.23. Comparison between analytical Newmark's, Rathje and Antonakos (2011) and Bray and Travasarou (2007) displacements with the co-seismic horizontal displacements from the 2D dynamic analyses (sand slope)..... 139

Figure 5.24. Error (%) of the models in the median displacement estimation compared to the corresponding FLAC displacement calculation for rock outcropping accelerograms scaled at PGA=0.7g- clay slope (T_s=0.16sec) 140

Figure 5.25. Average error (%) of the predictive models in the median displacement estimation compared to the corresponding FLAC displacement calculation for rock outcropping accelerograms scaled at PGA=0.7g- clay slope (T_s=0.16sec) 140

Figure 5.26. Dispersion of the error (%) of the predictive models in the median displacement estimation in relation to the corresponding FLAC results for rock outcropping accelerograms scaled at PGA=0.7g- clay slope (T_s=0.16sec) 141

Figure 5.27. Comparison between analytical Newmark's, Rathje and Antonakos (2011) and Bray and Travasarou (2007) displacements with the co-seismic horizontal displacements from the 2D dynamic analyses (clay slope)..... 142

Figure 6.1. Parametric model under study 146

Figure 6.2. Upslope (a) and downslope (b) V_s variation with depth for the analyzed soil profiles (soil classification according to EC8)..... 148

Figure 6.3. Fragility curves as a function of PGA (left) and PGD (right) derived from the parametric analysis 157

Figure 6.4. Fragility curves for extensity damage as a function of PGA (left) and PGD (right) when varying slope inclination [β=f (Soil properties) = 15°, 30°, 45°] for sand slopes..... 160

Figure 6.5. Fragility curves for slight damage as a function of PGA (left) and PGD (right) when varying slope inclination [β=f (Soil properties) = 15°, 30°, 45°] for clayey slopes 160

Figure 6.6. Fragility curves as a function of PGA (left) and PGD (right) when varying slope height (H= 20, 40m) for sand slopes 162

Figure 6.7. Fragility curves as a function of PGA (left) and PGD (right) when varying slope height (H= 20, 40m) for clayey slopes 163

Figure 6.8. Fragility curves as a function of PGA (left) and PGD (right) when varying slope soil properties (sand, clay) for soft soil conditions (slope inclination β=15^o) 164

Figure 6.9. Fragility curves as a function of PGA (left) and PGD (right) when varying slope soil properties (sand, clay) for relatively stiff soil conditions (slope inclination β=30^o) 164

Figure 6.10. Fragility curves as a function of PGA (left) and PGD (right) when varying slope soil properties (sand, clay) for stiff soil conditions (slope inclination β=45^o) 165

Figure 6.11. Fragility curves as a function of PGA (left) and PGD (right) when varying the distance from the crest (L= 3, 5m) for sand slopes 166

Figure 6.12. Fragility curves as a function of PGA (left) and PGD (right) when varying the distance from the crest (L= 3, 5m) for clayey slopes 166

Figure 6.13. Proposed fragility curves as a function of PGA (left) and PGD (right) for high-code, low-rise RC frame buildings subjected to permanent landslide displacements 169

Figure 6.14. Fragility curves as a function of PGA (left) and PGD (right) when varying the hydraulic conditions (dry or partially saturated materials) for sand slopes 171

Figure 6.15. Fragility curves as a function of PGA (left) and PGD (right) when varying the hydraulic conditions (dry or partially saturated materials) for clayey slopes 171

Figure 6.16. Two dimensional behavior of a linear elastic-softening plastic material (Potts and Zbravkovi, 1999) 173

Figure 6.17. Idealization of the variation of cohesion, friction and dilation with plastic shear strain to simulate strain softening soil behavior 173

Figure 6.18. Fragility curves as a function of PGA (left) and PGD (right) when considering (or not) a strain softening material 173

Figure 6.19. Schematic view of the analyzed single bay-single storey RC bare-frame structures with flexible (left) and stiff (right) foundations 174

Figure 6.20. Fragility curves as a function of PGA (left) and PGD (right) when varying the flexibility of the foundation system for sand slopes 174

Figure 6.21. Fragility curves as a function of PGA (left) and PGD (right) when varying the flexibility of the foundation system for clayey slopes 175

Figure 6.22. Schematic view of the analyzed 1 bay- 2 storeys RC bare frame structures with flexible (left) and stiff (right) foundations 176

Figure 6.23. Fragility curves as a function of PGA (left) and PGD (right) when considering a one-storey and a two-storey structure on flexible foundations for sand slopes 176

Figure 6.24. Fragility curves as a function of PGA (left) and PGD (right) when considering a one-storey and a two-storey structure on flexible foundations for clayey slopes..... 177

Figure 6.25. Fragility curves as a function of PGA (left) and PGD (right) when considering a one-storey and a two-storey structure on stiff foundations for sand slopes 177

Figure 6.26. Fragility curves as a function of PGA (left) and PGD (right) when considering a one-storey and a two-storey structure on flexible foundations for clayey slopes..... 177

Figure 6.27. Schematic view of the analyzed 2 bays- 1 storey RC bare frame structures with flexible (top) and stiff (bottom) foundations 179

Figure 6.28. Fragility curves as a function of PGA (left) and PGD (right) when considering a one-bay and a two-bay structure on flexible foundations for sand slopes179

Figure 6.29. Fragility curves as a function of PGA (left) and PGD (right) when considering a one-bay and a two-bay structure on flexible foundations for clay slopes 179

Figure 6.30. Fragility curves as a function of PGA (left) and PGD (right) when considering a one-bay and a two-bay structure on stiff foundations for sand slopes ... 180

Figure 6.31. Fragility curves as a function of PGA (left) and PGD (right) when considering a one-bay and a two-bay structure on stiff foundations for clay slopes 180

Figure 6.32. Fragility curves as a function of PGA (left) and PGD (right) when varying the code design level 181

Figure 7.1. Comparison of the proposed fragility curves as a function of settlement for the building on flexible foundation with the corresponding empirical curves provided by Zhang and Ng (2005) 187

Figure 7.2. Comparison of the proposed fragility curves as a function of settlement for the building on stiff foundation with the corresponding empirical curves provided by Zhang and Ng (2005) 187

Figure 7.3. Comparison of the proposed fragility curves as a function of angular distortion for the building on flexible foundation with the corresponding empirical curves provided by Zhang and Ng (2005) 188

Figure 7.4. Comparison of the proposed fragility curves as a function of angular distortion for the building on stiff foundation with the corresponding empirical curves provided by Zhang and Ng (2005) 188

Figure 7.5. Comparison of the proposed fragility curves for extensive and complete damage as a function of permanent ground displacement (PGD) for the building on flexible foundation with the corresponding expert judgment curves provided by HAZUS (NIBS, 2004)..... 190

Figure 7.6. Comparison of the proposed fragility curves for extensive and complete damage as a function of permanent horizontal ground displacement (PHGD) for the building on flexible foundation with the corresponding expert judgment curves provided by HAZUS (NIBS, 2004) for ground failure due to lateral spreading 191

Figure 7.7. Comparison of the proposed fragility curves for extensive and complete damage as a function of permanent vertical ground displacement (PVGD) for the building on flexible foundation with the corresponding expert judgment curves provided by HAZUS (NIBS, 2004) for ground failure due to settlement..... 191

Figure 7.8. Comparison of the proposed fragility curves for extensive damage as a function of permanent ground displacement (PGD) for the building on stiff foundation with the corresponding expert judgment curves provided by HAZUS (NIBS, 2004)..... 192

Figure 7.9. Comparison of the proposed fragility curves for extensive and complete damage as a function of permanent horizontal ground displacement (PHGD) for the building on stiff foundation with the corresponding expert judgment curves provided by HAZUS (NIBS, 2004) for ground failure due to lateral spreading 192

Figure 7.10. Comparison of the proposed fragility curves for extensive and complete damage as a function of permanent vertical ground displacement (PVGD) for the building on stiff foundation with the corresponding expert judgment curves provided by HAZUS (NIBS, 2004) for ground failure due to settlement 193

Figure 7.11. Comparison of the proposed fragility curves as a function of differential ground displacement for the building on flexible foundation with the corresponding analytical curves provided by Negulescu and Foerster (2010) 195

Figure 7.12. Comparison of the proposed fragility curves as a function of differential ground displacement for the building on stiff foundation with the corresponding analytical curves provided by Negulescu and Foerster (2010) 195

Figure 7.13. Comparison of the harmonized proposed fragility curves as a function of PGA for low-rise, seismically designed, RC frame buildings exposed to co-seismic slope displacements with the corresponding curves provided by Ahmad et al. (2011) for the same building typologies when subjected to seismic ground shaking..... 199

Figure 7.14. Comparison of the harmonized proposed fragility curves as a function of PGA for low-rise, seismically designed, RC frame buildings exposed to co-seismic slope

displacements with the corresponding curves provided by Borzi et al. (2007) for the same building typologies when subjected to seismic ground shaking 199

Figure 7.15. Comparison of the harmonized proposed fragility curves as a function of PGA for low-rise, seismically designed, RC frame buildings exposed to co-seismic slope displacements with the corresponding curves provided by Kappos et al. (2003) for the same building typologies when subjected to seismic ground shaking..... 200

Figure 7.16. Comparison of the harmonized proposed fragility curves as a function of PGA for low-rise, seismically designed, RC frame buildings exposed to co-seismic slope displacements with the corresponding curves provided by Ozmen et al. (2010) for the same building typologies when subjected to seismic ground shaking..... 200

Figure 7.17. Comparison of the harmonized proposed fragility curves as a function of PGA for low-rise, seismically designed, RC frame buildings exposed to co-seismic slope displacements with the corresponding curves provided by Rossetto and Elnashai (2003) for the same building typologies when subjected to seismic ground shaking..... 201

Figure 7.18. Comparison of the harmonized proposed fragility curves as a function of PGA for low-rise, seismically designed, RC frame buildings exposed to co-seismic slope displacements with the corresponding curves provided by Tsionis et al. (2011) for the same building typologies when subjected to seismic ground shaking..... 201

Figure 7.19. Comparison of the harmonized proposed fragility curves as a function of PGA for low-rise, seismically designed, RC frame buildings exposed to co-seismic slope displacements with the corresponding curves provided by Akkar et al. (2005) for the same building typologies when subjected to seismic ground shaking..... 202

Figure 7.20. Comparison of the harmonized proposed fragility curves as a function of PGA for low-rise, seismically designed, RC frame buildings exposed to co-seismic slope displacements with the corresponding curves provided by Erberik (2008) for the same building typologies when subjected to seismic ground shaking 202

Figure 7.21. Comparison of the harmonized proposed fragility curves as a function of PGA for low-rise, seismically designed, RC frame buildings exposed to co-seismic slope displacements with the corresponding curves provided by Nuti et al. (1998) for the same building typologies when subjected to seismic ground shaking 203

Figure 7.22. Comparison of the harmonized proposed fragility curves as a function of PGA for low-rise, seismically designed, RC frame buildings exposed to co-seismic slope displacements with the corresponding curves provided by Fotopoulou et al. (2012) for the same building typologies when subjected to seismic ground shaking..... 203

Figure 7.23. Fault of the June 8, 2008 sequence (black) (determined by analysis of the main shock and aftershock distribution) and already mapped faults (red).The red circle

denotes the epicenter of the main shock. Towns affected by the earthquake are denoted by squares. (Margaris et al., 2010). 205

Figure 7.24. Strong motion stations located near the ruptured fault segment. Distance of Kato Achaia town from the surface projection of the fault. 205

Figure 7.25. Geographical distribution of the buildings (black circles) that suffered severe damage in Kato Achaia 206

Figure 7.26. Topographic map (original scale 1:5000) of Kato Achaia area and position of A-A' cross section. 207

Figure 7.27. Soil model used for the 2D finite difference dynamic analysis of the Kato-Achaia slope 208

Figure 7.28. 2D FLAC dynamic model adopted for the Kato-Achaia slope 208

Figure 7.29. Shear wave velocity variation with depth for the selected recording stations. 210

Figure 7.30. Modulus reduction and damping curves of Darendeli (2001) used for the 1D deconvolution analysis 210

Figure 7.31. Input outcropping horizontal accelerations used in the dynamic analysis 211

Figure 7.32. Differential horizontal ground displacements at the building's foundation level for low and high excitation level. 212

Figure 7.33. Fragility curves proposed for the specific site and structural characteristics 214

Figure 7.34. General plan of the area of Corniglio affected by the landslide phenomena during the years 1995-2000. The indicated displacements (ADG = Absolute Ground Displacement) are obtained by aerial photo interpretation ("Lama" area) and inclinometer readings (Village) (Callerio et al., 2007) 216

Figure 7.35. Geotechnical profile B-B (see Fig. 7.34) of the Corniglio case history used for the analysis 217

Figure 7.36. Representative physical damage to buildings in Corniglio village (Callerio et al., 2007)..... 218

Figure 7.37. Location of inclinometers, geodetic and crack measurements on buildings. Buildings are denoted by red polygons whereas the ones that suffered damages due to the landslide movement are filled in red. (Callerio et al., 2007)..... 219

Figure 7.38. Correlation between absolute ground displacement (from nearby Inclinometer A3-2), building n. 17 and 18 displacement (from geodetic levelling) and crack opening (compared to the defined damage levels) as a function of time (Callerio et al., 2007)..... 221

Figure 7.39. Correlation between absolute ground displacement (from nearby Inclinometer A2-2), building n. 23 and 25 displacement (from geodetic levelling) and crack opening (compared to the defined damage levels) as a function of time (Callerio et al., 2007)..... 222

Figure 7.40. Correlation between absolute ground displacement (from nearby Inclinometer A2-6), building n. 27 displacement (from geodetic levelling) and crack opening (compared to the defined damage levels) as a function of time (Callerio et al., 2007)..... 223

Figure 7.41. Correlation between absolute ground displacement (from nearby Inclinometer A2-1), building n. 27 displacement (from geodetic levelling) and crack opening (compared to the defined damage levels) as a function of time (Callerio et al., 2007)..... 223

Figure 7.42. Correlation between absolute ground displacement (from nearby Inclinometers A2-1 and A3-3), building n. 35 displacement (from geodetic levelling) and crack opening (compared to the defined damage levels) as a function of time (Callerio et al., 2007)..... 224

Figure 7.43. Correlation between absolute ground displacement (from nearby Inclinometers A3-1 and A3-3), building n. 63 displacement (from geodetic levelling) and crack opening (compared to the defined damage levels) as a function of time (Callerio et al., 2007)..... 224

Figure 7.44. Closer view of building with ID 17 and the nearby inclinometer A3-2 within the Corniglio area. The geodetic and crack monitored points on the buildings are also shown (in green)..... 225

Figure 7.45. Representative fragility functions derived from the parametric analyses 227

Figure 7.46. Slope configuration adopted for the geotechnical profile B-B 229

Figure 7.47. Simplified 2D FLAC dynamic model adopted for the geotechnical profile B-B 230

Figure 7.48. Linear 5%-damped acceleration response spectra of the records selected for numerical analyses. The average and median spectra are also shown. 232

Figure 7.49. Differential horizontal (a) and vertical (b) ground displacements at the building's foundation level for input accelerograms scaled at 0.15 g..... 232

Figure 7.50. Schematic view of the studied building in Corniglio village 233

Figure 7.51. Maximum recorded steel strain as a function of permanent ground displacement vector at the foundation level for the studied building in Corniglio village 234

Figure 7.52. Fragility curves for the studied RC frame building in Corniglio village 235

Figure 8.1. Structural deterioration due to reinforcement corrosion 238

Figure 8.2. Schematic illustration of the evolution of the reinforced concrete corrosion 239

Figure 8.3. Carbonation in concrete (Beushausen and Alexander, 2010) 240

Figure 8.4. Carbonation induced corrosion (Beushausen and Alexander, 2010) 241

Figure 8.5. Typical chloride profile in concrete (Beushausen and Alexander, 2010) ... 246

Figure 8.6. Chloride induced corrosion of reinforcement (Beushausen and Alexander, 2010) 247

Figure 8.7. Information needed to determine the variables C_S and $C_{S,\Delta x}$ (FIB- CEB Task Group 5.6, 2006) 250

Figure 8.8. Reference analyzed RC frame buildings 253

Figure 8.9. Distribution of carbonation induced corrosion initiation time T_{ini} (mean = 36.40years, Standard Deviation = 20.85 years)..... 256

Figure 8.10. Distribution of chloride corrosion initiation time T_{ini} (mean = 2.96 years, Standard Deviation = 2.16 years)..... 256

Figure 8.11. Distribution of normalized time variant area of the reinforcement (a) for carbonation and (b) chloride induced deterioration 258

Figure 8.12. Fragility curves in terms of PGA for different points in time (0, 40, 60 and 90 years), for slight (LS_1), moderate (LS_2), extensive (LS_3) and complete (LS_4) limit states considering carbonation induced corroded buildings on flexible foundations. 262

Figure 8.13. Fragility curves in terms of PGD for different points in time (0, 40, 60 and 90 years), for slight (LS_1), moderate (LS_2), extensive (LS_3) and complete (LS_4) limit states considering carbonation induced corroded buildings on flexible foundations. 263

Figure 8.14. Time-dependent quadratic fit of median values of PGA for the slight, moderate, extensive and complete limit states considering carbonation induced corroded buildings on flexible foundations 264

Figure 8.15. Time-dependent quadratic fit of median values of PGD for the slight, moderate, extensive and complete limit states considering carbonation induced corroded buildings on flexible foundations 264

Figure 8.16. Fragility surfaces as a function of time and PGA for slight, moderate, extensive and complete limit states (fit: Interpolant) considering carbonation induced corroded buildings on flexible foundation 265

Figure 8.17. Fragility surfaces as a function of time and PGD for slight, moderate, extensive and complete limit states (fit: Interpolant) considering carbonation induced corroded buildings on flexible foundations..... 266

Figure 8.18. Fragility curves in terms of PGA for different points in time (0, 40, 60 and 90 years), for slight (LS_1), moderate (LS_2), extensive (LS_3) and complete (LS_4) limit states considering carbonation induced corroded buildings on stiff foundations..... 267

Figure 8.19. Fragility curves in terms of PGD for different points in time (0, 40, 60 and 90 years), for slight (LS_1), moderate (LS_2) and extensive (LS_3) limit states considering carbonation induced corroded buildings on stiff foundations..... 268

Figure 8.20. Time-dependent quadratic fit of median values of PGA for the slight, moderate, extensive and complete limit states considering carbonation induced corroded buildings on stiff foundations 268

Figure 8.21. Time-dependent quadratic fit of median values of PGD for the slight, moderate, extensive and complete limit states considering carbonation induced corroded buildings on stiff foundations 269

Figure 8.22. Fragility surfaces as a function of time and PGA for slight, moderate, extensive and complete limit states (fit: Interpolant) considering carbonation induced corroded buildings on stiff foundations 270

Figure 8.23. Fragility surfaces as a function of time and PGD for slight, moderate, extensive and complete limit states (fit: Interpolant) considering carbonation induced corroded buildings on stiff foundations 270

Figure 8.24. Fragility curves in terms of PGA for different points in time (0, 20, 40, 60 and 90 years), for slight (LS_1), moderate (LS_2), extensive (LS_3) and complete (LS_4) limit states considering chloride induced corroded buildings on flexible foundations..... 272

Figure 8.25. Fragility curves in terms of PGD for different points in time (0, 20, 40, 60 and 90 years), for slight (LS_1), moderate (LS_2), extensive (LS_3) and complete (LS_4) limit states considering chloride induced corroded buildings on flexible foundations..... 272

Figure 8.26. Time-dependent quadratic fit of median values of PGA for the slight, moderate, extensive and complete limit states considering chloride induced corroded buildings on flexible foundations..... 273

Figure 8.27. Time-dependent quadratic fit of median values of PGD for the slight, moderate, extensive and complete limit states considering chloride induced corroded buildings on flexible foundations..... 274

Figure 8.28. Fragility surfaces as a function of time and PGA for slight, moderate, extensive and complete limit states (fit: Interpolant) considering chloride induced corroded buildings on flexible foundations..... 274

Figure 8.29. Fragility surfaces as a function of time and PGD for slight, moderate, extensive and complete limit states (fit: Interpolant) considering chloride induced corroded buildings on flexible foundations 275

Figure 8.30. Fragility curves in terms of PGA for different points in time (0, 20, 40, 60 and 90 years), for slight (LS_1), moderate (LS_2), extensive (LS_3) and complete (LS_4) limit states considering chloride induced corroded buildings on stiff foundations. 276

Figure 8.31. Fragility curves in terms of PGD for different points in time (0, 20, 40, 60 and 90 years), for slight (LS_1), moderate (LS_2) and extensive (LS_3) limit states considering chloride induced corroded buildings on stiff foundations. 277

Figure 8.32. Time-dependent quadratic fit of median values of PGA for the slight, moderate, extensive and complete limit states considering chloride induced corroded buildings on stiff foundations 278

Figure 8.33. Time-dependent quadratic fit of median values of PGD for the slight, moderate, extensive and complete limit states considering chloride induced corroded buildings on stiff foundations 278

Figure 8.34. Fragility surfaces as a function of time and PGA for slight, moderate, extensive and complete limit states (fit: Interpolant) considering chloride induced corroded buildings on stiff foundations 279

Figure 8.35. Fragility surfaces as a function of time and PGD for slight, moderate, extensive and complete limit states (fit: Interpolant) considering chloride induced corroded buildings on stiff foundations 280

Figure A.1. Slope geometrical configuration 1- Models 1 to 4 310

Figure A.2. Slope geometrical configuration 2- Models 5 to 9 311

Figure A.3. Slope geometrical configuration 3- Models 9 to 12 312

Figure A.4. Slope geometrical configuration 4- Models 13 to 16 313

Figure A.5. Slope geometrical configuration 5- Models 17 to 20 314

Figure A.6. Slope geometrical configuration 6- Models 21 to 24 315

Figure B.1. Proposed fragility curves as a function of PGA (left) and PGD (right) for low-code, low-rise RC frame buildings subjected to permanent landslide displacements.... 319

Σχήμα Ι.1. Διάγραμμα ροής της προτεινόμενης μεθοδολογίας για την εκτίμηση της τρωτότητας κτιρίων οπλισμένου σκυροδέματος 323

Σχήμα I.2. Τυπικό δισδιάστατο αριθμητικό προσομοίωμα που χρησιμοποιείται για την ανελαστική σεισμική ανάλυση 325

Σχήμα I.3. Αντιπροσωπευτικά πλαισιακά κτίρια Ο/Σ χαμηλού ύψους με εύκαμπτο και δύσκαμπτο σύστημα θεμελίωσης και περιγραφή της φόρτισης κινηματικού τύπου για τη διεξαγωγή της μη-γραμμικής, ψευδοστατικής ανάλυσης..... 326

Σχήμα I.4. Μέγιστες τιμές αναπτυχθείσας παραμόρφωσης συναρτήσει της PGA (αριστερά) και PGD (δεξιά) για ένα πλαισιακό κτίριο Ο/Σ χαμηλού ύψους σχεδιασμένου βάσει σύγχρονου κανονισμού με εύκαμπτο σύστημα θεμελίωσης, τοποθετημένο εγγύς της στέψης ενός αμμώδους πρανούς 327

Σχήμα I.5. Συγκριτική παρουσίαση τυπικών καμπυλών τρωτότητας συναρτήσει της PGA (αριστερά) και PGD (δεξιά) με βάση την μέθοδο της παλινδρόμησης (RA) και την μέθοδο της μέγιστης πιθανοφάνειας (ML) 327

Σχήμα I.6. Συγκριτική παρουσίαση των διαφορετικών μοντέλων για την εκτίμηση των σεισμικών μετακινήσεων των πρανών θεωρώντας μια άκαμπτη ολισθαίνουσα εδαφική μάζα (T_s=0.032 sec) 329

Σχήμα I.7. Συγκριτική παρουσίαση των διαφορετικών μοντέλων για την εκτίμηση των σεισμικών μετακινήσεων των πρανών θεωρώντας μια παραμορφώσιμη ολισθαίνουσα εδαφική μάζα (T_s=0.16 sec) 329

Σχήμα I.8. Σύγκριση των μετακινήσεων των Newmark's, Rathje και Antonakos (2011) και Bray και Travasarou (2007 με τις παραμένουσες σεισμικές μετακινήσεις των μη-γραμμικών δυναμικών αναλύσεων για την περίπτωση ενός δύσκαμπτου αμμώδους πρανούς..... 330

Σχήμα I.9. Σύγκριση των μετακινήσεων των Newmark's, Rathje και Antonakos (2011) και Bray και Travasarou (2007 με τις παραμένουσες σεισμικές μετακινήσεις των μη-γραμμικών δυναμικών αναλύσεων για την περίπτωση ενός εύκαμπτου αργιλώδους πρανούς..... 331

Σχήμα I.10. Το υπό μελέτη παραμετρικό μοντέλο 333

Σχήμα I.11. Προτεινόμενες καμπύλες τρωτότητας συναρτήσει της PGA (αριστερά) και της PGD (δεξιά) για τυπικά πλαισιακά κτίρια Ο/Σ χαμηλού ύψους σχεδιασμένα με συγχρόνους κανονισμούς που υπόκεινται σε παραμένουσες εδαφικές μετακινήσεις λόγω πιθανής κατολίσθησης 335

Σχήμα I.12 Καμπύλες τρωτότητας συναρτήσει της PGA (αριστερά) και της PGD (δεξιά) όταν μεταβάλλεται το επίπεδο του υπόγειου νερού (ξηρά ή μερικώς κορεσμένα εδαφικά υλικά) 336

Σχήμα Ι.13. Καμπύλες τρωτότητας συναρτήσει της PGA (αριστερά) και της PGD (δεξιά) για θεωρούμενο (ή όχι) υλικό κατολίσθησης που «χαλαρώνει» με την παραμόρφωση (strain softening material) 337

Σχήμα Ι.14. Καμπύλες τρωτότητας συναρτήσει της PGA (αριστερά) και της PGD (δεξιά) όταν μεταβάλλεται η ευκαμψία του συστήματος θεμελίωσης..... 337

Σχήμα Ι.15. Καμπύλες τρωτότητας συναρτήσει της PGA (αριστερά) και της PGD (δεξιά) για μονώροφα και διώροφα πλαισιακά κτίρια Ο/Σ ενός ανοίγματος 337

Σχήμα Ι.16. Καμπύλες τρωτότητας συναρτήσει της PGA (αριστερά) και της PGD (δεξιά) όταν για μονώροφα πλαισιακά κτίρια Ο/Σ ενός και δύο ανοιγμάτων 338

Σχήμα Ι.17. Καμπύλες τρωτότητας συναρτήσει της PGA (αριστερά) και της PGD (δεξιά) όταν μεταβάλλεται το επίπεδο σχεδιασμού της κατασκευής 338

Σχήμα Ι.18. Σύγκριση αντιπροσωπευτικών προτεινόμενων καμπυλών συναρτήσει της καθίζησης (ολικής κατακόρυφης μετακίνησης) με τις εμπειρικές καμπύλες των Zhang και Ng (2005) 339

Σχήμα Ι.19. Σύγκριση αντιπροσωπευτικών προτεινόμενων καμπυλών για εκτενείς βλάβες και ολική κατάρρευση συναρτήσει της παραμένουσας εδαφικής μετακίνησης (PGD) με τις καμπύλες του HAZUS (NIBS, 2004)..... 339

Σχήμα Ι.20. Σύγκριση αντιπροσωπευτικών προτεινόμενων καμπυλών συναρτήσει της διαφορικής μετακίνησης με τις αναλυτικές καμπύλες των Negulescu και Foerster (2010) 340

Σχήμα Ι.21. Συσχέτιση των εναρμονισμένων προτεινόμενων καμπυλών τρωτότητας συναρτήσει της PGA για χαμηλού ύψους, πλαισιακά κτίρια Ο/Σ σχεδιασμένων βάσει σύγχρονων κανονισμών που εκτίθενται σε παραμένουσες σεισμικές μετακινήσεις λόγω πιθανής κατολίσθησης με τις αντίστοιχες των Kappos et al. (2003), Tsionis et al. (2011), Erberik (2008) και Fotopoulou et al. (2012) για τις ίδιες τυπολογίες κτιρίων που υπόκεινται σε σεισμική ταλάντωση 341

Σχήμα Ι.22. Προτεινόμενες καμπύλες τρωτότητας αντιπροσωπευτικές της περιοχής μελέτης και των χαρακτηριστικών των κατασκευών της περιοχής..... 342

Σχήμα Ι.23. Συσχετίσεις μεταξύ της μόνιμης μετατόπισης του υπό μελέτη κτιρίου από μετρήσεις γεωδαιτικής χωροστάθμησης (geodetic levelling), της παραμένουσας εδαφικής μετακίνησης από το κοντινότερο σε σχέση με τη θέση του κτιρίου ινκλινόμετρο καθώς και των μετρήσεων ανοίγματος των ρωγμών του κτιρίου (συγκρινόμενα με τις οριζόμενες στάθμες βλάβης) συναρτήσει του χρόνου (Callerio et al., 2007) 344

Σχήμα Ι.24. Αντιπροσωπευτικές αναλυτικές καμπύλες τρωτότητας που προέκυψαν από την παραμετρική διερεύνηση για κλίση πρανούς $\beta=30^{o}$ (αριστερά) και $\beta=45^{o}$ (δεξιά) .. 344

Σχήμα I.25. Καμπύλες τρωτότητας που προτείνονται για το υπό μελέτη κτίριο στην περιοχή του Corniglio 345

Σχήμα I.26. Μεταβολή της κανονικοποιημένης επιφάνειας του οπλισμού με το χρόνο λόγω του φαινομένου της διάβρωσης για τα σενάρια (α) της ενανθράκωσης του χάλυβα και (β) της επίδρασης χλωριόντων 347

Σχήμα I.27. Χρονικά εξαρτώμενες καμπύλες και επιφάνειες τρωτότητας συναρτήσει του PGD, για μικρές (LS_1), μέτριες (LS_2), εκτενείς (LS_3) βλάβες και ολική κατάρρευση (LS_4), για ένα τυπικό χαμηλού ύψους πλαισιακό κτίριο Ο/Σ επί εύκαμπτου συστήματος θεμελίωσης, για το σενάριο της διάβρωσης που σχετίζεται με τη διείσδυση χλωριόντων 348

Σχήμα I.28. Αναπαράσταση της χρονικά εξαρτώμενης διαμέσου (σε όρους PGD) των καμπυλών με πολυώνυμο $2^{ου}$ βαθμού για την περίπτωση των μικρών (LS_1), μέτριων (LS_2), εκτενών (LS_3) βλαβών και για ολική κατάρρευση (LS_4), για ένα τυπικό χαμηλού ύψους πλαισιακό κτίριο Ο/Σ επί εύκαμπτου συστήματος θεμελίωσης, για το σενάριο της διάβρωσης που σχετίζεται με τη διείσδυση χλωριόντων..... 349

LIST OF TABLES

Table 2.1. Detailed list of sites and villages with remarkable ground failures (Pavlides et al., 2004)..... 19

Table 2.2. Characteristics of earthquake-induced landslides (Keefer, 2002) 22

Table 2.2. (Continued) - Characteristics of earthquake-induced landslides (Keefer, 2002) 23

Table 2.3. Geometric characteristics of earthquake-induced landslides (Rodríguez et al., 1999). 24

Table 2.4. Guidelines for selecting appropriate sliding-block analysis (Jibson, 2011) ... 35

Table 3.1. Damage Criteria based on angular distortion (after Bjerrum, 1963) 51

Table 3.2. Classification of visible damage to walls with particular reference to ease of repair of plaster and brickwork masonry (after Burland, 1995). 52

Table 3.3. Structural damage state descriptions for RC frame buildings (Crowley et al., 2004; Bird et al., 2005) 54

Table 3.4. Suggested mean post-yield limit state strains for steel (ε_s) and concrete (ε_c) for poorly confined (poor) and well confined (good) RC frame buildings subject to ground deformations (Bird et al., 2005) 54

Table 3.5. Suggested limit states for rigid body settlement and rotation due to earthquake induced ground deformations (Bird et al., 2005) 54

Table 3.6. Damage expected from slow-moving slides to urban communities versus movement rate (Mansour et al., 2011) 55

Table 3.7. Data and their relevant raw and standardized scores (after Papathoma et al., 2007) 58

Table 3.8. Building value and vulnerability considering exposure to different landslide types within the Fanhões-Trancão test site (Zêzere et al., 2008) 59

Table 3.9. Values of susceptibility factor for structural typology (Uzielli et al., 2008)... 60

Table 3.10. Values of susceptibility factor for state of maintenance (Uzielli et al., 2008) 60

Table 3.11. Possible sets of values for kinetic and kinematic relevance factors for structures (Uzielli et al., 2008) 61

Table 3.12. Proposed tentative vulnerabilities at different foundation depths (Li et al., 2010) 63

Table 3.13. HAZUS Building Damage Relationship to PGD - Shallow Foundations 66

Table 3.14. Existing methods to assess building vulnerability to slides in relation to the methodological framework adopted 67

Table 4.1. Soil properties of the analyzed slopes 76

Table 4.2. Foundation properties 79

Table 4.3. Interface properties 79

Table 4.4. Selected outcropping records used for the dynamic analyses 80

Table 4.5. Structural damage state descriptions for RC frame buildings (Crowley et al. 2004) 95

Table 4.6. Definition of limit states for "low" and "high" code design RC buildings 95

Table 4.7. Parameters of fragility functions for PGA based on the regression analysis method 100

Table 4.8. Parameters of fragility functions for PGD based on the regression analysis method 100

Table 4.9. Parameters of fragility functions for PGA based on the Maximum likelihood method 106

Table 4.10. Parameters of fragility functions for PGD based on the Maximum likelihood method 106

Table 5.1. Parameters describing the characteristics of the ground motions and the slope dynamic response used for the analyses 126

Table 5.2. Parameters of the models for rock outcropping accelerograms scaled at PGA=0.7g- sand slope (T_s=0.032sec) 136

Table 5.3. Comparison of FLAC horizontal displacements to analytical Newmark rigid block method, Rathje and Antonakos (2010) decoupled approach and Bray and Travasarou (2007) coupled stick-slip displacement method for rock outcropping accelerograms scaled at PGA=0.7g sand slope (T_s=0.032sec) 136

Table 5.4. Error (%) of the models in the displacement estimation compared to the corresponding FLAC displacement calculation for rock outcropping accelerograms scaled at PGA=0.7g- sand slope (T_s=0.032sec) 137

Table 5.5. Parameters of the models for rock outcropping accelerograms scaled at PGA=0.7g- clay slope (T_s=0.16sec) 139

Table 5.6. Comparison of FLAC horizontal displacements to analytical Newmark rigid block method, Rathje and Antonakos (2011) decoupled approach and Bray and Travasarou (2007) coupled stick-slip displacement method for rock outcropping accelerograms scaled at PGA=0.7g- clay slope (T_s=0.16sec) 139

Table 5.7. Error (%) of the models in the displacement estimation compared to the corresponding FLAC displacement calculation for rock outcropping accelerograms scaled at PGA=0.7g- clay slope (T_s=0.16sec)..... 140

Table 6.1. Model features for the parametric analysis..... 150

Table 6.2. Varying soil properties of the analyzed slope configurations..... 151

Table 6.3. Parameters of fragility functions for all the analyzed models when using PGA as an intensity measure 158

Table 6.4. Parameters of fragility functions for all the analyzed models when using PGD as an intensity measure 159

Table 6.5. Parameters of the proposed fragility functions using PGA as an intensity measure 169

Table 6.6. Parameters of the proposed fragility functions using PGD as an intensity measure 169

Table 7.1. Summary of tolerable and intolerable settlements on buildings considering different foundation types (adapted from Zhang and Ng, 2005) 184

Table 7.2. Summary of tolerable and intolerable settlements on buildings considering different foundation types (adapted from Zhang and Ng, 2005) 185

Table 7.3. Statistics of intolerable and limiting tolerable settlement and angular distortion of buildings (adapted from Zhang and Ng, 2005) 185

Table 7.4. Fragility parameters of the proposed curves in terms of settlement and angular distortion..... 186

Table 7.5. Suggested log-normally distributed fragility parameters of HAZUS for shallow/unknown foundations 189

Table 7.6. Fragility parameters of the proposed curves in terms of PGD, PHGD and PVGD 190

Table 7.7. Fragility parameters of the numerically derived curves provided by Negulescu and Foerster (2010) 194

Table 7.8. Fragility parameters of the proposed curves in terms of differential ground displacement 194

Table 7.9. Main parameters of the literature seismic fragility curves used for the comparison 198

Table 7.10. Fragility parameters of the harmonized proposed fragility curves used for the comparison (sand soil, flexible foundation) 199

Table 7.11. Soil properties used for the 2D finite difference cross-section 209

Table 7.12. Definition of Limit states for "low-code" RC buildings 213

Table 7.13. Parameters of the representative fragility functions 226

Table 7.14. Assumed soil properties for the geotechnical profile B-B 229

Table 7.15. Ground motion records used in the numerical simulations derived from the SHARE database 231

Table 7.16. Parameters of fragility functions for the studied building in Corniglio village based on the Maximum likelihood method 234

Table 8.1. Statistical characteristics of parameters affecting the carbonation induced corrosion deterioration of RC elements 245

Table 8.2. Statistical characteristics of parameters affecting the chloride induced corrosion deterioration of RC elements 252

Table 8.3. Statistical characteristics of parameters affecting the carbonation induced corrosion deterioration of RC elements adopted in the present study 255

Table 8.4. Statistical characteristics of parameters affecting the chloride induced corrosion deterioration of RC elements adopted in the present study 255

Table 8.5. Definition of limit states for the buildings at different points in time for the carbonation induced deterioration scenario 259

Table 8.6. Definition of limit states for the buildings at different points in time for the chloride induced deterioration scenario 260

Table 8.7. Parameters of fragility functions over time as a function of PGA and PGD for buildings with flexible foundation system considering carbonation induced reinforcement corrosion 261

Table 8.8. Percent (%) changes in median PGA/PGD and dispersion β values with aging for buildings with flexible foundation system considering carbonation induced reinforcement corrosion 262

Table 8.9. Parameters of fragility functions over time as a function of PGA and PGD for buildings with stiff foundation system considering carbonation induced reinforcement corrosion 266

Table 8.10. Percent (%) changes in median PGA/PGD and dispersion β values with aging for buildings with stiff foundation system considering carbonation induced reinforcement corrosion 266

Table 8.11. Parameters of fragility functions over time as a function of PGA and PGD for buildings with flexible foundation system considering chloride induced reinforcement corrosion 271

Table 8.12. Percent (%) changes in median PGA/PGD and dispersion β values with aging for buildings with flexible foundation system considering chloride induced reinforcement corrosion 271

Table 8.13. Parameters of fragility functions over time as a function of PGA and PGD for buildings with stiff foundation system considering chloride induced reinforcement corrosion 275

Table 8.14. Percent (%) changes in median PGA/PGD and dispersion β values with aging for buildings with stiff foundation system considering chloride induced reinforcement corrosion 276

Table B.1. Parameters of the proposed fragility functions using PGA as an intensity measure 320

Table B.2. Parameters of the proposed fragility functions using PGD as an intensity measure 320

CHAPTER 1

Introduction

1.1 Motivation and objectives of the research

Landslides triggered by earthquakes represent a major threat to the population and the built environment in most mountainous and hilly regions of the world. Marano et al. (2010) observed that landslides are both the most abundant and the most deadly secondary effect of earthquakes, being responsible for 71.1% of the non-shaking deaths. For instance, the 2008 Wenchuan earthquake in China is estimated to have triggered more than 15000 landslides of various types covering an area of 50,000 km^2, causing approximately 20,000 fatalities and tremendous economic losses (Yin et al., 2009). Therefore, there is an increasing requirement for effective evaluation, management and mitigation of the risk associated with earthquake-induced landslides.

In any landslide risk assessment study, the focus is on the asset, i.e., *the element at risk that may suffer damage from a harmful landslide* and not on the single slope or the mapping unit where landslides can occur. As a consequence, to determine landslide risk information on slope failures and their expected evolution, which is generally the product of a hazard or susceptibility assessment study, is necessary but not enough. The landslide risk estimation also requires information regarding the type, spatial and temporal distribution and vulnerability of the elements at risk in the study area.

Although Quantitative Risk Assessment (QRA) procedures are well established for earthquakes and river floods hazards, in the case of landslides, QRA methodologies have been developed only recently and they are far from being routinely used by the scientific and technical community. The main reason for this is that several key components of risk are uncertain and/or difficult to obtain (Corominas and Mavrouli, 2011b). Among them, the quantitative evaluation of the vulnerability of the exposed elements is affected by a great deal of uncertainty due to its multifaceted and dynamic nature that constraints its assessment in an objective way and makes its integration into the risk equation, a challenge.

In this context, the main goal of this thesis is to propose and quantify an innovative analytical methodology to assess the vulnerability of reinforced concrete buildings subjected to earthquake-induced slow-moving slides. Various sets of probabilistic fragility curves are proposed that might be used by scientists and practitioners for efficient implementation within a probabilistic risk assessment framework from site specific to local scales. The method is verified through the comparison of representative suggested curves with reference literature curves and real event damage data.

Traditionally, seismic and landslide vulnerability assessment studies implicitly refer to the intact, as-built structure assuming an optimum plan of maintenance. Nevertheless, the real, dynamic vulnerability modeling of structures due to landslides may be significantly affected by aging considerations, anthropogenic actions, cumulative damage from past landslide events and retrofitting measures. To bridge this gap, the proposed approach is also extended to account for the evolution of building vulnerability over time by proposing time-dependent fragility curves for RC buildings exposed to earthquake – induced landslide hazard.

Partial objectives and associated results are summarized as follows:

- Identification of the basic categories in which the earthquake triggered landslides are classified as well as the key parameters affecting seismic slope stability
- Critical review of methods to assess earthquake induced landslide hazards
- Literature review of existing quantitative methodologies to assess building vulnerability to slides
- Description on the methods to derive fragility curves, on the selection of appropriate intensity measures for different landslide types, on the extent and mechanisms of building damage to slow-moving slides and on the definition of structural and non-structural damage/limit states
- Proposition and quantification of an innovative procedure to assess the vulnerability of reinforced concrete (RC) structures due to earthquake induced slow-moving slides based on an uncoupled numerical modeling approach and adequate statistical analysis
- Comparison of the computed numerical results derived from the proposed approach, in terms of permanent horizontal displacement, with Newmark-type displacement-based methods
- Development of various sets of fragility curves accounting for different building typologies, slope configurations and soil conditions through an extensive parametric investigation and sensitivity analysis

- Validation of the developed method via comparison of the suggested fragility curves with literature ones derived from different approaches i.e. empirical, expert judgment and analytical.
- Correlations of representative fragility curves proposed in this research for buildings located on the top of topographic features subjected to earthquake induced slides to respective curves for buildings on horizontally layered soil deposits subjected to ground shaking.
- Reliability assessment of the method through comparison of the developed fragility functions to the damage data on typical buildings recorded in two real case histories: Kato Achaia slope in Peloponnese –Greece and the Corniglio village-Italy case study
- Development of more realistic fragility curves for a typical building in Corniglio village. Validation of the curves through comparison of the predicted damage by the curves to the corresponding damage observed for the measured level of displacement.
- Broadening of the developed methodological framework to account for the evolution trends of building vulnerability to earthquake induced landslide hazard over time-Proposition of time-dependent fragility functions.

1.2 Outline of the Thesis

This thesis is organized into nine chapters with the following contents:

In the present chapter (**Chapter 1**) the motivation and main goals that aspire to fulfill this thesis are presented. The organization of the remaining chapters is following.

In **Chapter 2** an overview on landslides triggered by earthquakes is presented. First, a summary of some of the most pronounced, from an engineering point of view, seismically induced landslides experienced worldwide and in Greece is provided. Furthermore, particular effort is devoted in identifying the basic categories in which the earthquake triggered landslides are classified as well as the key parameters affecting seismic slope stability. The Chapter ends with the description of different methods to assess earthquake induced landslide hazards that vary from simplified empirical or semi-empirical methods (e.g. pseudo-static analyses, Newmark- type displacement models) to more sophisticated numerical approaches. The importance of estimating the extent of permanent ground deformation along the sliding surface of the slope that may govern its serviceability level after an earthquake and cause structural distress and damage to affected buildings and infrastructures is emphasized.

In **Chapter 3** a critical review of existing quantitative methodologies to assess building vulnerability to slides is presented. Various concepts and aspects of physical vulnerability to slides are discussed and analyzed regarding the development of fragility curves, the selection of appropriate intensity measures for different landslide types, the extent and mechanisms of building damage to slow-moving slides and the definition of structural and non-structural damage/limit states. The general lack of methods to quantify the physical vulnerability of structures to slides based on analytical relationships and numerical analysis is highlighted.

Chapter 4 focuses on the proposition and quantification of an analytical procedure to assess the vulnerability of reinforced concrete (RC) structures due to earthquake induced slow-moving slides. Vulnerability is expressed in terms of probabilistic fragility curves, which describe the probability (P_i) of exceeding each limit state (LS_i) of a RC building located next to the crest of the potentially unstable slope, versus the landslide intensity measure e.g. peak ground acceleration at the assumed "seismic bedrock" or permanent ground/foundation displacement at the slope area, allowing for the quantification of various sources of uncertainty. The proposed methodological framework is described with a simplified case study. In terms of numerical computations, a two-step uncoupled analysis is performed. In the first step, the deformation demand, i.e. total and differential displacements considering the actual weight and stiffness of the building and its foundation, due to the landslide hazard is assessed using an adequate non-linear finite difference dynamic slope model. In the second step, the building response to the statically imposed landslide differential displacement is estimated using a Finite Element code. Modeling issues and associated assumptions concerning both analysis steps are addressed in full detail. Two alternative analytical procedures amenable to estimate the parameters of fragility functions are presented and compared to stress the influence of epistemic uncertainty on the fragility analysis.

In **Chapter 5** three different Newmark-type displacement models are presented and compared, namely the conventional analytical Newmark rigid block, the Rathje and Antonakos (2011) decoupled and Bray and Travasarou (2007) coupled model, to assess their relative predictive capability in estimating the expected slope displacements for certain earthquake scenarios. Then, to enhance the reliability and robustness of the computed numerical results derived from the non-linear dynamic analysis (Chapter 4), they are compared, in terms of permanent horizontal displacements, with the corresponding predicted displacements from the three Newmark-type models for the step-like slope configurations and soil conditions presented in Chapter 4 in the absence of any structure near its crest.

In **Chapter 6** different sets of fragility functions for a variety of RC building typologies, soil conditions and slope configurations are proposed, based on the analytical method described in Chapter 4, with potential application from site specific to local/regional scales. To this aim, an extensive parametric study is performed by considering different idealized finite slope geometries, soil geological settings and distances of the structure to the slope's crest. The effect of the various analyzed features on the structural performance is investigated, highlighting trends on the building's behavior to the permanent co-seismic slope deformations. Generic fragility curves as a function of PGA at the outcrop and PGD at the slope area that could be used for several practical applications are then suggested based on the parameters that are proved to most significantly affect the structure's vulnerability. Moreover, a sensitivity analysis is conducted to gain insight into the influential role of various additional parameters, namely the water table level, the consideration of a strain softening landslide material, the flexibility of the foundation system, the number of bays and storeys of the building and the code design level on the structure's fragility.

Chapter 7 aims at verifying the validity of the proposed methodology (Chapter 4) and of the respective fragility curves (Chapter 6). It is divided into three main parts. In the first part, the reliability and accuracy of the proposed methodology (Chapter 4) is assessed through the comparison of representative proposed fragility curves (Chapter 6) with corresponding literature curves derived by different approaches (empirical, expert judgment, analytical). The second part provides approximate correlations between the fragility curves suggested in this research for RC buildings subjected to co-seismic permanent slope displacement and literature ones derived for low-rise RC buildings on horizontally layered soil deposits subjected to ground shaking. Overall, the comparisons allow gaining further insight into the relative extent of damage and the associated prevailing damage mechanisms for structures impacted by co-seismic slope deformation and ground shaking respectively. In the third part, the reliability and applicability of the proposed methodological framework and the corresponding fragility curves is also assessed through its application to two real case histories: Kato Achaia slope in Peloponnese –Greece and the Corniglio village-Italy case study. In particular, the recorded damage data on typical buildings is compared with the corresponding damage predicted by the developed fragility functions. In addition, to enhance the effective implementation of the proposed methodological framework within a probabilistic risk assessment study, more realistic fragility curves are constructed for a representative building in Corniglio village based on straightforward numerical computations. The curves were validated through their direct comparison with the observed building damage data for the measured level of displacement.

In **Chapter 8** the proposed methodological framework (Chapter 4) is extended to account for the evolution trends of building vulnerability to earthquake induced landslide hazard over time. In particular, the aging of typical RC buildings is considered by including probabilistic models of corrosion deterioration of the RC elements within the vulnerability modeling framework. Two potential adverse corrosion scenarios are examined: chloride and carbonation induced corrosion of the steel reinforcement. An application of the proposed methodology to reference low-rise RC buildings exposed to the combined effect of seismically induced landslide differential displacements and reinforcement corrosion is provided. Both buildings with stiff and flexible foundation system standing near the crest of a potentially precarious soil slope are examined. The method results to the construction of time-dependent fragility curves/surfaces as a function of PGA at the seismic bedrock or PGD at the slope area for both chloride and carbonation induced deterioration scenarios.

Chapter 9 summarizes the main findings and contributions of the work. Recommendations for future research are also provided.

1.3 Evidence of originality of the Thesis

The work's main originality principally lies in the following points:

- To the author's knowledge, this is the first time that a comprehensive analytical method to assess the vulnerability of RC buildings subjected to earthquake induced slow-moving slides is proposed.
- Furthermore, an unusually extensive set of numerical computations is performed to estimate vulnerability for a variety of RC building typologies, soil conditions and slope configurations. These computations provide insight into the influential role of the various analyzed features on the structure's fragility.
- It 's also the first time that fragility curves for RC buildings exposed to earthquake induced slow-moving landslides are proposed. Such curves allow for an efficient quantitative estimation of vulnerability within a probabilistic risk assessment framework from site specific to local/regional scales.
- The validation of the method and of the corresponding fragility curves with high-quality, recoded damage and displacement data and the proposition of more realistic fragility curves for a representative building in Corniglio village, based on straightforward numerical computations, offer a substantial and *original* contribution to scientific research in the quantitative risk assessment field.

- Finally, the dynamic nature of vulnerability has been traditionally neglected in any vulnerability assessment study. A major contribution and novelty of the present work is thus the expansion of the proposed method to account for the evolution of building's vulnerability over time exposed to the combined effect of earthquake – induced landslide and aging. Preliminary time –dependent fragility curves for different damage states are analytically evaluated at different points in time, considering different structural deterioration scenarios.

CHAPTER 2

Landslides triggered by earthquakes

2.1 Introduction

The destructive impact of earthquakes can be greatly enhanced by the induced triggering of landslides during or after the shaking (Bommer and Rodrıguez, 2002). Strong earthquakes can potentially trigger landslides that can induce catastrophic losses in terms of human lives and infrastructure damage. Marano et al. (2010) observed that landslides are both the most abundant and the most deadly earthquake-induced secondary effect, being responsible for 71.1% of the non-shaking deaths (see Fig. 2.1). According to Wen et al. (2004), around 20% of the registered landslides are triggered by earthquakes. In particular, China is the country characterized by significant casualties associated to slides triggered by earthquakes (Huang and Li, 2011) and many seismic active countries around the world present records of slope failures causing tremendous damages and casualties. Therefore, there is an urgent need for efficient landslide hazard, vulnerability and risk assessment and management at different scales.

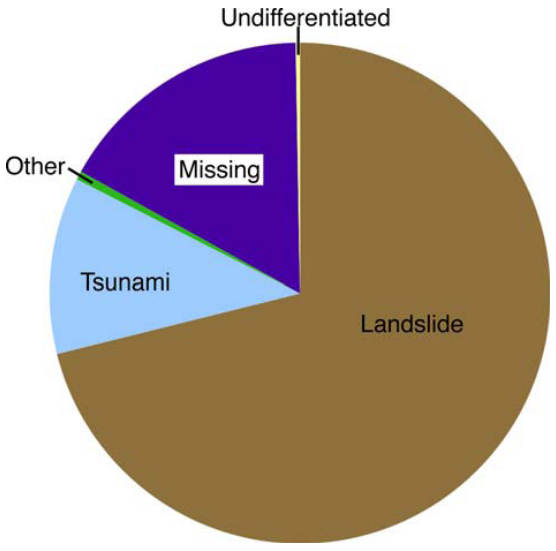


Figure 2.1. Non-shaking earthquake fatalities for all deadly earthquakes between September 1968 and June 2008, with deaths from the 2004 Sumatra event removed (source: Marano et al., 2010)

2.1.1 Worldwide destructive earthquake induced landslides

Earthquake induced landslides have been documented from at least as early as 1789 BC in China (Hansen and Franks, 1991) and 372 BC in Greece (Seed, 1968). Geographic Information Systems (GIS) and remote sensing have significantly improved the ability to map earthquake-induced landslides. Various earthquake triggered slides have been mapped and analyzed in California, Taiwan, Japan, Italy and elsewhere. With the aid of the GIS incorporating various models (geotechnical parameters, geology, hydrology, digital elevation model (DEM), land use, lithology, seismic parameters), analyses of the landslide susceptibility, hazard and risk in local, regional and national scales have been performed in a deterministic or probabilistic sense. The implementation of GIS tool in the landslide susceptibility, hazard and risk zoning at different scales is discussed among others by Wang et al. (2008), Van Westen et al. (2008), Hasegawa et al. (2009) and Miles and Keefer (2009).

Some of the most pronounced recently occurred seismically induced landslides worldwide that present particular interest from an engineering viewpoint are briefly outlined below.

The 13th January **2001 El Salvador earthquake** (Mw=7.7) caused widespread damage to buildings and infrastructure due to ground shaking and earthquake-induced ground failures, including several large-scale landslides. The most tragic among them and one of the most destructive landslides ever recorded was the **Las Colinas landslide** (Fig. 2.2), occurred on the steep northern flank of the Bálsamo Ridge, involving a total volume of about 180,000 m^3 of stratified volcanic deposits (Crosta et al., 2005). Once triggered, the landslide developed into a flowslide, traveling northward an abnormally long distance of about 700 m into the Las Colinas neighborhood of Santa Tecla. It covered hundreds of residential houses, resulting in about 500 casualties (Konagai et al., 2009).



Figure 2.2. Las Colinas landslide in El Salvador

The 23th October **2004 Niigata–Ken Chuetsu earthquake** (Mw=6.8) in Japan caused more than 4000 slope failures within the area about 200 km North of the city of Tokyo. Among the great number of slope failures during the 2004 earthquake, 282 ground failures exceeded 10^4 m^3 and 10 exceeded 10^5 m^3 in terms of the affected areas. The **Higashi-Takezawa landslide** (Fig. 2.3) activated by the earthquake was a large-scale rapid landslide involved a soil volume of about 1,200,000 m^3 (Kokusho and Ishizawa, 2005). The landslide mass filled a valley and stopped a river flow forming a large natural reservoir. One part of the sliding mass spread across the road and hit a school (Fig. 2.4). The surprisingly large (100m) and rapid runoff of the soil mass motivated several researchers (Tsukamoto and Ishihara, 2005; Sassa et al., 2005; Kokusho et al., 2009) to study the Higashi– Takezawa landslide, providing different interpretations of the sliding process.



Figure 2.3. General view of the Higashi Takezawa landslide and the head scarp of past landslide (Sassa et al., 2005)



Figure 2.4. School building hit by the landslide mass (Sassa, 2005)

Except for the destructive impact of the Higashi-Takezawa landslide, many other slope failures induced significant direct and indirect losses to the built environment as a result of the 2004 Niigata–Ken Chuetsu earthquake. For instance, a large number of houses were affected by the slope instability at the **Takamachi housing complex** in southeast Nagaoka City triggered by the earthquake. In particular, fill slopes around the complex underwent significant deformation resulting to extensive ground cracks and to the complete collapse of four slopes. Ohtsuka et al. (2009) analyzed the correlation among fill thickness, ground cracks and damage to houses. They found that most of the damaged houses were distributed throughout the fill area. Moreover, they revealed a strong correlation between the damage to houses and the observed ground cracks, indicating that many houses were suffered structural damage due to differential settlement and lateral deformation. Figure 2.5(a) shows an example of a house that sustained severe damage due to uneven settlement and lateral displacement of its foundation system. Figure 2.5(b) illustrates the differential settlement of a periphery road in the fill area whereas Figure 2.5(c) shows a house at the edge of the main scarp of a fill slope that suffered significant damage.



Figure 2.5. (a) Damage to houses as a result of ground deformation (b) Differential settlement of periphery road (c) Slope failure of valley fill (Ohtsuka et al., 2009)

The 21st September **1999 Chi-Chi Taiwan earthquake** (M_L=7.3, M_W=7.6) caused severe damage including more than 11,000 casualties and over US$11.8 billion capital lost (4% of Taiwan's GNP). After the earthquake, over 20,000 landslides totaling approximately 113 km^2 had occurred in an area of 2400 km^2 in central Taiwan. More than 90% of the landslides were smaller than 0.01 km^2 in scale, and most were shallow debris slides, although a few being large and deep-seated (Lin et al., 2003). Figure 2.6 shows representative slope failures resulting to severe damage to a building and the road network respectively. The **Jiufengershan landslide** (Fig. 2.7) was one of the major large and deep-seated landslides triggered by the earthquake (Shou and Wang, 2003). The slide affected weathered, jointed rock and soil materials, which slide along the bedding plane, generating a catastrophic rockslide-avalanche. The avalanche which created a debris deposit with maximum thickness of 110 m dammed two small rivers and created three small lakes located upstream, resulting to 39 casualties (Chang et al., 2005).



Figure 2.6. Damage to the built environment as a result of the 1999 Chi-Chi Taiwan earthquake induced landslides



Figure 2.7. General view of the Jiufengershan landslide (Dong et al., 2007)

The 8th October **2005 Kashmir earthquake** in Pakistan caused severe damage to the infrastructure and to the landscape including approximately 80,000 fatalities (Schneider, 2008). The earthquake triggered thousands of landslides throughout the region in an area of 7500 km^2, causing approximately 1000 fatalities, destroying roads, and disrupting communications. These were mainly rock falls and debris falls, although translational rock and debris slides also occurred (Owen et al., 2008). The largest landslide associated with the earthquake was the 68×10^6 m^3 **Hattian Bala rock avalanche** (Fig. 2.8) that destroyed a village. The reported death toll varies greatly; it is estimated to be a few hundreds to around 1000 people (Dunning et al., 2007; Schneider, 2008).



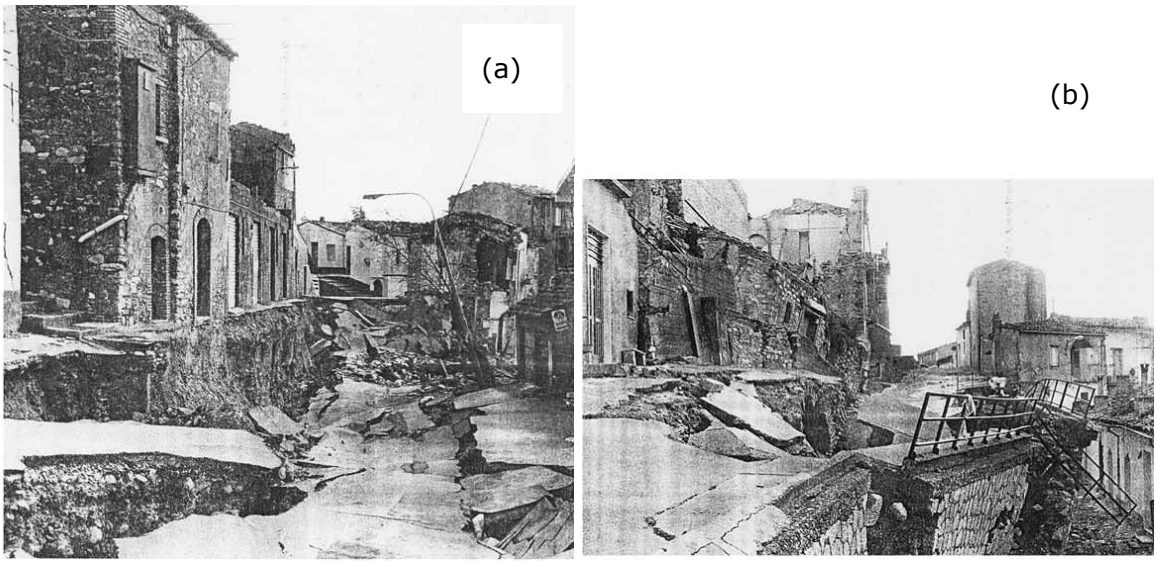
Figure 2.8. View to the source of the Hattian Bala rock avalanche (Dana Hill) from the high point of the dam crest (Dunning et al., 2007).

On May 12th, 2008, the catastrophic Ms 8.0 **Wenchuan earthquake** occurred in east Sichuan Province of China, causing more than 69000 casualties and extensive structural damage to the built environment. It was the strongest earthquake and the most costly natural disaster recognized to be occurred in China in the past 100 years. The earthquake triggered more than 15,000 geohazards in the form of earthslides, rockfalls and debris flows which resulted in about 20,000 deaths. Among the landslides activated by the earthquake, the **Chengxi landslide** (Fig. 2.9), which is located at the west side of the Beichuan County Town, is the most severe one; the landslide was characterized by its high speed and long runout (considering air-cushion effect) and involved a volume of around 2 million m^3. It buried a large portion of the southwest part of the old Beichuan resulting to 1,600 fatalities and significant economic losses (Yin et al., 2009).



Figure 2.9. Oblique aerial view (a) and vertical air photo (b) of the Chengxi landslide in Beichuan (Yin et al., 2009)

The 23 November **1980 Ms =6.9 Irpinia earthquake** in Southern Italy remobilized numerous mass movements. Among them, one of the most pronounced was the reactivation of the **Calitri landslide**, which was repeatedly reactivated by earthquakes since 1694. The landslide destroyed or seriously damaged over 100 houses and caused the death of 7 people. The town of Calitri in Irpinia (Southern Italy) located at the top of an approximately EW-trending hilly relief on the left bank of the Ofanto river, was severely damage by the landslide. Figures 2.10 a, b, c and d present damages to buildings and infrastructures in the town due to the landslide. The highest measured vertical displacement was reported to be equal to over 4 m and caused the sinking of a house; at the end of the sinking, the roof of the building lay at the same elevation as the road (Martino and Scarascia Mugnozza, 2005). The event, although not so devastating as the previous ones, presents particular interest for the European context.



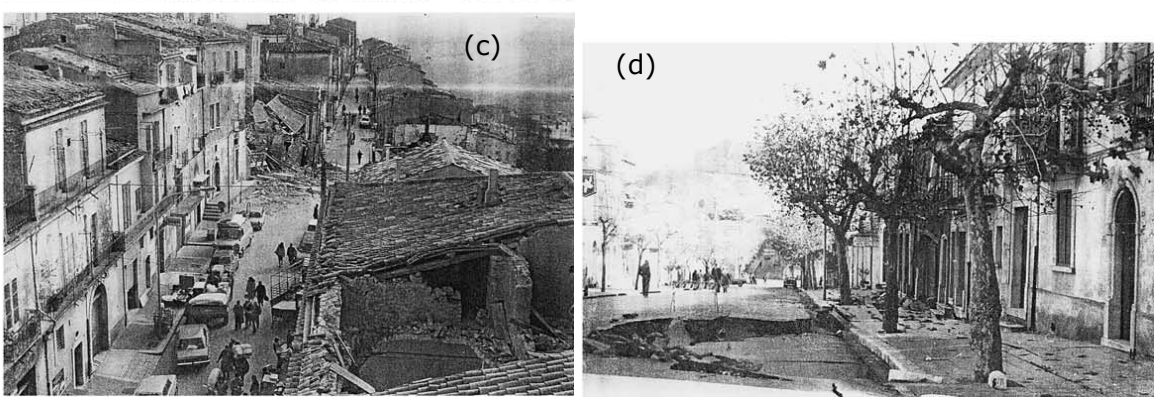


Figure 2.10. Calitri landslide activation in 1980, producing damage: on the Francesco De Sanctis main street (a), on the Torre street (b), along the landslide scarp at the Giacomo Matteotti main street (c), on the Garibaldi main street (d) (Martino and Scarascia Mugnozza, 2005)

2.1.2 Experience from earthquake induced landslides in Greece

In Europe, there are few and not well documented cases of earthquake induced landslides. Most of them are concentrated on the Mediterranean region (Greece and Italy). Papadopoulos and Plessa (2000) compiled a data set of 47 earthquake-induced landslides occurring in Greece from AD 1650 to 1995 and examined their distribution. The spatial distribution indicates landslides occurrence almost everywhere in Greece with the exception of the north Greek mainland, which is likely due to the low occurrence frequency of large earthquakes. Moreover, they examine the landslide distribution in relation to various earthquake parameters (earthquake magnitude, epicentral distance) and compare their result with those obtained by other authors for other seismotectonic regions of the world (Keefer, 1984; Ambraseys, 1988).

Some examples of landslides triggered by seismic events occurring in Greece over the last two decades as well as their consequences to the built environment are presented hereafter.

The June **1995 Aegion earthquake** (Ms=6.2) caused significant destruction, including human losses, structural damage, liquefaction and ground ruptures. The earthquake also triggered numerous landslides accompanied by debris flows and block rotations (Fig. 2.11). Reconstruction of the pre-earthquake topographic profiles along the main axis of the landslides indicates that the failure zones extended to a maximum depth of 6 to 10m within the loose alluvial deposits which cover the seabed. Post-earthquake landslides occurred for ground slopes as low as 12.0 %, corresponding to a static factor of safety of 2.0. At almost all sites, ground failures were triggered by excess pore pressure build up in very thin liquefied silty sand layers, with average thickness between 0.24 and 0.36m (Bouckovalas et al., 1995).

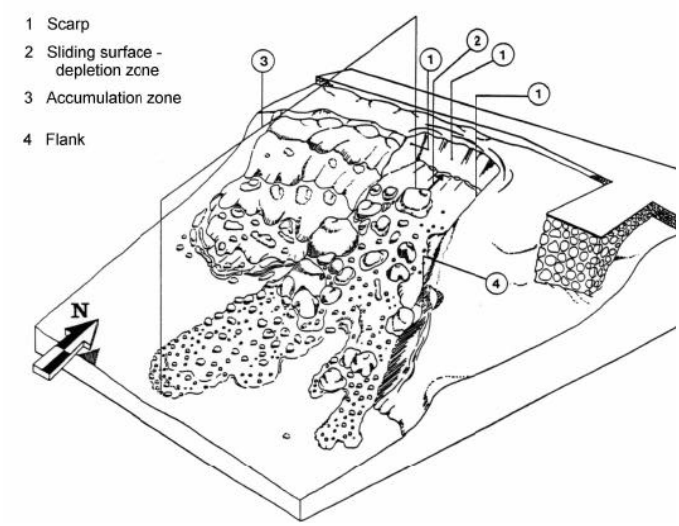


Figure 2.11. 3D perspective of a typical earthquake-induced landslide at Eratini Gulf (Bouckovalas et al., 1995)

The 7 September **1999 Athens earthquake** (Ms=5.9) was one of the most damaging events of the modern history of Greece (Bouckovalas and Kouretsis, 2001) causing the death of 143 people (Papadopoulos et al., 2000, Pavlides et al., 2002). Significant structural damage was noted, particularly in the area to the West of Athens. However, from the geotechnical point of view, the earthquake is not remembered for any spectacular ground failure. Ground damage, such as small-scale fissures and cracks as well as very local landslides, was observed in only a few spots. Ground fissures 5–10 cm wide and rockfalls of the order of 103 m^3 affected an area less than 1 km^2 in Agios Kyprianos monastery (Fig. 2.12). Cracks 5 cm wide and 5–6 cm deep were observed at Kleiston convent (Moni Kleiston), while similar cracks were observed close to the cable car station on Parnitha Mountain. A few local landslides of length 20–30 m also were reported in the same area (Fokaefs and Papadopoulos, 2007).



Figure 2.12. Rockfalls in Agios Kyprianos (Fokaefs and Papadopoulos, 2007)

The 14 August **2003 Lefkada earthquake** (Mw=6.2), due to the very steep morphology of the region, triggered a large number of landslides; the vast majority of them on the island road network can be categorized as rock falls, rock slides, and disrupted slides, with volume ranging from several cm^3 to some (5 to 10) m^3. Landslides were detected on both natural and cut slopes, as well as on downstream road embankment slopes. The slides were mainly observed at the central and northern part of the island, as well as in the steep western coastal zone along the road joining the town of Lefkada with Tsoukalades, Agios Nikitas, Kathisma, Kalamitsi, Chortata, Dragano and Komilio (Fig. 2.13). The steep morphology of the west coast, observed at the Ionian Islands, due to the active tectonism of the area, and the highly fractured rock mass played an important role in the appearance of such phenomena. The most characteristic rockfalls, with diameters up to 4 m, were observed along the 6 km long road of Tsoukalades-Agios Nikitas, which was very close to the epicentral area (EERI, 2003). In Table 2.1 a detailed list of sites and villages with remarkable ground failures is presented (Pavlides et al., 2004).



Figure 2.13. Rockfalls due to detachment and possible overturn at the Agios Nikitas (left); Cars were buried under landslides near the same area (right)

After the 8 January **2006 Kythira earthquake** (M=6.9) a number of landslides, rockfalls and rock slidings were detected on natural slopes, which resulted in cutting off parts of the road network and caused significant damage (fractures) of the road surface, and in some cases, local failure of road embankments. The largest landslides and rockfalls took place at Mitata village and its surroundings. Plan and side view of this natural slope landslide is shown in Figure 2.14.

Table 2.1. Detailed list of sites and villages with remarkable ground failures (Pavlides et al., 2004)

Id	NAME	LATDD	LONGDD	REMARKS
1.	NIKIANA	38.7745	20.7229	ROCK FALLS
2.	LYGIA	38.7873	20.7210	LIQUEFACTION –settlement
3.	AMMOGLOSSA	38.845	20.714	LIQUEFACTION- Settlement, mud ejection
4.	BRIDGE	38.839	20.711	GROUND CRACKS
5.	PARKING	38.8315	20.7080	LIQUEFACTION – mud ejection
6.	PORT	38.8320	20.7086	LIQUEFACTION
7.	PORT	38.8327	20.7103	LIQUEFACTION – Settlement
8.	PORT	38.8342	20.7119	Settlement – ROAD
9.	PORT	38.8350	20.7119	Settlement – PIER
10.	PORT	38.8355	20.7096	Settlement
11.	TSOUKALADES	38.8179	20.6413	ROCK FALLS
12.	KARYA	38.76	20.645	ROCK FALLS
13.	KAVALLOS	38.7918	20.6540	ROAD CRACKS
14.	ASPROGERAKAS	38.8028	20.6340	SLIDE
15.	ASPROGERAKAS	38.7909	20.6505	ROCK FALLS
16.	DRIMONAS	38.7877	20.6352	ROCK FALLS
17.	KALAMITSI	38.7704	20.6171	SLIDE
18.	AGNIKITAS	38.7898	20.6150	ROCK FALLS
19.	PEFKOULIA	38.8035	20.6310	LIQUEFACTION – Sand crater
20.	NYDRI	38.7115	20.7173	LIQUEFACTION –Sand boils
21.	NYDRI	38.7079	20.7122	LIQUEFACTION
22.	BASILIKI	38.6272	20.6069	LIQUEFACTION
23.	BASILIKI	38.6255	20.6066	LIQUEFACTION -Settlement
24.	BASILIKI	38.629	20.60	LIQUEFACTION – Mud Volcanoes
25.	AG.PETROS	38.6825	20.5968	SLIDE – ROCK FALL
26.	TSELIGAS	38.6285	20.5617	SLIDE OVER EGREMNOI BEACH



Figure 2.14. Plan (left) and side (right) view of the natural slope landslide at the main square of Mitata village (Karakostas et al., 2006)

The slope movements (rockfalls, disrupted slides etc) associated with the 8 June **2008 NW Peloponnese earthquake** (Mw=6.4) were spread over a wide area. The epicentral area was mainly affected by rockfalls along the steep slopes of the very impressive Scollis mountain, which caused damages on roads and houses around Santoneri (Fig. 2.15) and Portes village. The road network was affected in many areas, either by failures or rockfalls (Chatzipetros et al., 2008).



Figure 2.15. Santomeri village: location of the detached rock block that toppled (left) - the rock block itself (volume 6 to 7 cubic meters) that caused severe structural damage at one of the houses of the village (right) (Margaris et al., 2008)

2.2 Landslide classification and mechanisms

2.2.1 General classification of earthquake induced landslides

The term "landslide" describes a wide variety of ground processes that result in the downward and outward movements of slope-forming materials, including rock, soil, artificial filling, or a combination of these. Landslide classification is a very complex topic oriented by research purpose. Although the impact of a given landslide type is not always predictable, the class of landslide does present an indication of the type of movement and its destructive potential (Glade and Crozier, 2005). Starting from the work of Varnes (1978), Cruden and Varnes (1996) proposed a taxonomic classification of landslides which considers, in addition to the movement mechanism at the initial stage of motion, the material, the state of activity and the rate of movement (Fig. 2.16). However, they do not distinguish between the different triggering landslide mechanisms. In a pioneering study, Keefer (1984; 2002), based on the principles and terminology by Varnes (1978), classified the earthquake triggered landslides into three main categories on the basis of type of material, landslide movement, degree of internal disruption of the landslide mass and geologic environment (see Tab. 2.2):

Category I: Disrupted Landslides, which occur fast and at high inclinations (>35°) in discontinuous rock masses or weakly cemented materials.

Category II: Coherent Landslides either in rock or soil with deep slip weakened surfaces or with a relatively broad distributed shear zone, reported for inclinations >15°
Category III: Lateral Spreads and flows slides, associated to liquefaction in granular materials; if residual strengths are lower than static shear stresses, flow slides can develop at very low inclinations.

Keefer (1984) studied the landslides triggered by 40 historic earthquakes globally with magnitudes varying from 5.2 to 9.2 and found that the frequency of the seismically

induced landslides increases with increasing earthquake magnitudes. Three types of disrupted landslides – i.e. rock falls, disrupted soil slides, and rock slides - were found to be the most abundant, comprising about 80 percent of the earthquake induced landslides as reported in Keefer (2002). Rodriguez and co-workers (Rodriguez et al., 1999), after studying the landslides that occurred after 36 earthquakes worldwide, summarized the typical geometric characteristics of some of the most common slide categories (Table 2.3) including ranges of depth to the slip surface and the geometry of the slide in terms of the aspect ratio and the shape of the slip surface.

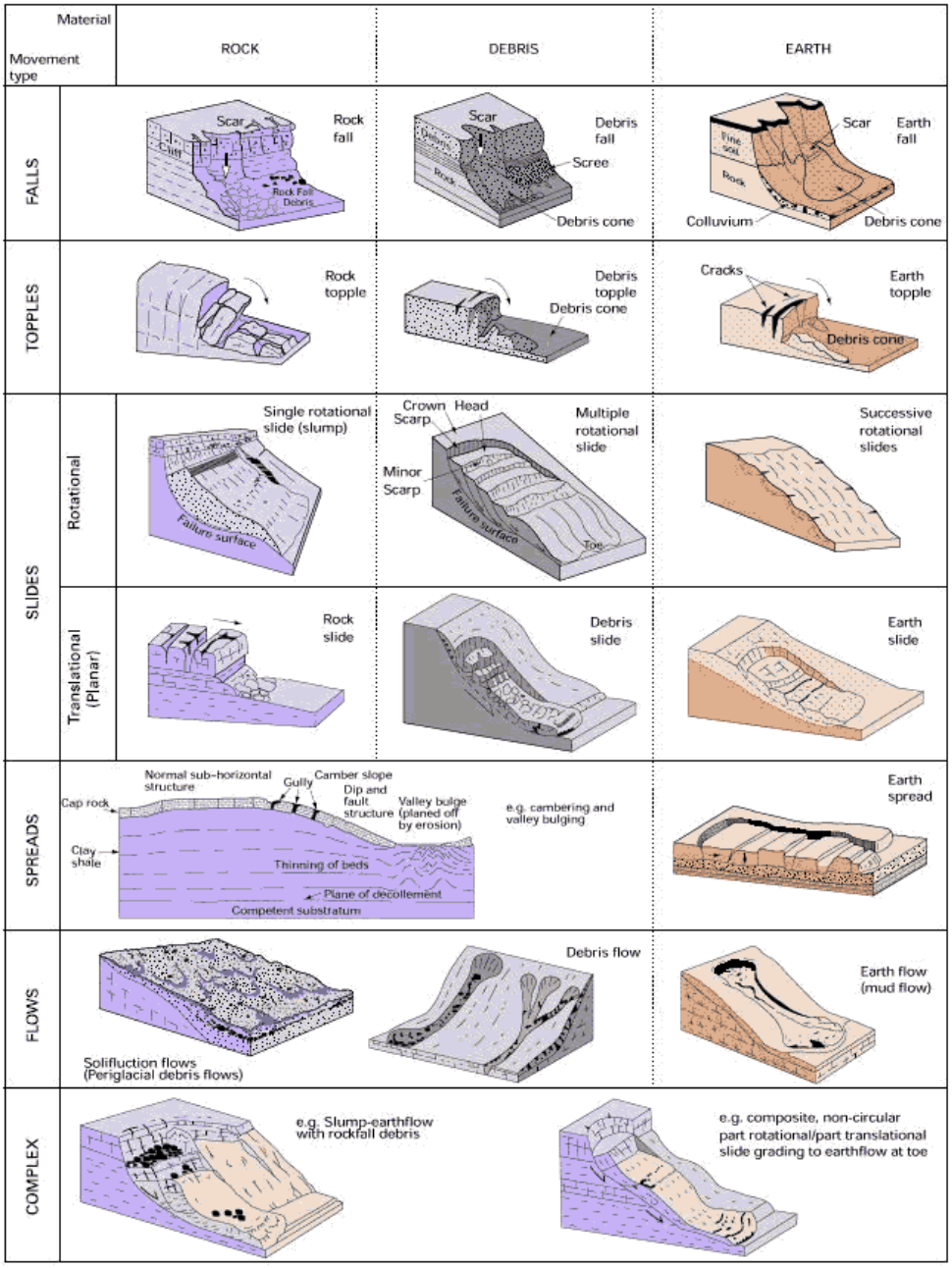


Figure 2.16. Classification of landslides (Modified after Varnes, 1978)

Table 2.2. Characteristics of earthquake-induced landslides (Keefer, 2002)

Name	Type of movement	Internal disruption	Water content				Typical depths	Minimum slope (°)	Typical velocities	Typical volumes	Typical displacements
			D	U	PS	S					
Disrupted landslides											
Rock falls	Bouncing, rolling, free fall	High or very high	×	×	×	×	Shallow	40	Extremely rapid	Most less than 1×10^4 m^3; maximum reported 2×10^7 m^3	May fall to base of steep source slope and move as far as several tens or hundreds of meters farther, on relatively gentle slopes
Disrupted rock slides	Translational sliding	High	×	×	×	×	Shallow	35	Rapid to very rapid	Most less than 1×10^4 m^3; maximum reported 2×10^9 m^3	May slide to base of steep source slope and several tens or hundreds of meters farther, on relatively gentle slopes
Rock avalanches	Complex, involving sliding, flow, and occasionally free fall	Very high	×	×	×	×	Deep	25	Very rapid to extremely rapid	5×10^5–2×10^8 m^3 or more	Several kilometers
Soil falls	Bouncing, rolling, free fall	High or very high	×	×	×	×	Shallow	40	Extremely rapid	Most less than 1,000 m^3; maximum volumes not well documented	Most come to rest at or near bases of steep source slopes
Disrupted soil slides	Translational sliding	High	×	×	×	×	Shallow	15	Moderate to rapid	Most less than 1×10^4 m^3; maximum reported 4.8×10^7 m^3	May slide to base of steep source slope and several tens or hundreds of meters farther, on relatively gentle slopes
Soil avalanches	Complex, involving sliding, flow, and occasionally free fall	Very high	×	×	×	×	Shallow	25	Very rapid to extremely rapid	Volumes not well documented; maximum reported 1.5×10^8 m^3	Several tens of meters to several kilometers beyond steep source slopes
Coherent landslides											
Rock slumps	Rotational sliding	Slight or moderate	?	×	×	×	Deep	15	Slow to rapid	Most between 100 and a few million m^3; maximum at least tens of millions of m^3	Typically less than 10 m; occasionally 100 m or more
Rock block slides	Translational sliding	Slight or moderate	?	×	×	×	Deep	15	Slow to rapid	Most between 100 and a few million m^3; maximum at least tens of millions of m^3	Typically less than 100 m; maximum displacements not well documented
Soil slumps	Rotational sliding	Slight or moderate	?	×	×	×	Deep	7	Slow to rapid	Most between 100 and 1×10^5 m^3; occasionally 1×10^5 to several million m^3	Typically less than 10 m; occasionally 100 m or more
Soil block slides	Translational sliding	Slight or moderate	?	?	×	×	Deep	5	Slow to very rapid	Most between 100 and 1×10^5 m^3; maximum reported 1.12×10^8 m^3	Typically less than 100 m; maximum displacements not well documented
Slow earth flows	Translational sliding and internal flow	Slight			×	×	Generally shallow; occasionally deep	10	Very slow to moderate; occasionally, with very rapid surges	Most between 100 and 1×10^6 m^3; maximum reported between 3×10^7 and 6×10^7 m^3	Typically less than 100 m; maximum displacements not well documented

Table 2.2. (Continued) - Characteristics of earthquake-induced landslides (Keefer, 2002)

Continued

Name	Type of movement	Internal disruption	Water content D	U	PS	S	Typical depths	Minimum slope (°)	Typical velocities	Typical volumes	Typical displacements
Lateral spreads and flows											
Soil lateral spreads	Translation on fluid basal zone	Generally moderate; occasionally slight or high			×	×	Variable	0.3	Very rapid	Most between 100 and 1×10^5 m^3; largest reported 9.6 $\times 10^6$ m^3.	Typically less than 10 m; maximum reported 600 m
Rapid soil flows	Flow	Very high		?	?	×	Shallow	2.3	Very rapid to extremely rapid	Volumes not well documented; largest are at least several million m^3.	A few m to several km
Subaqueous landslides	Generally lateral spreading or flow; occasionally sliding	Generally high or very high; occasionally moderate or slight			×	×	Variable	0.5	Generally rapid to extremely rapid; occasionally slow to moderate	Volumes not well documented; largest are at least tens of millions of m^3.	Not well documented, but some move more than 1 km

* Notes: Names: "rock" signifies bedrock that is relatively firm and intact prior to landslide initiation, and "soil" signifies loose, unconsolidated or poorly cemented aggregates of particles that may or may not contain organic materials. Internal disruption: "slight" signifies landslide consists of one or a few coherent blocks; "moderate" signifies several coherent blocks; "high" signifies numerous small blocks and individual soil grains and rock fragments; "very high" signifies nearly complete disaggregation into individual soil grains or small rock fragments. Depth: shallow signifies generally < 3 m deep; deep signifies generally > 3 m deep. Water content: D = dry; U = moist but unsaturated; PS = partly saturated; S = saturated. Velocity: very slow = 1×10^{-6}–3 $\times 10^{-6}$ m/min; slow = 3×10^{-6}–3×10^{-5} m/min; moderate = 3×10^{-5}–0.001 m/min; rapid = 0.001–0.3 m/min; very rapid = 0.3–180 m/min; extremely rapid = >180 m/min. (Terminology after Varnes, 1978).

Table 2.3. Geometric characteristics of earthquake-induced landslides (Rodríguez et al., 1999).

Slide type	Slide depth (m)	Slide shape factor (d/L)[a]	Slip surface shape
Rock falls	3–5, depending on discontinuities spacing	= 0.15, only one data reported	Planar on outward dipping discontinuities
Disrupted rock slides	(No representative data)	(No representative data)	Predominantly planar, but other shapes were also reported
Coherent rock slides	20–50, given by geological features, such as weakness zones	0.08–0.10, apparent relationship with ground shaking	Circular or planar on outward dipping discontinuities
Disrupted soil slides	3–100, depending on geological setting	0.005–0.3, apparently dependent on ground shaking	Predominantly complex mechanism (rotational–translational), single mechanisms commonly planar
Coherent soil slides	6–50, apparently dependent on ground shaking	0.04–0.3, apparently dependent on ground shaking	Circular
Soil spreads and flows	6–40, depending on the ground shaking	0.007–0.20, depending on geological setting	Predominantly planar, some circular cases also reported

[a] (d/L = depth/length ratio)

2.2.2 Parameters affecting seismic slope stability

Many factors may influence the seismic stability of slopes and the characteristics of the landslides induced by earthquakes. Among these, the most important parameters affecting seismic slope stability are:

- physical, mechanical and dynamic properties of the ground;
- geometry of the slope
- characteristics of shaking primarily related to M, R, PGA, local soil conditions and topographic effects.

2.2.2.1. Ground Properties

According to Keefer (2002), geomaterials most susceptible to earthquake-induced landslides are:

(1) Weakly cemented, weathered, sheared, intensely fractured, or closely jointed rocks,

(2) Better-indurated rocks having prominent discontinuities,

(3) Sandy residual or colluvial soils,

(4) Saturated volcanic soils containing sensitive clay,

(5) Loess,

(6) Cemented soils,

(7) Granular deltaic sediments,

(8) Granular flood-plain alluvium, and

(9) Uncompacted, or poorly compacted, granular artificial fill

Data on the involved geomaterials may be derived from previously published documents such as geologic maps, field reconnaissance survey, laboratory tests and in situ monitoring.

Under the influence of earthquake loading, inertial forces and pore pressure build-up may contribute to increased shear stresses and reduced shear strength along the potential sliding mass leading to instability and/or permanent deformations. Soils that exhibit significant reduction of shear strength due to cyclic loading are loose soils and soils with particles that are weakly bonded into loose structures. Saturated soft cohesionless soils may liquefy under cyclic loading, lose temporaly all strength, and behave as viscous fluids.

The presence of pre-existing shear zones and the degree of brittleness is particularly important in determining the potential of a landslide mass (Hutchinson, 1995). Considering that the brittleness on preexisting shears is generally low or zero, the reactivation of landslide movement on such shears is usually slow.

Groundwater when present may play a definite role as well. In Italy, Wasowski et al. (2002) observed that during the Irpinia earthquake (1980) the change in the groundwater condition (seismically induced pore-water pressure rise) was a major controlling parameter in the spatial landslide distribution.

Shear strain softening of soil materials, which can be related in its effectiveness to the number of (equivalent uniform) excitation cycles N, result to the degradation of the stiffness and strength properties of the soils: it may be considered as one of the major causes of most of the slides induced by earthquakes (Ishihara, 1996). If landslide materials display strain-softening behavior, their kinetic energy can reach catastrophic proportions and long runout distances (Leroueil et al., 1996). In these materials, a progressive failure can occur owing to a reduction of strength with increasing strain. Progressive failure involves non-uniform straining of brittle materials resulting in a nonuniform mobilisation of the shear strength along the potential slip surface (Bjerrum 1967; Troncone, 2005). General failure of the slope usually takes place before the residual strength has developed everywhere along the sliding mass. Thus, the average strength of the mass at failure is less than the peak strength of the soil and greater than the residual one (Dounias, 1988; Troncone, 2005; Conte et al., 2010; Kourkoulis et al., 2010).

Knowledge of the effect of rate of displacement on the residual strength is important when studying the kinematics of a potential sliding mass. Three types of variation of the fast residual strength with an increasing rate of displacement have been identified (Tika et al., 1996): (a) neutral rate effect—soils showing a constant residual strength irrespective of the rate of displacement; (b) negative rate effect—soils showing a significant drop in strength when sheared at rates higher than a critical value; and (c) positive rate effect—soils showing an increase in residual strength above the slowly (static) drained residual value at increasing rates of displacement. Soils with small clay

fractions (sands and soils with PI<10%) have shown neutral rate effect. In soils of increasing clay fraction (or plasticity), however, negative and positive rate effects have been observed.

There is a possibility of delayed initiation or reactivation of landslide movement subject to ground shaking, especially in coherent materials, associated with the potential reduction of the in situ shear strength and the variation of groundwater conditions. As an example, this was the case of the Irpinia earthquake occurred in Italy (M= 6.9), where several large earth flows and other coherent slides began their movement few hours to few days after the main shock. The post-earthquake movement of these landslides was inferred to be caused by the increased spring flow and pore-water pressures regime, associated with the tectonic deformation of the interested area (Keefer, 2002).

A comprehensive overview of the dynamic strength characteristics of granular and cohesive soils playing a role in the slope seismic stability and related induced displacements, may be found in Ishihara (1996) and Pitilakis (2010, in Greek).

2.2.2.2. Size of landslides

Expect for the parameters described in Table 2.2, landslide size may be related to the earthquake magnitude (Fig. 2.17), shaking intensity, and epicentral distance (Keefer, 2002). Hancox et al. (2002) reported that only landslides having volumes < 104 m^3 occurred in New Zealand earthquakes with M < 6, whereas landslides having volumes > 108 m^3 occurred only in earthquakes with M > 7.5 and intensities of MMI IX or higher. The size of landslides induced by an earthquake can be also correlated to the relation between slope aspect and ground shaking intensity during the strong motion phase (Li, 1978 in Wen et al., 2004).

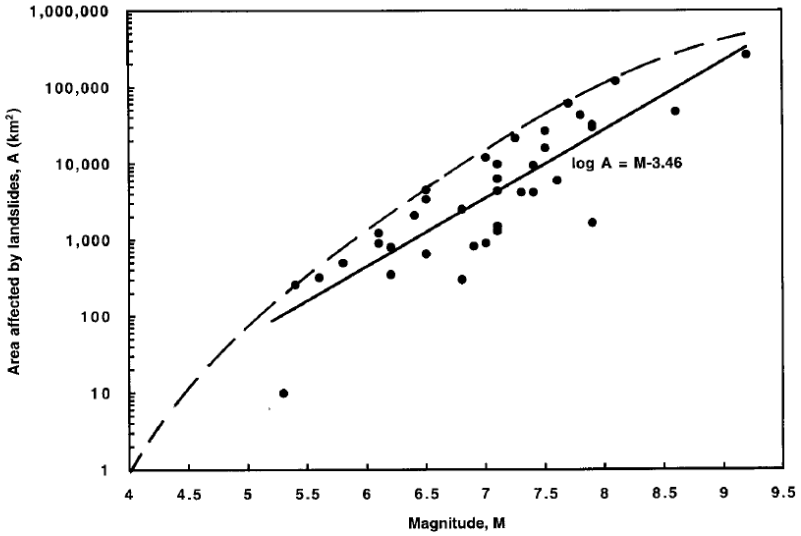


Figure 2.17. Relations between area affected by landslides and earthquake magnitude (Keefer, 2002)

2.2.2.3. Shaking characteristics

Magnitude

According to Keefer (1984, 2002), the minimum magnitude of an earthquake that would cause landslides of various types is (see Fig. 2.18):

~4.0 for rock falls, rock slides, soil falls and disrupted soil slides

~4.5 for soil slumps and soil block slides;

~5.0 for soil lateral spreads, rapid soil flows, subaqueous landslides, rock slumps, rock block slides, and slow earth flows;

~6.0 for rock avalanches; and

~6.5 for soil avalanches.

Modified (generally lower) values were proposed by Rodríguez et al. (1999) for the earthquake magnitude that can trigger a landslide of various types. These minimum magnitude thresholds have been empirically derived and as such they are approximate in nature. However, they are important as they reveal general trends. Smaller earthquake events can occasionally trigger landslides in correlation with non seismic causes (e.g intense precipitation). Hence, if a slope is in a marginally stable state, even a weak earthquake (M<4) can trigger the landslide mass movement. Several examples of low magnitude induced landslides have been reported in the literature (e.g. Keefer, 1984; Rodríguez et al., 1999; Papadopoulos and Plessa, 2000).

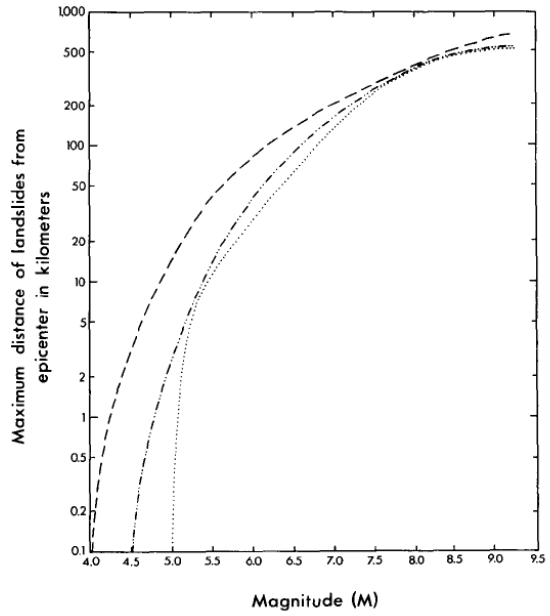


Figure 2.18. Maximum epicentral distance as a function of the event magnitude for the three landslide categories (dashed line: disrupted landslides, dash-double-dot line: coherent landslides, dotted line: lateral spreads and flows) (Keefer, 1984)

Epicentral Distance

Keefer (1984) proposed a set of upper bound curves for the maximum distance as a function of the event magnitude for the three landslide categories (disrupted, coherent, flows) (Fig. 2.18). Recent studies showed that these curves are appropriate in most cases, although some outliers were observed for disrupted and coherent type landslides at moderate to low magnitudes (Delgado et al., 2011).

Statistical analysis of the landslide distribution showed a strong correlation between landslide concentration, on the one hand, and distance from the epicenter, distance from the fault rupture, and slope inclination, on the other (Keefer, 2000). Landslide abundance showed an exponential decrease with increasing distance from the fault-rupture zone (Fig. 2.19a) but not with increasing epicentral distance (Fig. 2.19b) (Keefer, 2002). Later studies (e.g. Huang and Li, 2009; Sato and Harp, 2007) also report that the distribution of earthquake-triggered landslides is more related to the distance from the surface projection of the fault plane and the surface projection up-dip edge of the fault rather than the distance from the epicenter.

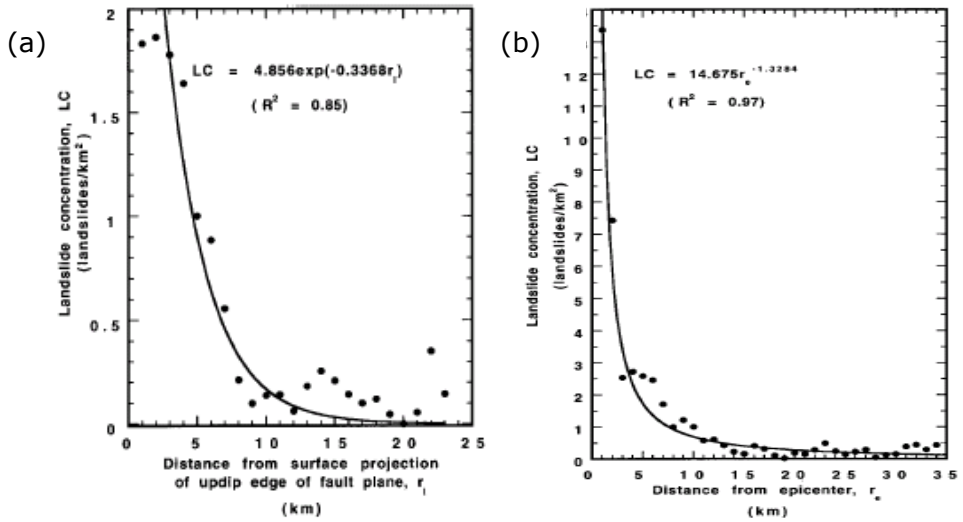


Figure 2.19. Relation of landslide concentration to the distance from the fault rupture zone (a) and to the epicentral distance (b) for landslides in the southern Santa Cruz Mountains triggered by the 1989 Loma Prieta, California, earthquake (Keefer, 2002)

Site and Topographic effects

The specific properties and geometrical features of the soil deposits can modify the characteristics (amplitude, frequency content and duration) of the travelling wave field, generating extra amplification (aggravation factor in the seismic input characteristics), attenuation or tensional effects in the ground influencing the deformation and, eventually, ground failure. Soil nonlinearity, material damping, the impedance contrast

between sediments and the underlying bedrock, and the characteristics of incident wavefield are considered to represent the governing factors for site amplification (Kramer and Stewart, 2004; Pitilakis, 2004; 2010). A fundamental period of the earthquake close to the natural period of the site can lead to resonance phenomena and, consequently, to an amplified energy content of the ground motion. The slope failure potential assumes its highest values for a combination of a low-frequency seismic input motion together with a resonance phenomenon in the low-frequency range (Bourdeau et al., 2004; Bourdeau and Havenith, 2008).

Topographic irregularities can considerably affect the amplitude and frequency content of ground motions. In the case of hills or slopes this can be related to the triggering forces acting upon them, since amplified surface accelerations behind the crest may present larger destabilizing forces, potentially causing higher landslide risk (Paolucci, 2002). Amplification of both horizontal and vertical ground motion components normally takes place over a narrow zone near the crest of the slope. This is due, among other factors, to the diffraction at the surface irregularities and surface wave generation: it can be observed both in the time domain (as an increase in the maximum observed amplitude near the crest, with respect to the maximum observed amplitude of the free-field) as well as in the frequency domain (as a spectral amplification over a narrow band of frequencies corresponding to wavelengths similar to the horizontal dimension of the slope) (e.g. Assimaki and Gazetas, 2004; Assimaki et al. 2005; Bouckovalas and Papadimitriou, 2005; Ktenidou, 2010).

While landslides triggered by precipitation are generally distributed uniformly along the slopes, landslides triggered by earthquakes tend to be clustered near ridge crests and hill slope toes. Densmore and Hovius (2000) in Peng et al. (2009) attributed this ridge- crest clustering to topographic effects (as described above), and the clustering at hill slope toes to dynamic pore-pressure changes in the water-saturated material of lower hill slopes.

Ashford et al. (1977), Bouckovalas and Papadimitriou (2005), Papadimitriou and Chaloulos (2010) and Lenti and Martino (2010, 2012), among others, investigated parametrically the effect of step-like slope topography that may lead to intense amplification and de-amplification irregularly along the slope, depending on its geometry and its geological setting as well as on the wavelength of the impinging excitation with respect to the slope's height. Bozzano et al. (2008a, 2010) also pointed out the role of "self-excitation" process due to local seismic amplification resulting from the structural setting of the stiff bedrock and the pre-existing landslide masses, in the reactivation of far field pre-existing large landslides. As the authors demonstrated, the frequency content of the incoming seismic wave field in relation to the geological setting of the

slope is fundamental to the occurrence of this phenomenon. According to Del Gaudio and Wasowski (2011), amplification in potentially unstable slopes may have a pronounced directional character causing a re-distribution of shaking energy with maxima oriented along potential sliding directions. However, more research is needed to identify the critical factors controlling these phenomena.

2.3 Methods to assess earthquake induced landslide hazards

According to the Association of Professional Engineers and Geoscientists of British Columbia guidelines (APEGBC, 2010), there are various methods to assess earthquake induced landslide hazards. These include, but are not limited to, estimating:

- The likelihood or probability of occurrence of a landslide,
- The factor of safety of a slope,
- The slope displacement along a slip surface.

In order for the results of the above estimate to be incorporated in a Quantitative Risk Assessment (QRA) methodology, they must be combined with an estimate of landslide run-out distance (for residential development at the bottom of the slope), or an estimate of where the main scarp of the landslide will intersect the ground (for residential development on, or at the top of, the slope) (APEGBC, 2010).

2.3.1 Likelihood or probability of occurrence of a landslide

When assessing the probability of a particular slope experiencing landsliding within a reference period and within a given area, the recognition of the geotechnical, hydro-geological, topographic conditions that caused the slope to become unstable, and the mechanisms that triggered the landslide movement is of primary importance. The triggering variables (e.g. the seismological characteristics) shift the slope from a marginally stable to an unstable state and thereby initiating failure in an area of given susceptibility (Dai et al., 2002). They are time-dependent factors that may change over a very short period of time. The historic frequency of landslides in an area can be determined to provide realistic estimates of landslide probability of occurrence throughout a region where landslides have caused a significant amount of damage. The trigger/landsliding and frequency–magnitude relations that help understanding landslide probabilities may be derived from landslide inventories. Considering that landslide inventories are usually incomplete or inaccurate, the use of aerial photographs and/or satellite images in conjunction with the landslide inventories may give further insight in

the documentation of the landslide occurrence and the interpretation of the main landslide triggering processes.

The frequency of seismically induced landslides may be related to the peak ground acceleration at the site, the magnitude of the earthquake and the distance from the earthquake epicenter (Fell et al., 2008). Studies by Keefer (1984, 2002), Harp and Jibson (1996), Rodriguez et al. (1999), Jibson et al. (2000), Papadopoulos and Plessa (2000), have shown that there is a threshold magnitude, peak ground acceleration and distance from the earthquake epicenter above which landsliding will occur. This varies for different landslide types and sizes (see subsection 1.2.2.3). One problem with the characteristics of the expected ground shaking is that strong-motion stations are not usually widely distributed in areas where landslides are most likely to occur. Hence, the interpolation of the available data from the few stations available to grid points in mountainous areas is difficult and sometimes ineffective.

2.3.2 Factor of safety of a slope

For site-specific slopes, the probability of failure is usually considered as simply the probability that the factor of safety is less than unity. The factor of safety of a slope may be defined as the ratio of the shear resistance to the shear stress mobilized. In simple terms, a FS=1 is assumed when failure occurs and values successively greater than 1 suggest increasing stability and hence lower susceptibility to failure. When an earthquake occurs, the slope material is subjected to horizontal and vertical acceleration with reverse cycles. The inertial forces associated with these accelerations may momentarily reduce the factor of safety below 1.0 by increasing the shear stresses and possibly decreasing the shear resistance of the material, initiating downslope movement. If the accelerations are large enough or continue for a long period of time, they may lead to instability and/or extensive permanent deformations.

There are many different ways to compute the factor of safety of a slope including limit equilibrium (e.g. Fellenius, Bishop, Janbu, Morgenstern and Price, Spencer, Sarma methods) and strength reduction method (SRM) (e.g. Dawson and Roth, 1999; Griffiths and Lane, 1999). For simple homogenous soil slopes, it is found that the results from these methods are generally in good agreement. The strength reduction method, utilized in many finite element and finite difference codes (e.g. Plaxis, FLAC 2D, FLAC 3D, Phase etc.), does not require any pre-definition of the sliding surface. Instead, the failure surface develops "naturally" based on the selected yield criterion (e.g. Mohr Coulomb, Hoek-Brown etc.). Nevertheless, the strength reduction method is incapable of determining other failure surfaces, which may be only slightly less critical than the SRM

solution. It is also sensitive to nonlinear solution algorithms/flow rule for some special cases (Cheng et al., 2007). For this reason, it is generally advisable to perform both methods in parallel when dealing with critical problems.

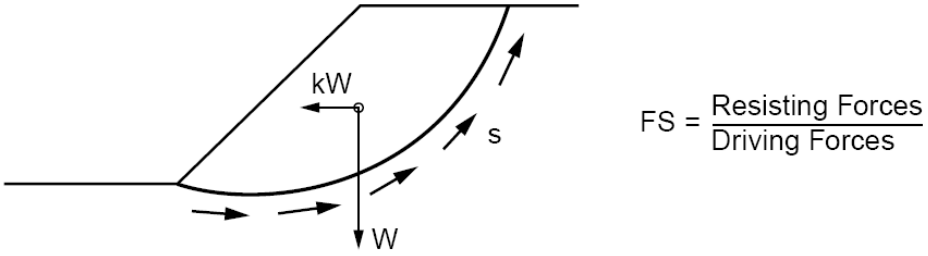


Figure 2.20. Pseudostatic slope stability analysis

In a conventional limit equilibrium slope stability analysis, such as the ordinary method of slices, simplified Bishop's method, and simplified Janbu's method, an additional horizontal static force is applied to simulate earthquake shaking. Analyses that model the earthquake as an equivalent static force are commonly referred to as pseudo-static analyses (Fig. 2.20). For pseudo-static analyses, the horizontal static force is calculated by multiplying the soil weight by a seismic coefficient, k that represents the earthquake shaking. Seismic coefficients used in pseudo-static analyses are empirically derived to represent an equivalent seismic load. The selection of the proper value of the seismic coefficient is fundamental, as this value controls the inertial forces on the soil masses. According to Terzaghi (1950), who first introduced the pseudo-static (PS) approach, the values of the seismic coefficient should be k=0.1 for severe earthquakes, k=0.25 for violent-destructive earthquakes, and k=0.5 for catastrophic earthquakes. In all cases the author suggested that the design safety factor with respect to strength, Fs, may be close to 1.0. In contemporary seismic norms, e.g. Eurocode 8 (EC8 2004), the pseudostatic slope stability analysis is widely adopted for the design of natural and engineered slopes due to its simplicity. The selection of a seismic coefficient equal to a specific portion of the design peak ground acceleration at the site of interest is prescribed depending on the earthquake magnitude and peak ground acceleration values as well as the acceptable level of seismic performance of the studied slope. However, a main limitation of the pseudostatic approach is that it provides only a single numerical threshold below which no displacement is predicted and above which total, but undefined, failure is predicted. Moreover, the fact that an equivalent static force models the earthquake does not permit the actual dynamic response of the structure to be taken into account, and thus, the real response and stability of the geo-structure cannot be accurately assessed during a moderate or severe seismic event. Lagaros et al. (2009) recognized that in cases where the local site conditions play an important role (e.g. sensitive clays, loose saturated silty

sands), more sophisticated non-linear dynamic analysis procedures should be used. According to APEGBC (2010) guidelines, pseudostatic analysis can be used for preliminary analyses and screening procedures and for the evaluation of seismic slope stability using a slope displacement-based seismic coefficient equivalent to the prescribed tolerable slope displacement along the slip surface (Bray and Travasarou, 2009).

2.3.3 Slope displacement along a slip surface

It is common practice in geotechnical earthquake engineering to assess the expected seismic performance of slopes and earth structures by estimating the potential for seismically induced permanent displacements using one of the available displacement-based analysis procedures. Considering that (total and/or differential) displacements ultimately govern the serviceability level of a slope after an earthquake, the use of such approaches is strongly recommended. Moreover, for a landslide risk assessment study it is the extent of permanent ground deformation that is the most important parameter, since the assessment of landslide potential (e.g. probability of landslide occurrence) on its own is of little relevance if the consequent ground deformations are not expected to cause distress and damage to buildings and infrastructure. The later represents one of the most important principles on which this study has been based. Typically, two different approaches of increased complexity are proposed to assess permanent ground displacements in case of seismically triggered slides:

- Newmark-type displacement methods
- Advanced stress- strain dynamic methods

2.3.3.1. Newmark-type displacement methods

Starting from the landmark study of Newmark (Newmark, 1965), the first class includes simplified or advanced displacement based approaches that generally differ with respect to the assumptions and idealizations used to represent the mechanism of earthquake-induced displacement. They are intended for soil slopes and they can be grouped into three main types (Jibson, 2011): rigid-block, decoupled, and coupled.

The rigid-block model originally proposed by Newmark (1965) treats the potential landslide block as a rigid mass (no internal deformation) that slides in a perfectly plastic manner on an inclined plane (Fig. 2.21). The mass experiences no permanent displacement until the base acceleration exceeds the critical (yield) acceleration of the block, which is the threshold base acceleration, required to overcome the shear resistance of the slope and initiate failure; then, the block begins to move downslope. Cumulative displacements are estimated by double-integrating the parts of an acceleration-time history that lie above the critical acceleration. The original Newmark

rigid sliding block assumption is employed in many of the available simplified slope displacement procedures (e.g., Lin and Whitman, 1986; Ambrasseys and Menu, 1988; Yegian et al. 1991; Jibson, 2007; Saygili and Rathje, 2008 etc.). The dynamic site response and the sliding block displacements are computed separately in the 'decoupled' approach (e.g. Makdisi and Seed, 1978; Bray and Rathje, 1998; Ausilio et al., 2008; Rathje and Antonakos, 2011) or simultaneously in the 'coupled' stick-slip analysis (Rathje and Bray, 2000; Bray and Travasarou, 2007) (Fig. 2.22). Some of the most commonly applicable seismic displacement procedures that account for the soil deformability (both coupled and decoupled) are discussed in Bray (2007). In general, coupled analysis yields reliable results for slopes of all dynamic stiffness and strength, but, of course, is the most complex to conduct. Rigid-block analysis is appropriate for analyzing thin, stiff landslides but yields quite unconvervative results for deep, flexible slopes. The decoupled approach is generally considered to slightly overestimate displacements compared to the fully nonlinear, coupled stick-slip analysis. However, it was found non-conservative primarily for projects undergoing intense, near-fault ground motions (Rathje and Bray, 1999; 2000). Jibson (2011) provides guidelines for selecting the most appropriate sliding-block analysis based on the T_s/T_m, i.e. the ratio of the fundamental site period (T_s) to the mean period of the earthquake motion (T_m) (Tab. 2.5). APEGBC (2010), based on the concept of tolerable slope displacement, proposed the use of Bray and Travasarou (2007) simplified coupled method for the seismic analysis of soil slopes.

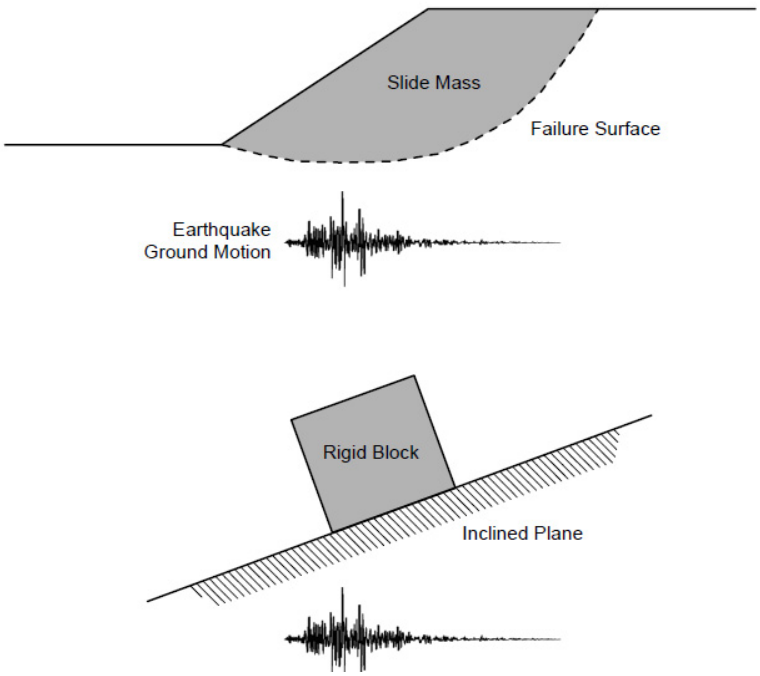


Figure 2.21. Newmark Sliding-block analogy

The significance of modeled displacements must be judged by their probable effect on a potential landslide (Jibson, 2011). According to the California Geological Survey's (2008) general guidelines, Newmark displacements of 0-15cm are unlikely to correspond to serious landslide movement and damage; displacements of 15-100cm could be serious enough to cause serious ground cracking or strength loss and continuing failure; and displacements greater than 100 cm are very likely to correspond to damaging landslide

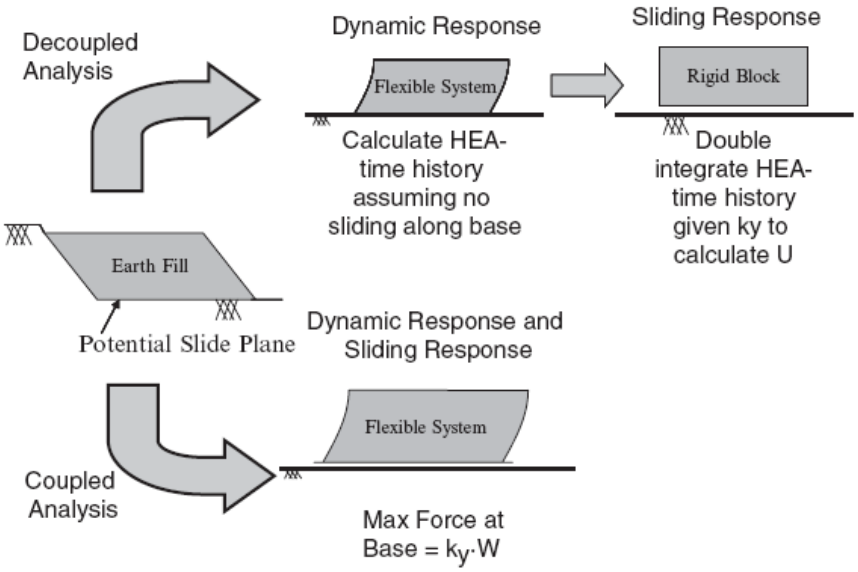


Figure 2.22. Decoupled dynamic response/rigid sliding block analysis and fully coupled analysis (Bray, 2007)

Table 2.4. Guidelines for selecting appropriate sliding-block analysis (Jibson, 2011)

Slide type	T_s/T_m	Rigid-block analysis	Decoupled analysis
Stiffer, thinner slides	0–0.1	Best results	Good results
↓	0.1–1.0	Unconservative	Conservative to very conservative
↓			
Softer, thicker slides	1.0–2.0	Conservative	Conservative
	>2.0	Very conservative	Conservative to unconservative

T_s is the site period.
T_m is the mean period of the earthquake shaking.

movement, including possible catastrophic failure. However, it is important to note the fact that the estimated range of seismic induced permanent displacement from semi-analytical and/or semi-empirical procedures both coupled and uncoupled, should be considered as an index of the expected seismic performance. Seismic displacement estimates will always be approximate in nature due to the complexities of the dynamic

response of the soil materials involved and the variability of the earthquake ground motion (Bray, 2007). Moreover, it's worth noticing that the yield coefficient k_y is assumed to be constant during seismic shaking. Thus, Newmark-type approaches should not be followed when significant strength loss is anticipated in the slope soil material (e.g. liquefaction) (e.g. Kramer 1996). In the later, a more sophisticated numerical analysis capable to account for soil nonlinearity is recommended for use.

2.3.3.2. Advanced stress- strain dynamic methods

Advanced stress-deformation analyses based on continuum (finite element (FEM), finite difference (FDM), boundary element method (BEM)) or discontinuum (e.g. Distinct Element Method (DEM) and Discontinuous Deformation Analysis (DDA)) formulations usually incorporating complicated constitutive models, are becoming more and more attractive, as they can provide approximate solutions to problems which otherwise cannot be solved by conventional methods e.g. the complex geometry including topographic and basin effects, material anisotropy and non-linear behavior under seismic loading, in situ stresses, pore water pressure built-up, progressive failure of slopes due to strain localization, soil-structure interaction. Numerical methods have been applied to model the dynamic response of slopes using different constitutive models (e.g. Mohr Coulomb, strain softening, hysteretic model etc.), boundary conditions and dynamic input motions (real or synthetic accelerograms, simplified wavelets).

Many investigators implemented continuum FE (e.g. ABAQUS, Opensees, PLAXIS etc.) or FD (e.g. FLAC 2D, 3D) codes to evaluate the residual ground displacements of soil slopes using elastic–plastic constitutive models. Martino and Scarascia Mugnozza (2005) examined the effect of seepage and frequency content of dynamic input motion on the histories of permanent co-seismic displacements and excess pore pressures of the Calitri landslide (Southern Italy) by means of the explicit finite difference program FLAC2D. Siyahi and Arslan (2008) investigated the dynamic behavior and earthquake resistance of Alibey earth dam (Istanbul, Marmara Region, Turkey) taking into account the effects of liquefaction and cyclic mobility. They performed displacement-pore pressure coupled FE analyses using OpenSees (Open System for Earthquake Engineering Simulation) platform. Marchi et al. (2011) performed a sensitivity analysis on the influence of the strength, stiffness and damping parameters of the soil on the seismic response (in terms of permanent displacements) of Las Colinas slope (El Salvador) using the finite element code PLAXIS. Kourkoulis et al. (2010) used the FE code ABAQUS to estimate the co-seismic displacements of an idealized slope with strain- softening behavior considering soil-foundation-interaction. Han and Hart (2010) studied the seismic stability of reservoir-/earth dam/pore fluid systems and predicted the potential liquefied regions, earthquake-induced settlement and lateral spreading for a realistic reservoir dam

experiencing seismic loading using the explicit difference program FLAC2D (Itasca, 2011). Taiebat et al. (2011) estimated the seismic response (in terms of shear strains and horizontal displacements) of a saturated clay slope based on an advanced modified isotropic modified Cam-Clay model to account for anisotropy and destructuration. The model was numerically implemented in the 3D explicit finite-difference program FLAC3D. Fotopoulou et al. (2011) used the explicit finite difference code FLAC2D to assess the permanent ground displacement of the Kato-Achaia slope - western Greece as a consequence of the Ilia-Achaia, Greece 2008 (Mw= 6.4) earthquake, considering the presence of a structure near the cliff.

To analyze the seismic stability of rock slopes both continuum or discontinuum methods are possible. An overview of the advantages and disadvantages of these approaches are presented in Stead et al. (2006). When the seismic stability of rock is controlled by movement of joint-bounded blocks and/or intact rock deformation then the use of discontinuum discrete-element codes is generally preferable. The predominant discontinuum method that has been used to investigate a wide variety of rock slope failure mechanisms is the distinct-element code UDEC (Itasca, 2004).

The accuracy of advanced numerical methods is highly dependent upon the quality of the input parameters and the level of model validation performed by the user for similar applications. One basic limitation is that the parameters required for the definition of the constitutive models are not easily quantified in the laboratory or in situ. Moreover, due to their complexity, they are generally more appropriate for specific case studies and not for a parametric analysis aiming to evaluate the landslide risk at local and regional scale. Finally, it should be emphasized that numerical modeling is a very powerful tool in the identification and comprehension of the coupled processes and complex mechanisms leading to instability of a given slope but it should be combined with engineering experience and critical judgment in order to yield reliable results.

2.3.4 Discussion

The choice of the most appropriate method to assess earthquake induced landslide hazard should primarily rely on the scale of the problem, data availability and quality concerning the geometrical, hydro-geological and the geotechnical characteristics of the site, the seismic motion parameters and soil dynamic properties (e.g. residual dynamic shear strength), the criticality of the structure and engineering judgment. A simplified empirical or semi-empirical method (e.g. pseudo-static analyses, Newmark- type displacement models) is generally preferable for the landslide hazard assessment in small scales (e.g. regional scale) while a more sophisticated method (e.g. numerical model) is usually adopted in large and detailed scales. Within the framework of this research, the

numerical approach is selected as it is reportedly more accurate than any empirical method and it permits the direct estimation of absolute and/or differential ground displacements at the slope area, which represent the main cause of damage.

CHAPTER 3

Literature review on assessing building vulnerability to landslides

3.1 Introduction

The present chapter aims at providing a critical review of existing methodologies to quantify building vulnerability to slides. Various concepts and aspects of physical vulnerability to slides are discussed and analyzed regarding the development of fragility curves, the selection of appropriate landslide intensity measures, the extent and mechanisms of building damage to slides and the definition of structural and non-structural damage/limit states.

3.2 Physical vulnerability to landslides

Different disciplines use multiple definitions and different conceptual frameworks of the term of vulnerability. In engineering and natural sciences, physical vulnerability is commonly expressed as the degree of loss (expressed on a scale of 0: no loss to 1: total loss) to a given element or set of elements at risk (i.e. buildings and infrastructures), resulting from the occurrence of a specified hazard of given magnitude. The term of vulnerability [V], closely related to the consequences of natural hazards, is generally enclosed in the definition of risk [R] through the following simple formulation (Varnes, 1984):

$$[R]= [H] \times [V] \times [E] \quad (3.1)$$

Where [H]: hazard, [E]: value (or cost) of the element at risk.

However, in many cases the estimation of landslide vulnerability depends on the hazard evaluation and therefore the vulnerability term should be conditioned on the hazard term. Thus, the previous relationship can be transformed as follows:

$$[R]= [H] \times [V/H] \times [E] \quad (3.2)$$

Within the context of a landslide risk assessment methodology, physical (technical) vulnerability comprises a key component that still requires significant research (Leone et al., 1996; Dai et al., 2002; Cascini et al., 2005; Van Westen et al., 2006; Mavrouli and Corominas, 2010). The explanation lies in the first place in the scarcity of available damage data in quantitative terms and the inherent uncertainties associated with them (Van Westen et al. 2006). The heterogeneity of vulnerable elements to similar landslide mechanisms, the wide range of processes (e.g. rockfalls, debris flows, earth slides etc.) and their possible characteristics (e.g. size, shape, velocity, momentum) as well as the numerous categories of damages and their inherent dynamic nature have also contributed to the insufficient and somewhat subjective treatment of landslide vulnerability. Physical vulnerability may be defined as the degree of loss (in terms of percentage % of structural damage) of the affected built structures subjected to a landslide event of a given type and intensity. It depends on the structural properties of the exposed elements (e.g. typology, construction quality, state of maintenance, use etc), but also on the mechanism and intensity of the landslide processes. An additional important factor is the geographic location of the exposed elements with respect to the the landslide area (e.g. within or outside the unstable mass), given the variation of the soil movement and the consequent interaction with the structures and infrastructures, or in the case of rock falls, the location and the extent of the rock fall impact on the exposed elements. For instance, buildings subject to the same landslide event may experience different vulnerability values owing to their particular different structural (strength and stiffness) characteristics. Furthermore, buildings having exactly the same typological and structural properties may suffer less or more damage, determined by the landslide type and mechanism and their location in relation to the landslide zone. Thus, they might sufficiently accommodate the impact of a falling block but they cannot avoid development of tension cracks due to differential displacements produced by a translational slide (Fell et al, 2008). Figure 3.1 presents a schematic overview of landslide damage types, related to different types of landslides, elements at risk and the location of the elements at risk in relation to the landslide (Van Westen et al., 2006).

Physical vulnerability of the exposed elements to the different landslide hazards may be expressed both in qualitative and quantitative terms. Whether qualitative or quantitative assessments are more suitable depends on both the desired accuracy of the outcome and the nature of the problem, and should be compatible with the quality and quantity of available data (Dai et al., 2002). When sufficient data is available, a quantitative analysis (QRA) is preferable compared to qualitative, as it allows for a more explicit characterization of the causes of damage (in terms of permanent deformation, tension cracks, number of fatalities, monetary values etc.) and offers an improved basis for

communication among the research community, local authorities and emergency planners (AGS, 2007; Uzielli et al., 2008).

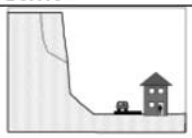
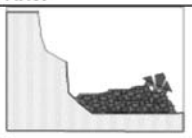
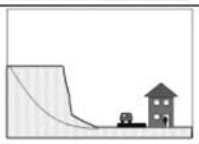
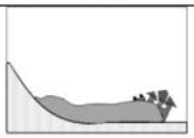
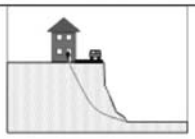
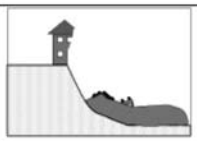
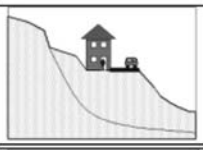
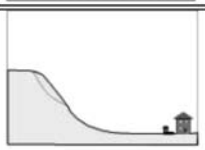
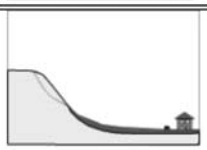
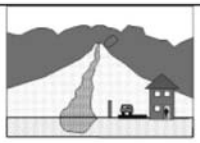
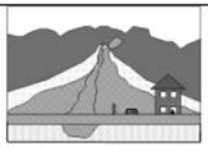
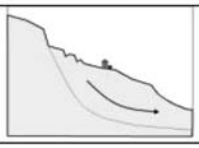
Type	Before	After	Likely damage to elements at risk	Factors determining risk
Impact by large rockmass			**Buildings:** Total collapse likely **Persons in buildings:** Loss of life/ major injury likely **Infrastructure:** Coverage and obstruction / destruction of surface **Persons in traffic:** Loss of life/ major injury possible	• Volume of rockfall mass • Location of source zone • Distance to Elements at risk • Triggering factors • Local topography along track • Intermediate obstacles • Precursory events
Impact by single blocks			**Buildings:** Total collapse not likely. Localized damage **Persons in buildings:** Minor to major injury likely **Infrastructure:** Coverage and obstruction of traffic **Persons in traffic:** Loss of life/ major injury possible	• Volume of rockfall blocks • Number of rockfall blocks • Location of source zone • Distance to Elements at risk • Triggering factors • Local topography along track • Intermediate obstacles
Impact by landslide mass			**Buildings:** Collapse / major damage depending on volume **Persons in buildings:** None, persons are normally able to escape **Infrastructure:** Coverage and obstruction of traffic **Persons in traffic:** None, persons are normally able to escape	• Volume of landslide mass • Water content • Landslide material type • Triggering factors • Distance to Elements at risk • Local topography along track • Speed of landslide movement
Loss of support due to undercutting			**Buildings:** Collapse / major damage likely **Persons in buildings:** None, persons are normally able to escape **Infrastructure:** Complete destruction of road surface. **Persons in traffic:** None, persons are normally able to escape	• Volume of landslide mass • Water content • Landslide material type • Triggering factors • Retrogressive landslide • Cliff erosion • Speed of landslide movement
Differential settlement /tilting due to slow movement			**Buildings:** Tilted buildings with cracks. Normally no collapse **Persons in buildings:** None, slow movement. People not in danger **Infrastructure:** Tilting and cracks, traffic slowed down **Persons in traffic:** None, slow movement	• Volume of landslide mass • Water content • Landslide material type • Triggering factors • Speed of landslide movement • Amount of displacement
Impact by debris flow on slope			**Buildings:** Filled by mud, damage to contents **Persons in buildings:** Minor-major injuries. Depends on speed. **Infrastructure:** Coverage of road surface. Obstruction of traffic. **Persons in traffic:** Minor-major injuries. Depends on speed.	• Volume of landslide mass • Water content • Slope steepness • Local topography • Landslide material type • Triggering factors • Speed of movement • Size of blocks transported
Flooding by debris flow on alluvial fan			**Buildings:** Filled by mud, damage to contents **Persons in buildings:** None, persons are normally able to escape **Infrastructure:** Coverage **Persons in traffic:** None, persons are normally able to escape	• Volume of debris flow • Water & sediment content • Local topography of fan • Triggering factors • Distance from source • Distance from lahar channel • Speed
Impact by Sturzstrom			**Buildings:** Total collapse **Persons in buildings:** Loss of life **Infrastructure:** Total destruction **Persons in traffic:** Loss of life	• Volume of rockfall mass • Location of source zone • Distance to Elements at risk • Triggering factors • Local topography along track • Distance from source zone • Precursory events
Liquefaction			**Buildings:** Differential settlement, cracks **Persons in buildings:** Minor injuries or no-injuries **Infrastructure:** Differential settlement, cracks **Persons in traffic:** no-injuries	• Soil types • Soil strength • Grainsize distribution • Foundation types • Earthquake intensity • Water table
Deep seated creep movement			**Buildings:** Differential settlement, tilting, cracks **Persons in buildings:** Minor injuries or no-injuries **Infrastructure:** Differential settlement, cracks, broken pipes **Persons in traffic:** no-injuries	• Speed of movement • Local geological situation • Age of landslide • Seasonality of movement

Figure 3.1. Schematic overview of landslide damage types, related to different landslide types, elements at risk and the location of the exposed element in relation to the landslide (Van Westen et al., 2006)

3.2.1 Landslide intensity measures

According to Hungr (1997) landslide intensity represents a set of spatially distributed parameters that describe the destructiveness of a landslide. To quantify the landslide effect on the exposed element, proper intensity parameters should be used that link the landslide hazard to the response of the exposed element to it. Their selection should be made with consideration of their predictability, efficiency and sufficiency (Kramer, 2011), taking also into account the scale of the problem. Intensity measure predictability refers to the uncertainty with which an IM can be predicted for a given landslide event whereas intensity measure efficiency refers to the conditional uncertainty in the structural response given the landslide intensity. Sufficient IM is a measure for which consideration of additional intensity parameters does not reduce the uncertainty in predicted response.

Intensity (demand) of a given landslide event can be expressed in different ways depending on the landslide type (slow moving or rapid slide, rockfall, etc.), the relative position of the exposed element (e.g. uphill, downhill or inside the potential unstable slope) to the landslide as well as the initial trigger of the landslide event (e.g. earthquake, intense precipitation, erosion etc.). Commonly used intensity measures are defined in terms of the absolute or differential displacement, velocity, kinetic energy, volume of the landslide deposit, impact force, etc. The interaction of the affected structure with the underlying soil materials may play a definite role as well. For instance, the uniform (absolute) displacement or tilting may be the optimal intensity measure for a building on stiff foundations standing near the crest of a potentially unstable slope whereas the differential displacement is considered more appropriate for a building on flexible, weak foundations.

Intensity criteria have been proposed by Leone et al. (1996) according to the landslide type (Fig. 3.2). As shown in Figure 3.2, for certain landslide types (e.g. slides) more than one intensity parameters are possible based on the particular characteristics of the problem (e.g building typology, relative location to the slide etc.) and data availability. Uzielli et al. (2008) proposed a composite intensity parameter accounting for kinetic and kinematic characteristics of the interaction between the sliding mass and the reference area. Li et al. (2010) estimated the landslide intensity as a function of dynamic and geometric intensity factors. Different geometric intensity factors were considered for structures located within and outside the landslide area. Recommendations for selecting proper landslide intensity criteria can be found in Corominas and Mavrouli (2011a).

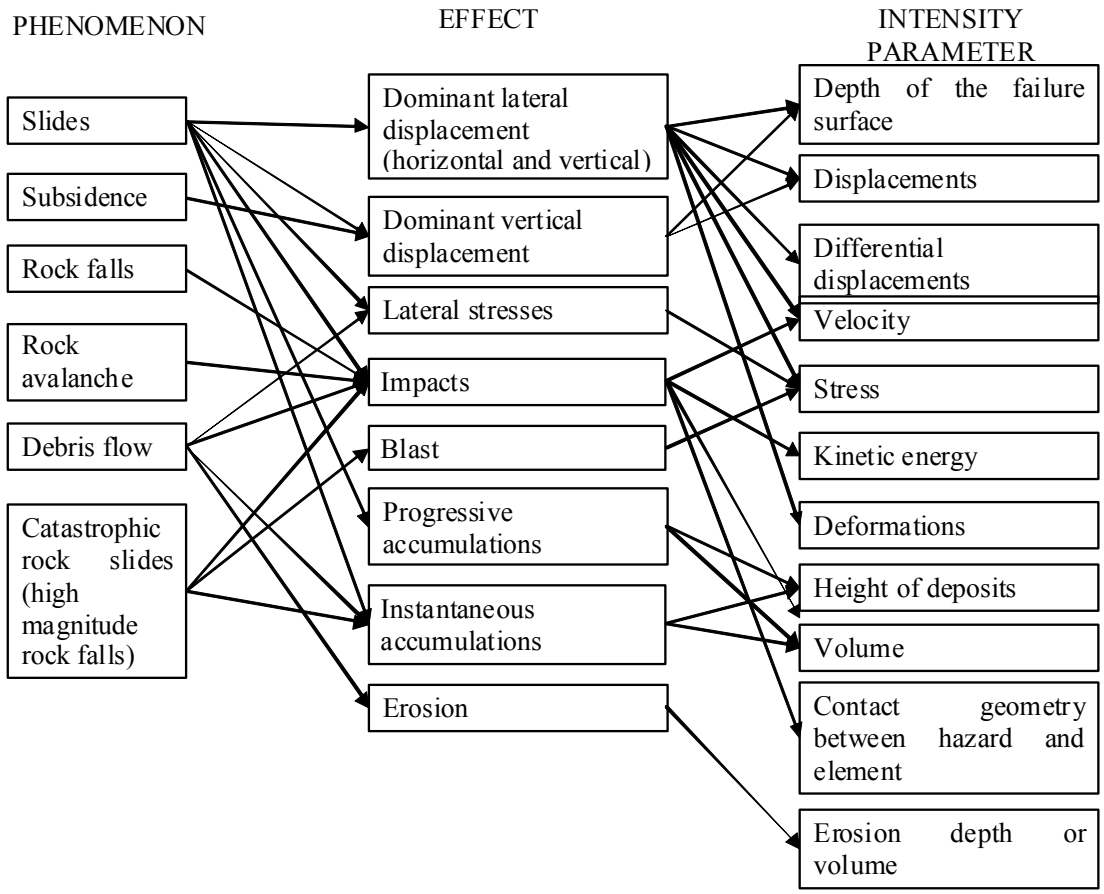


Figure 3.2. Landslide intensity criteria (after Leone et al. 1996)

3.2.2 Damage to structures impacted by slow moving slides

It is acknowledged that the expected damage of a structure due to the landslide hazard depends not only on its typology and its specific features but also on the landslide type and intensity and its relative position to the unstable zone. In the ensuing, the damage to buildings is described with respect to a basic landslide mechanism, namely slow moving slide. An extensive description of damage of various elements at risk (buildings, roads, population) concerning different landslide mechanisms (slow moving slides, debris flows, rock falls etc) is presented by Corominas and Mavrouli (2011a).

According to Cruden and Varnes (1996) established criteria, slow slides are classified as extremely slow moving slides (rates 0 to 16 mm/year), very slow moving slides (rates 16 mm/year to 1.6 m/year) and slow-moving slides (rates 1.6 to 160 m/year). While damage to the built environment resulting from the occurrence of rapid landslides such as debris flows and rock falls is generally the highest and most severe as it may lead to the complete destruction of any structure within the affected area, slow-moving slides also have adverse effects on affected facilities (Mansour et al., 2011; Argyroudis et al., 2011).

The damage caused by a slow moving slide on a building is mainly attributed to the cumulative permanent (absolute or differential) displacement and it is concentrated within the unstable area. For instance, a slow moving slide may produce tension cracks due to differential displacement to a building that may result to the partial or complete disruption of the structure's serviceability and stability. The type of response to permanent total and differential ground deformation depends primarily on the foundation type. A structure on a deep foundation compared to shallow foundations often has higher resistance ability and hence a lower vulnerability (Ragozin and Tikhvinsky, 2000). For shallow foundations (Fig. 3.3), the distinction is between rigid or flexible/unrestrained foundation systems. When the foundation system is rigid (e.g. continuous raft foundation), the building is expected rather to rotate as a rigid body and a failure mainly attributed to the loss of functionality of the structure is anticipated. In that case, the building can be rendered uninhabitable by the effect of a landslide without suffering any significant structural damage to the load-bearing system. On the contrary, when the foundation system is flexible (e.g. isolated footings), the various modes of differential deformation produce structural damage (e.g. cracks) to the building members (Bird et al, 2006). The interaction between the structure and the soil is also a key factor as the influence of the building stiffness is likely to modify its deformation demand compared to the predicted free field movement (Pitilakis D. et al., 2012). The structural system is a further crucial parameter that could potentially control the magnitude and distribution of damage due to the landslide movement. For instance, a bare frame structure would generally be more affected by the ground displacement than a structure with reinforced concrete walls supported with stiff floor system. Other typological parameters which determine the capacity of the building to withstand the landslide deformation demand are the geometry, material properties, the state of maintenance, code design level, superstructure details, number of floors etc.

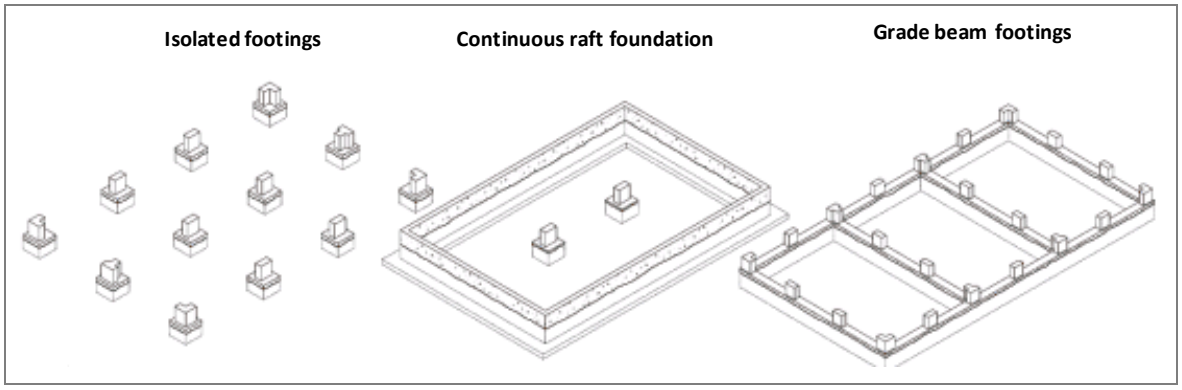


Figure 3.3. Typical shallow foundation systems - Types and layout

The extent and type of damage of a structure should also be regarded with respect to the mechanical properties of the soil beneath its foundation and its relative location to the potential unstable slope. A ductile failure (usually associated with deep sliding surfaces) is expected for a slope consisting of clayey material leading to rather homogenous movements for a building situated next the slope's crest (within the unstable mass). Such movements are generally more pertinent to operational and not to structural damage. On the other hand, a relative brittle failure (associated to shallow sliding surfaces) is anticipated for a slope consisting of sand or rock materials that could result to significant differential deformation demand for the building standing at the edge and consequently to structural distortion and/or tilting.

Figure 3.4 presents various types of damage of different severity for buildings located within the unstable area of a deep sited landslide in Austria. Similarly, Figure 3.5 (a-d) illustrates examples of damage to houses including structural cracks and rigid body deformation caused by mass movements in Umbria. Figure 3.6 presents the main damage patterns of buildings located on top or within residential unstable slopes composed by cut and fills triggered by the 2011 Great East Japan Earthquake. Extensive structural damage was observed on the fill part of slopes (e.g. Fig. 3.7), mainly attributed to the formation of a soft layer between the original ground and the fill.



Figure 3.4. Building damage due to a deep sited landslide in Austria (Geological Survey of Austria)

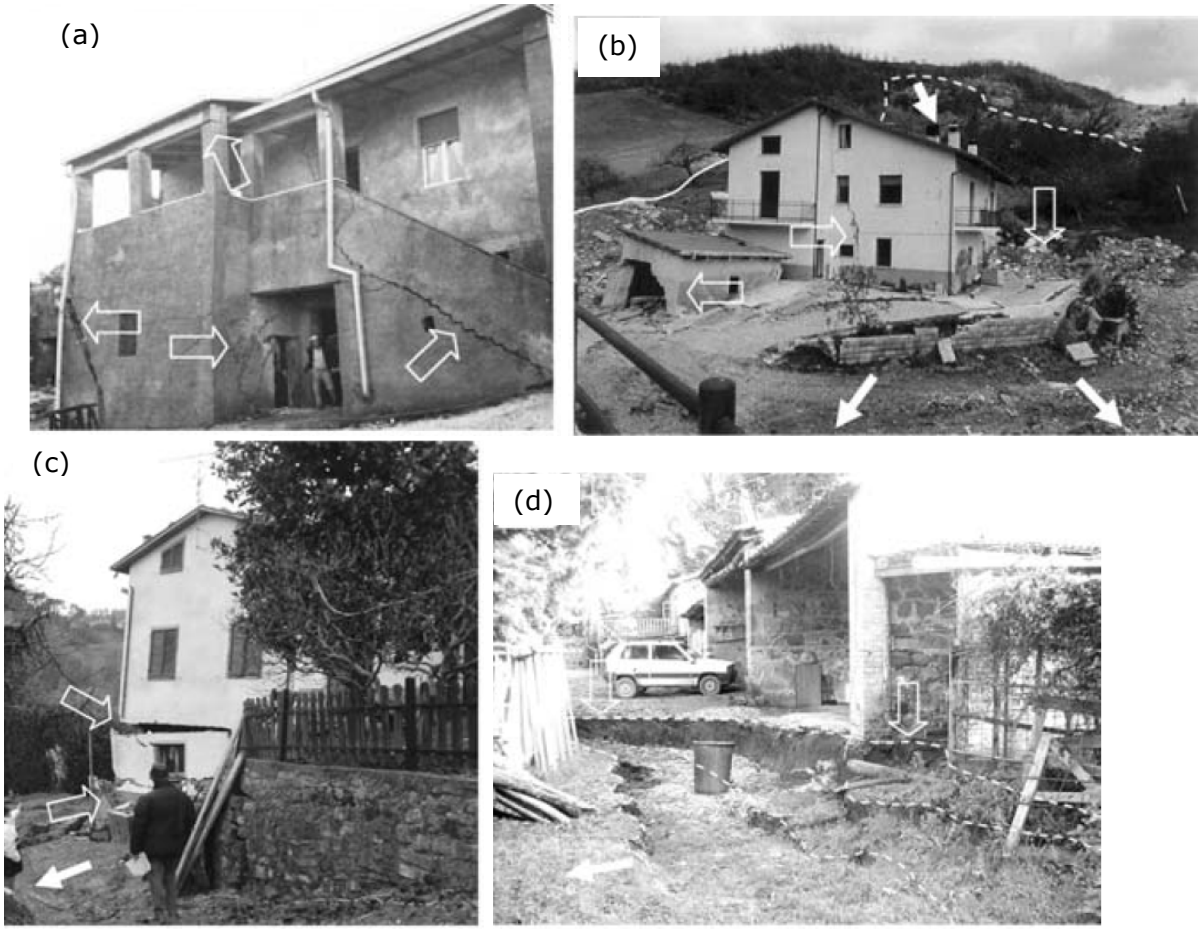


Figure 3.5. (a) Structural damage caused by deep-seated slide at Monteverde on December 22, 1982. (b) Total damage caused by deep-seated slide at Valderchia on January 6, 1997. (c) Total damage caused by deep-seated slide at Nuvole di Morra on December 9, 2005. (d) Functional damage caused by deep-seated slide at Badia and Podere Cipresso (Orvieto) on December 6, 2004. Open arrows show location of damage, filled arrows show approximate direction of landslide movement (Galli and Guzzetti, 2007).

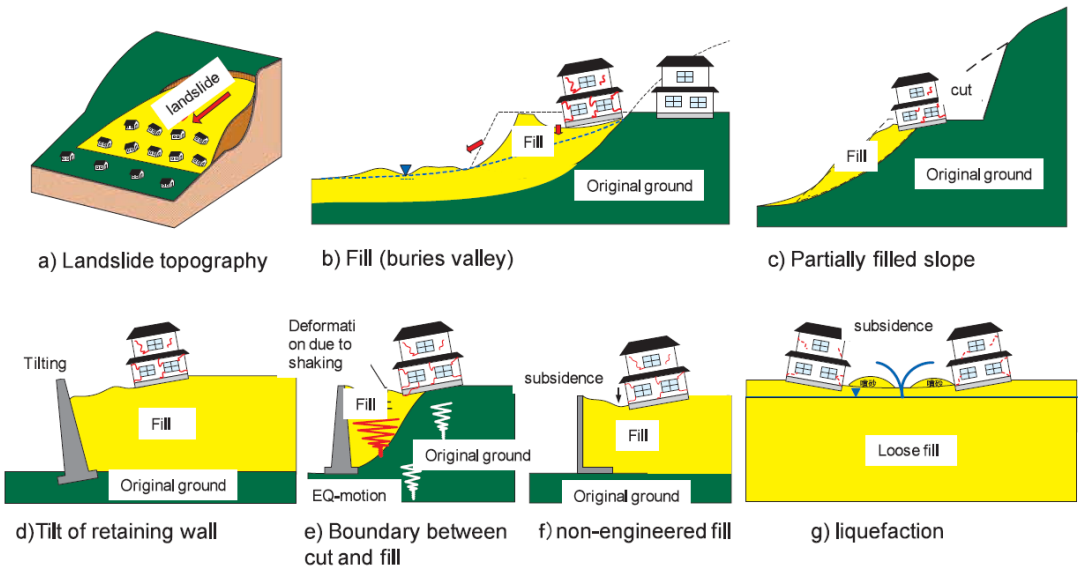


Figure 3.6. Classification of building damage mechanisms impact by slope instability triggered by the 2011 Great East Japan Earthquake (Japanese Geotechnical Society, 2011).



Figure 3.7. Building damage due to differential displacement in Sendai City, Japan following the 2011 Great East Japan Earthquake (Japanese Geotechnical Society, 2011).

Summarizing, the vulnerability of buildings to slow moving slides may depend on (a) the hazard level (b) the rate of movement (relative slow to extremely slow moving slides) (c) the type of materials controlling the movement (d) the triggering mechanism (intense rainfall, earthquake, erosion, construction activities etc), (e) the specific typological, strength and geometrical characteristics of the exposed buildings (determining its capacity), (f) their position and potential interaction in relation to the potential sliding surface.

3.3 Quantification of physical vulnerability to slides

3.3.1 Fragility functions

The physical vulnerability of elements at risk to landslides may be described through fragility functions. Fragility curves provide for every element at risk (i.e. building, infrastructure), the conditional probability for the element to be in or exceed a certain damage state, under a landslide event of a given type and intensity, taking into account various sources of uncertainty (both aleatory and epistemic). Fragility relationships are essential components of quantitative risk assessment (QRA) studies as they allow for the estimation of risk within a probabilistic performance or consequence-based framework. However, in contrast to other natural processes such as earthquakes, the use of fragility curves in landslide vulnerability and risk assessment studies has not received much attention and remains somewhat primitive. This thesis is intended as a step to bridge this

gap, providing various sets of analytical fragility curves for buildings to earthquake induced relative slow moving earth slides (see Chapter 6). Figure 3.8 illustrates a conceptual form of fragility function. Different mathematical procedures for developing fragility curves have been proposed in the literature (e.g. ATC-13, 1985; Shinozuka et al., 2000; Cornell et al., 2002; NIBS, 2004; Nielson and DesRoches, 2007; Porter et al., 2007 etc.). The determination of an appropriate statistical distribution is of major importance to deal with various sources of uncertainty. A two-parameter lognormal distribution function is usually adopted due to its simple parametric form to represent a fragility curve for a predefined damage/limit state (Koutsourelakis, 2010).

The methods used to estimate fragility curves can be classified into four categories – empirical, engineering judgmental, analytical, and hybrid – based on the scale of the study area, the availability and quality of input data and the local technology in construction practice.

Damage observation from previous landslide events are the main source of information for empirical curves that are generally more realistic compared to the other categories as they fit real-event data. The most common problem when applying a purely empirical approach is the unavailability of (sufficient and reliable) statistical data for several landslide types and intensities. Empirical fragility curves based on damage data survey on over 300 buildings of various classes were developed by Zhang and Ng (2005) in terms of limiting building settlement and angular distortion.

Engineering judgmental fragility relationships resort to expert opinion (ATC-13, 1985; Smith et al., 2012). The reliability of judgment-based curves is questionable due to their dependence on the individual experience and the number of the experts consulted. HAZUS (NIBS, 2004) provide fragility curves for extensive/complete building damage due to ground failure as a function of permanent ground displacement principally based on expect judgment.

Analytical fragility curves are essentially based on numerical modeling (e.g. Nielson and DesRoches, 2007; Argyroudis and Pitilakis 2012; Kakderi, 2011; Fotopoulou and Pitilakis, 2012). Analytical fragility relationships offer a higher level of detail compared to the previous ones. With the expansion of computational power and the development of reliable analysis tools, the limitations in the analytical derivation of vulnerability curves are decreasing. A first attempt to derive analytical fragility curves for RC buildings to differential settlements due to landslides has been made by Negulescu and Foerster (2010) largely inspired from the work of Bird et al. (2005).

Hybrid relationships attempt to compensate for the scarcity of observational data, subjectivity of judgmental data and modeling deficiencies of analytical procedures by combining observed data and analytical estimations (Kappos et al., 2006).

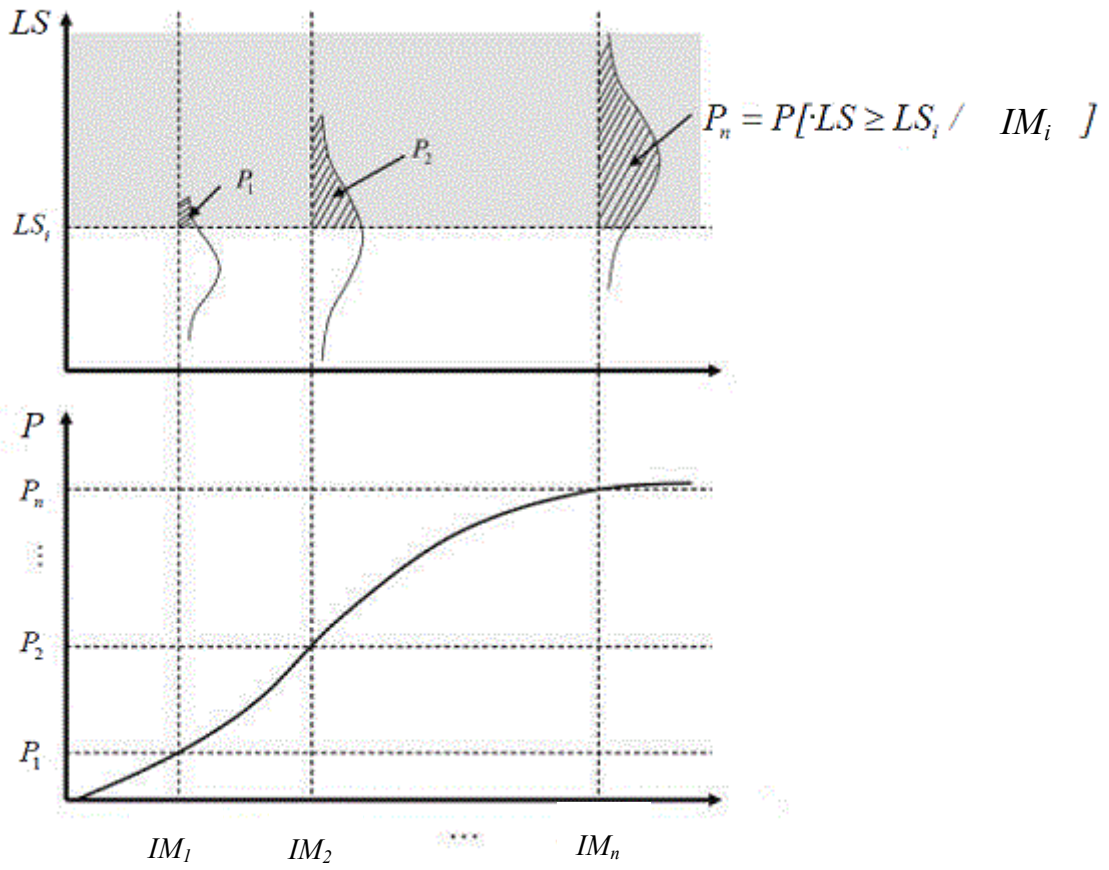


Figure 3.8. Concept of fragility curve

3.3.1.1. Damage states

Damage states express the average level of damages to specific elements at risk (buildings, lifelines, infrastructures) for different intensity levels. They imply a relationship between the response of the structure and its capacity to resist that response. They often describe different fragility curves for slight, moderate, extensive and complete damage (collapse). Typically multiple damage (or performance) criteria need to be satisfied. The number of damage states is normally between two and six, depending on the element at risk (typology, state of maintenance, use etc.) and the available data. They are defined by a threshold value of the damage index that could be a limit value of a component strain, joint displacement, inter-story drift, foundation displacement/rotation or other fragility criteria related to the loss of functionality and/or stability (Pitilakis et al. 2006a and b). The threshold value for each damage state and element at risk is commonly defined based on engineering judgment and damage observations. However, calibration of the adopted limit values with experimental data and large-scale laboratory tests is certainly desirable to enhance their credibility and reduce the associated subjectivity and uncertainty. Figure 3.9 presents the form of

HAZUS (NIBS, 2004) fragility curves to estimate seismic vulnerability of buildings for different damage states as well as the expected building performance for each damage state. When considering the impact of a slow moving slide, intensity could be related to the cumulative (absolute or differential) permanent foundation/ground movement or to the initial trigger of the landslide (e.g. Peak ground acceleration in case of earthquake induced landslides).

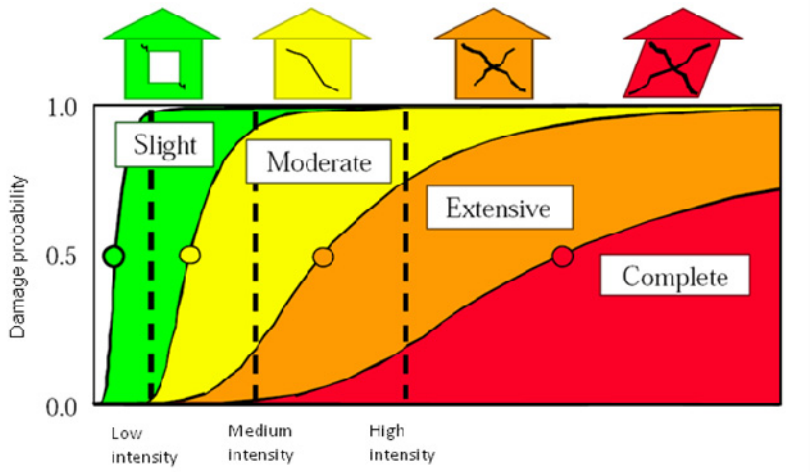


Figure 3.9. HAZUS fragility curves derived for buildings for different damage states (NIBS, 2004)

Various investigators have proposed different damage criteria for buildings subjected to ground movements related to slides as well as to other causes such as the dead weight of the buildings, adjacent excavation and tunneling activities, ground heaving, liquefaction etc. A review of the proposed damage indicators and the associated damage states is following.

Over half a century ago, Skempton and MacDonald (1956) based on settlements and damage observations on buildings due to their own weight suggested a range of limit values depending on the type of building or foundation, to determine the magnitude of differential foundation movement that will cause cosmetic, i.e. architectural damage to structures, or more seriously, structural damage. The damage criterion they used was the "angular distortion" defined as the ratio of the differential settlements and the distance between two points after eliminating the influence of the tilt on the building. Limits were selected empirically at 1/300 for preventing cracks in walls and 1/150 for avoiding structural damage. These recommendations proved to be in reasonable agreement with further studies (Burland and Worth, 1974), especially for frame buildings. Bjerrum (1963) based on the work of Skempton and MacDonald (1956) and

additional empirical data proposed damage criteria for different building types by relating angular distortion to building's performance (Tab. 3.1).

Polshin and Tokar (1957) defined limit performance criteria for different types of buildings which depend on the "slope" (difference of settlement of two adjacent supports relative to the distance between them), the "relative deflection" (ratio of deflection to the deflected part length) and the average settlement under the building, based on field observations on building damage and respective modes of deformation. These criteria were in accordance with the values proposed by Skempton and MacDonald (1956) and were also in agreement with the results obtained later by Burland and Worth (1974). Limit values proposed by Polshin and Tolkar (1957) were incorporated into the 1955 Building Code of the URSS.

Table 3.1. Damage Criteria based on angular distortion (after Bjerrum, 1963)

Angular distortion	Damage assessment
1/100	Limit where structural damage is to be feared. Safe limit for flexible brick walls with h/L<0.25. Considerable cracking in panel walls and brick walls.
1/250	Limit where tilting of high rigid buildings may become visible.
1/300	Limit where difficulties with overhead cranes can be expected.
1/500	Safe limit for buildings where cracking is not permissible.
1/600	Danger limit for frames with diagonals.
1/750	Lower limit for sensitive machinery.

Burland and Worth (1974), based on the results from a number of large scale tests on masonry panels and walls, showed that, for a given material, the onset of visible cracking is associated with a well defined value of average tensile strain which is not sensitive to the mode of deformation. They reported average values of strain at which cracking becomes evident of 0.05-0.1% for brick and 0.03-0.05% for concrete noting, however, that these values were much larger than the local tensile strain corresponding to tensile failure. Burland and Worth (1974) and Burland et al. (1977) applied the concept of limiting tensile strain to elastic beam theory to study the relation between building deformation and onset of cracking. Burland et al. (1977) pointed out that the visual building damage is difficult to quantify due to its subjective nature and thus they proposed the ease of repair as the key factor to determine the category of damage (Tab. 3.2). The ease of repair was then related to the measure of crack opening.

Boscardin and Cording (1989) complemented Burland and Wroth's concepts by including the effect of horizontal strain developing in the ground due to settlements. They noted that this effect depends on the lateral stiffness of the structure. Based on the results of their study, they defined categories of damage by developing relationships between the horizontal strain and the angular distortion (Fig. 3.10).

Table 3.2. Classification of visible damage to walls with particular reference to ease of repair of plaster and brickwork masonry (after Burland, 1995).

Category of damage	Normal degree of severity	Description of typical damage (Ease of repair is printed *italic*) Note: Crack width is only one factor in assessing category of damage and should not be used on its own as a direct measure of it
0	Negligible	Hairline cracks less than about 0.1 mm
1	Very Slight	*Fine cracks which are easily treated during normal decoration.* Damage generally restricted to internal wall finishes. Close inspection may reveal some cracks in external brickworks or masonry. Typical crack widths up to 1 mm.
2	Slight	*Cracks easily filled. Re-decoration probably required. Recurrent cracks can be masked by suitable linings.* Cracks may be visible externally and *some repointing may be required to ensure weathertightness.* Doors and windows may stick slightly. Typical crack width up to 5 mm.
3	Moderate	*The cracks require some opening up and can be patched by mason. Repointing of external brickwork and possibly a small amount of brickwork to be replaced.* Doors and windows sticking. Service pipes may fracture. Weathertightness often impaired. Typical crack widths are 5 to 15 mm or several up to 3 mm.
4	Severe	*Extensive repair work involving breaking-out and replacing sections of walls, especially over doors and windows.* Windows and door frames distorted, floor sloping noticeably[1]. Walls leaning[1] or bulging noticeably, some loss of bearing in beams. Service pipes disrupted. Typical crack widths are 15 to 25 mm but also depends on the number of cracks.
5	Very severe	*This requires a major repair job involving partial or complete rebuilding.* Beams lose bearing, walls lean badly and require shoring. Windows broken with distortion. Danger of instability. Typical crack widths are greater than 25 mm but depends on the number of cracks.

[1] **Note:** Local deviation of slope, from the horizontal or vertical, of more than 1/100 will normally be clearly visible. Overall deviations in excess of 1/150 are undesirable.

Boone (1996) adopted the crack width as an indicator of damage severity to assess the building damage considering ground deformation pattern, structure design and geometry, strain superposition and critical strains of building materials. The estimated damage for a number of examined case histories was found to be in good agreement with the actual observed building damage.

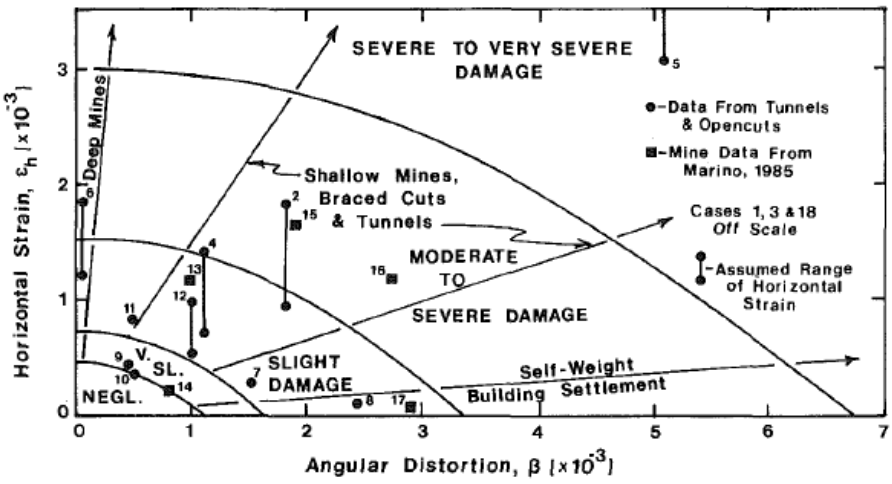


Figure 3.10. Correlation of Damage level to Angular Distortion and Horizontal Extension Strain (after Boscardin and Cording, 1989)

Bird et al. (2005; 2006) suggested different damage states for buildings subjected to seismically induced ground deformations based on the flexibility of the foundation system (flexible, rigid) and the deformation mode (uniform, differential). Where building response to ground failure comprised structural damage, damage states were classified using the same schemes used for structural damage caused by ground shaking (Table 3.3). In that case, limit states were defined in terms of threshold values of steel and concrete material strain. The first limit state was specified as steel bar yielding whereas suggested possible mean values for post-yield limit states for steel (ε_s) and concrete (ε_c) material for both poorly confined (poor) and well confined (good) RC frame buildings are presented in Table 3.4. The damage state of a building subjected to rigid body deformation was described using empirical solutions, classifying the damage level in terms of functionality and reparability. Table 3.5 presents the corresponding proposed rotational and settlement limits for grouping the rigid body response of buildings to ground failure into similar ranges that coincide with structural damage definitions. According to the authors these limits should be related to the extent of settlement, the ease of repair and the repair cost ratio. The authors acknowledge, however, that these limits involve a considerable degree of uncertainty owning to the lack of available data on repair methods and costs for settled and rotated buildings.

Table 3.3. Structural damage state descriptions for RC frame buildings (Crowley et al., 2004; Bird et al., 2005)

Structural damage band	**Description**
None to slight	Linear elastic response, flexural or shear type hairline cracks (<1.0 mm) in some members, no yielding in any critical section
Moderate	Member flexural strengths achieved, limited ductility developed, crack widths reach 1.0 mm, initiation of concrete spalling
Extensive	Significant repair required to building, wide flexural or shear cracks, buckling of longitudinal reinforcement may occur
Complete	Repair of building not feasible either physically or economically, demolition after earthquake required, could be due to shear failure of vertical elements or excessive displacement

Table 3.4. Suggested mean post-yield limit state strains for steel (ε_s) and concrete (ε_c) for poorly confined (poor) and well confined (good) RC frame buildings subject to ground deformations (Bird et al., 2005)

Limit state	***Poor* Buildings**		***Good* Buildings**	
	ε_s	ε_c	ε_s	ε_c
2	0.0125	0.0045	0.0125	0.0045
3	0.0225	0.0075	0.05	0.015

Table 3.5. Suggested limit states for rigid body settlement and rotation due to earthquake induced ground deformations (Bird et al., 2005)

Damage State	**Structural damage (see Table 3.1 for full description)**	**Additional description (rigid body deformation)**	**Settlement (Δ) only**	**Rotation (θ) only**
Slight	Hairline cracks only	Repairs may be necessary for aesthetic reasons	$\Delta \leq 0.1$m	$\theta \leq 0.6^o$ 1/100
Moderate	Some cracks in load-bearing elements	Repairable damage, Serviceability and/or functionality affected	0.1m $<\Delta \leq 0.3$m	$0.6^o < \theta \leq 2.3^o$ 1/100 to 1/25
Extensive	Wide cracks and buckling of longitudinal reinforcement	Uninhabitable, but repairable	0.3m $<\Delta \leq 1.0$m	$2.3^o < \theta \leq 4.6^o$ 1/25 to 1/12.5
Complete	Repair not feasible, shear failures or excessive displacement	Demolition cheaper than repair. Structural integrity affected, possible instability	≥ 1.0m	$\theta \geq 4.6^o$ ≥1/12.5

Mansour et al. (2011), based on an extensive literature survey on slow moving slides, their initial triggers and their impacts, proposed qualitative relations between the expected extent of damage and the movement rate for urban structures and facilities (Table 3.6).

Table 3.6. Damage expected from slow-moving slides to urban communities versus movement rate (Mansour et al., 2011)

Movement rate (mm/year)	Extent of Damage
0–10	Minor or no damage
10–100	Cracks in streets, footpaths and nearby embankments
	General signs of distress like bent trees
	House walls disjunction and badly working casings
	May cause damage to small dwelling houses
100–300	Cracks are wide to the extent that houses start to suffer a noticeable damage
	Rupture of service utilities
300–800	House walls buckling, bending of doors and windows and various damages in houses
800–4,000	Severe damage and failures to slopes or retaining walls supporting buildings
	If no warning system is implemented, human losses may occur
>4,000	Complete collapse of buildings

Finally, although not directly associated to damage caused by ground instability (due to landslides), inter-storey drift limits of a superstructure may provide, in conjunction with other damageability criteria, an index of the approximate performance of the structure, in terms of both structural stability and serviceability. Various structural codes and research provide insight on the relationship between the drift ratio limits and damage levels for different structural typologies (e.g. SEAOC, 1995; FEMA, 2000; UBC, 1997; NIBS, 2004; Rossetto and Elnashai, 2003; Ghobarah, 2004 etc.).

3.3.2 Review of quantitative methodologies to assess building vulnerability to slides

It is recognized that there is a lack of a unified and simple methodological framework to address the quantification of vulnerability due to different landslide hazards (Glade, 2003). Hollenstein (2005) observed that while there were numerous studies (>1000) on earthquake and wind (>100) related vulnerability models, there were only a few (<20) ones for gravitational hazards such as landslides, debris flows, snow avalanches and even floods. Methodologies are usually classified with regard to the landslide type (slide, debris flow, rockfall etc.), the element at risk (buildings, roads, lifelines etc.), the scale of

analysis (site specific, local, regional, national) and the methodological framework adopted (empirical, judgmental/heuristic, analytical). However, focusing in particular on slides, it is seen that most of the existing methodologies resort to expert judgment and empirical data providing fixed vulnerability values and hence they are principally applicable to studies at regional and local scales. Uncertainty (both epistemic and aleatory) that is inherent in such studies is not properly accounted for. Very few models are available in the literature to quantify the vulnerability of structures impacted by slides using analytical relationships and/or numerical simulations with potential application within a probabilistic framework. Such models may allow to study, in controlled conditions, the structure's behavior under the different landslide schemes considering various sources of uncertainty.

An overview of the available procedures found in the literature for quantitatively assessing vulnerability of buildings to slides is provided in the following.

Leone et al. (1996) introduced damage matrices that provide correlation, in terms of vulnerability, between the exposed elements and the characteristics of landslides. Structural vulnerability was related to the characteristics of the landslide and the technical resistance of the building, such as the type, nature, age, etc. The effective applicability of the method requires statistical analysis of detailed records on landslides and their consequences on the affected structures. *Dai et al. (2002)* also proposed the use of damage matrices due to their flexibility in different situations and reduced subjectivity.

Heinimann (1999) based on investigation of past landslide events, attributed vulnerability values to buildings considering different structural typologies and their resistance to different magnitudes of the landslide processes. However, as Heinimann stated, a major limitation of the approach is that most of the data have to be assumed.

Few years later, *Australian Geological Survey Organization (AGSO 2001)* proposed fixed vulnerability values for buildings subjected to landslides on hill slopes, proximal and distal debris fans. The capacity of the structure to resist the impact of different landslide mechanisms is not considered for assessing their vulnerability.

More recently, *Galli and Guzzetti (2007)* used historical damage data to buildings and roads caused by slow moving slides and slide-earth flows in Umbria region in central Italy to establish correlation between the landslide area and the vulnerability to landslides for the different elements at risk (buildings, major roads, secondary roads). Figure 3.11 presents the derived empirical vulnerability threshold curves for buildings in Umbria defined as the proportion of landslide damage (D_L) to buildings as a function of the landslide area (A_L). The authors observed that the amount of damage generally increases with increasing landslide area. However, they recognized that this trend is highly non-

linear while they revealed considerable variability in the data and in the corresponding curves. Simple, two-parameter power-law functions were selected to represent the lower and upper threshold curves.

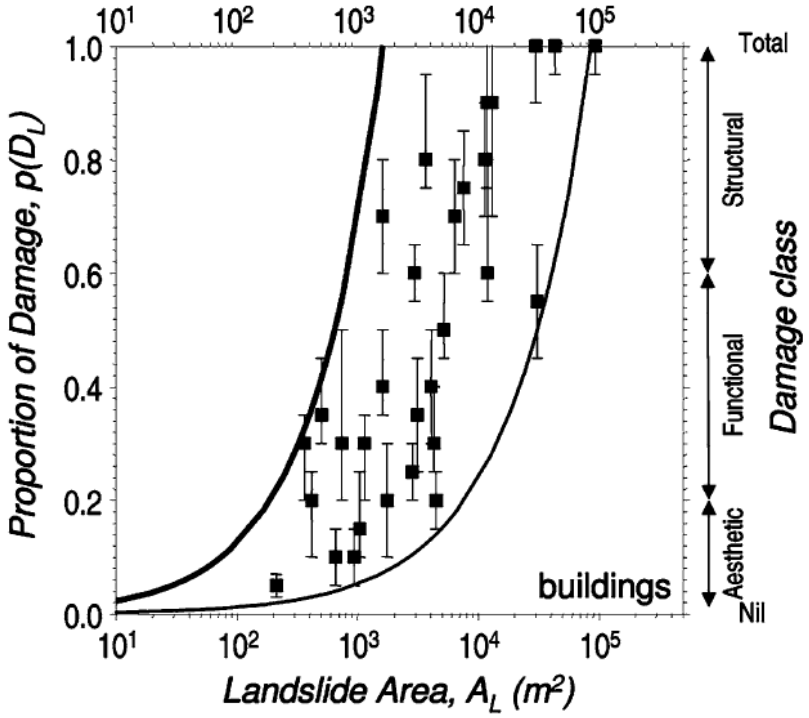


Figure 3.11. Proportion of landslide damage (DL) as a function of landslide area (AL) for different elements at risk in the Umbria region, central Italy (Galli and Guzzetti, 2007).

Papathoma et al. (2007) introduced a framework to undertake the assessment of vulnerability of buildings to different landslide hazards based on a Weighted Linear Combination Method. The specific framework was first developed for tsunami related disasters and was properly modified by the authors for landslides. The proposed approach was applied to a landside prone area in Lichtenstein, south Germany. Physical (direct) vulnerability of buildings to landslides was related to different factors based on the construction material, the existence of surrounding wall, the number of floors, the presence of warning signs and the side of the building facing the unstable slope. Table 3.7 presents the description of the various factors considered for the vulnerability assessment of the buildings in Lichtenstein area as well as their relevant raw and standardized scores defined by expert knowledge and judgment. The authors proposed the use of different weightings of the factors according to the priorities and final purpose of the vulnerability assessment.

The method presents some major shortcomings mainly associated with the pre-existence of landslide susceptibility/hazard maps, availability and costs of the required data,

weighting of the factors, inclusion of landslide related phenomena etc. The results are highly sensitive to the weighting of the parameters introducing considerable uncertainties owning to the subjective manner to which these are assigned. A non-linear regression sensitivity analysis to determine which attribute influences more the overall vulnerability of the building is proposed by the authors as a potential future improvement of their study. Recently, Mousavi et al. (2011) also applied this framework to assess the vulnerability of buildings exposed to earthquake induced landslides in Emamzadeh Ali area, Iran by carrying out a detailed investigation of each building in the affected zone.

Table 3.7. Data and their relevant raw and standardized scores (after Papathoma et al., 2007)

Field	Description of field	Description categories	Raw score (code)	Standardised score
Material	Material of which the building is made	Concrete	1	0.33
		Masonry	2	0.66
		Other (poor material such as wood and stone)	3	1
Surround	Surrounding walls or protection especially on the side of the slope	Strong high wall	1	0.33
		Medium wall	2	0.66
		No/low surrounding wall	3	1
Floors		More than one	1	0.5
		One floor	2	1
Warning	Presence of warning signs of landslides	Yes	1	0.5
		No	2	1
Slope side	Description of the side of the building facing the slope	Only wall	1	0.33
		Small windows	2	0.66
		Large windows	3	1

Zêzere et al. (2008) estimated the vulnerability of buildings in a small test site in the area north of Lisbon (Portugal) under different landslide hazards based on empirical or historic data, in conjunction with available data on buildings concerning age (state of maintenance), construction material and function. Vulnerability values (0-1) for the various building typologies were derived with respect to the different types of landslide processes (shallow translational slides, translational slides, rotational slides) and considering their estimated cost of reconstruction (Table 3.8).

Table 3.8. Building value and vulnerability considering exposure to different landslide types within the Fanhões-Trancão test site (Zêzere et al., 2008)

Building type	Value €		Vulnerability		
	m2	Pixel	Shallow translational slides	Translational slides	Rotational slides
Poor traditional masonry buildings	600	15,000	0.5	1	1
Poor adobe stone or taipa buildings	600	15,000	0.5	1	1
Poor other resistant elements (wood, metallic) buildings	600	15,000	0.4	1	1
Usual traditional masonry buildings	1197	29,925	0.5	1	1
Usual reinforced concrete buildings	1197	29,925	0.3	1	1
Luxurious reinforced concrete buildings	2186	54,650	0.3	1	1
Heritage traditional masonry	2217	55,425	0.5	1	1

Remondo et al. (2008) performed a detailed inventory of exposed buildings to the study area of Bajo Deba in northern Spain to quantitatively assess landslide vulnerability and risk implemented in a GIS platform. Vulnerability values (0–1) for a given landslide magnitude scenario were obtained by comparing damages experienced in the past (last 50 years) by each type of building with its actual momentary value. The derived vulnerability values express the degree of potential monetary loss with respect to the total value of the element.

Uzielli et al. (2008) developed a method for scenario-based, quantitative estimation of physical vulnerability of structures to landslides based on expert judgment and empirical data. Vulnerability is defined quantitatively as a product of the landslide intensity I and the susceptibility S of vulnerable elements using the following simple relationship:

$$V = I \times S \quad (3.3)$$

Within their framework, susceptibility of a structure quantifies its capacity to withstand the landslide action. It was related to two different factors depending on the structure's typological features and its state of maintenance through an analytical expression. Values of the partial susceptibility factor for structural type ξ_{STY} were subjectively assigned for six categories of structures based on the work of Heinimann (1999) (Table 3.9). The susceptibility factor for state of maintenance ξ_{SMN} was expressed as the reduced capacity of structures in comparison with the "very good" category in which maximum capacity is expected. The authors proposed indicative values that are given in Table 3.10.

Table 3.9. Values of susceptibility factor for structural typology (Uzielli et al., 2008)

Structural typology	Resistance	ξ_{STY}
Lightest, simple structures	None	1.00
Light structures	Very low	0.90
Rock masonry, concrete and timber	Low	0.70
Brick masonry, concrete structures	Medium	0.50
Reinforced concrete structures	High	0.30
Reinforced structures	Very high	0.10

Table 3.10. Values of susceptibility factor for state of maintenance (Uzielli et al., 2008)

State of maintenance	ξ_{SMN}
Very poor	0.50
Poor	0.40
Medium	0.25
Good	0.10
Very good	0.00

The landslide intensity was defined accounting for both kinetic (e.g. kinetic energy of the sliding mass) and kinematic (e.g. displacement) characteristics of the interaction between the sliding mass and the reference area. The proposed general model for the intensity of a landslide acting on the element at risk was specified as:

$$I = k_S \cdot [r_K \cdot I_K + r_M \cdot I_M] \quad (3.4)$$

Where

$$k_S = A_i / A_t \quad (3.5)$$

k_S is the spatial impact ratio; A_i is the area pertaining to the category that is affected by the landslide; A_t is the total area pertaining to the category; r_K is the kinetic relevance factor of the category; r_M is the kinematic relevance factor of the category; I_K is the kinetic intensity parameter of the category; and I_M is the kinematic intensity parameter of the category. Relevance factors were assumed to be dependent on the characteristics of the particular landslide event and the expected induced damage to the exposed element. In any case, they need to comply with the constraint: $r_K + r_M = 1$.

The authors acknowledged that the damage caused by a slow moving landslide on a building is mainly due to the displacement (i.e. kinematic parameter), while kinetic characteristics could be predominant in case of a rapid movement. In Table 3.11 proposed possible combinations of values for kinetic and kinematic relevance factors are given for structures for different landslide types (rapid, slow). Figure 3.12 presents the suggested kinetic and kinematic intensity models for structures (in which C is the velocity in mm/s of the sliding mass at impact, D_G is the absolute displacement in mm of the

ground and $D_{G,t}$ is a threshold value of D_G above which complete structural damage or loss of functionality may be supposed).

Table 3.11. Possible sets of values for kinetic and kinematic relevance factors for structures (Uzielli et al., 2008)

Landslide type	r_K	r_M
Rapid	0.90	0.10
Slow	0.15	0.85

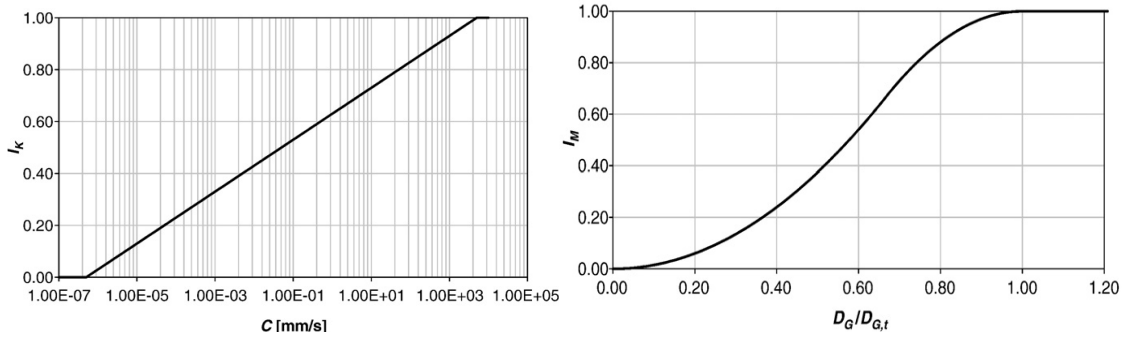


Figure 3.12. Kinetic and kinematic intensity models (Uzielli et al., 2008)

The method allows explicit consideration of the uncertainties in the parameters and models. However, due to its expert-based nature, critical judgment and objective data should accompany its application. Kaynia et al. (2008) explored the applicability of this methodology based on the First-Order Second-Moment (FOSM) approach to estimate landslide risks to the village of Lichtenstein- Unterhausen in Germany. They acknowledged that the methodology could be improved by inserting more accurate and precise models and objective data without requiring modification of its general probabilistic framework.

Li et al. (2010) based on the work of Uzielli et al. (2008) and Kaynia et al. (2008) suggested a new quantitative model for vulnerability of buildings based on landslide intensity I and resistance ability R of the structure to withstand the landslide impact.

The proposed model reads:

$$V = f(I,\ R) = \begin{cases} 2\dfrac{I^2}{R^2} & \dfrac{I}{R} \le 0.5 \\ 1.0 - \dfrac{2(R-I)^2}{R^2} & 0.5 < \dfrac{I}{R} \le 1.0 \\ 1.0 & \dfrac{I}{R} > 1.0 \end{cases} \tag{3.6}$$

Figure 3.13 shows the proposed theoretical changing trend of vulnerability as a function of intensity / resistance (a) and intensity for different resistance values (b).

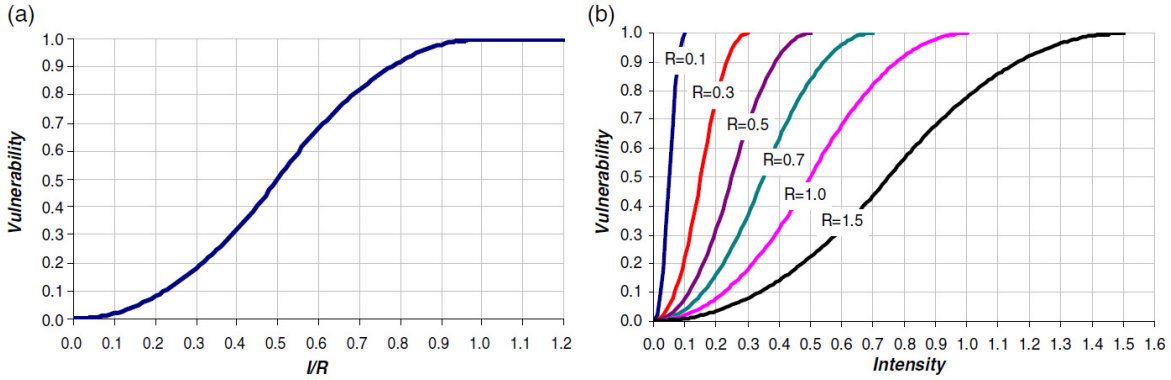


Figure 3.13. Theoretical changing trend of Vulnerability with Intensity/Resistance (a) and Intensity (b) (Li et al., 2010)

Landslide intensity was defined as a function of dynamic and geometric intensity factors depending on the relative location of the structure to the landslide area:

$$I = \begin{cases} I_{dyn} \cdot I_{dpt} & \text{For structures outside landslide area} \\ I_{dyn} \cdot I_{dfm} & \text{For structures within landslide area} \end{cases} \quad (3.7)$$

where I_{dyn} is the dynamic intensity factor, I_{dpt} is the debris-depth factor (used to evaluate the elements outside rapid landslide area), and I_{dfm} is the deformation factor (mainly used to evaluate the structures within the sliding mass of a slow landslide).

The dynamic intensity factor was related to the velocity of the sliding mass. For stationery elements (e.g. structures) the following expression was proposed:

$$I_{dyn-s} = \begin{cases} 0.00 & C \le 5 \times 10^{-7} \ (mm/s) \\ \frac{1}{36}\left(\log_{10} C + 6.30\right)^2 & C > 5 \times 10^{-7} \ (mm/s) \end{cases} \quad (3.8)$$

The debris-depth factor was estimated in proportion to the debris depth (in meters) at the location of a building. The later was also correlated to the foundation depth of the structure based on a previous work (Ragozin and Tikhvinsky, 2000) to allow them to assign tentative vulnerability values at different foundation depths (see Table 3.12). The deformation factor for structures is defined as the ratio of $D_S/D_{S,T}$, where D_S is the displacement index of foundation or structure and $D_{S,T}$ is a threshold value of D_S above which complete structural damage or loss of functionality may be expected.

The resistance of the building was related to four different factors, namely the foundation depth ξ_{sfd}, structure type ξ_{sty}, maintenance state ξ_{smn}, and height ξ_{sht} through the following expression:

$$R_{str} = \left(\xi_{sfd} \cdot \xi_{sty} \cdot \xi_{smn} \cdot \xi_{sht}\right)^{1/4} \quad (3.9)$$

Table 3.12. Proposed tentative vulnerabilities at different foundation depths (Li et al., 2010)

Depth of foundation (including piles), m	Landslide debris depth, m	Vulnerability
≤2	<2	1.0
>2	<2 0	0.0
Less than a landslide depth	2–10	1.0
10–13	2–10	0.5–1.0
>13	2–10	0.0–0.5
Any	>10	1.0

The author recommended values for the last three factors that range from 0.1 (very low resistance) to 1.5 (very high resistance) whereas they proposed a continuous function with a minimum of 0.05 and without upper limit for the resistance factor of foundation depth. Beyond a certain depth, an increase in the foundation depth yielded a marginal influence on the resistance.

As the previously discussed method proposed by Uzielli et al. (2008), the main limitation of this method lies again on its expert- based and therefore subjective origin. However, this approach is generally improved compared to the previous one owning to the introduction of more refined models and factors concerning both the characterization of the landslide intensity and the resistance of the structures.

Das et al. (2011) developed a methodology for stochastic landslide vulnerability modeling and applied it in a region of northern Himalaya, India. A logistic regression method was adopted for calculating building vulnerability to landslides. This incorporates the occurrence of landslides as a discrete and dichotomous response variable, and the locations of the buildings as explanatory variables to generate a conceptually rational function. The proposed logistic regression model applied to landslide vulnerability of the buildings was modeled as:

$$\Pr\ [V_{b(i)}(s)] = 1 / (1 + \exp(\alpha_1(E_{b(i)}(s) + \alpha_0) \quad (3.10)$$

where $V_{b(i)}(s)$ is the spatial vulnerability of the buildings, $E_{b(i)}(s)$ the maximum unit cost of the building and coefficients a_0 and a_1 the intercept and coefficient of a Logit function obtained from the analysis of damage data from the study area. Equation (3.10) represents a sigmoid curve and assumes that the property accumulation fits a Logit curve. Historical records of damage information of buildings were assessed while generating the vulnerability conditions. $V_{b(i)}(s)$ values were assessed on the basis of expected loss considering the maximum building cost for a complete damage condition.

Obtained Pr [$V_{b(i)}(s)$] values were then used to generate the building vulnerability map (Fig. 3.14).

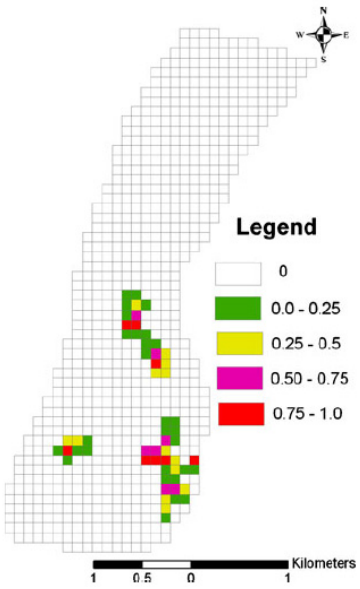


Figure 3.14. Building vulnerability map in a region of northern Himalaya, India (Das et al., 2011)

The authors claim that the proposed stochastic vulnerability framework may form the basis for a quantitative landslide risk assessment study. However, although the model offers a comprehensive modeling of uncertainties, a robust building vulnerability assessment still remains a challenge principally due to the randomness, complexities and site specific nature of the landslide processes and the particular characteristics of the vulnerable structures (e.g. typology, age, height, use etc.).

An interesting approach for the quantification of building vulnerability to landslides is made by *Negulescu and Foerster (2010)*. The authors proposed an analytical methodology to estimate the vulnerability of RC buildings to differential settlements due to different landslide hazards. To this aim, a series of 2-dimensional non-linear static time-history parametric analyses of a reference single bay- single storey structure were performed in order to identify one or several response parameters (foundation type e.g. different links, cross-section geometry, reinforcement degree, displacement magnitudes and displacement inclination angles) that govern the structural behavior when subjected to differential settlements. The input to the building model was a displacement load increasing linearly up to a certain value imposed quasi-statically at one of its supports to simulate the differential displacement demand of the structure impact by a landslide. The results of the parametric studies revealed that the parameters mostly affecting the behavior of the frame elements are the displacement magnitude and inclination angle

both related to the landslide deformation demand. Structural damage levels were defined as a function of the local strain limits of steel and concrete constitutive models. Preliminary fragility curves were constructed as a function of differential displacement for an encasing RC frame building (Fig. 3.15).

They authors compare their curves with other empirical ones proposed in the literature (HAZUS 2003; Zhang and Ng, 2005) and they found relatively good correlations. However, one must note that the derived curves use a different intensity parameter (i.e. the differential displacement) compared to the literature curves (HAZUS use the permanent ground displacement while Zhang and Ng (2005) the absolute settlement at the foundation level). Considering that, their direct comparison (as performed) involves a great deal of uncertainty and should be made with caution.

The proposed approach, although is a crucial step in the estimation of landslide vulnerability performed by means of straightforward analytical simulations, it focuses solely on the analysis of the building response to assess the settlement induced damage of buildings. Important factors such as the landslide type and mechanism, the triggering mechanism, the soil –structure interaction, the relative location of the building to the potential unstable slope and the corresponding uncertainties associated with them are not considered in the analysis. The development of analytical fragility curves expressing building vulnerability to different landslide hazards constitutes also a significant step in landslide vulnerability research community. However, the use of differential displacement as an intensity measure generally involves an even greater uncertainty than the estimation of uniform or average movements (at the foundation level or the sliding mass) as sufficient field data are often missing.

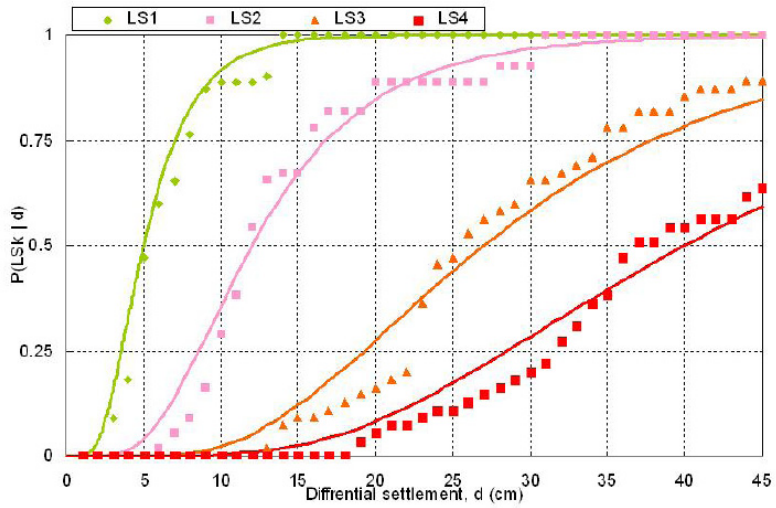


Figure 3.15. Fragility curves obtained for a one bay-one storey encasing RC frame building, considering 4 damage limit states: Slight (LS1), Moderate (LS2), Extensive (LS3) and Complete (LS4) (Negulescu and Foerster, 2010)

HAZUS (NIBS 2004) multi-hazard loss estimation methodology is maybe the only available practical tool to tackle the problem of estimating physical vulnerability of buildings affected by earthquake triggered landslides. The building damage is estimated through the use of simplified fragility curves that relate the permanent ground displacement (PGD) to the probability of exceeding a certain damage state. Different fragility curves that distinguish between ground failure due to lateral spreading and ground failure due to ground settlement, and between shallow and deep foundations were proposed considering one combined Extensive/Complete damage state.

Table 3.13. HAZUS Building Damage Relationship to PGD - Shallow Foundations

P[E or C| PGD]	Settlement PGD (cm)	Lateral Spread PGD (cm)
0.10	5.10	30.50
0.5 (median)	25.40	152.40

Table 3.13 presents the HAZUS Building Damage Relationship to PGD for buildings with shallow foundations (e.g., spread footings). Thus, lateral spread is judged to require significantly more PGD to effect severe damage than ground settlement. According to HAZUS methodology, median PGD values given in the table can be used with a lognormal standard deviation value of β_{PGD} = 1.2 to estimate P [E or C|PGD] for buildings on shallow foundations or buildings of unknown foundation type.

The aforementioned methodology, which is exclusively based on expert judgment, involves a high degree of subjectivity and simplification as it does not account various landslide types and mechanisms, soil type, building typology, stiffness of the foundation as well as different damage states.

3.3.2.1. Discussion

Table 3.14 summarizes all existing approaches for quantifying building vulnerability to slides with respect to the methodological framework used (e.g. empirical, engineering judgemental or analytical). It is seen that almost all methods are classified as empirical or judgemental while some methods are included in both categories. This may be attributed to the scarce and discrete historic damage data as well as to the great deal of randomness, uncertainty and complexity associated with them. Only one purely analytical model based on numerical simulations is found in the literature (Negulescu and Foerster, 2010) that involves, however, as discussed previously some basic limitations. It is noticed that even though some recently developed approaches provide analytical relationships that allow for implementation within a probabilistic framework (e.g. Li et al.,

2010; Das et al., 2011), their origin is either empirical or heuristic and thus they cannot be regarded as principally analytical methods.

Table 3.14. Existing methods to assess building vulnerability to slides in relation to the methodological framework adopted

Methodology to assess vulnerability to slides		
Empirical	**Judgmental/Heuristic**	**Analytical**
Galli and Guzzetti (2007) , Zêzere et al. (2008) , Remondo et al. (2008), Uzielli et al. (2008), Li et al. (2010), Das et al. (2011)	Leone et al. (1996), Heinimann (1999), AGSO 2001, Papathoma et al. (2007), HAZUS (NIBS, 2004), Uzielli et al. (2008), Li et al. (2010)	Negulescu and Foerster (2010)

Based on the above classification, it is recognized that there is a lack of analytical methodologies to quantify physical vulnerability of structures to slides. This gap aspires to bridge this thesis by proposing an analytical methodology for the quantification of the vulnerability of buildings to relative slow moving slides at site specific/local scales (Chapter 4). Analytical fragility curves are developed for various buildings typologies interacting with different landslide materials and slope configurations (Chapter 6).

CHAPTER 4

Vulnerability assessment methodology

4.1 Introduction

In the present chapter an analytical procedure to assess the vulnerability of RC structures due to earthquake induced landslide displacements is proposed. Part of this research has recently been published in Landslides scientific journal (Fotopoulou and Pitilakis, 2012). Vulnerability is described in terms of probabilistic fragility curves, which describe the probability (P_i) of exceeding each limit state (LS_i) of a specific element at risk (i.e. RC building), on a given slope, versus the given landslide intensity measure, allowing for the quantification of various sources of uncertainty.

In the following sections, the proposed methodological framework is described with a simplified case study. In terms of numerical computations, a two-step uncoupled analysis is performed. In the first step, the deformation demand, i.e. total and differential displacements considering the actual weight and stiffness of the building and its foundation, due to the landslide hazard is assessed using an adequate non-linear finite difference dynamic slope model. In the second step, the building response to the statically imposed landslide differential displacement is estimated using a Finite Element code. Modeling issues concerning both analysis steps are described in detail. Finally, two different analytical procedures to develop fragility functions are presented and applied to quantitatively evaluate the structural vulnerability in landslide risk analysis of specific RC building typologies and soil conditions.

4.2 Conception and description of the method

The proposed methodology, largely inspired from earthquake risk analysis, is applicable for the vulnerability assessment of low-rise RC frame buildings impacted by seismically induced relative slow moving earth slides. It is based on a comprehensive set of numerical computations and adequate statistical analysis. In terms of numerical simulation, a two-step uncoupled analysis is conducted. In the first step, a nonlinear Soil-

Foundation-Interaction analysis is performed using FLAC2D (Itasca, 2008) finite difference code. Slope dynamic models are subjected to several properly selected ground motions at their base to estimate the differential permanent displacements at the building's foundation level. Soil properties are adequately selected to consider modulus degradation with shear strains, initial shear stresses and other parameters involved in the dynamic analysis (Ishihara, 1996; Pitilakis, 2010). Then, the building's response for different statically applied ground/foundation differential displacements induced by the different earthquake time histories with progressively increasing intensities is assessed. To this aim, the previously computed differential displacements are directly applied as input quasi-static loads to an appropriate building nonlinear model at the foundation level. The numerical non-linear static analysis of the building is performed through the Finite Element code SeismoStruct (Seismosoft, SeismoStruct 2011). It is worth noticing that the complex issue of combined damages on the building by ground shaking and ground failure due to landslide is not taken into account in the evaluation of the building's vulnerability, which is assessed only for the effect of the permanent co-seismic displacement. In other words, it is supposed that the building is properly designed to resist even severe ground shaking following modern seismic codes and consequently no initial damage to the building's structural members (e.g. in terms of stiffness and strength degradation) is assumed to occur due to ground shaking.

Appropriate limit states are defined in terms of threshold values of building's material strain, based on engineering judgment and the associated work of Crowley et al. (2004), Bird et al. (2005) and Negulescu and Foerster (2010). Different limit strains are adopted for "low" and "high" code designed structures.

The fragility curves are estimated in terms of peak ground acceleration (PGA) recorded on rock outcrop or permanent ground displacement (PGD) at the slope area versus the probability of exceedance of each limit state. The selection of the most appropriate landslide intensity measure is generally recommended to be made with consideration of its predictability, efficiency and sufficiency (Kramer, 2011) (see Chapter 3, § 3.2.1). It is noticed, however, that when the rock outcropping PGA is used as an intensity parameter the local soil conditions, surface geology, soil and topographic amplification are directly included in the fragility analysis. Its use is consistent with the modern seismic hazard assessment methods applied in the most recent approaches (see SHARE, http://www.share-eu.org/ and OpenQuake, http://openquake.org/). On the other hand, PGD that is obtained from the response of the landslide to ground shaking is better correlated to structural deformation and damage. In addition, its use as an intensity parameter may allow for direct application to non-earthquake related landslide hazards. Other parameters such as the maximum differential permanent displacement at the

foundation level could potentially be used as measures of the landslide intensity. However, their accurate estimation generally involves a higher degree of uncertainty. Thus, their use is justified for site-specific applications on critical structures where adequate data from field measurements and/or detailed numerical analysis are available.

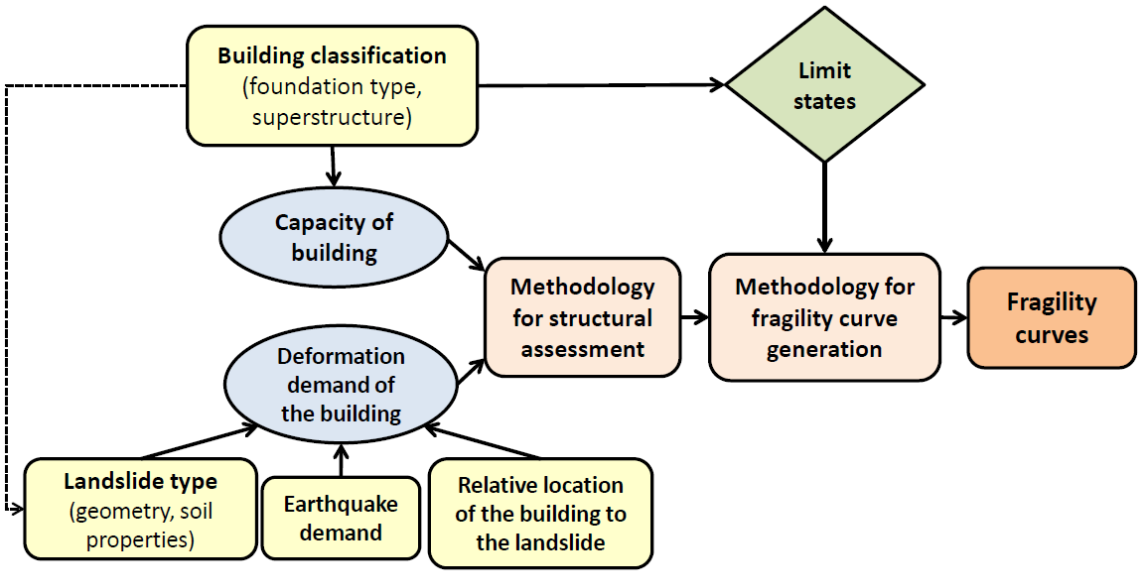


Figure 4.1. Flowchart for the proposed framework of fragility analysis of RC buildings

Figure 4.1 illustrates the framework of the method. The "capacity" of each building is defined by the building classification (foundation and superstructure type, and geometry, material strength), while the "demand" is described in terms of induced permanent ground deformation (slow moving slide) depending on the landslide type, soil conditions and the relative location of the building to the potential unstable slope. It is noted that the soil-foundation relative stiffness may also control in a certain degree the deformation demand for the building (e.g. for the case of a stiff foundation resting on soft soil material). Thus, the soil-foundation compliance and the geometric constraints imposed by the rigidity of the foundation system, as well as its potential slippage and/or detachment with respect to the underlying soil, may alter the free-field displacement pattern, modifying the deformation demand for the structure. These two components i.e. building capacity, deformation demand, can be considered as inputs to the simulation engine, which is the third major component, providing the methodology for structural assessment. Structural response data obtained by analyzing the building capacity under the deformation demand is processed to generate fragility curves. Limit states, which are determined with respect to the building classification and structural characteristics, selected empirical criteria and expert judgment, are required at this step. The final step is the construction of the analytical fragility relationships. Similar flowcharts may be

defined for other triggering mechanisms (intense rainfall, erosion etc.). It is also possible to construct synthetic flowcharts combining different triggering mechanisms. Further discussion on the conceptual features of the proposed methodological framework is highlighted in the following paragraphs. It is noted that some of these features have already been thoroughly discussed in previous chapters but they are shortly repeated herein to provide a link with the proposed approach.

The landslide type (rock fall, debris flow, earth slide, etc) is a crucial parameter of the proposed methodology as landslides of different types and sizes usually require different and complementary methods to estimate vulnerability. While most devastating damages to the built environment are probably resulting from the occurrence of rapid landslides such as debris flows and rock falls, slow-moving slides also have adverse effects to buildings and lifelines and critical facilities (Mansour et al., 2011; Argyroudis et al., 2011). The damage caused by a slow moving slide on a single building is mainly attributed to the cumulative permanent (absolute or differential) displacement and it is concentrated within the unstable area (see Chapter 3, §3.2.2). A relative slow moving earth slide that will produce tension cracks due to differential displacement to a RC building, exposed to the landslide hazard, is considered in this study. Note, however, that the time scale related to non-earthquake and earthquake induced slow moving slides studied in this research is different. In particular, the landslide processes associated with earthquake triggering mechanisms are naturally more rapid as they involve seismic cyclic loading that may usually last from several seconds to few minutes. Yet, they are classified herein as "relative slow moving slides" to differentiate them from the earthquake induced landslides that involve the complete failure of the slope and displacements of tens of meters.

The characteristics of the earthquake ground motion in terms of amplitude, frequency content and duration, in relation to the soil dynamic properties and stratigraphy, can significantly affect the deformation demand for the building. Soil nonlinearity, material damping, impedance contrast between sediments and underlying bedrock and the characteristics of incident wavefield are the main governing factors for site amplification/attenuation (Kramer and Stewart, 2004; Pitilakis, 2010). The slope failure potential assumes its highest values for a combination of a low-frequency seismic input motion with a resonance phenomenon in the low-frequency range (Bourdeau et al., 2004). In general, a fundamental period of the input earthquake close to the natural period of the site can lead to resonance phenomena and, consequently, to an amplified energy content of the ground motion (see also Chapter 2, §2.2.2.3 for detailed description).

The position of the building with respect to the landslide area is also a very important contributing factor. Topographic effects may alter the amplitude and frequency content of the ground motions along slopes (Bouckovalas and Papadimitriou, 2005; Ktenidou, 2010) (see Chapter 2, §2.2.2.3 for details). Moreover, the effect of soil-structure interaction due to the presence of a structure at a cliff can further modify the seismic response at the topographic irregularity with respect to the free-field case (i.e. in the absence of any structure), depending on the soil-structure impedance contrast, the geometry of the slope and the dynamic characteristics of the building itself (Assimaki and Kausel, 2007; D. Pitilakis and Tsinaris, 2010). In the current study, RC buildings of different stiffness characteristics standing near the slope's crest, where the seismic ground motion due to topographic effects is generally amplified, are explicitly considered in the analysis.

For a given landslide mechanism and hazard intensity, the typology of the exposed structure is also a key factor. A building's geometry and number of floors, material properties, state of maintenance, code design level, soil conditions and mainly the foundation and structure details are the critical parameters which determine the capacity of the building to withstand co-seismic landslide displacements. The response to permanent total and differential ground deformation depends primarily on the foundation type (see also Chapter 3, § 3.3.2). A structure on a deep foundation (e.g. piles) compared to shallow foundations is more resilient and often experiences higher resistance ability and hence a lower vulnerability. For shallow foundations, a rigid foundation, i.e. continuous raft foundation is less vulnerable than a flexible one, i.e. isolated footings. The soil-foundation relative stiffness is also a dominant parameter. When the foundation system is rigid the building is expected to rotate as a rigid body and the anticipated damages or failure is mainly attributed to loss of functionality. In this case, the damage states are defined empirically, as there is limited structural demand to the members of the building (apart from possible P-Δ effects at larger rotations). On the contrary, when the foundation system is flexible enough allowing differential movement of the walls or columns (e.g. isolated footings), the various modes of differential deformation produce structural damage (e.g. cracks) to the building members (Bird et al., 2005; 2006).

To derive the vulnerability of a building exposed to seismically induced slow-moving slides, an analytical procedure analogous to that of the response due to seismic oscillation is proposed. When building response to ground failure and permanent ground deformations comprises structural damage, damage states can be classified using the same schemes used for structural damage caused by ground shaking. Limit states could be defined in terms of limit value of a component's strain based on damage observation from previous earthquake events, the existing knowledge related to earthquake damage

levels, and published tolerances for non-earthquake related foundation deformations (Crowley et al., 2004; Bird et al., 2005). Different limit strains are assigned based on the construction quality of the building and code adopted in the design.

In the probabilistic approach proposed herein, several uncertainties are involved with respect to the capacity of the building, the definition of the limit states and the deformation demand (differential permanent displacement). The uncertainty in the permanent displacement capacity is a function of the material properties, geometric characteristics, and the yield strain of steel and post-yield strain capacities of the steel bars and concrete. The uncertainty in the demand is associated with the ground motion estimation and additional uncertainties associated with the landslide type and size, the relative position of the building in the landslide area, the variability in soil parameters in space and time during the loading, the stratigraphy and the epistemic uncertainties associated with the assessment of ground deformations.

4.3 Layout- Numerical example

4.3.1 Dynamic analysis of the slope

The conceptual features of the methodology outlined in the previous section are described in detail through an idealized, yet realistic, example. The deformation demand in terms of permanent seismic displacements can be estimated either empirically (e.g. Newmark type methods) or numerically. The numerical approach applied herein is selected for two reasons: (a) it is more accurate than any empirical method and (b) it permits the direct estimation of the differential ground/foundation displacements, which are the main cause of damage. For completeness reasons, the computed total permanent displacements for specific slope configurations, material properties and seismic inputs are compared with different Newmark-type displacement approaches in Chapter 5, §5.2.3.

4.3.1.1. Numerical model

In order to evaluate the permanent differential ground/foundation displacements (deformation demand) for the building on a given slope, the dynamic non-linear analyses are performed using the two dimensional (2D) finite difference code FLAC 6.0 (Itasca, 2008). The 2D dynamic calculation is based on the explicit finite difference scheme to solve the full equations of motion, using lumped gridpoint masses derived from the real density of surrounding zones. FLAC2D (Fast Lagrangian Analysis of Continua) has been widely used by many investigators to study the non-linear dynamic response of slopes and embankments in plane strain conditions (e.g. Bourdeau et al., 2004; Chugh and Stark, 2006; Bozzano et al., 2008b; Barani et al., 2010; Fotopoulou et al., 2011; Lenti

and Martino, 2012 etc.) due to its efficiency in modeling nonlinearity, large-strain problems and physical instability.

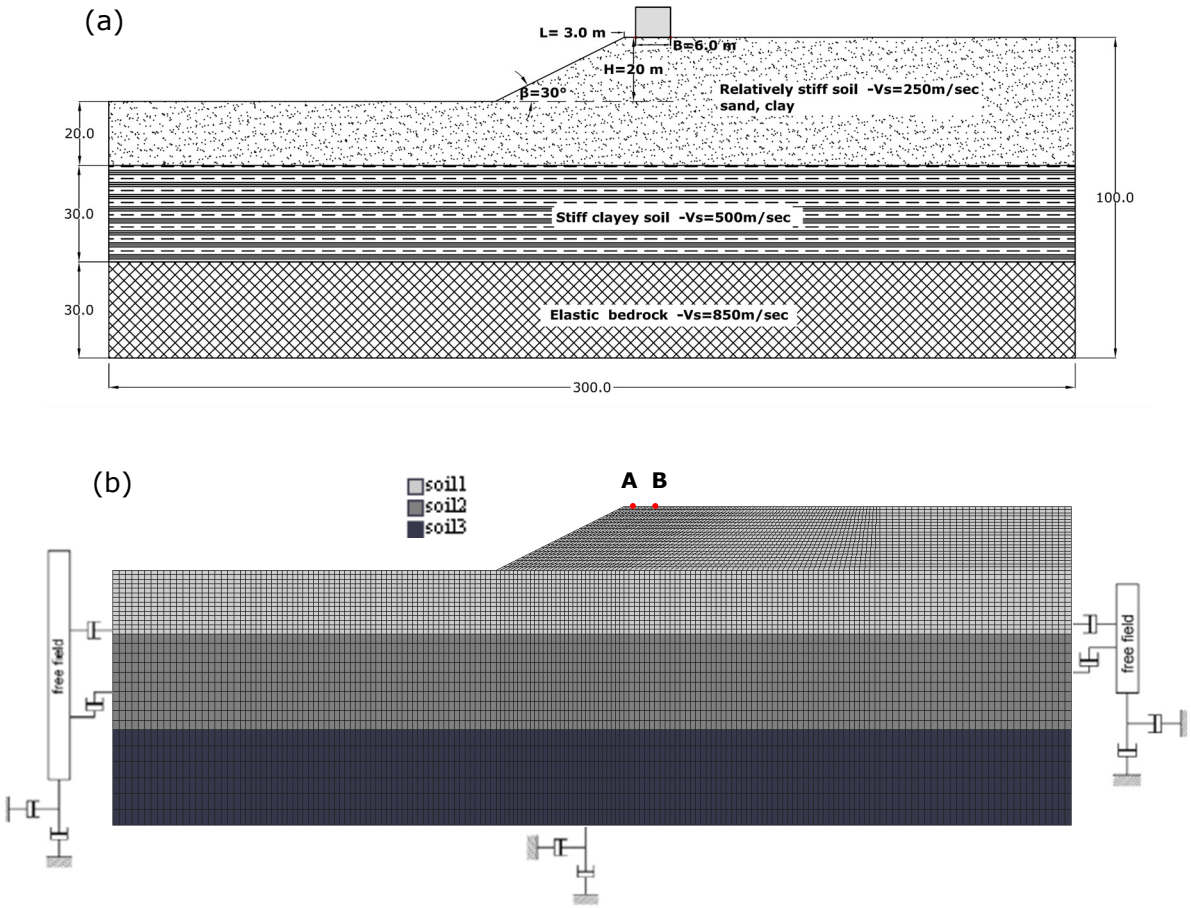


Figure 4.2. (a) Slope and foundation configuration used for the numerical modeling (b) and FLAC 2D dynamic model

A schematic representation of the reference finite slope geometrical and geological features and the corresponding 2D dynamic slope model used to study the irreversible deformation demand for the building located near its crest is illustrated in Figures 4.2 a and b respectively. The model has a total length of 300m and width of 100 m, while the slope height and inclination are 20m and 30^{o} respectively. It contains approximately 9000 four-node quadrilateral elements of various sizes determined by the shear wave velocities of the medium and the frequency content of the incident motions. Kuhlemeyer and Lysmer (1973) showed that for accurate representation of wave transmission through a model, the element size must be smaller than approximately one-tenth to one-eighth of the wavelength associated with the highest frequency component of the input wave. In the present study, the discretization allows for a maximum frequency of at least

10Hz to propagate through the grid without distortion. A finer discretization is adopted in the slope area, whereas towards the lateral boundaries of the model the mesh is coarser.

The soil materials are modeled using an elastoplastic constitutive model with the Mohr-Coulomb failure criterion (shear yield) with tension cutoff (tension yield function), assuming a zero dilatancy non-associated flow rule for shear failure and an associated rule for tension failure. The use of such simple model within the framework of this study is justifiable as it allows more clearly identifying the basic parameters that influence the estimation of the differential displacement demand for the building. Besides, it serves as a useful reference against which more complex soil behavior may be compared. Soil strength properties are properly selected to account for the dynamic ground response. The influence of the initial shear stress in the strength values is directly taken into account. It is noticed that the sliding surface is not pre-defined but "emerges" naturally, following the elastoplastic constitutive law. Two different soil types are selected for the surface deposits to represent homogenous dry, purely frictional and cohesive materials corresponding to soil category C of EC8 (CEN-European Committee for Standardization 2003). A stiffer clayey layer (V_s=500 m/sec) is assumed to underlie the surface deposits. The elastic bedrock (V_s=850 m/sec) lies at 70 m. The mechanical characteristics for the soil materials and elastic bedrock are presented in Table 4.1.

Table 4.1. Soil properties of the analyzed slopes

	Relatively stiff soil		**Stiff soil**	**Elastic bedrock**
	sand	**clay**		
Dry density (kg/m^3)	1800	1800	2000	2300
Young's modulus (KPa)	2.93E+05	2.93E+05	1.30E+06	4.32E+06
Poisson's ratio	0.3	0.3	0.3	0.3
Drained Bulk modulus K (KPa)	2.44E+05	2.44E+05	1.08E+06	3.60E+06
Shear modulus G (KPa)	1.13E+05	1.13E+05	5.00E+05	1.66E+06
Cohesion c (KPa)	0	10	50	-
Friction angle φ (degrees)	36	25.0	27	-
Dilation angle (degrees)	0	0	0	0
P-wave velocity V_p (m/sec)	468	468	935	1590
Shear wave velocity V_s (m/sec)	250	250	500	850

The static factor of safety of the slope is calculated through a limit equilibrium approach using the Spencer's method (Spencer, 1967) as Fs=1.45 for the sand and Fs =1.38 for the cohesive soil material. The critical failure surfaces during seismic loading cover a wide range from shallow in the case of surface sand deposits to relatively deep for the surface clayey materials.

Rayleigh type damping is used in conjunction to the stress-strain constitutive model for an approximate representation of cyclic energy dissipation. A damping matrix, *C*, is used, with components proportional to the mass (M) and stiffness (K) matrices:

$$[C] = \alpha [M] + \beta [K] \quad (4.1)$$

where

α = the mass-proportional damping constant; and

β = the stiffness-proportional damping constant.

Although Rayleigh damping involves two viscous elements in which the absorbed energy is dependent on frequency, the frequency-dependent effects can be canceled out over a restricted range of frequencies with the appropriate choice of parameters.

When irreversible strain accumulation takes place the energy dissipation is intended to be captured through the yield model. However, while stiffness-proportional damping is turned off when plastic failure occurs within a FLAC zone, mass proportional damping remains active. Thus, if excessive failure occurs in a model, the mass proportional term may inhibit yielding as rigid-body motions that occur during failure modes are erroneously resisted (Itasca, 2008). In this study, a considerable amount of energy dissipation is represented by the yield constitutive model considering that extensive plastic deformation is expected to occur during ground shaking. In this way, the selection of Rayleigh damping parameters is tend to be less critical to the outcome of the analysis. Based on the above, a small amount of mass and stiffness -proportional Rayleigh damping (1 to 3% for the soil materials and 0.5% for the elastic bedrock) is assigned to account for the energy dissipation during the elastic part of the cyclic response. The center frequency of the Rayleigh damping (f_{min}) is selected to lie between the natural modes of the model, f_1= 1.52 Hz and $f_2=5 \cdot f_1=7.6$ Hz based on common practice (e.g. Kwok et al., 2007). This range includes the model's natural frequencies (defined by the downhill and uphill resonant frequencies respectively) and the predominant frequencies of the input motions. Figure 4.3 presents the specification of critical damping ratio (for $\xi_{min}=3\%$) and central (minimum) frequency adopted in this study.

Note that hysteretic damping is an alternative algorithm in FLAC to account for the non-linear hysteretic soil behavior prior yielding. It is considered conceptually more realistic as it is based on the implementation of fitted G-γ-D curves that yield different shear stiffness and damping levels as a function of cyclic strain. However, its use was abandoned after some preliminary trial investigation as it was found to be performed outside its expected range of application, resulting to unrealistically high strain accumulation and to numerical instability, for the large irreversible deformations anticipated in the analyzed cases.

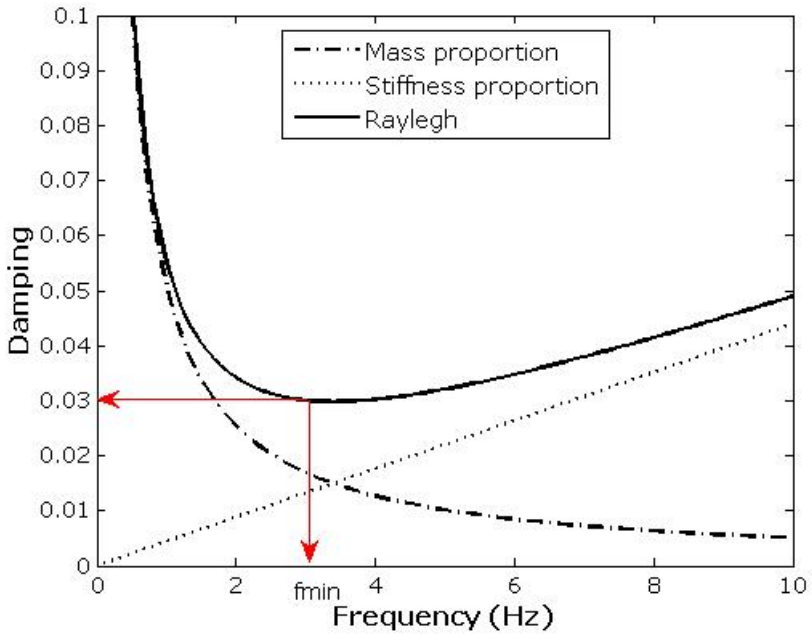


Figure 4.3. Specification of FLAC Rayleigh damping parameters for the present study (ξ_{min}=3%, f_{min}=3.1 Hz)

Free field absorbing boundaries (Cundall et al. 1980) are applied along the lateral boundaries whereas quiet boundaries (Lysmer and Kuhlemeyer, 1969) are applied along the bottom of the dynamic model to minimize the effect of artificially reflected waves (see Fig. 4.2). Free field absorbing boundaries involve the execution of a one-dimensional free-field calculation in parallel with the main-grid analysis. The coupling of the free-field grid to the main grid is achieved by viscous dashpots. In this way, plane waves propagating upward suffer (almost) no distortion at the boundary because the free-field grid supplies conditions that are identical to those in an infinite model. Quiet (viscous) boundaries consist of dashpots attached independently in the normal and shear directions (Lysmer and Kuhlemeyer, 1969). In order to apply quiet boundary conditions along the same boundary as the dynamic input, the seismic motions must be applied as stress loads combining with the quiet (absorbing) boundary condition using the following relationships:

$$\begin{aligned} \sigma_n &= 2 \cdot \rho \cdot C_p \cdot v_n \\ \sigma_s &= 2 \cdot \rho \cdot C_s \cdot v_s \end{aligned} \tag{4.2}$$

where σ_n and σ_s are the applied normal and shear stresses, respectively, ρ is the material density, C_P and C_S are the P- and S-wave velocities, respectively, and v_n and v_s are the input normal and shear particle velocities. The factor of two in Eqs. 4.1 accounts for the fact that the amplitude of the applied stress waves must be doubled to keep into account that half the input energy is absorbed by the viscous boundary.

A RC building is assumed to be located 3m away from the slope crest. Two different shallow foundation systems are considered (Tab. 4.2): isolated footings and a uniform

loaded continuous slab foundation. In the first case, the foundation is simulated with concentrated loads at the footings' links. As a consequence, no relative slip and/or separation between foundation and subsoil are allowed. In the second case, the foundation system is modeled as a deformable elastic beam connected to the soil elements' grid through appropriate interface elements that can approximate the potential Coulomb sliding and/or tensile separation of the beam. The relative interface movement is controlled by interface stiffness values in the normal (k_n) and tangential directions (k_s) as well as the maximum interface shear resistance between the soil and the foundation. The interface properties adopted for the present study are presented in Table 4.3. A first series of analyses is also conducted for the free-field case, i.e. in the absence of any structure, to assess the influence of Soil-Foundation Interaction in altering the seismic slope response in the vicinity of the crest.

Table 4.2. Foundation properties

Properties	Foundation system	
	Stiff foundation	Flexible foundation
Element	beam	
Width (m)	6	
Density (KN/m^3)	25	
Young's modulus (KPa)	$2.90 \cdot 10^7$	
Moment of inertia I (m^3)	0.0053	
Area (A) (m^2)	0.4	
Load (KN/m)	Uniform distributed q=25KN/m^2	Concentrated P=50KN/m

Table 4.3. Interface properties

Properties	Surface soil layer	
	Sand	Clay
Normal stiffness k_n (KN/m)	$2 \cdot 10^6$	$2 \cdot 10^6$
Shear stiffness k_s (KN/m)	$1 \cdot 10^6$	$1 \cdot 10^6$
Cohesion c (KPa)	0.0	7.0
Friction angle φ (degrees)	24	17
Dilation angle (degrees)	0.0	0.0

4.3.1.2. Seismic loading

Prior to the dynamic simulations, a static analysis is carried out to establish the initial effective stress field throughout the model. The dynamic input motion consists of SV waves vertically propagating from the base. Seven different earthquake records are used for the dynamic analyses (Tab. 4.4). They all refer to outcrop conditions as it is normally proposed in modern seismic codes (i.e. EC8). No specific soil amplification

factors are applied, as this is explicitly taken into consideration through the numerical analysis. The records are selected to cover a wide range of seismic motions in terms of the seismotectonic environment, amplitude, frequency content and significant duration. Figure 4.4 presents the normalized 5%-damped elastic response spectra of the input motions together with the proposed elastic design spectrum of EC8 (CEN-European Committee for Standardization 2003) for soil type A (rock).

Table 4.4. Selected outcropping records used for the dynamic analyses

Earthquake	Record station	M_w	R (km)	PGA (g)
Valnerina, Italy 1979	Cascia	5.9	5.0	0.15
Parnitha, Athens 1999	Kypseli	6.0	10.0	0.12
Montenegro 1979	Hercegnovi Novi	6.9	60.0	0.26
Northridge, California 1994	Pacoima Dam	6.7	19.3	0.41
Campano Lucano, Italy 1980	Sturno	7.2	32.0	0.32
Duzce, Turkey 1999	Mudurno_000	7.2	33.8	0.12
Loma Prieta, California 1989	Gilroy1	6.9	28.6	0.44

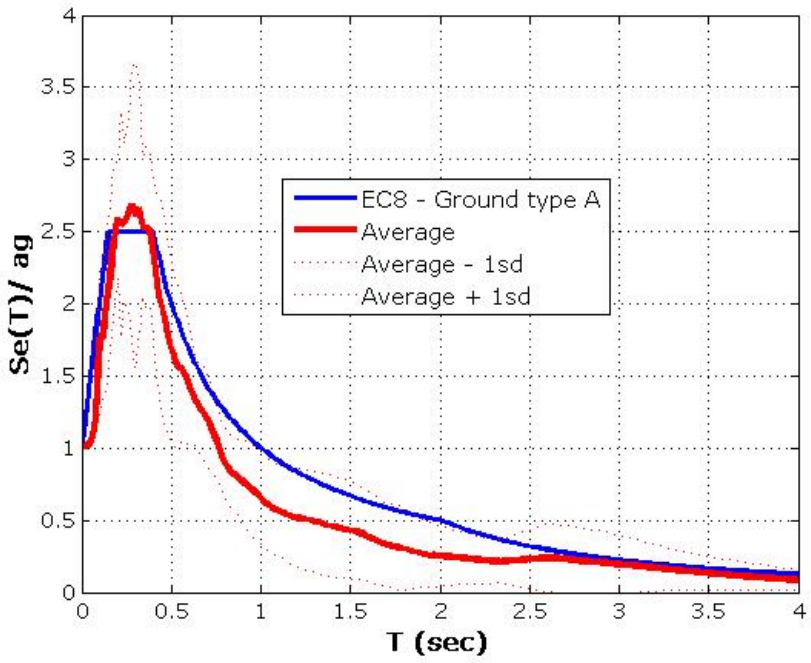


Figure 4.4. Normalized average elastic response spectrum of the input motions in comparison with the corresponding elastic design spectrum for soil type A (rock) according to EC8

Before applying the selected outcropping records (target motions) the appropriate dynamic loading for the base of the FLAC model needs to be determined. Thus, the time histories are first subjected to baseline correction and filtering to assure an accurate representation of wave transmission through the model. In particular, a Butterworth bandpass 4^{th} order filter type in the frequency range from f_1=0.25 Hz to f_2=10 Hz and a

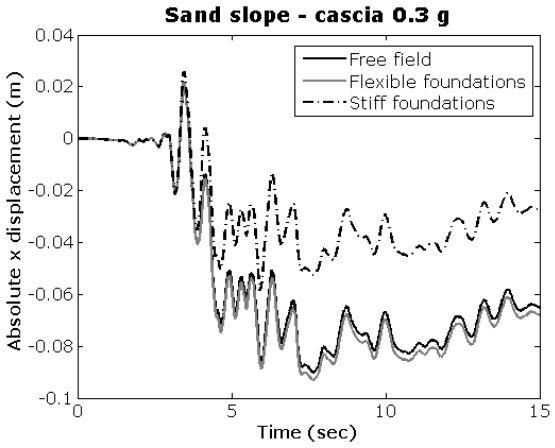
linear type baseline correction were applied to all records using Seismosignal computer software (Seismosoft, Seismosignal 2011). Moreover, due to the compliant base used in the model the appropriate input excitation corresponds to the upward propagating wave train that is taken as one-half of the target outcrop motion (Mejia and Dawson, 2006). Note that the acceleration time histories at the base are integrated to obtain velocities which are then converted into stress histories using Eq. 4.2. The selected input time histories are scaled to four levels of peak ground acceleration, namely PGA=0.3, 0.5, 0.7 and 0.9g. This is done in order to assess the building response for a range of ground differential displacement and to allow the evaluation of fragility curves for different limit damage states.

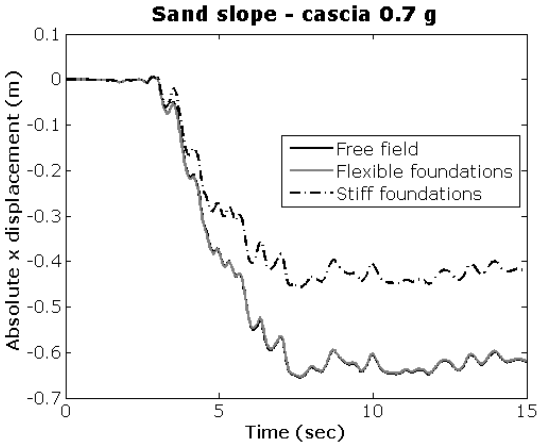
4.3.1.3. Results

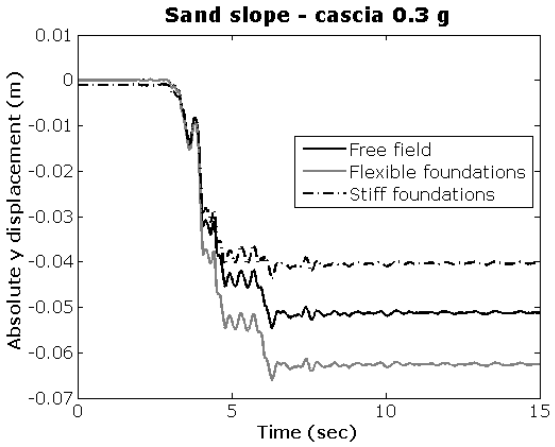
Numerical computations are carried out in large-strain mode to ensure sufficient accuracy considering that large deformations are expected to occur.

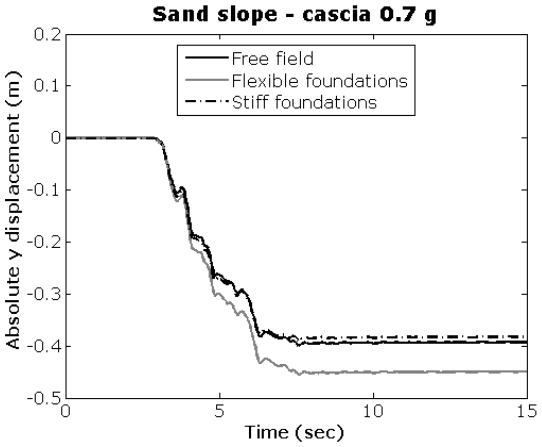
Figures 4.5 and 4.6 present representative graphs of the maximum absolute (point A in Fig. 4.2b) and differential (A-B, Fig. 4.2b) horizontal and vertical permanent displacement time histories at the closest edge of the assumed building from the slope' crest (i.e. 3 m) considering stiff and flexible foundations for the building and at the same location in the absence of any structure (free field conditions). A variety of such graphs is given for both sand and clayey surface slope layers and for two different input motions (cascia, pacoima) scaled at two PGA levels, namely 0.3 g and 0.7 g. Various trends are revealed from these comparative plots. A first general observation is that the presence of a structure next to the slope's crest may contribute in altering the free field response of the slope and the corresponding deformation demand for the building. The level of this differentiation depends primary on the foundation type (flexible, stiff). The building on flexible foundations seems to follow more closely the free field movement both in terms of absolute and differential displacement. On the other hand, when the soil-foundation interaction (building on stiff foundations) is considered, the differential horizontal displacements at the beam foundation are practically zero and the total (vector) differential displacement demand for the building is generally decreased due to the continuity and stiffness of the foundation slab. The displacement patterns are also greatly influenced by the surface soil conditions (sand, clay). As shown in the figures, for the sand slope case the building founded on flexible foundations displays larger absolute and differential displacements compared to the free field conditions and the corresponding building on continuous stiff foundation. On the contrary, for the clayey slope case, while the free field absolute movement is generally reduced, the corresponding differential movement is larger compared to the stiff and flexible foundation conditions. Thus, the presence of the structure's foundation near the crest of the clay slope is found to shift

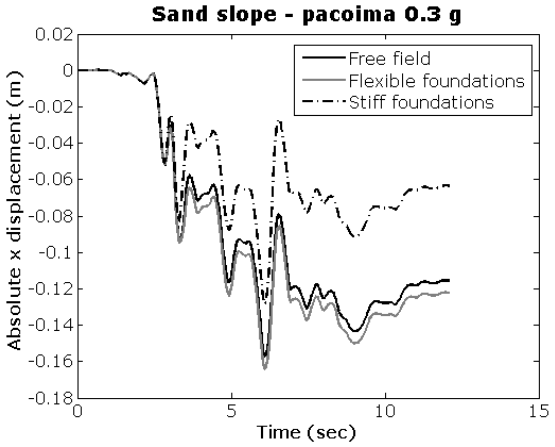
the original free field position of the sliding surface towards the inner part of the slope resulting to more uniform movements and reduced differential deformation potential for the assumed building. The characteristics of the input motion (cascia, pacoima) as well as the level of shaking (0.3g, 0.7g) are also important influential parameters yielding to modified absolute and differential displacement patterns with respect to the free field response. Finally, it's worth noting that the flattening of the displacement versus time curves is representative of zero residual velocities after the action of seismic shaking implying that the a general landslide resulting to the complete failure of the slope has not occurred.

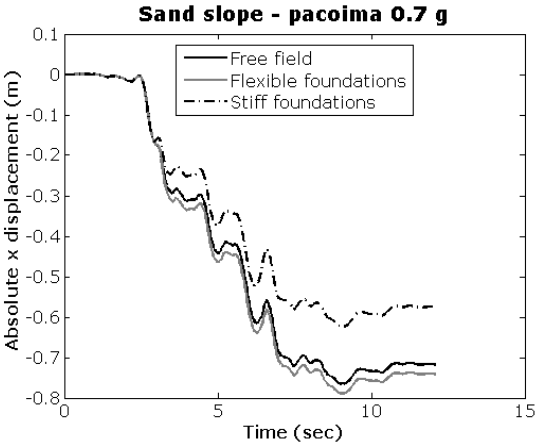


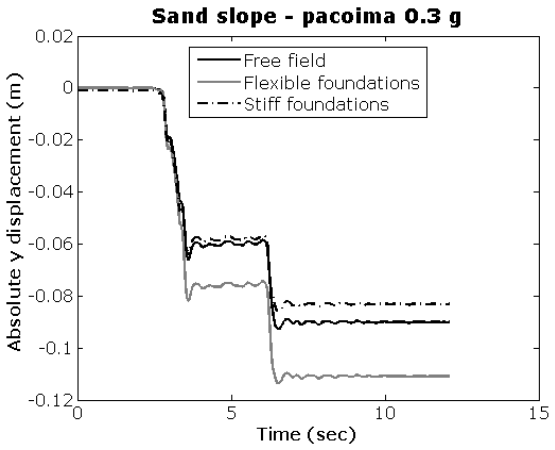


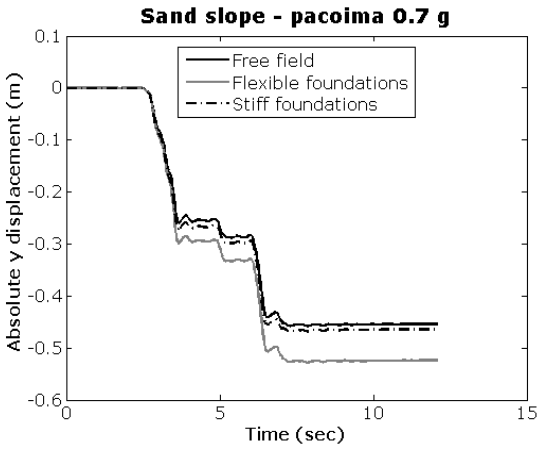


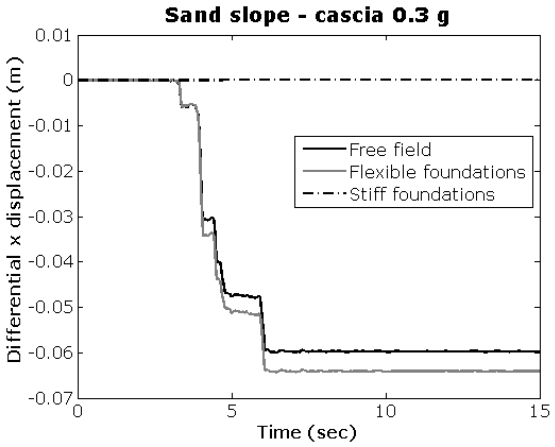


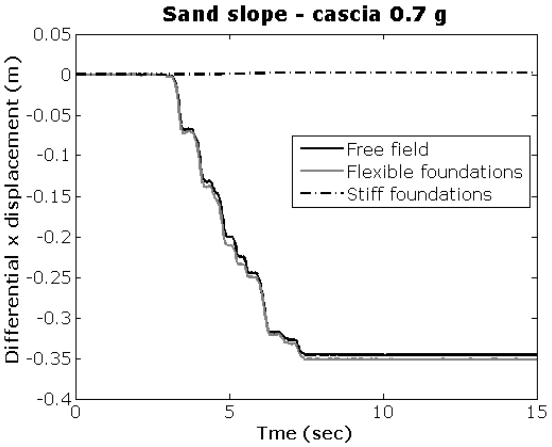


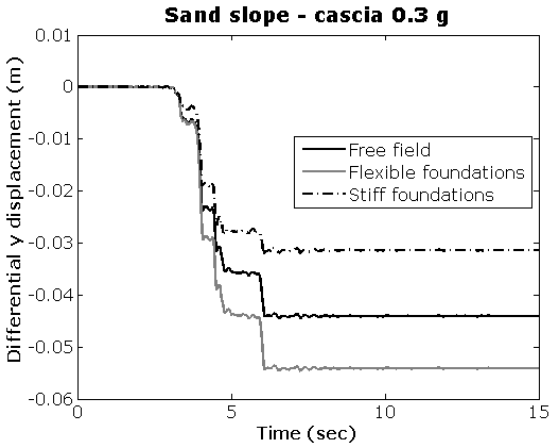


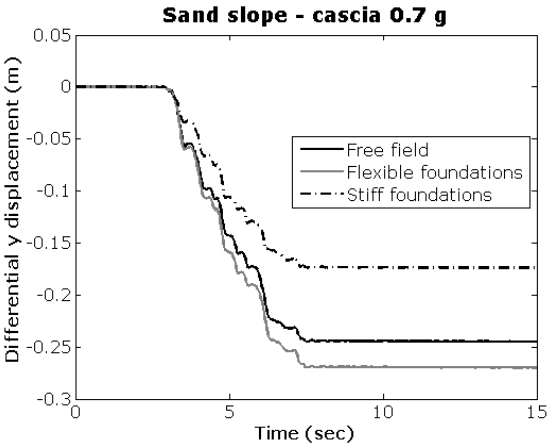

Sand slope - pacoima 0.3 g
Free field
Flexible foundations
Stiff foundations
Absolute y displacement (m)
Time (sec)

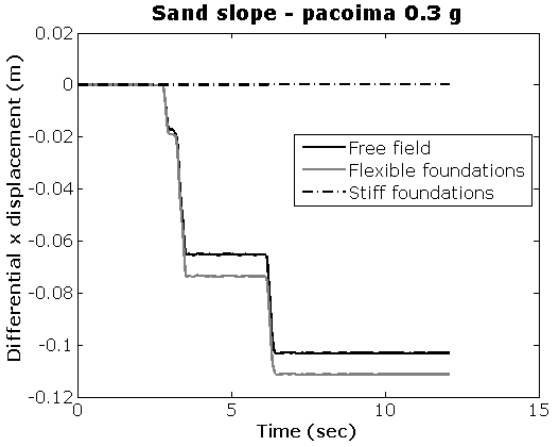

Sand slope - pacoima 0.7 g
Free field
Flexible foundations
Stiff foundations
Absolute y displacement (m)
Time (sec)

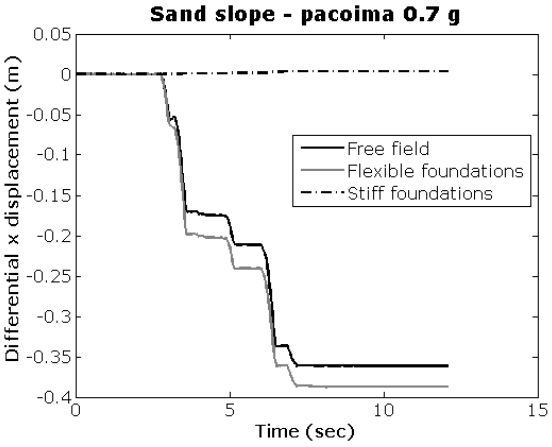

Sand slope - cascia 0.3 g
Free field
Flexible foundations
Stiff foundations
Differential x displacement (m)
Time (sec)


Sand slope - cascia 0.7 g
Free field
Flexible foundations
Stiff foundations
Differential x displacement (m)
Tme (sec)


Sand slope - cascia 0.3 g
Free field
Flexible foundations
Stiff foundations
Differential y displacement (m)
Time (sec)


Sand slope - cascia 0.7 g
Free field
Flexible foundations
Stiff foundations
Differential y displacement (m)
Time (sec)


Sand slope - pacoima 0.3 g
Free field
Flexible foundations
Stiff foundations
Differential x displacement (m)
Time (sec)


Sand slope - pacoima 0.7 g
Free field
Flexible foundations
Stiff foundations
Differential x displacement (m)
Time (sec)

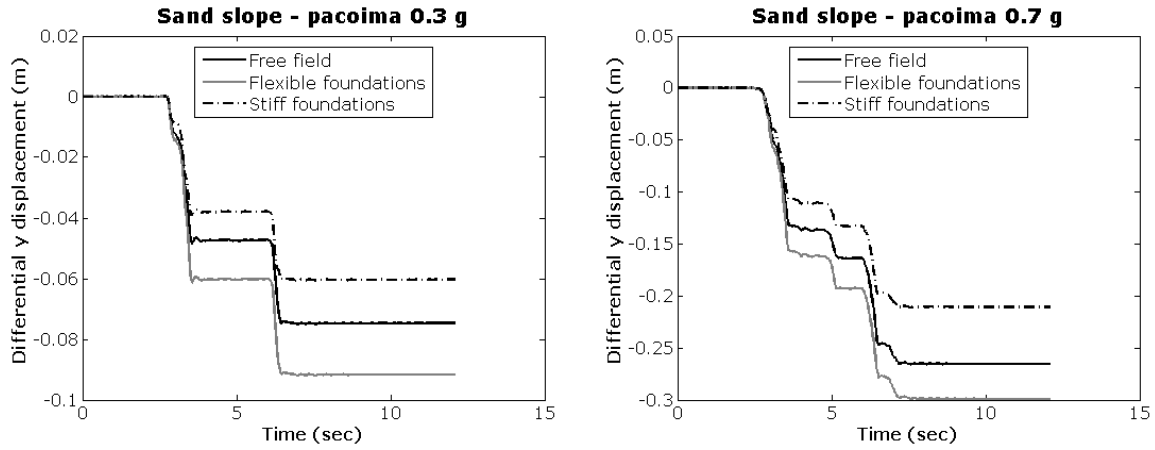
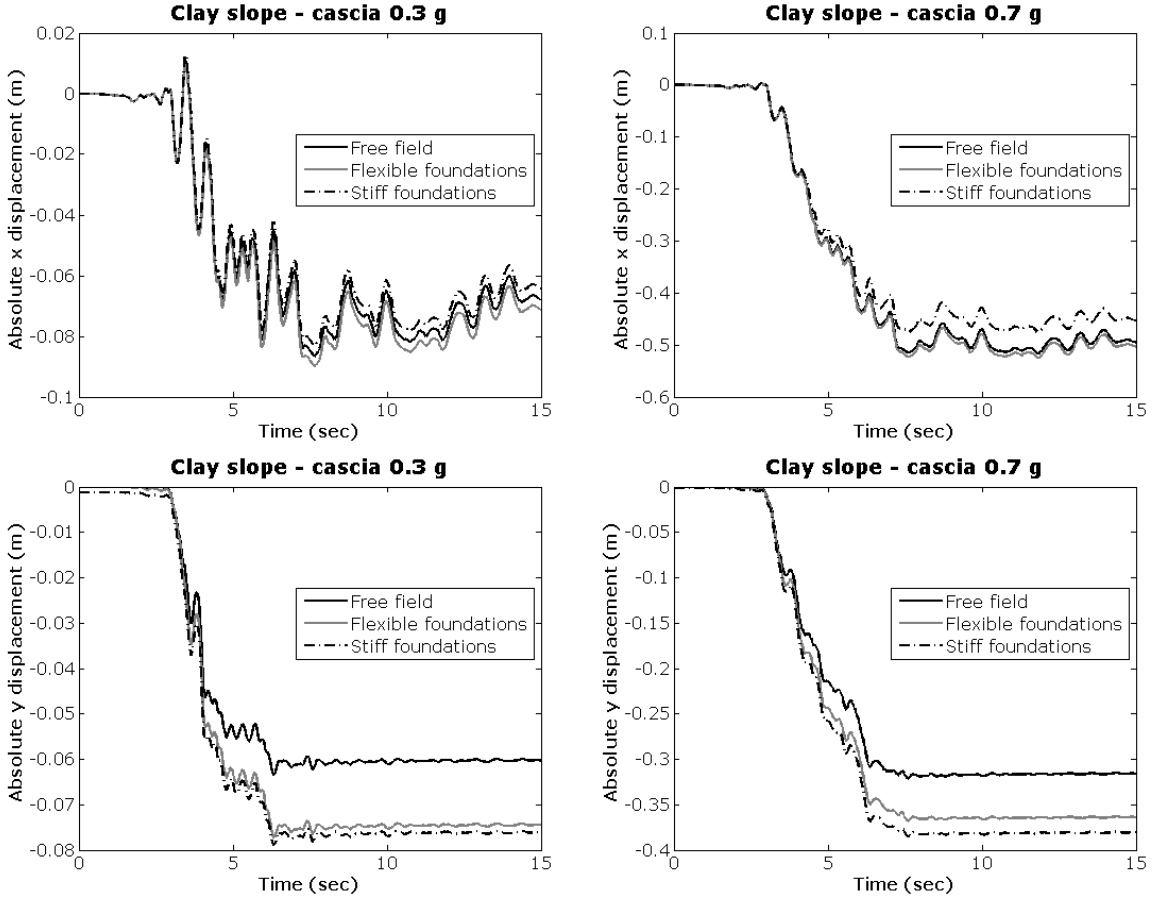
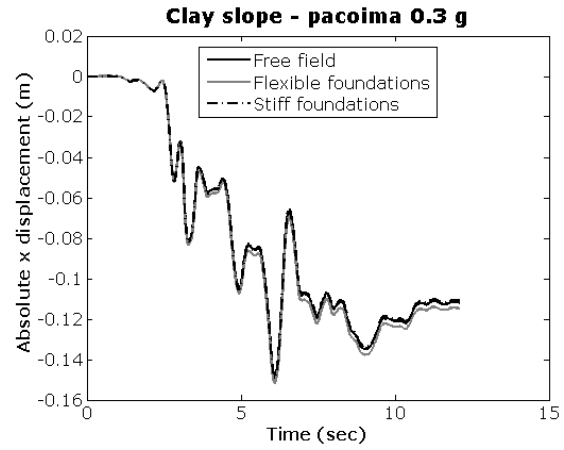
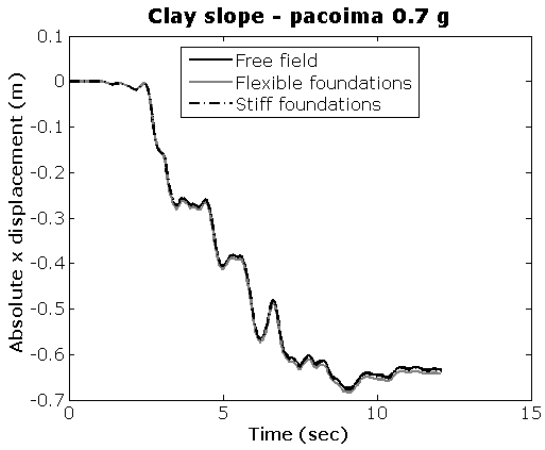
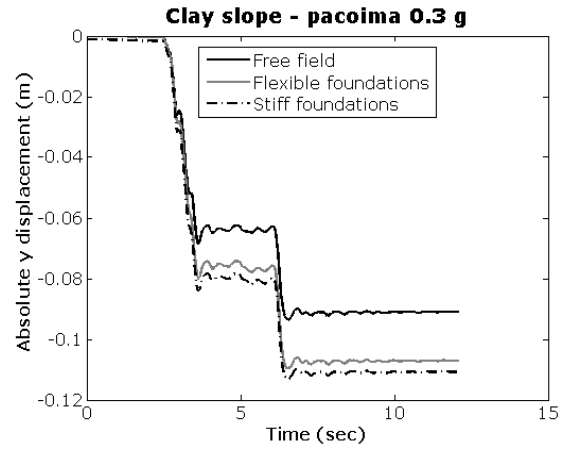


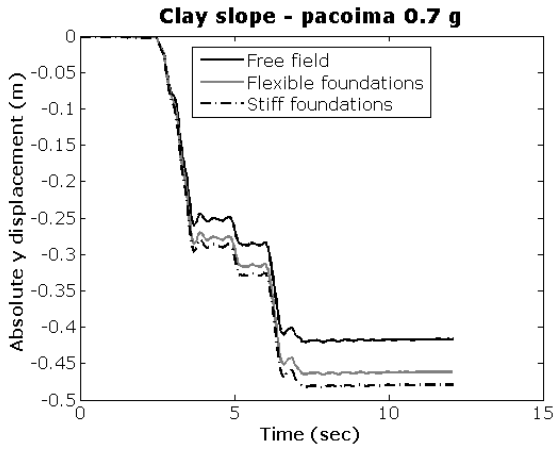
Figure 4.5. Absolute and differential horizontal and vertical displacement time histories at the closest edge of the assumed building from the slope' crest (i.e. 3.0 m) considering stiff and flexible foundations for the building and at the same location in the absence of any structure for two different input motions (cascia, pacoima) scaled at two PGA levels (0.3, 0.7 g) (sand slope).

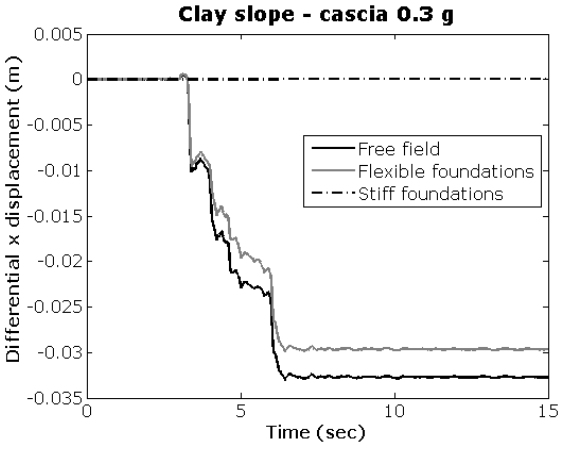


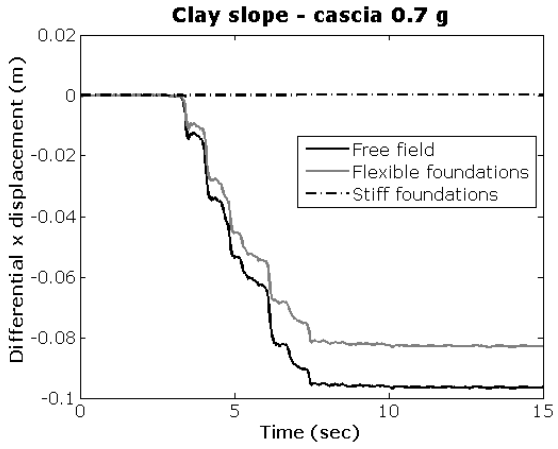

Clay slope - pacoima 0.3 g
Free field
Flexible foundations
Stiff foundations
Absolute x displacement (m)
Time (sec)

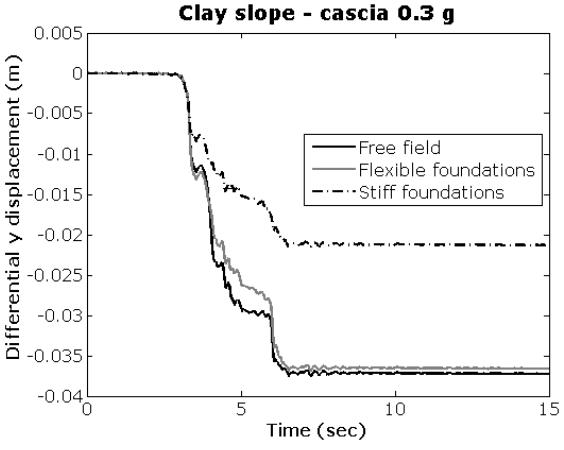

Clay slope - pacoima 0.7 g
Free field
Flexible foundations
Stiff foundations
Absolute x displacement (m)
Time (sec)

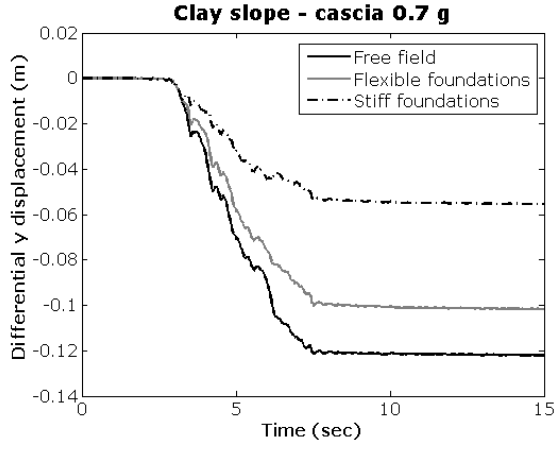

Clay slope - pacoima 0.3 g
Free field
Flexible foundations
Stiff foundations
Absolute y displacement (m)
Time (sec)


Clay slope - pacoima 0.7 g
Free field
Flexible foundations
Stiff foundations
Absolute y displacement (m)
Time (sec)


Clay slope - cascia 0.3 g
Free field
Flexible foundations
Stiff foundations
Differential x displacement (m)
Time (sec)


Clay slope - cascia 0.7 g
Free field
Flexible foundations
Stiff foundations
Differential x displacement (m)
Time (sec)


Clay slope - cascia 0.3 g
Free field
Flexible foundations
Stiff foundations
Differential y displacement (m)
Time (sec)


Clay slope - cascia 0.7 g
Free field
Flexible foundations
Stiff foundations
Differential y displacement (m)
Time (sec)

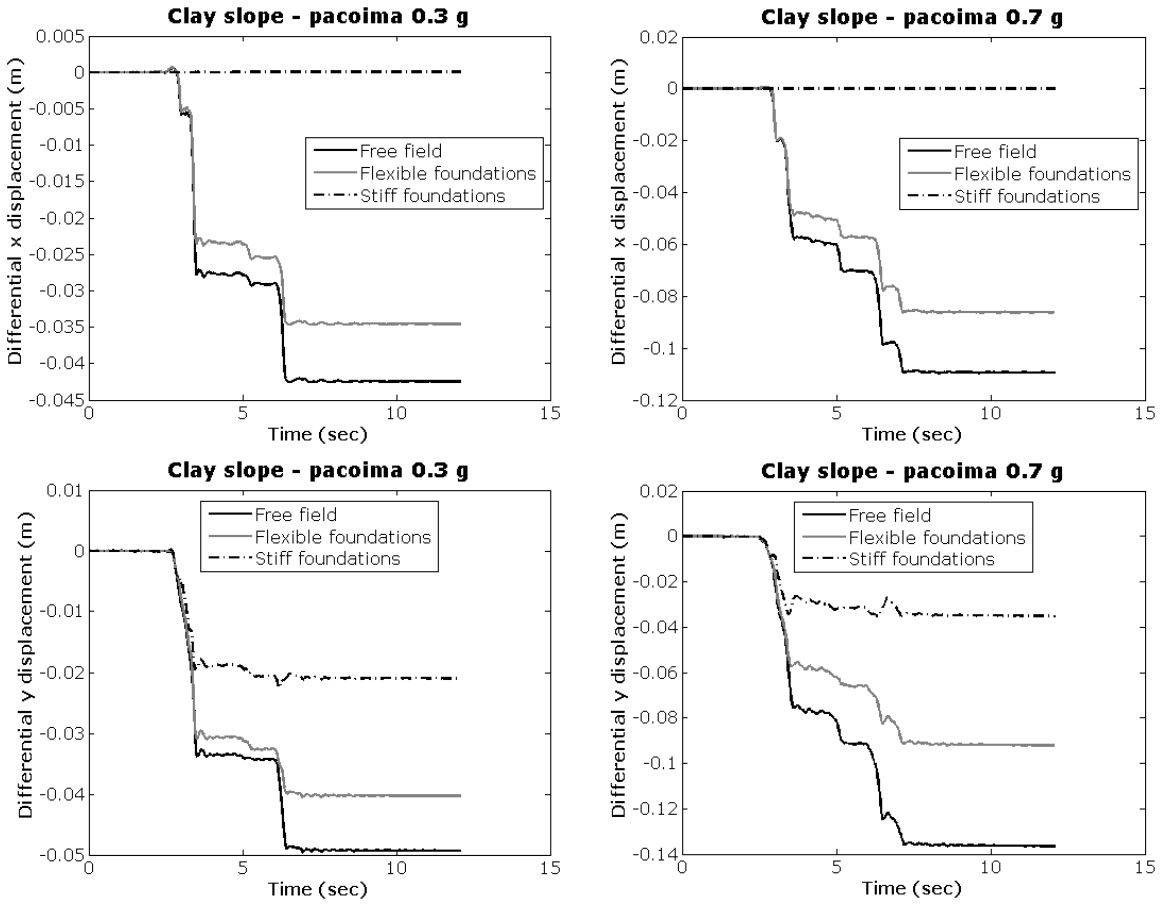


Figure 4.6. Absolute and differential horizontal and vertical displacement time histories at the closest edge of the assumed building from the slope' crest (i.e. 3.0 m) considering stiff and flexible foundations for the building and at the same location in the absence of any structure for two different input motions (cascia, pacoima) scaled at two PGA levels (0.3, 0.7 g) (clay slope).

Figures 4.7 and 4.8 present the maximum computed values of permanent ground displacement at the slope area in relation to the corresponding differential displacements at the foundation level for the different foundation configurations and soil types. A strong, linear correlation between the two variables is detected in all cases. Thus, differential deformation can be easily determined by the residual maximum slope displacement using an appropriate linear expression. While the maximum calculated slope displacements are found to be of the same order of magnitude for both sand and clay slopes, the resulting differential displacement for the building is strongly reduced for slopes consisting of cohesive soil material, implying that in that case the building is primarily expected to move uniformly as a rigid body rather than to distort differentially.

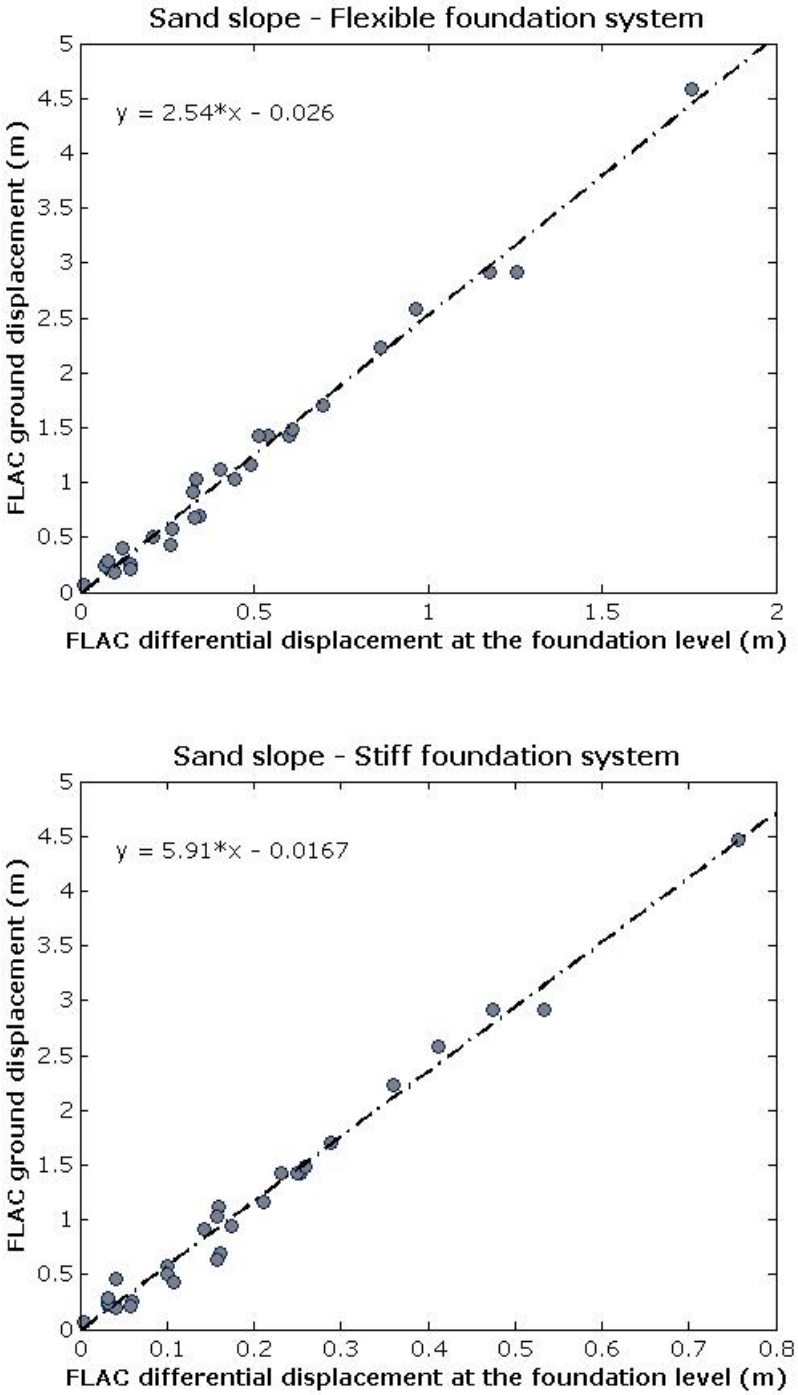


Figure 4.7. Regression of differential displacement vector for buildings with flexible (top) and stiff (bottom) foundation system on the maximum computed permanent ground displacement (sand slope).

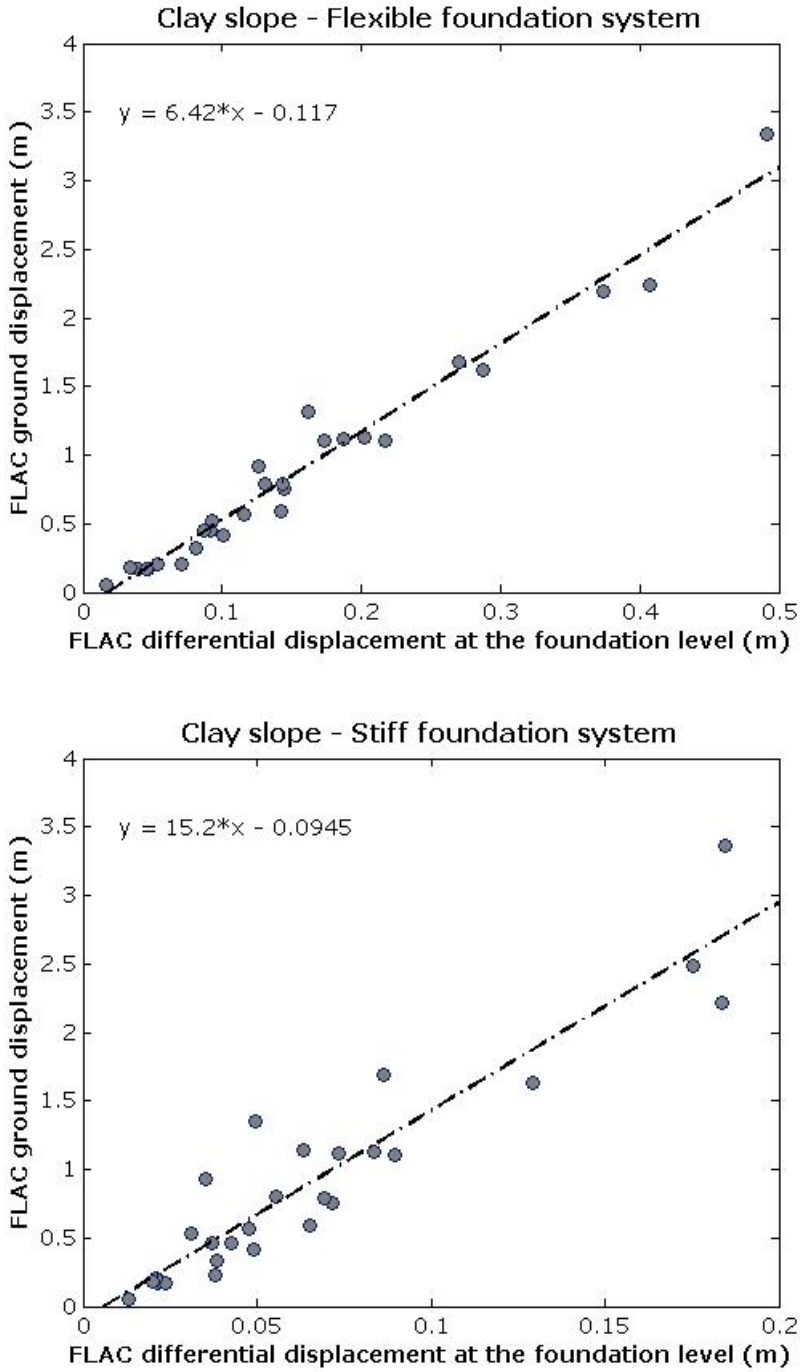


Figure 4.8. Regression of differential displacement vector for buildings with flexible (top) and stiff (bottom) foundation system on the maximum computed permanent ground displacement (clay slope).

Figures 4.9 and 4.10 depict the maximum values of differential displacements for the building with flexible and stiff foundation system founded on sand and clay soil respectively. It is observed that the specific characteristics (frequency content and duration) of the seismic ground motions can significantly affect the magnitude of the computed differential displacement at the foundation level. In particular, for all analyzed

cases, the maximum and minimum differential displacements are estimated when applying the sturno and gilroy time histories respectively.

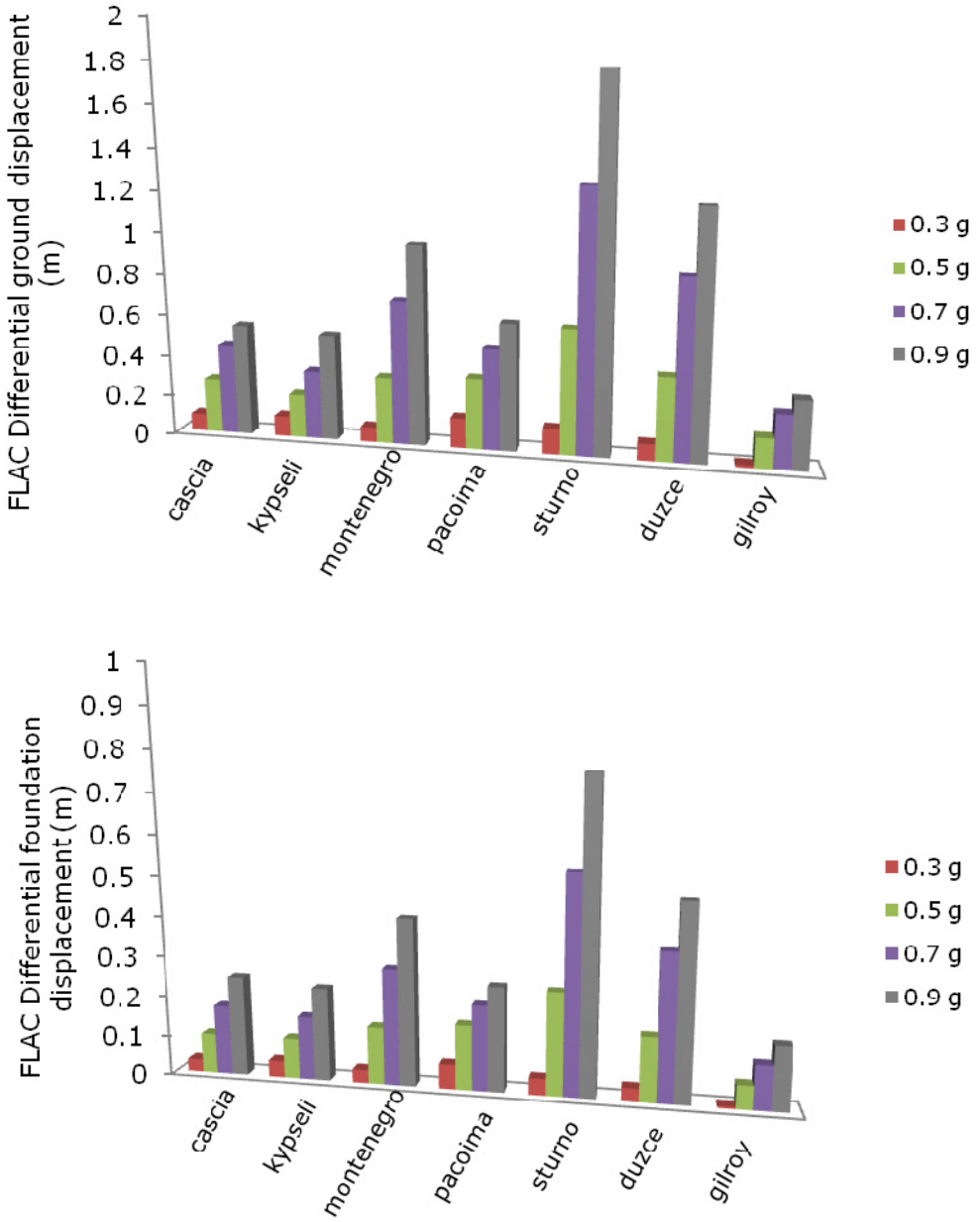


Figure 4.9. Maximum values of differential displacement vector for buildings with flexible (top) and stiff (bottom) foundation system (sand slope).

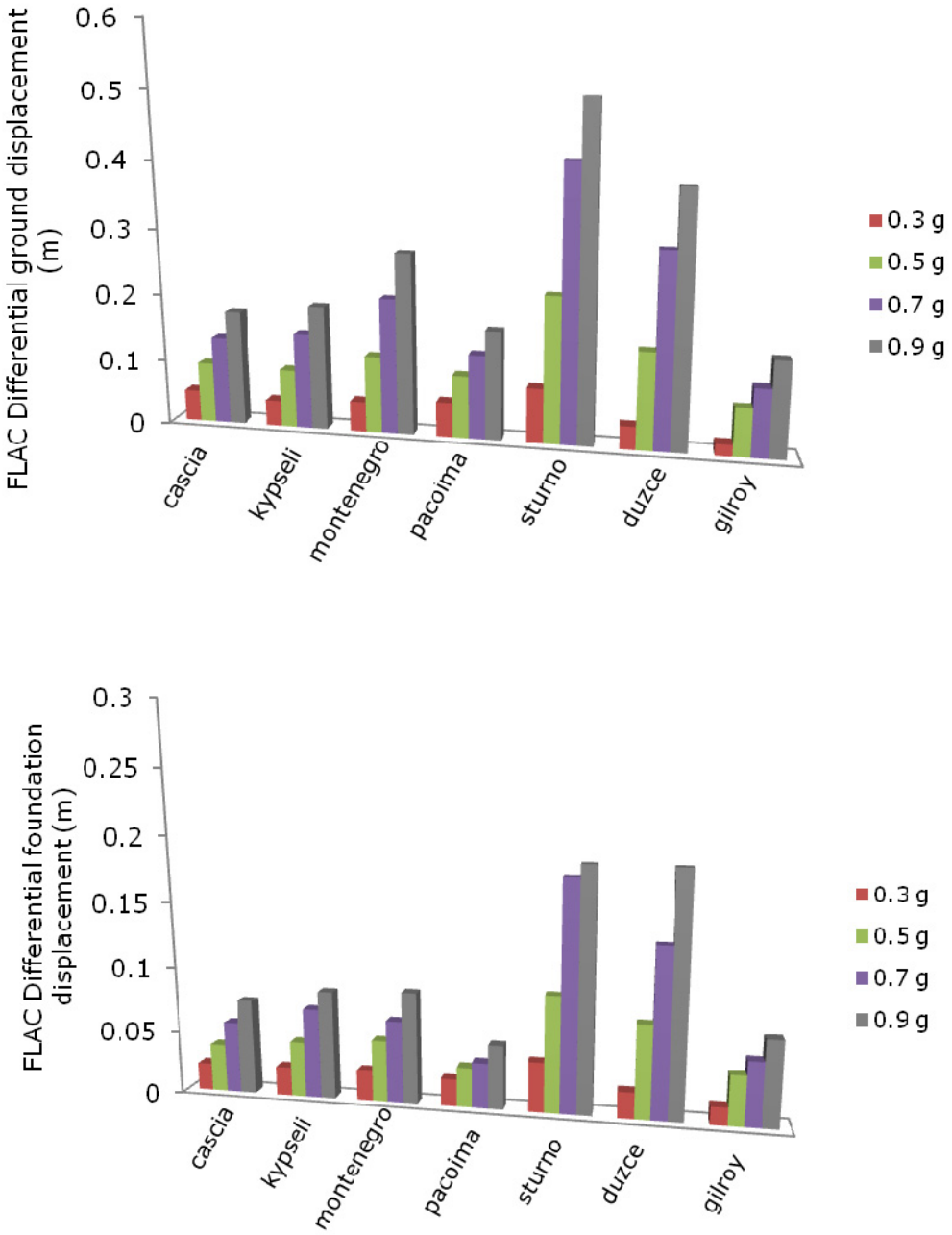


Figure 4.10. Maximum values of differential displacement vector for buildings with flexible (top) and stiff (bottom) foundation system (clay slope).

4.3.2 Non linear static analysis of the RC structures

The analysis of the building is conducted using the finite element code SeismoStruct (Seismosoft, SeismoStruct 2011), which is capable of calculating the large displacements of space frames under static or dynamic loading, taking into account geometric nonlinearities and material inelasticity. The code is widely and successfully used in structural earthquake engineering. Both local (beam-column effect) and global (large displacements/rotations effects) sources of geometric nonlinearity are automatically taken into account. Distributed elements are used based on the so-called "fibre approach" to represent the cross-section inelastic behaviour, where each fibre is associated with a uni-axial stress-strain relationship (see Fig. 4.11). The sectional stress-strain state of beam-column elements is then obtained through the numerical integration of the nonlinear uni-axial stress-strain response of the individual fibres (typically 300-400) in which the section has been subdivided. In displacement-based (DB) finite element formulation using nonlinear models, structural elements should be subdivided into a number of segments (typically 4 to 5) and the delimiting sections follow the Navier-Bernoulli approximation (plane sections remain plane). In the present analysis, the frame sections have been discretized into 300 fibres and the structural members, into 4 elements. Nonlinear static time-history analyses are performed for all numerical simulations. The differential permanent displacement curves, directly extracted from the FLAC dynamic analysis, are statically imposed at one of the RC frame supports (see Fig. 4.12).

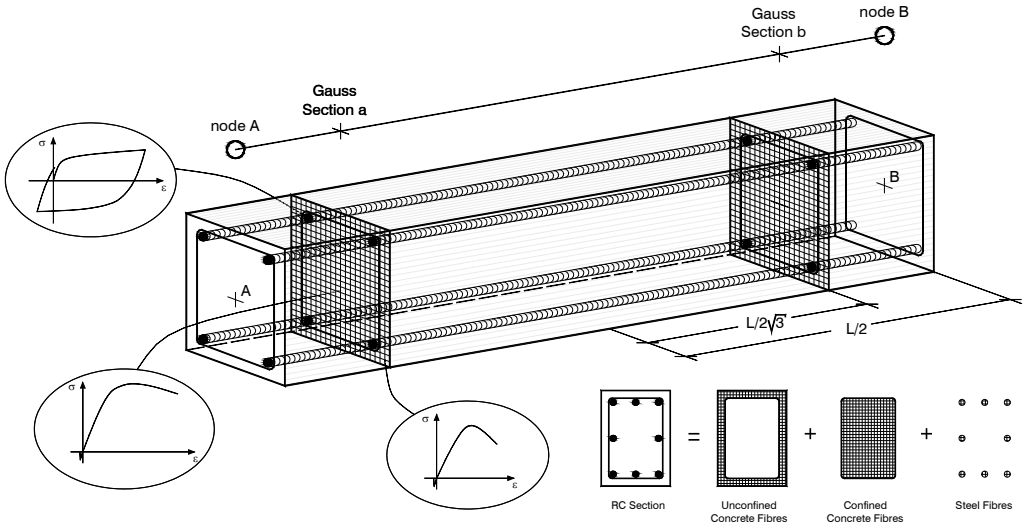


Figure 4.11. Discretisation in fibre modelling of a typical reinforced concrete cross-section (Seismosoft, Seismostruct 2011)

The herein studied buildings are single bay-single storey RC bare frame structures with two foundation types: flexible foundation system (isolated footings) and stiff but not

completely rigid foundation system (continuous uniformly loaded foundation of finite stiffness characteristics) (Fig. 4.12). The beneficial contribution of masonry infill walls to the building capacity is not considered in this study. The building's height and length are 3.0 m and 6.0 m respectively. All columns and beams have rectangular cross sections (beam: 0.30x 0.50 m, column: 0.40x 0.40m). The structures have been designed according to the provisions of the Greek Seismic Code (EAK, 2000), for a design acceleration A_d = 0.36 g, and a behavior factor q = 3.5. The adopted dead and live loads (g = 1.3 kN/m^2 and q = 2 kN/m^2) are typical values for residential buildings. The longitudinal section reinforcement degree used is 1% for the columns and 0.75% for the beams.

The use of single bay-single storey structures is justified from the observation that the number of storeys and bays do not seem to comprise crucial parameters in the determination of the building's performance subjected to permanent ground displacements. The latter is also discussed in Bird et al. (2005) and Negulescu and Foerster (2010) for the vulnerability assessment of RC buildings due to differential settlements. Hence, one bay-one storey RC structures despite their simplicity are found to be adequately representative of the performance of real low-rise RC frame buildings.

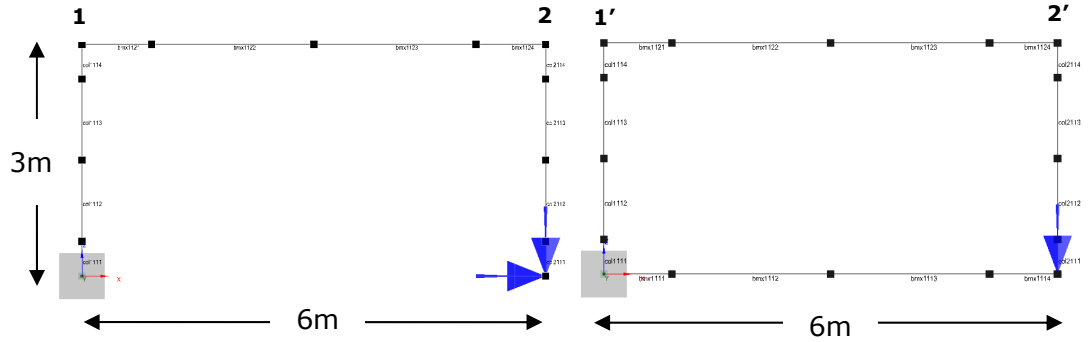


Figure 4.12. Single bay-single storey RC frame buildings with flexible (a) and stiff (b) foundation system and displacement loading pattern considered for the non-linear quasi-static analysis

The material properties assumed for the structural members of the reference RC buildings are described below. A uni-axial nonlinear constant confinement model (Fig. 13a) is used for the concrete material (f_c=20MPa, f_t=2.1MPa, strain at peak stress 0.002mm/mm, confinement factor =1 for unconfined and 1.2 for confined concrete, specific weight=24KN/m^3), assuming a constant confining pressure throughout the entire stress-strain range (Mander et al., 1988). For the reinforcement, a uni-axial bilinear stress-strain model with kinematic strain hardening (Fig. 13b) is utilized (f_y=400MPa, E=200GPa, strain hardening parameter μ =0.005, specific weight=78KN/m^3). This model

is characterized by easily identifiable calibrating parameters and by its computational efficiency. Note that only nonlinear models are suitable for the analysis since cracking and irreversible deformation is expected to govern the behavior of the RC structural members.

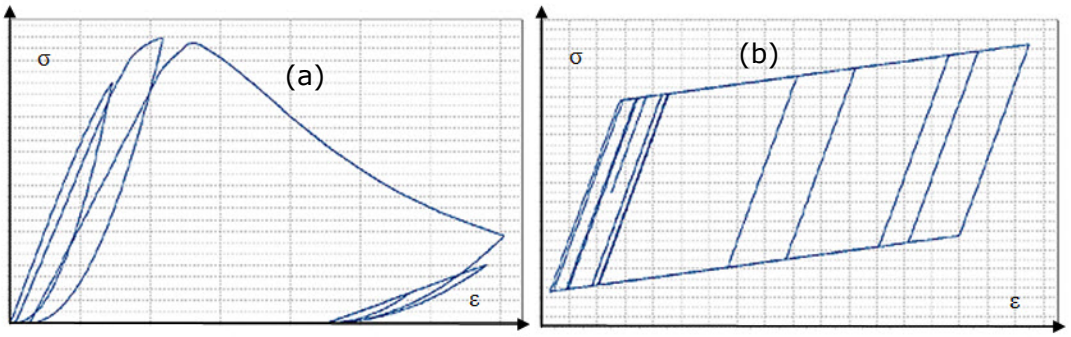


Figure 4.13. Stress-strain models for concrete (a) and steel (b) material

A sensitivity analysis is performed for the reference building cases, which allows for indentifying the influence of different parameters on the structural response and to develop a probabilistic framework for the damage estimation. The parameters selected to vary are the following: yield strength of steel (f_y=210, 400, 500 MPa), compressive (f_c=16, 20, 30 MPa) and tensile (f_t=2.0, 2.1, 3.0 MPa) strength of concrete, reinforcement ratio (ρ=0.8%, 1%, 1.2% for columns and ρ=0.55%, 0.75%, 0.95% for beams) and confinement factor (1.0, 1.2, 1.3). The analyses are conducted for progressively increasing levels of differential displacements provided by the computed dynamic stress strain analysis for increasing amplitudes of input acceleration time histories. For each analysis, the peak response of the structures in terms of maximum strain is recorded. The yield strength of steel material is proved to be the most influential factor for both buildings with stiff and flexible foundations resulting to an average variation on the results of 25% for the stiff and 20% for the flexible foundations.

The deformed shapes of buildings with flexible foundation system are essentially the same irrespective of the variability in the strength parameters and the level of the displacement demand in terms of imposed differential ground/foundation deformations, observation that is in accordance with Bird et al. (2005). The same trend is observed for the buildings with stiff foundation (Fig. 4.14). In both building typologies, a column failure mechanism is detected. The reason is that the axial stiffness of the beams is generally much higher compared to the flexural stiffness of the columns. Moreover, in the case of buildings with flexible foundations, the applied differential displacement vector is mainly governed by the horizontal component that governs the deformation mode (Fig. 4.14a). On the contrary, in buildings with stiff foundation system the applied

displacements are practically vertical (Fig. 4.14b). Thus, the inclination of the applied differential permanent displacement constitutes a fundamental parameter in determining the deformed shape of the building when subjected to a permanent displacement at the foundation level.

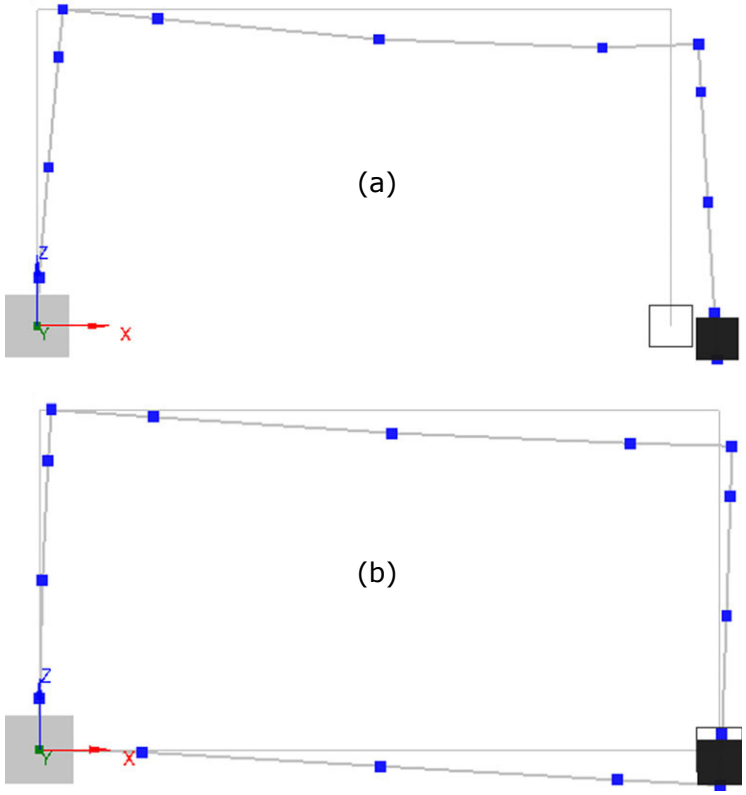


Figure 4.14. Deformed shapes for buildings with flexible (b) and stiff (b) foundations

4.4 Fragility functions

Analytical fragility curves are derived for low-rise (single bay- single storey) RC buildings with varying stiffness of the foundation system founded in the vicinity of a slope consisting of two different soil materials: a typical sand and a typical clay. Different methodologies are applied to estimate the parameters of fragility functions, namely the regression analysis method (e.g. Nielson and DesRoches, 2007; Argyroudis and Pitilakis, 2012) and the maximum likelihood method (e.g. Shinozuka et al., 2000), to investigate the influence of epistemic uncertainties (stem from lack of knowledge) on the fragility estimates. The landslide intensity is expressed in terms of peak horizontal ground acceleration (PGA) at the seismic bedrock that is the initial triggering force of the slow moving slide or alternatively in terms of permanent ground displacement (PGD) at the slope area (i.e. a product of PGA). The latter one is generally better correlated to

structural damage and allows for direct comparisons to non-earthquake related landslide damages to buildings. It is worth noting that the final deformation demand for the building will be the permanent differential displacements at the foundation level, irrespective of the intensity measure used in the fragility analysis.

4.4.1 Definition of limit states

The definition of limit states constitutes an important step in the construction of the fragility curves. The definition and selection of realistic limit damage states are of paramount importance since these values have a direct effect on the evaluation of the fragility curve parameters. In this study, a local damage index (DI) describing the steel and concrete material strains is introduced to identify the building performance in terms of damages and to construct the corresponding fragility curves. Within the context of a fibre-based modelling approach, as implemented in SeismoStruct, material strains usually constitute the best parameter for identifying the performance state of a given structure (Seismosoft, SeismoStruct 2011). In all cases analyzed, the steel strain (ε_s) yields more critical results. Thus, it was decided to adopt only this parameter as a damage index. In this way, it is possible to establish a relationship between the damage index (ε_s) and the landslide intensity defined in terms of PGA at the seismic bedrock or PGD at the slope area, for different building typologies and consequently to assign a median value of PGA or PGD to each limit state.

The next step is the definition of the limit states. Based on the work of Crowley et al. (2004), Bird et al. (2005; 2006), Negulescu and Foerster (2010) and proper engineering judgment, 4 limit states (LS_1, LS_2, LS_3, LS_4) are defined. Considering that low code RC buildings are poorly constructed structures characterized by a low level of confinement, the limit steel strains needed to exceed post yield limit states should have lower values compared to high code properly constructed buildings. As a consequence, it was decided to adopt different limit state values to derive exceedance of extensive and complete damage for low and high code frame RC buildings. A qualitative description of each damage state for reinforced concrete frames is given in Table 4.5, while the limit state values finally adopted are presented in Table 4.6. They describe the exceedance of minor, moderate, extensive and complete damage of the RC building. The first limit state is specified as steel bar yielding that is the ratio between yield strength and modulus of elasticity of the steel material. For the rest, mean values of post-yield limit strains for steel reinforcement and concrete material (for completeness) are suggested, as shown in Table 4.6.

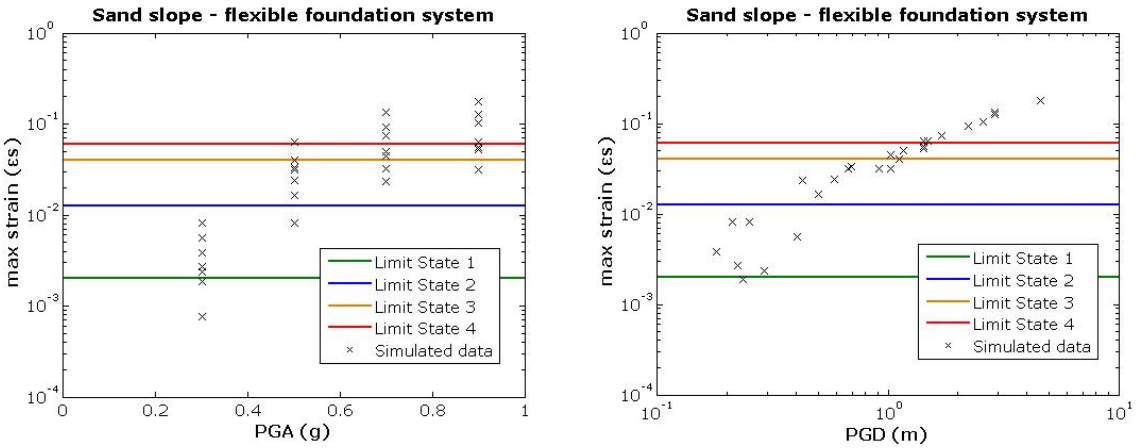
Table 4.5. Structural damage state descriptions for RC frame buildings (Crowley et al. 2004)

Structural damage band	Description
None to slight	Linear elastic response, flexural or shear type hairline cracks (<1.0 mm) in some members, no yielding in any critical section
Moderate	Member flexural strengths achieved, limited ductility developed, crack widths reach 1.0 mm, initiation of concrete spalling
Extensive	Significant repair required to building, wide flexural or shear cracks, buckling of longitudinal reinforcement may occur
Complete	Repair of building not feasible either physically or economically, demolition after earthquake required, could be due to shear failure of vertical elements or excessive displacement

Table 4.6. Definition of limit states for "low" and "high" code design RC buildings

Limit state	Limit strains –low code		Limit strains –high code	
	Steel strain (ε_s)	Concrete strain (ε_c)	Steel strain (ε_s)	Concrete strain (ε_c)
Limit State 1	Steel bar yielding	-	Steel bar yielding	-
Limit State 2	0.0125	0.0045	0.0125	0.005
Limit State 3	0.025	0.006	0.04	0.010
Limit State 4	0.045	-	0.06	-

Figures 4.15 and 4.16 present representative plots of damage evolution expressed in terms of maximum strain as a function of PGA and PGD for low-rise, "high code" designed RC frame buildings with stiff and flexible foundation system resting close to the crest of the sand and clay slopes respectively. The corresponding threshold values of steel strain for each limit state are also shown.



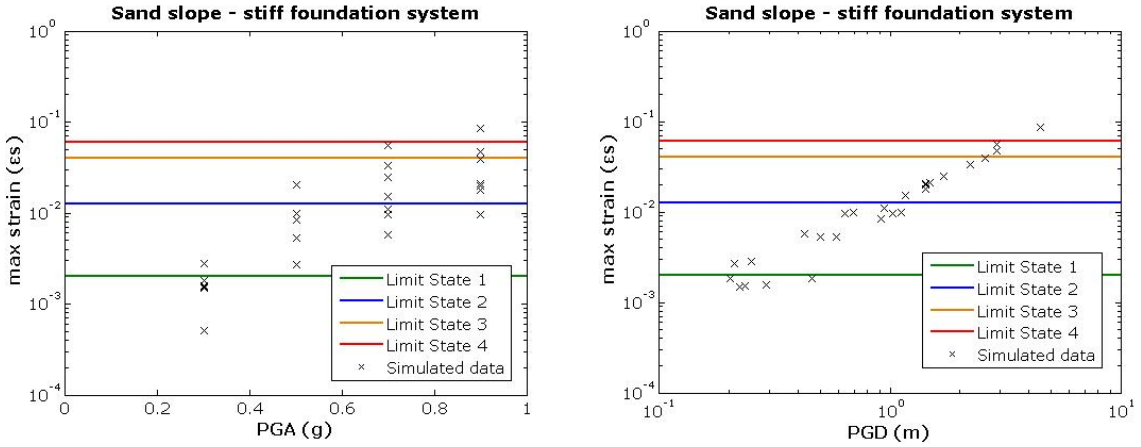


Figure 4.15. Maximum recorded strain as a function of PGA (left) and PGD (right) for 1bay-1story RC frame buildings with stiff and flexible foundation system on top of a sand slope

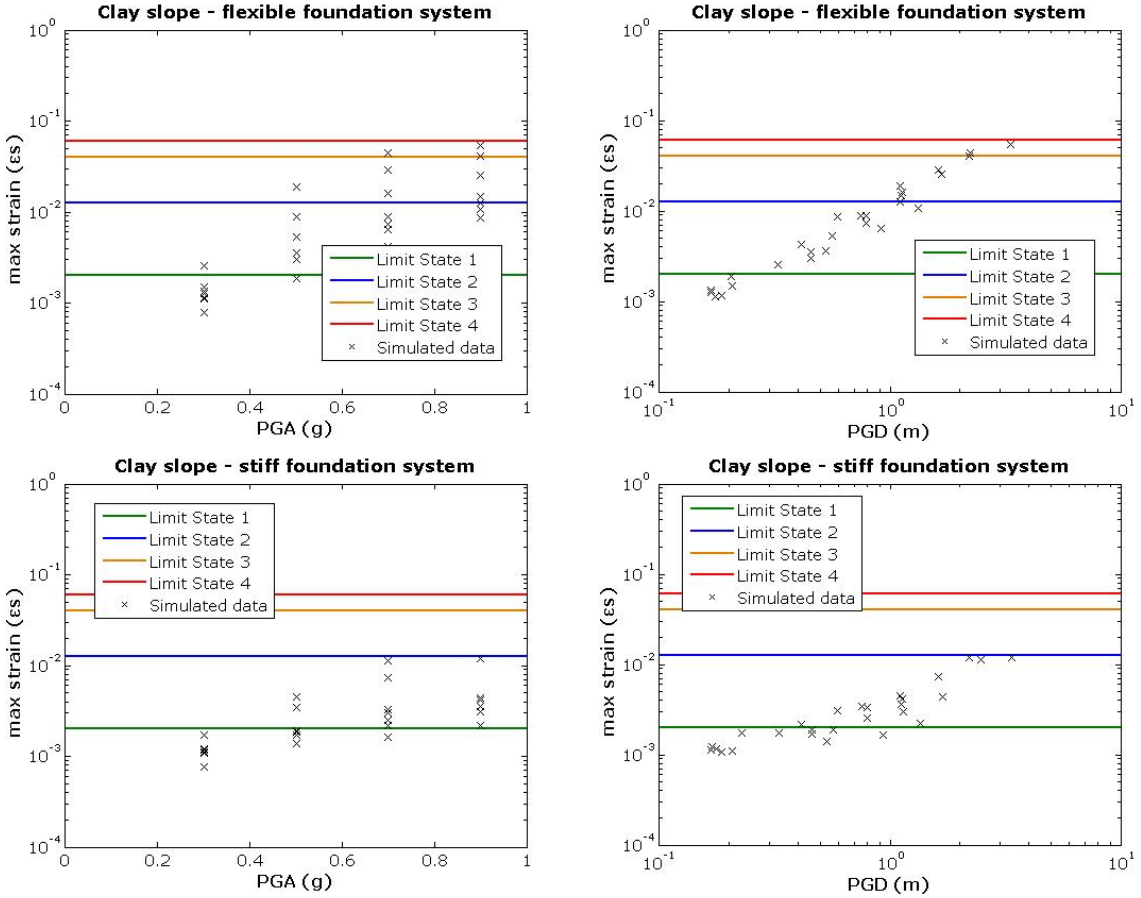


Figure 4.16. Maximum recorded strain as a function of PGA (left) and PGD (right) for 1bay-1story RC frame buildings with stiff and flexible foundation system on top of a clay slope

4.4.2 Construction of the fragility curves

To construct the fragility relationships, appropriate cumulative distribution functions have been generated, in line to previous studies (e.g. Shinozuka et al. 2000; NIBS, 2004; Pinto, 2007; Nielson and DesRoches, 2007; Koutsourelakis, 2010; Argyroudis and Pitilakis, 2012 etc.). The probability of exceeding a given limit state LS_i, of the structural damage, for a given intensity measure (IM) is mathematically expressed as a two-parameter cumulative lognormal distribution function:

$$F(IM) = \Phi\left[\frac{1}{\beta_i} In\left(\frac{IM}{\overline{IM_i}}\right)\right] \quad (4.3)$$

Where:

IM is the intensity measure in terms of PGA at the outcrop or PGD at the slope area

Φ[·] is the standard normal cumulative distribution function,

$\overline{IM_i}$ is the median value of PGA or PGD at which the building reaches the limit state, i,

β_i is the standard deviation of the natural logarithm of PGA or PGD for limit state, i.

The median values of peak ground acceleration or permanent ground displacement that correspond to each limit state can be defined as the values that corresponds to the 50% probability of exceeding each limit state. The standard deviation values (β) describe the total variability associated with each fragility curve. The most commonly analyzed uncertainty sources are associated to the structure‘s capacity and demand and the definition of damage limit states (e.g. NIBS, 2004; Pinto, 2007). A common β value is usually adopted for all limit states, assuring the coherence in probability for the different damage limit states (e.g. Shinozuka et al., 2003).

Two different procedures are applied herein to estimate the fragility parameters (median and log-standard deviation) given the simulated damage data. The first one, is based on a regression analysis method (e.g. Nielson and DesRoches, 2007; Argyroudis and Pitilakis, 2012) whereas the second is based on a purely statistical approach, i.e. the maximum likelihood method.

4.4.2.1. Regression analysis method

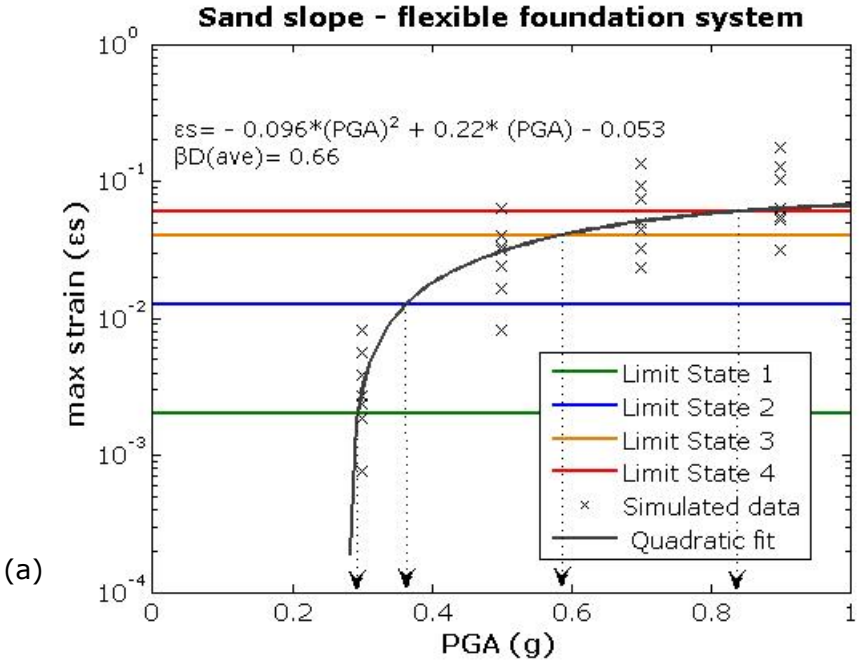
The method is basically based on the establishment of an analytical relationship between the calculated damage index in terms of maximum steel strain (demand on the structure) and the landslide intensity parameter (PGA or PGD) to assign median $\overline{IM_i}$ for

each limit state. This relationship describes the evolution of damage for an increasing level of seismic intensity.

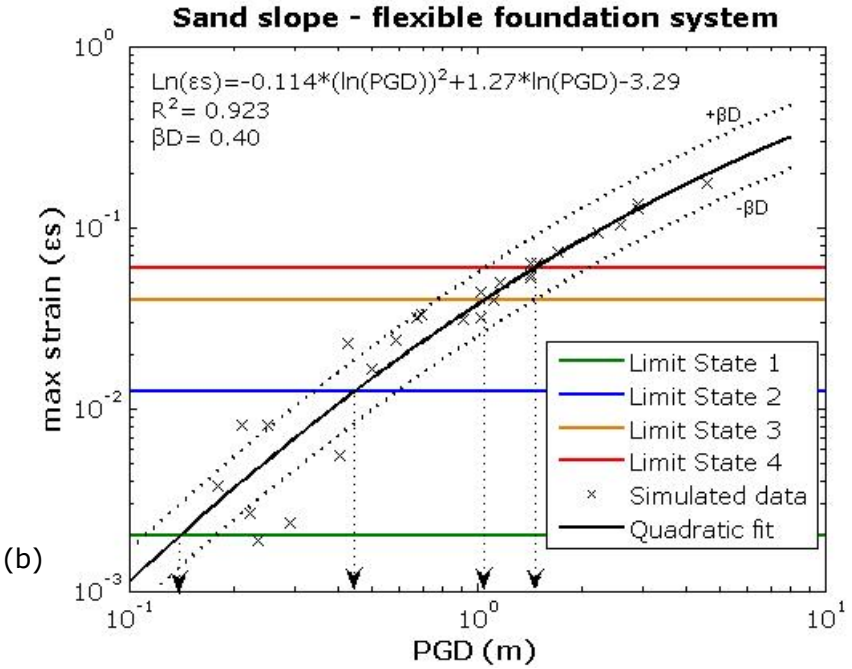
According to HAZUS (NIBS, 2004) three primary sources contribute to the total variability for any given limit state, namely the variability associated with the definition of the limit state value, the capacity of each structural type and the demand (seismic demand, landslide type, relative position of the structure to the landslide). The uncertainty in the definition of limit states (β_{LS}), for all building types and limit states, is assumed to be equal to 0.4 while the variability of the capacity (β_C) is assumed to be 0.3 for "low code" and 0.25 for "high code" buildings (NIBS, 2004). The third source of uncertainty associated with the demand (β_D), is taken into consideration by calculating the variability in the results of the numerical simulation (in terms of maximum steel strain). It should be mentioned that this variability is different for the different intensity measures considered. Assuming that these three component dispersions are statistically independent, the total uncertainty (β) is estimated as the root of the sum of the squares of the component dispersions (NIBS, 2004).

A slightly different procedure is used to assess the fragility parameters when using PGA and PGD as measures of the landslide intensity, following the work of Kwon and Elnashai (2007). In the former case, a lognormal probabilistic distribution of the damage index is assumed for the different applied input motions at each intensity level (0.3, 0.5, 0.7, 0.9g). The log-standard deviation associated with the demand β_D is estimated as the average dispersion of the damage index for the different applied input motions at each PGA level. The median values of PGA for the predefined limit states are estimated through an applied non-linear regression fit (see Fig. 4.17a). In the latter case, a quadratic relationship between the PGD and the steel strain (in the log-log space) is established and the median PGD values for each limit state are assigned based on the non-linear regression analysis and the specified limit states. The log-standard deviation on the demand β_D (corresponding to confidence interval 68%) is estimated from the dispersion of the simulated data around the estimated median curve (see Fig. 4.17b).

Figure 4.17 presents representative plots of PGA- $\ln(\varepsilon_s)$ and ln(PGD)- $\ln(\varepsilon_s)$ analytical relationships for the building with flexible foundation system resting close to the crest of the sand slope. The process of obtaining the median PGA and PGD values for each limit state is also shown.



(a)



(b)

Figure 4.17. PGA- ln(ε_s) (a) and ln(PGD)- ln(ε_s) (b) relationships for the building with flexible foundation system resting close to the crest of the sand slope.

The median and β values of each limit state for buildings with flexible and stiff foundation system located near the crest of the sand and clay slope are given in Tables 4.7 and 4.8 for IM in terms of PGA at the outcrop and PGD at the slope area respectively.

It is noted that some extrapolation of the median regression curve beyond the limits of the data set was performed to allow for the derivation of median PGA and PGD values for all limit states. For certain analysis cases (e.g. clay slope- stiff foundation system),

however, median values of LS_3 and LS_4 are not provided. This is due to the fact that the simulated maximum strains in that cases are much lower compared to the corresponding predefined limit state values and thus further extrapolation to higher PGA/PGD levels would possibly lead to unrealistic predictions of the median PGA and PGD values of LS_3 and LS_4.

Figures 4.18 to 4.21 illustrate the derived sets of fragility curves for the different building configurations and soil types. "High code" designed RC structures are considered herein. Similar fragility relationships, which are generally associated with a more rapid transition from low levels of damage to collapse, could also be constructed for "low code" structures.

Table 4.7. Parameters of fragility functions for PGA based on the regression analysis method

Soil type	Foundation type	Median PGA (g)				Dispersion β
		LS1 (g)	LS2 (g)	LS3 (g)	LS4 (g)	
Sand	Flexible	0.29	0.36	0.59	0.84	0.81
	Stiff	0.31	0.62	1.70	-	0.82
Clay	Flexible	0.38	0.83	1.41	1.71	0.82
	Stiff	0.53	1.78	-	-	0.69

Table 4.8. Parameters of fragility functions for PGD based on the regression analysis method

Soil type	Foundation type	Median PGD (m)				Dispersion β
		LS1 (m)	LS2 (m)	LS3 (m)	LS4 (m)	
Sand	Flexible	0.14	0.45	1.06	1.47	0.62
	Stiff	0.25	1.07	2.53	3.36	0.55
Clay	Flexible	0.25	1.09	2.27	2.87	0.53
	Stiff	0.52	3.31	-	-	0.55

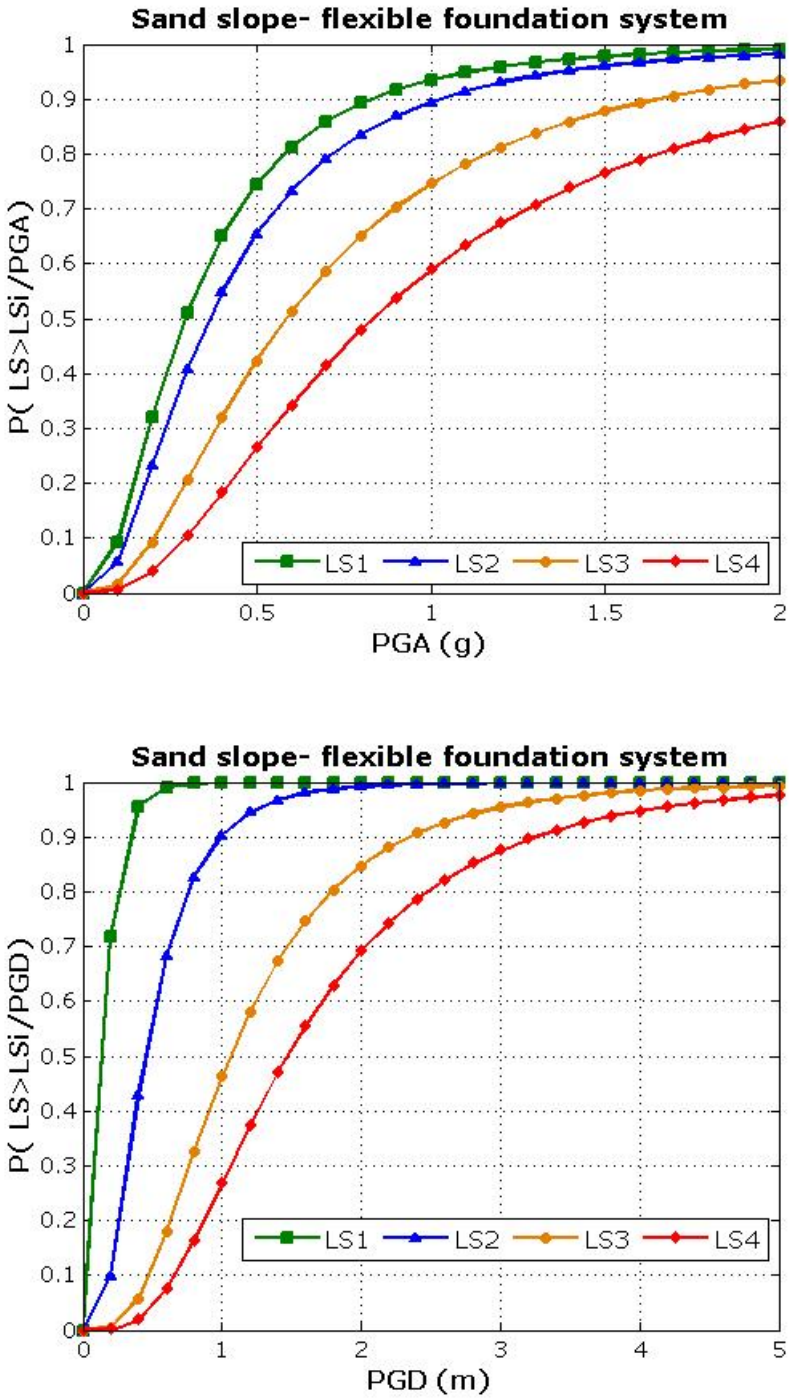


Figure 4.18. Fragility curves for low rise-RC buildings with flexible foundation system on sand slope based on the regression analysis method

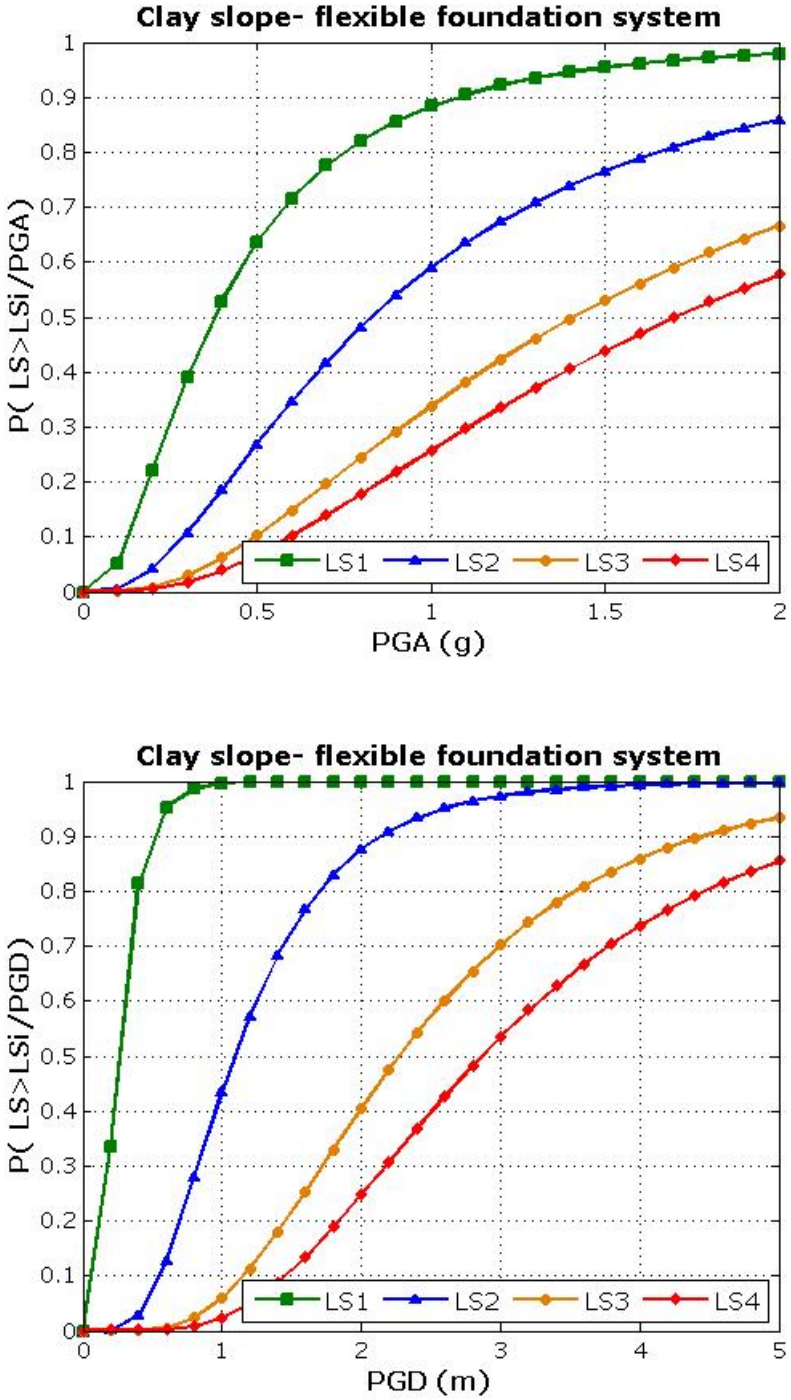
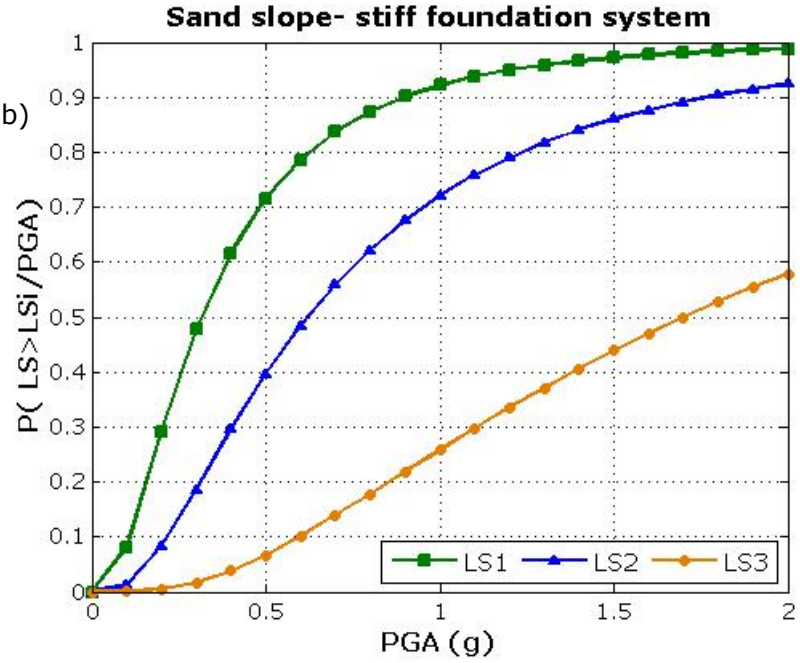


Figure 4.19. Fragility curves for low rise-RC buildings with flexible foundation system on clay slope based on the regression analysis method

(b)



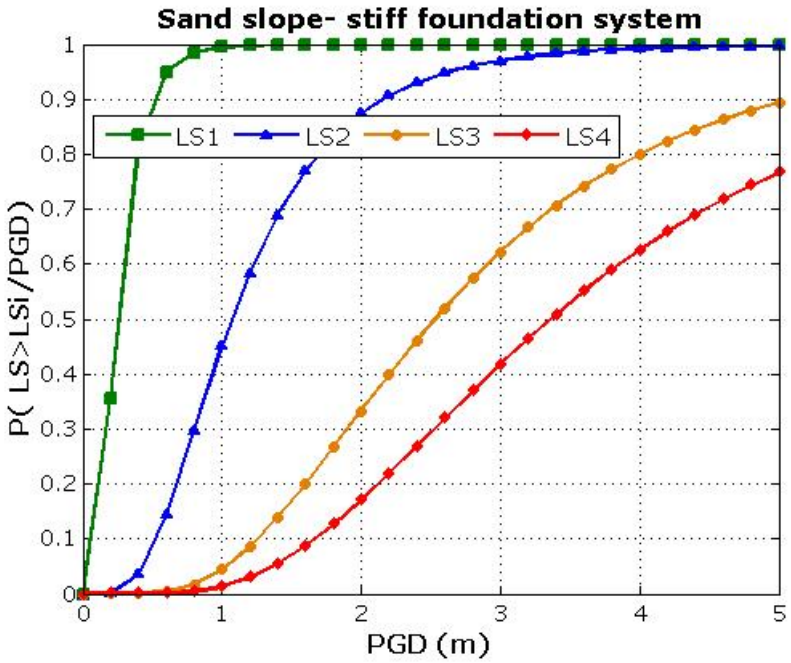


Figure 4.20. Fragility curves for low rise-RC buildings with stiff foundation system on sand slope based on the regression analysis method

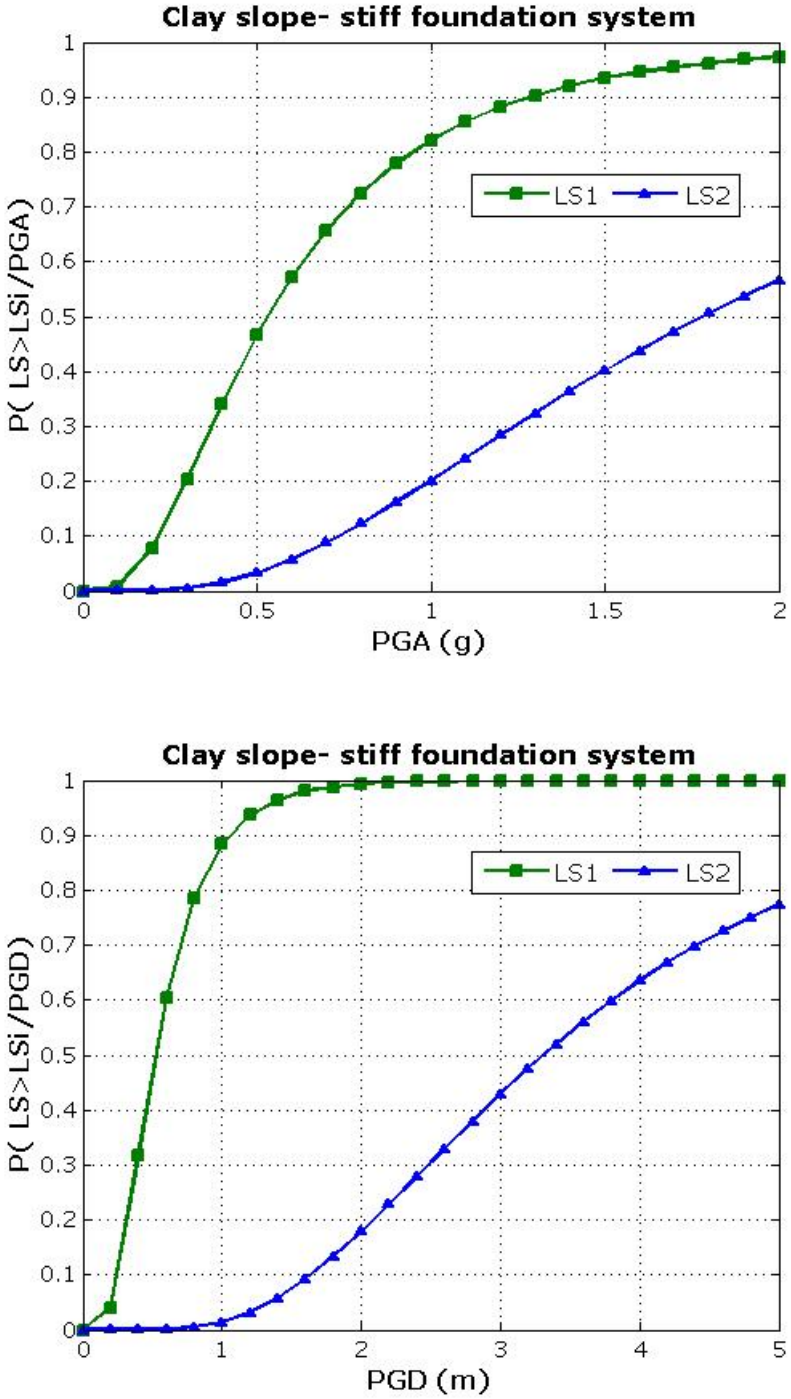


Figure 4.21. Fragility curves for low rise-RC buildings with stiff foundation system on clay slope based on the regression analysis method

4.4.2.2. Maximum likelihood method

The Maximum Likelihood (ML) method is a commonly used approach to estimate the log-normal parameters of the fragility curves (median and log-standard deviation). The maximum likelihood function gives, among the possible values of the fragility parameters, the ones that maximize the likelihood of obtaining the simulated dataset. The likelihood function is expressed as (Shinozuka, 2000):

$$L = \prod_{i=1}^{N} \left[F(IM_i)\right]^{y_i} \left[1 - F(IM_i)\right]^{1-y_i} \quad (4.4)$$

F (.): represents the lognormal fragility distribution for a certain limit state (see Eq. 4.3)

IM_i: is the intensity measure in terms of PGA at the outcrop or PGD at the slope area

y_i: represents the realization of the Bernouilli random variable Y_i with y_i = 1 or 0 depending on whether or not the structure sustains the specific state of damage under the IM equal to IM_i and N is the total number of simulations.

The two fragility parameters $\overline{IM}$ *and* β (see Eq. 4.3) are computed so as to maximize ln*L (*and hence *L)* satisfying the following equations:

$$\frac{d\ lnL}{d\overline{IM}} = \frac{d\ lnL}{d\beta} = 0 \quad (4.5)$$

Considering a common β for all limit damage states the likelihood function can be introduced as (e.g. Shinozuka et al 2003; Argyroudis, 2010):

$$L\left(IM_1, IM_2, IM_3, IM_4, \beta\right) = \prod_{i=1}^{N} \prod_{j=0}^{4} P_j\left(IM_i; E_j\right)^{y_{ij}} \quad (4.6)$$

Where

E_j the specified damage state for no damage (j=0), at least slight damage (j=1), at least moderate damage (j=2), at least extensive damage (j=3) and complete damage (j=4).

y_{ij}=1 if the damage state E_j occurs for the i simulation of the structure subject to the landslide intensity IM_i and 0 otherwise. The computation is performed numerically using a standard optimization algorithm.

As already discussed previously, three primary sources of uncertainty contribute to the total variability:

- the uncertainty on the demand that is taken into account from the dispersion of the recorded damage indices (maximum strain) as a function on the selected IM,
- the damage state definition uncertainty that is accounted for by performing a Monte Carlo simulation for the simulated damage data considering a lognormal distribution for the specified limit states in accordance to the pertinent literature

(Crowley et al., 2004) with median the already defined limit state values (see Tab. 4.6) and coefficient of variation equal to 0.4.

- the capacity uncertainty is added to the results of the analysis through the following expression:

$$\beta = \sqrt{\beta'^2 + \beta_C^2} \quad (4.7)$$

Where β' the variability associated with the demand and the definition of limit states and β_c is taken equal to 0.25 or 0.30 depending on the code design level of the structures (e.g. NIBS, 2004).

Table 4.9. Parameters of fragility functions for PGA based on the Maximum likelihood method

Soil type	Foundation type	Median PGA (g)				Dispersion β
		LS1 (g)	LS2 (g)	LS3 (g)	LS4 (g)	
Sand	Flexible	0.22	0.39	0.58	0.81	0.37
	Stiff	0.34	0.75	1.12	1.61	0.40
Clay	Flexible	0.29	0.61	1.0	1.37	0.39
	Stiff	0.45	1.51	-	-	0.51

Table 4.10. Parameters of fragility functions for PGD based on the Maximum likelihood method

Soil type	Foundation type	Median PGD (m)				Dispersion β
		LS1 (m)	LS2 (m)	LS3 (m)	LS4 (m)	
Sand	Flexible	0.14	0.37	0.80	1.54	0.42
	Stiff	0.25	0.99	2.29	-	0.45
Clay	Flexible	0.24	0.96	2.35	-	0.46
	Stiff	0.42	3.86	-	-	0.74

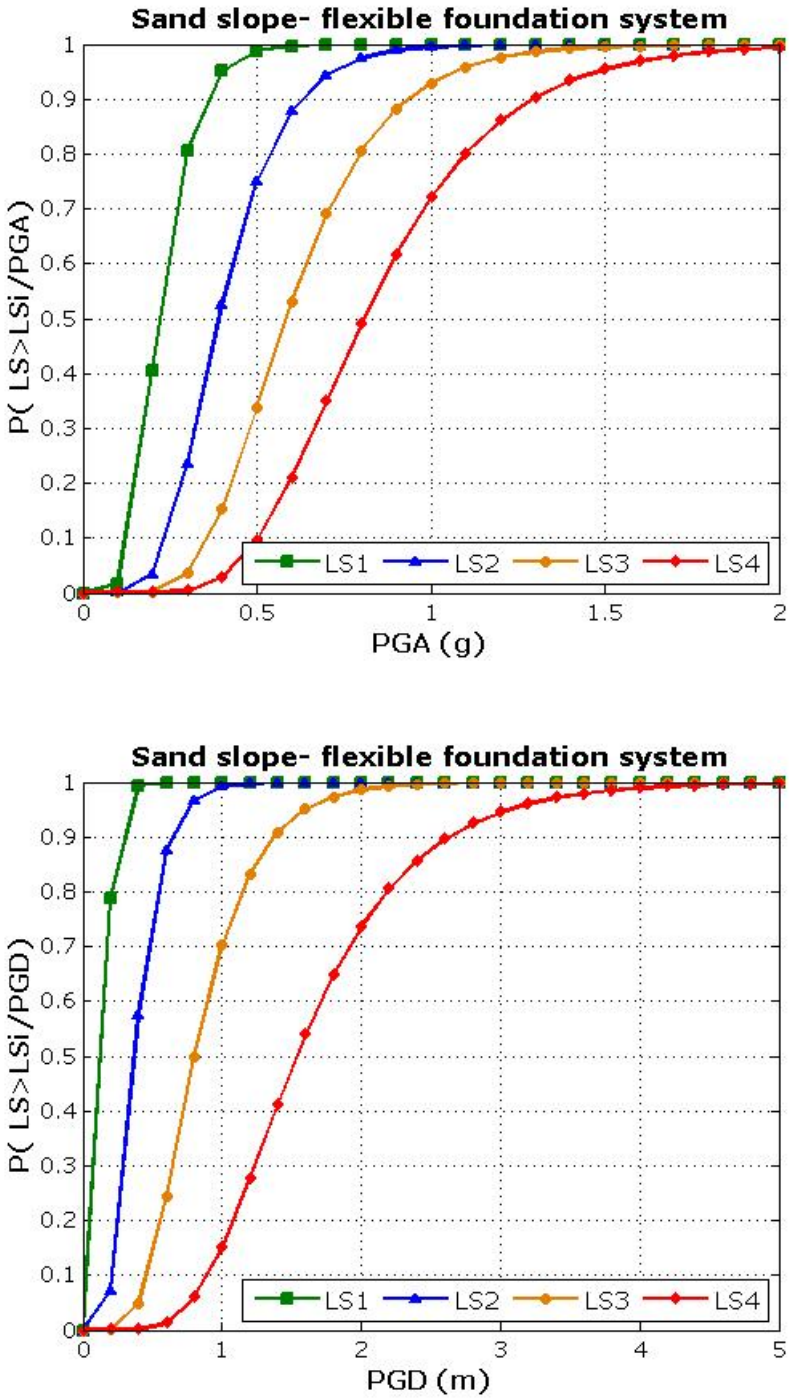


Figure 4.22. Fragility curves for low rise-RC buildings with flexible foundation system on sand slope based on the Maximum likelihood method

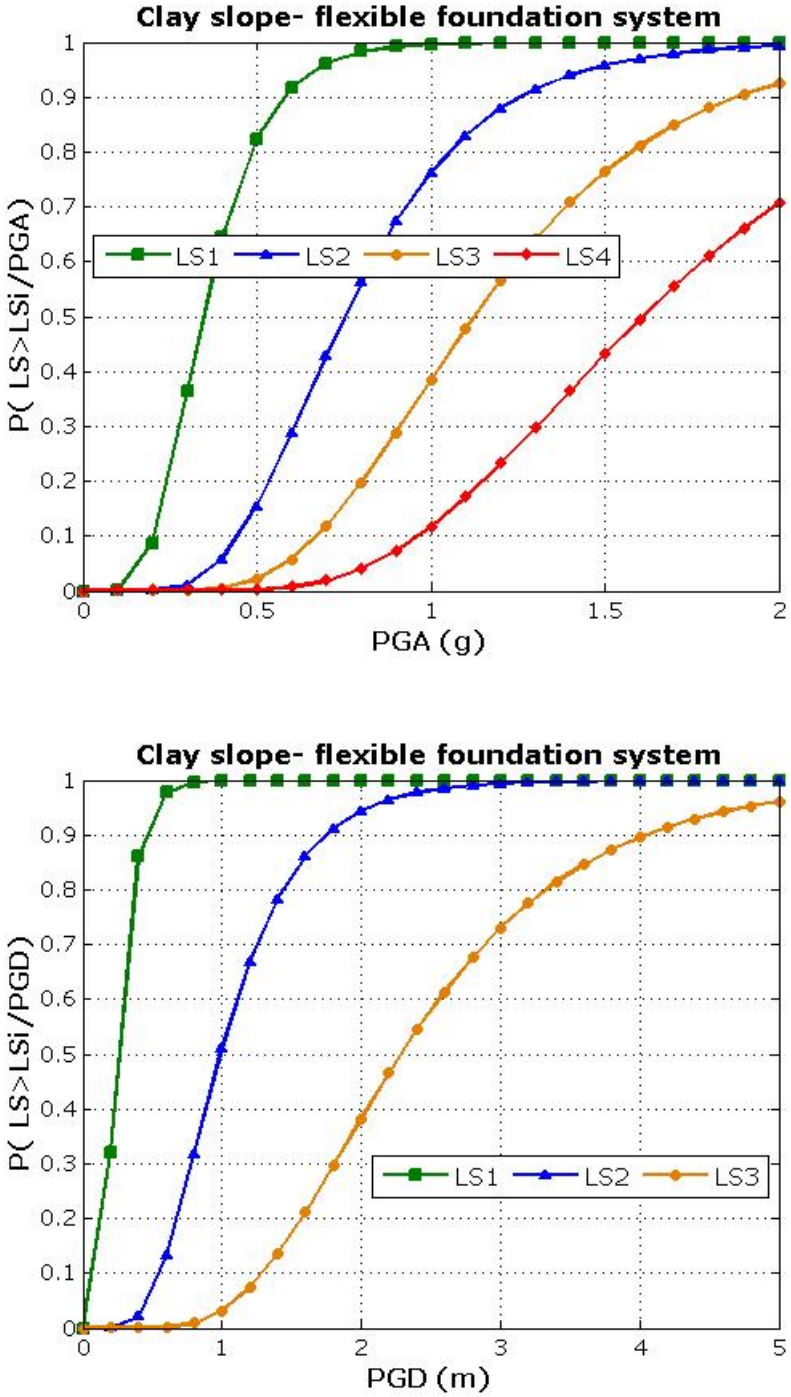


Figure 4.23. Fragility curves for low rise-RC buildings with flexible foundation system on clay slope based on the Maximum likelihood method

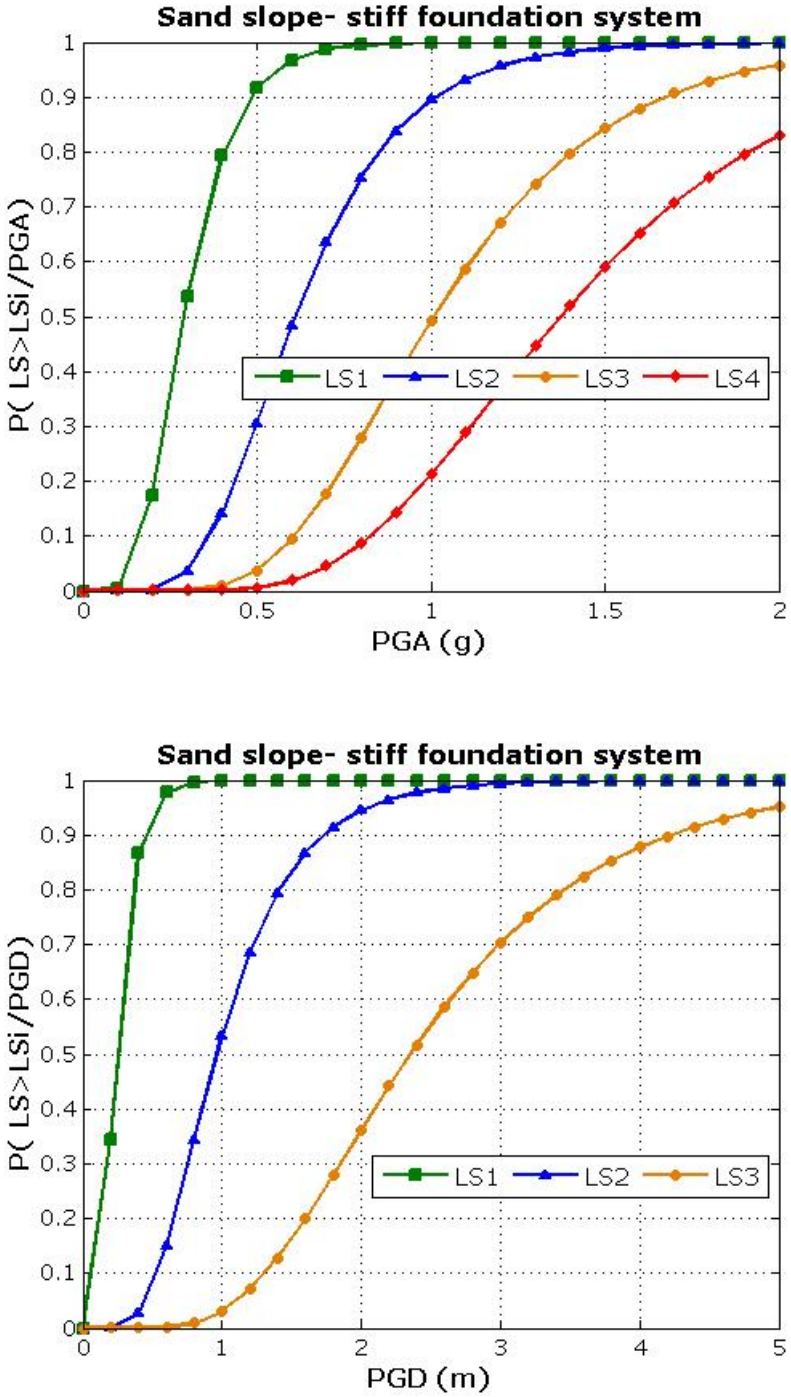


Figure 4.24. Fragility curves for low rise-RC buildings with stiff foundation system on sand slope based on the Maximum likelihood method

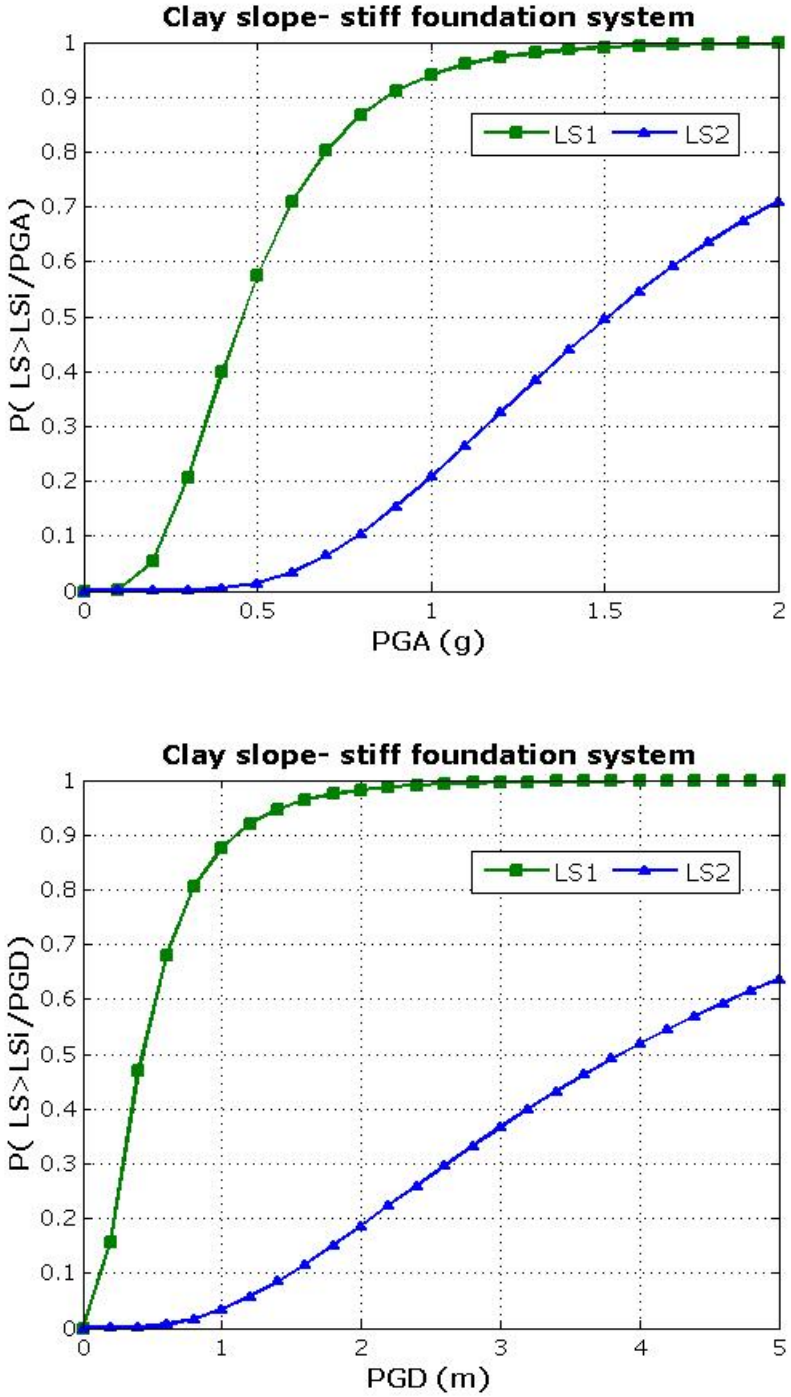
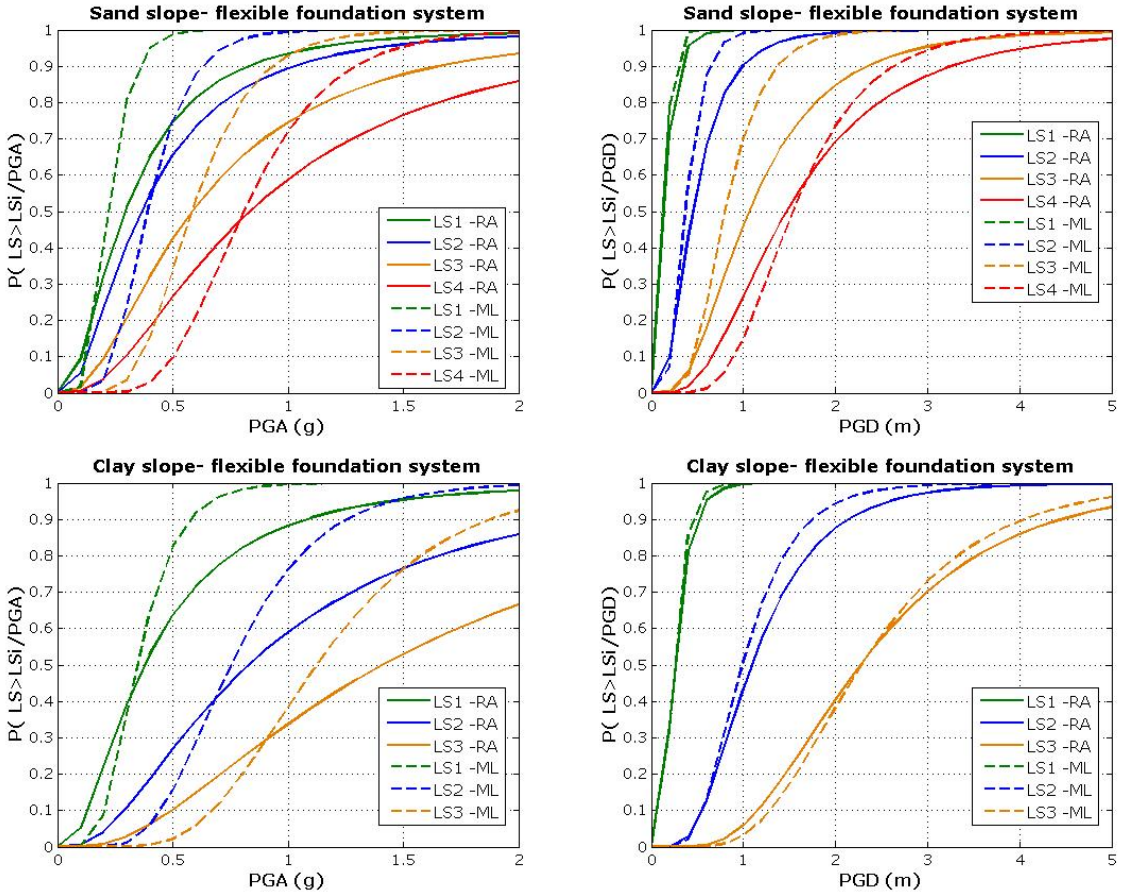


Figure 4.25. Fragility curves for low rise-RC buildings with stiff foundation system on clay slope based on the Maximum likelihood method

4.4.2.3. Comparison between the methods

The differences on the fragility curves when applying the two different approaches are due to the different assumptions adopted in each method and clearly identify the influence of epistemic uncertainty on the fragility analysis. In particular, the two methods estimate medians in terms of PGA and PGD that are generally in good agreement. The estimated β values from the two methods are quite similar when using PGD as a landslide intensity measure whereas it presents a large dispersion in case that the PGA is used as an intensity parameter. More specifically, it is shown that the maximum likelihood method predicts quite smaller log-normal standard deviations. In that sense, it may be concluded that for the given dataset the maximum likelihood method is more efficient compared to the regression analysis method when considering PGA as a measure of the landslide intensity.



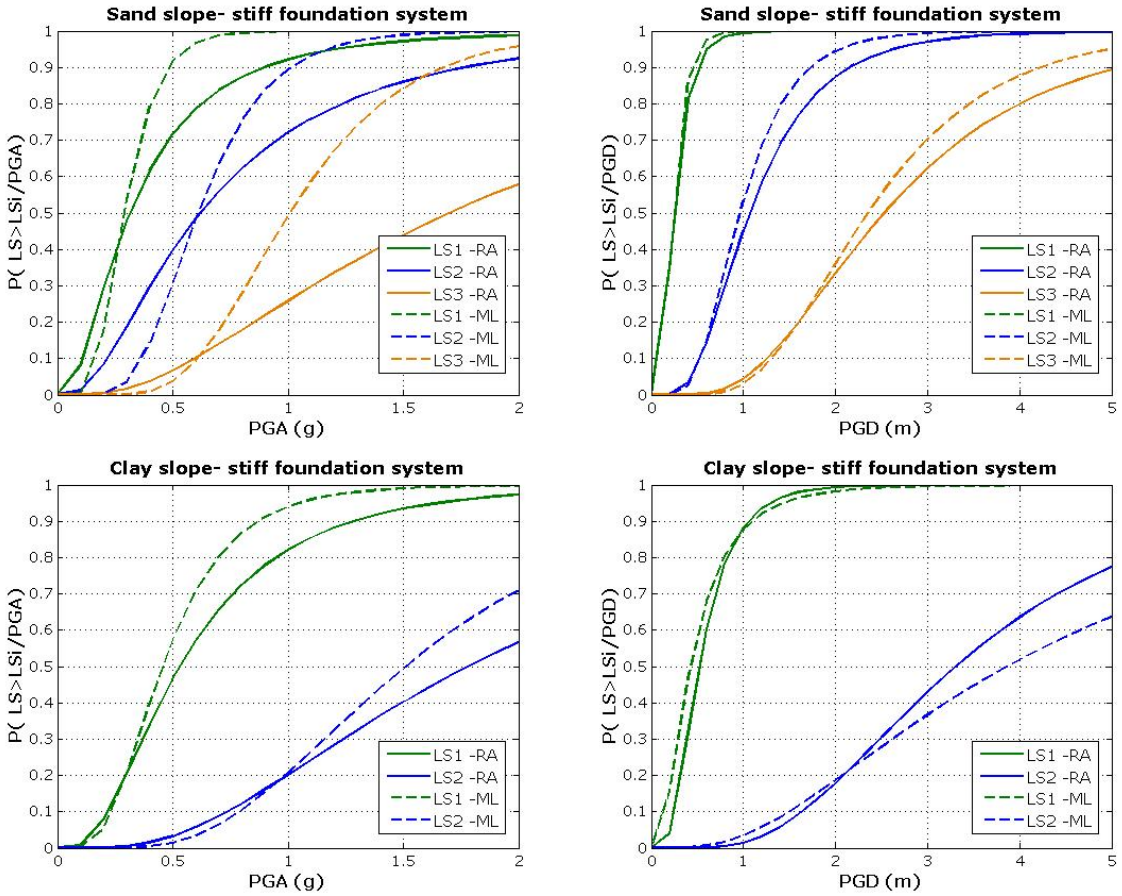


Figure 4.26. Comparison of Fragility curves in terms of PGA (left) and PGD (right) developed based on the regression Analysis (RA) and the Maximum likelihood (ML) methods

4.4.3 Discussion

As expected, the building with stiff foundation system would sustain less damage due to earthquake induced slow moving slides, compared to the same building with the flexible foundation system. The soil type (dry sand or clay in our case) is also proved to play a significant role in assessing the building's vulnerability standing near the crest of potentially precarious slopes. It is observed that buildings with the same structural and stiffness characteristics located on slopes of cohesive material behave much better compared to sandy slopes when subject to differential deformation. More specifically, among the structures analyzed, the ones with flexible foundations located on sand slopes present the highest vulnerability whereas the corresponding ones with stiff foundations located on clay slopes appear to be the least susceptible to damage.

It should be noted that only the structural damage of the building members is considered in this research. The total damage (structural and non-structural) will be quite different (certainly larger) in case of the building with the stiff foundation as a considerable amount of damage may be attributed to the rotation of the whole building as a rigid

body. In the latter, the damage can only be defined using empirical criteria and expert opinion (Bird et al., 2005). Furthermore, it is worth pointing out that the complex issue of combined damages due to ground shaking and ground failure is not taken into account in the evaluation of building's vulnerability. Thus, no strength or stiffness degradation to the building's structural members due to the effect of ground shaking is assumed to occur. Neither are aging effects such as concrete or steel corrosion considered in the present chapter. It is implicitly assumed that the maintenance of the building is conducted in an optimal manner. A first attempt to include these effects within the vulnerability assessment framework and to propose time-variant fragility functions is presented in Chapter 8.

The derived fragility curves are valid only for the specific combination of geometry, material properties and limit states used herein; their use to other geometric configurations and site conditions should be made with caution. In order to derive generic fragility functions for the assessment of the seismic risk and to design appropriate mitigation measures at building or aggregate scale, an extensive numerical parametric analysis considering various building typologies, slope configurations and soil properties should be carried out. Such analysis is presented in Chapter 6.

The reliability and accuracy of the proposed methodology is assessed through the comparison of the analytically derived fragility curves with literature ones and recorded building damage data from two real case histories: Kato Achaia slope in Peloponnese – Greece and Corniglio village-Italy case study (Chapter 7).

CHAPTER 5

Newmark- type displacement methods: Comparison with numerical results

5.1 Introduction

The sliding-block analogy proposed by Newmark (1965) still provides the conceptual basis on which all displacement-based methods have been developed. Since then, however, several variations of Newmark's method have been proposed with the aim to yield more accurate estimates of slope displacement. This has been accomplished by proposing more efficient ground motion intensity measures (e.g. Crespelllani et al., 1998; Jibson, 2007; Watson-Lamprey and Abrahamson, 2006; Saygili and Rathje, 2008), improving the modeling of dynamic resistance of the slope characterized by its yield coefficient (e.g. see Bray, 2007) and by analyzing the dynamic slope response more rigorously (e.g. Bray and Travasarou, 2007; Ausilio et al., 2008; Rathje and Antonakos, 2011). In terms of their assumptions to analyze the dynamic slope response, displacement based methods can be classified into three main types (Jibson, 2011): rigid block, decoupled and coupled.

A short description of the different types of Newmark-type displacement methods as well as recommendations for the selection of the most appropriate ones have already been presented in Chapter 2, § 2.3.3. The focus in this chapter is first on the description of three different displacement –based models (one of each type): the conventional analytical Newmark rigid block, the Rathje and Antonakos (2011) decoupled and Bray and Travasarou (2007) coupled model that have been selected to assess the expected slope displacements. Then, after providing a short literature review on the reliability assessment of various displacement based methods for site specific applications, a comparison of the three Newmark-type procedures is attempted to assess their relative predictive capability considering various earthquake scenarios and different compliance of the sliding surface. Finally, the computed FLAC numerical results derived from the non-linear dynamic analysis (see Chapter 4, §4.3.1), in terms of permanent horizontal

displacements, are compared with the predicted displacements from the three models for the case of a 30° inclined sand and clayey slope.

5.1.1 Analytical Newmark rigid block model

In his 1965 seminal Rankine Lecture, Newmark (1965) proposed that seismic stability of earth dams and embankments could be assessed in terms of earthquake-induced deformations which occur whenever the inertia forces on a potential slide mass are large enough to overcome the frictional resistance at the "failure" surface. He formulated this concept by proposing the analogue of a rigid block on inclined plane as a simple way of analytically obtaining approximate estimates of these deformations.

Newmark (1965) computed rigid block displacements for four earthquake motions and showed that displacement was a function of yield coefficient (k_y), peak ground acceleration and peak ground velocity.

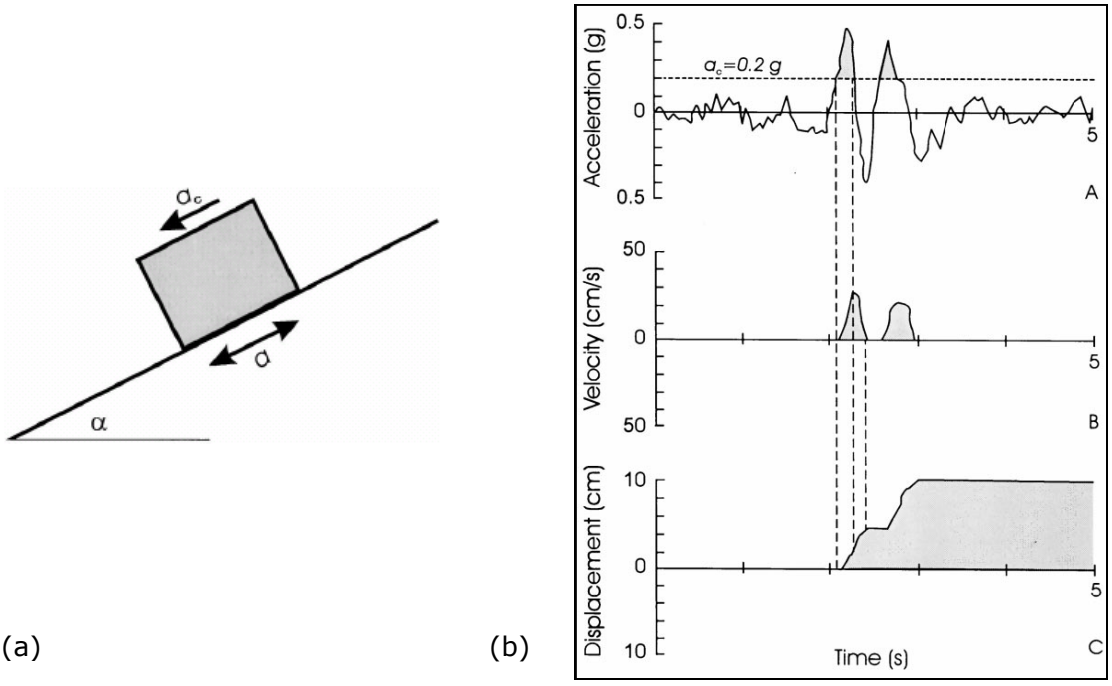


Figure 5.1. (a) Newmark Sliding-block model (b) Newmark algorithm for seismically-induced permanent displacements (adapted from Wilson and Keefer, 1983).

The basic assumption of Newmark's method is that the potential landslide block behaves as a rigid mass that slides in a perfectly plastic manner on an inclined plane (Fig. 5.1a). This assumption is reasonable for relatively thin landslides in stiff or brittle materials, but it introduces significant errors as landslides become thicker and material becomes softer (Jibson, 2011). Cumulative landslide displacements are estimated by integrating twice with respect to time the parts of an earthquake acceleration-time history that exceed the

critical or yield acceleration, a_c ($k_y \cdot g$), that is the threshold acceleration required to overcome basal resistance and initiate sliding. Figure 5.1b presents a schematic description of the rigorous Newmark Sliding Block procedure (adapted from Wilson and Keefer, 1983) for estimating permanent co-seismic landslide displacements. The critical (yield) acceleration may be determined through a pseudostatic analysis or by a simplified empirical relationship (e.g. Bray, 2007).

Expect for the rigid block key assumption, several other simplifying assumptions were imposed (see e.g. Newmark, 1965; Makdisi and Seed, 1978; Chang et al., 1984; Ambraseys and Menu, 1988); these include:

- Static and dynamic material shear strengths are taken to be the same
- Seismic yield coefficient (k_y) is not strain dependent and thus remains constant during sliding implying that the soil does not undergo significant strength loss as a result of shaking
- The upslope resistance is taken to be infinitely large such that displacements occur in the downslope direction only
- The effects of dynamic pore pressures are neglected
- Yield behavior of the material is non-elastic, perfectly-plastic (implied by the use of k_y);
- Displacements are assumed to occur along a single, well-defined slip surface (typically the LEM critical pseudostatic surface);
- Accelerations and corresponding inertial forces act in the direction of initial movement at the center of gravity of the slide mass.

Newmark conventional analytical rigid block method is used in this study to predict cumulative slope displacements obtained by double integration of the accelerograms recorded on rock outcrop condition. The freeware software by Jibson and Jibson (2003) was used for that calculation.

5.1.2 Rathje and Antonakos (2011) decoupled model

Rathje and Antonakos (2011) decoupled model is based on the recent empirical displacement models of Saygili and Rathje (2008) and Rathje and Saygili (2009) and thus a brief description of the aforementioned models is first provided.

Saygili and Rathje (2008) presented a suite of empirical predictive models for rigid block sliding displacements developed using a database of more than 2000 acceleration time histories with moment magnitudes that range from 5.0 to 7.9 and four values of yield

coefficient. These models consider various single ground motion parameters (PGA, PGV, I_a, T_m) and vectors of ground motion parameters (e.g. PGA, PGV, I_a, T_m, D_{5-75}, D_{5-95}) to estimate the sliding displacements with the goal of minimizing the standard deviation in the displacement prediction. Rathje and Sayligi (2009) slightly modified the single parameter PGA model of Saygili and Rathje (2008) by adding a term related to earthquake magnitude.

The authors recommended (among others) the use of the two parameter vector (PGA, PGV) model due to its ability to significantly reduce the variability in the displacement prediction. The derived (PGA, PGV) displacement model is given by the following equation (Saygili and Rathje, 2008):

$$\ln(D) = -1.56 - 4.58\left(\frac{k_y}{PGA}\right) - 20.84\left(\frac{k_y}{PGA}\right)^2 + 44.75\left(\frac{k_y}{PGA}\right)^3 - 30.50\left(\frac{k_y}{PGA}\right)^4 + -0.64\ln(PGA) + 1.55\ln(PGV) + \varepsilon\,\sigma_{InD} \quad (5.1)$$

Were D=sliding displacement (cm); k_y =yield coefficient (g); PGA is the peak ground acceleration (g); PGV is the peak ground velocity (cm/sec); σ_{InD}= standard deviation in natural log units; and ε= standard normal variate with zero mean and unit standard deviation.

The standard deviation of the (PGA, PGV) model σ_{InD} is a function of k_y/PGA is and given by:

$$\sigma_{InD} = 0.41 + 0.52\left(\frac{k_y}{PGA}\right) \quad (5.2)$$

Rathje and Antonakos (2011) presented a unified framework that extends these models for application to flexible sliding masses following a decoupled approximation. The decoupled approach estimates the effect of dynamic response of the slide mass on permanent sliding displacement in a two-step procedure: first, a dynamic response analysis of the slope is performed assuming no failure surface to estimate the equivalent acceleration time history within the slide mass and then the resulting time history is input into a rigid block analysis and the permanent displacements are estimated.

To use the rigid block predictive expressions (Saygili and Rathje, 2008; Rathje and Sayligi, 2009) for deformable sliding masses appropriate seismic loading parameters were specified. In particular, for the two vector (PGA, PGV) model, k_{max} (e.g. peak value of the average acceleration time history within the sliding mass) was used to replace PGA and k-vel_{max} (e.g. peak value of the k-vel time history provided by numerical integration of the k-time history) to replace PGV. The authors presented predictive models for k_{max} and k-vel_{max} based on one-dimensional site response analysis of five sites subjected to 80 input ground motions (Antonakos, 2009). The computed k_{max} values were

normalized by the input PGA and correlated to T_s/T_m ; the ratio of the fundamental site period (T_s) to the mean period of the earthquake motion (T_m). The derived model predicts $\ln(k_{max}/PGA)$ as a function of $\ln(T_s/T_m)$ and PGA:

For $T_s/T_m \geq 0.1$:

$$\ln\left(k_{max}/PGA\right) = (0.459 - 0.702 \cdot PGA) \cdot \left[\frac{\ln\left(\frac{T_s}{T_m}\right)}{0.1}\right] + (-0.228 + 0.076 \cdot PGA) \cdot \left[\frac{\ln\left(\frac{T_s}{T_m}\right)}{0.1}\right]^2 \quad (5.3)$$

For $T_s/T_m < 0.1$ (nearly rigid conditions):

$$\ln\left(k_{max}/PGA\right) = 0$$

A similar predictive model was developed for $k\text{-}vel_{max}/PGV$ given by:

For $T_s/T_m \geq 0.2$:

$$\ln\left(k\text{-}vel_{max}/PGV\right) = (0.240) \cdot \left[\frac{\ln\left(\frac{T_s}{T_m}\right)}{0.2}\right] + (-0.091 - 0.171 \cdot PGA) \cdot \left[\frac{\ln\left(\frac{T_s}{T_m}\right)}{0.2}\right]^2 \quad (5.4)$$

For $T_s/T_m < 0.2$:

$$\ln\left(k\text{-}vel_{max}/PGV\right) = 0$$

The standard deviation for these models in natural log units is 0.25.

In addition to the change in seismic loading parameters, the rigid block predictive models (Saygili and Rathje, 2008; Rathje and Sayligi, 2009) were further modified to account for the differences in frequency characteristics between acceleration-time histories and k-time histories. This modification is a function of T_s and increases the predicted displacement.

The resulting modification to the (PGA, PGV) model to account for flexible sliding is:

For $T_s/T_m \leq 0.5$:

$$\ln\left(D_{flexible}\right) = \ln\left(D_{PGA,PGV}\right) + 1.42 \cdot T_s$$

For $T_s/T_m > 0.5$: (5.5)

$$\ln\left(D_{flexible}\right) = \ln\left(D_{PGA,PGV}\right) + 0.71$$

where $D_{PGA,PGV}$ represents the median displacement predicted by the (PGA, PGV) rigid sliding block model where k_{max} is used in lieu of PGA and $k\text{–}vel_{max}$ is used in lieu of PGV.

A revised linear relationship is used to predict σ_{lnD} for flexible sliding masses for the (PGA, PGV) model:

$$\sigma_{InD} = 0.40+0.284\left(\frac{k_y}{k_{max}}\right) \quad (5.6)$$

Figure 5.2 depicts the plots of displacements as a function of T_s for k_y=0.05 and 0.1 for the revised (PGA, PGV) Rathje and Antonakos (2011) model.

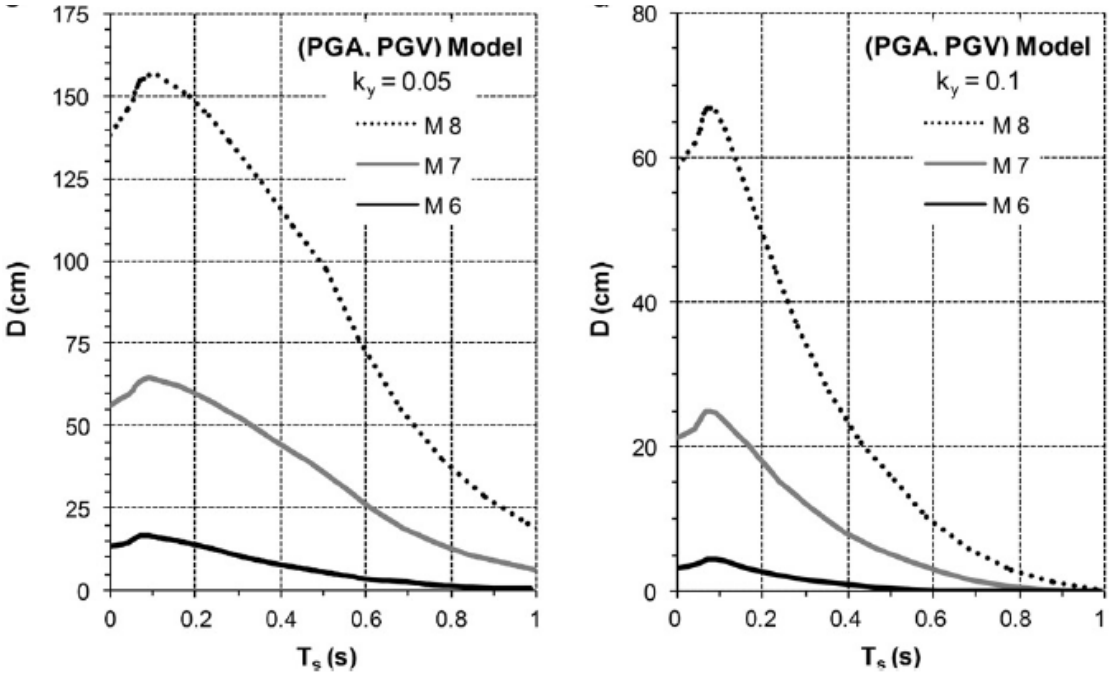


Figure 5.2. Predicted values of sliding displacement as a function of T_s with k_y=0.05(a) and k_y=0.1 (b) for the (PGA, PGV) Rathje and Antonakos (2011) model

It's worth noting that the (PGA, PGV) model is recommended for use in practice by Rathje and Antonakos (2011) because of the significant frequency content information provided by PGV (for rigid sliding) and by k-vel_{max} (for flexible sliding) resulting in the minimization of the uncertainty in the displacement estimation. Considering that, this method is used in this study to predict co-seismic slope displacements for different earthquake scenarios.

5.1.3 Bray and Travasarou (2007) coupled model

Bray and Travasarou (2007) proposed a simplified semi-empirical method to estimate earthquake deviatoric- induced displacements of rigid and deformable soil slopes. Displacements were calculated using the nonlinear fully coupled stick-slip deformable sliding block model proposed by Rathje and Bray (2000) to capture the dynamic

response of an earth-waste structure (Fig. 5.3). In a fully coupled analysis, as proposed by the authors, the dynamic response of the sliding mass and the permanent displacement are modeled together so that the effect of plastic sliding displacement on ground motions is taken into account. Thus, the fully coupled stick-slip deformable sliding block model offers a conceptual improvement over the decoupled approximation.

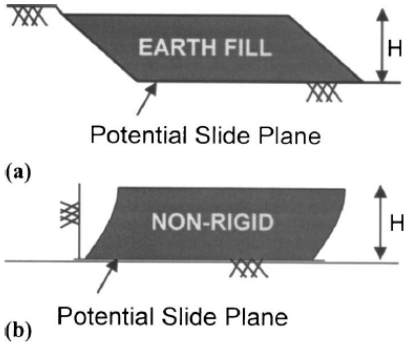


Figure 5.3. Generic seismic slope displacement problem of height H and initial stiffness Vs and (b) idealized nonlinear stick with one-way sliding used in Bray and Travasarou (2007).

The model used is based on an equivalent-linear visco-elastic one dimensional analysis to allow for the use of a large number ground motions with wide range of properties of the potential sliding mass. Vucetic and Dobry (1991) shear modulus and damping curves for PI=30 were used. 688 recorded ground motions from 41 earthquakes with moment magnitudes (M_w) that range from 5.5 to 7.6, has been used to compute co-seismic displacements (Travasarou, 2003). The predictive seismic displacement model parameters include the system's yield coefficient (k_y), its initial fundamental period (T_s), and the ground motion's spectral acceleration at a degraded period equal to $1.5T_s$. The slope's yield coefficient (k_y) and initial fundamental period (T_s) were selected to represent the dynamic strength and stiffness, respectively, of the earth/waste slope in the seismic displacement model. The seismic displacements were computed for ten values of k_y (0.02-0.4) and eight values of T_s (0 - 2 s) for the entire set of used ground motions. The slope's yield coefficient (k_y) can be estimated through a psedostatic analysis or by a simplified expression as a function of the slope geometry, weight and strength (e.g. Bray et al., 1998). The initial fundamental period of the sliding mass can normally be estimated using the expression T_s=4H/Vs, where H= average height of the potential sliding mass, Vs=average shear wave velocity of the sliding mass. A modified expression should be used in case of a triangular –shaped sliding mass (Bray, 2007). In Bray and Travasarou (2007), average H varied from 12 to 100m and V_s from 200 to 425m/sec. The spectral acceleration at a degraded period equal to 1.5 times the initial fundamental period of the slope, i.e., S_a ($1.5T_s$), was found to represent (among others) an efficient

measure of the seismic intensity for minimizing the variability of displacement predictions (Travasarou and Bray, 2003). Note that the model has been developed for S_a ($1.5T_s$) values from 0.002 to 2.7 g and should be used within these ranges to provide reasonable and reliable estimates of the slope displacements. The degraded fundamental period is considered to capture the overall average stiffness reduction for the earth/waste slopes. It is also important to notice that the Bray and Travasarou (2007) expressions do not model the foundation conditions (e.g. rock, stiff soil) that can moderately effect the computed displacements.

The model separates the probability of "zero" displacement occurring from the distribution of "non-zero" displacement, so that to exclude from the results values of calculated displacement <1 cm that are assumed to be of no engineering significance.

The probability of negligible "zero" displacement is estimated as:

$$P(D = "0") = 1 - \Phi\left(-1.76 - 3.22\ln(k_y) - 0.484T_s\ln(k_y) + 3.52\ln(S_a(1.5T_s))\right) \quad (5.7)$$

where P(D=0): probability (as a decimal number) of occurrence of zero displacements; D-seismic displacement; Φ: standard normal cumulative distribution function; k_y: yield coefficient; T_s: initial fundamental period of the sliding mass in seconds, and $S_a(1.5T_s)$: the spectral acceleration of the input ground motion at a period of $1.5T_s$ in terms of g.

The likely amount of nonzero seismic displacement (*D)* is given by the following equation:

$$\begin{aligned}\ln(D) = {} & -1.10 - 2.83\ln(k_y) - 0.333(\ln(k_y))^2 + 0.566\ln(S_a(1.5T_s)) \\ & + 3.04\ln(S_a(1.5T_s)) - 0.244(\ln(S_a(1.5T_s)))^2 + 1.50T_s + 0.278(M - 7) \pm \varepsilon\end{aligned} \quad (5.8)$$

where the k_y, T_s, and $S_a(1.5T_s)$ are defined as previously for Eq. (5.7), and ε is a normally distributed random variable with zero mean and standard deviation σ=0.66.

For the nearly Newmark rigid sliding block case ($T_s \approx 0$), Eq. (5.8) is transformed as follows:

$$\begin{aligned}\ln(D) = {} & -0.22 - 2.83\ln(k_y) - 0.333(\ln(k_y))^2 + 0.566\ln(PGA) \\ & + 3.04\ln(PGA) - 0.244(\ln(PGA))^2 + 1.50T_s + 0.278(M - 7) \pm \varepsilon\end{aligned} \quad (5.9)$$

where PGA is the peak ground acceleration of the ground motion (i.e., $S_a(T_s=0)$).

The model can be implemented rigorously within a fully probabilistic framework for the estimation of the probability of exceedance of a selected threshold of displacement (d) for a specified earthquake scenario and slope properties.

The probability of the seismic displacement (*D)* exceeding a specified displacement threshold (*d)* is expressed as:

$$P(D > d) = \left[1 - P(D = "0")\right] P(D > d / D > "0") \quad (5.10)$$

The term $P(D=0)$ is computed using Eq. (2). The term P (D>d/D>0) may be computed assuming that the estimated displacements are lognormally distributed as:

$$P(D > d / D > "0") = 1 - P\left(D \le d / D > "0"\right) = 1 - \Phi\left(\frac{\ln d - \ln \hat{d}}{\sigma}\right) \quad (5.11)$$

where $\ln \hat{d}$ is computed using Eq. (3); σ is the standard deviation of the random error, which in this case is 0.66; and Φ is the standard normal cumulative distribution function. Some trends in the estimates from the model are shown in Figure 5.4.

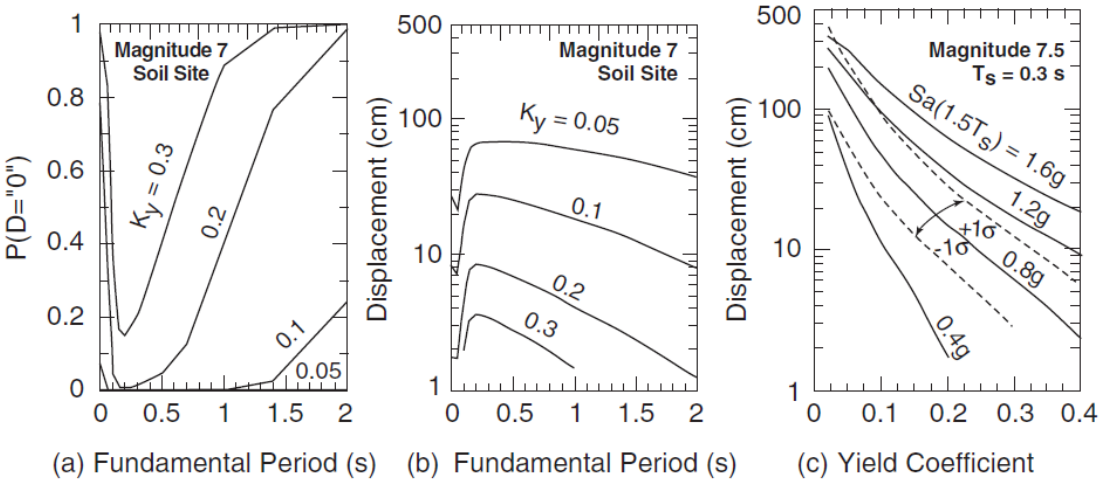


Figure 5.4. Trends from the Bray and Travasarou (2007) model: (a) probability of negligible displacements and (b) median displacement estimate for a M_w = 7 strike-slip earthquake at a distance of 10 km, and (c) seismic displacement as a function of yield coefficient for several intensities of ground motion (M_w = 7.5) for a sliding block with T_s = 0.3 s (adopted from Bray, 2007)

The Bray and Travasarou (2007) seismic displacement model has shown to predict reliably the seismic performance observed at 16 earth dams and solid-waste landfills. The authors also found that the values of predicted displacements were not inconsistent with other simplified methods. This method is also used in this study to predict sliding displacements for various earthquake scenarios.

5.2 Comparison between the displacement-based methods and with the numerical approach

5.2.1 Literature review

Several investigators have applied Newmark-type deformation procedures of different complexity as well as advanced 2D dynamic stress-strain methods to case studies to

compare the results among the different approaches and with the actual field performance. This comparison allows assessing the reliability of the various methods to predict the expected co-seismic displacements and to judge their relative degree of conservativeness.

Wilson and Keefer (1983) applied the Newmark method to a landslide triggered by the 1979 Coyote Creek, California earthquake using a real acceleration time history recorded at the landslide area and they found that the predicted Newmark landslide displacement agreed well with the observed displacement.

Chugh and Stark (2006) applied 2D FD dynamic analysis and analytical Newmark rigid block method to assess the seismically induced slope deformations of the Quaternary landslide (Qls-18) in California. They found that the obtained permanent displacements of both methods are in good agreement with the field observations.

Pradel et al. (2005) compared the post earthquake field performance of a pre-existing coherent landslide reactivated after the Northridge earthquake with the seismic displacements calculated using the analytical decoupled Newmark approximation as well as the simplified decoupled empirical relationships suggested by Makdisi and Seed (1978) and Bray and Rathje (1998). The authors showed that decoupled Newmark- type sliding block analyses can result in reasonable estimates of the observed displacement.

Bray and Travasarou (2007) confirmed the reliability of their model by providing estimations of the seismic displacements for 16 earth dams and solid-waste landfills that are correlated quite well with the observed seismic performance. The authors also found that the values of predicted displacements are not inconsistent with other simplified decoupled approaches (Makdisi and Seed, 1978; Bray and Rathje, 1998).

Austilio et al. (2009) evaluated the seismic displacements of the Calitri landslide (southern Italy) reactivated after the Irpinia earthquake (1980), based on simplified and analytical decoupled Newmark-type approaches, a 1D stick-slip coupled model (Austilio et al., 2008) and 2D FD dynamic analyses. They observed that the displacements predicted by simplified and analytical decoupled procedures for four different soil profiles seemed to capture the average value of displacement recorded at Calitri after the earthquake while the 1D coupled method generally yielded more conservative results. Moreover, they showed that the 2D FD dynamic analysis for the certain case history predicted the largest displacements, constant for all soil profiles that are comparable with the maximum observed values.

Strenk (2010) applied a suite of 20 deformation based methods of different categories (rigid block, decoupled and coupled) to assess their reliability in predicting the observed seismically-induced displacements at three case studies in California, USA : Calabasas

landslide triggered by the 1994 Northridge earthquake and Ditullio and Upper Laurel landslides triggered by the 1989 Loma Prieta earthquake. By comparing the median predictions obtained from each method to the actual measured displacement observed at each landslide he concluded that no method (or category of methods) is drastically more accurate than any of the others while he observed an overall tendency for nearly all deformation-based methods to under-predict the recorded field displacement (73% of the total number of predictions were reported to be near or below the actual measured displacement). He proposed the use of more recent simplified rigid-block methods that are derived using larger ground motion databases and robust mathematical regression techniques. Moreover, he recommended the use of the analytical-versions over the simplified versions of all deformation based methods as he recognized that simplified methods make more assumptions associated with the reduction of the analytical approach into a simplified mathematical equation or chart that can introduce significant bias on the computed displacements.

5.2.2 Implementation of the selected displacement-based predictive models

After providing a short literature review on the different displacement based approaches to site-specific applications, the three different procedures described in section 5.1 are used to predict the permanent slope deformation: the conventional analytical Newmark rigid block model (Newmark 1965), the decoupled Rathje and Antonakos (2011) model and the coupled Bray and Travasarou (2007) sliding block model. The main goal is to identify the influence of the earthquake characteristics and the dynamic response of the slope on the magnitude of the residual slope displacements using the aforementioned predictive models. In this respect, permanent displacements as a function of the critical acceleration ratio (e.g. k_y/k_{max} or k_y/PGA) were computed using the three different approaches considering different earthquake scenarios and compliance of the sliding surface. Comparisons between the methods were allowed to be made to assess their relative degree of conservatism. Mean displacements were calculated using the Newmark rigid block model whereas median values ±1 standard deviation and median and 16^{th} - 84^{th} percentiles were derived for the decoupled and coupled approximations respectively.

The applied seismic input consists of two real acceleration time histories characterized by quite different frequency content recorded at rock outcropping conditions (Fig. 5.5). These are scaled at two different levels of PGA, namely 0.3 and 0.7g. Table 5.1 presents the parameters describing some basic characteristics (amplitude, frequency content) of the ground motions and the flexibility of the potential sliding surface. Moment magnitude values for the Bray and Travasarou model were approximately taken to be consistent to

the level of shaking and considering the initial shaking characteristics of the given earthquake events. The displacement were computed for nearly rigid (T_s=0.032sec) and relatively flexible (Ts=0.16 sec) sliding masses.

The derived permanent displacements for the three different predictive models and for the different considered earthquake scenarios plotted as a function of the critical acceleration ratio, PGA (or k_{max})/k_y, are illustrated in Figures 5.6 to 5.8 and 5.13 to 5.14 for the nearly rigid and relatively flexible sliding surfaces respectively. Comparative plots between the methods are shown as well (Figs. 5.9-5.12 and 5.15-5.18 for the nearly rigid and relatively flexible sliding surfaces respectively).

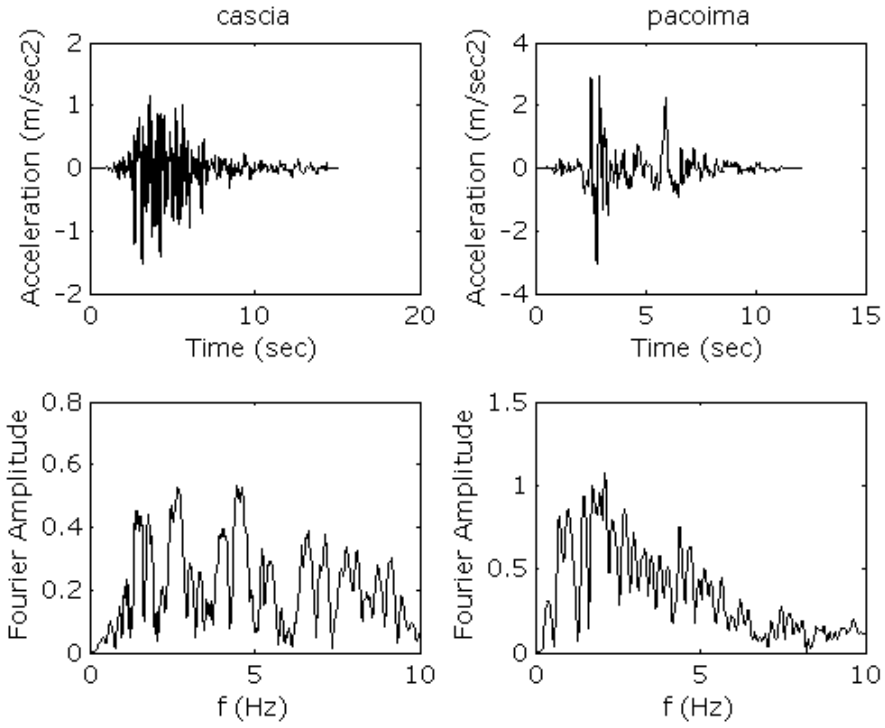


Figure 5.5. Input acceleration time histories (before scaling) and Fourier spectra

Table 5.1. Parameters describing the characteristics of the ground motions and the slope dynamic response used for the analyses

Earthquake record name	Valnerina 1979-Cascia_L		Northridge 1994-Pacoima Dam_L	
Earthquake code	cascia		pacoima	
Fundamental frequency of the input motion f_p (Hz)	4.44		2.1	
Fundamental period of the input motion T_p (sec)	0.23		0.48	
Mean Period of the input motions T_m (sec)	0.295		0.507	
Scaled outcropping PGA (g)	0.3	0.7	0.3	0.7
PGV (cm/sec)	10.3	30.9	14.6	43.9
Fundamental period of the sliding mass T_s (sec)	0.16	0.032	0.16	0.032
$S_a(1.5T_s)$/PGA	2.9265	1.073	2.2572	1.033
T_s/T_m	0.542	0.106	0.316	0.063

The results stress the influential role of the amplitude and frequency content of the earthquake as well as the compliance of the sliding surface on the magnitude of the computed displacements. As observed for all the applied approaches, time histories scaled at 0.7g produce larger displacements compared to those scaled at 0.3g for the same critical acceleration ratios. Moreover, the lower frequency input motion (Pacoima- f_p=2.1 Hz) yields larger displacements in relation to the higher frequency input motion (cascia- f_p=4.4 Hz). For the Newmark and Bray and Travasarou models this trend becomes more pronounced as the critical acceleration ratio increases whereas for the Rathje and Antonakos model this trend does not seem to be influenced by the critical acceleration ratio. Bray and Travasarou (2007) coupled model generally predicts larger displacements compared to conventional analytical Newmark rigid block and Rathje and Antonakos decoupled model. In particular, the difference in the displacement prediction is by far more noticeable for the flexible (Ts=0.16sec) compared to the nearly rigid (Ts=0.032sec) sliding masses. Displacements computed using Rathje and Antonakos (2011) predictive equations are more in line with the Newmark rigid block method. More specifically, the higher frequency input motion (cascia) yields displacements that match fairly well with the Newmark analytical rigid block approach (especially for the low level of shaking). On the contrary, the lower frequency input motion (pacoima) can predict larger or smaller displacements compared to the Newmark rigid block model depending on the ratio of k_y/k_{max} (or PGA).

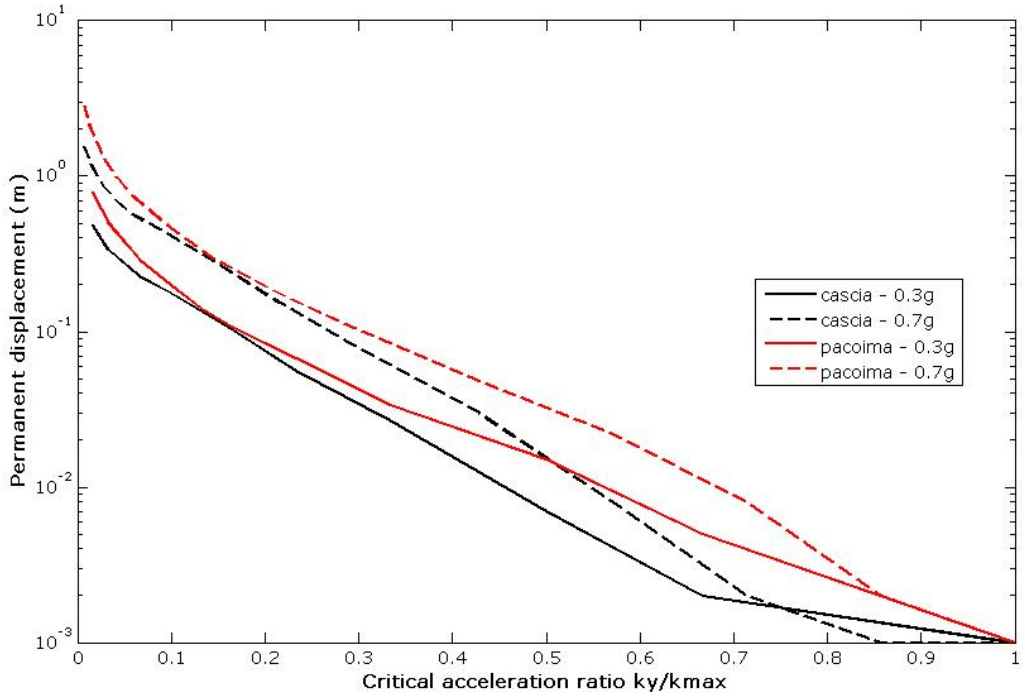


Figure 5.6. Newmark displacement versus critical acceleration ratio k_y/k_{max} for different acceleration time histories (cascia, pacoima) scaled at different levels of PGA (PGA=0.3g, 0.7g)

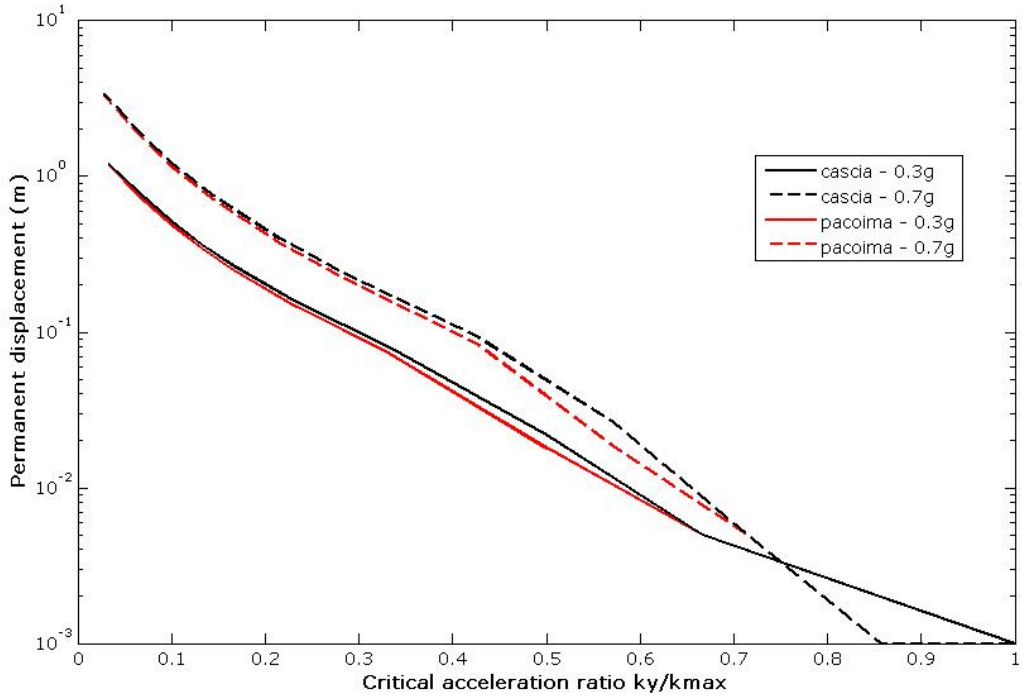


Figure 5.7. Bray and Travasarou (2007) displacement versus critical acceleration ratio k_y/k_{max} considering a nearly rigid sliding mass (T_s=0.032 sec) for different acceleration time histories (cascia, pacoima) scaled at different levels of PGA (PGA=0.3g, 0.7g)

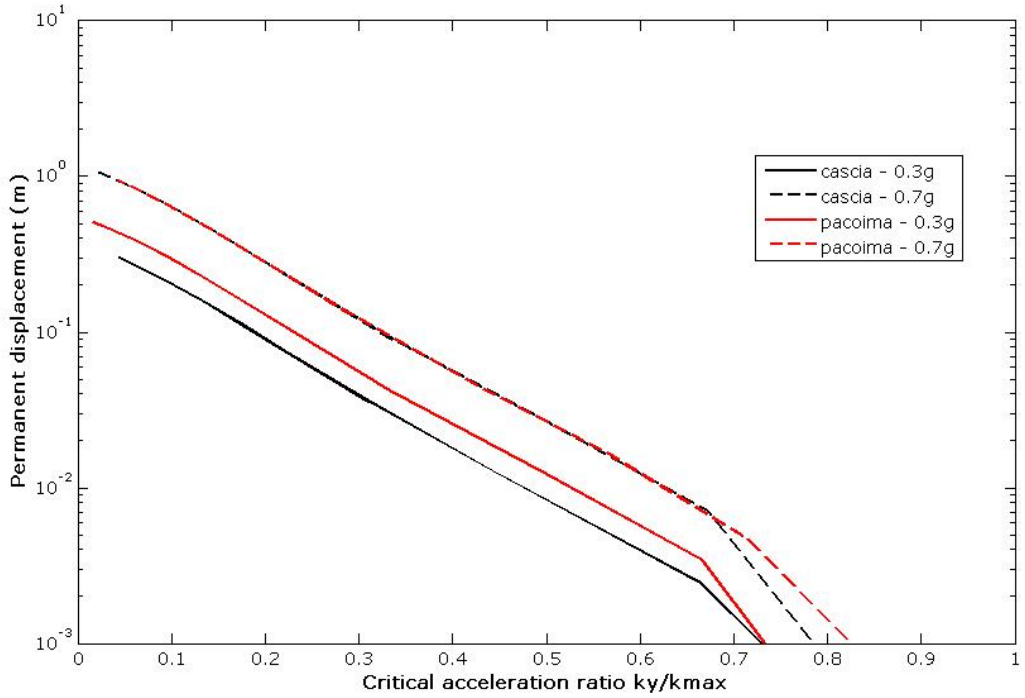


Figure 5.8. Rathje and Antonakos (2011) displacement versus critical acceleration ratio k_y/k_{max} considering a nearly rigid sliding mass (T_s=0.032 sec) for different acceleration time histories (cascia, pacoima) scaled at different levels of PGA (PGA=0.3g, 0.7g)

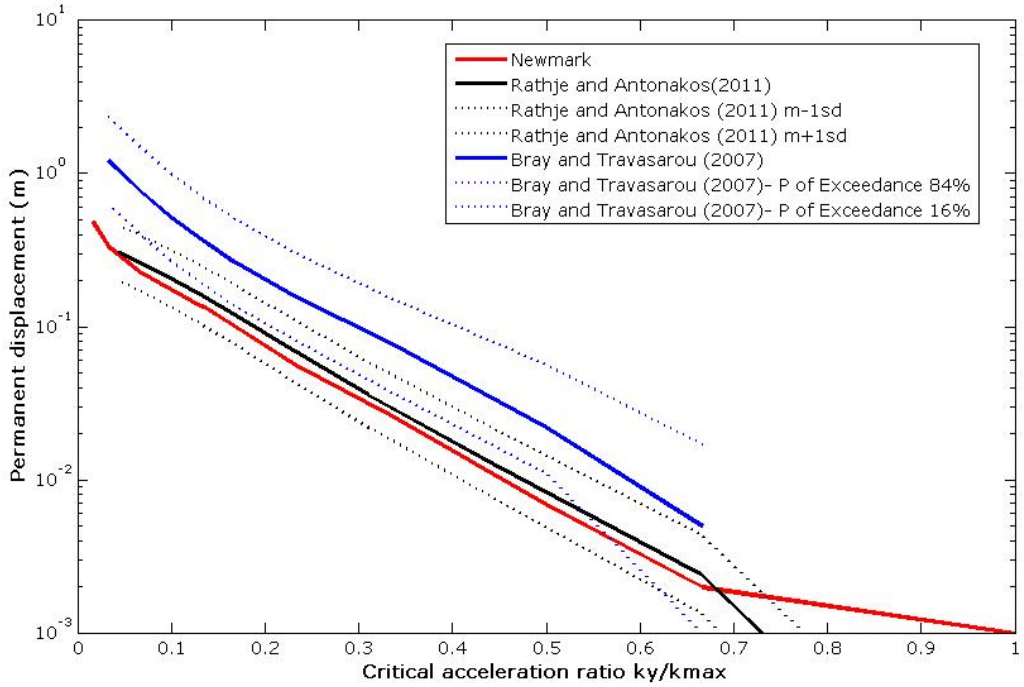


Figure 5.9. Comparison of the different predictive models for permanent slope displacement considering a nearly rigid sliding mass (T_s=0.032 sec) for a certain earthquake scenario (cascia scaled at 0.3g)

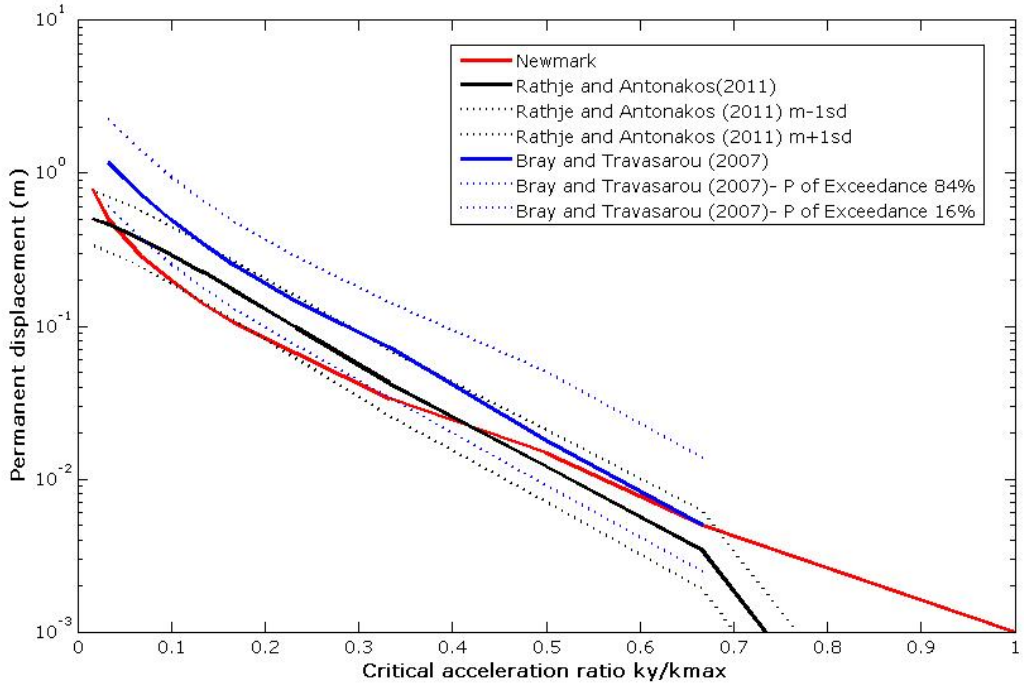


Figure 5.10. Comparison of the different predictive models for permanent slope displacement considering a nearly rigid sliding mass (T_s=0.032 sec) for a certain earthquake scenario (pacoima scaled at 0.3g)

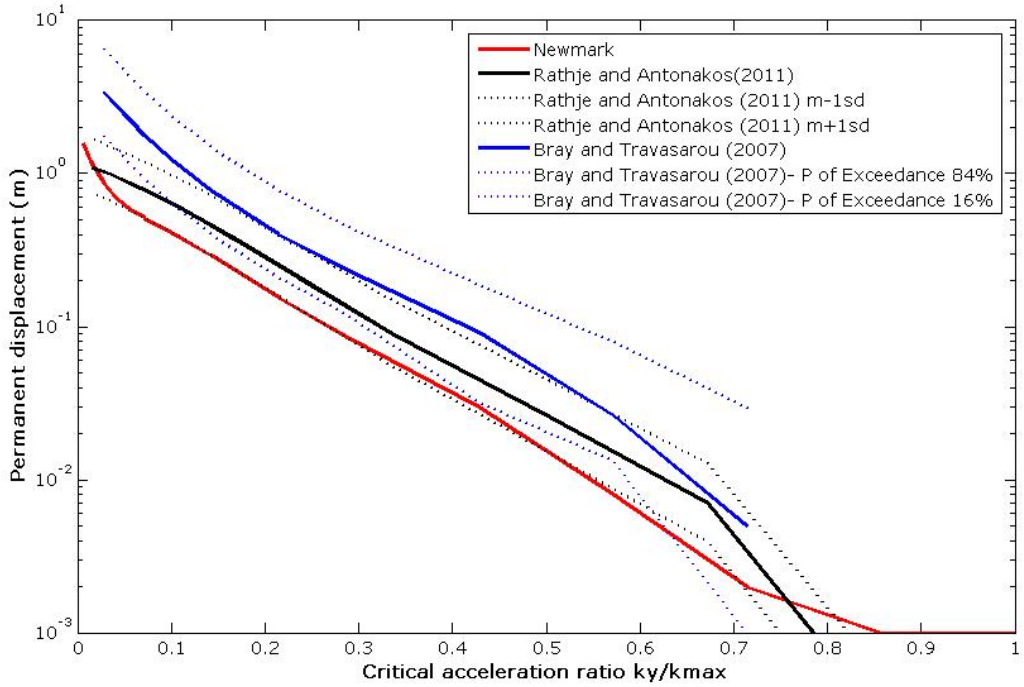


Figure 5.11. Comparison of the different predictive models for permanent slope displacement considering a nearly rigid sliding mass (T_s=0.032 sec) for a certain earthquake scenario (cascia scaled at 0.7g)

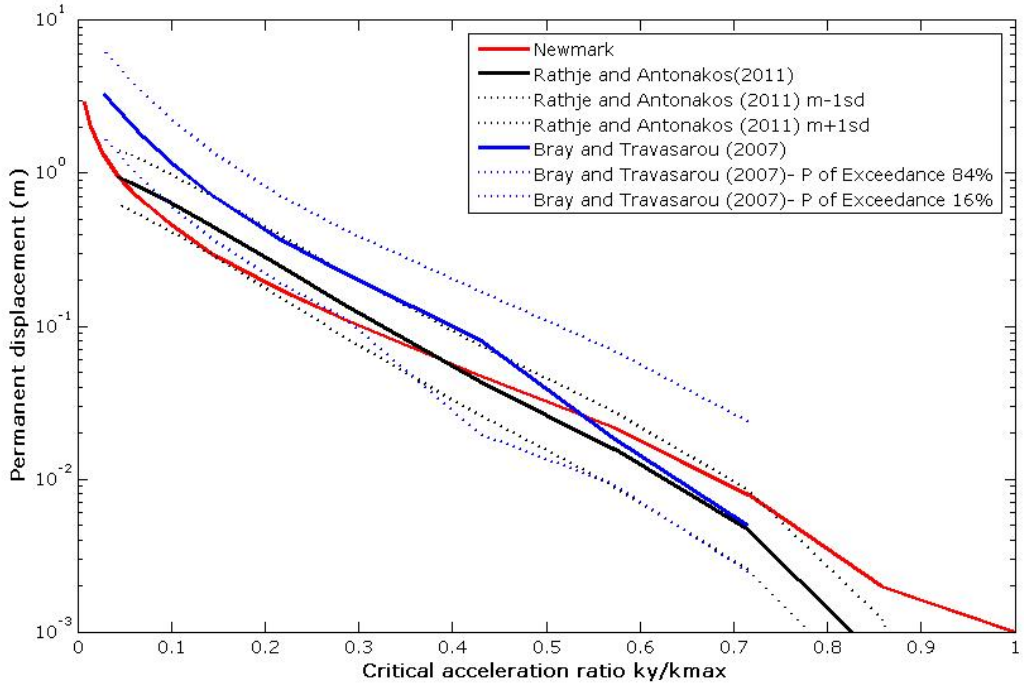


Figure 5.12. Comparison of the different predictive models for permanent slope displacement considering a nearly rigid sliding mass (Ts=0.032 sec) for a certain earthquake scenario (pacoima scaled at 0.7g)

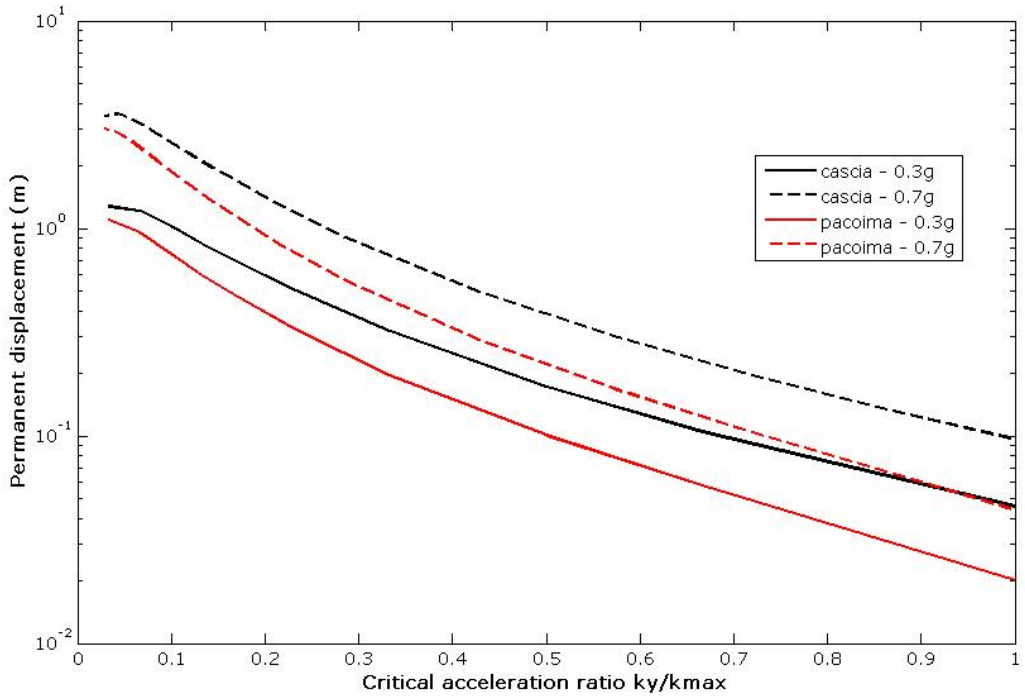


Figure 5.13. Bray and Travasarou (2007) displacement versus critical acceleration ratio k_y/k_{max} considering a deformable sliding mass (T_s=0.16 sec) for different acceleration time histories (cascia, pacoima) scaled at different levels of PGA (PGA=0.3g, 0.7g)

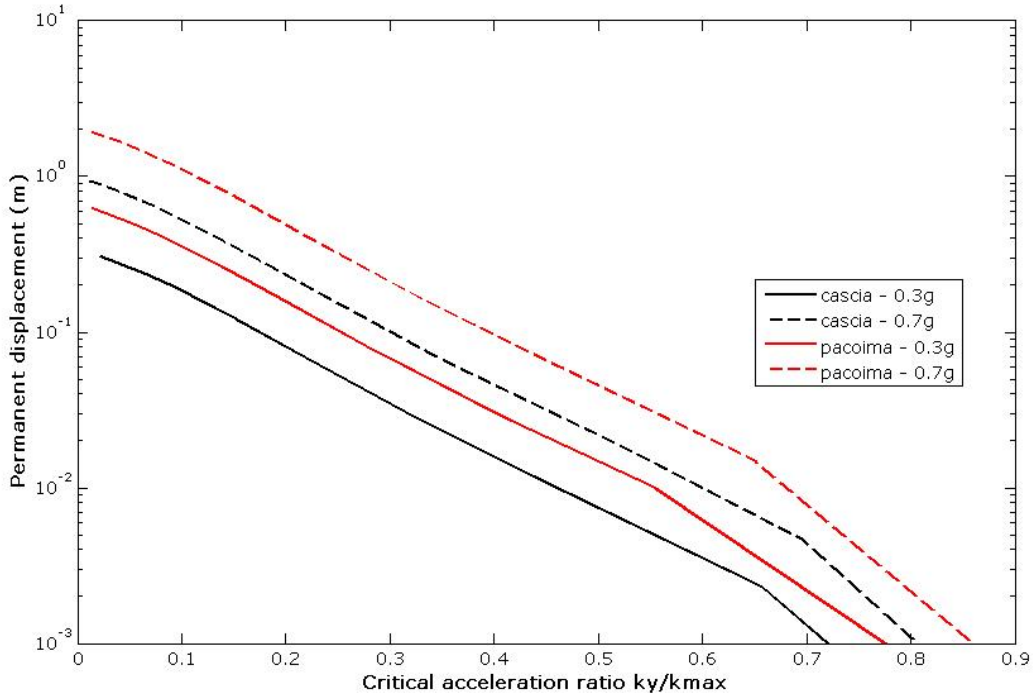


Figure 5.14. Rathje and Antonakos (2011) displacement versus critical acceleration ratio k_y/k_{max} considering a deformable sliding mass (T_s=0.16 sec) for different acceleration time histories (cascia, pacoima) scales at different levels of PGA (PGA=0.3g, 0.7g)

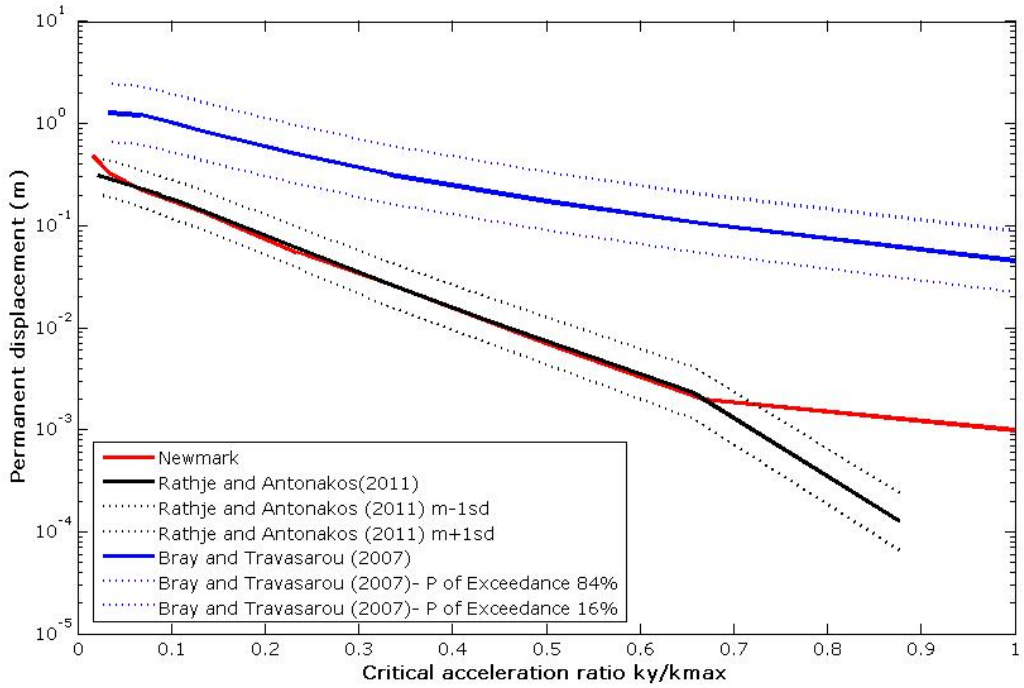


Figure 5.15. Comparison of the different predictive models for permanent slope displacement considering a deformable sliding mass (T_s=0.16 sec) for a certain earthquake scenario (cascia scaled at 0.3g)

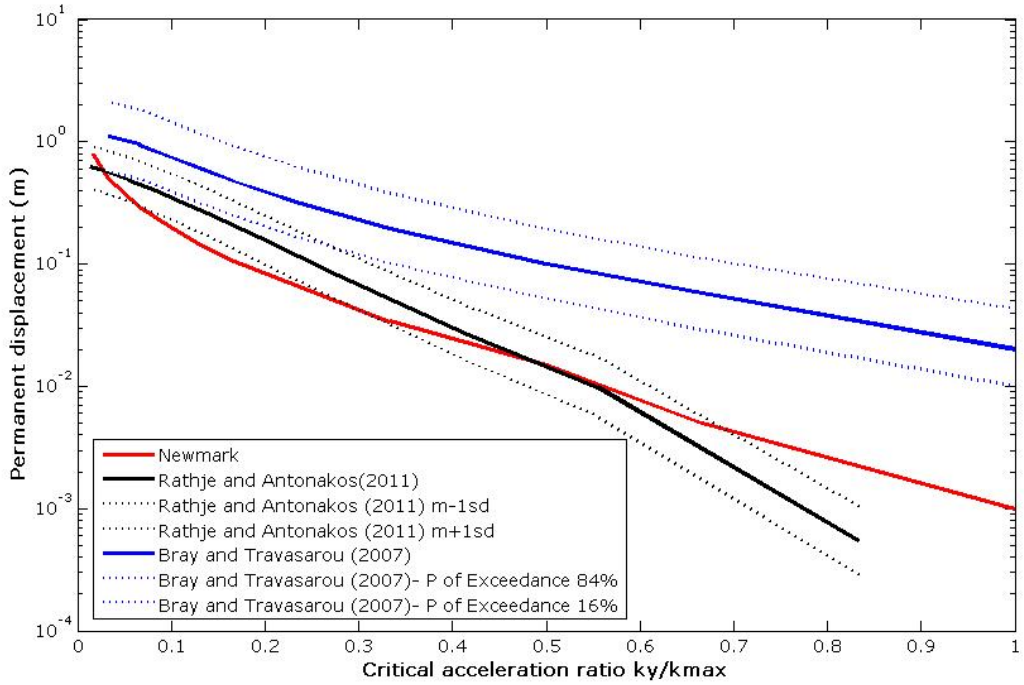


Figure 5.16. Comparison of the different predictive models for permanent slope displacement considering a deformable sliding mass (T_s=0.16 sec) for a certain earthquake scenario (pacoima scaled at 0.3g)

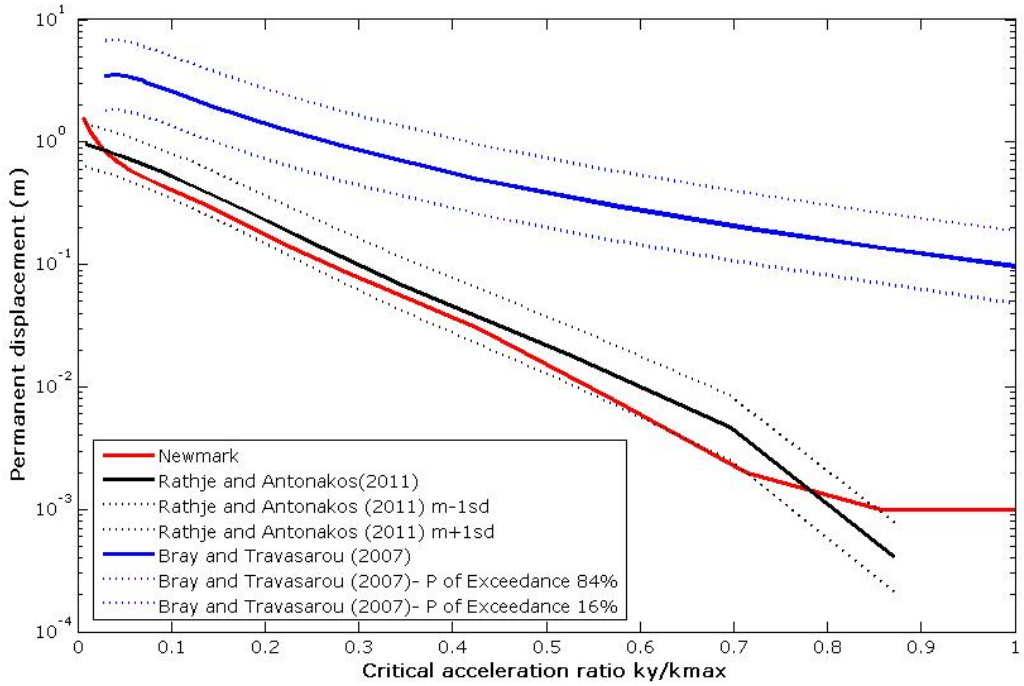


Figure 5.17. Comparison of the different predictive models for permanent slope displacement considering a deformable sliding mass (T_s=0.16 sec) for a certain earthquake scenario (cascia scaled at 0.7g)

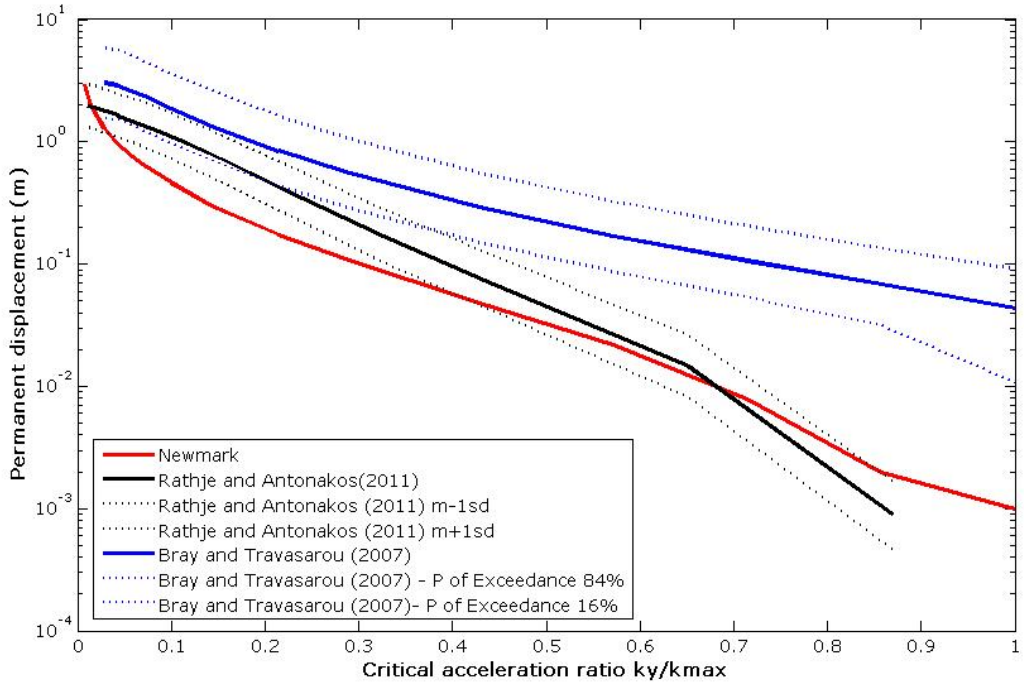


Figure 5.18. Comparison of the different predictive models for permanent slope displacement considering a deformable sliding mass (T_s=0.16 sec) for a certain earthquake scenario (Pacoima scaled at 0.7g)

5.2.3 Comparison of displacements estimated by displacement-based methods and dynamic analyses

In the previous section an application of the selected displacement based approaches was performed for different earthquake scenarios for both deformable and nearly rigid sliding surfaces highlighting prevailing trends in the displacement prediction.

In this section, 2 dimensional fully non-linear FLAC numerical results (see Chapter 4) are compared in terms of permanent horizontal displacement along the unstable slope area, with the Newmark-type displacement methods. The aim is, on the one hand, to gain confidence on the results of the numerical analysis and, on the other hand, to assess the predictive capability of the different displacement based approaches with respect to the FLAC dynamic analysis. As described above, the conventional analytical Newmark rigid block model (Newmark 1965), the decoupled Rathje and Antonakos (2011) model and the coupled Bray and Travasarou (2007) sliding block model are used for this purpose to calculate permanent displacements of the slide mass. These are compared with the FLAC permanent horizontal displacements within the sliding mass derived from the dynamic analysis for the free-field conditions (in the absence of any structure) for the two idealized step-like slopes analyzed in Chapter 4 (see Fig. 5.19), which characterized by sand and clayey soil materials respectively that overlay a stiff clayey layer. The elastic bedrock lies at 70 m. The mechanical characteristics for the soil materials and elastic bedrock have been presented in Chapter 4, Table 4.1. Details regarding the numerical modeling and the computed permanent FLAC displacements have already been discussed in Chapter 4 and will not be repeated herein.

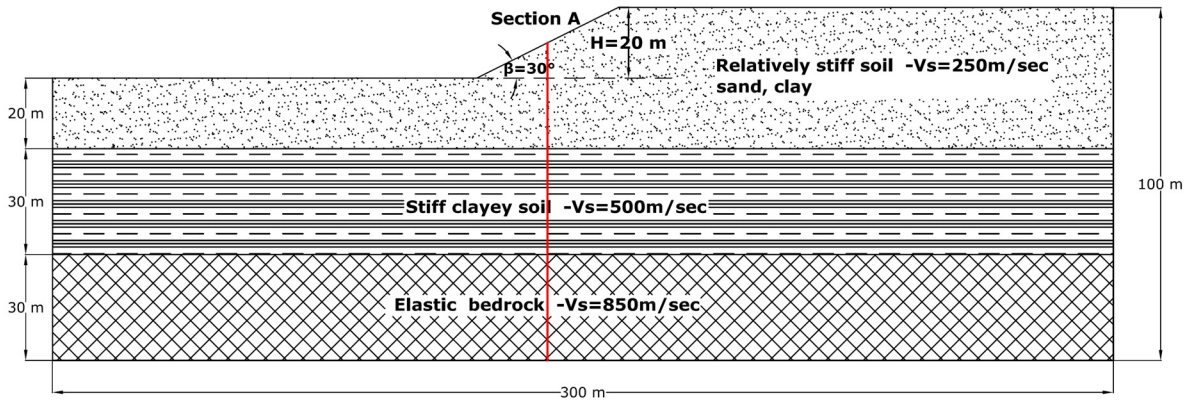


Figure 5.19. Slope configuration used for the numerical modeling

The initial fundamental period of the sliding mass (T_s) has been estimated using the simplified expression: $T_s = 4H/V_s$, where H is the height and V_s is the shear wave velocity

of the potential sliding mass. Different heights of the landslide mass have been evaluated for slopes consisting of sand (H=2 m) and clay material (H=10 m) by means of a LEM pseudostatic analysis based on the more critical sliding surfaces.

The horizontal yield coefficient, k_y, has been computed via a pseudostatic slope stability analysis using Spencer method of slides (Spencer, 1967) that satisfied full equilibrium. The k_y values are estimated as 0.16 and 0.15 for the 30^o inclined slopes consisting of sand and clay soil material respectively.

The seismic input applied along the base of the dynamic model consists of a set of 7 real acceleration time histories from different earthquakes worldwide recorded on rock outcrop (see Chapter 4, Tab. 4.4). Two of them (Valnerina –Cascia_L, Northridge - Pacoima Dam_L) have also been used in the previous section to predict permanent slope deformation using different Newmark-type displacement methods. To obtain the appropriate inputs for the Newmark-type displacement based methods that include the effect of soil conditions, the selected acceleration time histories were first propagated up to the depth of the potential sliding surface through a 1D non-linear site response analysis considering the same soil properties as in the 2D dynamic analysis. It is noticed that the 1D soil profile is located at the section that approximately corresponds to the maximum slide mass thickness of the slope (Section A, see Fig. 5.19). The bottom of the sliding surface is taken be consistent to the estimated fundamental period of the sliding mass (T_s) that is different for the clay and sand slopes. It's worth noting that the thickness of the landslide mass may also vary with respect to the characteristics of the earthquake and the level of shaking. This effect, however, was not taken into account and thus only average predictions of the cumulative co-seismic displacement can be made.

Tables 5.2 and 5.5 present the computed parameters of the models for outcropping accelerograms scaled at PGA_{rock}=0.7g for the sand (T_s=0.032sec) and clay (T_s=0.16sec) slopes respectively. Tables 5.3 and 5.6 present the predicted FLAC horizontal displacements in comparison to those calculated using the conventional analytical Newmark rigid block method, Rathje and Antonakos (2011) decoupled approach and Bray and Travasarou (2007) coupled stick-slip displacement method for rock outcropping accelerograms scaled at PGA=0.7g for the hypothesized sand (T_s=0.032 sec) and clay (T_s=0.16 sec) slopes. The error (%) of the Newmark-type models in the displacement estimation compared to the corresponding FLAC displacement calculation for input accelerograms scaled at PGA=0.7g are presented in Table 5.4 for sand nearly rigid sliding mass (T_s=0.032 sec) and in Table 5.7 for clay deformable sliding mass (T_s=0.16 sec). Relative error (%) of the models in the median displacement estimation as well as the corresponding average error (%) to the FLAC displacement calculation are depicted in

Figures 5.20 and 5.21 for the sand and in Figures 5.24 and 5.25 for the clay slope respectively. The dispersion of the corresponding error is presented in Figures 5.22 and 5.26 for the sand and clay slope respectively. Finally, Figures 5.23 and 5.27 show a direct comparison between analytical Newmark's , Bray and Travasarou (2007) and Rathje and Antonakos (2011) displacements with the maximum horizontal displacements from the 2D dynamic analyses for rock outcropping accelerograms scaled at different levels of PGA (0.3, 0.5, 0.7, 0.9 g) for sand and clay slopes.

Table 5.2. Parameters of the models for rock outcropping accelerograms scaled at PGA=0.7g-sand slope (T_s=0.032sec)

Earthquake code	PGA_{rock} (g)	PGA sliding surface (g)	PGV sliding surface (cm/sec)	T_m (sec)	T_s/T_m	k_{max} (g) (Eq. 5.3)	k-vel_{max} (cm/sec) (Eq. 5.4)	$S_a(1.5T_s)$ (g)
cascia	0.70	0.89	61.70	0.42	0.08	0.89	61.70	0.96
kypseli	0.70	0.91	70.60	0.45	0.07	0.91	70.60	1.00
montenegro	0.70	0.75	66.30	0.49	0.07	0.75	66.30	0.81
pacoima	0.70	0.86	72.60	0.56	0.06	0.86	72.60	0.93
sturno	0.70	1.04	91.70	0.55	0.06	1.04	91.70	1.12
duzce	0.70	0.84	60.20	0.41	0.08	0.84	60.20	0.94
gilroy	0.70	0.81	52.10	0.36	0.09	0.81	52.10	0.93

Table 5.3. Comparison of FLAC horizontal displacements to analytical Newmark rigid block method, Rathje and Antonakos (2010) decoupled approach and Bray and Travasarou (2007) coupled stick-slip displacement method for rock outcropping accelerograms scaled at PGA=0.7g sand slope (T_s=0.032sec)

Earthquake code	FLAC horizontal displacement (m)	Average Newmark displacement (m)	Rathje and Antonakos displacement (m)			Bray and Travasarou displacement (m)		
			Median $D_{flexible}$	Median -1sd (m)	Median +1sd (m)	Median (m)	84^{th} percentile (m)	16^{th} percentile (m)
cascia	0.60	0.64	0.40	0.62	0.25	0.60	0.31	1.16
kypseli	0.50	0.55	0.50	0.78	0.32	0.65	0.34	1.25
montenegro	0.90	0.70	0.37	0.59	0.24	0.42	0.22	0.81
pacoima	0.70	0.53	0.49	0.78	0.31	0.57	0.29	1.09
sturno	1.70	1.38	0.83	1.29	0.53	0.81	0.42	1.55
duzce	1.10	0.94	0.36	0.57	0.23	0.57	0.30	1.10
gilroy	0.20	0.23	0.28	0.44	0.18	0.57	0.29	1.09

Table 5.4. Error (%) of the models in the displacement estimation compared to the corresponding FLAC displacement calculation for rock outcropping accelerograms scaled at PGA=0.7g- sand slope (T_s=0.032sec)

Earthquake code	Error (%)						
	Newmark (m)	Rathje and Antonakos (2011)			Bray and Travasarou (2007)		
		Median $D_{flexible}$	Median -1sd (m)	Median +1sd (m)	Median (m)	84th percentile (m)	16th percentile (m)
cascia	7.25	-34.10	3.48	-58.03	0.25	-48.00	93.26
kypseli	10.60	0.02	56.82	-36.21	29.65	-32.75	149.93
montenegro	-22.56	-58.46	-34.17	-73.78	-53.24	-75.75	-9.85
pacoima	-24.00	-29.57	10.80	-55.23	-19.28	-58.13	55.62
sturno	-18.85	-51.44	-24.33	-68.84	-52.56	-75.39	-8.55
duzce	-14.95	-67.03	-48.09	-79.06	-48.26	-73.16	-0.26
gilroy	14.00	39.39	119.94	-11.67	182.89	46.74	445.35

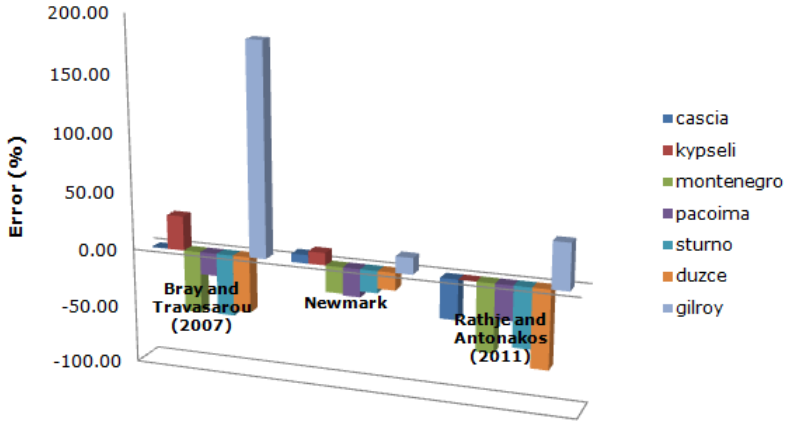


Figure 5.20. Error (%) of the predictive models in the median displacement estimation compared to the corresponding FLAC displacement calculation for rock outcropping accelerograms scaled at PGA=0.7g- sand slope (T_s=0.032sec)

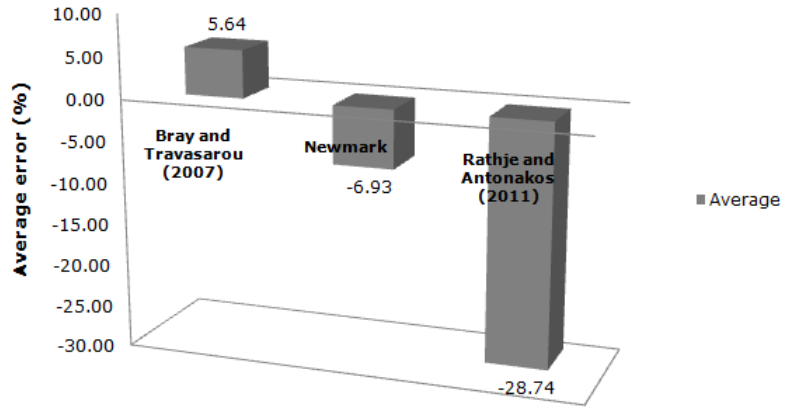


Figure 5.21. Average error (%) of the predictive models in the median displacement estimation compared to the corresponding FLAC displacement calculation for rock outcropping accelerograms scaled at PGA=0.7g- sand slope (T_s=0.032sec)

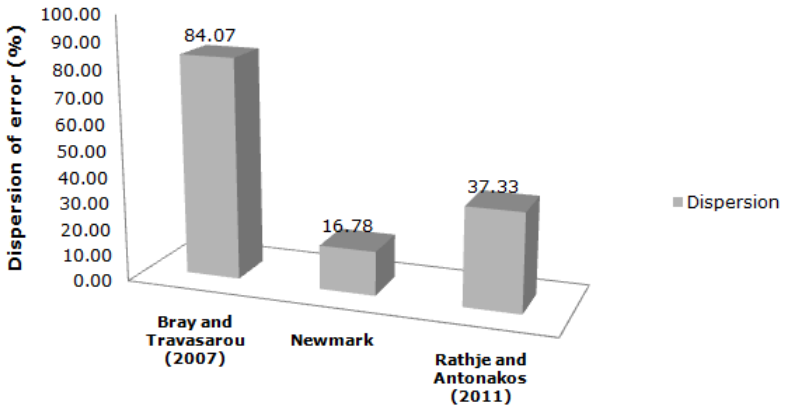
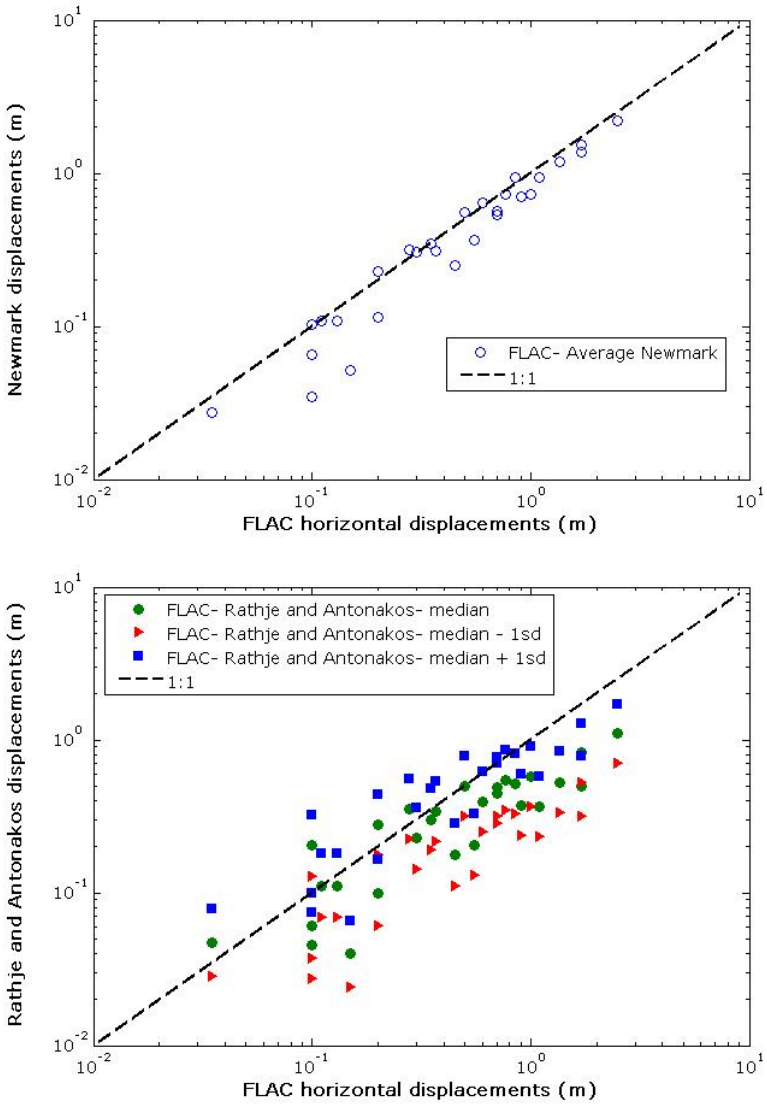


Figure 5.22. Dispersion of the error (%) of the predictive models in the median displacement estimation in relation to the corresponding FLAC results for rock outcropping accelerograms scaled at PGA=0.7g- sand slope (T_s=0.032sec)



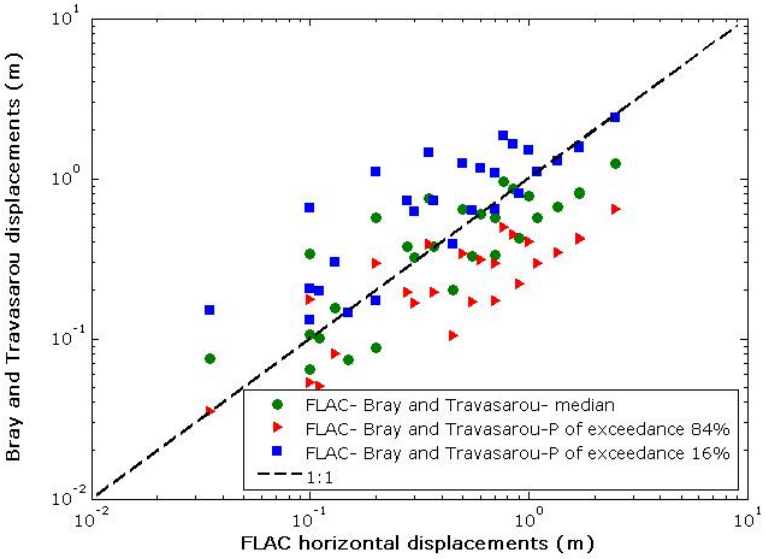


Figure 5.23. Comparison between analytical Newmark's, Rathje and Antonakos (2011) and Bray and Travasarou (2007) displacements with the co-seismic horizontal displacements from the 2D dynamic analyses (sand slope)

Table 5.5. Parameters of the models for rock outcropping accelerograms scaled at PGA=0.7g- clay slope (T_s=0.16sec)

Earthquake code	PGA_{rock} (g)	PGA sliding surface (g)	PGV sliding surface (cm/sec)	T_m (sec)	T_s/T_m	k_{max} (g) (Eq. 5.3)	k-vel_{max} (cm/sec) (Eq. 5.4)	$S_a(1.5T_s)$ (g)
cascia	0.70	0.57	24.90	0.50	0.32	0.44	54.67	1.27
kypseli	0.70	0.57	34.00	0.53	0.30	0.43	50.93	1.22
montenegro	0.70	0.63	24.30	0.58	0.28	0.43	58.12	1.45
pacoima	0.70	0.62	31.90	0.63	0.25	0.41	68.95	1.53
sturno	0.70	0.69	38.50	0.68	0.23	0.41	82.33	1.44
duzce	0.70	0.58	22.70	0.49	0.33	0.45	54.59	1.90
gilroy	0.70	0.47	20.70	0.45	0.35	0.44	37.43	1.24

Table 5.6. Comparison of FLAC horizontal displacements to analytical Newmark rigid block method, Rathje and Antonakos (2011) decoupled approach and Bray and Travasarou (2007) coupled stick-slip displacement method for rock outcropping accelerograms scaled at PGA=0.7g- clay slope (T_s=0.16sec)

Earthquake code	FLAC horizontal displacement (m)	Average Newmark displacement (m)	Rathje and Antonakos displacement (m)			Bray and Travasarou displacement (m)		
			Median $D_{flexible}$	Median -1sd (m)	Median +1sd (m)	Median (m)	84^{th} percentile (m)	16^{th} percentile (m)
cascia	0.50	0.36	0.16	0.27	0.10	0.57	0.30	1.11
kypseli	0.45	0.28	0.14	0.23	0.08	0.53	0.27	1.02
montenegro	0.82	0.47	0.16	0.27	0.10	0.72	0.37	1.39
pacoima	0.62	0.35	0.19	0.32	0.12	0.79	0.41	1.53
sturno	1.40	0.90	0.25	0.42	0.15	0.71	0.37	1.37
duzce	0.85	0.48	0.16	0.27	0.10	1.16	0.60	2.24
gilroy	0.20	0.09	0.09	0.15	0.05	0.55	0.28	1.05

Table 5.7. Error (%) of the models in the displacement estimation compared to the corresponding FLAC displacement calculation for rock outcropping accelerograms scaled at PGA=0.7g- clay slope (T_s=0.16sec)

Earthquake code	Error (%)						
	Newmark (m)	Rathje and Antonakos (2011)			Bray and Travasarou (2007)		
		Median $D_{flexible}$	Median -1sd (m)	Median +1sd (m)	Median (m)	84th percentile (m)	16th percentile (m)
cascia	-27.30	-67.52	-46.66	-80.22	14.80	-40.45	121.31
kypseli	-37.22	-69.14	-49.21	-81.25	17.23	-39.19	126.00
montenegro	-43.23	-80.03	-67.08	-87.89	-11.96	-54.33	69.72
pacoima	-43.55	-68.69	-48.15	-81.10	28.10	-33.55	146.95
sturno	-35.68	-81.90	-70.01	-89.07	-49.07	-73.58	-1.83
duzce	-43.65	-80.61	-68.17	-88.18	36.53	-29.17	163.20
gilroy	-53.00	-55.76	-27.28	-73.09	173.31	41.78	426.86

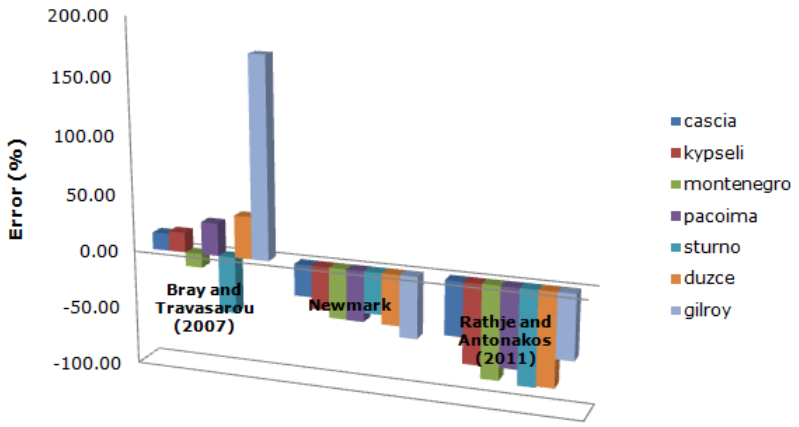


Figure 5.24. Error (%) of the models in the median displacement estimation compared to the corresponding FLAC displacement calculation for rock outcropping accelerograms scaled at PGA=0.7g- clay slope (T_s=0.16sec)

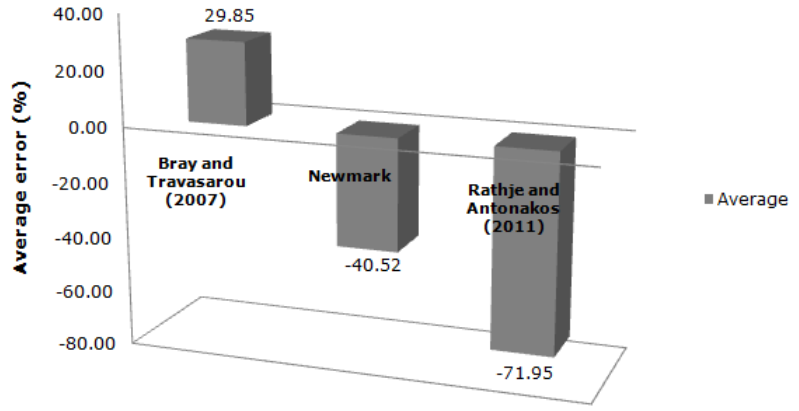


Figure 5.25. Average error (%) of the predictive models in the median displacement estimation compared to the corresponding FLAC displacement calculation for rock outcropping accelerograms scaled at PGA=0.7g- clay slope (T_s=0.16sec)

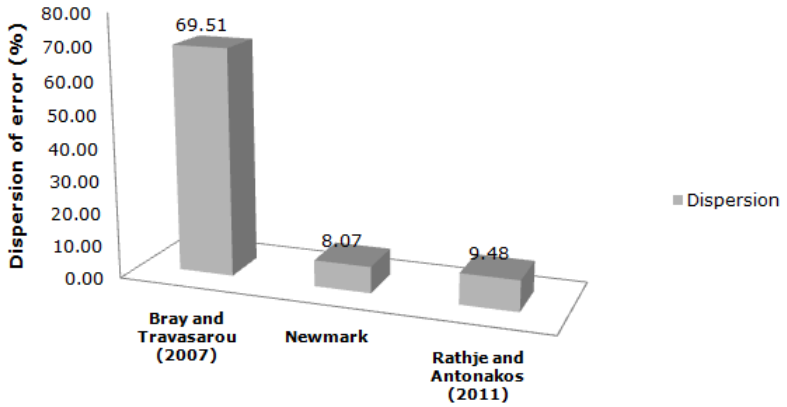
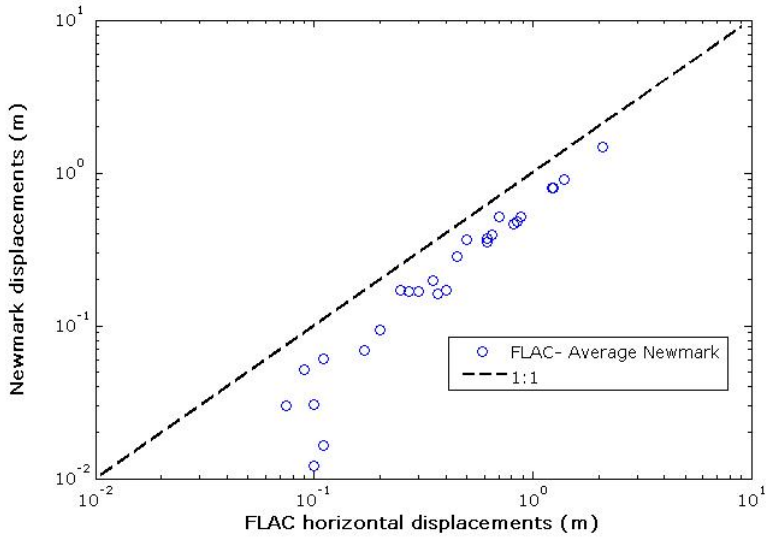
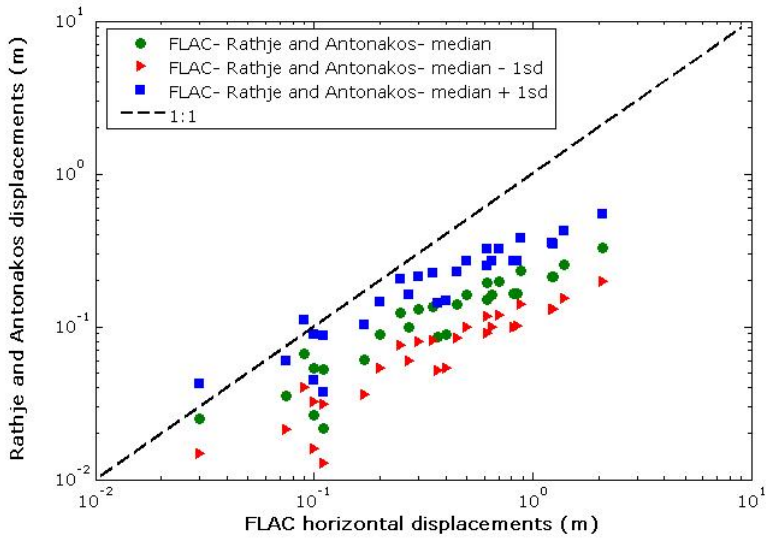


Figure 5.26. Dispersion of the error (%) of the predictive models in the median displacement estimation in relation to the corresponding FLAC results for rock outcropping accelerograms scaled at PGA=0.7g- clay slope (T_s=0.16sec)





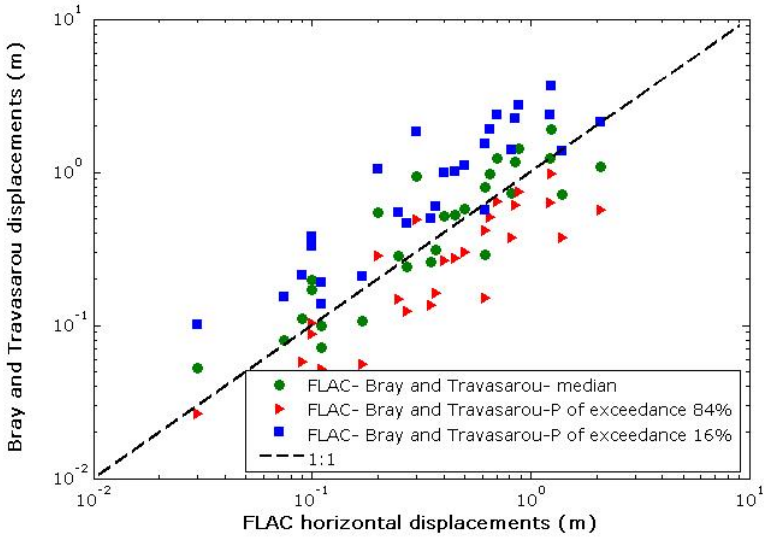


Figure 5.27. Comparison between analytical Newmark's, Rathje and Antonakos (2011) and Bray and Travasarou (2007) displacements with the co-seismic horizontal displacements from the 2D dynamic analyses (clay slope)

5.2.3.1. Discussion- Concluding remarks

FLAC displacements generally are not inconsistent with the predicted Newmark-type displacements enhancing the reliability and robustness of the dynamic analysis results. All three displacement based models predict displacements that are generally in good agreement with the FLAC results for the sand stiff slope case. On the contrary, for the clay more flexible slope the correlation is not so good. In particular, Bray and Travasarou (2007) model tend to predict generally larger displacements with respect to the dynamic analysis whereas Newmark rigid block and Rathje and Antonakos (2011) models underpredict the corresponding displacements.

Among the three methods, Bray and Travasarou model was found to present the minimum average predictive error (%) in relation to the dynamic analysis for both sand nearly rigid and clay relatively flexible slope cases. This is in line with the inherent coupled stick-slip assumption adopted in the method that offers a conceptual improvement over the rigid block and decoupled approaches for modeling the physical mechanism of earthquake-induced landslide deformation.

Newmark analytical approach shows the minimum dispersion (minimum standard deviation of the error in the displacement prediction) compared to the Bray and Travasarou and Rathje and Antonakos models. This may be justified by the fact that Newmark analytical method uses the entire time history to characterize the seismic loading as opposed to the Bray and Travasarou and Rathje and Antonakos models that use one [$S_a(1.5\ T_s)$] and two (PGA, PGV) intensity parameters respectively. As such,

uncertainties associated to the selection of the ground motion intensity parameters disappear in the Newmark conventional analytical approach.

Overall, the differences in the displacement prediction between the models are larger for the more ductile clay slope. Thus, the compliance of the failure surface in relation to the frequency content of the input earthquake scenarios allows for some bias to be introduced on the results.

Summarizing, Newmark-type displacement methods display a valuable compromise between simplistic pseudostatic approaches and sophisticated numerical modeling techniques in providing a rough estimate of the seismic slope performance. They can be efficiently implemented in the prediction of earthquake induced landslide displacements for regional seismic hazard analysis (e.g. Jibson et al., 2000). However, as shown in this study, their use in site specific problems should be made with caution, acknowledging the simplified assumptions associated with them. In any case, a stochastic framework to account for the (generally large) uncertainty in the displacement prediction is recommended.

CHAPTER 6

Fragility curves for low-rise RC buildings subjected to slow-moving slides

6.1 Introduction

The present chapter, stemming from the general lack of existing fragility curves for buildings subjected to slow-moving slides (see Chapter 3), aspires to propose different sets of fragility functions for a variety of RC building typologies, soil conditions and slope configurations, based on the analytical method described in Chapter 4, with potential application from site specific to local/regional scales.

To this aim, an extensive parametric study is performed by considering different idealized slope geometries, soil geological settings and distances of the structure to the slope's crest. The effect of the various analyzed features on the structural performance is investigated, highlighting trends on the building's behavior to the permanent co-seismic slope deformations. Generic fragility curves as a function of PGA at the outcrop and PGD at the slope area that could be used for several practical applications are then suggested based on the parameters that are proved to most significantly contribute to the structure's vulnerability. Moreover, a sensitivity analysis is conducted to stress the influential role of various additional parameters, namely the water table level, the consideration of a strain softening landslide material, the flexibility of the foundation system, the number of bays and storeys of the building and the code design level on the structure's fragility. Some of these parameters may, under certain circumstances, control the structural response to the permanent landslide displacement.

6.2 General description of the parametric investigation

In order to construct an abacus of fragility curves applicable to various RC building typologies, soil conditions and slope configurations, an extensive parametric investigation is performed based on the method proposed in Chapter 4. The main parameters selected to vary are associated to:

- The geometry of the finite slope (slope height H, inclination β) (Fig. 6.1).
  - Slope height H=20, 40 m
  - Slope inclination θ =f (Soil properties) = 15°, 30°, 45°
- The soil properties of the slope material (soft to stiff clayey and sand soils corresponding to soil categories B, C and D according to EC8)
- The relative position of the building with respect to the slope crest (L=3, 5 m) (Fig. 6.1).

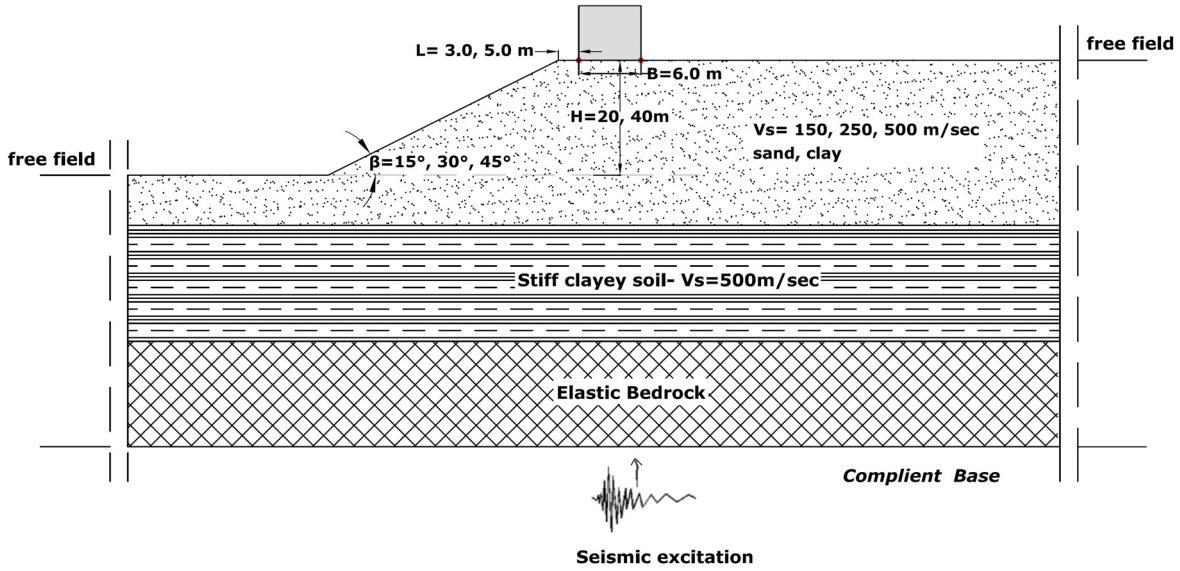


Figure 6.1. Parametric model under study

Six simplified –yet realistic- step-like slope configurations are considered for the present study. For each geometry, 4 different models are developed that vary on the soil conditions (sand, clay) and the relative location of the assumed building to the slope crest (L=3, 5 m) (see Annex A for the corresponding sketches). Table 6.1 presents the considered features of the 24 analyzed models.

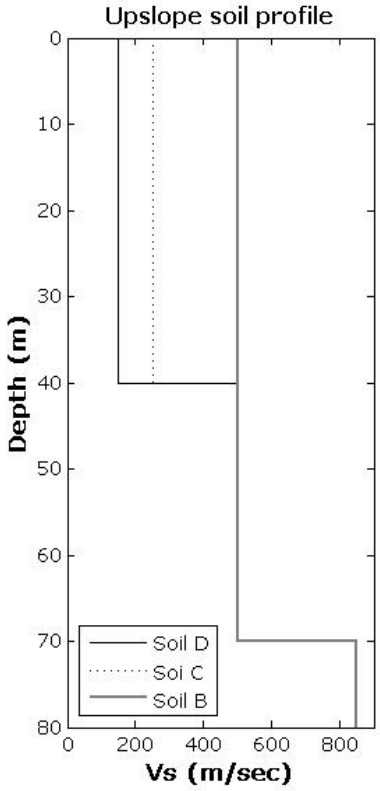
It is noticed that the first two models have already been analyzed in Chapter 4 to demonstrate the proposed methodological framework for the vulnerability assessment of the representative RC buildings to earthquake induced slow moving slides. It is also important to note that the soil properties of the slope materials are taken to be consistent with the considered inclination angles to ensure static slope stability. Thus, it doesn't make any sense to analyze steep slopes with soft soil as the slope would be already unstable in static conditions. Finally, it's worth noting that only the cases that result to the highest susceptibility to landsliding are modeled. For instance, slopes with small inclination (β=15°) on stiff soil are not investigated as the resulting permanent

deformation and consequently the building expected damage would be negligible and thus out of the scope of this study.

Figure 6.2 shows the considered upslope and downslope variation of shear wave velocity V_s with depth whereas Table 6.2 presents the assumed properties for the soil materials and the elastic bedrock. As thoroughly presented in Chapter 4, the numerical analysis is based on an uncoupled approach and involves two consecutive steps. First, the differential permanent displacements at the building's foundation level are estimated using a plane strain FLAC2D (Itasca 2008) finite difference non-linear dynamic slope model considering the foundation compliance. The seismic input applied along the base of the dynamic model consists of a suite of 7 real acceleration time histories from different earthquakes worldwide recorded on rock outcropping conditions and scaled at different level of PGA i.e. 0.3 g, 0.5g, 0.7g and 0.9g (see Chapter 4, §4.3.1). Some additional analyses for lower levels of PGA (e.g. 0.1 g) were deemed necessary for certain models (e.g. model 21) in order to obtain reliable results for all damage states. Then, the calculated differential displacements are imposed to the Seismostruct (Seismosoft, SeismoStruct 2011) building model at the foundation level to assess the building's response for the different applied landslide displacements induced by the earthquake. A high code designed single bay-single storey structure with flexible foundation system located in the vicinity of the slope's crest (L=3, 5 m) is considered in all analyzed cases herein. Its geometrical, strength and stiffness characteristics are identical to the ones of the structure on isolated footings described in Chapter 4, §4.3.2. Limit states are defined in terms of threshold values of steel and concrete material strain for both "low" and "high" code designed RC buildings (see Chapter 4, § 4.4.1). The results are presented in terms of fragility curves as a function of PGA at the outcrop or PGD at the slope area. Two different methodologies to derive the log-normally distributed parameters of the fragility functions are presented in Chapter 4, § 4.4.2. These have been found to yield results that are generally in good agreement and as such they can be equally implemented to construct the fragility curves.

It 's worth noting that the computational demand for the derivation of fragility curves is very large. Analysis time for the 24 models subjected to the two-step numerical approach is about 1000 hours on a fast PC (Intel Core i7-2600 CPU, 3.4 GHz, 4.0 GByte of RAM) at the time of the current study.

(a)



(b)

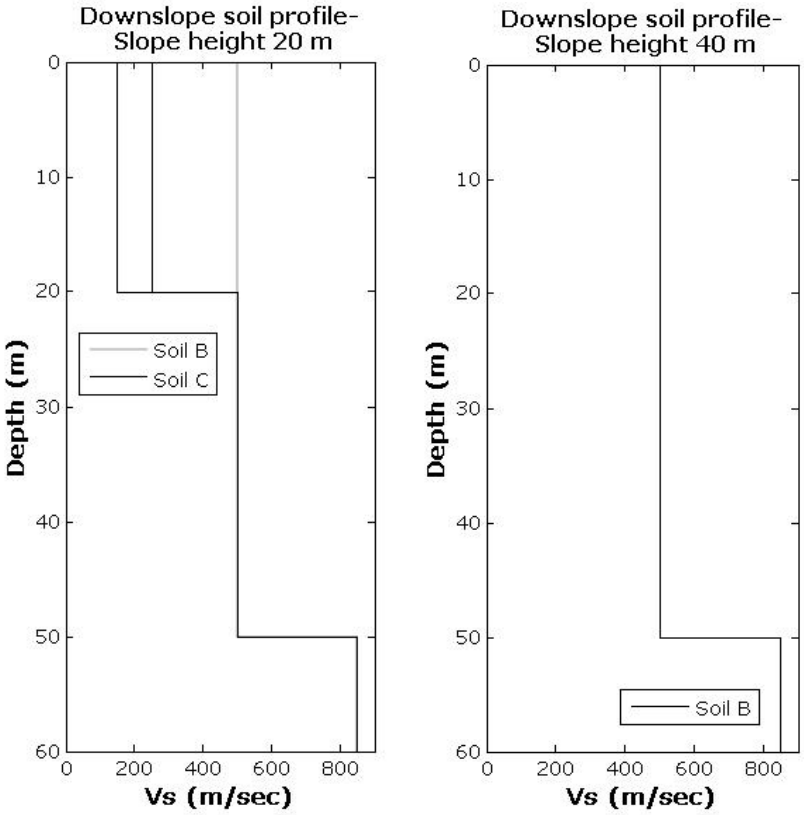


Figure 6.2. Upslope (a) and downslope (b) V_s variation with depth for the analyzed soil profiles (soil classification according to EC8)

6.2.1 Derivation of fragility curves

The parametric analysis results to the construction of fragility curves (Figure 6.3) as a function of PGA at the outcrop and PGD at the slope area for the different investigated models presented in Table 6.1. The Maximum Likelihood method as described in Chapter 4, section 4.4.2.2 is used herein to estimate the log-normal parameters (median and log-standard deviation) of the fragility relationships. Tables 6.3 and 6.4 present the derived median and log-standard deviation for all the analyzed models when using PGA at the outcrop and PGD at the slope area as a metric of the landslide intensity respectively.

The fragility curves presented below can be used to assess the vulnerability of low-rise, "high-code" RC buildings on isolated footings subjected to seismically induced slow moving slides for a variety of slope configurations and site conditions. Similar curves, generally associated with a more rapid transition from slight damage to collapse could be derived for "low-code" RC frame structures (see section 6.3.5 and Annex B).

It is noted that PGD refers to the response of the landslide to cyclic loading (and not to the initial triggering force) that is then correlated to differential permanent displacement at the foundation level and to structural distortion and damage. Thus, the derived curves as a function of PGD at the slope area, although initially developed to deal with earthquake induced landslide displacements, they can also be implemented to buildings impacted by non-earthquake related slow-moving slides.

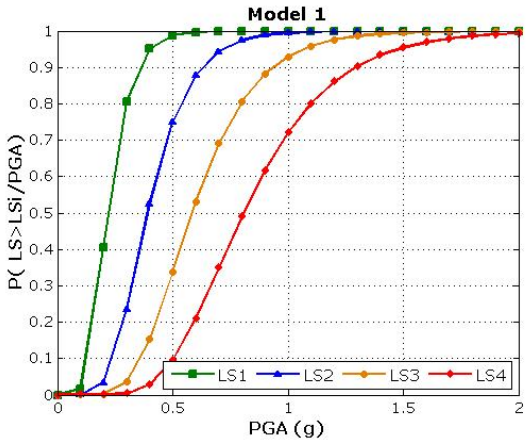
It is seen that the structure's vulnerability may vary significantly with respect to the various considered features. A first comparison is facilitated by looking at just the medians of the various analyzed models. Thus, among the analyzed cases, models 23 and 21 would suffer the highest vulnerability whereas models 20 and 18 would sustain the lowest vulnerability measured in terms of expected median values of PGA and PGD respectively. The estimated β-values that represent the dispersion of the results are found to vary from 0.25 to 0.56 and from 0.36 to 0.94 when considering PGA and PGD respectively as an intensity parameter. To better illustrate the influential role of each parameter to the building's expected damage level several comparative plots of fragility functions are presented in the following subsections.

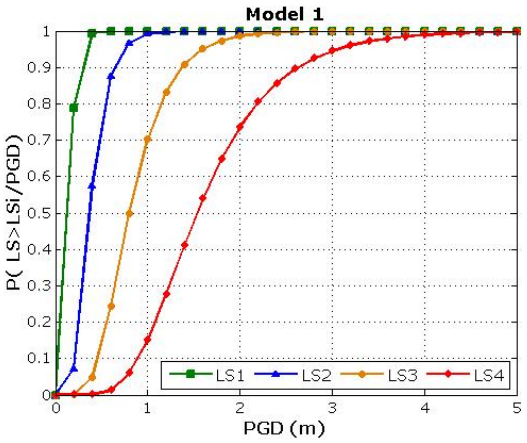
Table 6.1. Model features for the parametric analysis

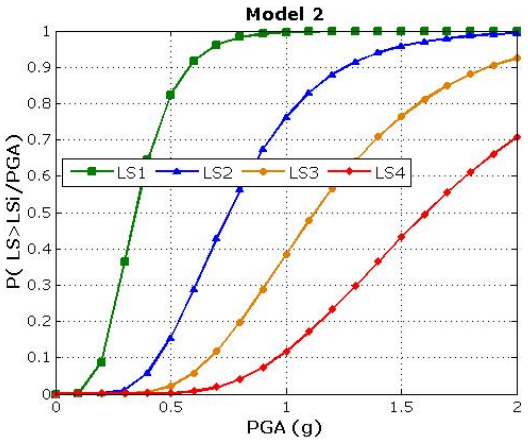
Geometry	model	Slope inclination β (degrees)	Slope height H (m)	$V_{s,30}$ (m/sec)	Soil	Distance from the crest L (m)
Geometry 1	model 1	30	20	250	medium dense sand	3
	model 2	30	20	250	relatively stiff clay	3
	model 3	30	20	250	medium dense sand	5
	model 4	30	20	250	relatively stiff clay	5
Geometry 2	model 5	30	40	250	medium dense sand	3
	model 6	30	40	250	relatively stiff clay	3
	model 7	30	40	250	medium dense sand	5
	model 8	30	40	250	relatively stiff clay	5
Geometry 3	model 9	15	20	150	loose sand	3
	model 10	15	20	150	soft clay	3
	model 11	15	20	150	loose sand	5
	model 12	15	20	150	soft clay	5
Geometry 4	model 13	15	40	150	loose sand	3
	model 14	15	40	150	soft clay	3
	model 15	15	40	150	loose sand	5
	model 16	15	40	150	soft clay	5
Geometry 5	model 17	45	20	500	dense sand	3
	model 18	45	20	500	stiff clay	3
	model 19	45	20	500	dense sand	5
	model 20	45	20	500	stiff clay	5
Geometry 6	model 21	45	40	500	dense sand	3
	model 22	45	40	500	stiff clay	3
	model 23	45	40	500	dense sand	5
	model 24	45	40	500	stiff clay	5

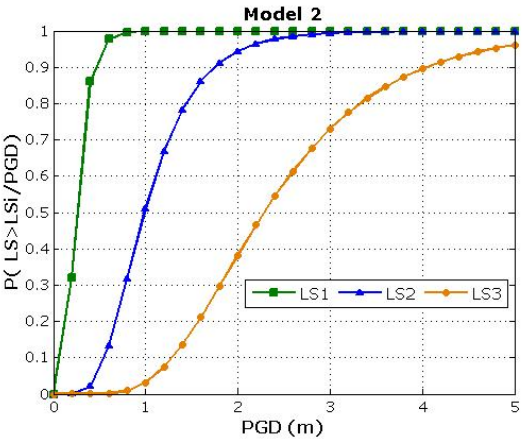
Table 6.2. Varying soil properties of the analyzed slope configurations

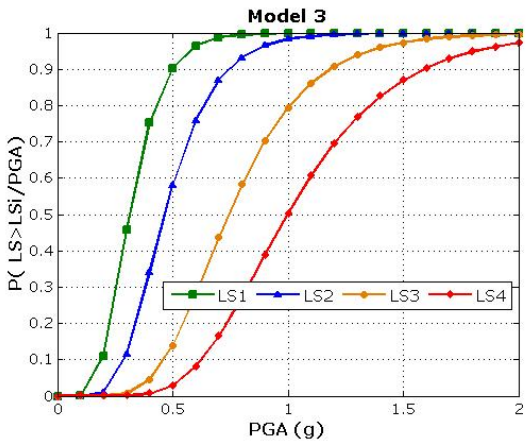
	Elastic bedrock	**Stiff soil**		**Relatively stiff soil**		**Soft soil**	
		sand	**clay**	**sand**	**clay**	**sand**	**clay**
Constitutive model	Elastic	Mohr Coulomb	Mohr Coulomb	Mohr Coulomb	Mohr Coulomb	Mohr Coulomb	Mohr Coulomb
Dry density (kg/m^3)	2300	2000	2000	1800	1800	1700	1700
Young's modulus (KPa)	$4.321 \cdot 10^6$	$1.300 \cdot 10^6$	$1.300 \cdot 10^6$	$2.925 \cdot 10^5$	$2.925 \cdot 10^5$	$9.945 \cdot 10^4$	$9.945 \cdot 10^4$
Poisson's ratio	0.3	0.3	0.3	0.3	0.3	0.3	0.3
Drained Bulk modulus K (KPa)	$3.600 \cdot 10^6$	$1.0833 \cdot 10^6$	$1.083 \cdot 10^6$	$2.438 \cdot 10^5$	$2.438 \cdot 10^5$	$8.288 \cdot 10^4$	$8.288 \cdot 10^4$
Shear modulus G (KPa)	$1.662 \cdot 10^6$	$5.0000 \cdot 10^5$	$5.000 \cdot 10^5$	$1.125 \cdot 10^5$	$1.125 \cdot 10^5$	$3.825 \cdot 10^4$	$3.825 \cdot 10^4$
Cohesion c (KPa)	-	10	50	0	10	0	5
Friction angle φ (degrees)	-	44	27	36	25	25	15
Hydraulic conductivity (m·sec^{-1})	$5 \cdot 10^{-07}$	$1 \cdot 10^{-05}$	$1 \cdot 10^{-07}$	$1 \cdot 10^{-05}$	$1 \cdot 10^{-07}$	$1 \cdot 10^{-05}$	$1 \cdot 10^{-07}$
P-wave velocity V_p (m/sec)	1590.20	935.41	935.41	467.71	467.71	280.62	280.62
Shear wave velocity V_s (m/sec)	850.00	500.00	500.00	250.00	250.00	150.00	150.00
Max. allowed zone size (m)	8.50	5.00	5.00	2.50	2.50	1.50	1.50
Max. Allowed frequency	10.00	10.00	10.00	10.00	10.00	10.00	10.00

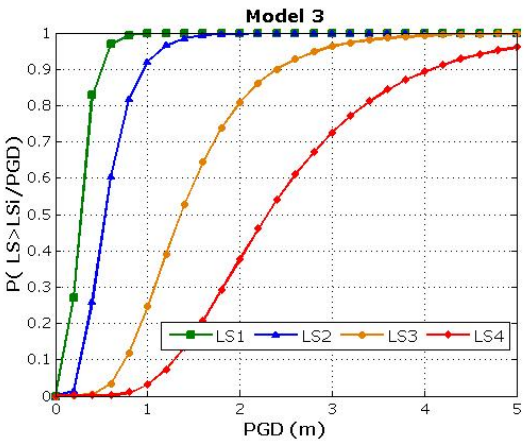

Model 1
P(LS>LSi/PGA)
PGA (g)
LS1
LS2
LS3
LS4

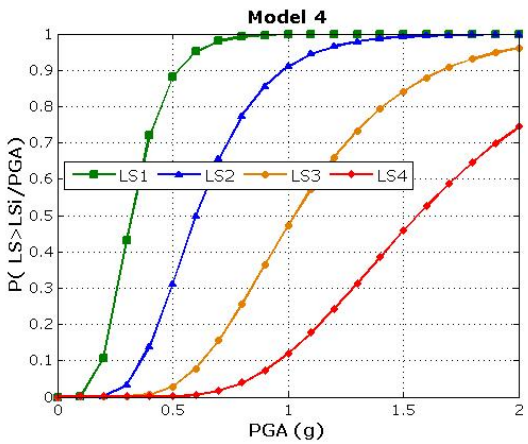

Model 1
P(LS>LSi/PGD)
PGD (m)
LS1
LS2
LS3
LS4

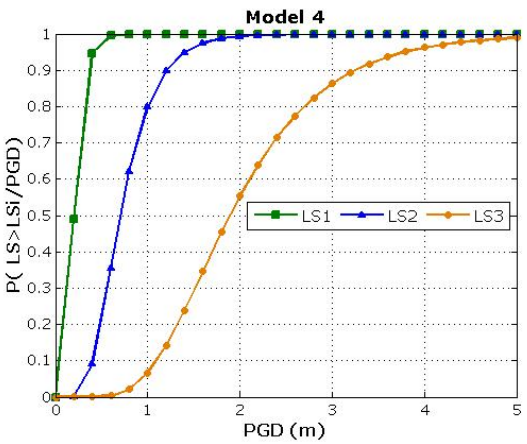

Model 2
P(LS>LSi/PGA)
PGA (g)
LS1
LS2
LS3
LS4

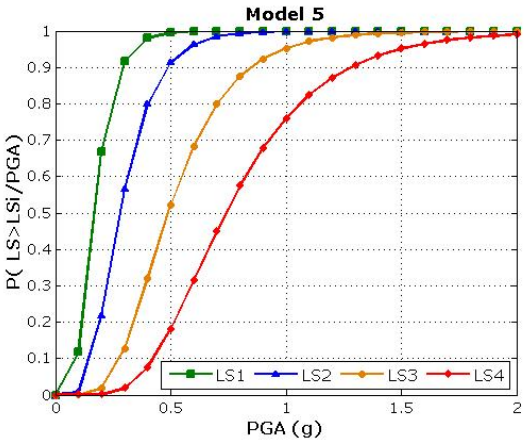

Model 2
P(LS>LSi/PGD)
PGD (m)
LS1
LS2
LS3

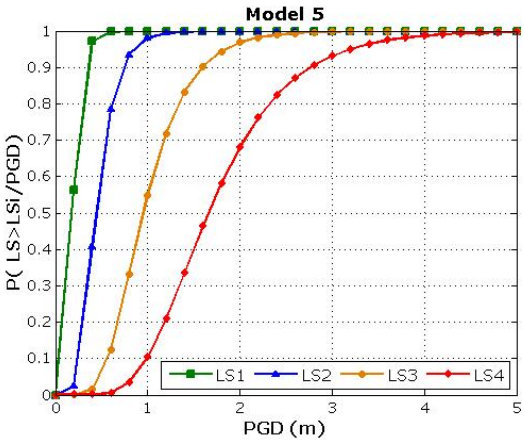

Model 3
P(LS>LSi/PGA)
PGA (g)
LS1
LS2
LS3
LS4

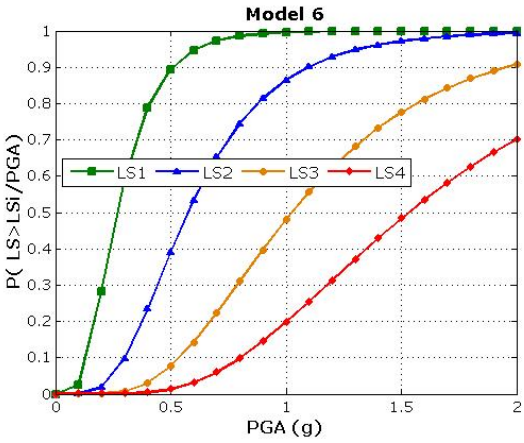

Model 3
P(LS>LSi/PGD)
PGD (m)
LS1
LS2
LS3
LS4

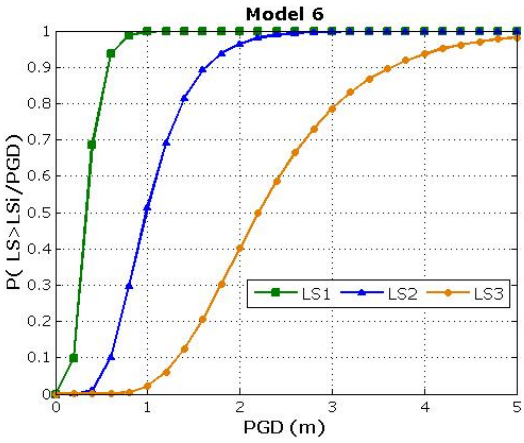

Model 4
P(LS>LSi/PGA)
PGA (g)
LS1
LS2
LS3
LS4

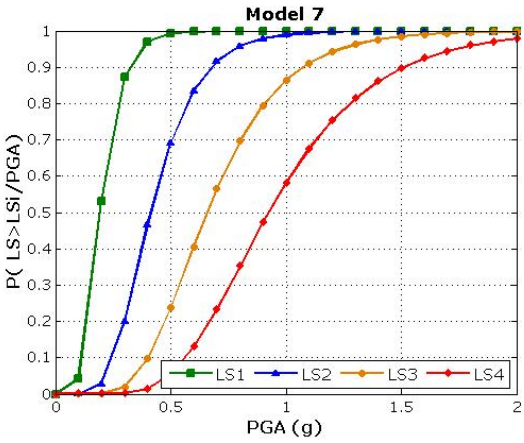

Model 4
P(LS>LSi/PGD)
PGD (m)
LS1
LS2
LS3

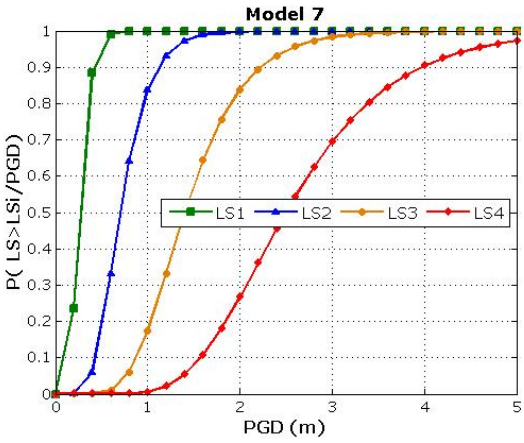

Model 5
P(LS>LSi/PGA)
PGA (g)
LS1
LS2
LS3
LS4

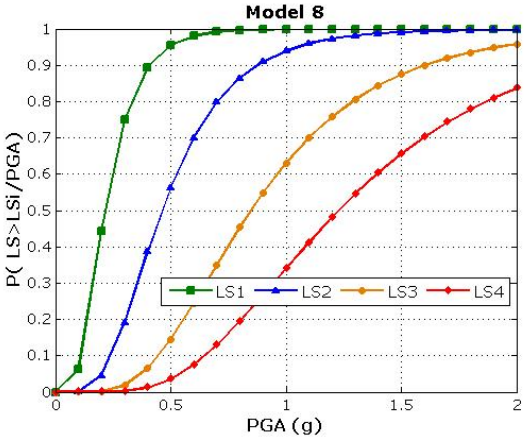

Model 5
P(LS>LSi/PGD)
PGD (m)
LS1
LS2
LS3
LS4

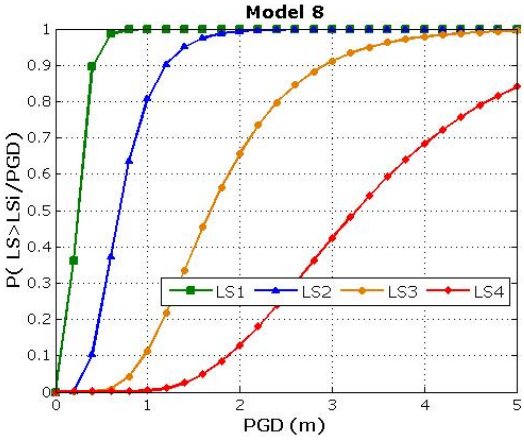

Model 6
P(LS>LSi/PGA)
PGA (g)
LS1
LS2
LS3
LS4

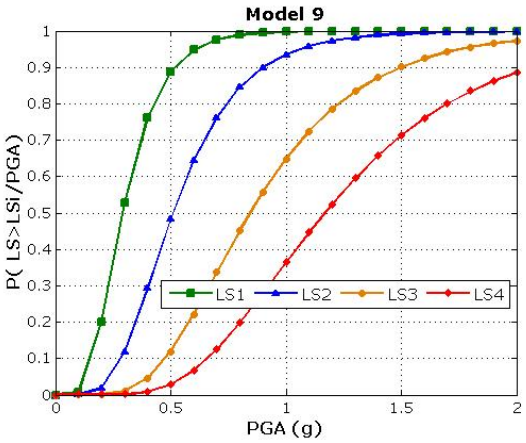

Model 6
P(LS>LSi/PGD)
PGD (m)
LS1
LS2
LS3

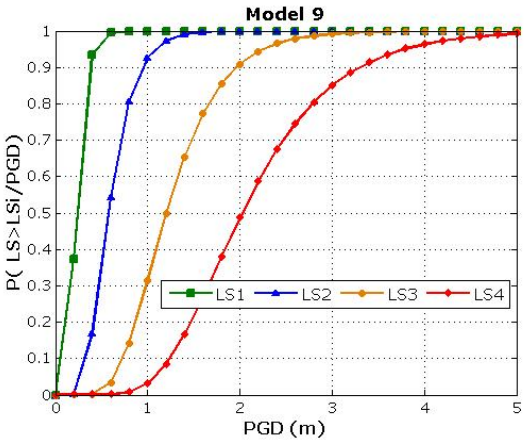

Model 7
P(LS>LSi/PGA)
PGA (g)
LS1
LS2
LS3
LS4

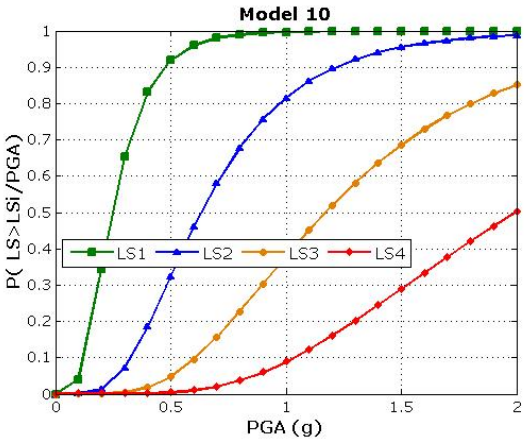

Model 7
P(LS>LSi/PGD)
PGD (m)
LS1
LS2
LS3
LS4

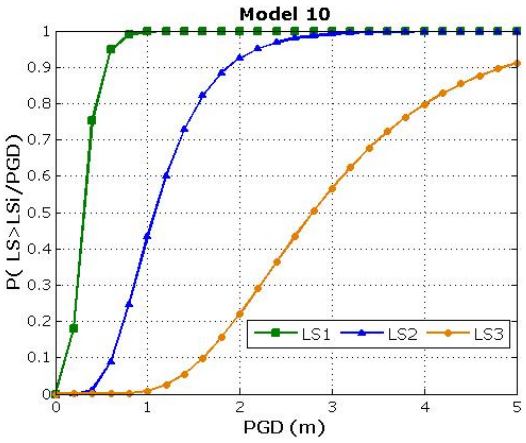

Model 8
P(LS>LSi/PGA)
PGA (g)
LS1
LS2
LS3
LS4

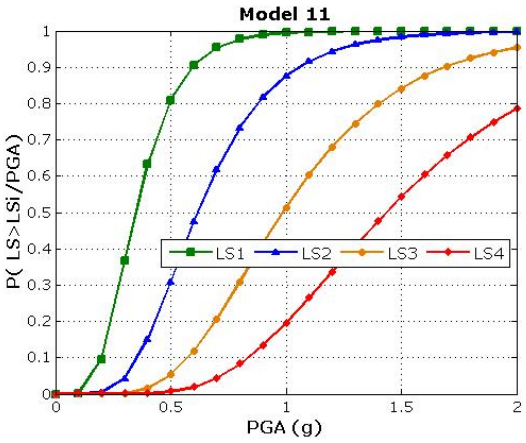

Model 8
P(LS>LSi/PGD)
PGD (m)
LS1
LS2
LS3
LS4

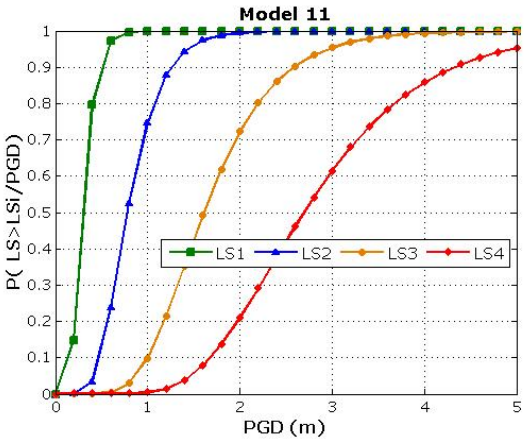

Model 9
P(LS>LSi/PGA)
PGA (g)
LS1
LS2
LS3
LS4

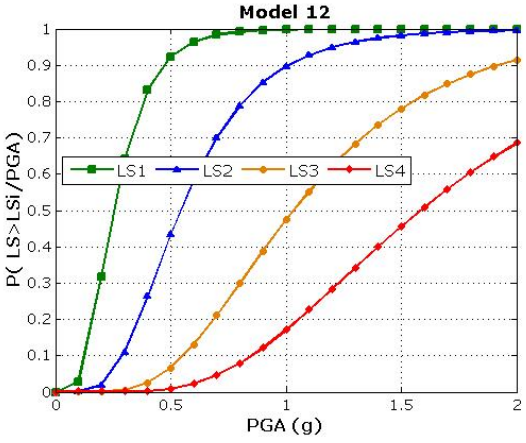

Model 9
P(LS>LSi/PGD)
PGD (m)
LS1
LS2
LS3
LS4

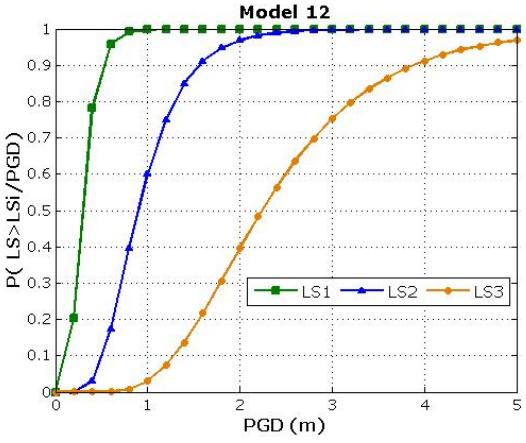

Model 10
P(LS>LSi/PGA)
PGA (g)
LS1
LS2
LS3
LS4

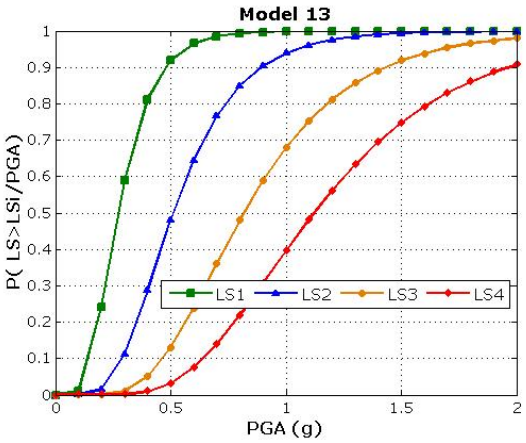

Model 10
P(LS>LSi/PGD)
PGD (m)
LS1
LS2
LS3

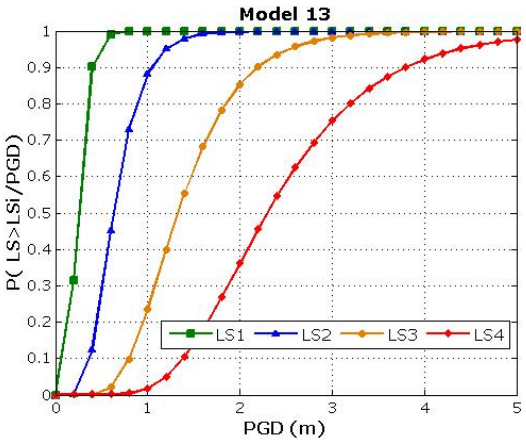

Model 11
P(LS>LSi/PGA)
PGA (g)
LS1
LS2
LS3
LS4

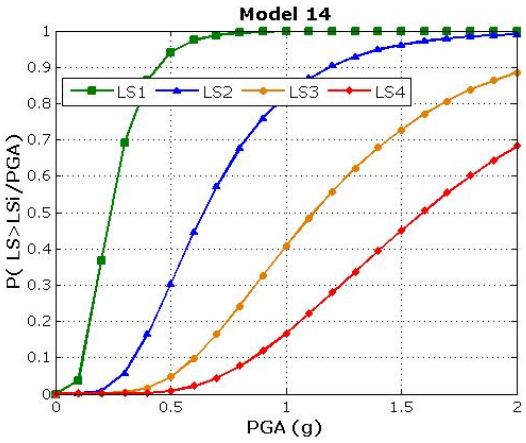

Model 11
P(LS>LSi/PGD)
PGD (m)
LS1
LS2
LS3
LS4

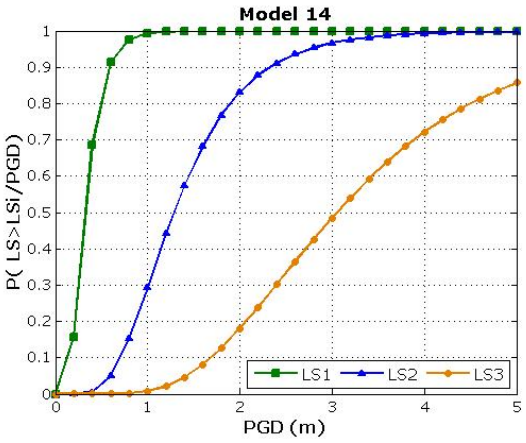

Model 12
P(LS>LSi/PGA)
PGA (g)
LS1
LS2
LS3
LS4

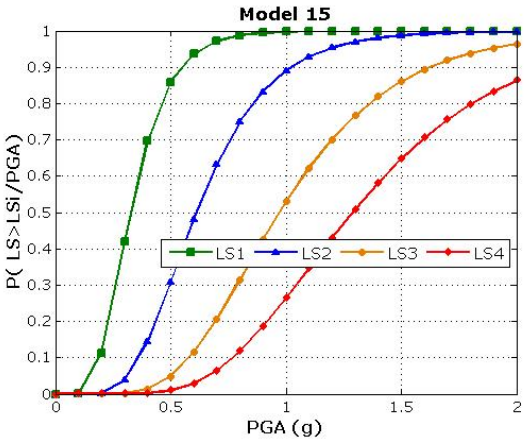

Model 12
P(LS>LSi/PGD)
PGD (m)
LS1
LS2
LS3

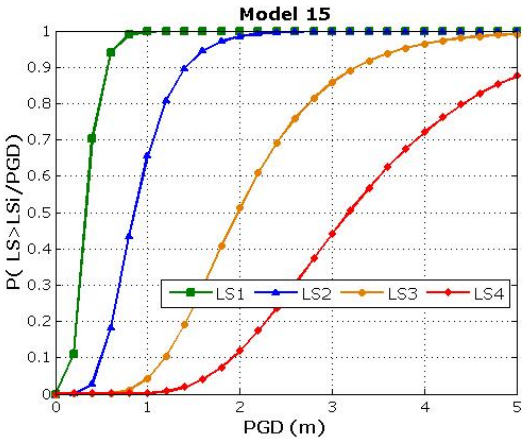

Model 13
P(LS>LSi/PGA)
PGA (g)
LS1
LS2
LS3
LS4

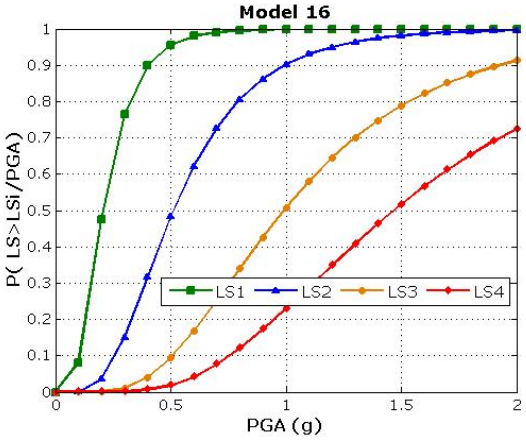

Model 13
P(LS>LSi/PGD)
PGD (m)
LS1
LS2
LS3
LS4

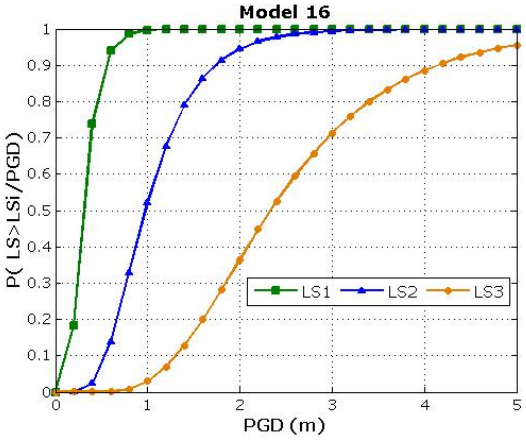

Model 14
P(LS>LSi/PGA)
PGA (g)
LS1
LS2
LS3
LS4

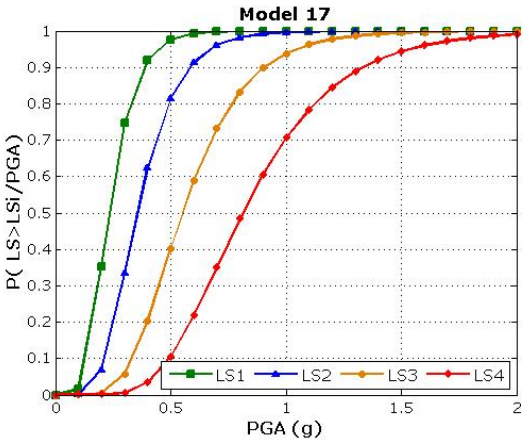

Model 14
P(LS>LSi/PGD)
PGD (m)
LS1
LS2
LS3

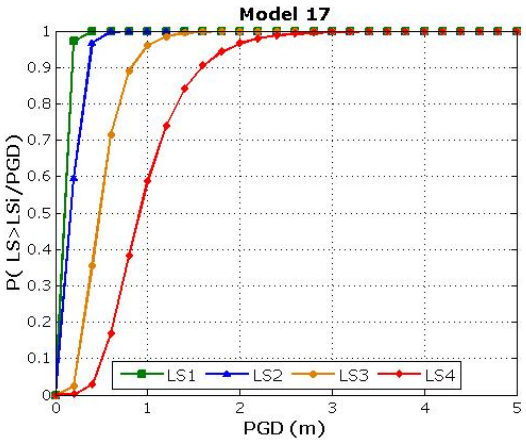

Model 15
P(LS>LSi/PGA)
PGA (g)
LS1
LS2
LS3
LS4

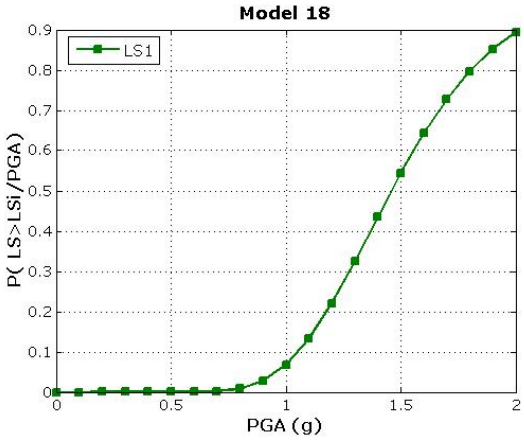

Model 15
P(LS>LSi/PGD)
PGD (m)
LS1
LS2
LS3
LS4

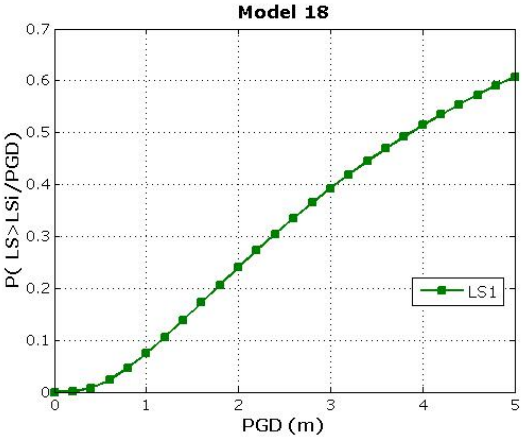

Model 16
P(LS>LSi/PGA)
PGA (g)
LS1
LS2
LS3
LS4

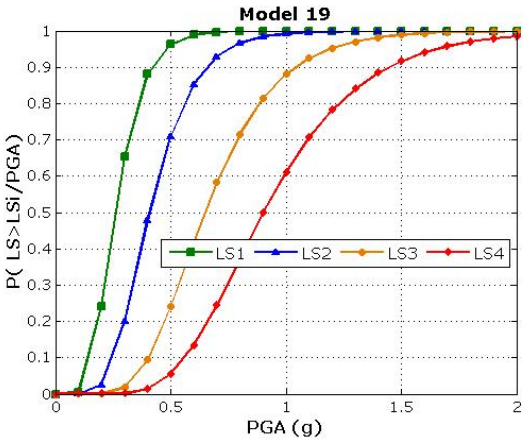

Model 16
P(LS>LSi/PGD)
PGD (m)
LS1
LS2
LS3

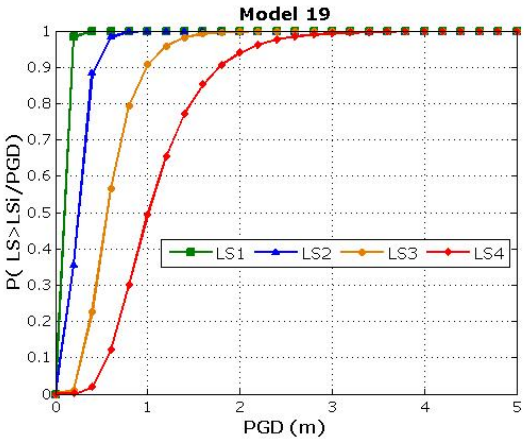

Model 17
P(LS>LSi/PGA)
PGA (g)
LS1
LS2
LS3
LS4

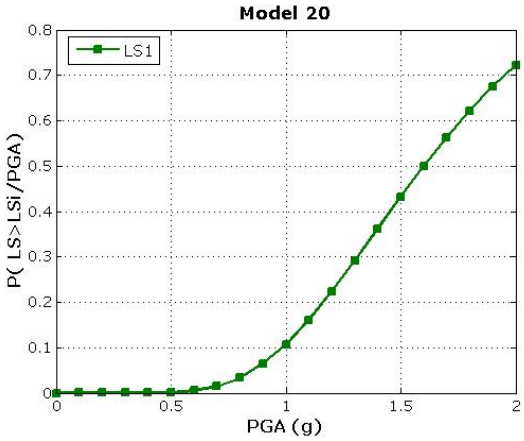

Model 17
P(LS>LSi/PGD)
PGD (m)
LS1
LS2
LS3
LS4

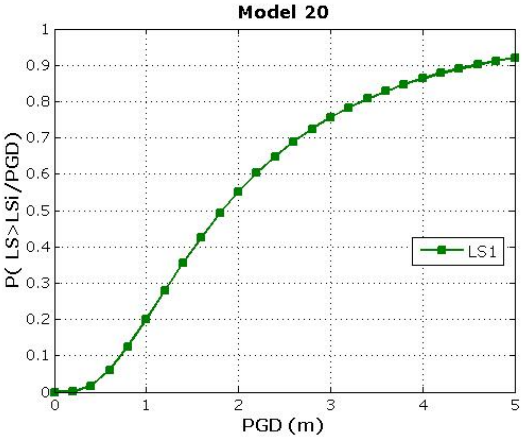

Model 18
P(LS>LSi/PGA)
PGA (g)
LS1


Model 18
P(LS>LSi/PGD)
PGD (m)
LS1


Model 19
P(LS>LSi/PGA)
PGA (g)
LS1
LS2
LS3
LS4


Model 19
P(LS>LSi/PGD)
PGD (m)
LS1
LS2
LS3
LS4


Model 20
P(LS>LSi/PGA)
PGA (g)
LS1


Model 20
P(LS>LSi/PGD)
PGD (m)
LS1

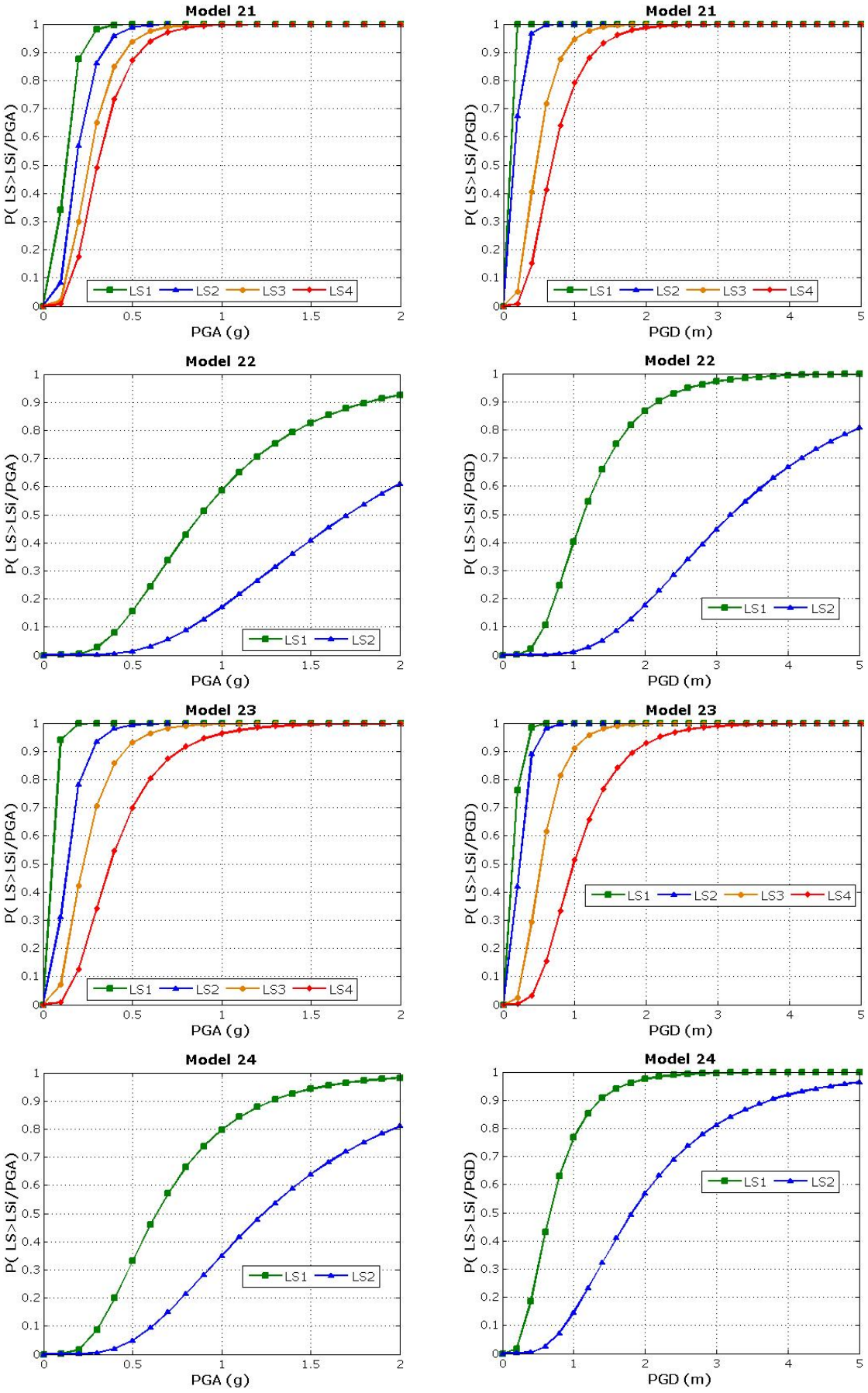


Figure 6.3. Fragility curves as a function of PGA (left) and PGD (right) derived from the parametric analysis

Table 6.3. Parameters of fragility functions for all the analyzed models when using PGA as an intensity measure

Model	Median PGA (g)				Dispersion β
	LS1 (g)	LS2 (g)	LS3 (g)	LS4 (g)	
1	0.22	0.39	0.58	0.81	0.37
2	0.34	0.75	1.12	1.61	0.40
3	0.31	0.46	0.74	1.00	0.36
4	0.34	0.75	1.12	1.61	0.40
5	0.17	0.28	0.49	0.74	0.43
6	0.27	0.57	1.03	1.53	0.50
7	0.19	0.41	0.66	0.92	0.38
8	0.21	0.46	0.85	1.23	0.50
9	0.29	0.51	0.84	1.17	0.45
10	0.25	0.63	1.17	2.00	0.51
11	0.35	0.62	0.99	1.43	0.42
12	0.25	0.54	1.03	1.58	0.48
13	0.27	0.51	0.82	1.12	0.44
14	0.24	0.64	1.12	1.59	0.48
15	0.32	0.61	0.97	1.29	0.40
16	0.21	0.51	0.99	1.47	0.52
17	0.23	0.35	0.55	0.81	0.39
18	1.46	-	-	-	0.25
19	0.26	0.41	0.65	0.90	0.37
20	1.60	-	-	-	0.38
21	0.12	0.19	0.25	0.30	0.44
22	0.88	1.71	-	-	0.56
23	0.04	0.13	0.22	0.38	0.55
24	0.63	1.24	-	-	0.55

Table 6.4. Parameters of fragility functions for all the analyzed models when using PGD as an intensity measure

Model	Median PGD (m)				Dispersion β
	LS1 (m)	LS2 (m)	LS3 (m)	LS4 (m)	
1	0.14	0.37	0.80	1.54	0.42
2	0.25	0.99	2.29	-	0.45
3	0.26	0.53	1.36	2.30	0.45
4	0.25	0.99	2.29	-	0.45
5	0.19	0.44	0.95	1.66	0.40
6	0.33	0.99	2.20	-	0.39
7	0.26	0.70	1.40	2.50	0.36
8	0.23	0.69	1.68	3.26	0.43
9	0.23	0.58	1.20	2.02	0.38
10	0.30	1.07	2.79	-	0.43
11	0.29	0.78	1.61	2.70	0.37
12	0.29	0.90	2.24	-	0.43
13	0.24	0.63	1.33	2.30	0.39
14	0.32	1.28	3.05	-	0.46
15	0.32	0.85	1.97	3.18	0.39
16	0.30	0.98	2.33		0.45
17	0.09	0.18	0.47	0.91	0.43
18	3.87	-	-	-	0.94
19	0.08	0.24	0.56	1.01	0.44
20	1.83	-	-	-	0.72
21	0.04	0.16	0.45	0.67	0.50
22	1.13	3.21	-	-	0.51
23	0.14	0.22	0.52	0.99	0.48
24	0.66	1.82	-	-	0.56

6.2.1.1. Effect of slope inclination

The influence of the slope inclination to the fragility curves in terms of PGA and PGD are presented in Figures 6.4 and 6.5 respectively for varying slope inclinations (15^o, 30^o, 45^o) considering both sand (models 1, 9 and 17) and clayey slopes (models 2, 10 and 18). In particular, the fragility curves for extensive (Figs. 6.4) and slight (Figs. 6.5) damage are presented for the sand and clayey slope respectively. As shown in Table 6.1, soft, relatively stiff and stiff soil materials are considered for the 15^o, 30^o and 45^o slope configurations respectively that distinguish different mechanical parameters for the sand and clay slopes (see Table 6.2). The height of the slope for the herein examined models is 20 m.

It is shown that the slope inclination plays a fundamental role in the fragility analysis of the building standing next to the slope's edge. However, it should be regarded in conjunction to the slope soil properties to obtain meaningful conclusions. Thus, for the sand slope, the building would suffer more damage as the slope inclination increases.

On the contrary, for the clayey slope, the building is expected to sustain less structural damage when standing on the 45° inclined slope compared to the gentler ones due to the stiff cohesive soil conditions assumed for the steep slope configuration.

These trends are generally evident when considering both PGA and PGD as intensity measures.

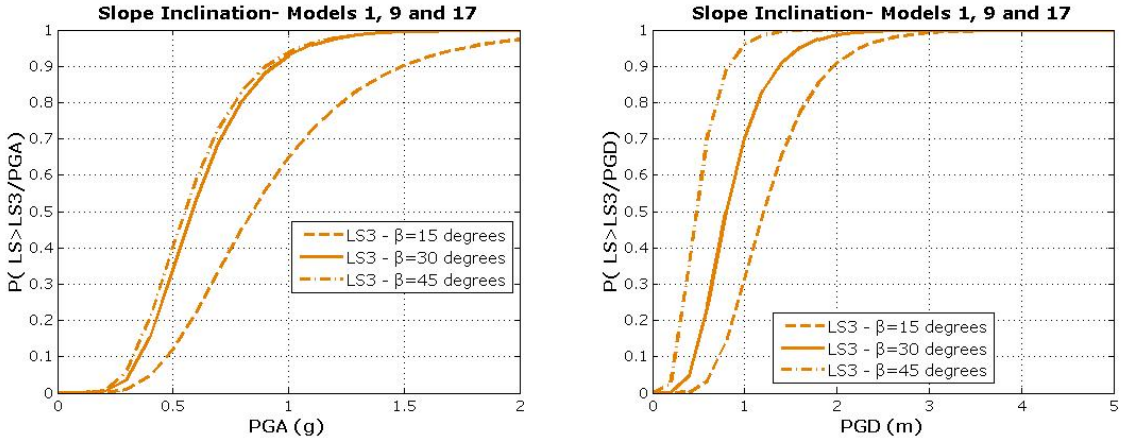


Figure 6.4. Fragility curves for extensity damage as a function of PGA (left) and PGD (right) when varying slope inclination [β=f (Soil properties) = 15°, 30°, 45°] for sand slopes

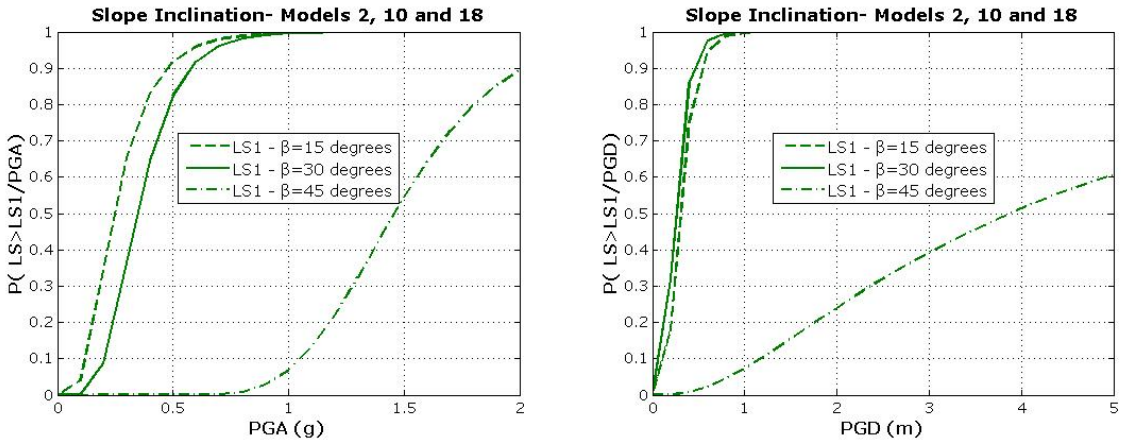


Figure 6.5. Fragility curves for slight damage as a function of PGA (left) and PGD (right) when varying slope inclination [β=f (Soil properties) = 15°, 30°, 45°] for clayey slopes

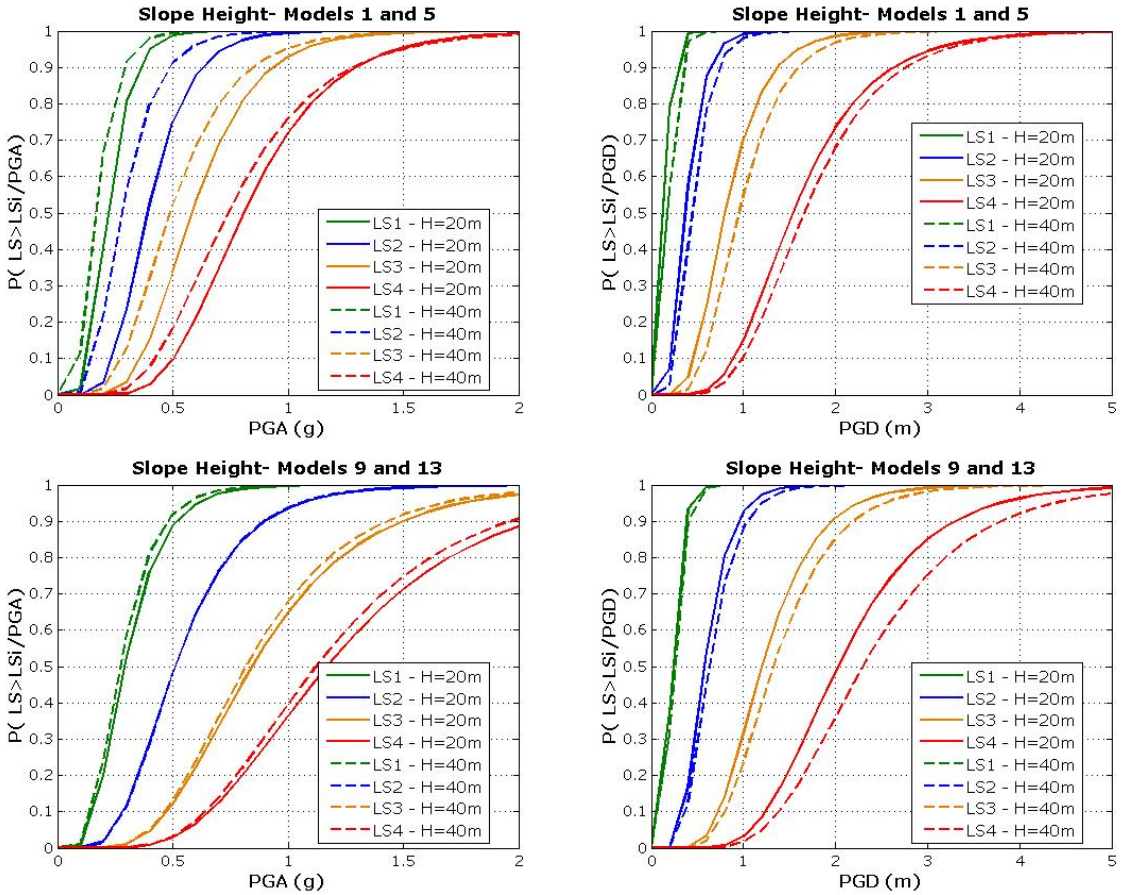
6.2.1.2. Effect of slope height

To demonstrate the influence of the slope height on the vulnerability of the building to permanent ground displacement due to the landslide impact, comparative plots of

fragility curves as a function of PGA and PGD when varying slope height (H= 20, 40m) for sand and clayey slopes are presented in Figures 6.6 and 6.7 respectively.

In overall, the slope height can moderately affect the structure's fragility. Different trends are revealed depending on the selected intensity measure (PGA or PGD) and the inclination angle of the analyzed slopes (15°, 30°, 45°). These trends seem to hold irrespective of the type (sand or clayey) of the slope soil materials involved.

When using PGA as an intensity parameter, it is seen that the vulnerability of the building increases with the slope height. As it would be normally expected, this increase is more pronounced for the 45° steep slope configurations (e.g. models 17, 18, 23, 24) whereas it is far less important for the 15° inclined slopes (e.g. models 9, 10, 13, 14). In contrast, the use of PGD as intensity measure, apart from some exceptions, is associated to lower vulnerability values of the building with increased slope heights. A plausible explanation of the latter is that in the case of higher slopes the mobilized sliding mass is larger and thus it affects more the building located close to the crest in terms of total displacements, which are larger, while the differential displacement demand on the building is reduced.



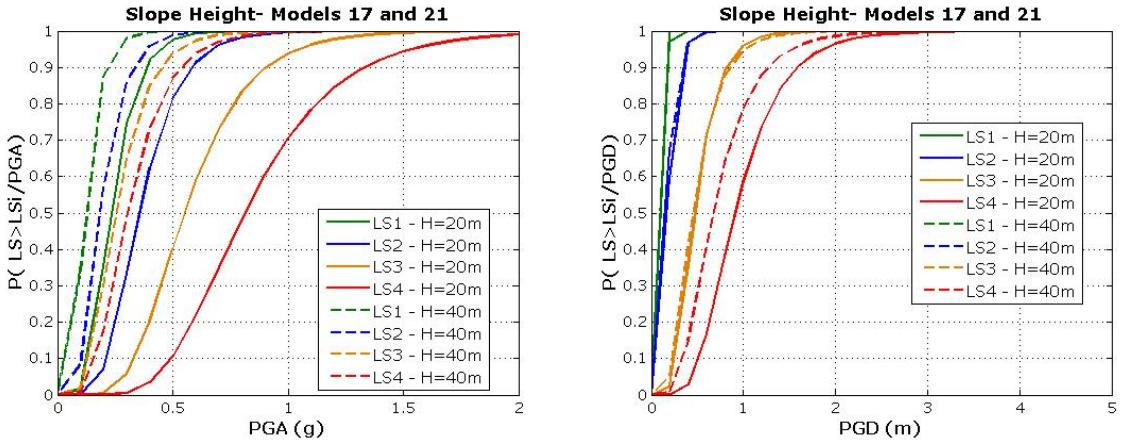
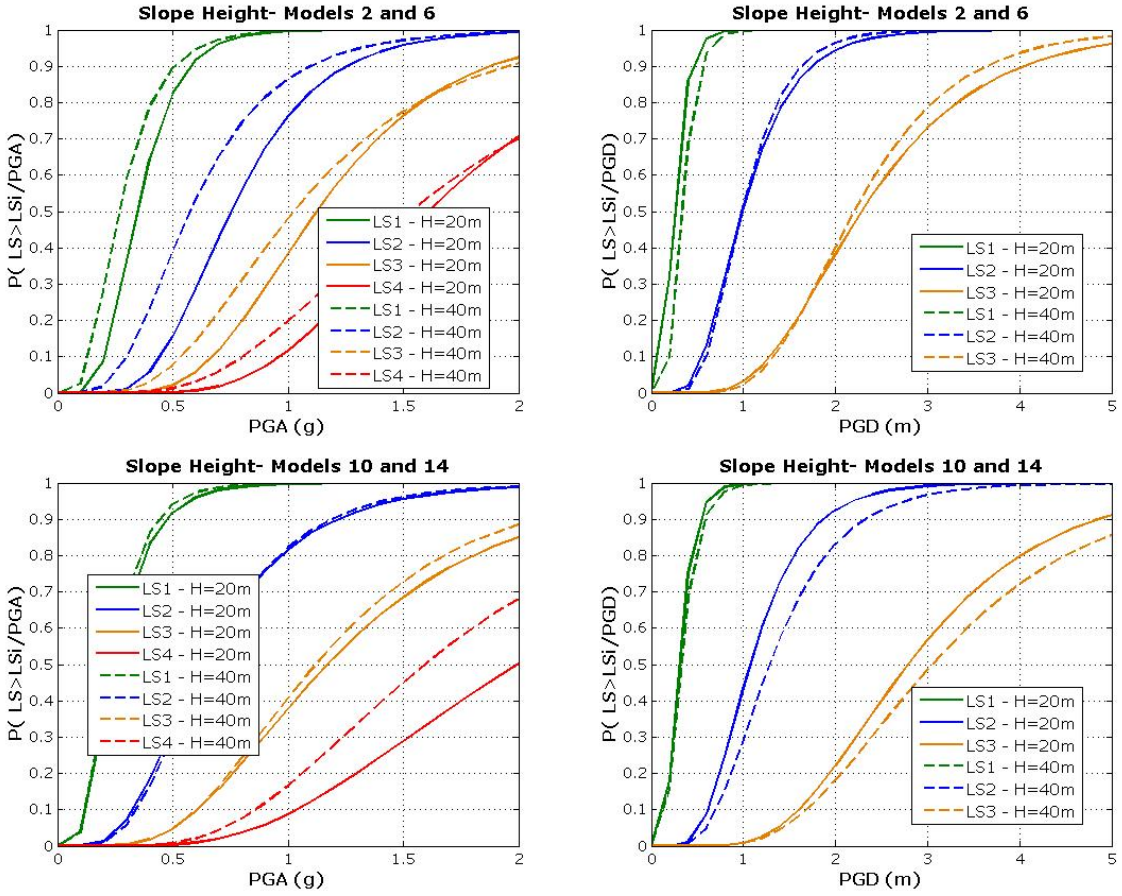


Figure 6.6. Fragility curves as a function of PGA (left) and PGD (right) when varying slope height (H= 20, 40m) for sand slopes



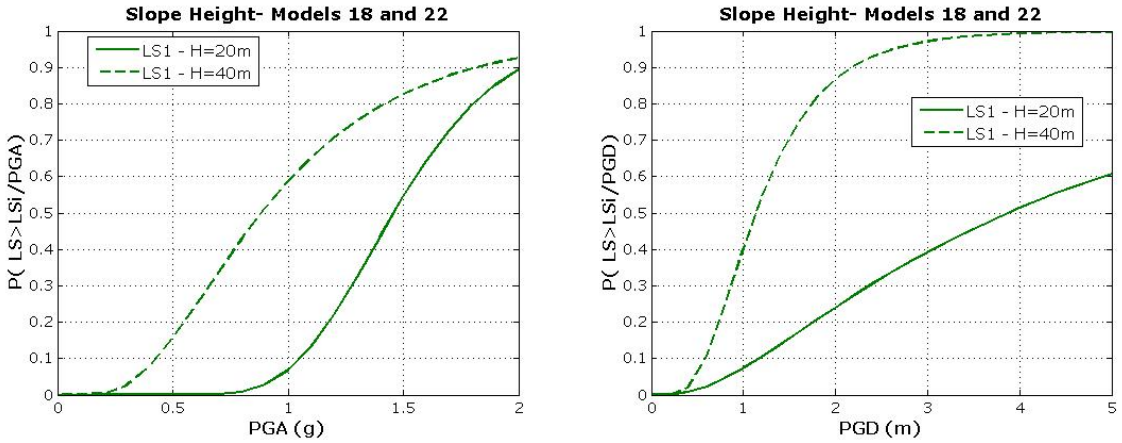
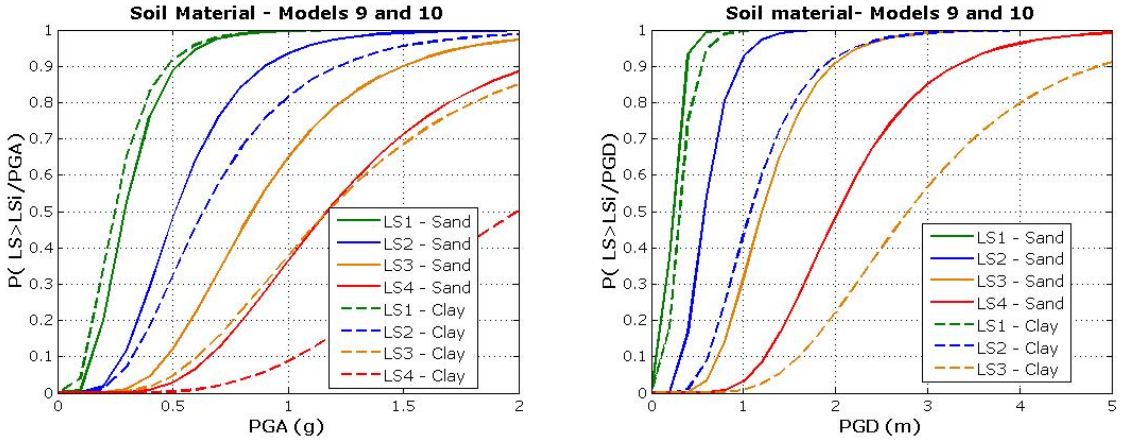


Figure 6.7. Fragility curves as a function of PGA (left) and PGD (right) when varying slope height (H= 20, 40m) for clayey slopes

6.2.1.3. Effect of soil material

The soil material is certainly a significant parameter in assessing building's vulnerability standing near the crest of a potentially precarious slope. Figures 6.8 to 6.10 present the derived sets of fragility curves, always given as a function of PGA and PGD, when varying slope soil properties (sand, clay) for the 15°, 30° and 45° slope configurations respectively. As shown in Table 6.2, soft, relatively stiff and stiff (sand or clay) soil conditions are considered for the 15°, 30° and 45° inclined slopes respectively.

It is observed that slopes consisting of clay material generally demonstrate better performance compared to sands when subjected to differential permanent ground displacements, resulting to lower vulnerability levels for the building. This is largely due to the inherent cohesive behavior of clay soil material that is associated to the formation of larger and deeper sliding surfaces. Thus, the considered one-bay building located at a close distance (i.e. 3m) from the slope's crest would be practically within the sliding mass and therefore it is primarily expected to move uniformly with the landslide mass rather than to distort differentially. The above observation is more noticeable as the slope inclination increases, i.e. for the stiffer clayey soil materials.



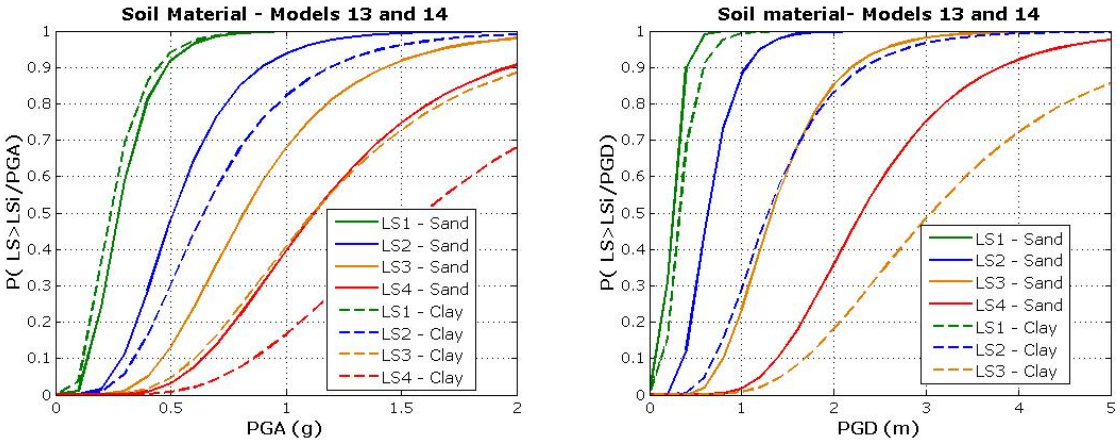


Figure 6.8. Fragility curves as a function of PGA (left) and PGD (right) when varying slope soil properties (sand, clay) for soft soil conditions (slope inclination β=15°)

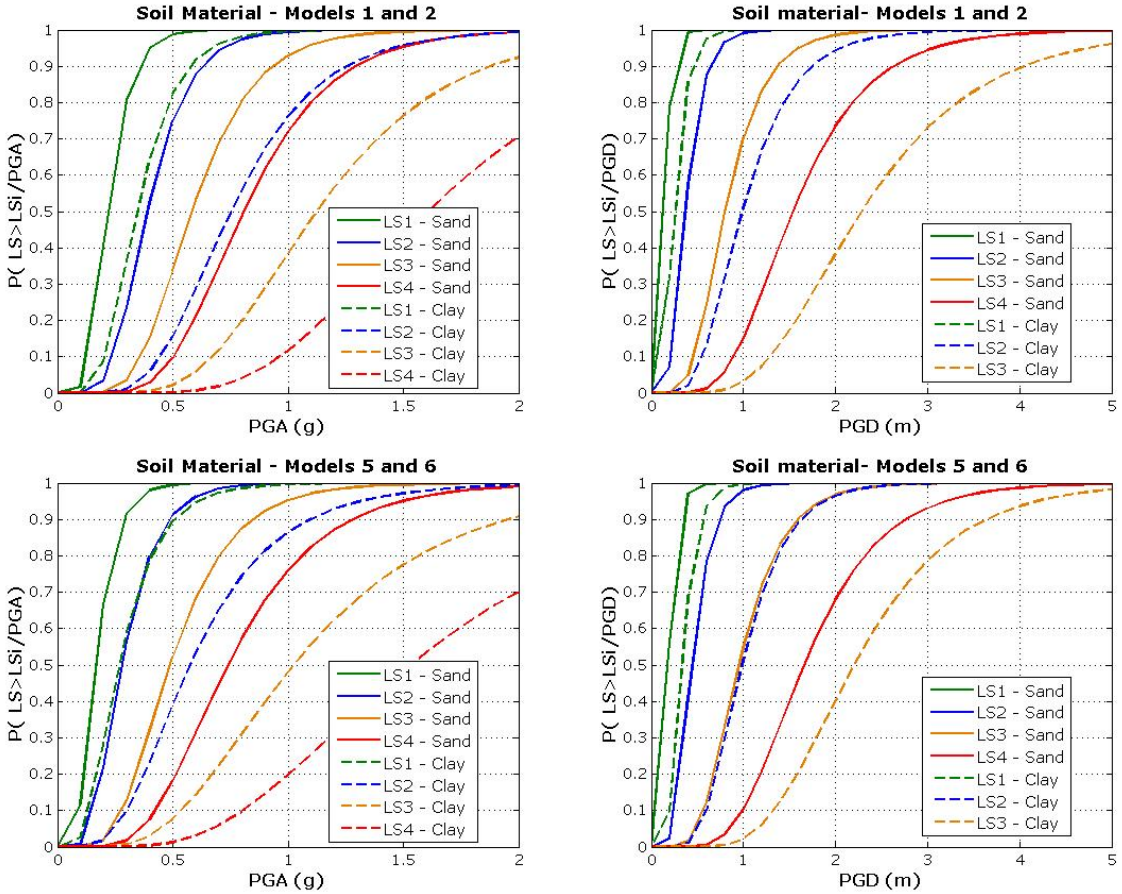


Figure 6.9. Fragility curves as a function of PGA (left) and PGD (right) when varying slope soil properties (sand, clay) for relatively stiff soil conditions (slope inclination β=30°)

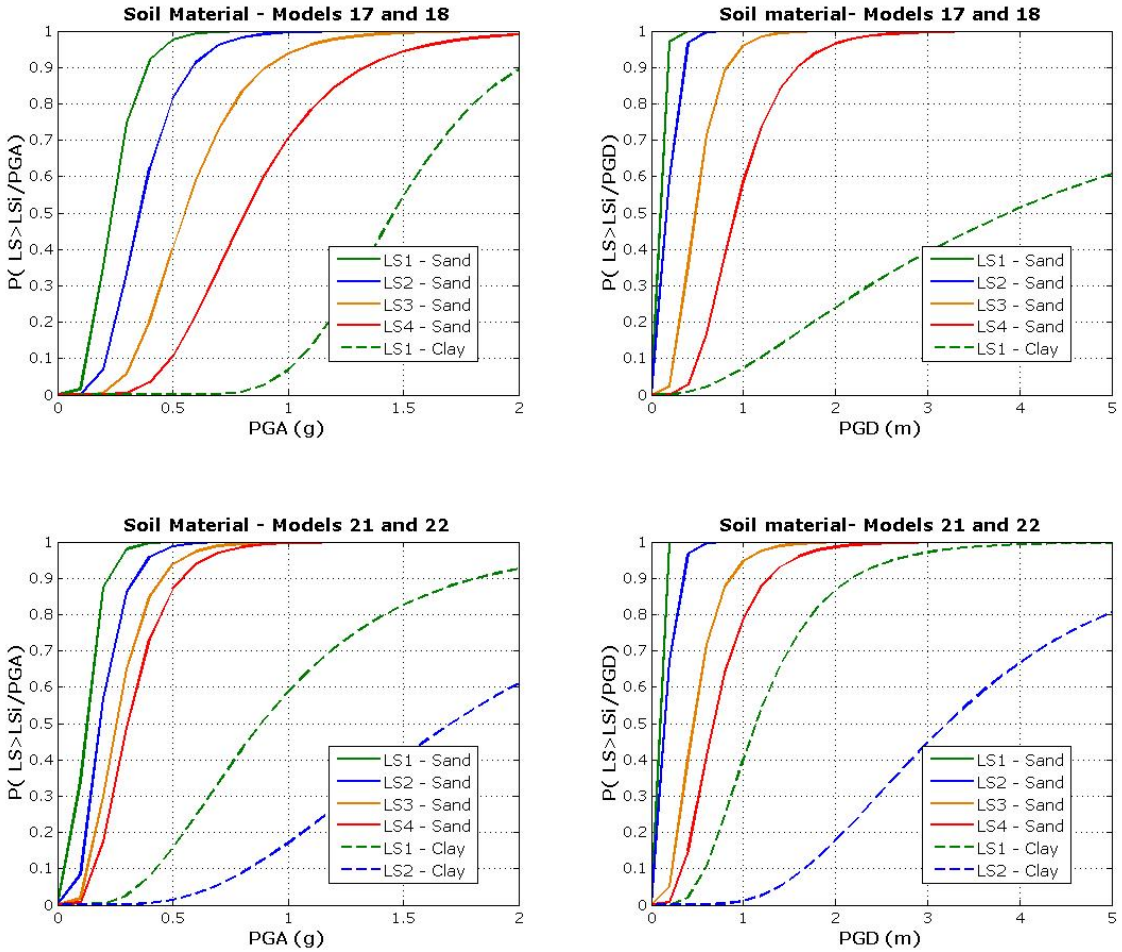


Figure 6.10. Fragility curves as a function of PGA (left) and PGD (right) when varying slope soil properties (sand, clay) for stiff soil conditions (slope inclination β=45°)

6.2.1.4. Effect of the foundation location with respect to the slope's crest

The distance of the assumed building from the crest of the slope may also considerably influence its vulnerability to the permanent landslide displacement. Figures 6.11 and 6.12 display the derived sets of fragility curves when varying the distance from the crest (L= 3, 5m) for sand and clayey slopes respectively. Different observations can be made depending on the type of the considered slope soil materials. For sand slopes, the building is expected to suffer less damage as the distance from the crest increases. On the contrary, for the clayey slopes, the more distant building from the crest would be more vulnerable. This differentiation lies again on the nature of the slope soil materials involved that are associated to the formation of sliding surfaces that may vary for very small and shallow for sands brittle slopes to large and deep for clayey deformable slopes. Thus, the assumed one-bay building standing at 3m from the crest of the clayey slope is basically within the landslide mass and moves rather uniformly as a rigid body whereas for increasing distances from the crest (5 m) the building shifts (partially) outside the

landslide mass and therefore it exhibits more differential (rather than uniform) ground displacements and hence more structural damage. On the other hand, the building located at the closest distance from the crest (i.e. 3m) of the sand slope is outside the landslide mass and consequently it is subjected to extensive differential deformation demand that is gradually decayed as the distance from the crest increases.

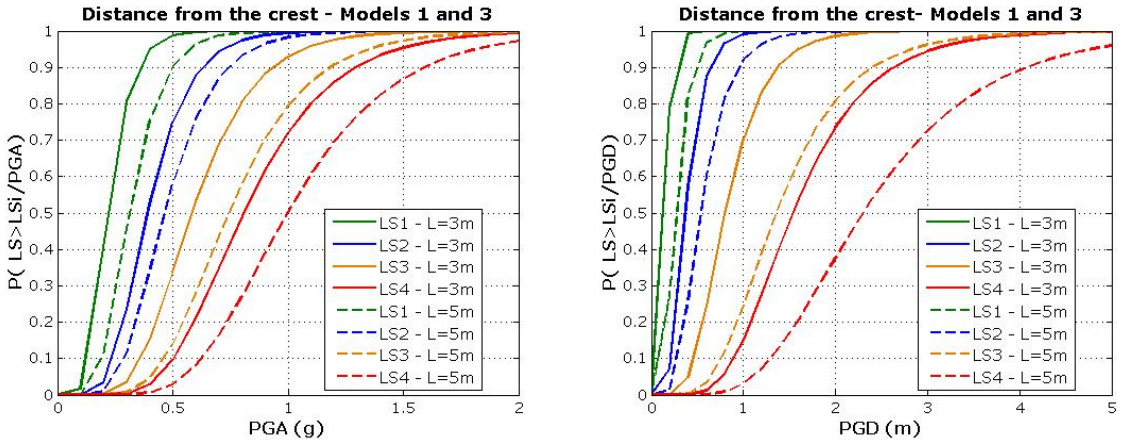


Figure 6.11. Fragility curves as a function of PGA (left) and PGD (right) when varying the distance from the crest (L= 3, 5m) for sand slopes

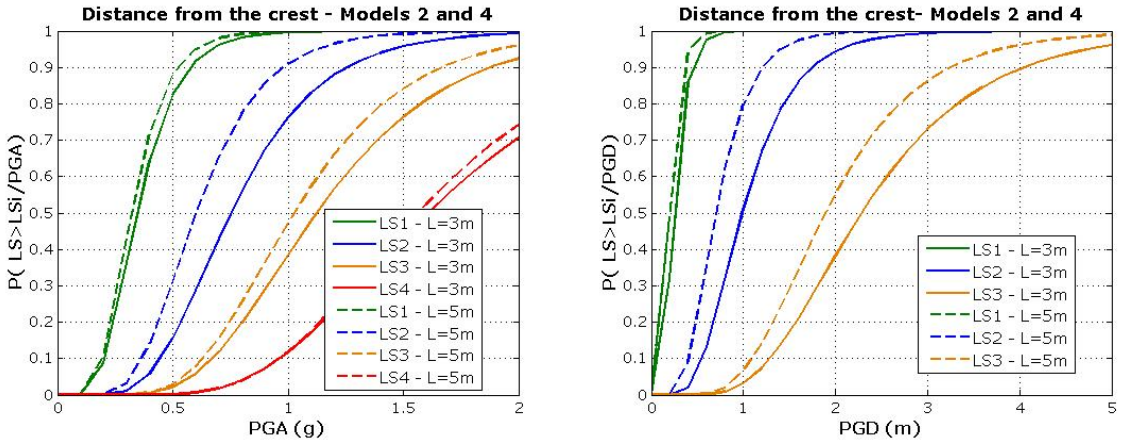
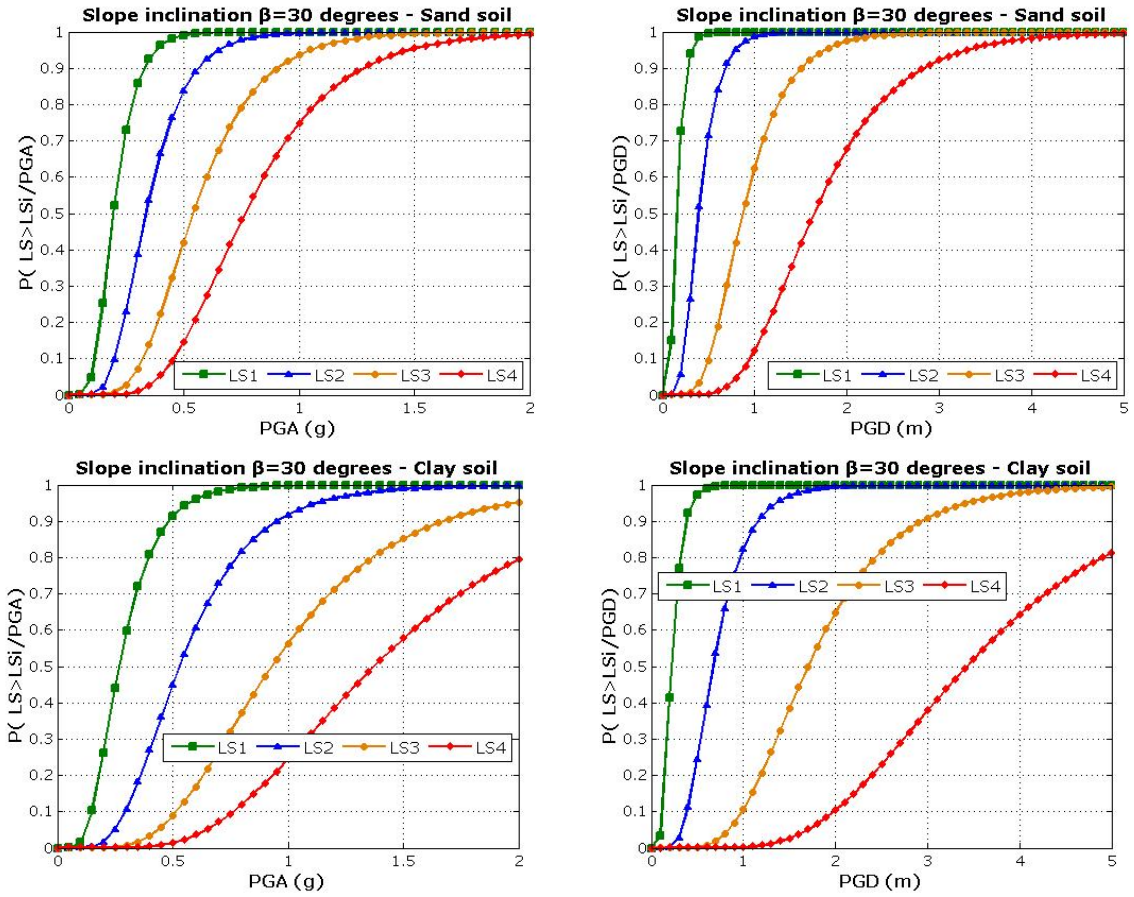
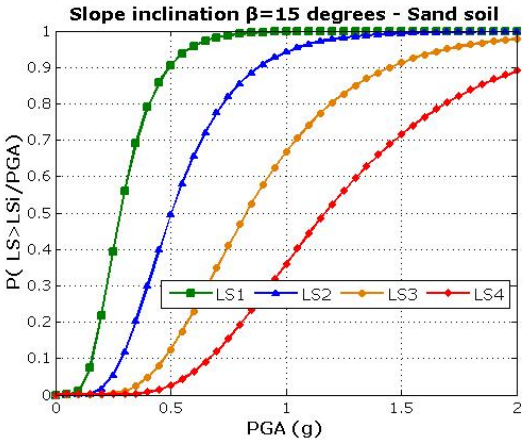


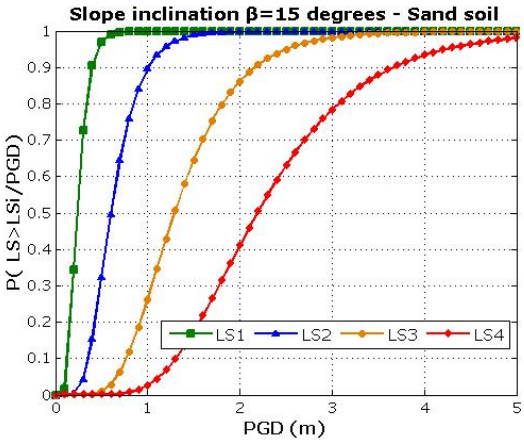
Figure 6.12. Fragility curves as a function of PGA (left) and PGD (right) when varying the distance from the crest (L= 3, 5m) for clayey slopes

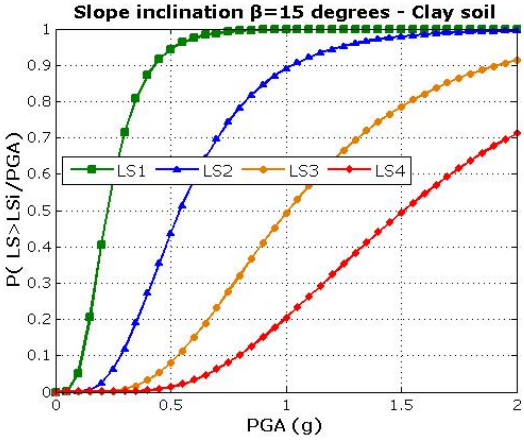
6.2.2 Generalized fragility curves

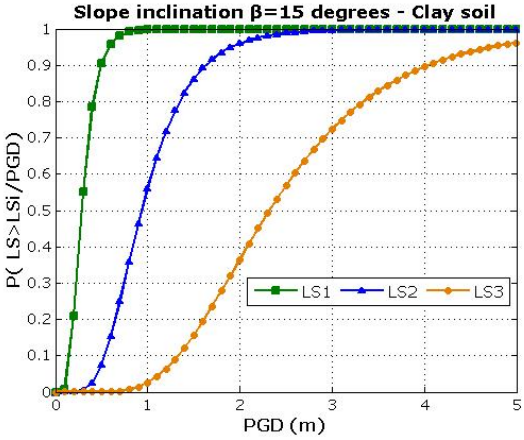
Seven sets of fragility curves both in terms of PGA and PGD (Fig. 6.13) are proposed herein that could be used for engineering applications based on the main features that proved to be the most influential in assessing the vulnerability of the building to the differential permanent deformation due to the landslide hazard. These are principally the slope inclination and the soil material of the slope that are found to be highly correlated. The slope height is also proved to be a significant contributor to the building's fragility for the steep sand slope configurations. Thus, for the 45° inclined sand slopes fragility curves are also differentiated with respect to the considered slope height (H=20, 40 m). The latter curves are probably less accurate than the others as they are based on a smaller simulated dataset. It is noted that the proposed curves have been constructed considering the most adverse position of the building with respect to the landslide that was found to be different for sand and clay slopes. It is also important to note that the curves presented herein refer to "high-code", adequately confined RC frame structures. The corresponding suggested curves accounting for "low-code", poorly confined frames are presented in Annex B. Tables 6.5 and 6.6 present the median and dispersions of the suggested curves when using PGA and PGD as an intensity measure respectively.

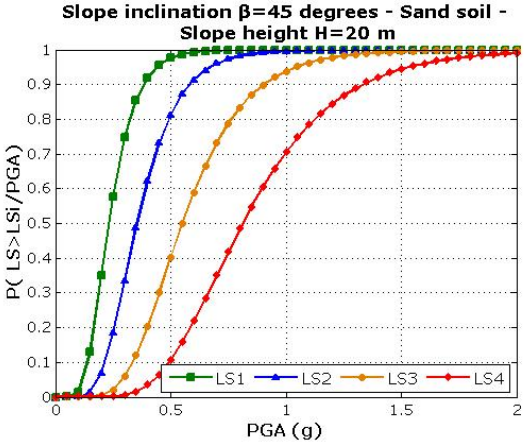


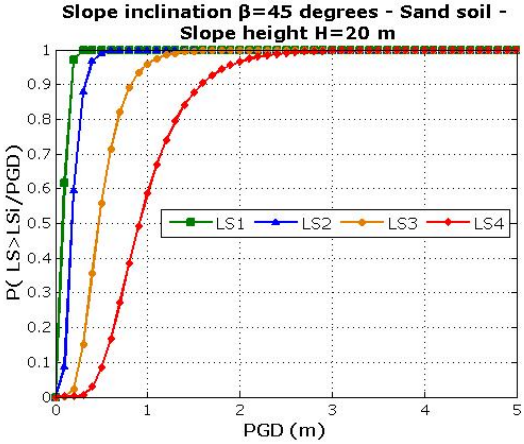

Slope inclination β=15 degrees - Sand soil
P(LS>LSi/PGA)
PGA (g)
LS1
LS2
LS3
LS4

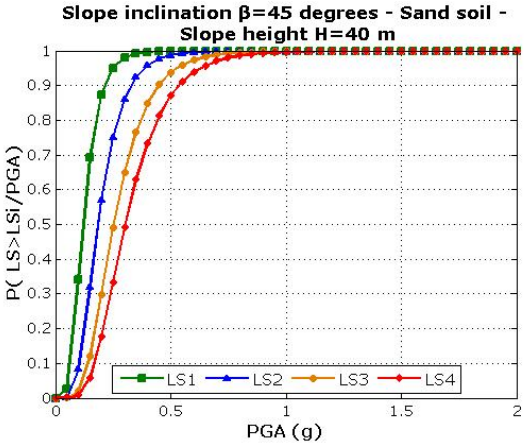

Slope inclination β=15 degrees - Sand soil
P(LS>LSi/PGD)
PGD (m)
LS1
LS2
LS3
LS4

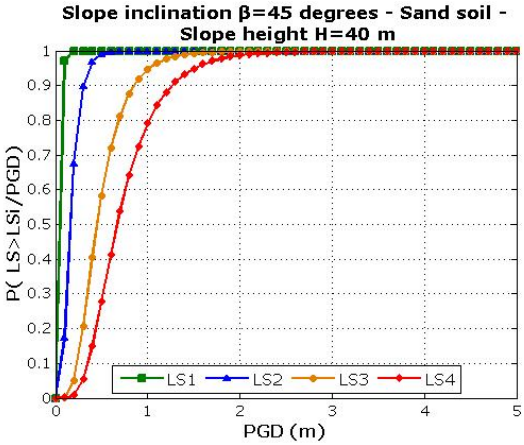

Slope inclination β=15 degrees - Clay soil
P(LS>LSi/PGA)
PGA (g)
LS1
LS2
LS3
LS4


Slope inclination β=15 degrees - Clay soil
P(LS>LSi/PGD)
PGD (m)
LS1
LS2
LS3


Slope inclination β=45 degrees - Sand soil -
Slope height H=20 m
P(LS>LSi/PGA)
PGA (g)
LS1
LS2
LS3
LS4


Slope inclination β=45 degrees - Sand soil -
Slope height H=20 m
P(LS>LSi/PGD)
PGD (m)
LS1
LS2
LS3
LS4


Slope inclination β=45 degrees - Sand soil -
Slope height H=40 m
P(LS>LSi/PGA)
PGA (g)
LS1
LS2
LS3
LS4


Slope inclination β=45 degrees - Sand soil -
Slope height H=40 m
P(LS>LSi/PGD)
PGD (m)
LS1
LS2
LS3
LS4

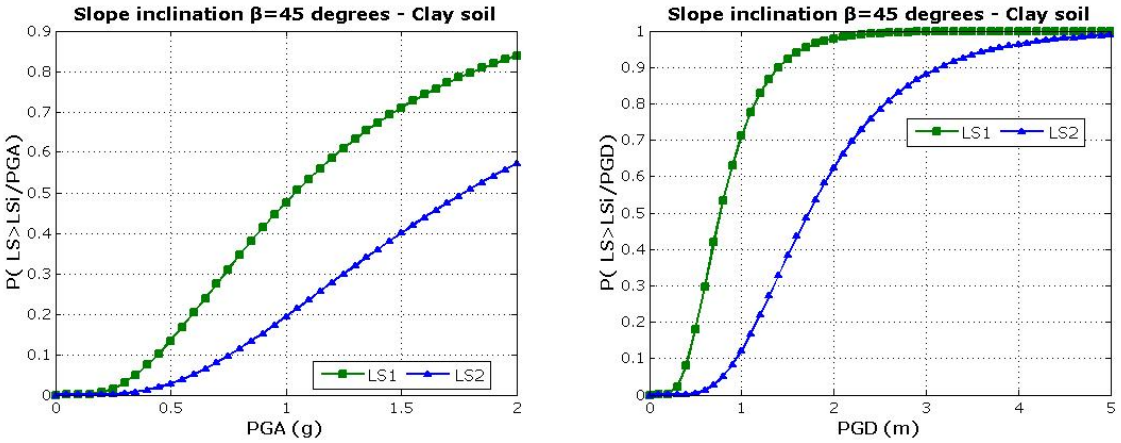


Figure 6.13. Proposed fragility curves as a function of PGA (left) and PGD (right) for high-code, low-rise RC frame buildings subjected to permanent landslide displacements

Table 6.5. Parameters of the proposed fragility functions using PGA as an intensity measure

Parametric models	Median PGA (g)				Dispersion β
	LS1 (g)	LS2 (g)	LS3 (g)	LS4 (g)	
sand_β30	0.20	0.34	0.54	0.76	0.40
clay_β30	0.27	0.53	0.93	1.37	0.46
sand_β15	0.28	0.50	0.83	1.17	0.44
clay_β15	0.23	0.54	1.01	1.51	0.50
sand_β45_H20	0.23	0.35	0.55	0.81	0.39
sand_β45_H40	0.12	0.19	0.25	0.30	0.44
clay_β45	1.04	1.77	-	-	0.66

Table 6.6. Parameters of the proposed fragility functions using PGD as an intensity measure

Parametric models	Median PGD (m)				Dispersion β
	LS1 (m)	LS2 (m)	LS3 (m)	LS4 (m)	
sand_β30	0.15	0.39	0.87	1.64	0.43
clay_β30	0.22	0.67	1.70	3.43	0.43
sand_β15	0.24	0.60	1.29	2.19	0.40
clay_β15	0.28	0.94	2.32	-	0.43
sand_β45_H20	0.09	0.18	0.47	0.91	0.43
sand_β45_H40	0.04	0.16	0.45	0.67	0.50
clay_β45	0.77	1.72	-	-	0.47

As already shown, the building founded upon sand slopes is expected to demonstrate a greater damaging potential than the respective clayey ones. The corresponding curves referring to sand slopes are generally shifted to the left compared to clays and they are associated with a more rapid transition from slight to complete damage limits. These differences are becoming much more pronounced as the slope inclination increases.

Among the considered cases, the sand steep, high-rise slope and clay steep slope configurations are producing the most and the least damage respectively on the building. The dispersion of the suggested curves is found to vary from 0.39 to 0.66 and from 0.40 to 0.50 when considering PGA and PGD respectively as an intensity parameter. As shown on the tables presented above, the larger β values are expected for the 45^o slope configurations and for clayey soil materials.

6.3 Sensitivity analysis

Apart from the main parametric investigation, a sensitivity analysis is also conducted to examine the relative influence of various additional parameters on the structure's performance and fragility. In all analyzed cases hereafter we refer to a 30^o inclined and 20m high slope configuration consisting of a relatively stiff upslope soil material corresponding to soil class C according to EC8 (Vs=250 m/s), to allow for direct comparison with the already analyzed reference models 1 to 4 (see Table 6.1) .

6.3.1 Effect of water table

The influence of groundwater in altering the slope's seismic response and the extent of ground and foundation irreversible deformation and consequently the expected structural damage is investigated herein. In particular, two hydraulic conditions are examined: a first one with no water (dry materials, models 1 and 2) and a second with a water table level located at 80% of the slope height (saturated materials underneath the water table and dry materials above). Non-liquefiable upslope soil deposits are considered in this research as the proposed methodology (Chapter 4) is dealing with slow movements. The analyzed slope dynamic models ($\beta=30^o$, H=20m, Vs=250m/sec) vary only in the hydrological and soil conditions studied. A single bay-single story bare frame RC building with flexible foundation system standing 3m from the slope's crest is considered for all the analysis cases.

The results are given in terms of fragility functions that account for dry and partially saturated soil conditions. The corresponding plots of the fragility diagrams are illustrated in Figures 6.14 and 6.15 for slopes consisting of sand and clay soil materials respectively. For sand soil conditions, the presence of water results in a slight increase on the total and differential displacement imposed to the building at the foundation level that causes a shift of the respective curves to the left (Fig. 6.14). On the contrary, the corresponding displacement is decreased in case of clayey materials yielding to lower vulnerability levels (Fig. 6.15). A reasonable explanation could be the following: the presence of

groundwater might potentially reduce the static factor of safety of the slope giving rise to instability and/or permanent displacement that was found to be more pronounced for higher permeability values i.e. for the sand soil material (Srivastava et al., 2010). In addition, its presence is associated with the formation of larger sliding surfaces that, in relation to the proximity of the structure to the slope's crest, results to reduced differential displacements for the specified building (located 3m from the crest) resting on the clay slope and to slightly increased differential deformation for the building on the sand slope.

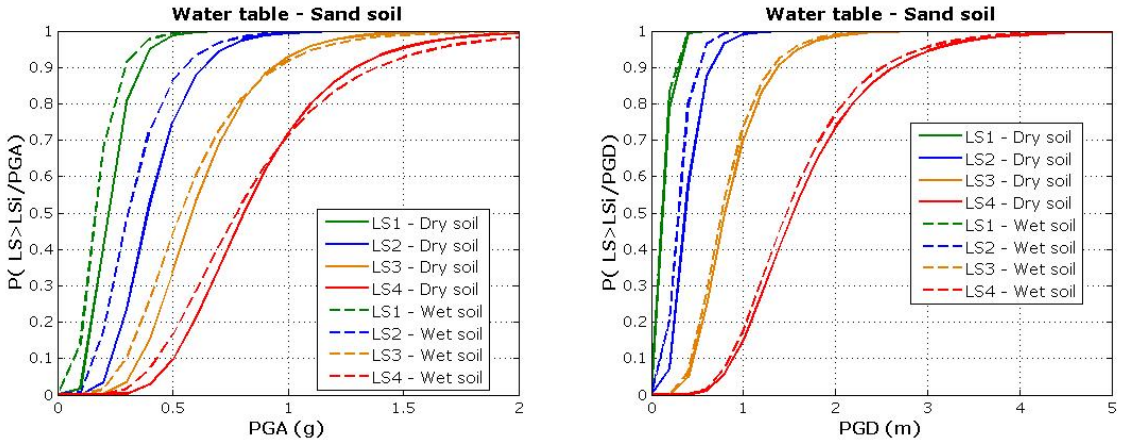


Figure 6.14. Fragility curves as a function of PGA (left) and PGD (right) when varying the hydraulic conditions (dry or partially saturated materials) for sand slopes

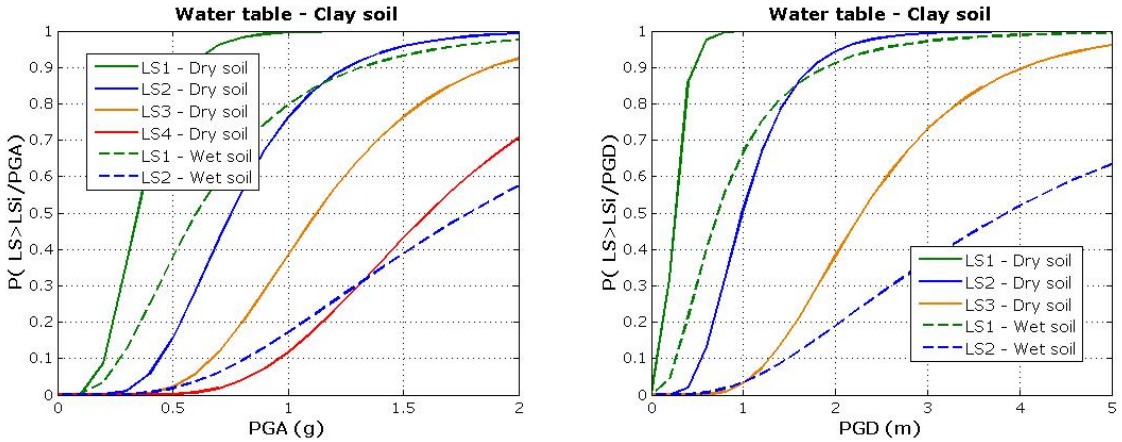


Figure 6.15. Fragility curves as a function of PGA (left) and PGD (right) when varying the hydraulic conditions (dry or partially saturated materials) for clayey slopes

6.3.2 Effect of strain softening in slope soil material

In all analyses performed so far non-softening slope soil materials are considered. However, quite often brittle soils in slopes may exhibit a strain softening behavior when subjected to cyclic loading. In these materials, a progressive failure can occur owing to

the reduction of strength with increasing strain (e.g. Bjerrum, 1967; Dounias, 1988; Troncone, 2005; Conte et al., 2010; Kourkoulis et al., 2010).

In order to capture such phenomena, a simple elastoplastic constitutive model of the Mohr-Coulomb type coupled with an isotropic strain-softening rule, able to simulate the reduction of the strength parameters after the onset of plastic yield, may be used (Fig. 6.16). The use of such models allows for simulating the formation of shear zones in which strain localized and hence are capable to reproduce a progressive failure process along a potential rupture surface in slopes. The model requires the specification of peak and residual strength as a function of the deviatoric plastic strain. A piecewise-linear variation of strength parameters with plastic shear strain is adopted herein to simulate the strain softening law (Fig. 6.17). The determination of peak and residual values of cohesion, friction angle and dilation as well as the yield and failure plastic strains depend on the soil type and should be based on appropriate laboratory and in situ tests. From a computational point of view, the adaptation of such a model presents many difficulties associated with lack of convergence due to numerical/physical instability and mesh dependency (e.g. Troncone 2005; Conte et al, 2010; Kourkoulis et al., 2010). In the present study, the proper element size of the slope dynamic model in the slope area was determined through a parametric analysis to balance between accuracy and computational efficiency as discussed in Kourkoulis et al. (2010).

Following the calibration procedure discussed in Anastasopoulos et al. (2007) to model medium dense Fontainebleau sand, the softening behavior of sand soil is determined utilizing the values for strength and plastic strain given below: $\varphi_p=39^o$, $\psi_p=11^o$, $\varphi_r=30^o$, $\psi_r=0^o$, $\gamma_y=2\%$, $\gamma_p=13.5\%$. The derived dynamic model, expect for the considered strain softening slope material, distinguishes the same features with the analyzed model 1 (see Table 6.1) to allow for direct comparisons. Figure 6.18 presents the derived sets of fragility curves as a function of PGA and PGD considering a non-softening (model 1) and a softening soil material. As we may see, the curves accounting for the slope soil materials with strain softening behavior are more close together and are generally associated with increased steepness and higher vulnerability levels. A physical interpretation of this lies on the inherent softening behavior of the sand soil material, which is simulated by reducing its friction angle and dilation from peak to residual with increasing deviatoric shear strain.

More research is needed to analyze strain softening behavior of slopes in different soil conditions (e.g. a stiff clay) and slope configurations. However, it‘s worth noting that such analyzes are computationally expensive and therefore they are often warranted only for site specific applications where detailed information on the soil parameters and strain thresholds are available from in-situ or laboratory tests.

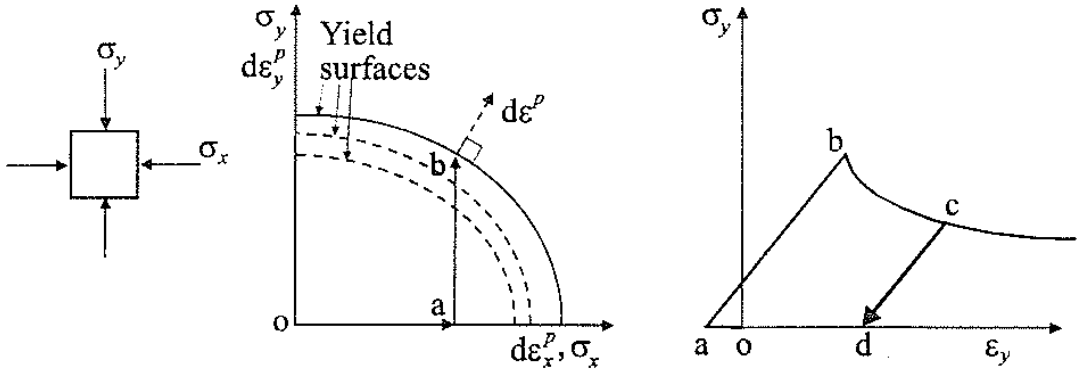


Figure 6.16. Two dimensional behavior of a linear elastic-softening plastic material (Potts and Zbravkovi, 1999)

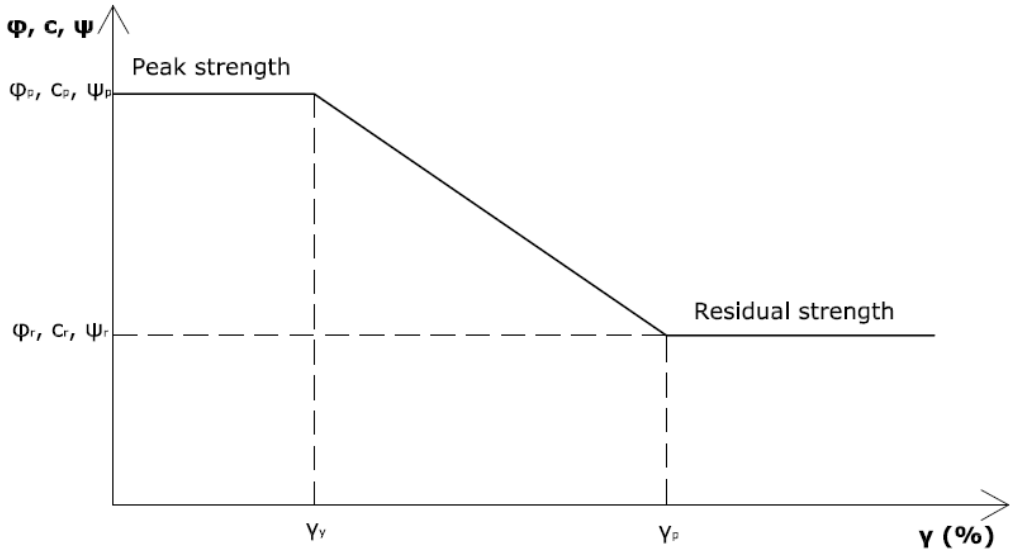


Figure 6.17. Idealization of the variation of cohesion, friction and dilation with plastic shear strain to simulate strain softening soil behavior

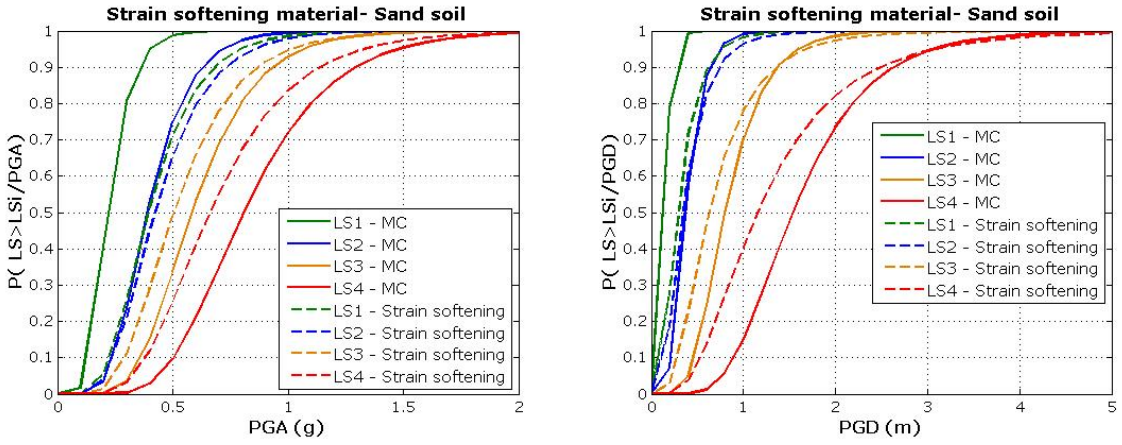


Figure 6.18. Fragility curves as a function of PGA (left) and PGD (right) when considering (or not) a strain softening material

6.3.3 Effect of foundation compliance

The parametric analyses conducted in section 6.2 refer to a simple single bay-single storey RC bare frame structure founded on flexible foundation system (e.g. isolated footings). However, as it has been thoroughly discussed Chapter 4, the stiffness of the foundation system may considerably modify the deformation demand for the building and its resistance ability and therefore its vulnerability.

The fragility curves (Figs. 6.20 and 6.21), as developed in Chapter 4, are also presented herein for the building founded on two different foundation systems (Fig. 6.19), namely isolated footings (models 1 and 2) and a continuous raft foundation, to stress the significant role of foundation flexibility in assessing the vulnerability of the building to the differential permanent displacement due to the landslide hazard. The building is assumed to be standing 3 m from the crest of a potentially unstable sand and clayey slope. It is noticed that simulation issues, concerning e.g. the modeling of the foundation system, have been extensively presented in Chapter 4 and are not repeated herein.

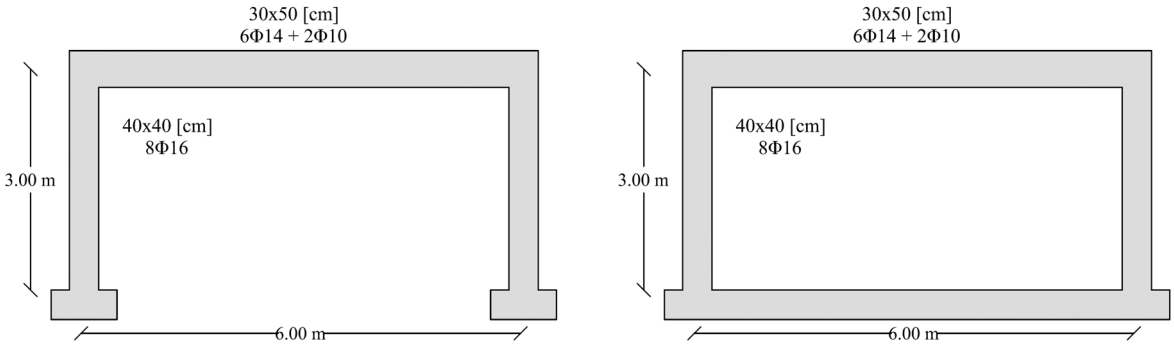


Figure 6.19. Schematic view of the analyzed single bay-single storey RC bare-frame structures with flexible (left) and stiff (right) foundations

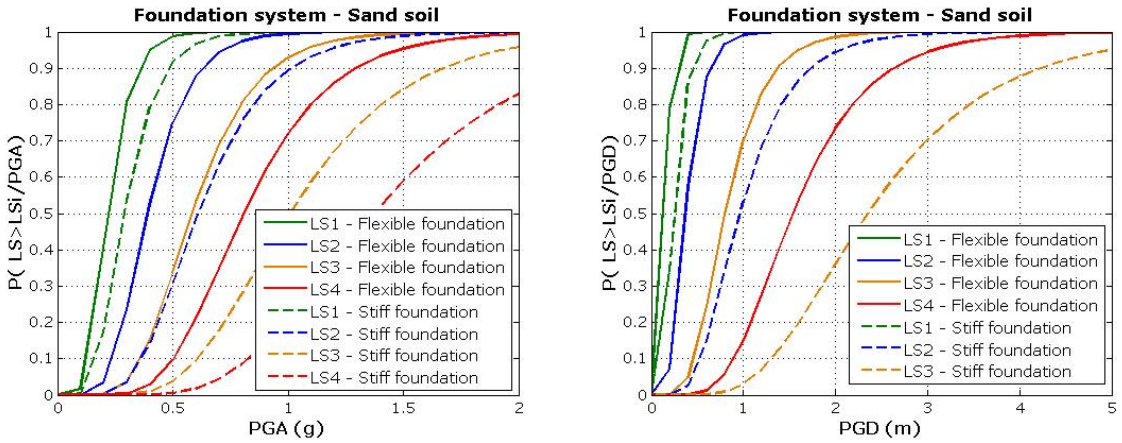


Figure 6.20. Fragility curves as a function of PGA (left) and PGD (right) when varying the flexibility of the foundation system for sand slopes

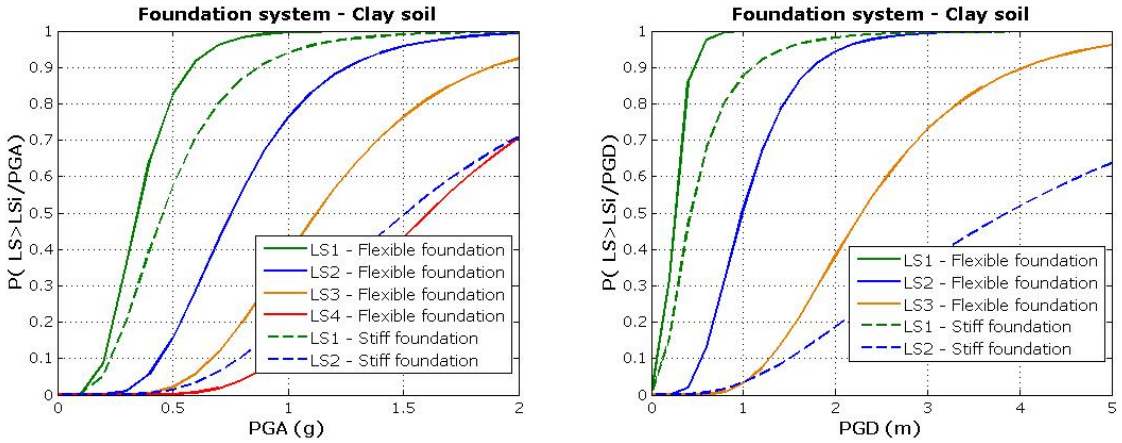


Figure 6.21. Fragility curves as a function of PGA (left) and PGD (right) when varying the flexibility of the foundation system for clayey slopes

Overall, the computed fragility curves display an important reduction on the structure's expected damages when a stiff foundation system rather than a flexible one is considered. This observation is noticeable for both slopes consisting of sand and clay material. Thus, the fragility curves proposed in 6.2.2 that refer to buildings on flexible foundation are expected to be always on the safe site. Once the type and relative stiffness of the foundation system is adequately known (e.g. for site specific applications and critical structures), the suggested curves for flexible foundations (isolated footings) could be properly modified to capture the influence of the foundation flexibility on the structure's performance and vulnerability.

6.3.4 Effect of building geometry

One-bay one-storey RC frame buildings have been investigated so far. Such simple structures have been found to adequately capture the performance of the low-rise RC frame buildings to permanent ground deformations (e.g. Bird et al. 2005; 2006; Negulescu and Foerster 2010).

However, for the sake of completeness, it was decided to carry out a sensitivity analysis on the geometry of the building (e.g. number of storeys, number of bays) considering different foundation systems and slope material properties to identify possible trends in its vulnerability.

6.3.4.1. Number of storeys

The effect of number of storeys on the expected differential deformation demand for the building and consequently on its structural response and vulnerability is explored herein considering different foundation types and slope soil materials. To this aim, 1 bay - 2 storey RC bare frame structures are analyzed (Fig. 6.22) assuming the same slope dynamic properties (i.e. see models 1 and 2) and typological parameters as for the

respective 1 bay- 1 storey buildings (see Fig. 6.19 for the corresponding sketches). Worthy of note is the fact that the load applied on the foundation system of the two-storey frames is doubled with respect to the corresponding load on the one-storey frame structure resulting to increased slope and foundation deformations.

Figures 6.23 to 6.26 depict the derived sets of fragility curves when considering a one-storey and a two-storey structure accounting for different foundation systems (flexible, stiff) and slope soil materials (sand, clay).

In all cases, the two-storey building is expected to sustain more damage compared to the corresponding one-storey building. This is largely due to the heavier loaded foundation assumed in the simulation of the two-storey building that gives rise to increased permanent displacements at the slope area. In this regard, it might deem necessary to modify the proposed curves in 6.2.2 for weightily loaded structures.

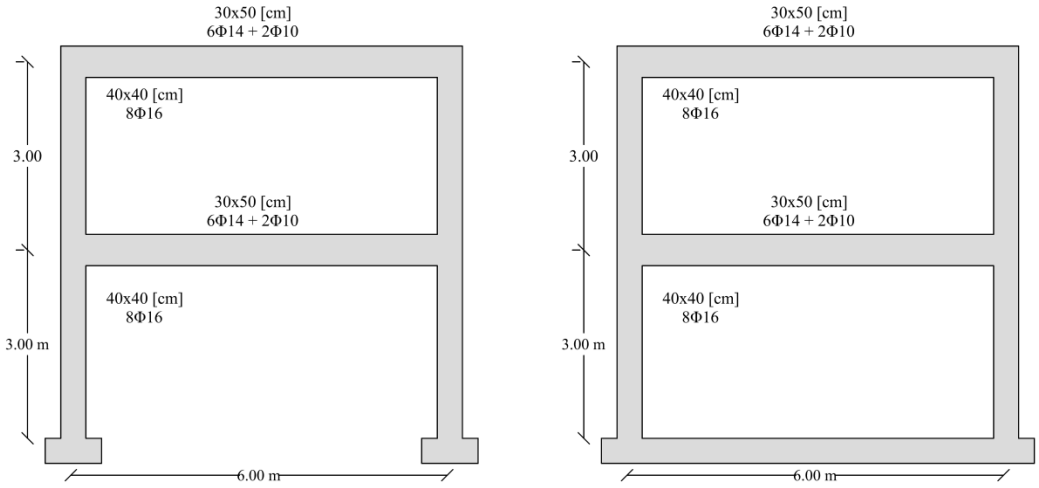


Figure 6.22. Schematic view of the analyzed 1 bay- 2 storeys RC bare frame structures with flexible (left) and stiff (right) foundations

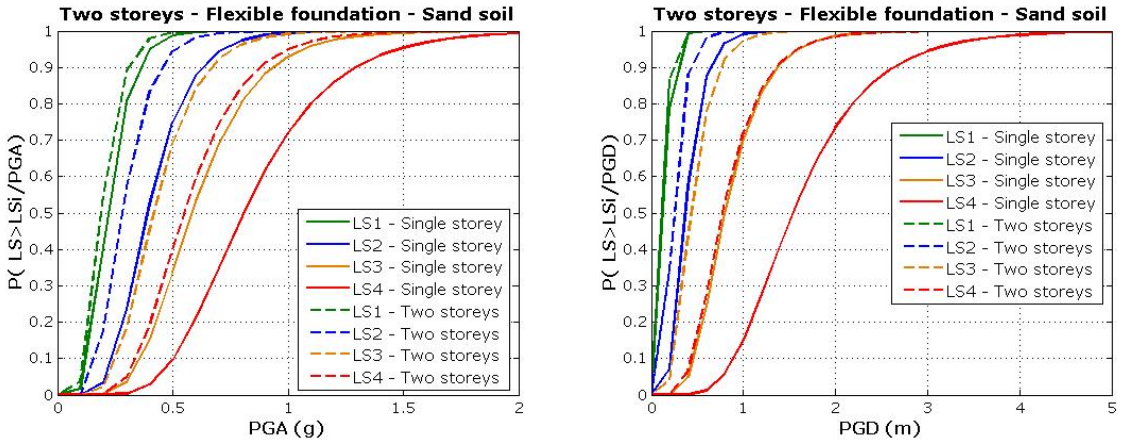


Figure 6.23. Fragility curves as a function of PGA (left) and PGD (right) when considering a one-storey and a two-storey structure on flexible foundations for sand slopes

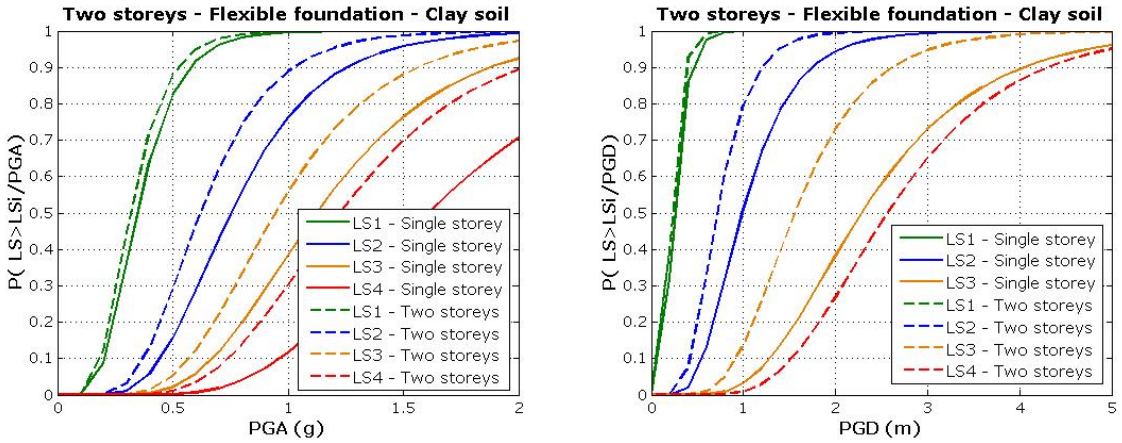


Figure 6.24. Fragility curves as a function of PGA (left) and PGD (right) when considering a one-storey and a two-storey structure on flexible foundations for clayey slopes

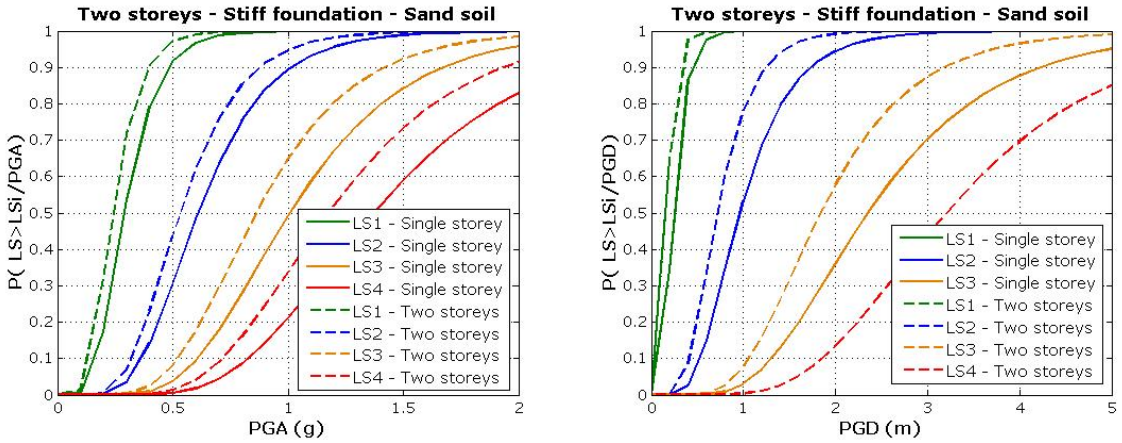


Figure 6.25. Fragility curves as a function of PGA (left) and PGD (right) when considering a one-storey and a two-storey structure on stiff foundations for sand slopes

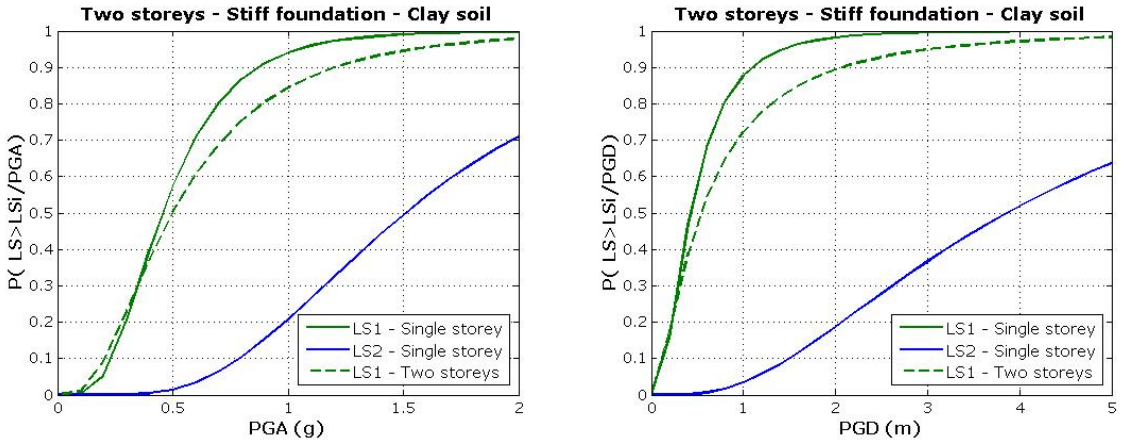


Figure 6.26. Fragility curves as a function of PGA (left) and PGD (right) when considering a one-storey and a two-storey structure on flexible foundations for clayey slopes

6.3.4.2. Number of bays

The number of bays of the considered building is an additional parameter that is selected to vary in this research. In particular, 2-bay RC bare frames are also studied considering different foundation systems and slope soil conditions. A schematic view of the analyzed two-bay structures is illustrated in Figure 6.27.

The performance of these structures is compared with the corresponding performance of the single-bay frames (see Fig. 6.19) by means of fragility functions considering common features for the slope dynamic models (model 1 and 2) and the structural typology. The building is assumed to be located 3m from the crest of the slope. It is noticed that the surcharge load on the foundation of the two-bay frame that is applied to an extended zone (determined by the foundation width), may contribute in deviating the path of excessive shearing deformation and consequently in altering the potential sliding surface exhibited.

A graphical representation of the fragility relationships is given in Figures 6.28 to 6.31. It is seen that, for the sand slope case, the two-bay frame would be less vulnerable compared to the corresponding single-bay frame building. On the contrary, for the clay slopes, the two-bay frame would suffer more damages than the single-bay one. These observations hold true irrespective of the foundation typology considered; they are associated to the relative position of the foundation to the potential sliding surface as well as to the zone in which the surcharge load is applied. For the slopes consisting of clayey soil material, the zone of the applied load on the foundation for the two-bay building would be comparable in dimensions with the potential sliding surface and thus the building would be partially outside the landslide mass resulting to increased differential deformation compared to the single-bay case where a rather more uniform movement of the building is anticipated. On the other hand, for the sand slope materials this zone is quite larger than the expected possible sliding surface and therefore a generally reduced differential deformation demand for the building is more likely.

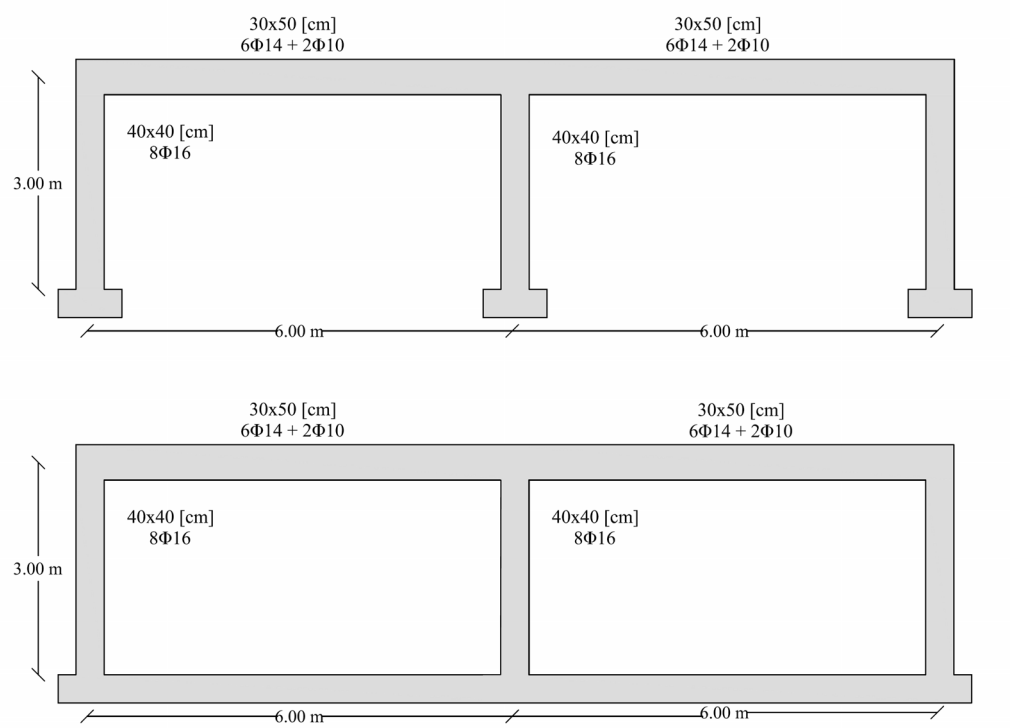


Figure 6.27. Schematic view of the analyzed 2 bays- 1 storey RC bare frame structures with flexible (top) and stiff (bottom) foundations

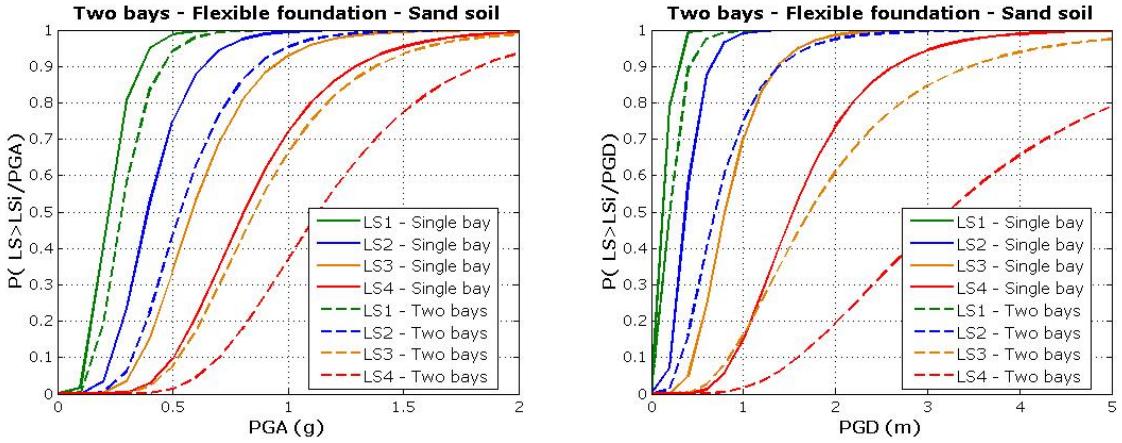


Figure 6.28. Fragility curves as a function of PGA (left) and PGD (right) when considering a one-bay and a two-bay structure on flexible foundations for sand slopes

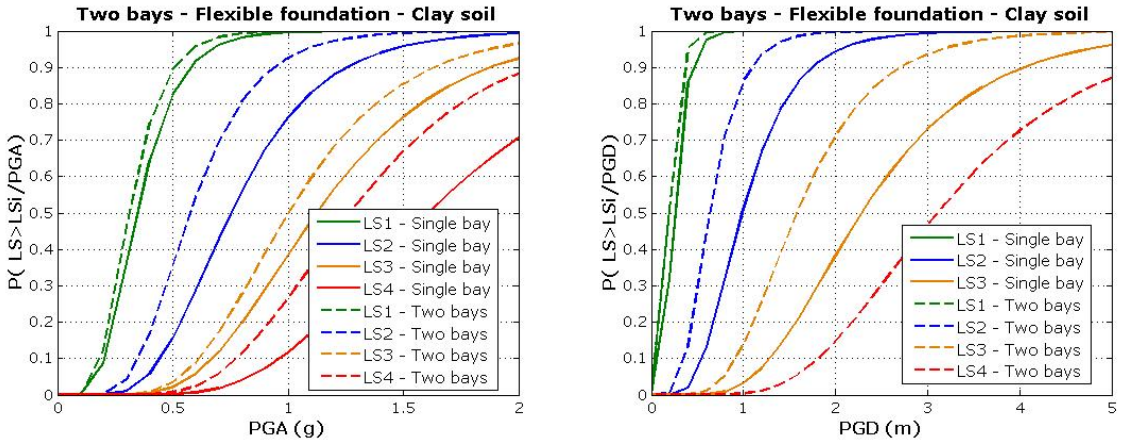


Figure 6.29. Fragility curves as a function of PGA (left) and PGD (right) when considering a one-bay and a two-bay structure on flexible foundations for clay slopes

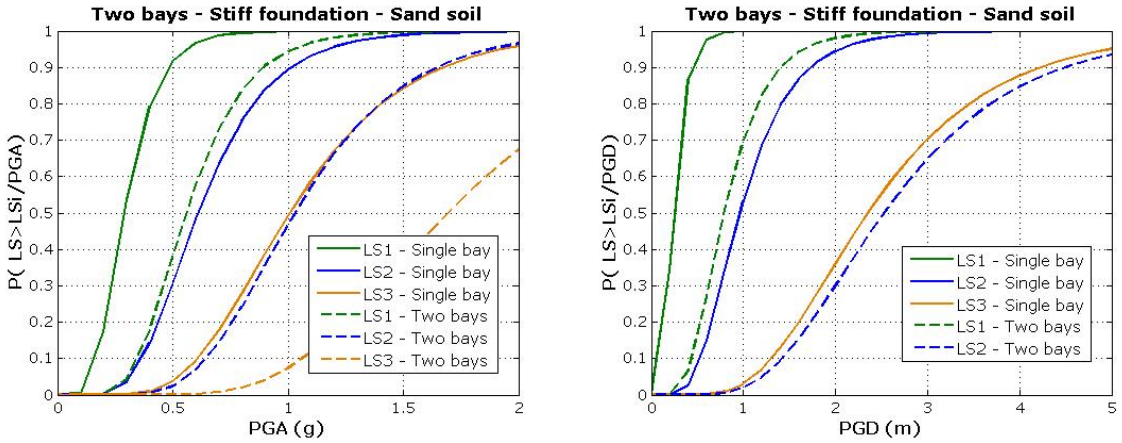


Figure 6.30. Fragility curves as a function of PGA (left) and PGD (right) when considering a one-bay and a two-bay structure on stiff foundations for sand slopes

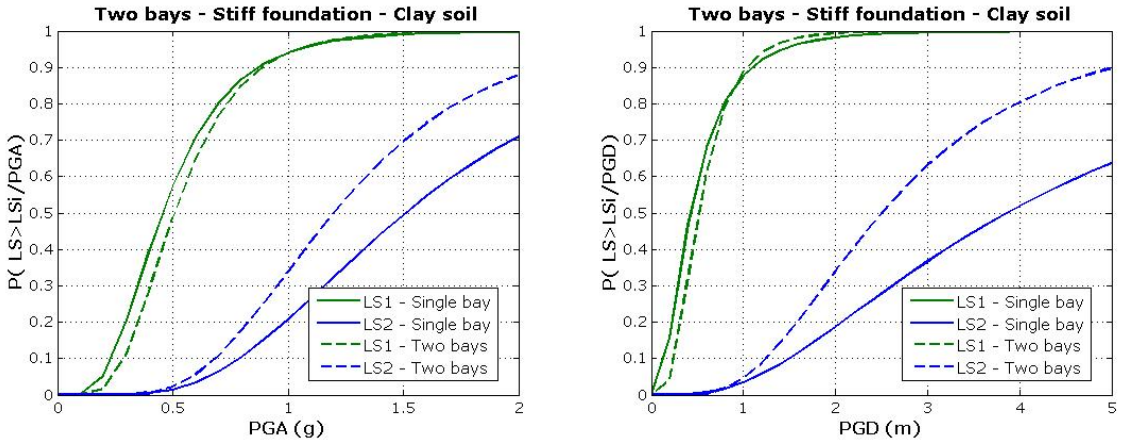


Figure 6.31. Fragility curves as a function of PGA (left) and PGD (right) when considering a one-bay and a two-bay structure on stiff foundations for clay slopes

6.3.5 Effect of building code design level

The code design level is another important parameter in assessing the vulnerability of RC frame structures to the irreversible landslide displacement. Considering that low-code RC buildings are poorly constructed structures characterized by a low level of confinement, the limit steel strains needed to exceed post yield limit states should have lower values compared to high-code, properly constructed RC buildings. As a consequence, different limit state values were adopted for exceedance of extensive and complete damage for low- and high-code frame RC buildings (see Chapter 4, Table 4.6) based on the work of Crowley et al. (2004), Bird et al. (2005), Negulescu and Foerster (2010) and engineering judgement. The corresponding fragility functions for the high- and low-code designed buildings as a function of PGA and PGD assuming the same geometrical and hydro-geological conditions (model 1) are depicted in Figure 6.32.

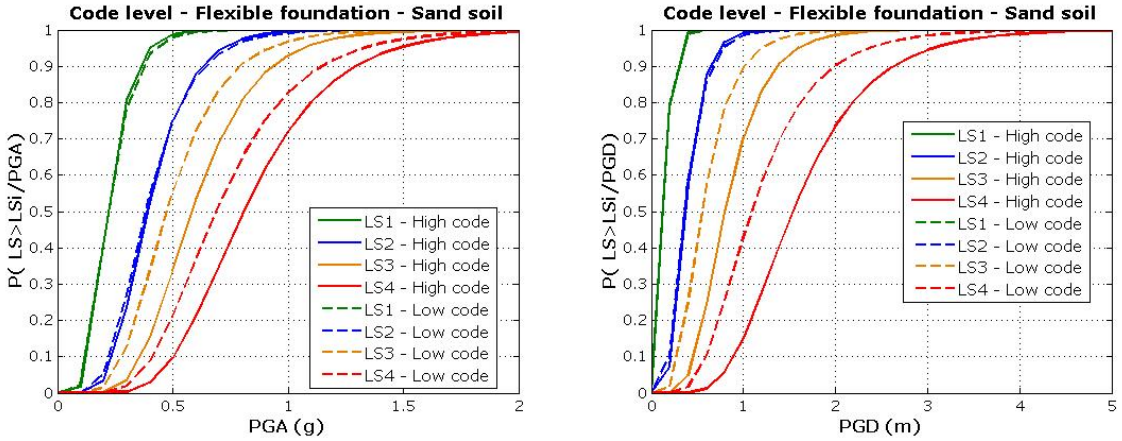


Figure 6.32. Fragility curves as a function of PGA (left) and PGD (right) when varying the code design level

It is observed that for the 1st and 2nd limit states, low- and high-code RC frame buildings experience quite similar performance. However, when extensive or complete damage to the building members is anticipated, the deviation in the building performance for low- and high-code designed buildings is expected to increase resulting to higher vulnerability levels for low code buildings. This is due to the low levels of attainable limit strains assumed for low-code building compared to high code, adequately confined structures. Several portfolios of fragility curves for low-code buildings based on the most crucial analyzed features are given in Annex B.

6.4 Conclusive remarks

Generic fragility curves both in terms of PGA and PGD have been proposed based on an extensive parametric investigation and sensitivity analysis of various slope configurations, soil properties and distances of the building with respect to the slope's crown. The features that have proved to affect more drastically the vulnerability of the building to the differential permanent deformation due to the seismically induced landslide hazard are the slope inclination in conjunction with the slope soil material. The slope height has also turned out to significantly influence the building's fragility for the steep sand slope configurations. Based on the above observations, seven sets of fragility curves have been suggested considering the most adverse position of the building with respect to the landslide that was found to be different for sand and clay slopes.

Several additional parameters, namely the water table level, the consideration of a strain softening landslide material, the flexibility of the foundation system, the number of bays and storeys of the building and the code design level, have also been studied for specific finite slope geometries and soil conditions, to illustrate the relative influence of each one of them on the structure's fragility. The influence of each parameter may vary with respect to the slope soil material (e.g. for the water table) and the foundation compliance (e.g. for the building geometry). Overall, their effect might potentially control the structure's fragility. It is noted, however, that a more in depth analysis of each of the additional features is generally warranted only for case histories where adequate quantitative data on the soil properties, slope geometry and building typologies are available.

CHAPTER 7

Validation of the proposed method

7.1 Introduction

The reliability and accuracy of the proposed methodology (Chapter 4) is assessed through the comparison of the analytically derived fragility curves with literature curves and recorded building damage data from two real case histories: Kato Achaia slope in Peloponnese –Greece and the Corniglio-Italy case study. In addition, in order to increase the applicability band of the proposed methodological framework, more realistic fragility curves are suggested for a representative building in Corniglio village.

7.2 Comparison of the developed fragility curves with literature curves

The validity of the developed curves is assessed through their comparison with respective literature curves derived by different approaches. In particular, fragility curves based on empirical damage data (Zhang and Ng, 2005), engineering judgement (NIBS, 2004) and on numerical simulations (Negulescu and Foerster, 2010) are used for that comparison.

Moreover, fragility curves derived for buildings subjected to ground shaking on horizontally layered soil deposits are used for approximate correlations with the ones proposed in this study. The purpose of this comparison is twofold: first, to assess the reliability of the proposed curves (mainly in terms of the order of magnitude) and second to gain better insight into the relative extent of damage and the associated failure mechanisms that dominate the structural response and fragility for structures subjected to ground shaking and co-seismic slope deformation respectively.

Among the developed curves, the ones that are selected for the comparison refer to a low-rise, high-code RC frame building resting on a shallow foundation of varying stiffness characteristics (i.e. isolated footings, continuous raft foundation) located next to the crest (i.e. 3m) of a 30^{o} inclined sand slope (see Chapter 4). These curves generally

represent a somewhat moderate case in terms of the expected vulnerability of the building to the permanent landslide displacement (see Chapter 6).

7.2.1 Comparison with empirical curves

Zhang and Ng (2005), based on statistical analysis of the actual observed displacement on over 300 buildings, proposed empirical fragility curves as a function of the limiting tolerable settlement (maximum vertical foundation displacement) and angular distortion (the average slope of the associated differential settlement of the building). The authors used the term "intolerable" to describe the displacements (settlements and angular distortions) that affect the safety, function and appearance of the structure. The buildings were classified into two main categories according to their foundation type (shallow or deep foundation). Among the studied buildings, they found that 95 experienced certain settlement and 205 certain angular distortion. The authors did not mention the origin of these displacements (e.g. due to landslide hazard). Tables 7.1 and 7.2 provide a summary of the limiting tolerable and intolerable displacements of these buildings (shallow foundation and all foundations cases are shown herein) in terms of settlements and angular distortions respectively. Table 7.3 presents the corresponding mean and standard deviations of these displacements.

Table 7.1. Summary of tolerable and intolerable settlements on buildings considering different foundation types (adapted from Zhang and Ng, 2005)

Settlement interval (cm)	All foundations		Shallow foundations	
	Tolerable	Intolerable	Tolerable	Intolerable
0–2.5	25	0	18	0
2.6–5	16	0	10	0
5.1–10	10	6	7	4
10.1–15	2	3	2	3
15.1–20	2	0	1	0
20.1–25	1	7	1	5
25.1–30	1	3	1	3
30.1–40	0	8	0	7
40.1–50	1	2	1	2
50.1–150	0	8	0	6
0-150 (all)	58	37	41	30

Table 7.2. Summary of tolerable and intolerable settlements on buildings considering different foundation types (adapted from Zhang and Ng, 2005)

Angular distortion	All foundations		Shallow foundations	
	Tolerable	Intolerable	Tolerable	Intolerable
0–0.001	23	2	18	0
0.0011–0.002	28	10	21	4
0.0021–0.003	17	13	14	7
0.0031–0.004	8	21	7	17
0.0041–0.005	2	10	2	6
0.0051–0.006	2	8	1	7
0.0061–0.008	1	12	1	9
0.0081–0.010	0	20	0	19
0.011–0.050	0	25	0	18
0.051–0.100	0	3	0	2
0-0.10 (all)	81	124	64	89

Table 7.3. Statistics of intolerable and limiting tolerable settlement and angular distortion of buildings (adapted from Zhang and Ng, 2005)

Statistics	All foundations		Shallow foundations	
	Mean	Standard deviation	Mean	Standard deviation
Observed intolerable settlement (cm)	40.3	33.4	39.9	32.3
Limiting tolerable settlement (cm)	12.3	7.3	12.9	7.2
Observed intolerable angular distortion	0.0116	0.0143	0.0119	0.0138
Limiting tolerable angular distortion	0.0028	0.0024	0.003	0.0015

To allow for direct comparisons of the fragility curves developed in this research to the corresponding curves provided by Zhang and Ng (2005), the proposed curves were properly modified as a function of the induced settlement and angular distortion respectively. The Maximum Likelihood method as described in Chapter 4 is used to estimate the log-normal distributed fragility parameters presented in Table 7.4. Comparative plots of the proposed curves for building on flexible and stiff foundations to the empirical ones as a function of settlement and angular distortion are given in Figures 7.1 to 7.4.

Table 7.4. Fragility parameters of the proposed curves in terms of settlement and angular distortion

		Limit state	Flexible foundation	Stiff foundation
Settlement (m)	Median	LS1	0.07	0.06
		LS2	0.21	0.32
		LS3	0.31	0.75
		LS4	0.49	1.36
	Dispersion β		0.39	0.42
Angular distortion	Median	LS1	0.006	0.007
		LS2	0.018	0.029
		LS3	0.037	0.061
		LS4	0.064	0.100
	Dispersion β		0.36	0.37

Overall, the comparison between the curves is judged satisfactory considering the large uncertainty and variability involved and the fact that the empirically derived curves are dealing with foundation movements irrespective of their origin (e.g. earthquake induced landslide hazard) and the superstructure typology.

A good correlation is observed between the empirical curves and the proposed fragility curves for the building when using Settlement as a metric of the landslide displacement. A better match is detected for buildings on flexible foundation rather than on stiff ones. The correlation is not so good when using Angular distortion as an intensity parameter. In particular, the empirical curves are generally shift to the left predicting quite low median values of limiting tolerable angular distortion and consequently increased expected building damage. These low values are probably associated to loss of functionality (e.g. due to tilting), which is not accounted for in the proposed numerically derived curves, and not to structural damage to the building members.

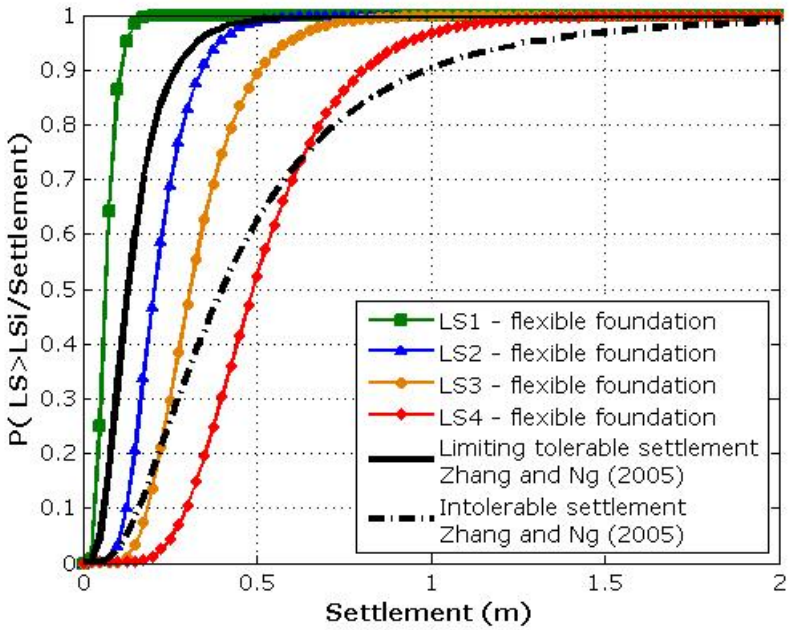


Figure 7.1. Comparison of the proposed fragility curves as a function of settlement for the building on flexible foundation with the corresponding empirical curves provided by Zhang and Ng (2005)

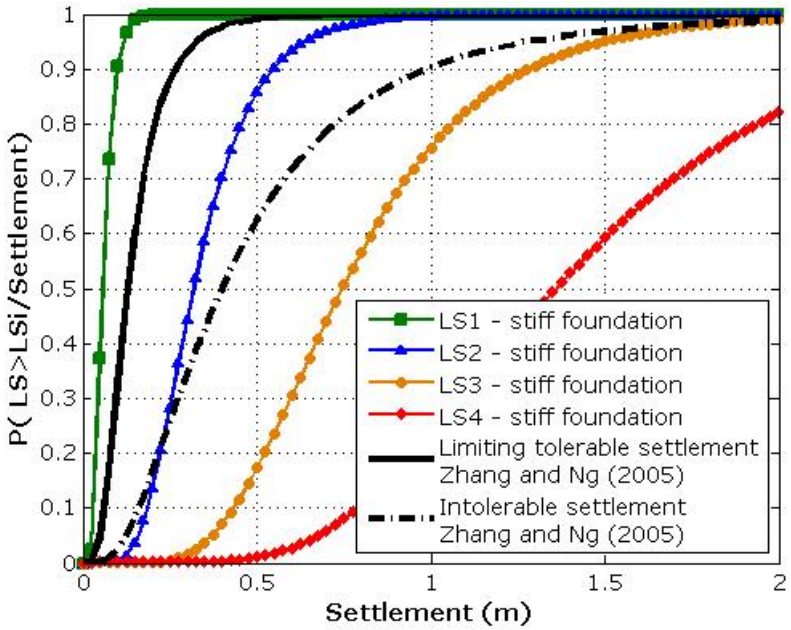


Figure 7.2. Comparison of the proposed fragility curves as a function of settlement for the building on stiff foundation with the corresponding empirical curves provided by Zhang and Ng (2005)

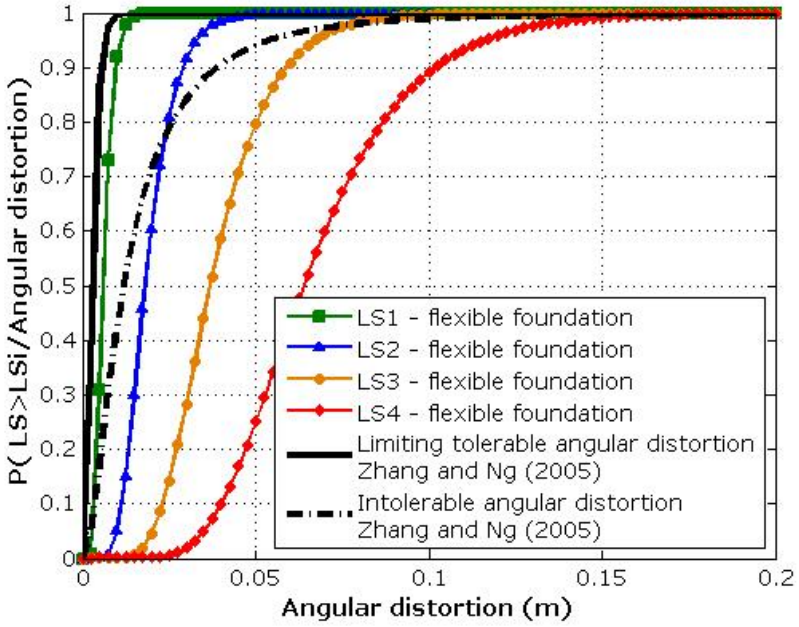


Figure 7.3. Comparison of the proposed fragility curves as a function of angular distortion for the building on flexible foundation with the corresponding empirical curves provided by Zhang and Ng (2005)

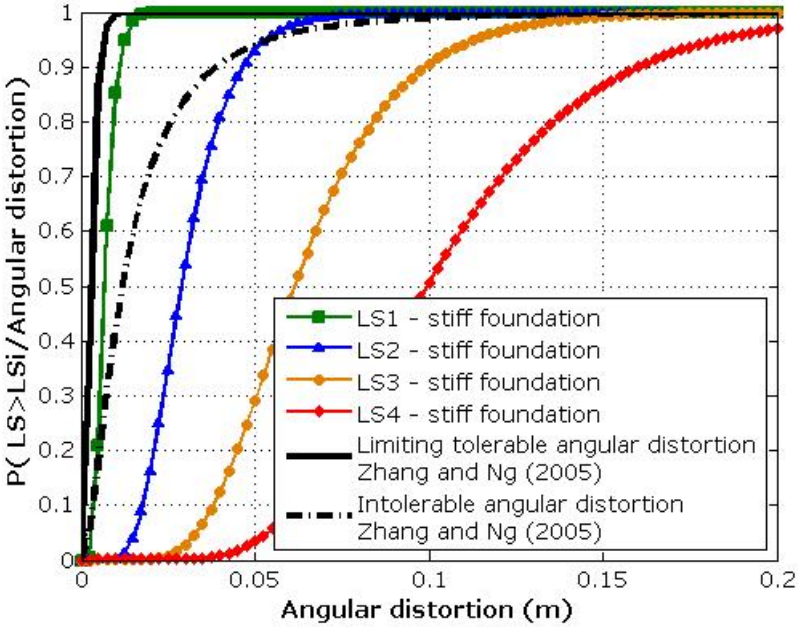


Figure 7.4. Comparison of the proposed fragility curves as a function of angular distortion for the building on stiff foundation with the corresponding empirical curves provided by Zhang and Ng (2005)

7.2.2 Comparison with expert judgment curves

HAZUS loss estimation methodology (NIBS, 2004) provided fragility curves for structures subjected to earthquake-induced ground failure taking into account the expected mode of failure and the foundation type (see also Chapter 3, § 3.3.2). Separate fragility curves

distinguishing between ground failure due to lateral spreading and ground failure due to ground settlement, and between shallow and deep foundations were proposed. Only one combined Extensive/Complete damage state was considered. In essence, according to HAZUS, buildings were assumed to be either undamaged or severely damaged due to ground failure. Fragility curves were derived as a function of permanent ground displacement (PGD) using a form similar to those used to estimate shaking damage. Engineering judgment was used to develop a set of assumptions, which define building fragility. Suggested median and lognormal standard deviation values in terms of PGD for buildings on shallow foundations or buildings of unknown foundation type are given in Table 7.5. As shown in the table, that lateral spread was judged to require significantly more PGD to effect severe damage than ground settlement. This is due to the fact that many buildings in lateral spread areas are generally expected to move with the spread, but not to be severely damaged until the spread becomes quite significant.

Table 7.5. Suggested log-normally distributed fragility parameters of HAZUS for shallow/unknown foundations

	Settlement PGD (m)	**Lateral Spread PGD (m)**
Median	0.254	0.1524
Dispersion β	1.2	1.2

The expert judgemental curves provided by HAZUS are compared with the numerically derived curves for extensive and complete damage for the building on flexible and stiff foundations (Figs. 7.5 to 7.10). The herein proposed curves are given as a function of the maximum permanent ground displacement vector (PGD), horizontal permanent ground displacement (PHGD) and vertical permanent ground displacement (PVGD) at the slope area, to permit the comparison with both HAZUS curves (Figs. 7.5 and 7.8) and separately with the curves which account for lateral spreading (principally horizontal movement) (Figs. 7.6 and 7.9) and settlement (principally vertical movement) (Figs. 7.7 and 7.10) respectively. The log-normal distributed fragility parameters of the proposed curves in terms of PGD, PHGD and PVGD are presented in Table 7.6.

A good agreement between the proposed curves for the building on flexible foundation and the respective HAZUS curves is observed, with the latter generally predicting larger vulnerability values. However, the comparison is not satisfactory when considering a building on stiff foundations. In particular, HAZUS curves are found to be far more conservative, highlighting the influential role of foundation stiffness (that is not taken into account in HAZUS methodology) in modifying (generally reducing) the building vulnerability to the permanent landslide displacement.

Table 7.6. Fragility parameters of the proposed curves in terms of PGD, PHGD and PVGD

		Limit state	Flexible foundation	Stiff foundation
PGD (m)	Median	LS1	0.14	0.24
		LS2	0.37	0.96
		LS3	0.80	2.35
		LS4	1.54	-
	Dispersion β		0.42	0.46
PHGD (m)	Median	LS1	0.12	0.19
		LS2	0.31	0.81
		LS3	0.67	2.08
		LS4	1.35	3.66
	Dispersion β		0.46	0.47
PVGD (m)	Median	LS1	0.08	0.13
		LS2	0.22	0.49
		LS3	0.43	1.15
		LS4	0.80	1.88
	Dispersion β		0.40	0.40

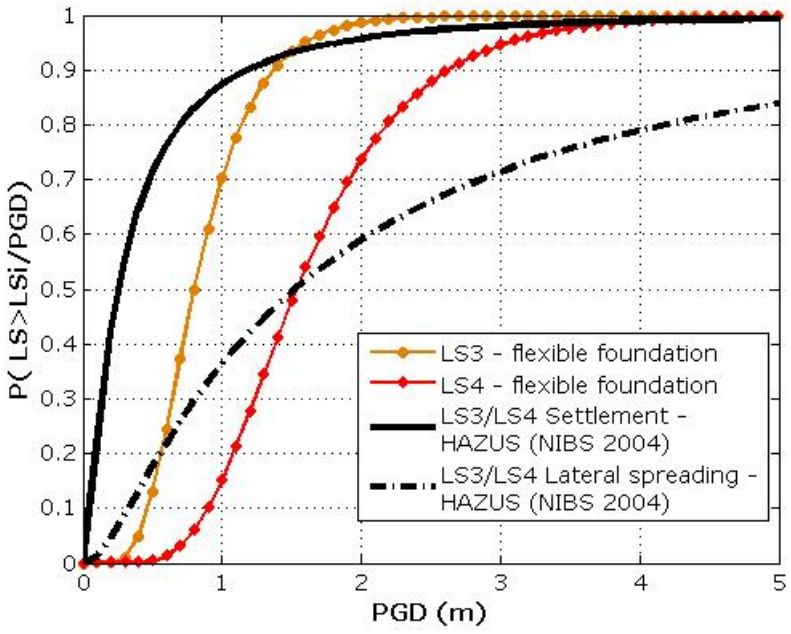


Figure 7.5. Comparison of the proposed fragility curves for extensive and complete damage as a function of permanent ground displacement (PGD) for the building on flexible foundation with the corresponding expert judgment curves provided by HAZUS (NIBS, 2004)

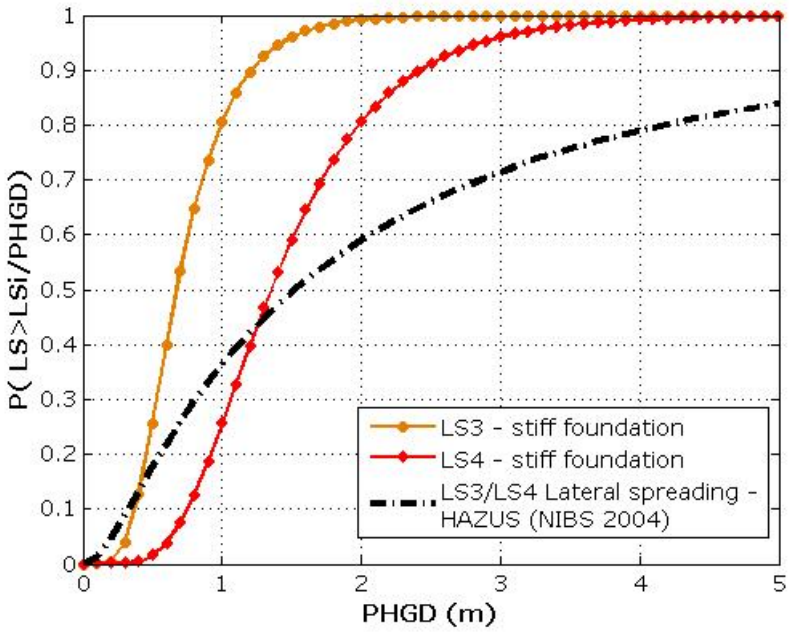


Figure 7.6. Comparison of the proposed fragility curves for extensive and complete damage as a function of permanent horizontal ground displacement (PHGD) for the building on flexible foundation with the corresponding expert judgment curves provided by HAZUS (NIBS, 2004) for ground failure due to lateral spreading

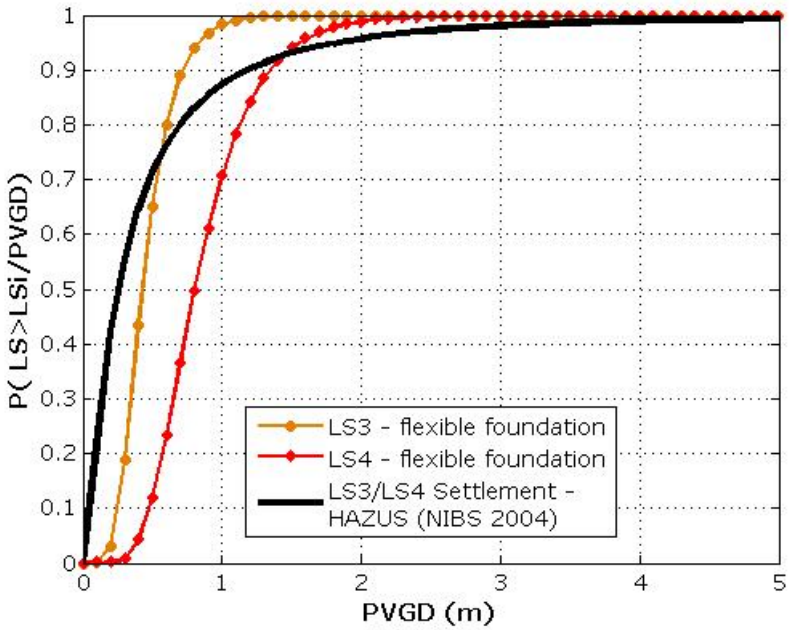


Figure 7.7. Comparison of the proposed fragility curves for extensive and complete damage as a function of permanent vertical ground displacement (PVGD) for the building on flexible foundation with the corresponding expert judgment curves provided by HAZUS (NIBS, 2004) for ground failure due to settlement

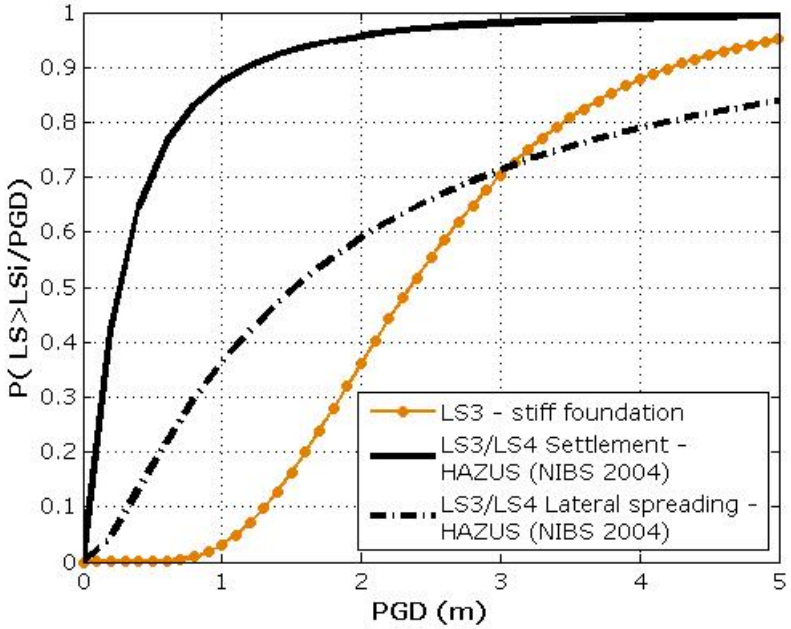


Figure 7.8. Comparison of the proposed fragility curves for extensive damage as a function of permanent ground displacement (PGD) for the building on stiff foundation with the corresponding expert judgment curves provided by HAZUS (NIBS, 2004)

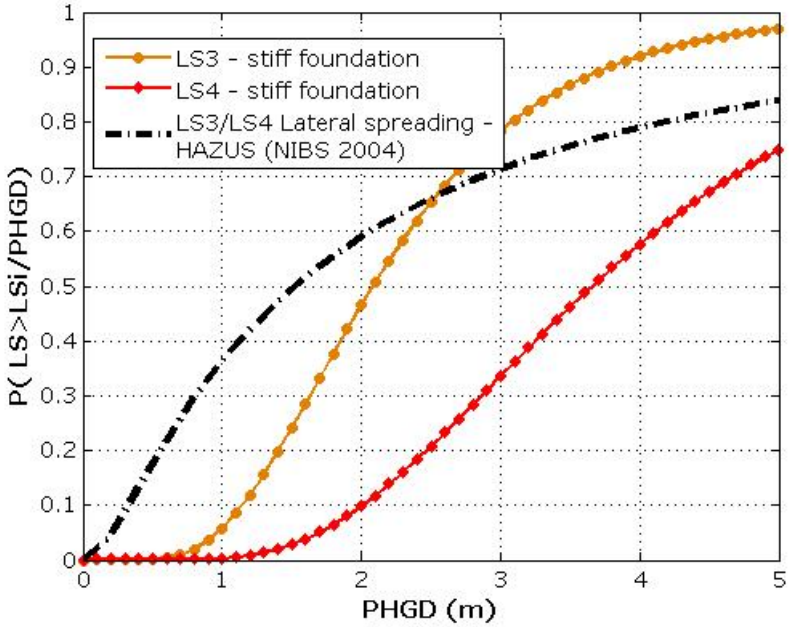


Figure 7.9. Comparison of the proposed fragility curves for extensive and complete damage as a function of permanent horizontal ground displacement (PHGD) for the building on stiff foundation with the corresponding expert judgment curves provided by HAZUS (NIBS, 2004) for ground failure due to lateral spreading

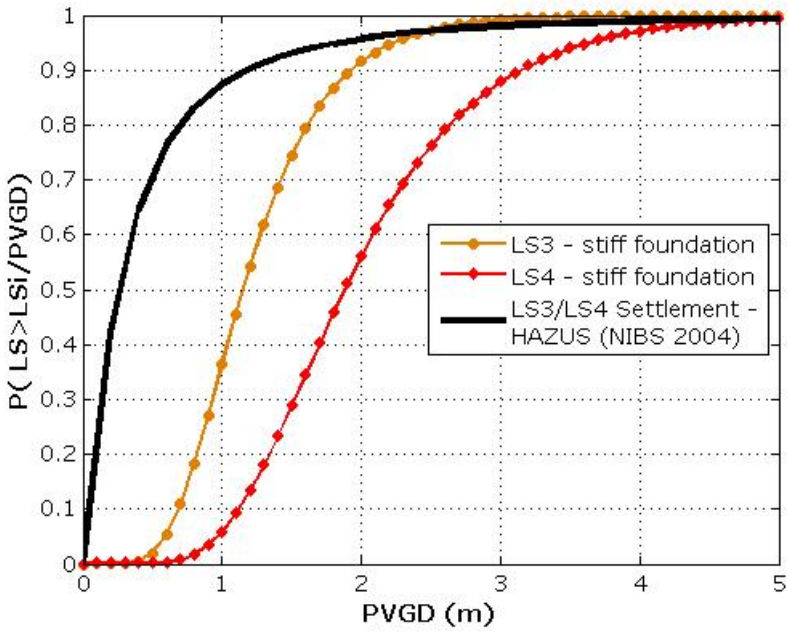


Figure 7.10. Comparison of the proposed fragility curves for extensive and complete damage as a function of permanent vertical ground displacement (PVGD) for the building on stiff foundation with the corresponding expert judgment curves provided by HAZUS (NIBS, 2004) for ground failure due to settlement

7.2.3 Comparison with numerically derived curves

Negulescu and Foerster (2010) proposed a simplified analytical methodology to assess the vulnerability of simple RC frame structures subjected to free-field differential ground displacement based on 2-D nonlinear static time-history analyses (see also Chapter 3, § 3.3.2). They examined different parameters that could influence structural behavior: foundation type (i.e. different combinations of links), cross-section geometry, section reinforcement degree, displacement magnitudes and displacement inclination angles. Structural damage levels were considered, as in the present study, based on the local strain limits of steel and concrete constitutive materials. A set of preliminary fragility curves was derived considering encasing links for the foundation to represent a continuous surface foundation or a building with a basement. Table 7.7 shows the fragility parameters used to construct the fragility curves.

To assess the validity of the curves proposed in this research, they are also compared with the curves given in Negulescu and Foerster (2010). For the purpose of this comparison, the herein proposed curves are modified in terms of differential ground displacement at the foundation level. The corresponding medians and dispersions of these curves for the building on flexible and stiff foundations, are presented in Table 7.8. As we may see from the table, the expected median differential ground displacement

values are increased as the stiffness of the foundation system increases, resulting to reduced vulnerability values for the building on stiff foundations.

Figures 7.11 and 7.12 shows comparative graphs of the proposed fragility curves as a function of differential ground displacement for the building on flexible foundation and stiff foundations respectively with the corresponding analytical curves given in Negulescu and Foerster (2010). It is observed that the suggested curves in this research for the building on flexible foundation are in good correlation with the Negulescu and Foerster's curves, taking also into account the different assumptions and uncertainties associated with them. On the contrary, for the curves referring to a building on stiff foundations the correlation is not so good. In particular, the building resting on stiff foundations is expected to sustain less structural damage compared to the Negulescu and Foerster's curves, highlighting the importance of modeling the soil-foundation-interaction in that case. It 's worth noting, however, that, for the stiff foundation case, the total building damage (structural and non-structural) is generally expected to be significantly larger as a considerable amount of damage would be attributed to rigid body movement reducing the serviceability level of the building.

Table 7.7. Fragility parameters of the numerically derived curves provided by Negulescu and Foerster (2010)

		Limit state	
Differential displacement (m)	Median	LS1	0.05
		LS2	0.12
		LS3	0.27
		LS4	0.40
	Dispersion β		0.50

Table 7.8. Fragility parameters of the proposed curves in terms of differential ground displacement

		Limit state	Flexible foundation	Stiff foundation
Differential displacement (m)	Median	LS1	0.07	0.08
		LS2	0.17	0.34
		LS3	0.34	0.86
		LS4	0.59	1.38
	Dispersion β		0.36	0.38

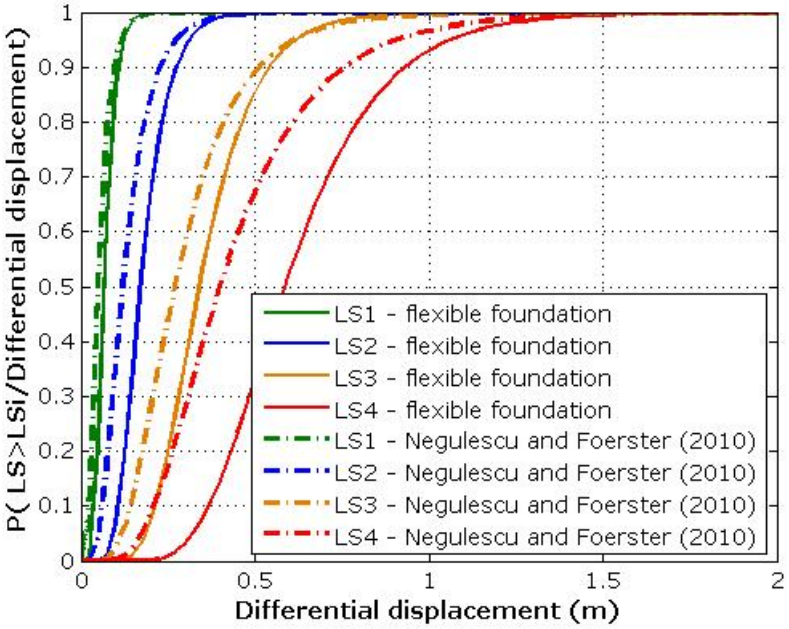


Figure 7.11. Comparison of the proposed fragility curves as a function of differential ground displacement for the building on flexible foundation with the corresponding analytical curves provided by Negulescu and Foerster (2010)

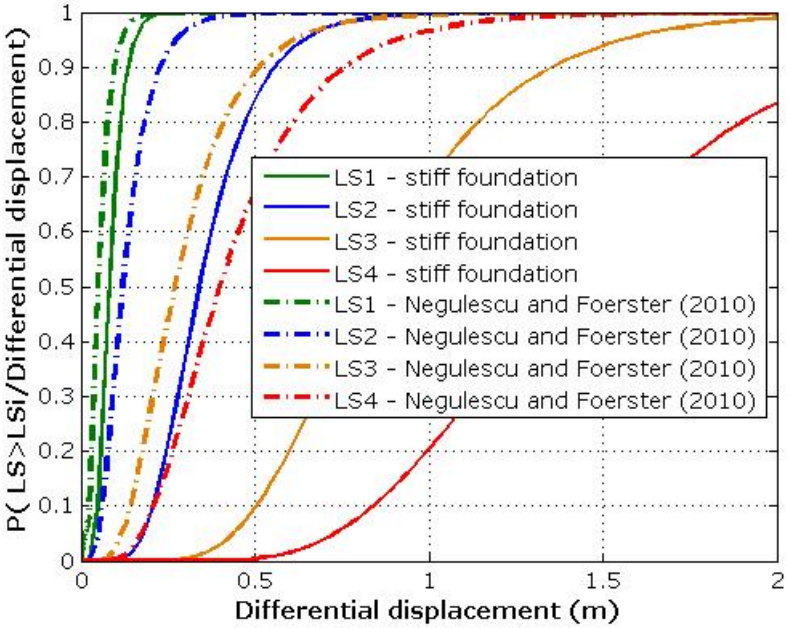


Figure 7.12. Comparison of the proposed fragility curves as a function of differential ground displacement for the building on stiff foundation with the corresponding analytical curves provided by Negulescu and Foerster (2010)

7.2.4 Comparison with seismic fragility curves for horizontally layered soil media

It is also particularly interesting from an engineering viewpoint to compare the fragility curves proposed in this research for buildings standing near the crest of a slope that are exposed to co-seismic irreversible slope displacements to the ones for buildings on horizontally layered soil deposits (without any topographic irregularity) subjected to cyclic loading due to an earthquake.

To accomplish this, an analytical code developed within the framework of Syner-G European project is used. The so-called Syner-G Fragility Function Manager (Crowley et al. 2011- SYNER-G project) is an efficient tool able to store, harmonize and compare different sets of fragility curves. It is based on the collection of existing fragility functions and the identification of categories for grouping buildings (taxonomy) and for harmonizing different intensity measures and limit states. Except for the already available fragility functions in the code, the recently developed fragility curves by Fotopoulou et al. (2012) for seismically designed RC frame buildings were stored and harmonized to permit correlations. It 's worth noting that the fragility curves in Syner-G Fragility Function Manager tool have been constructed for buildings subjected to ground shaking and not to earthquake induced differential permanent ground displacement, as proposed in this research, and thus only approximate comparisons, focusing e.g. on the order of magnitude, are possible.

The selected curves were harmonized both in terms of the intensity measure and the number of limit states to permit direct comparison. In particular, the harmonization in terms of the intensity measure was performed using PGA at the outcrop as the target intensity measure and considering appropriate conversion equations depending on the initial intensity parameter and the region of interest (see Table 7.9). The harmonization in terms of limit states is conducted by considering two different limit states, namely yielding and collapse, based on the reasonable assumption that yielding will almost always be either the first or the second curve whilst the collapse limit state is usually the last curve in the set (Crowley et al. 2011- SYNER-G project). Table 7.9 presents the basic references and assumptions associated with that curves. Table 7.10 presents the harmonized fragility parameters of the curves proposed in this thesis (see Chapters 4 and 6) referring to low-rise, seismically designed, RC moment-resisting bare frame buildings on flexible foundations subjected to co-seismic permanent landslide differential displacement for the yielding and collapse limit states. Comparative plots between the proposed curves for the yielding and collapse limit states and the harmonized literature seismic fragility curves are presented in Figures 7.13 to 7.22.

It is shown that for the yielding limit state most of the literature curves predict larger damages for the building (the curves given by Ozmen et al. (2010) and Rossetto and Elnashai (2003) represent an exception). This is reasonable considering that the building is generally expected to suffer some (usually slight) initial damage due to ground shaking before the onset of the landslide movement. On the contrary, it is observed that for the collapse limit state most of the literature curves estimate lower vulnerability values for the building with respect to the ones proposed in this study. Thus, it is implicitly shown that once the landslide has triggered by the earthquake, it may become the prevailing damage mechanism resulting to larger damages for the building near collapse.

Overall, the comparisons are judged satisfactory revealing, however, the high aleatory and epistemic uncertainty associated with the different fragility curves found in the literature.

Table 7.9. Main parameters of the literature seismic fragility curves used for the comparison

Reference	Region of applicability	Methodology	Intensity measure	Intensity measure type conversion	Cumulative distribution function
Ahmad et al. 2011	Euro-Mediterranean Regions (Greek, Italy, Turkey)	Analytical – Nonlinear Static	PGA	-	Lognormal
Borzi et al. 2007	Italy	Analytical – Nonlinear Static	PGA	-	Lognormal
Kappos et al. 2003	Greece	Hybrid	PGA	-	Lognormal
Ozmen et al. 2010	Turkey	Analytical – Nonlinear Dynamic	PGA	-	Lognormal
Rossetto and Elnashai 2003	Europe	Empirical	PGA	-	$P=1-\exp(-\alpha GM\beta)$
Tsionis et al. 2011	Euro-Mediterranean Regions	Analytical – Nonlinear Dynamic	PGA	-	Lognormal
Akkar et al. 2005	Turkey	Analytical – Nonlinear Dynamic	PGV	Bommer and Alarcon 2006 & IBC 2006	Lognormal
Erberik 2008	Turkey	Analytical – Nonlinear Dynamic	PGV	Bommer and Alarcon 2006 & IBC 2006	Lognormal
Nuti et al. 1998	Italy	Empirical	MCS Scale (Mercalli – Cancani – Sieberg)	Margottini et al. 1992	Lognormal
Fotopoulou et al. 2012	Euro-Mediterranean Regions	Analytical – Nonlinear Dynamic	PGA	-	Lognormal

Table 7.10. Fragility parameters of the harmonized proposed fragility curves used for the comparison (sand soil, flexible foundation)

PGA (g)		
Median		Dispersion β
Yielding	Collapse	
0.22	0.81	0.37

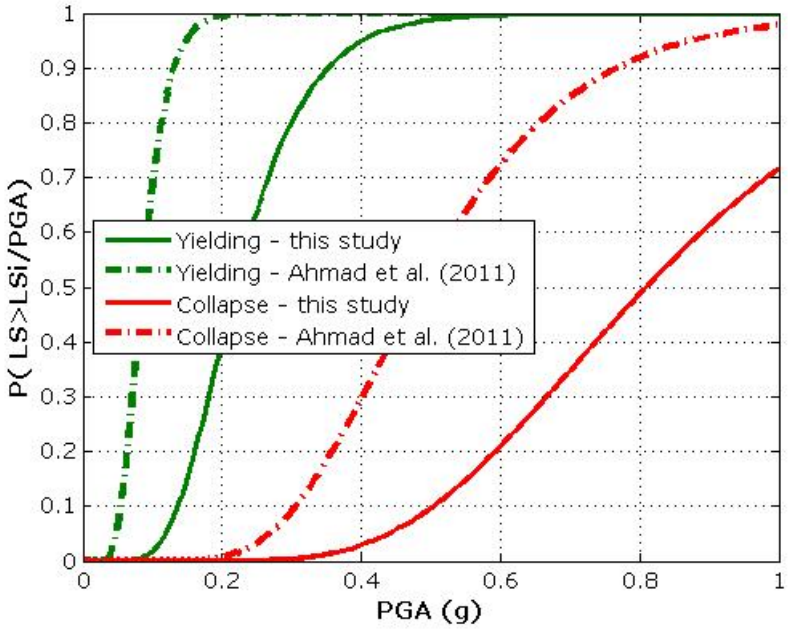


Figure 7.13. Comparison of the harmonized proposed fragility curves as a function of PGA for low-rise, seismically designed, RC frame buildings exposed to co-seismic slope displacements with the corresponding curves provided by Ahmad et al. (2011) for the same building typologies when subjected to seismic ground shaking

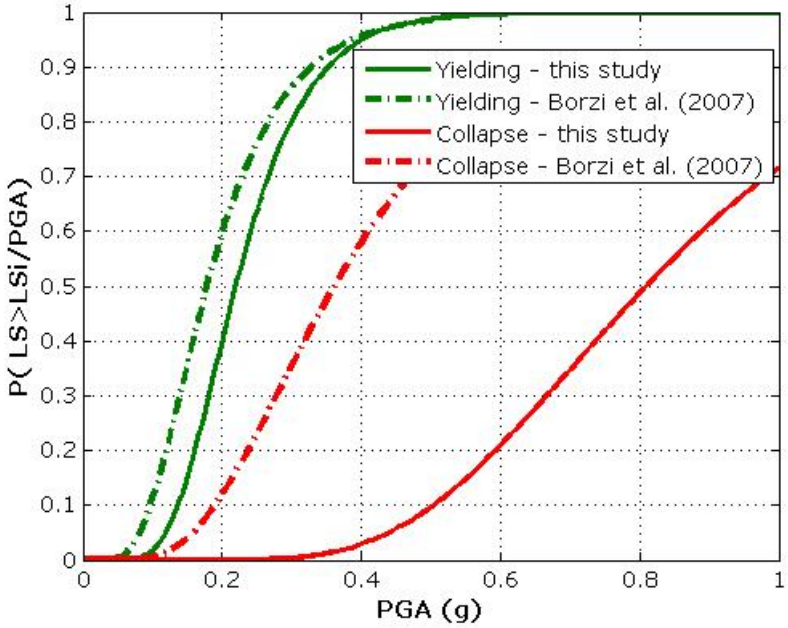


Figure 7.14. Comparison of the harmonized proposed fragility curves as a function of PGA for low-rise, seismically designed, RC frame buildings exposed to co-seismic slope displacements with the corresponding curves provided by Borzi et al. (2007) for the same building typologies when subjected to seismic ground shaking

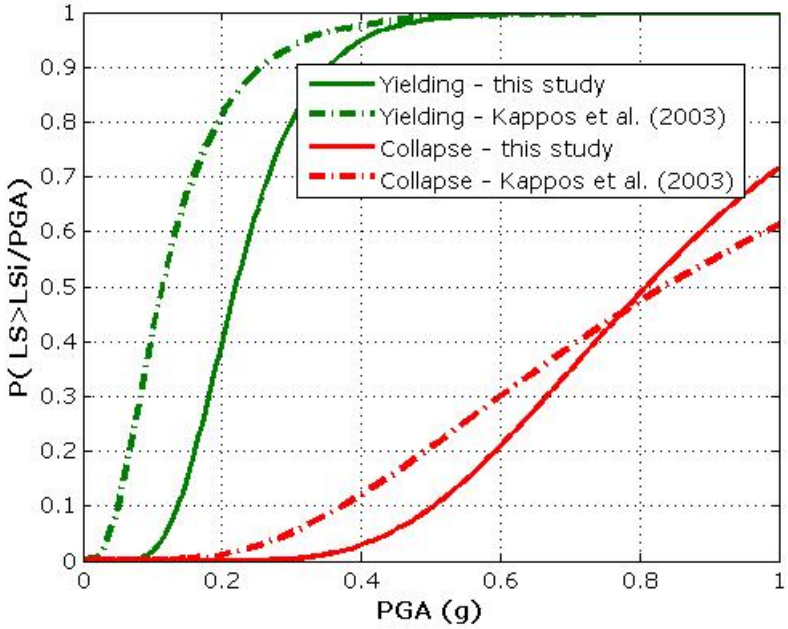


Figure 7.15. Comparison of the harmonized proposed fragility curves as a function of PGA for low-rise, seismically designed, RC frame buildings exposed to co-seismic slope displacements with the corresponding curves provided by Kappos et al. (2003) for the same building typologies when subjected to seismic ground shaking

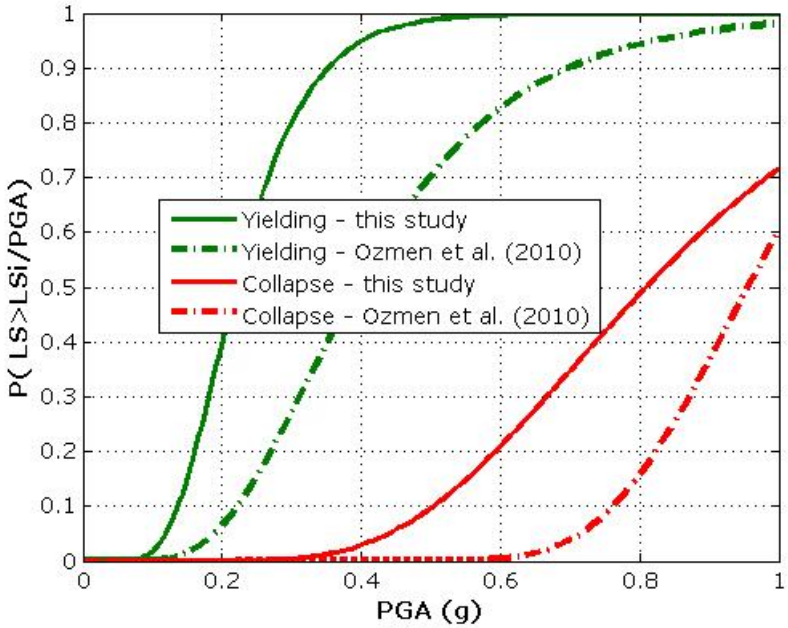


Figure 7.16. Comparison of the harmonized proposed fragility curves as a function of PGA for low-rise, seismically designed, RC frame buildings exposed to co-seismic slope displacements with the corresponding curves provided by Ozmen et al. (2010) for the same building typologies when subjected to seismic ground shaking

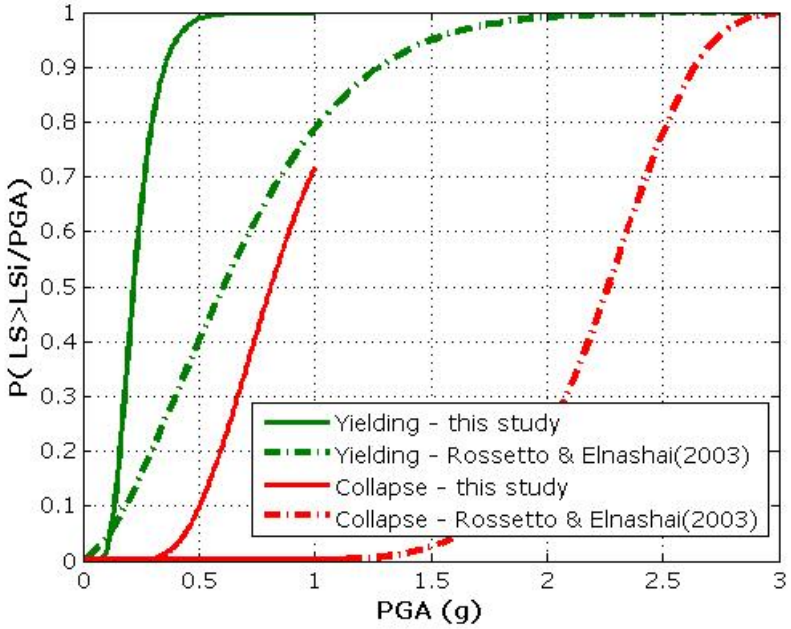


Figure 7.17. Comparison of the harmonized proposed fragility curves as a function of PGA for low-rise, seismically designed, RC frame buildings exposed to co-seismic slope displacements with the corresponding curves provided by Rossetto and Elnashai (2003) for the same building typologies when subjected to seismic ground shaking

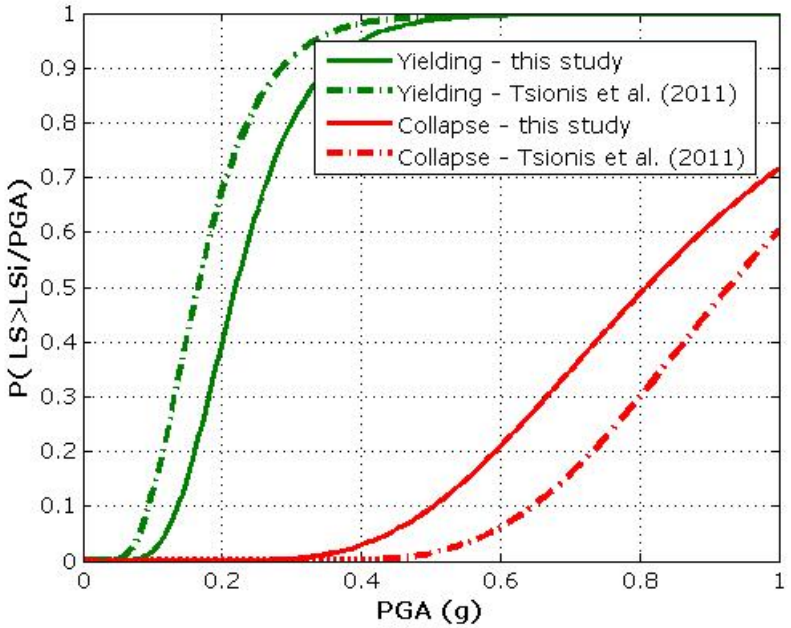


Figure 7.18. Comparison of the harmonized proposed fragility curves as a function of PGA for low-rise, seismically designed, RC frame buildings exposed to co-seismic slope displacements with the corresponding curves provided by Tsionis et al. (2011) for the same building typologies when subjected to seismic ground shaking

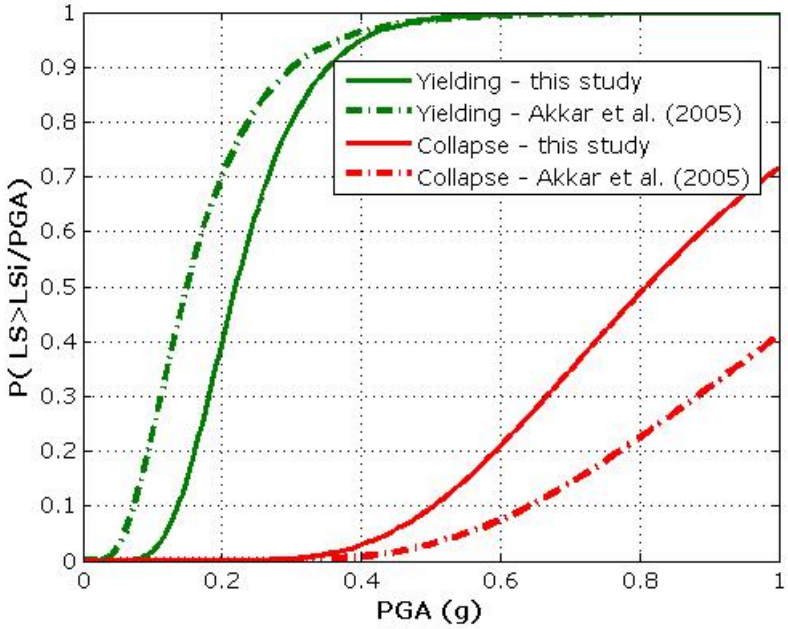


Figure 7.19. Comparison of the harmonized proposed fragility curves as a function of PGA for low-rise, seismically designed, RC frame buildings exposed to co-seismic slope displacements with the corresponding curves provided by Akkar et al. (2005) for the same building typologies when subjected to seismic ground shaking

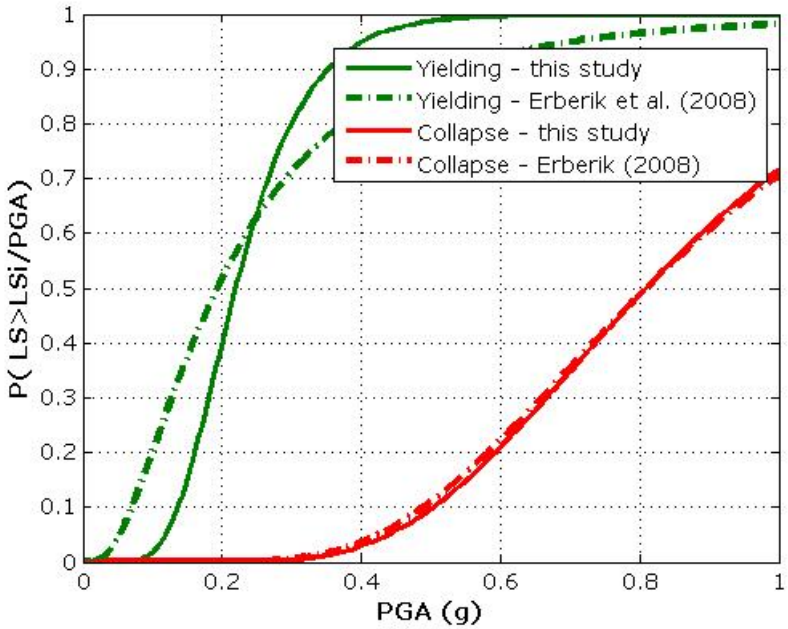


Figure 7.20. Comparison of the harmonized proposed fragility curves as a function of PGA for low-rise, seismically designed, RC frame buildings exposed to co-seismic slope displacements with the corresponding curves provided by Erberik (2008) for the same building typologies when subjected to seismic ground shaking

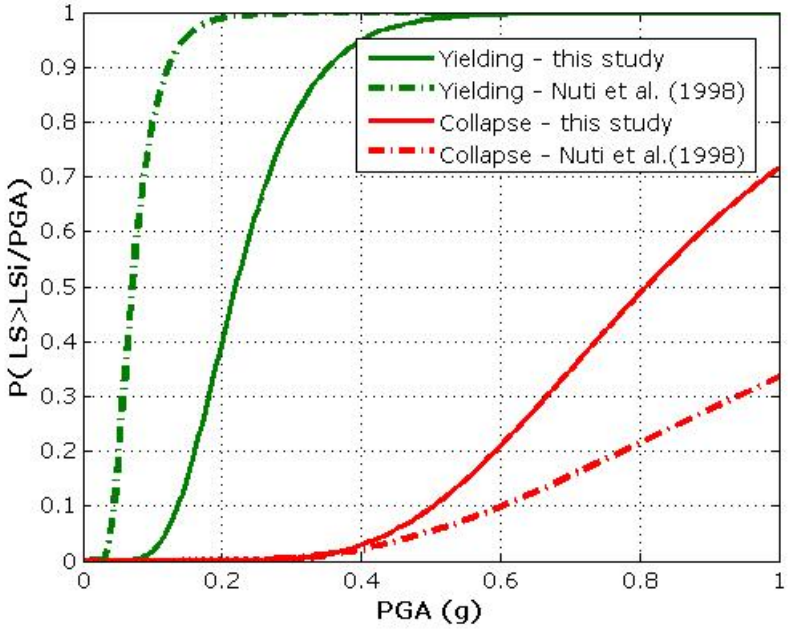


Figure 7.21. Comparison of the harmonized proposed fragility curves as a function of PGA for low-rise, seismically designed, RC frame buildings exposed to co-seismic slope displacements with the corresponding curves provided by Nuti et al. (1998) for the same building typologies when subjected to seismic ground shaking

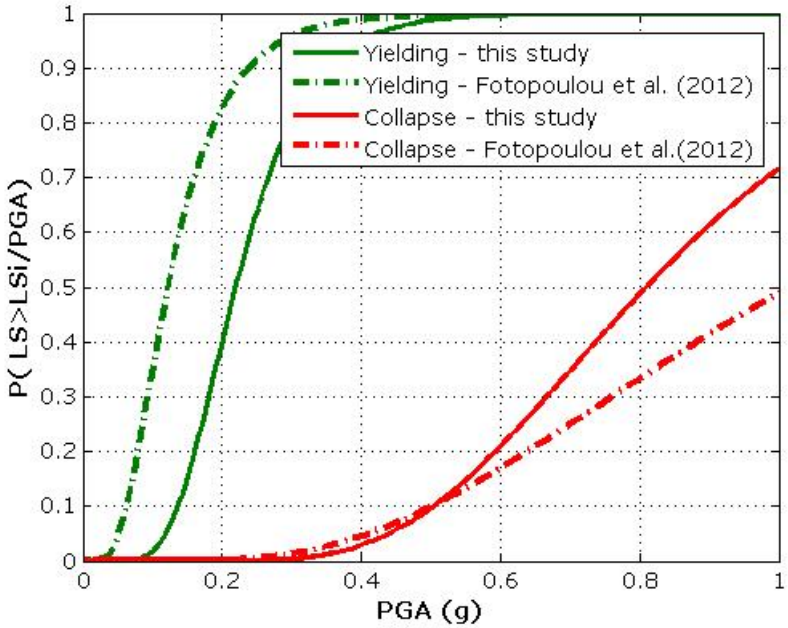


Figure 7.22. Comparison of the harmonized proposed fragility curves as a function of PGA for low-rise, seismically designed, RC frame buildings exposed to co-seismic slope displacements with the corresponding curves provided by Fotopoulou et al. (2012) for the same building typologies when subjected to seismic ground shaking

7.3 Application to Kato Achaia slope- western Greece

7.3.1 Introduction

The reliability and applicability of the proposed fragility curves is also explored through its application to real case histories. More specifically, the approach is implemented to a reference RC building located in the vicinity of the Kato Achaia slope's ridge, where most of the building damages were observed as a result of the Ilia-Achaia, Greece 2008 (Mw= 6.4) earthquake. The ultimate goal of the analysis is to assess the validity of the developed fragility curves via comparison with recorded and simulated building damage data.

7.3.2 The Earthquake of 8 June 2008 in Achaia-Ilia, Greece

On 8 June 2008, an Mw 6.4 strong earthquake occurred in the area of northwest Peloponnese, western Greece, at a distance of about 17 km southwest of the town of Patras on a dextral strike slip fault (Fig. 7.23). The main shock was recorded by 27 strong motion instruments at distances ranging approximately from 15 to 350 km from the surface projection of the fault. Of those 27 stations, six are within a relatively small region in Patras (Margaris et al., 2010). The event caused considerable structural damage to buildings and infrastructures. Ground failure was widely observed within approximately 15 km of the fault, taking the form of landslides (mostly rockfalls), liquefaction, coastal subsidence, and settlement of fills (Margaris et al., 2008).

The town of Kato Achaia is located approximately 20 km from the epicenter of the main shock and from the town of Patras (Fig. 7.23). The minimum distance from the surface projection of the fault was estimated as R_{jb} = 6 km (Fig. 7.24). The site along the coast of Kato Achaia was found to suffer extensive ground deformation due to liquefaction. However, it is not our objective here to study liquefaction phenomena. Preliminary investigation on Kato Achaia area indicates peak horizontal ground acceleration values on the order of 0.3g, quite higher than the values recorded in Patras downtown.

An important concentration of severe building damages is observed near the edge of the cliff that comprises the northern boundary of Kato Achaia town (Fig. 7.25). This is probably due to simple site amplification in the vicinity of the crest as it is illustrated by the amplification of the horizontal acceleration and the generation of parasitic vertical acceleration near the top of the slope (Athanasopoulos G. and Pefani H., personal communication, 2010). However such models are not considering any effect from permanent ground displacements due to differential ground movements close to the

slope and the crest. In the present study, the possible presence of both phenomena is investigated.

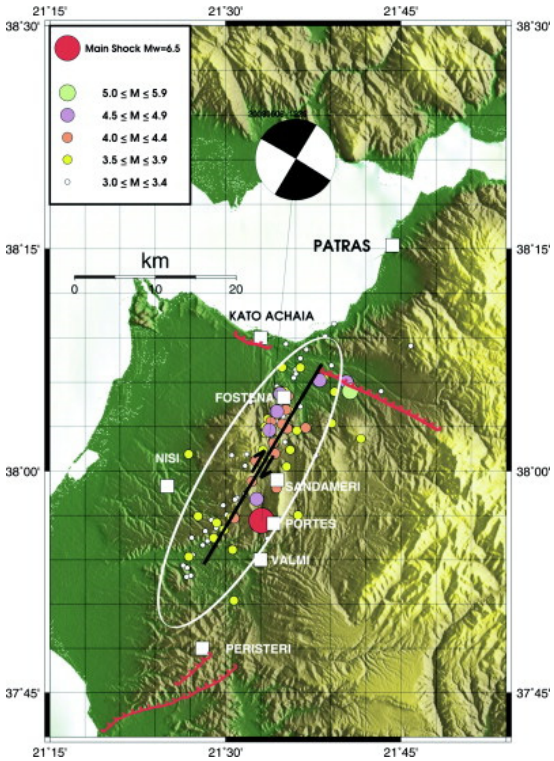


Figure 7.23. Fault of the June 8, 2008 sequence (black) (determined by analysis of the main shock and aftershock distribution) and already mapped faults (red).The red circle denotes the epicenter of the main shock. Towns affected by the earthquake are denoted by squares. (Margaris et al., 2010).

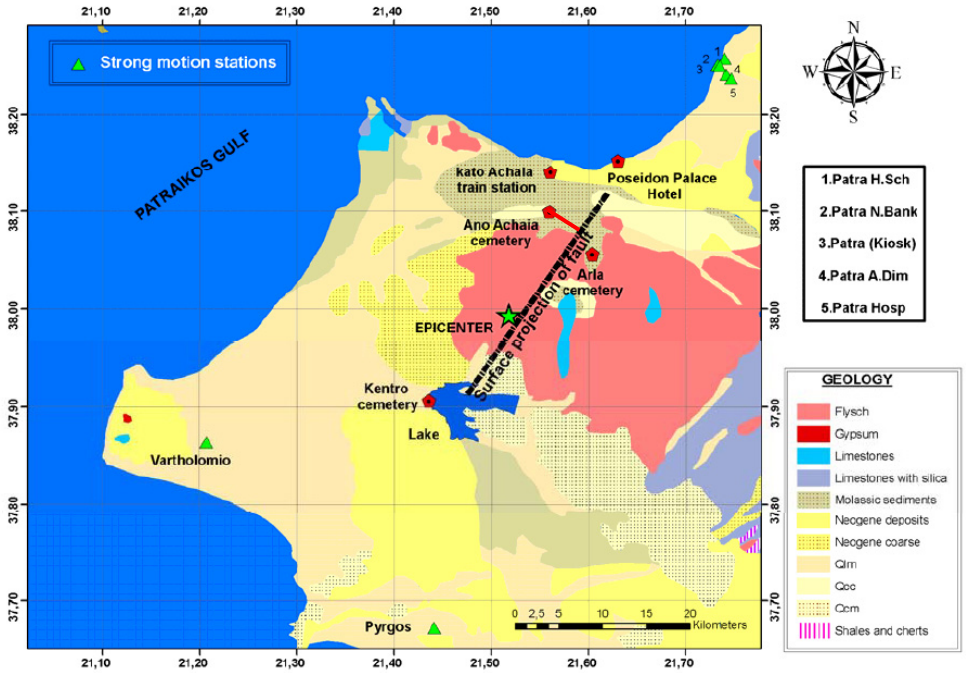


Figure 7.24. Strong motion stations located near the ruptured fault segment. Distance of Kato Achaia town from the surface projection of the fault.

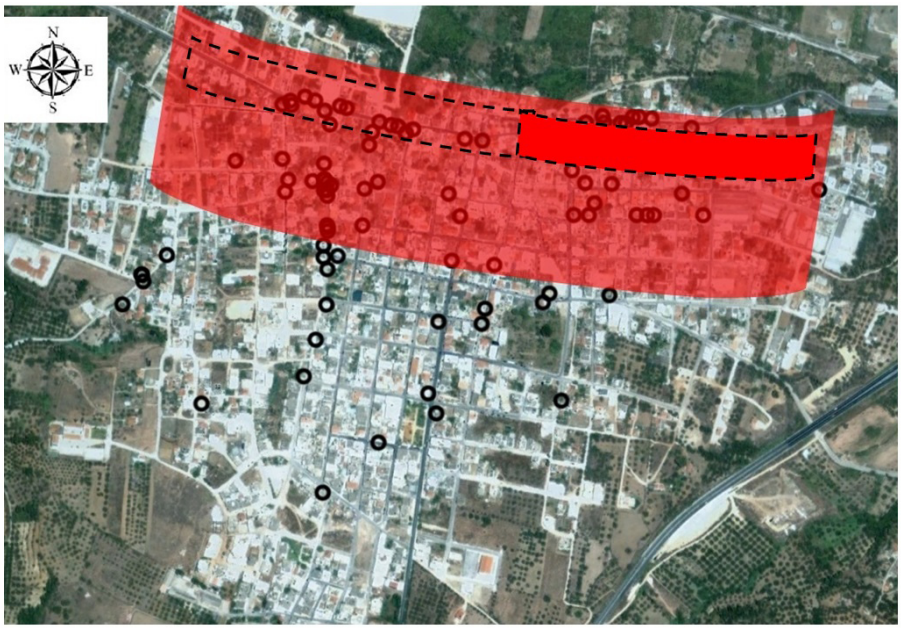


Figure 7.25. Geographical distribution of the buildings (black circles) that suffered severe damage in Kato Achaia

Figure 7.25 denotes the area with the larger concentration of damaged buildings (in red), while the narrow red zone indicates the area with complete collapses of the buildings. As expected for this level of shaking, the field reconnaissance survey revealed that the earthquake did not cause the complete failure of the slope; only limited permanent deformations were observed close to the slope's crest, implying that probably the building damage occurred primarily as a result of ground shaking and its amplification due to the topographic and complex site effects and not in consequence of extensive co-seismic irreversible slope deformation. However this has to be confirmed through numerical non-linear analysis.

7.3.3 Slope non-linear dynamic analysis

The present study aims at the investigation through numerical fully non-linear dynamic analysis of the Kato Achaia slope performance and the potential effects on the buildings located in the vicinity of the slope's crest; Different earthquake scenarios are examined. The main idea is first to verify through numerical nonlinear models that for the 8 June 2008 earthquake the observed building damages occurred primary as a result of amplified ground shaking; then, for a stronger earthquake hazard scenario (e.g. with a mean return period T_m of 1000 years) to assess the vulnerability due to permanent co-seismic slope displacement of a reference RC building standing near the slope's crown. The methodology proposed in this thesis (Chapter 4) for the vulnerability assessment of RC buildings subjected to earthquake induced slow moving slides is used.

In order to estimate structural vulnerability for a given earthquake triggered landslide scenario, one could directly use the proposed fragility curves derived via numerical

parametric analysis (see Chapter 6). These correspond to the simplified geometrical, geological and structural settings for the slope and the structure. Nevertheless, it was decided to reproduce the numerical simulation for the real slope geometrical, hydro-geotechnical, geological and shaking characteristics to check the reliability and applicability band of the proposed simplified curves.

Figure 7.26 presents the topographic map (original scale 1:5000) of the Kato Achaia area and the location of the 2 dimensional cross-section A-A' used to conduct the numerical dynamic analysis. A geotechnical and geophysical investigation has been performed by the University of Patras (Greece) Civil Engineering Department (UPatras; http://www.civil.upatras.gr/) in the broader area including geotechnical boreholes, N_{SPT} tests, Surface Waves tests (using ReMi, SASW and MASW techniques) and classical geotechnical laboratory tests on representative and undisturbed soil samples. Based on the above data provided by the University of Patras, Figure 7.27 presents the simplified 2-dimensional cross-section used for the dynamic analysis together with the (two) sites of geotechnical boreholes whereas Figure 7.28 presents the corresponding finite difference grid. The water table is found to be located 30 m below the slope's crest and 1m above the slope's toe. The geotechnical surveys reveal 9 different soil layers. The geotechnical characteristics assigned to each layer are summarized in Table 7.11. It should be noted that the investigation of the potential for liquefaction is beyond the scope of this study.



Figure 7.26. Topographic map (original scale 1:5000) of Kato Achaia area and position of A-A' cross section.

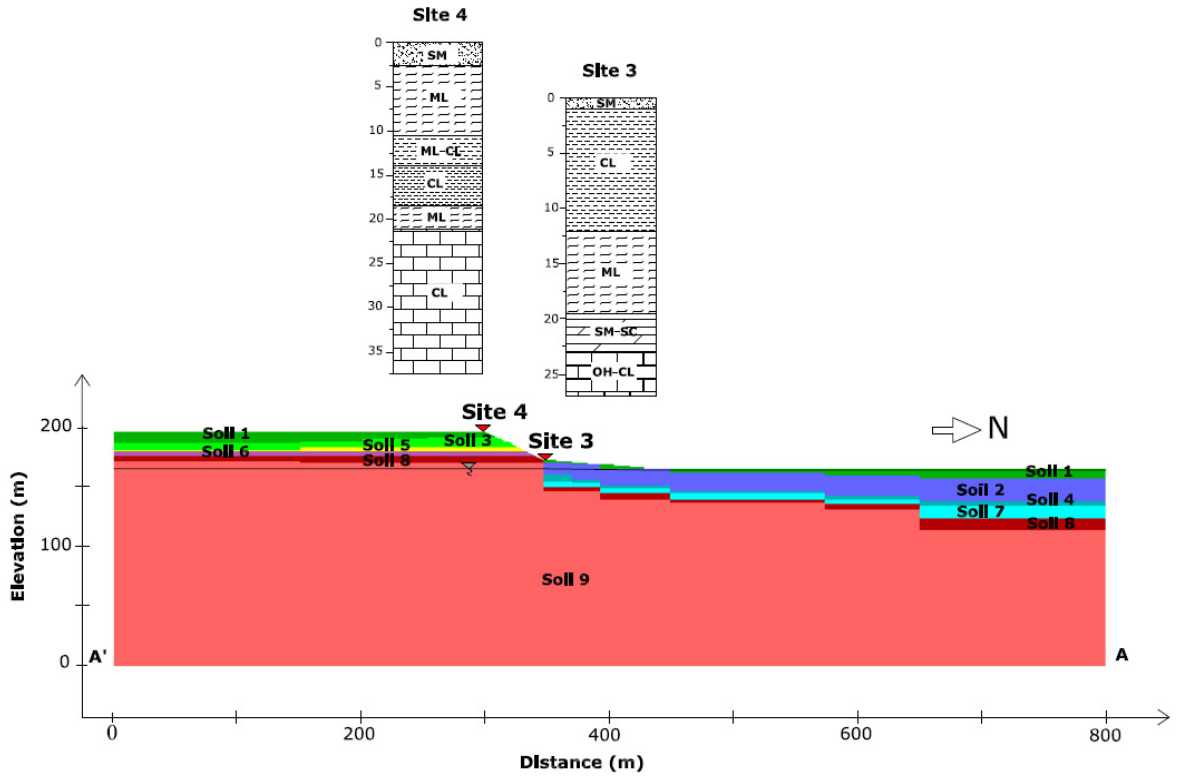


Figure 7.27. Soil model used for the 2D finite difference dynamic analysis of the Kato-Achaia slope

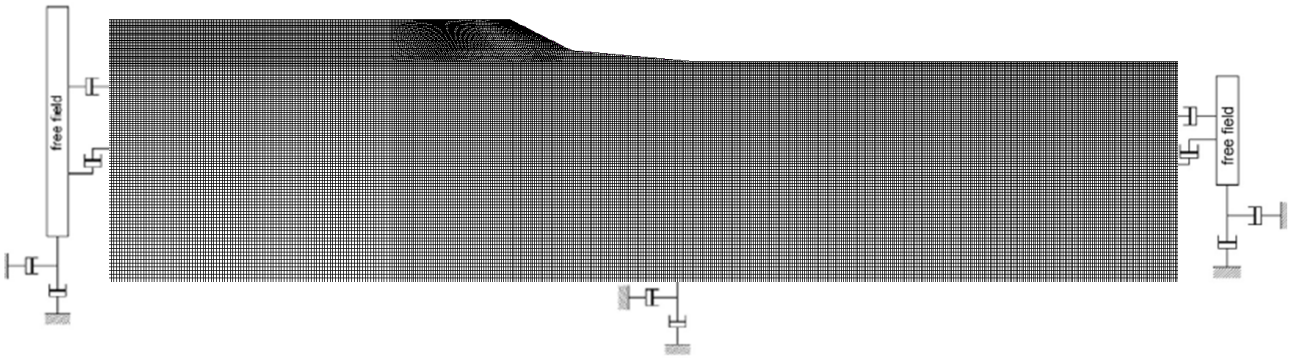


Figure 7.28. 2D FLAC dynamic model adopted for the Kato-Achaia slope

In order to establish correlation between the earthquake demand and the permanent differential displacements for the building, dynamic non-linear analyses were performed using the computer code FLAC 6.0 (Itasca, 2008). The soil materials are modeled using an elastoplastic constitutive model with the Mohr-Coulomb failure criterion, assuming a zero dilatancy non-associated flow rule. The discretization allows for a maximum frequency of at least 10Hz to propagate through the finite difference grid without distortion. A small amount of mass- and stiffness-proportional Rayleigh damping is also applied (0.5-2%), to account for the energy dissipation during the elastic part of the response and during wave propagation through the site. The center frequency of the

installed Rayleigh damping is selected to lie between the fundamental frequencies of the input acceleration time histories and the natural modes of the system. The 2D dynamic model is 800m wide and the elevations of ground surface vary from 160 to 195 m. The slope's height and inclination are estimated at 23 m and 28^o respectively.

Free field absorbing boundaries are applied along the lateral boundaries while quiet (viscous) boundaries are used along the bottom of the dynamic model to minimize the affect of reflected waves. In order to apply a compliant base along the same boundary as the dynamic input, the seismic motion is modeled as stress loads combining with the quiet (absorbing) boundary condition.

Table 7.11. Soil properties used for the 2D finite difference cross-section

Material	γ_d (KN/m^3)	γ_{sat} (KN/m^3)	Poisson's ratio	V_s (m/sec)	φ (^{o})	c (KPa)
Soil 1 (SM-CL)	18	20	0.4	150-250	27	5
Soil 2 (CL)	19	21	0.4	250-450	20	35
Soil 3 (ML)	19	21	0.4	450-550	34	5
Soil 4 (ML)	19	21	0.4	450-550	38	5
Soil 5 (CL-ML)	20	21	0.4	450-550	30	8
Soil 6 (ML)	20	21	0.4	550	24	15
Soil 7 (SM-SC)	20	21	0.4	550	40	8
Soil 8 (OL-CL-OH)	20	21	0.4	550	22	50
Soil 9 (OL-CL)	21	22	0.4	550-1000	28	80

A RC building is assumed to be located 3 m from the slope's crest. At this (first) stage of the numerical analysis, the building is modeled only by its foundation with a width of 6m (uncoupled approach). The combined effect of the soil-structure interaction and of the topographic irregularity on the dynamic response of the building (e.g. see Pitilakis 2009) is not taken into account in the analysis. A flexible foundation system (isolated footings) simulated with concentrated loads (P=50KN/m) at the footings' links is considered. Thus, no relative slip between foundation and subsoil is permitted.

Due to the lack of acceleration records within the slope area, two different strong motion time-histories recorded at the stations PAT3 – (Patra High School) and Pat_Hosp (Patras Hospital) of the town of Patras were used in the numerical simulations (see Fig. 7.24). The base motions imposed in the dynamic model were obtained by deconvolution of the motion recorded in Patras and appropriate scaling for distance. The code Cyberquake (BRGM Software, 1998) and the profiles of Figure 7.29 were used for this purpose. Site conditions for the selected stations were made available from previous geotechnical and geophysical investigations (Athanasopoulos G. and Pefani H., personal communication,

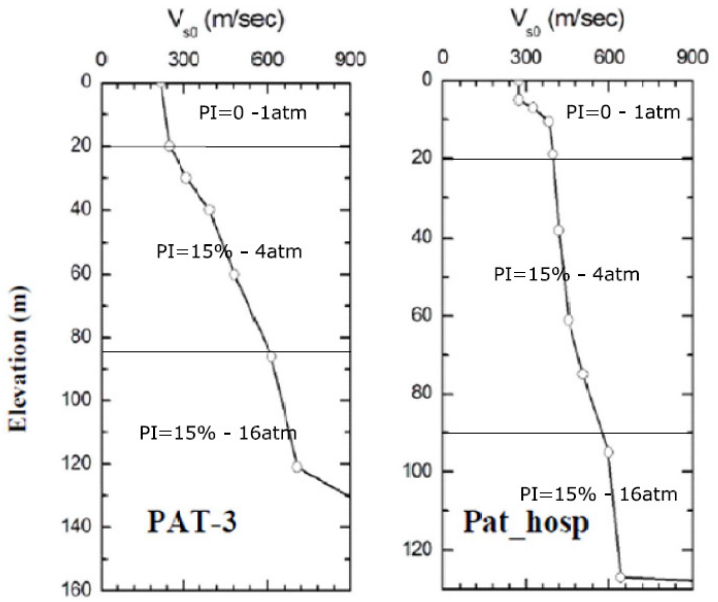


Figure 7.29. Shear wave velocity variation with depth for the selected recording stations.

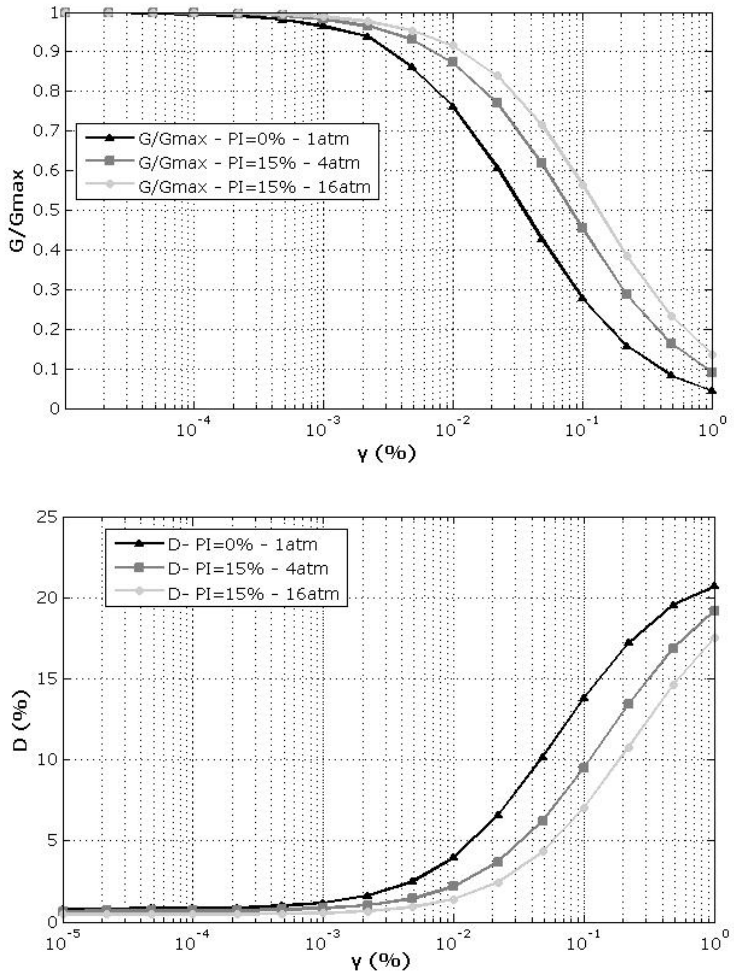


Figure 7.30. Modulus reduction and damping curves of Darendeli (2001) used for the 1D deconvolution analysis

2010). Three different sets of G-γ-D curves proposed by Darendeli (2001), which account for soil plasticity, OCR, and overburden pressure, were used for the deconvolution analysis (Fig. 7.30). The deconvoluted excitations which were obtained and used as seismic input are shown in Figure 7.31. Before applied to our Kato Achaia 2D model, they are subjected to appropriate correction (baseline correction and filtering) to allow for an accurate representation of wave transmission through the model.

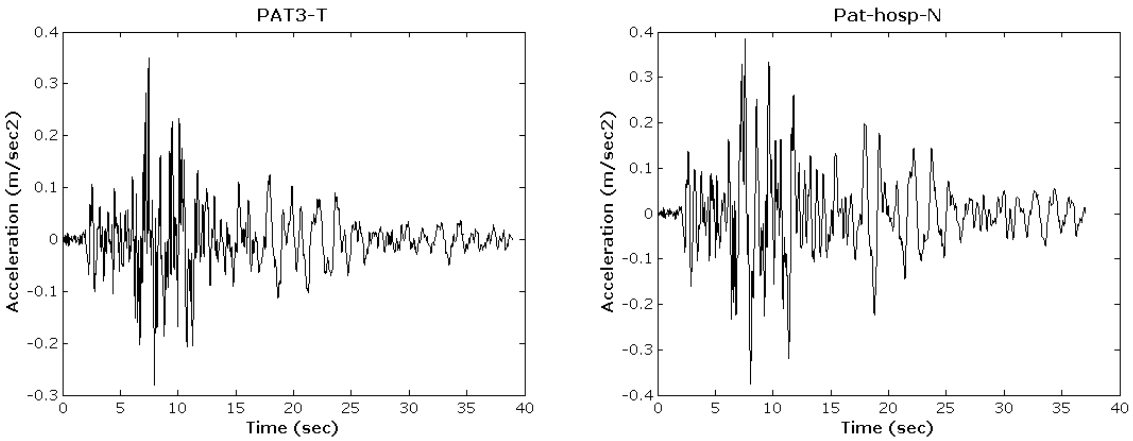


Figure 7.31. Input outcropping horizontal accelerations used in the dynamic analysis

Finally the input accelerograms are scaled for two levels of peak ground acceleration at the assumed seismic bedrock, namely 0.2 and 0.5g. The low level of excitation is taken to be consistent with the PGA values reported at the Kato Achaia area during the 2008 Ilia Achaia earthquake (reaching PGA values on the order of 0.3g at the free surface). The higher excitation level (0.5g) is considered in order to further investigate irreversible deformation beneath the building's foundation and finally to assess the vulnerability of the assumed building due to the differential permanent ground displacement induced by the landslide. The differential horizontal ground displacements at the foundation level derived from the 2D finite difference dynamic analysis by applying the PAT3-T and Pat_hosp-N accelerograms at the assumed seismic bedrock are schematically illustrated in Figure 7.32 for the two levels of excitation.

In accordance with the field observations carried out after the 2008 Achaia-Ilia earthquake, relatively small (<10cm) total and differential deformations at the building's foundation level are anticipated when applying the outcropping horizontal accelerograms scaled at 0.2g (Fig. 7.32- left). In contrast, for the stronger earthquake scenario (0.5g), significant differential permanent displacements (0.4m - 0.6m) are expected (Fig. 7.32- right).

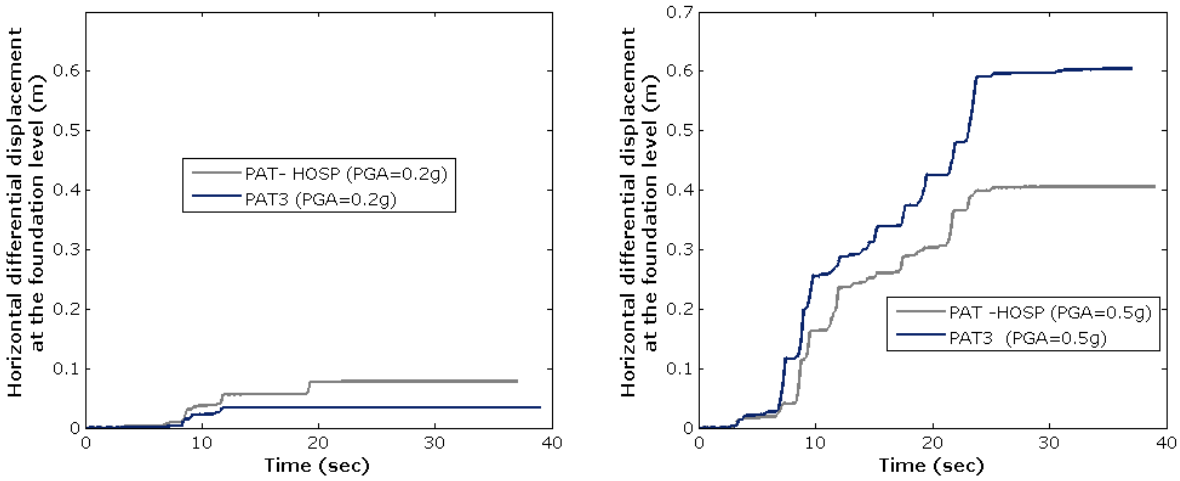


Figure 7.32. Differential horizontal ground displacements at the building's foundation level for low and high excitation level.

7.3.4 Fragility analysis of the building

The analysis of the building is conducted by means of the finite element code SeismoStruct (Seismosoft, SeismoStruct 2011), which is capable of calculating the large displacement behavior of space frames under static or dynamic loading, taking into account both geometric nonlinearities and material inelasticity. Both local (beam-column effect) and global (large displacements/rotations effects) sources of geometric nonlinearity are automatically taken into account. The spread of material inelasticity along the member length and across the section area is represented through the employment of a fibre-based modeling approach, implicit in the formulation of SeismoStruct's inelastic beam-column frame elements. Nonlinear static time-history analyses are performed for all numerical simulations. In particular, the differential permanent displacement (versus time) curves (Fig. 7.32), directly extracted from the FLAC dynamic analysis, are imposed as quasi-static loads at one of the RC frame supports.

The studied building is a "low-code", single bay-single storey RC bare frame structure, considering that most of the existing RC buildings found in the area are low rise, old, poorly constructed structures. The building's height and length are 3m and 6m respectively. A uni-axial nonlinear constant confinement model is used for the concrete material (f_c=20MPa, f_t=2.1MPa, strain at peak stress 0.002mm/mm, confinement factor 1.2), assuming a constant confining pressure throughout the entire stress-strain range (Mander et al, 1988). For the reinforcement, a uni-axial bilinear stress-strain model with kinematic strain hardening is utilized (f_y=400MPa, E=200GPa, strain hardening parameter μ =0.005). All columns and beams have rectangular cross sections (0.40x

0.40m). A low level of steel reinforcement is used (8Φ12) for all the cross sections considered.

Table 7.12. Definition of Limit states for "low-code" RC buildings

Limit state	Steel strain (ε_s) –low code design
Limit State 1	Steel bar yielding
Limit State 2	0.0125
Limit State 3	0.025
Limit State 4	0.045

The building structural response is obtained for the two different levels of excitation by analyzing the building capacity under the deformation demand (differential displacement time histories). In order to identify the building performance (damage) state, 4 limit states (LS1, LS2, LS3, LS4) are defined in terms of allowable values of steel reinforcement strain, based on the work of Crowley et al. (2004), Bird et al. (2005), Negulescu and Foerster (2010) and engineering judgment (Table 7.12). This concern exceedance of minor, moderate, extensive and complete damage of the "low-code" designed building.

The building's damage level is finally assessed by comparing the response of the critical member of the building (in terms of maximum steel bar strain) for the given hazard level to the specified threshold values for each limit state. As expected, the building will sustain slight damage (average maximum steel strain at the critical column $\varepsilon_{s,ave}$ =0.0027 >0.002=Es/fy) due to permanent ground deformation (landslide) for the low level of input excitation (0.2g), which most probably happened during the earthquake under consideration. This is in line with the minor permanent slope displacement observed after the 2008 Achaia-Ilia earthquake. On the contrary, for the strong earthquake scenario (0.5g), the structure is expected to suffer complete damage (average maximum steel strain at the critical column $\varepsilon_{s,ave}$ =0.0545> 0.045), making the repair of the building non feasible in physical or economical terms.

The fragility curves that are found to be more representative of the geotechnical, geological, geometrical and structural characteristics of the site and the building ("Low-code" building- Slope inclination 30^o- sand soil), derived via an extensive parametric analysis (Chapter 6), are depicted in Figure 7.33.

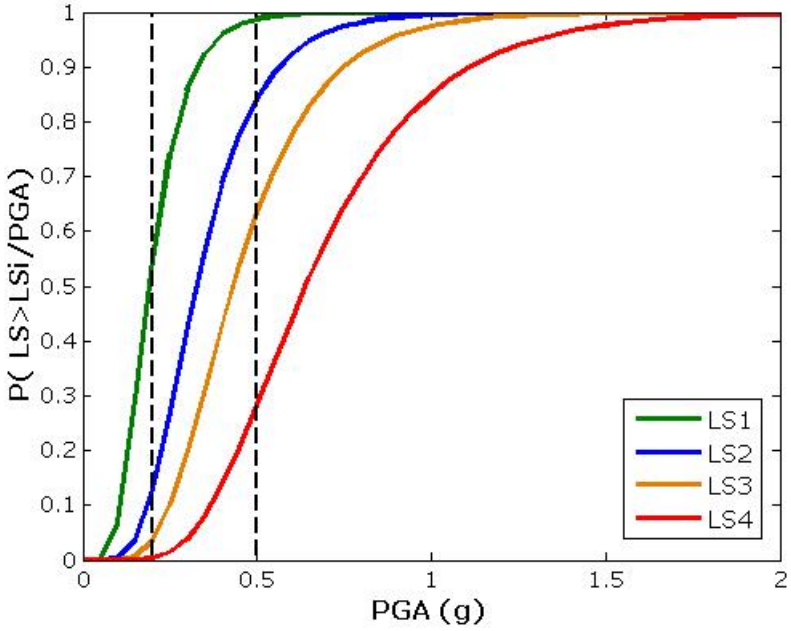


Figure 7.33. Fragility curves proposed for the specific site and structural characteristics

It is observed that the proposed curves predict that the typical building studied herein would suffer extensive or complete damage (estimated probabilities of being in extensive and complete damage state 0.34 and 0.29 respectively) for the high seismic hazard scenario (0.5g) and no or low damage for the low seismic hazard scenario (0.2g) (estimated probability of being in no damage and slight damage state 0.45 and 0.482 respectively). These observations are in fairly good agreement with the recorded (for the low hazard scenario) and simulated damages (for both hazard levels) of the typical building.

7.4 Application to buildings in Corniglio village- Italy

7.4.1 Introduction

Stemming from the valuable set of data (in terms of ground and building landslide displacement and measured building damage) which were made available and post-processed for a population of buildings in the village of Corniglio in the North-Western Italian Appennines (Callerio et al., 2007), the aim of the present study is twofold: first, to explore the reliability of the fragility curves derived via an extensive parametric investigation (Chapter 6) through their comparison with the observed damage data for a representative RC frame building at Coniglio village for the measured level of ground and building displacement and then, to enhance the applicability of the proposed methodological framework (Chapter 4), by comparing the more realistic fragility curves

derived for the Corniglio case history through straightforward numerical computations with the observed building damage data.

7.4.2 Landslide movement and building damage data in Corniglio village

The Corniglio Village is located in the northern part of the Appennines, at an altitude of about 700 m a.s.l., between the towns of Parma and La Spezia (as shown in Fig. 7.34). The morphology of the investigated area shows the characteristics features of an Appennine mountain site, with steep slopes alternating with narrow and deep valleys.

The Corniglio Village area is principally affected by two different slide movements (Lessloss, 2005): a deep rock block slide (cross section A-A in Fig.7.34) and a surface rotational landslide (cross section B-B in Fig. 7.34). The geological profile of B-B cross section, in which this study is focused, is presented in Figure 7.35. Several re-activations of the landslides have affected Corniglio village damaging buildings, roads and other infrastructures. The landslide movements are attributed mainly to a decrease of geomechanical parameters, caused by the weathering process due to intense precipitations and weak and moderate seismic activity.

The time period of interest in this study lies from September 1994 to December 1999 that was characterized by nearly continuous landslide activity. Through the entire period considered, the observed displacements reached tens of m on the main slide body, the so-called "Lama" (see Fig. 7.34), causing heavy damage to all sparse buildings in the Lama area. In Corniglio Village, the surface ground movements measured by inclinometers reached typically 20 to 25 cm, resulting to moderate/significant damage to the buildings located in the old centre of the village. The induced physical damage to the buildings in Corniglio included cracks in masonry vaults, opening of structural joints, cracking of retaining walls and in vertical and horizontal structural elements etc. Figure 7.36 illustrates representative observed building damages in Corniglio village. The most frequent structural typologies of Corniglio buildings, as it can be reasonably assumed on the basis of the pictures, are low-rise masonry buildings and low-rise RC frame buildings.

A substantial set of instrumental observations has been gathered mainly from the Emilia Romagna Regional Administration in charge of the monitoring and surveillance activities, including inclinometer data (monitoring ground movements in free field), geodetic levelling data on almost every building within the village area for the entire period of interest and crack aperture measurements in some susceptible to damage buildings.

The inclinometers position, the locations of the geodetic targeted points (and their ID's) and, for each building monitored, a letter from A to Z between brackets which indicates

the crack meters installed, are depicted in Figure 7.37. The most damaged buildings are denoted by red filled polygons.

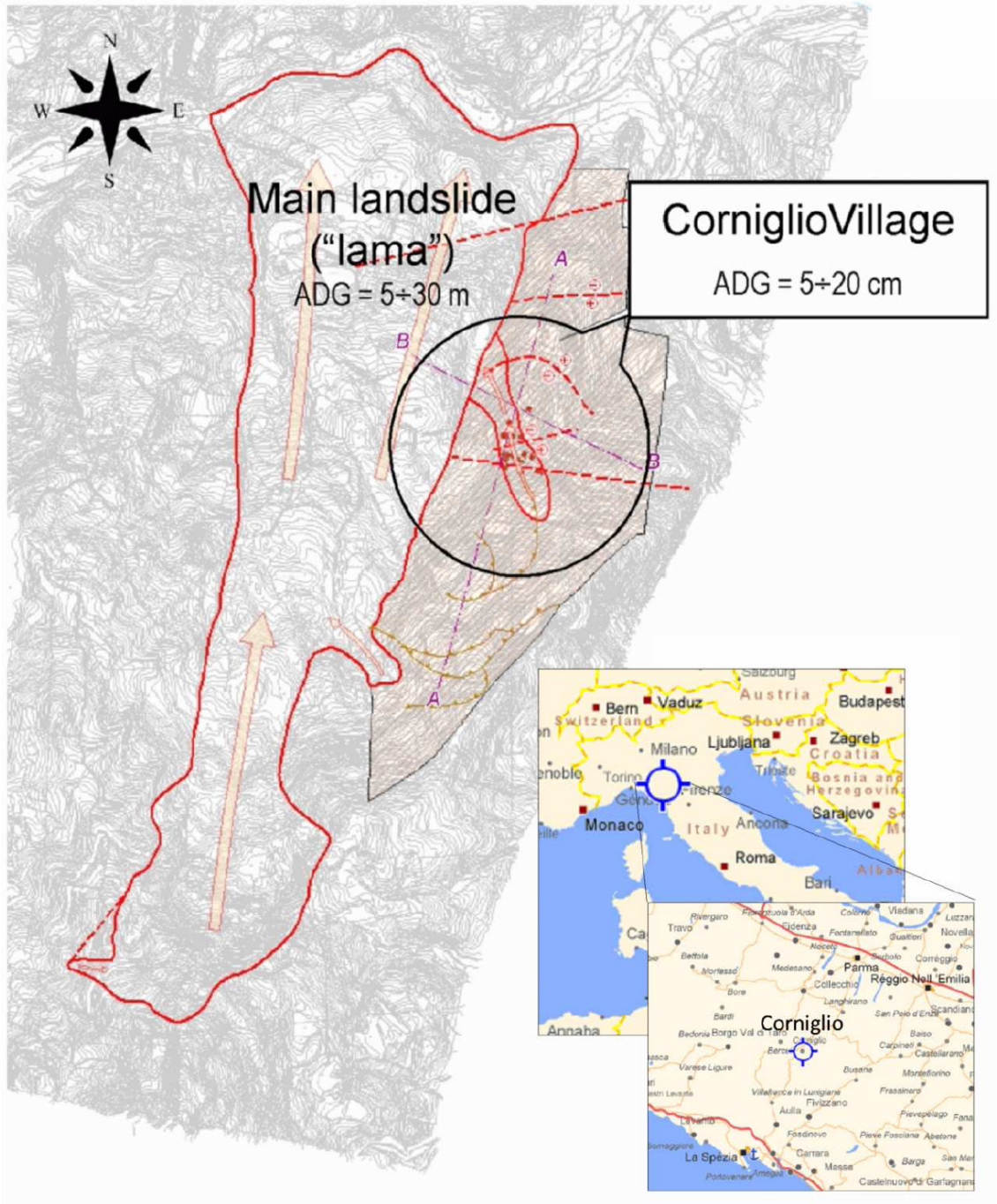


Figure 7.34. General plan of the area of Corniglio affected by the landslide phenomena during the years 1995-2000. The indicated displacements (ADG = Absolute Ground Displacement) are obtained by aerial photo interpretation ("Lama" area) and inclinometer readings (Village) (Callerio et al., 2007)

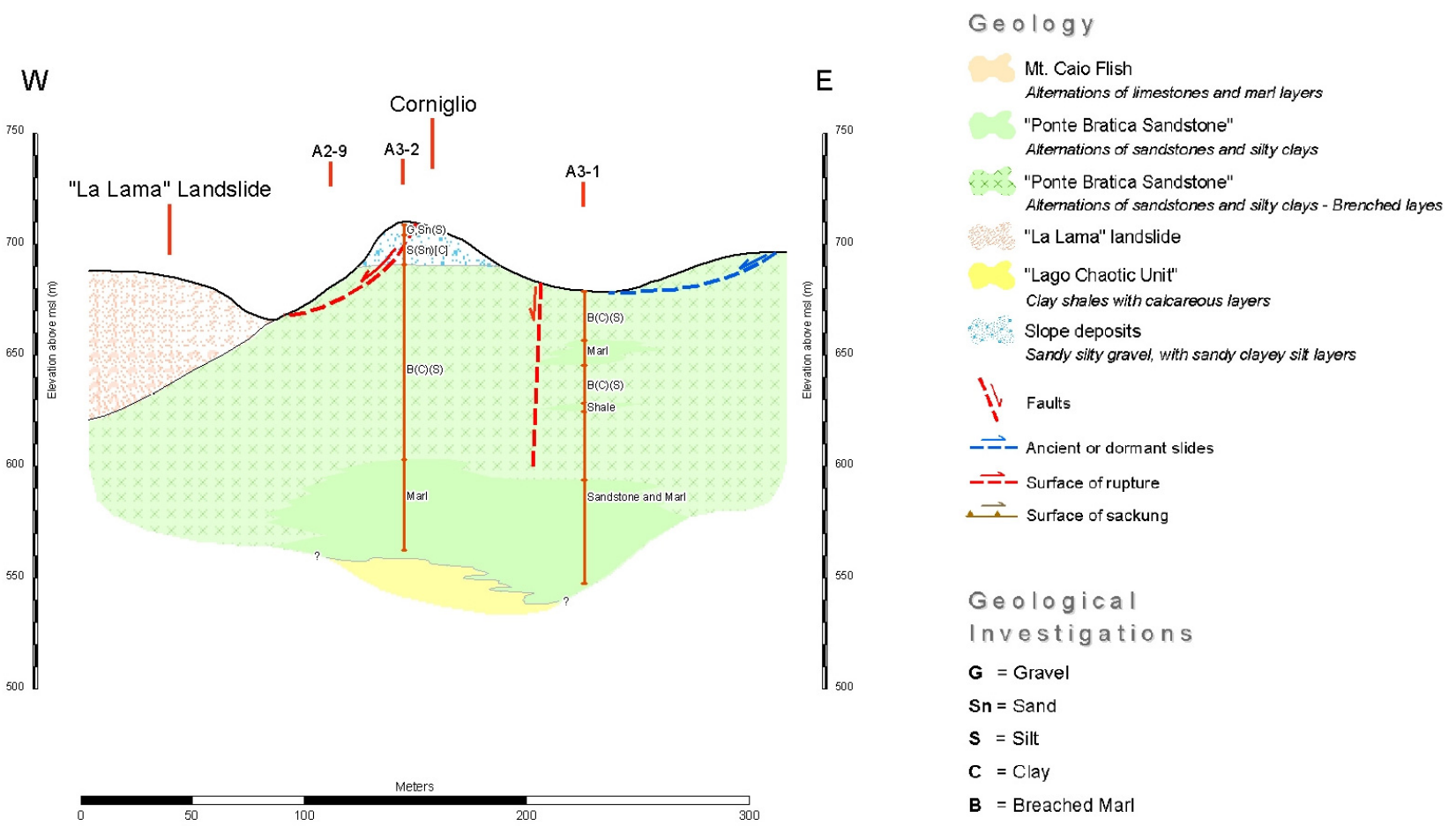


Figure 7.35. Geotechnical profile B-B (see Fig. 7.34) of the Corniglio case history used for the analysis

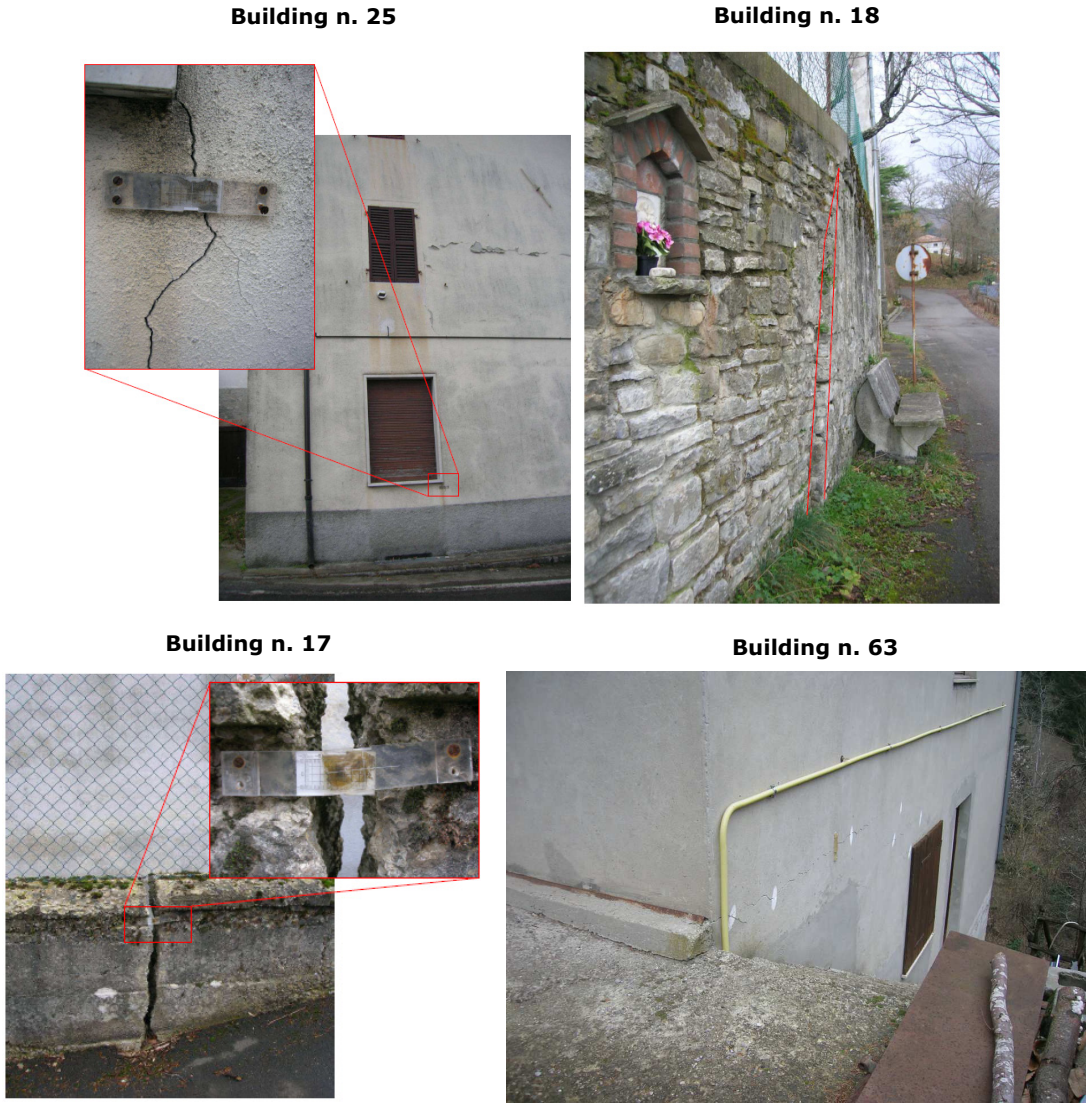


Figure 7.36. Representative physical damage to buildings in Corniglio village (Callerio et al., 2007)

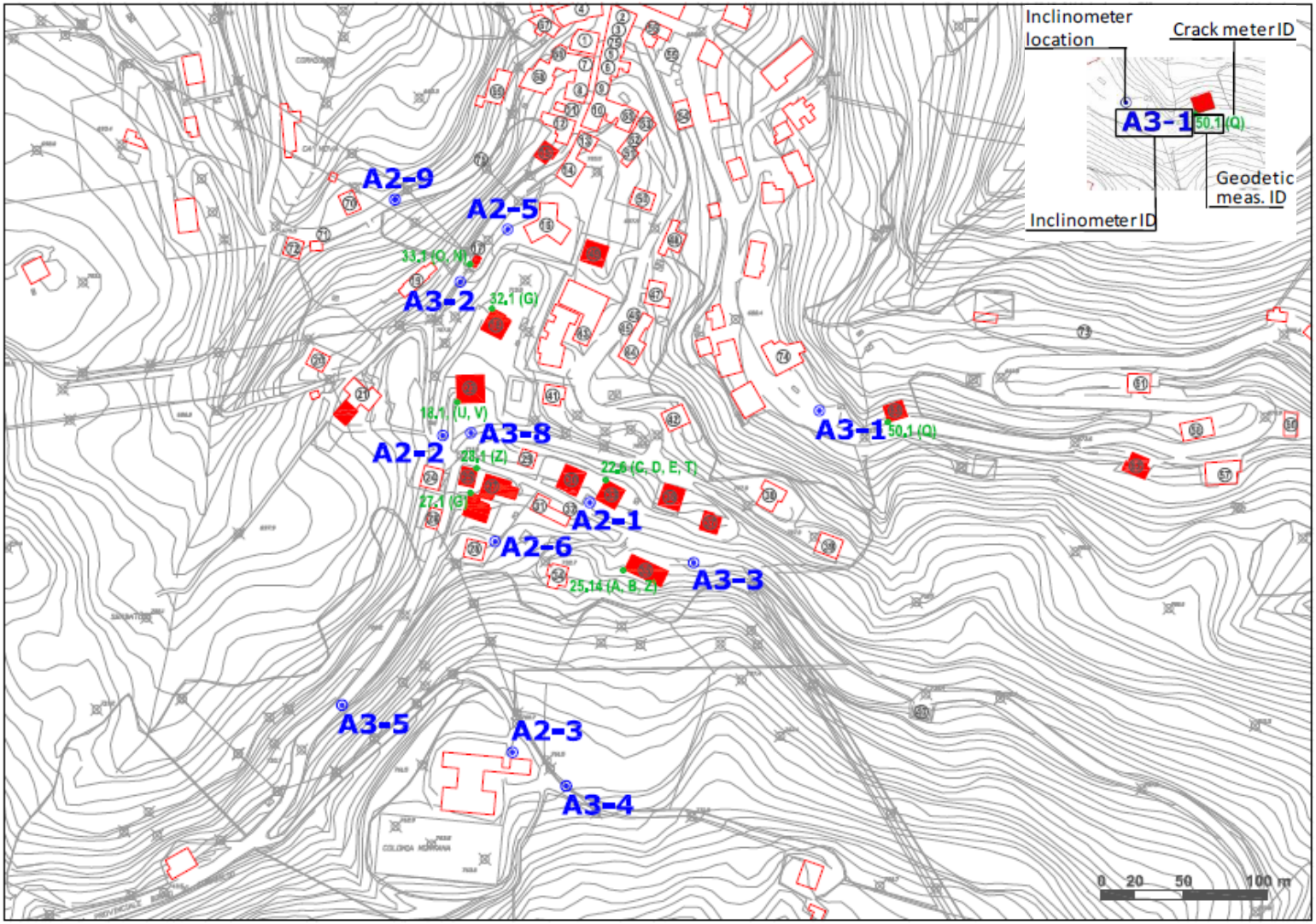


Figure 7.37. Location of inclinometers, geodetic and crack measurements on buildings. Buildings are denoted by red polygons whereas the ones that suffered damages due to the landslide movement are filled in red. (Callerio et al., 2007)

The processing of the data set was conducted by Callerio et al. (2007), focusing on establishing a correlation among ground displacement, building movements and damage induced during sliding so as to provide the basis for a probabilistically sound vulnerability assessment framework.

The damage levels observed in Corniglio were defined in terms of ease of repair, based on the scale proposed by Standing et al (1999), identifying 3 damage levels: negligible to slight, slight to moderate and moderate to severe. The ease of repair was then related to the measure of cracks opening.

Figures 7.38 to 7.43 display the ground displacement measured by the nearest inclinometer with respect to the building location, the building movement by geodetic levelling and the opening of each crack monitored on the structure. All the plots are over imposed on the damage scale in terms of cracks opening, to assess for each building the expected damage state. As it can be noticed from the figures, the ground displacement is not always linearly related to building movement. Moreover, the crack openings, which depend on various local factors (e.g. direction of crack opening, texture of the walls, precence of structural reinforcement etc.) are not directly related to ground displacement. A rather linear relationship between the building movement and crack opening is detected in some of the cases (i.e. for buildings 17, 23, 25).

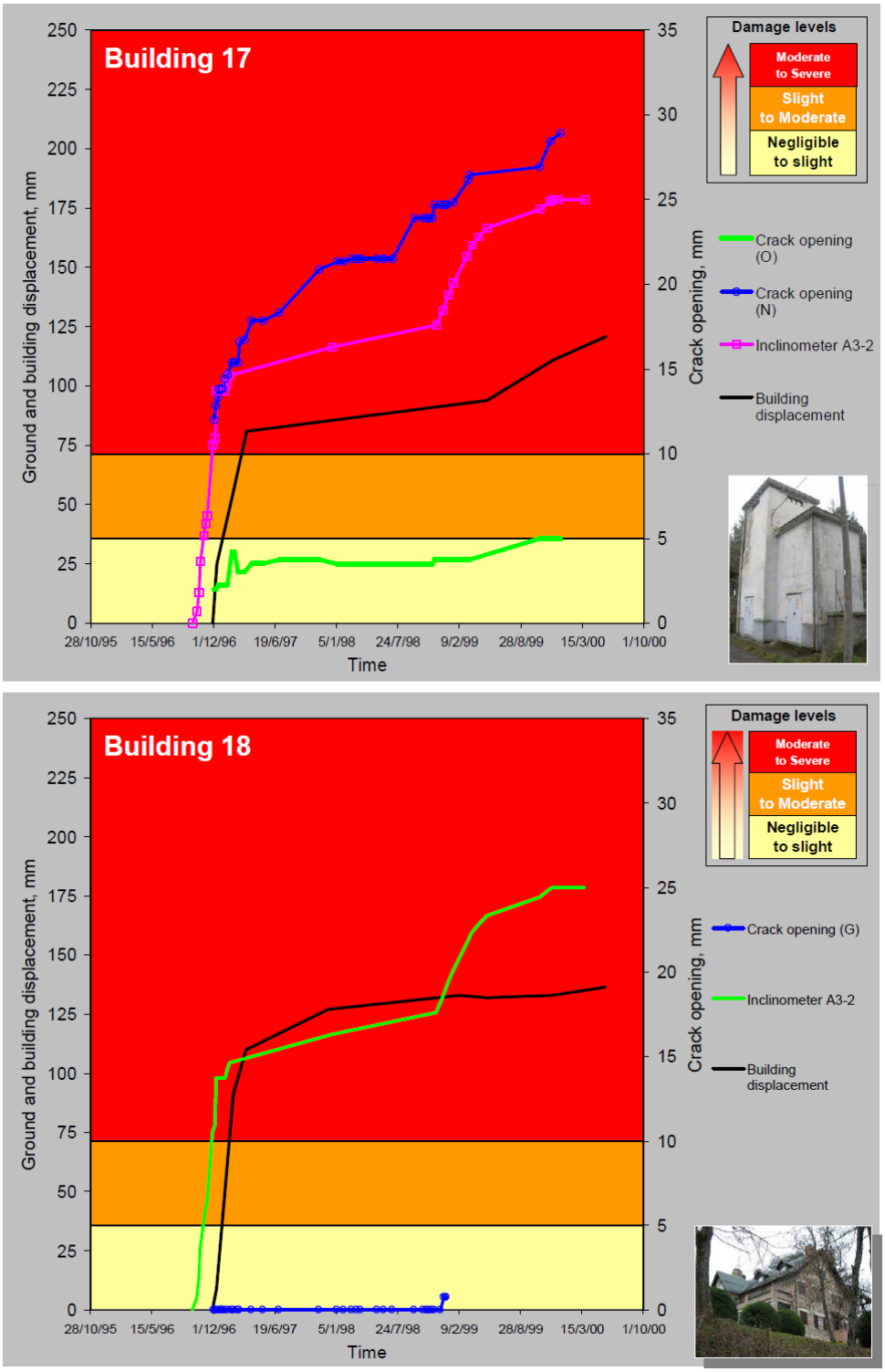


Figure 7.38. Correlation between absolute ground displacement (from nearby Inclinometer A3-2), building n. 17 and 18 displacement (from geodetic levelling) and crack opening (compared to the defined damage levels) as a function of time (Callerio et al., 2007)

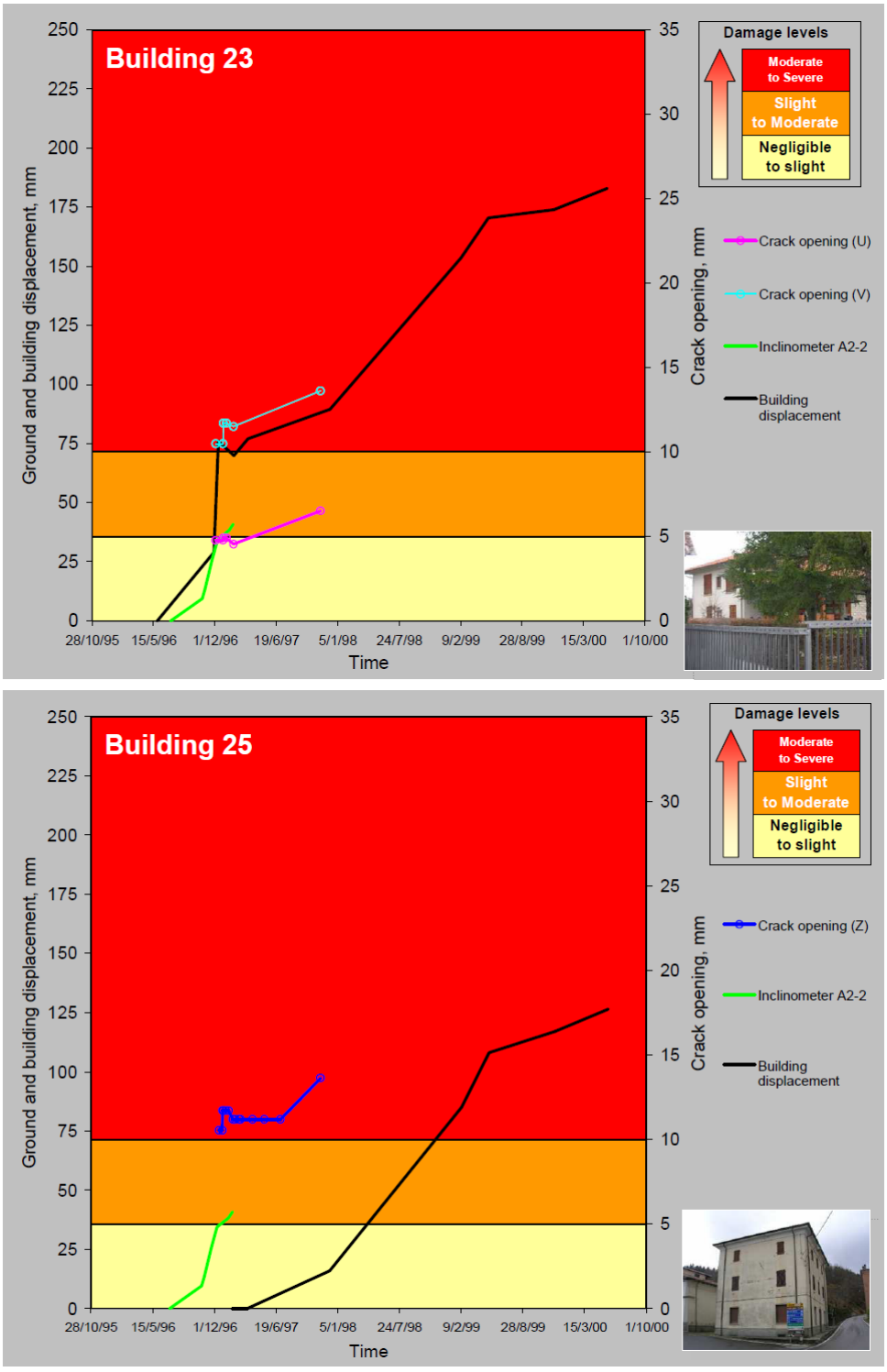


Figure 7.39. Correlation between absolute ground displacement (from nearby Inclinometer A2-2), building n. 23 and 25 displacement (from geodetic levelling) and crack opening (compared to the defined damage levels) as a function of time (Callerio et al., 2007)



Figure 7.40. Correlation between absolute ground displacement (from nearby Inclinometer A2-6), building n. 27 displacement (from geodetic levelling) and crack opening (compared to the defined damage levels) as a function of time (Callerio et al., 2007)

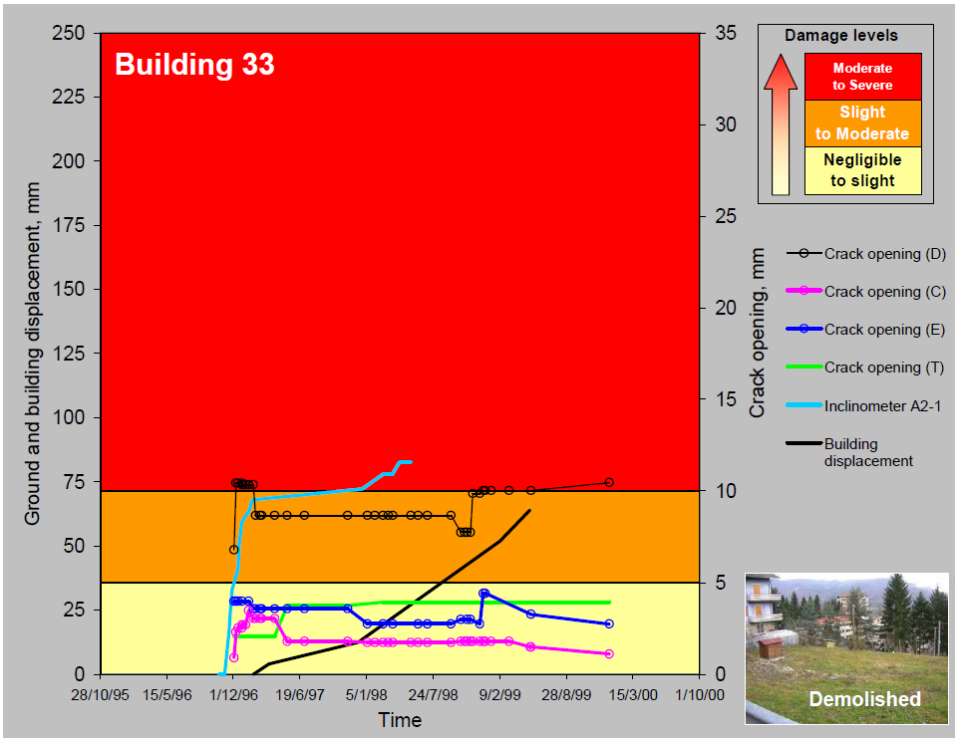


Figure 7.41. Correlation between absolute ground displacement (from nearby Inclinometer A2-1), building n. 27 displacement (from geodetic levelling) and crack opening (compared to the defined damage levels) as a function of time (Callerio et al., 2007)

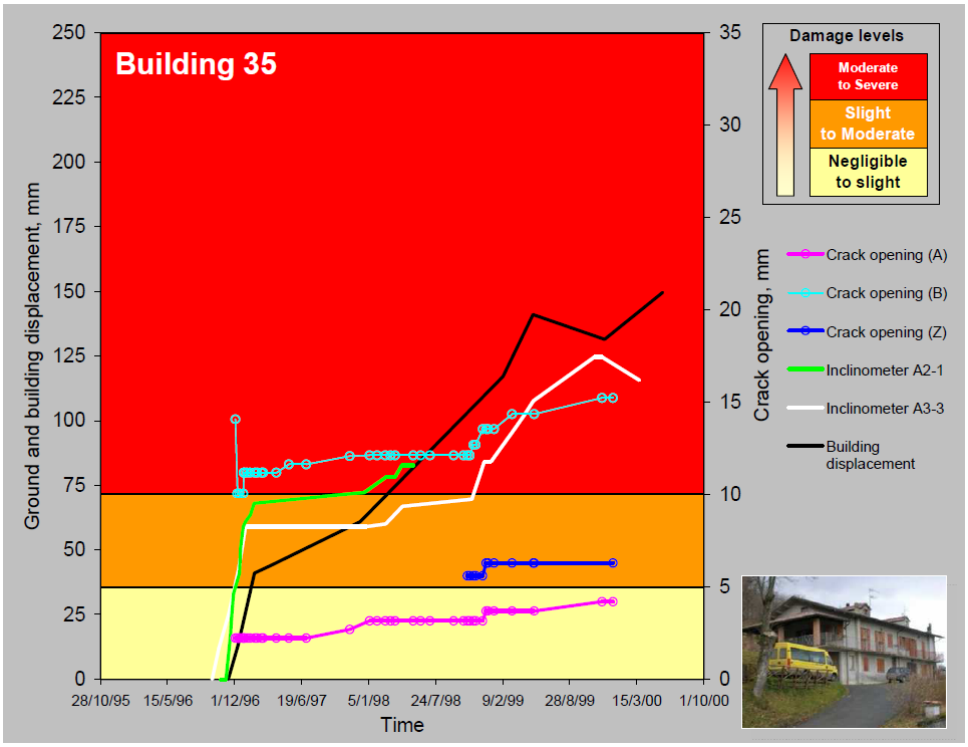


Figure 7.42. Correlation between absolute ground displacement (from nearby Inclinometers A2-1 and A3-3), building n. 35 displacement (from geodetic levelling) and crack opening (compared to the defined damage levels) as a function of time (Callerio et al., 2007)

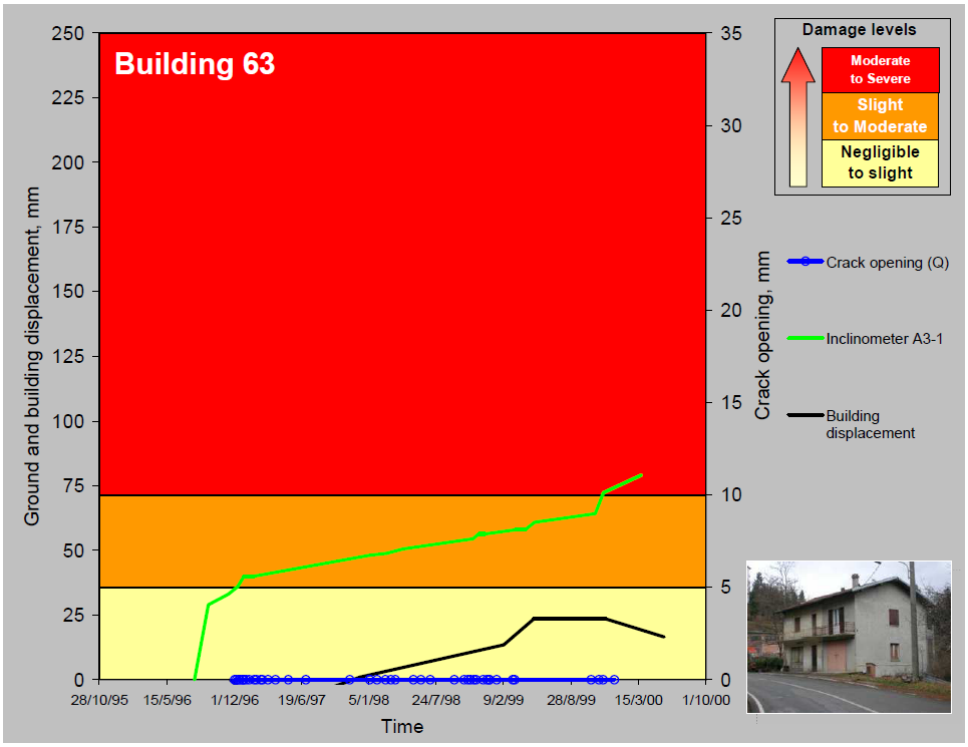


Figure 7.43. Correlation between absolute ground displacement (from nearby Inclinometers A3-1 and A3-3), building n. 63 displacement (from geodetic levelling) and crack opening (compared to the defined damage levels) as a function of time (Callerio et al., 2007)

7.4.3 Comparison of the observed building damage with the damage predicted by the proposed and simulated fragility curves

The present study is focused on the fragility analysis of building n. 17 due to its proximity to the inclinometer A3-2, which is installed near the slope crown of the geotechnical profile B-B of the Corniglio case history (see Fig. 7.35). As shown in Figure 7.38, building n. 17 is a rather simple two-storey RC frame structure with masonry infill walls. Figure 7.44 shows a closer view of building n. 17 and of the nearby inclinometer A3-2 within the Corniglio area.

Despite the proximity of building n.18 as well to the inclinometer A3-2 and the fact that the recorded displacements on both buildings 17 and 18 show more or less the same trends, building n. 18 is an upper class, well maintained masonry bearing wall structure with an heavy roof (A. Calerio, personal communication 2012), which is not considered appropriate for the herein fragility analysis, concentrated on RC buildings.

Other buildings, such as buildings n. 33 (RC frame 3 storey building, now demolished) and n. 35 (mixed RC frame, masonry structure), could potentially be suitable for this study. However, these buildings are not directly influenced by the landslide movement of the B-B cross section.

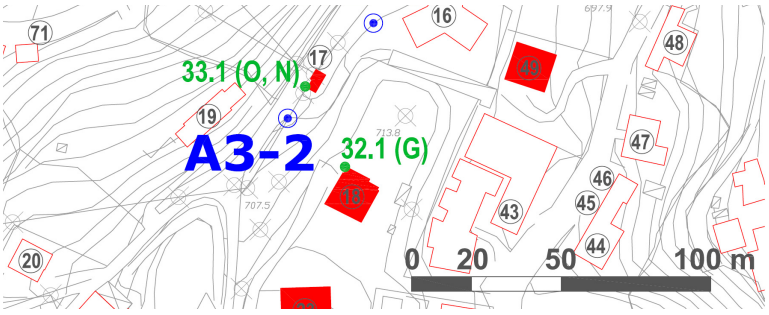


Figure 7.44. Closer view of building with ID 17 and the nearby inclinometer A3-2 within the Corniglio area. The geodetic and crack monitored points on the buildings are also shown (in green)

As it was expected, the given data do not exactly fit the proposed curves derived through the parametric analysis (Chapter 6). In particular, the studied slope configurations do not match very precisely to the given finite slope geometry and soil geotechnical properties of Corniglio case history (see Fig. 7.35, geotechnical profile B-B: average slope inclination≈ 37°, average height ≈43 m). Moreover, first-time failures where the sliding surface is allowed to be freely developed were analyzed in Chapter 6, as opposed to the Corniglio case study where a pre-existing landslide has to be simulated. Regarding all the above, two different approaches of increased complexity for the fragility analysis of building n. 17 in Corniglio village are presented in the ensuing.

7.4.3.1. Reliability assessment of the proposed fragility curves

As a first step analysis, two sets of the already developed curves, i.e. the ones that are more representative for the Corniglio case history, were selected to compare with the recorded building damage, for the measured level of building displacement (see Fig. 7.38). These curves have been developed for:

- slope height: 40 m,
- slope inclinations: 30^o and 45^o respectively
- sandy slope materials
- low code RC frame buildings with flexible foundations

A graph of the aforementioned developed curves is shown in Figure 7.45 for slope inclinations 30^o and 45^o respectively. It is noted that the curves are presented as a function of the maximum permanent displacement at the foundation level to allow for direct applications, considering the site-specific nature of the problem. The derived lognormal median and dispersions of the fragility functions are given in Table 7.13.

It 's also worth noting that the adoption of the steel and concrete strain as a damage index in this research (see Chapter 4) implies a structural damage (e.g. in terms of cracks) and a subsequent ductile failure of the building members. This is certainly the case for building n. 17 where extensive cracking was recorded (see Fig. 7.38).

Table 7.13. Parameters of the representative fragility functions

Limit strain	**Displacement at the foundation level (m)**			
	Slope inclination angle β=30^o		**Slope inclination angle β=45^o**	
	Median	**Dispersion β**	**Median**	**Dispersion β**
Limit State 1	0.075	0.51	0.031	0.49
Limit State 2	0.257		0.141	
Limit State 3	0.450		0.267	
Limit State 4	0.770		0.472	

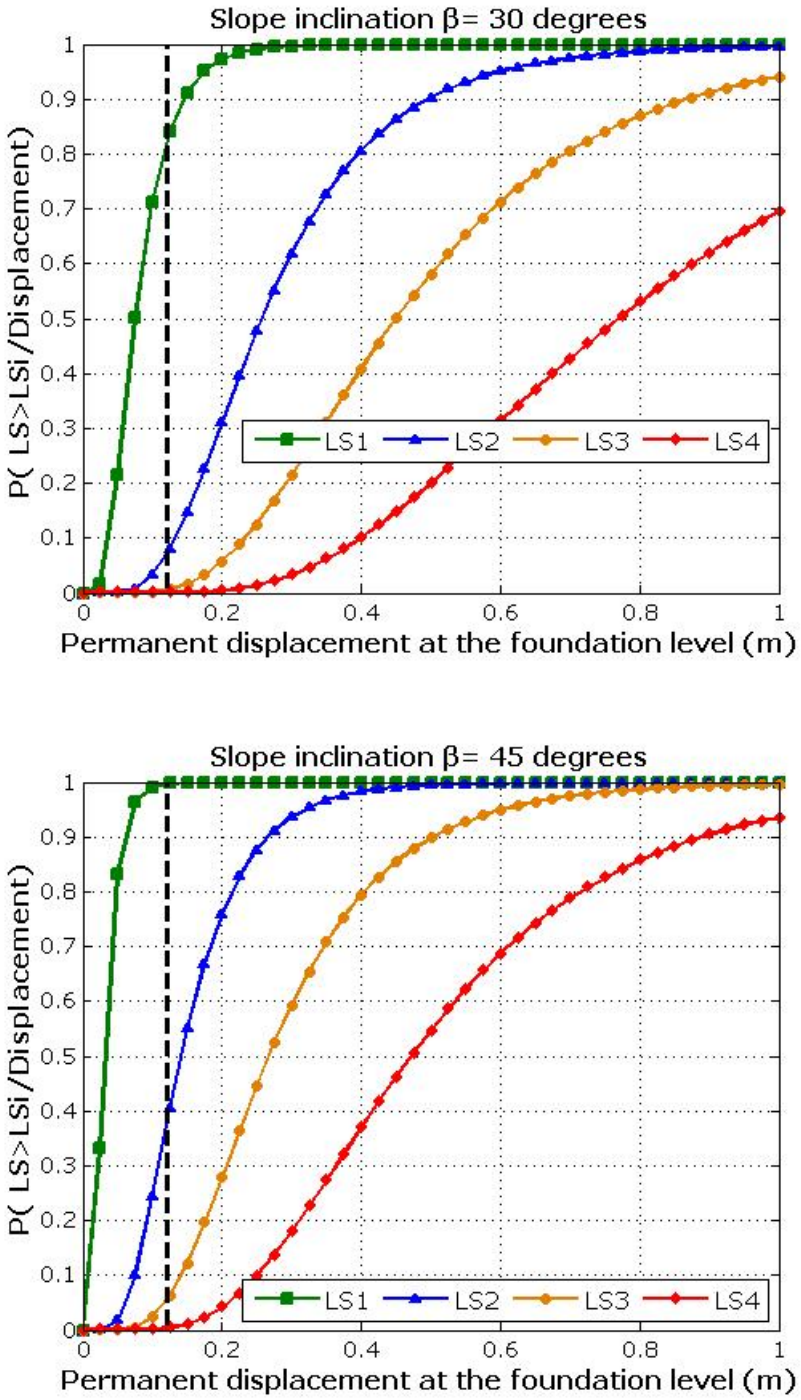


Figure 7.45. Representative fragility functions derived from the parametric analyses

The damages predicted by the curves are compared with the damages observed in building n. 17 for the recorded level of displacement, i.e. 0.121 m. As shown in Figure 7.38, for this level of displacement, the building would be in *"moderate to severe"* damage level according to the damage states proposed in Callerio et al. (2007).

The proposed curves predict *"slight to moderate" to "moderate to extensive"* damages that are in relatively good correlation with the corresponding assigned damage levels based on the field measurements and observations. As it can be easily seen in Figure 7.45, the expected damages when using the curves derived for 45^o slope inclinations are more in line with the observed structural performance. In particular, the estimated probabilities of exceeding slight and moderate damage are 1.0 and 0.4 respectively for the curves referring to the 45^o inclined slope whereas the corresponding probabilities are 0.84 and 0.08 respectively for the curves referring to the 30^o inclined slope.

7.4.3.2. Fragility curves for the Corniglio case study – Comparison with recorded damage data

Considering the relatively crude approximation that it may be achieved with the comparisons presented below, a more sophisticated analysis is performed herein resulting to the development of fragility curves for the Corniglio case history based on the data provided (e.g. geotechnical profile B-B, inclinometer A3-2 records associated with building n.17 geodetic and crack measurements). Fragility curves are derived from the response of the landslide to earthquake shaking that is in our case the differential displacement at the foundation level. The ultimate goal of the analysis is to get more reliable correlations between the observed and simulated damage of the building for the recorded displacement level so as to enhance the reliability and applicability band of the proposed methodology (Chapter 4).

In terms of numerical computations, a two-step uncoupled analysis is performed based on the methodological framework described in Chapter 4. The computer codes FLAC2D 7.0 (Itasca, 2011) and SeismoStruct (Seismosoft, SeismoStruct 2011) are used for the slope-foundation dynamic and structure's quasi-static analysis respectively.

Taking into account the various uncertainties involved due to lack of a detailed geotechnical investigation, the simplified finite slope geometry shown in Figure 7.46 is adopted to simulate the geotechnical profile B-B, characterized by three layers with different material properties (Soil 1, Soil 2, elastic bedrock) and a pre-existing sliding surface (Slide). The water table is assumed to lie at the base of the slope (-43m).

The soil materials overlaying the elastic bedrock were defined by the elasto-plastic Mohr Coulomb constitutive model coupled with the hysteretic damping scheme. In particular, FLAC 7.0 hysteretic damping formulation was implemented using the "default" model to account for the nonlinear hysteretic soil behavior prior yielding. The model approximately fits the damping and shear modulus curves over a reasonable range of strains (e.g. up to 0.2-0.3%) that are expected to occur in the herein dynamic analysis. In particular, the

Seed and Idriss (1970) sand-upper range curves were used for the slide and the upper soil formation (Soil 1) whereas Sun et al. (1988) clay-upper range curves were used for Soil 2. A small amount (e.g. 0.2%) of stiffness-proportional Rayleigh damping was also added to compensate for the low damping demonstrated by the program at small strains. In addition, for the elastic bedrock materials a constant 0.5% of Rayleigh-type damping was assigned. The geotechnical properties for the assumed 2D cross-section are summarized in Table 7.14.

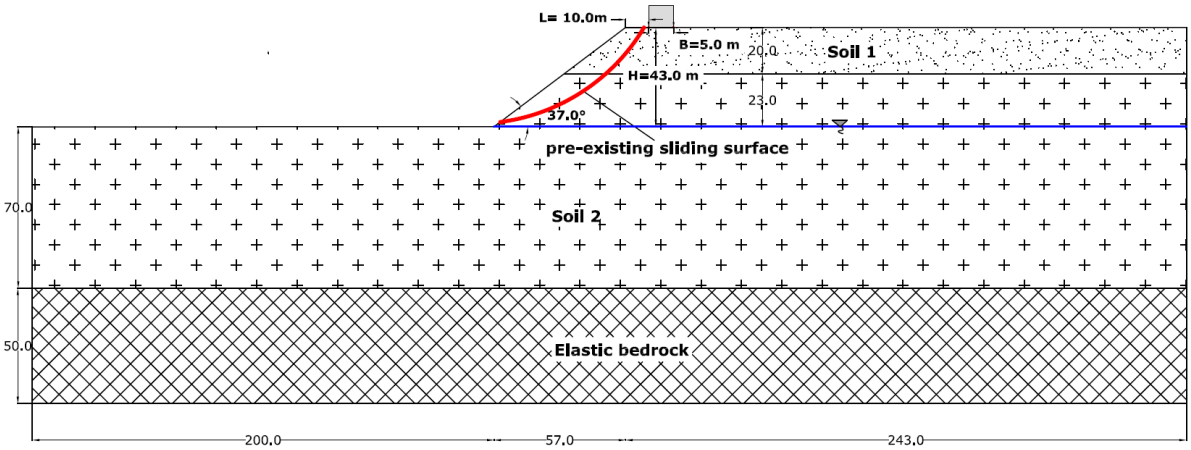


Figure 7.46. Slope configuration adopted for the geotechnical profile B-B

Table 7.14. Assumed soil properties for the geotechnical profile B-B

	Soil 1	Slide	Soil2	Elastic bedrock
Soil thickness (m)	20	1.0-2.0	93	40
Density ρ (kg/m^3)	1800	1700	2000	2300
Young's modulus E (KPa)	2.925E+05	4.420E+04	1.300E+06	4.321E+06
Poisson's ratio v	0.3	0.3	0.3	0.3
Bulk modulus K (KPa)	2.438E+05	3.683E+04	1.083E+06	3.600E+06
Shear modulus G (KPa)	1.125E+05	1.700E+04	5.000E+05	1.662E+06
K + 4G/3	3.900E+05	5.894E+04	1.733E+06	5.761E+06
Cohesion (KPa)	10	8	50	-
Friction angle (degrees)	35	35	30	-
P wave velocity Vp (m/sec)	465.48	186.19	930.95	1582.61
Shear wave velocity Vs (m/sec)	250.00	100.00	500.00	850.00
Max. allowed zone size (m)	2.50	1.00	5.00	8.50
Max. Allowed frequency	10.00	10.00	10.00	10.00

Free field absorbing boundaries are applied along the lateral boundaries while quiet (viscous) boundaries are applied along the bottom of the dynamic model to minimize the

effect of artificially reflected waves (Itasca, 2011). The simplified FLAC 2D dynamic model including mesh resolution and boundary conditions is illustrated in Figure 7.47.

A single bay-2 storey RC frame building was assumed to be standing 10 m from the crest to approximately model building n. 17. The building is modeled at this step with isolated loads at the footing links (P=80 KN). Thus, no relative slip or separation between the structure and the underlying soil materials was allowed. The assumed bay length and storey height are 5m and 3m respectively.

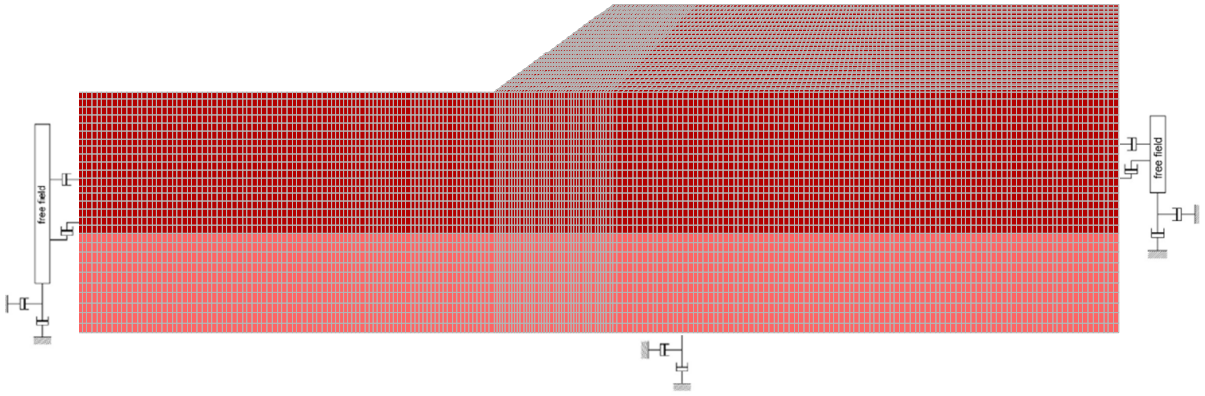


Figure 7.47. Simplified 2D FLAC dynamic model adopted for the geotechnical profile B-B

Prior to the dynamic simulations, a static analysis was carried out to establish the initial effective stress field throughout the model, and a stationary ground flow analysis was performed to establish the pore pressure distribution.

The seismic input applied along the base of the model consists of a suit of 13 real acceleration time histories extracted from SHARE database (Yenier et al., 2010; http://www.share-eu.org/) from Italian, Greek and USA earthquakes recorded at sites with average shear wave velocity in the upper 30 m, $V_{s,30}$, greater than 600 m/sec (Table 7.15). The 5%-damped acceleration response spectra of the selected records as well as the corresponding average and median spectra are shown in Figure 7.48.

To obtain the appropriate input motion at the base of the FLAC model, the selected time histories are first subjected to baseline correction and filtering (f_1=0.25Hz, f_2=10 Hz) to assure an accurate representation of wave transmission through the model. Moreover, due to the compliant base used in the model, the appropriate input excitation corresponds to the upward propagating wave train that is taken as one-half the target outcrop motion (Mejia and Dawson, 2006). The selected input time histories are scaled to three levels of peak ground acceleration, namely PGA=0.1, 0.15, 0.2g, in order to assess the building response for different ground differential displacement magnitudes to allow

the evaluation of different damage states for the building and at the end to construct the corresponding fragility curves. It is noted that due to the presence of a pre-existing sliding surface, the required amplitude of the input excitations able to cause extensive slope and foundation deformations is largely decreased compared to the corresponding amplitude considered for the first-time failures in Chapter 4.

Table 7.15. Ground motion records used in the numerical simulations derived from the SHARE database

Earthquake Name	Earthquake Country	Date	Epicetral distance R (km)	Magnitude M_W	Station Name	$V_{s,30}$ (m/s)	Database Code
Kalamata (Aftershock)	Greece	10/6/1987	17	5.36	Kyparrisia-Agriculture Bank	778	ESMD_126_H1
Ano Liosia	Greece	7/9/1999	17	6.04	Athens 4 (Kipseli District)	934	ESMD_335_H1
Kozani (Aftershock)	Greece	17/5/1995	16	5.3	Chromio-Community Building	623	ISESD_1210_H1
Friuli	Italy	6/5/1976	21.7	6.4	Tolmezzo-Diga Ambiesta	1030	ITACA_16_H1
Friuli (Aftershock)	Italy	15/9/1976	8.5	5.9	Tarcento	901	ITACA_116_H1
Umbria Marche (Aftershock)	Italy	14/10/1997	20	5.6	Norcia	681	ITACA_491_H2
App. Lucano	Italy	9/9/1998	6.6	5.6	Lauria Galdo	603	ITACA_613_H2
L Aquila Mainshock	Italy	6/4/2009	4.4	6.3	L Aquila - V. Aterno - Colle Grilli	685	ITACA_857_H2
San Fernando	USA	9/2/1971	20.04	6.61	Lake Hughes #12	602	NGA_71_H2
Coyote Lake	USA	6/8/1979	4.37	5.74	Gilroy Array #6	663	NGA_150_H2
Morgan Hill	USA	24/4/1984	36.34	6.19	Gilroy Array #6	663	NGA_459_H2
Loma Prieta	USA	18/10/1989	35.47	6.93	Gilroy Array #6	663	NGA_769_H1
Northridge-01	USA	17/1/1994	25.42	6.69	La - Griffith Park Observatory	971	NGA_994_H1

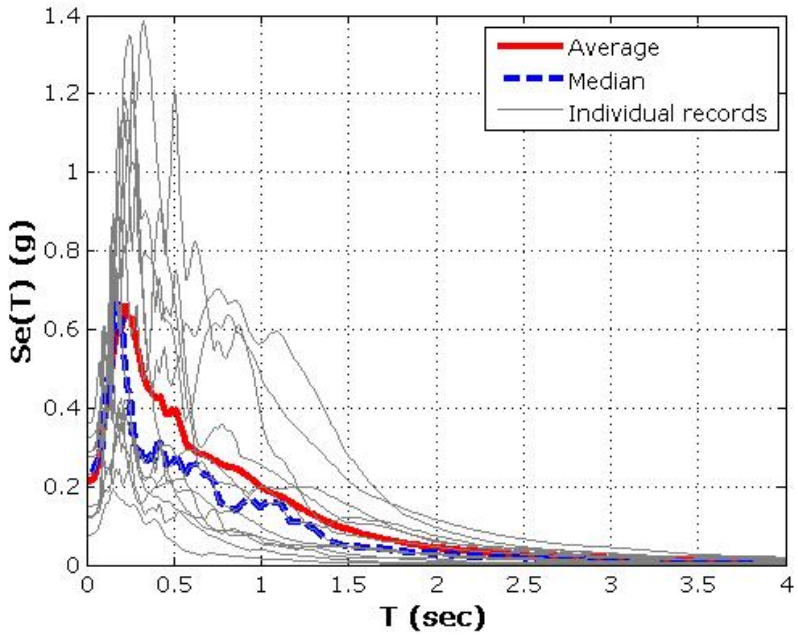


Figure 7.48. Linear 5%-damped acceleration response spectra of the records selected for numerical analyses. The average and median spectra are also shown.

Figures 7.49a and b depict the derived horizontal and vertical differential displacements time histories respectively at the closest edge of the assumed building from the slope's crest (i.e. 10 m) for input accelerograms scaled at 0.15 g. It is observed that the specific characteristics (frequency content and duration) of the seismic ground motions can significantly affect the history and the amplitude of the computed differential displacement demand at the foundation level.

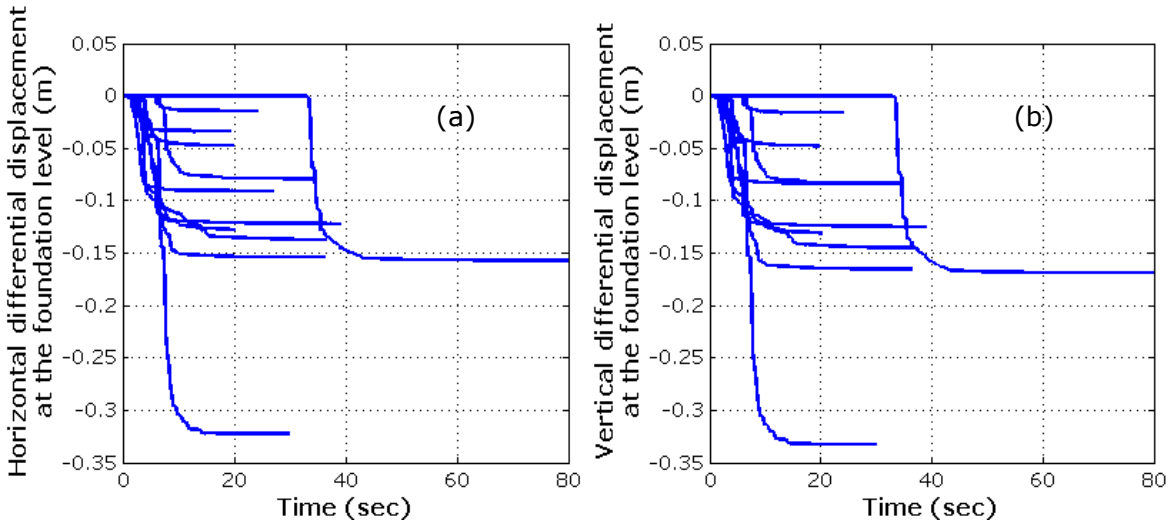


Figure 7.49. Differential horizontal (a) and vertical (b) ground displacements at the building's foundation level for input accelerograms scaled at 0.15 g

Then, a non-linear quasi-static analysis is performed for the studied 1 bay- 2 storey RC frame building model (Fig. 7.50) by means of the finite element code SeismoStruct (Seismosoft, SeismoStruct 2011). More specifically, the derived differential displacement time histories extracted from FLAC dynamic analysis (see Fig. 7.49) were directly applied as static loads at one of the RC frame supports. The beneficial contribution of masonry infill walls to the building capacity is not considered in this study.

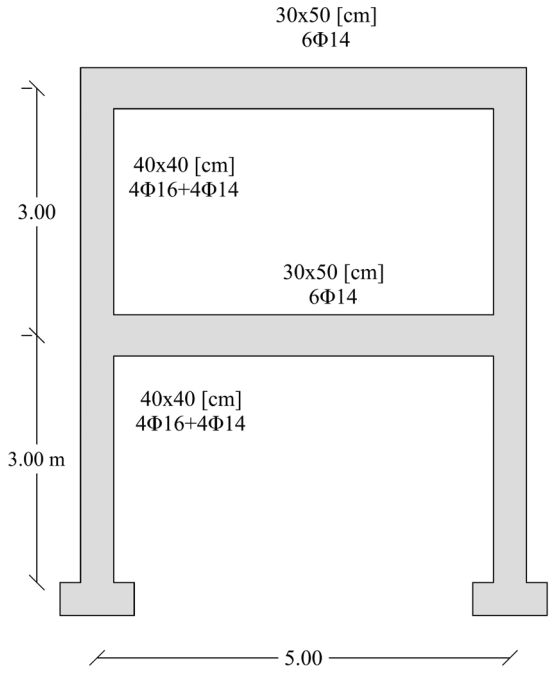


Figure 7.50. Schematic view of the studied building in Corniglio village

Non-linear fibre-based material properties are assumed for the structural members of the RC frame building under investigation. More specifically, a uni-axial nonlinear constant confinement model is used for the concrete material (f_c=20MPa, f_t=2.1MPa, strain at peak stress 0.002mm/mm, confinement factor =1 for unconfined and 1.2 for confined concrete, specific weight=24KN/m^3) and a uni-axial bilinear stress-strain model with kinematic strain hardening is used for the reinforcement (f_y=400MPa, E=200GPa, strain hardening parameter μ =0.005, specific weight=78KN/m^3).

Figure 7.51 presents representative plot of damage evolution expressed in terms of maximum steel strain (damage index) as a function of the maximum permanent ground displacement vector at the foundation level for the low-rise, "low code" designed RC frame building. The figure also shows the limit steel strains needed to exceed yield and post-yield limit states for low-code RC buildings characterized by a low level of confinement as defined in Chapter 4.

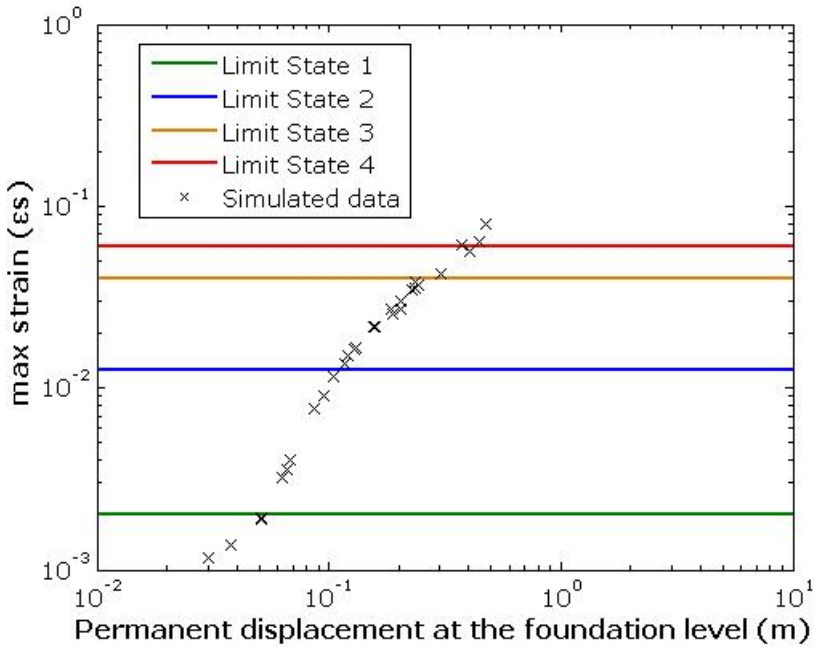


Figure 7.51. Maximum recorded steel strain as a function of permanent ground displacement vector at the foundation level for the studied building in Corniglio village

Finally, probabilistic fragility curves in terms of permanent displacement vector at the foundation level for building n. 17 in Corniglio village were derived using the Maximum likelihood Method (see Chapter 4 for details). Table 7.16 presents the lognormal parameters of the fragility functions whilst Figure 7.52 depicts the corresponding graphs.

Table 7.16. Parameters of fragility functions for the studied building in Corniglio village based on the Maximum likelihood method

	Permanent displacement at the foundation level (m)	
	Median (m)	**Dispersion β**
Limit State 1	0.042	0.41
Limit State 2	0.093	
Limit State 3	0.168	
Limit State 4	0.315	

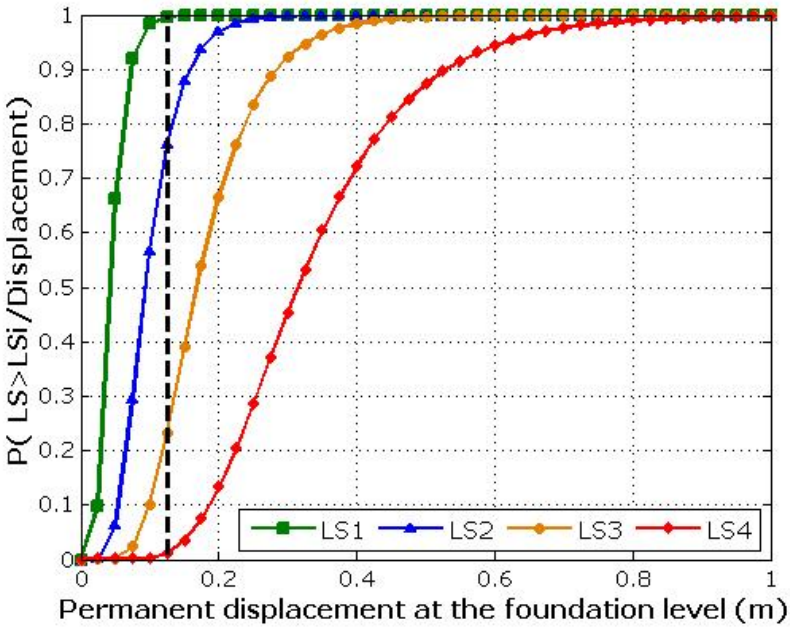


Figure 7.52. Fragility curves for the studied RC frame building in Corniglio village

The simulated fragility curves predict that the building n. 17 studied herein is more likely to suffer "moderate to extensive damage", for the measured level of displacement, i.e. 0.121 m. In particular, the estimated probabilities of exceeding moderate and extensive damage are 0.85 and 0.22 respectively. These observations are in fairly good agreement with the recorded building damages (see Fig. 7.38), verifying the validity of the derived curves and finally enforcing the credibility and applicability band of the proposed methodological framework.

7.5 Conclusive remarks

The validity the proposed method has been verified through the comparison of representative suggested fragility curves in this thesis with corresponding curves proposed in the literature derived by different approaches (empirical, expert judgment, analytical). The comparisons are generally judged satisfactory when considering a low-rise, high-code RC frame building resting on flexible foundations (e.g. isolated footings) whereas they are not so good in case of the building on stiff foundations (e.g. continuous raft foundation). In particular, the proposed curves generally predict lower vulnerability values for the building on stiff foundations compared to the literature ones. It should be noticed, however, that only the structural damage (e.g. in terms of cracks) to the building members could be estimated by the proposed curves even though, for the stiff

foundation case, a considerable amount of damage would be non structural (e.g. rigid body movement), reducing the serviceability level of the building.

Approximate correlations between the proposed fragility curves in this research for RC buildings subjected to co-seismic permanent slope displacement and different literature fragility curves derived for low-rise RC buildings subjected to ground shaking on horizontally layered soil deposits were also performed. Overall, the comparisons allow gaining better insight into the relative extent of damage and the associated dominating failure mechanism for structures subjected to co-seismic slope deformation and ground shaking respectively. More specifically, for the yielding limit state most of the literature curves predict larger damages for the building, implying that the building is generally expected to suffer some initial damage due to ground shaking before the onset of the landslide movement. For the collapse limit state, on the other hand, most of the literature curves estimate lower vulnerability values for the building with respect to the ones proposed in this study. Thus, the landslide, once triggered by the earthquake, may become the prevailing damage mechanism resulting to greater damages for the building near collapse.

The reliability and applicability of the proposed methodological framework and the corresponding fragility curves has been also assessed through its application to two real case histories: Kato Achaia slope in Peloponnese –Greece and the Corniglio village-Italy case study. The direct comparison of the recorded damage data on typical buildings with the corresponding damage predicted by the developed fragility functions proved that the proposed fragility curves could adequately capture the performance of the representative RC building affected by the slope co-seismic landslide differential displacement. In addition, to enhance the effective implementation of the proposed methodological framework within a probabilistic risk assessment study, more realistic fragility curves were constructed for a representative building in Corniglio village based on straightforward numerical computations. The curves were verified through their comparison with the observed building damage for the measured level of displacement.

CHAPTER 8

Evolution of building vulnerability over time

8.1 Introduction

The assessment of landslide risk depends on the evaluation of landslide hazard and the vulnerability of exposed structures which both change with time. The real, non-stationary vulnerability modeling of structures due to landslides may be significantly affected by various degradation mechanisms such as aging considerations, anthropogenic actions, cumulative damage from past landslide events and retrofitting measures. Such mechanisms, however, have been traditionally neglected in vulnerability assessment studies assuming an optimum plan of maintenance.

With the above in mind, the present work aims at the expansion of the proposed vulnerability assessment methodology in Chapter 4 to account for the evolution of building vulnerability over time exposed to earthquake –induced landslide hazard. In particular, the aging of typical RC buildings is considered in this research by including probabilistic models of corrosion deterioration of the RC elements within the vulnerability modeling framework. Two potential adverse corrosion scenarios are examined: chloride and carbonation induced corrosion of the steel reinforcement.

An application of the proposed methodology to reference low-rise RC buildings exposed to the combined effect of seismically induced landslide differential displacements and reinforcement corrosion is provided. Both buildings with stiff and flexible foundation system standing near the crest of a potentially precarious soil slope are examined. Non linear static time history analyses of the buildings are performed using a finite element code. The distribution for the corrosion initiation time is assessed through Monte Carlo simulation using appropriate probabilistic models for the carbonation and the chloride induced corrosion. Then, the loss of area of steel over time due to corrosion of the RC elements is modeled as a reduction in longitudinal reinforcing bar cross-sectional area in the fiber section model. Time dependent structural limit states are defined in terms of steel material strain. Fragility curves/surfaces are derived for different points in time as a

function of Peak Ground Acceleration PGA at the seismic bedrock or permanent co-seismic ground displacement PGD at the slope area for both chloride and carbonation induced deterioration scenarios.

8.2 Environmental deterioration of RC structures

8.2.1 Corrosion of reinforcement

The strength of the components of any structural system is in general a time dependent property which may decrease in resistance along the structure's service life. Potential reasons for structural strength and stiffness degradation can be attributed to multiple factors such as corrosion, erosion, other forms of chemical deterioration and fatigue (Melchers and Frangopol, 2008). Among these, reinforcement corrosion is undoubtedly, one of the most important causes of deterioration of reinforced concrete in Europe and worldwide. Corrosion is a complex process that may affect a RC structure in a variety of ways, including, among others, cover spalling, loss of steel-concrete bond strength and loss of reinforcement cross sectional area, potentially resulting to the reduction of the resistance and load bearing capacity of the structure and to the variation of the failure mechanism from ductile to fragile type (e.g. Saetta et al., 2008; Mohammed et al., 2011; Yalciner et al., 2012 etc.). Thus, it may affect both the safety and serviceability of RC structures in relation to their initial as-built state. Figure 8.1 presents typical structural failures as a result of reinforcement corrosion.



Figure 8.1. Structural deterioration due to reinforcement corrosion

Theoretically corrosion of the reinforcement should not occur as the reinforcement is supposedly well protected by the concrete cover and the alkalinity of the last. Non carbonated concrete has a high alkalinity (pH=13) that is a result of the presence of sodium, potassium and calcium hydroxides produced during the hydration of the cement. In this alkaline environment an oxide layer is formed on the steel surface, the so-called "passive film" that prevents the corrosion of the reinforcement. However, there are principally two processes that may break down this passive film: the *ingress of chlorides* and *carbon dioxide* (e.g. Zhong et al., 2010).

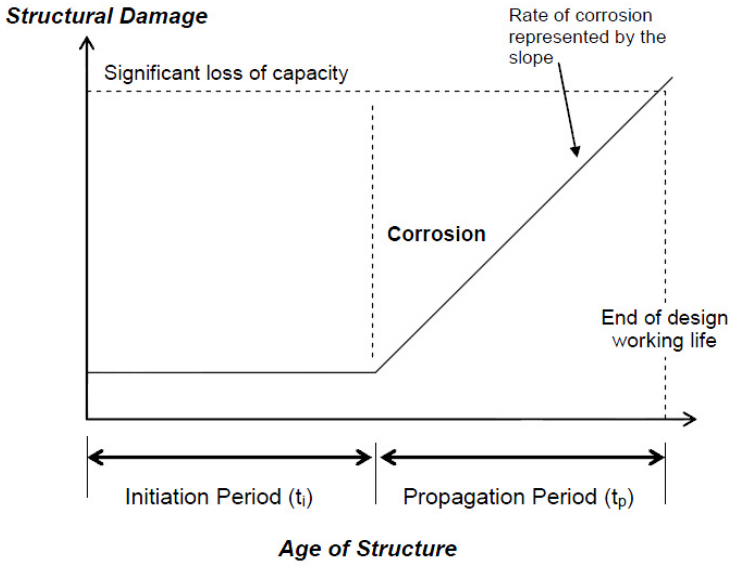


Figure 8.2. Schematic illustration of the evolution of the reinforced concrete corrosion (Tuutti, 1982)

The amount of structural damage due to corrosion of steel reinforcement as a function of the age of the structure can be expressed through a bilinear model as schematically illustrated in Figure 8.2. Deterioration caused by reinforcement corrosion is normally divided into two main time periods, the initiation period (t_i) and the propagation period (t_p). The initiation period is defined as the time until the reinforcement becomes depassivated either by the presence of chloride salts or by carbonation. As soon as the concrete at the depth of the reinforcement is carbonated or contains a critical amount of free chlorides the reinforcement becomes depassivated and corrosion may occur. This limit state defines the beginning of the propagation period. During the propagation period the reinforcement is corroding, which may lead to deterioration of the concrete as well. Expansive corrosion products provoke cracks along the reinforcement, and subsequently, spalling of the concrete cover may occur. Finally, the loss of cross section of the reinforcement may lead to reduction of the load bearing capacity.

8.2.2 Carbonation-induced corrosion

8.2.2.1. Mechanism

Concrete carbonation induces a decrease of the pH of the pore solution, which leads to dissolving the protective layer (Fig. 8.3). Then the corrosion of the reinforcement starts only if the reinforcing steel has significant electrical potential difference along with the presence of sufficient moisture and oxygen. Concrete carbonation is a complex physico-chemical process that develops in two distinct regions: the anode, where the passive layer is destroyed and the steel dissolved; and the cathode, where hydroxide ions are formed due to the combination of oxygen, water and the electrons coming from the anode. It includes the diffusion of CO_2 into the gas phase of the concrete pores and its reaction with the calcium hydroxyl $Ca(OH)_2$. As the high pH of uncarbonated concrete is mainly due to the presence of $Ca(OH)_2$, it is clear that the consumption of this species will lead to a pH drop, which can attain a value of 9 when the reaction is completed. In this environment, the oxide layer that protected the reinforcement bars is attacked and corrosion starts. In practice, CO_2 penetrates into the concrete mass by diffusion from the surface layer. Thus a carbonation front appears that moves into the structure (Fig. 8.4).

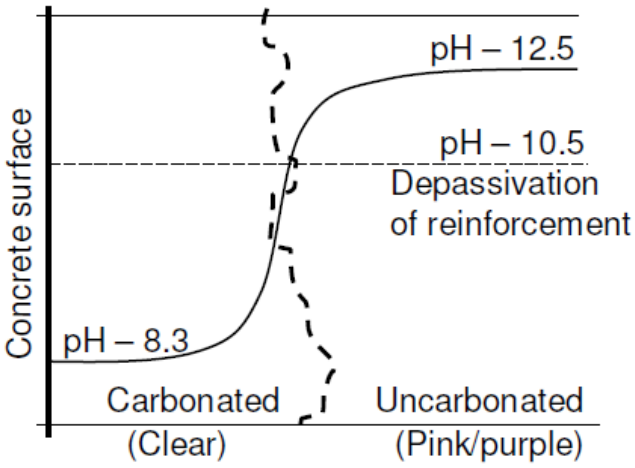


Figure 8.3. Carbonation in concrete (Beushausen and Alexander, 2010)

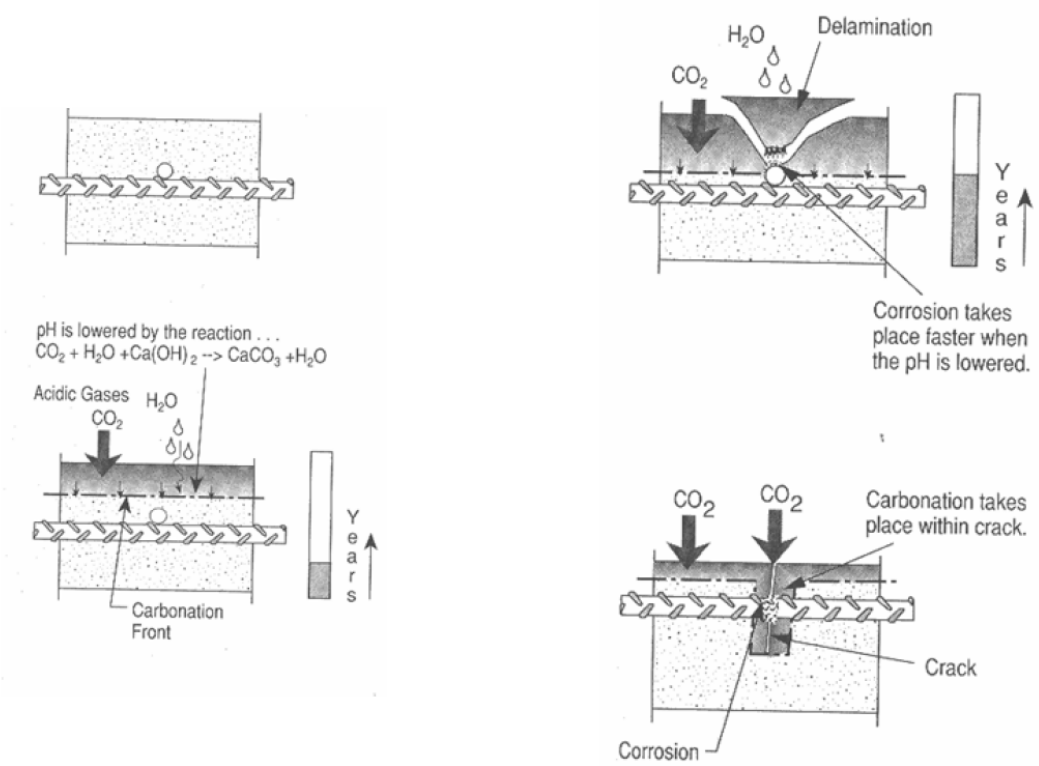


Figure 8.4. Carbonation induced corrosion (Beushausen and Alexander, 2010)

8.2.2.2. Probabilistic modeling of carbonation induced corrosion initiation

Probabilistic modeling of corrosion has much to offer with regard to practicality and reliability as compared with attempts at formulating purely deterministic models. Ditlevsen (1984) states: *"Probabilistic models are almost always superior to deterministic models of equal level of complexity in the sense that the former have considerable higher threshold of realism when dealing with phenomena taking place in uncertain environments"*.

Several methods have been proposed to model corrosion due to carbonation (e.g. Sudret et al. 2007; Peng and Stewart, 2008; Marques and Costa, 2010 etc.). The reliability-based model for computing the carbonation depth x_c proposed by FIB- CEB Task Group 5.6 (2006) is adopted in this study. The model has been developed within the research project DuraCrete and slightly revised in the research project DARTS, each project was funded by the European Union. It is based on diffusion as the prevailing transport mechanism within the concrete (Fick's 1st law of diffusion) assuming that the diffusion coefficient for carbon dioxide through the material is a constant material property.

$$x_c(t) = \sqrt{2 \cdot k_e \cdot k_c \cdot (k_t \cdot R_{ACC,0}^{-1} + \dot{a}_t) \cdot C_s} \cdot \sqrt{t} \cdot W(t) \qquad (8.1)$$

where

$x_c(t)$: carbonation depth at the time t [mm]

t: time [years]

k_e: environmental function [-]

k_c: execution transfer parameter [-]

k_t: regression parameter [-]

$R_{ACC,0}^{-1}$: inverse effective carbonation resistance of concrete [(mm^2/years)/(kg/m^3)]

a_t: error term,

C_S: CO_2-concentration [kg/m^3]

W(t): weather function [-]

It is supposed that corrosion immediately starts when carbonation has attained the rebar. Denoting by a (mm) the concrete cover, the time necessary for corrosion to start, called corrosion initiation time, is given as:

$$T_{init} = \left(\frac{2 \cdot k_e \cdot k_c \cdot (k_t \cdot R_{ACC,0}^{-1} + \dot{a}_t) \cdot C_s}{a^2} \cdot t_0^{2 \cdot w} \right)^{\left(\frac{1}{2 \cdot w - 1} \right)} \tag{8.2}$$

The environmental function k_e takes account of the influence of the humidity level on the diffusion coefficient and hence on the carbonation resistance of the concrete. The reference climate is T= +20°C/ 65% RH. It can be described by means of Equation 8.3.

$$k_e = \left(\frac{1 - \left(\frac{RH_{real}}{100} \right)^{f_c}}{1 - \left(\frac{RH_{ref}}{100} \right)^{f_c}} \right)^{g_c} \tag{8.3}$$

where

RH_{real}: weather nearest station data (daily mean value: 0 % < RH < 100 %)

RH_{ref} [%]: constant parameter, value: 65

g_c [-]: constant parameter, value: 2.5

f_c [-]: constant parameter, value: 5.0

The execution transfer parameter k_c takes the influence of curing on the effective carbonation resistance into account. It can be described by means of Equation 8.4, derived from Bayesian regression analysis.

$$k_c = \left(\frac{t_c}{7} \right)^{b_c} \tag{8.4}$$

k_c: execution transfer parameter [-]

b_c: exponent of regression [-], normally distributed variable

t_c: period of curing [d], constant parameter, value: period of curing

The inverse carbonation resistance of concrete $R_{ACC,0}^{-1}$ should be quantified using different direct and indirect testing methods. If no test data is available, literature data can be used for orientation purposes [Table B1-2, FIB- CEB Task Group 5.6 (2006)].

The factors k_t and a_t have been introduced in order to transform the results gained under "accelerated carbonation" conditions $R_{ACC,0}^{-1}$ into an inverse carbonation resistance $R_{NAC,0}^{-1}$ under "natural carbonation" conditions.

$$R_{NAC,0}^{-1} = k_t \cdot R_{ACC,0}^{-1} + \dot{a}_t \tag{8.5}$$

$R_{ACC,0}^{-1}$: inverse effective carbonation resistance of dry concrete, determined at a certain point of time t_0 on specimens with the accelerated carbonation test ACC [$(mm^2/years)/(kg/m^3)$], normally distributed variable.

$R_{NAC,0}^{-1}$: inverse effective carbonation resistance of dry concrete (65% RH) determined at a certain point of time t_0 on specimens with the normal carbonation test NAC [$(mm^2/years)/(kg/m^3)$]

k_t: regression parameter which considers the influence of test method on the ACC-test [-],normally distributed variable.

a_t: error term considering inaccuracies which occur conditionally when using the ACC test method [$(mm^2/years)/(kg/m^3)$], normally distributed variable.

The CO_2 concentration of the ambient air represents the direct impact on the concrete structure. The impact can be described by the following equation:

$$C_S = C_{S,atm} + C_{S,emi} \tag{8.6}$$

where

C_S: CO_2 concentration [kg/m^3]

$C_{S,atm}$.: CO_2 concentration of the atmosphere [kg/m^3]

$C_{S,emi}$.: additional CO_2 concentration due to emission sources [kg/m^3]

For usual structures, Equation 8.6 can be reduced to Equation 8.7:

$$C_S = C_{S,atm} \tag{8.7}$$

The atmospheric concentration of CO_2 can be quantified as a normally distributed variable (mean= 0.00082, s=0.0001).

The weather function W takes the meso-climatic conditions due to wetting events of the concrete surface into account.

$$W = \left(\frac{t_0}{t}\right)^{\frac{(p_{SR}\cdot ToW)^{b_w}}{2}} = \left(\frac{t_0}{t}\right)^{w} \tag{8.8}$$

t_0: time of reference [years]

w: weather exponent [-]

ToW: time of wetness [-], value: to be evaluated from weather station data

$$ToW = \frac{days\ with\ \text{rainfall}\ h_{Nd} \geq 2.5\ \text{mm per year}}{365} \tag{8.9}$$

p_{SR}: probability of driving rain [-],value: depending on the type of structural elements

b_w: exponent of regression [-],normally distributed variable

t_o [years]: constant parameter, value: 0.0767

The statistical quantification of the model parameters is provided in Table 8.1 based on the FIB- CEB Task Group 5.6 (2006) proposed model. For illustrational purposes, values for Portland Cement Concrete (PCC) and three different water/cement ratios (namely w/c=0.4,0.5 and 0.6) are given. Three different corrosion levels (low, medium, high) are considered in the table based on recent available literature (Marques and Costa, 2010).

Table 8.1. Statistical characteristics of parameters affecting the carbonation induced corrosion deterioration of RC elements

		Water to cement ratio (w/c)						Distribution	Reference
		0.4		0.5		0.6			
Parameters		Mean	cov	Mean	cov	Mean	cov		
Cover Depth (mm) a		25.00	0.32	25.00	0.32	25.00	0.32	Lognormal	FIB- CEB Task Group 5.6 (2006)
$Rh_{real,k}$ (% rel. humidity)		70.00	cov=0.1 , a=40.0, b=100	70.00	cov=0.1 , a=40.0, b=100	70.00	cov=0.1 , a=40.0, b=100	Beta	
exponent of regression b_c		-0.567	0.042	-0.567	0.042	-0.567	0.042	Normal	
Inverse carbonation resistance ($R_{acc,01}$) (mm^2/year) / (kg/m^3)		3.10E-11	0.15	6.80E-11	0.13	2.30E-10	0.10	Normal	
Influence of test method k_t		1.25	0.28	1.25	0.28	1.25	0.28	Normal	
Error term et (mm^2/years)		315.5	0.15	315.5	0.15	315.5	0.15	Normal	
$C_{s,\ atm}$ (kg/m^3)		0.000820	0.12	0.000820	0.12	0.000820	0.12	Normal	
Exponent of regression b_w		0.446	0.365	0.446	0.365	0.446	0.365	Normal	
Rate of Corrosion (r_{corr}) mA/cm^2	Low corrosion Level	0.1-0.5	0.25	0.1-0.5	0.25	0.1-0.5	0.25	Normal	Marques and Costa (2010)
	Medium corrosion Level	0.5-1		0.5-1		0.5-1			
	High corrosion Level	>1		>1		>1			

8.2.3 Chloride-induced corrosion

8.2.3.1. Mechanism

Chloride induced corrosion is reportedly the most serious and widespread deterioration mechanism of concrete structures, fib (2006). It can be attributed to the ingress of chloride ions from the concrete surface through the concrete cover to the reinforcing steel. Once the chlorides have penetrated the concrete cover and reached the surface of reinforcement, and their concentration exceeds a threshold value, corrosion is initiated (Figs. 8.5 and 8.6). According to DuraCrete (2000) two exposure environments are of main concern, namely marine and road environment. Within these, different zones are identified:

- the atmospheric
- the splash
- the tidal and
- the submerged zone

Chloride-induced corrosion causes extensive damage as the presence of salt and water creates the right conditions for rapid corrosion rates generating pits and expansive rust.

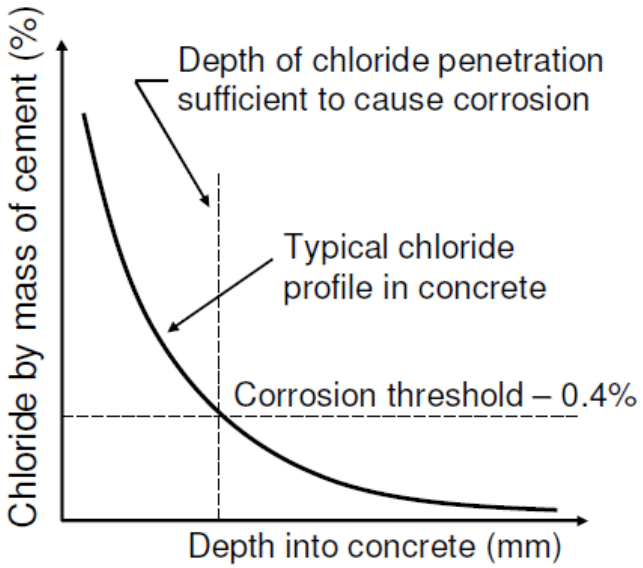


Figure 8.5. Typical chloride profile in concrete (Beushausen and Alexander, 2010)

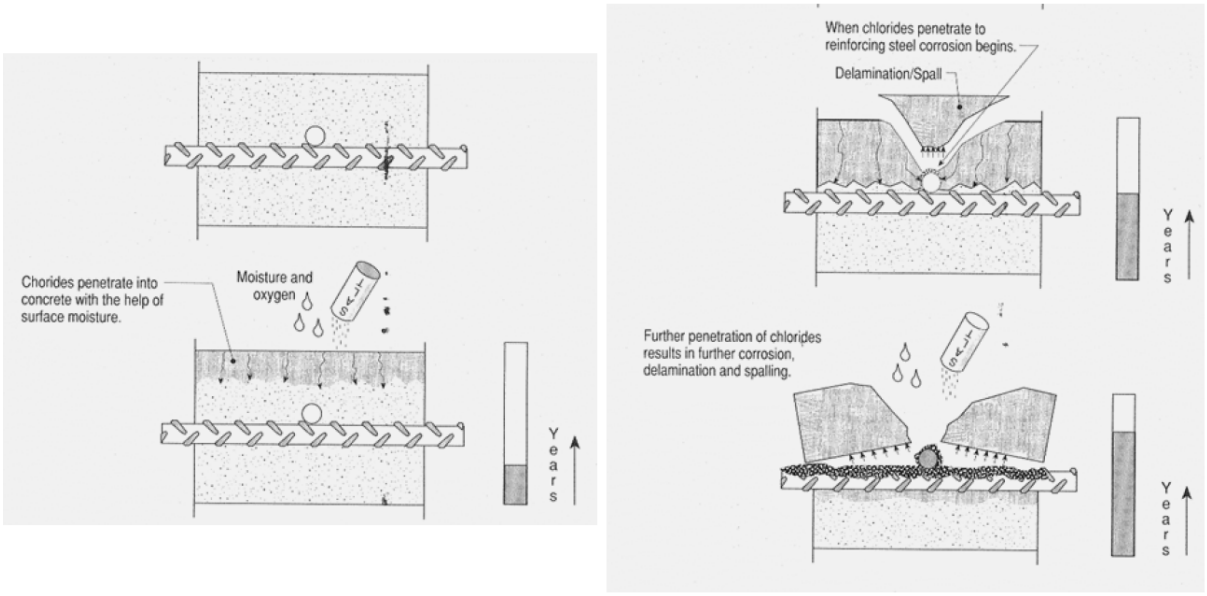


Figure 8.6. Chloride induced corrosion of reinforcement (Beushausen and Alexander, 2010)

8.2.3.2. Probabilistic modeling of chloride induced corrosion initiation

Several models have been proposed to quantify and account for corrosion in the design, construction, and maintenance of RC structures. A summary of these models can be found e.g. in DuraCrete (1998). Researchers tend to agree that corrosion phenomena are subject to severe uncertainties thus necessitating the use of probabilistic models. The probabilistic model proposed by FIB- CEB Task Group 5.6 (2006) for modeling corrosion initiation due to chloride ingress is adopted herein. It is based on the limit-state Equation 8.10, in which the critical chloride concentration C_{crit} is compared to the actual chloride concentration at the depth of the reinforcing steel at a time t C(x = a, t). The model has been developed within the research project DuraCrete and slightly revised in the research project DARTS, each project was funded by the European Union.

$$C_{crit.} = C(x = a, t) = C_0 + \left(C_{S,\Delta x} - C_0\right) \cdot \left(1 - erf \frac{a - \Delta x}{2 \cdot \sqrt{D_{app,C} \cdot t}}\right) \tag{8.10}$$

where

$C_{crit.}$: critical chloride content [wt.-%/c]

C(x,t): content of chlorides in the concrete at a depth x (structure surface: x = 0 m) and at time t [wt.-%/c]

C_0: initial chloride content of the concrete [wt.-%/c]

$C_{S,\Delta x}$: chloride content at a depth Δx and a certain point of time t [wt.-%/c]

x: depth with a corresponding content of chlorides C(x,t) [mm]

a: concrete cover [mm]

Δx: depth of the convection zone (concrete layer, up to which the process of chloride penetration differs from Fick's 2nd law of diffusion) [mm]

$D_{app,C}$: apparent coefficient of chloride diffusion through concrete [mm^2/years]

t: time [years]

erf: Gaussian error function

The apparent coefficient of chloride diffusion of concrete $D_{app,C}$ can be determined by means of Equation (8.11):

$$D_{app,C} = k_e \cdot D_{RCM,0} \cdot k_t \cdot A(t) \tag{8.11}$$

where

k_e: environmental transfer variable [-]

$D_{RCM,0}$: chloride migration coefficient [mm^2/a], normally distributed variable

k_t: transfer parameter [-], constant parameter, value: 1

A(t): subfunction considering the 'ageing' [-]

The model is based on Fick's 2nd law of diffusion, taking into account that most observations indicate that transport of chlorides in concrete is diffusion controlled. However, in order to still describe the penetration of chlorides for an intermittent load using Fick's 2nd law of diffusion, the data of the convection zone Δx (e.g. zone exposed to frequent change of wetting and subsequent evaporation), is neglected and Fick's 2nd law of diffusion is applied starting at a depth Δx with a substitute surface concentration $C_{s,\Delta x}$. With this simplification, Fick's 2nd law of diffusion yields a good approximation of the chloride distribution at a depth x ≥Δx.

The environmental transfer variable k_e has been introduced in order to take the influence of T_{real} on the diffusion coefficient $D_{app,C}$ into account. It is described by the following equation:

$$k_e = \exp\left(b_e \cdot \left(\frac{1}{T_{ref}} - \frac{1}{T_{real}}\right)\right) \tag{8.12}$$

where

b_e: regression variable [K], normally distributed variable

T_{ref}: standard test temperature [K], constant parameter, value: 293

T_{real}: temperature of the structural element or the ambient air [K], normally distributed variable, to be evaluated from nearby weather station data

The Chloride Migration Coefficient $D_{RCM,0}$ is one of the governing parameters for the description of the material properties in the chloride induced corrosion model. Suitable data for $D_{RCM,0}$ may be obtained from literature for different concrete mixtures to be used as starting variables in service life design or vulnerability assessment calculations [Table B2-1, FIB- CEB Task Group 5.6 (2006)].

The apparent diffusion coefficient $D_{app,C}$ is subject to considerable scatter and tends to reduce with increasing exposure time. In order to take this into account when modeling the initiation process, a transfer parameter k_t in combination with a so-called ageing exponent n has been introduced**.**

$$A(t) = \left(\frac{t_0}{t}\right)^n \tag{8.13}$$

n: ageing exponent [-], beta distributed variable, Table B2-2, FIB- CEB Task Group 5.6 (2006)

t_0: reference point of time [years], constant parameter, value: 0.0767

The chloride content in the concrete is not only caused by chloride ingress from the surface, but can also be due to chloride contaminated aggregates, cements or water used for the concrete production (initial chloride content C_0). In certain circumstances the chloride content of fine and coarse aggregates and water can be considerable.

The chloride content C_S at the concrete surface as well as the substitute surface content $C_{S,\Delta x}$ at a depth Δx are variables that depend on material properties (e.g. type of binder and the concrete composition) and on geometrical (e.g. geometry of the structural element and the distance to the chloride source) and environmental (e.g. equivalent chloride concentration of the ambient solution) conditions. The information needed to determine C_S and $C_{S,\Delta x}$ is briefly summarized in the flowchart given in Figure 8.7.

Under a continuous chloride impact of constant concentration, the chloride saturation concentration $C_{S,0}$ on the concrete surface is reached often in relative short time periods compared to the service life of the structure ($C_{S,0}$ = C_S). Based on these results, the conservative simplification that the variable C_S is from the beginning constant with time can be concluded for certain exposure conditions (e. g. for concrete continuously exposed to sea water).

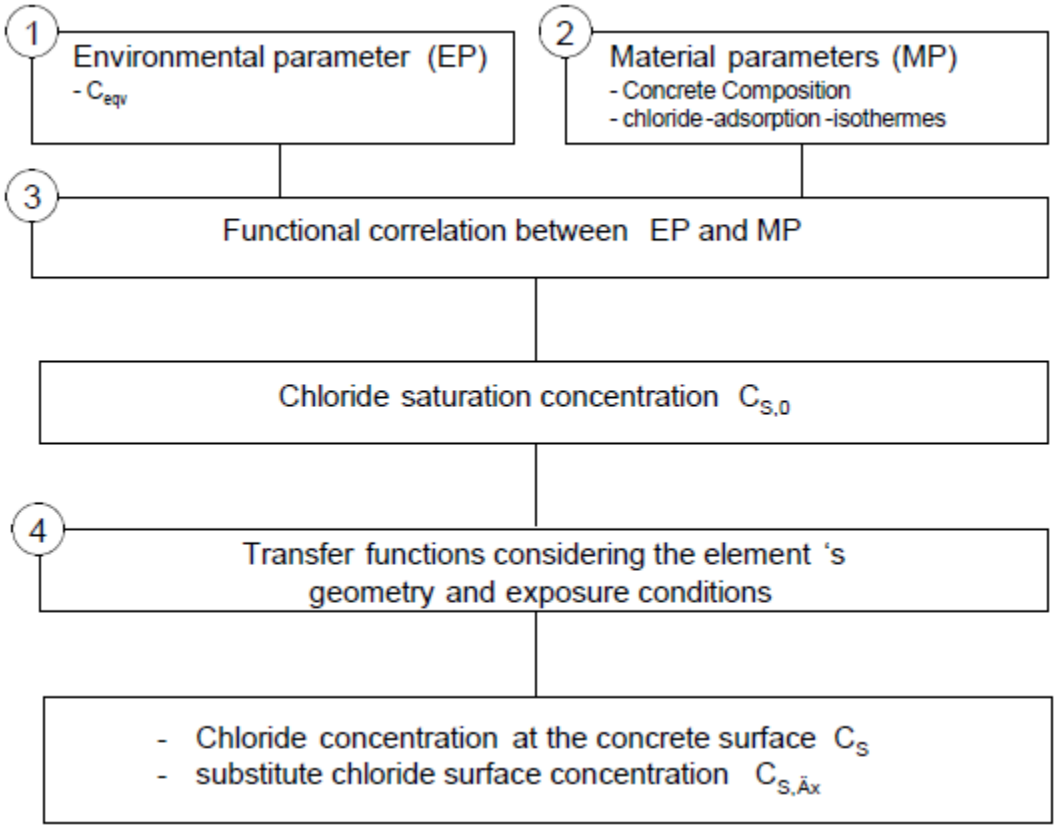


Figure 8.7. Information needed to determine the variables C_S and $C_{S,\Delta x}$ (FIB- CEB Task Group 5.6, 2006)

In order to quantify the substitute chloride surface concentration $C_{S,\Delta x}$, *the* transfer function Δx needs to be determined. For the different types of exposure conditions (splash, submerged, spray, tidal and atmospheric) Δx can be quantified based on the information provided in section B2.2.5.5 of FIB- CEB Task Group 5.6 (2006). Depending on the exposure condition $C_{S,\Delta x}$ may be defined as the maximum chloride content C_{max}. In cases when no Δx develops (e.g. spray zone), C_{max} represents the chloride content at the concrete surface C_S.

The critical chloride content C_{crit} is the critical chloride concentration that causes dissolution of the protective passive film around the reinforcement and initiates corrosion. A beta-distribution with a lower boundary of 0.20 wt.-%/cement, mean value of 0.60 wt.-%/cement and upper boundary of 2 wt.-%/cement was found to yield a sufficiently good description of the test results.

Based on Equation (8.10) and assuming that the chloride ion concentration near the concrete surface is constant, the time till corrosion initiation can be determined as:

$$T_{init} = \left(\frac{a^2}{4 \cdot k_e \cdot k_t \cdot D_{RCM,0} \cdot (t_0)^n} \cdot \left(erf^{-1} \left(1 - \frac{C_{crit}}{C_s} \right) \right)^{-2} \right)^{\left(\frac{1}{1-n}\right)} \quad (8.14)$$

where

T_{init}: the corrosion initiation time (years) and

Cs: the equilibrium chloride concentration at the concrete surface

The statistical quantification of the model parameters describing the corrosion initiation of the reinforced concrete elements is provided in Table 8.2 based on the FIB- CEB Task Group 5.6 (2006) proposed model. For illustrational purposes, values for Portland Cement Concrete (PCC) and three different water/cement ratios (namely w/c=0.4,0.5 and 0.6) are given. The values of surface chloride concentration C_S and of the temperature of the structural element or the ambient air T_{real} presented in the table are applicable to structures exposed to atmospheric chloride condition (Choe et al. 2009). Three different corrosion levels (low, medium, high) are considered in the table based on available literature (Stewart, 2004).

Table 8.2. Statistical characteristics of parameters affecting the chloride induced corrosion deterioration of RC elements

Parameter		water to cement ratio w/c						Distribution	Reference
		0.4		0.5		0.6			
		Mean	cov	Mean	cov	Mean	cov		
Cover Depth (mm) x		25	0.32	25	0.32	25	0.32	Lognormal	FIB- CEB Task Group 5.6 (2006)
Regression variable b_e [K]		4800	0.15	4800	0.15	4800	0.15	Normal	
Temperature of the structural element or the ambient air (T_{real}) [K]		286	0.20	286	0.20	286	0.20	Normal	
Chloride migration Coefficient ($D_{RCM,0}$) (m^2/s)		$8.9 \cdot 10^{-12}$	0.2	$1.58 \cdot 10^{-11}$	0.2	$2.5 \cdot 10^{-11}$	0.2	Normal	
Aging exponent n		0.3	cov=0.4, a=0.0, b=1.0	0.3	cov=0.4, a=0.0, b=1.0	0.3	cov=0.4, a=0.0, b=1.0	Beta	
Critical Chloride Concentration (C_{cr}) wt % cement		0.6	cov=0.25, a= 0.2, b=2.0	0.6	cov=0.25, a= 0.2, b=2.0	0.6	cov=0.25, a= 0.2, b=2.0	Beta	
Surface Chloride Concentration (C_s) wt % cement		1.026	0.2	1.2825	0.2	1.539	0.2	Normal	Choe et al. (2009)
Rate of Corrosion (i_{corr}) mA/cm^2	Low corrosion Level	0.1	0.25	0.1	0.25	0.1	0.25	Normal	Stewart (2004)
	Medium corrosion Level	1		1		1			
	High corrosion Level	10		10		10			

8.3 Application to reference RC buildings

8.3.1 Numerical modeling of the buildings

The proposed approach is described through its application to typical structures. The studied buildings (Fig. 8.8) are single bay- single story RC bare frame structures with varying strength and stiffness characteristics of the foundation system (isolated footings, continuous foundation). They have been designed according to the provisions of the Greek Seismic Code (EAK 2000), for a design acceleration A_d = 0.36 g, and a behavior factor q = 3.5. The adopted dead and live loads (g = 1.3 kN/m^2 and q = 2 kN/m^2) are typical values for residential buildings. The beneficial contribution of masonry infill walls to the building capacity is not considered in this study. The reference buildings are assumed to be standing near the crest of a potentially precarious sand soil slope (see Chapter 4 for details). Hence, for a certain earthquake scenario, the buildings may be subjected to a considerable amount of permanent differential displacement at the foundation level due to the effect of the earthquake triggered landslide hazard. The same methodology may be applied for other hazards (i.e. hydrogeological- intense precipitation). The analytical methodology for the vulnerability assessment of the as-built RC buildings subjected to earthquake induced slow moving soil slides as well as the proposition of adequate fragility functions for a variety of RC building typologies, slope configurations and soil conditions have been thoroughly described and discussed in Chapters 4 and 6 respectively.

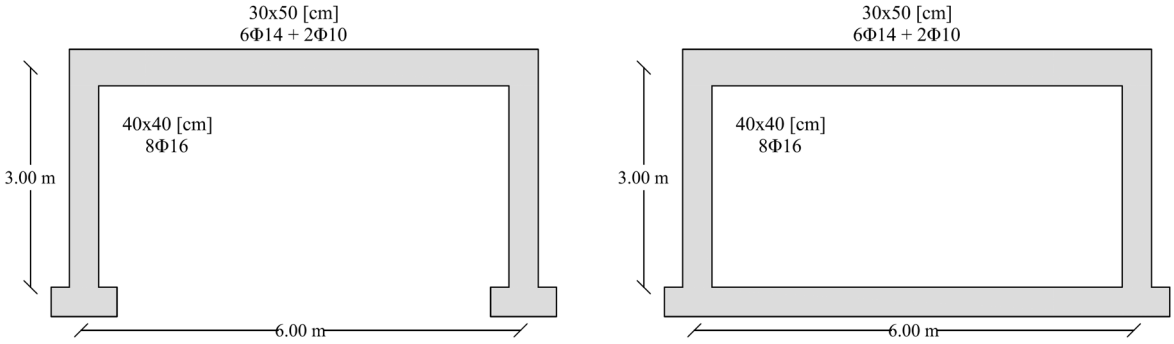


Figure 8.8. Reference analyzed RC frame buildings

The description of the numerical modeling of the typical RC buildings is also briefly outlined herein. It is noted that these models need to be updated with deteriorated component models to take into account the effect of aging. The analysis of the reference RC buildings are conducted using the finite element code SeismoStruct (Seismostruct, Seismosoft 2011). Non linear static time-history analyses are performed for all

numerical simulations. In this analysis type, the applied loads (displacements) at the foundation level vary in the pseudo-time domain, according to a load pattern prescribed as the differential permanent ground displacement (versus time) curves directly extracted from the seismic 2D dynamic analysis.

The material properties assumed for the members of the RC buildings are a uni-axial nonlinear constant confinement model for the concrete (f_c=20MPa, f_t=2.1MPa, strain at peak stress 0.002mm/mm, confinement factor 1.2) and a uni-axial bilinear stress-strain model with kinematic strain hardening for the reinforcement (f_y=400MPa, E=200GPa, strain hardening parameter μ =0.005). All columns and beams have rectangular cross sections (beam: 0.30x 0.50 m, column: 0.40x 0.40m). The initial longitudinal section reinforcement degree used is 1% for the columns and 0.75% for the beams.

8.3.2 Quantification of aging probabilistic parameters

The present study considers the aging of the typical RC buildings by including probabilistic models of carbonation and chloride induced corrosion deterioration of the RC elements within the proposed vulnerability modeling framework. The application of the fully probabilistic approach to the referred RC structures through a crude Monte Carlo simulation using the coefficient of variations proposed in FIB- CEB Task Group 5.6 (2006) was found to require large computational burden for practical problems and to yield to numerical errors and instability for usual sample sizes (e.g. 100000-500000). Hence, in an effort to equilibrate the computing efficiency and accuracy, for the probabilistic modeling of rebar corrosion of a specified RC building, it was decided to adopt the mean values of the parameters given in Tables 8.1 and 8.2 and to consider lower variability for the random variables. Tables 8.3 and 8.4 present the statistical characteristics of the parameters finally adopted for an adverse carbonation and chloride induced corrosion scenario (w/c=0.6, High corrosion Level) respectively. It should be noted that for the chloride corrosion scenario, an atmospheric exposure environment is assumed (e.g. k_e=0.67, Choe et al., 2009; 2010).

Table 8.3. Statistical characteristics of parameters affecting the carbonation induced corrosion deterioration of RC elements adopted in the present study

Parameter	Mean	COV	Distribution
Cover Depth (mm) a	25.00	0.20	Lognormal
$R_{hreal,k}$ (% rel. humidity)	70.00	cov=0.05, a=40.0, b=100	Beta
Exponent of regression bc	-0.567	0.035	Normal
Inverse carbonation resistance ($R_{acc,0}^{-1}$) (mm^2/year) / (kg/m^3)	$2.30 \cdot 10^{-10}$	0.10	Normal
Influence of test method k_t	1.25	0.10	Normal
Error term e_t (mm^2/years)	315.5	0.05	Normal
$C_{s,atm}$ (kg/m^3)	0.000820	0.10	Normal
Exponent of regression b_w	0.446	0.10	Normal
Rate of Corrosion (r_{corr}) mA/cm^2	2	0.20	Normal

Table 8.4. Statistical characteristics of parameters affecting the chloride induced corrosion deterioration of RC elements adopted in the present study

Parameter	Mean	COV	Distribution
Cover Depth (mm) x	25	0.2	Lognormal
Environmental tranfer variable k_e	0.67	0.1	Normal
Chloride migration Coefficient ($D_{RCM,0}$) (m^2/s)	$2.5 \cdot 10^{-11}$	0.1	Normal
Aging exponent n	0.3	cov=0.05, a=0.0, b=1.0	Beta
Critical Chloride Concentration (C_{cr}) wt % cement	0.6	cov=0.05, a= 0.2, b=2.0	Beta
Surface Chloride Concentration (C_s) wt % cement	1.539	0.1	Normal
Rate of Corrosion (i_{corr}) mA/cm^2	10	0.20	Normal

8.3.2.1. Corrosion initiation time

The corrosion initiation time depends on a number of parameters that can vary considerably for different structures depending on the deterioration mechanism, the structure location and environmental exposure condition. The distribution for the corrosion initiation time is assessed through Monte Carlo simulation having a sample size of 100000, using the equations 8.2 and 8.14 presented below for carbonation and chloride induced corrosion respectively. A lognormal distribution with mean 36.40 years and standard deviation of 20.85 years is found to be a good fit to the simulated data for the carbonation induced corrosion initiation time (Fig. 8.9). Similarly, a lognormal fit with mean 2.96 years and standard deviation of 2.16 years is adopted for the chloride induced corrosion initiation time (Fig. 8.10). These distributions will subsequently be used as key

inputs for probabilistic modeling of rebar corrosion due to presence of carbonation and chloride concentration.

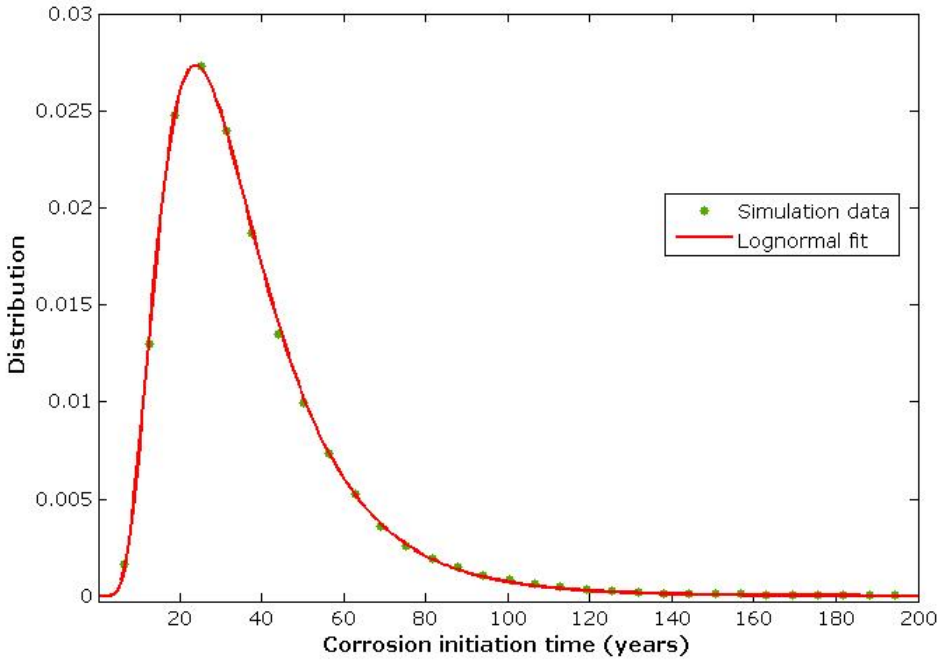


Figure 8.9. Distribution of carbonation induced corrosion initiation time T_{ini} (mean = 36.40years, Standard Deviation = 20.85 years)

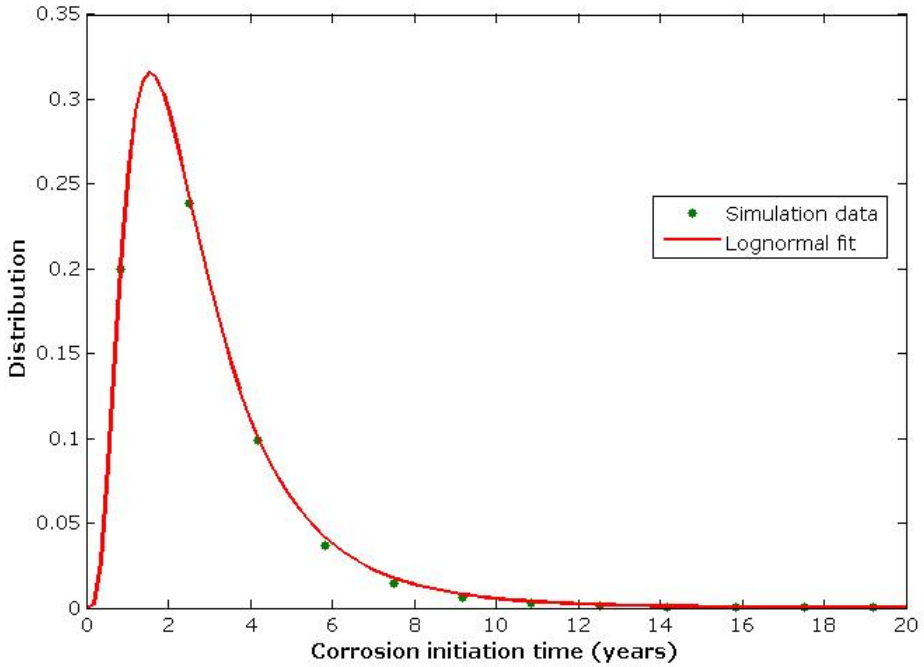


Figure 8.10. Distribution of chloride corrosion initiation time T_{ini} (mean = 2.96 years, Standard Deviation = 2.16 years)

8.3.2.2. Time dependent loss of reinforcement

Once the protective passive film around the reinforcement dissolves due to continued chloride ingress or carbonation, corrosion initiates and the time dependent loss of reinforcement cross-sectional area can be expressed as (e.g. Ghosh and Padgett, 2010):

$$A(t) = \begin{cases} n \cdot D_i^2 \cdot \frac{\pi}{4} & \text{if} \quad t \le T_{init} \\ \max\left[n \cdot \left(D(t)\right)^2 \cdot \frac{\pi}{4} \quad , 0 \right] & \text{if} \quad t \ge T_{init} \end{cases} \tag{8.15}$$

where, n is the number of reinforcement bars, D_i is the initial diameter of steel reinforcement, t is the elapsed time in years and D(t) is the reinforcement diameter at the end of (t-Ti) years , which can be represented as:

$$D(t) = \begin{cases} D_i & \text{if} \quad t \le T_{init} \\ \max[D_i - i_{corr} \cdot \kappa \cdot (t - T_{init}), 0] & \text{if} \quad t \ge T_{init} \end{cases} \tag{8.16}$$

If generalized corrosion is considered, the loss of metal due to corrosion is approximately uniform over the whole surface. In this case, Faraday's law indicates that a corrosion current density corresponds to a uniform corrosion penetration of κ = 11, 6μm/year. The rate of corrosion i_{corr} in this study is considered to be constant on average along the service life of the structure. Generally, the rate of corrosion due to carbonated concrete cover is slower compared to chloride-induced corrosion.

The loss of area of steel due to corrosion of the RC elements is modeled as a reduction in longitudinal reinforcing bar cross sectional area as compared to the elements in the initial nondegraded state. It is assumed that the corrosion will not affect the mechanical and material properties of the steel reinforcing bars. Figures 8.11 (a) and (b) show the probabilistic assessment of the time-dependent area reduction ratio, which is the area of reinforcing steel at time t, A(t), normalized by the initial area of reinforcement, $A(t_0)$ (for $D_{i=}$ 14 mm, n=6). As expected, the variability in the loss of area of reinforcing steel tends to increase with time due to the combined effect of the variability of the initial reinforcement diameter, rate of corrosion and corrosion initiation time.

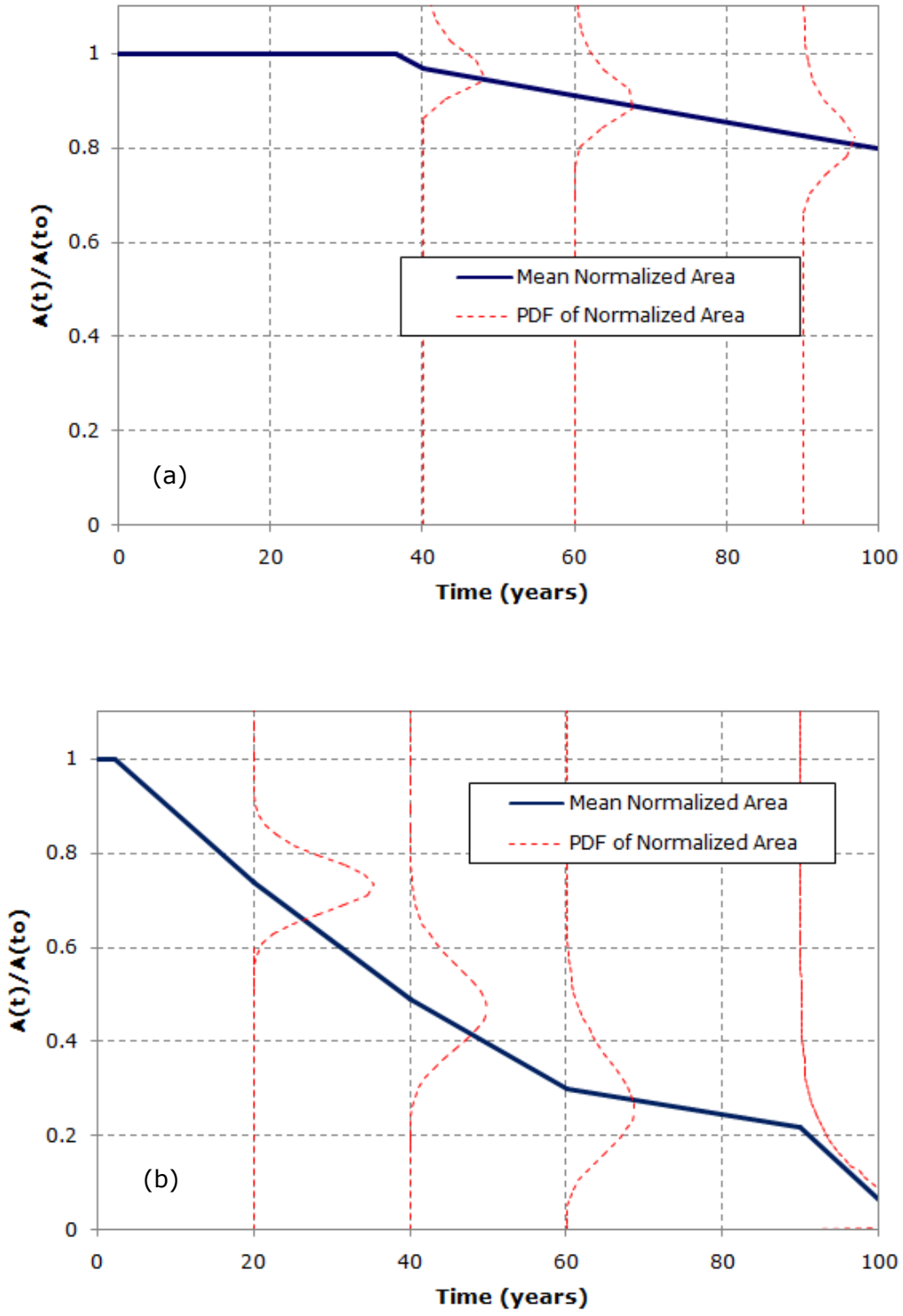


Figure 8.11. Distribution of normalized time variant area of the reinforcement (a) for carbonation and (b) chloride induced deterioration

8.3.3 Time-dependent fragility functions

In order to identify the building performance at different points in time and to construct the corresponding time-dependent fragility curves, a time-variant local damage index (DI) is introduced, describing the steel and concrete material strains. In all cases analyzed the steel strain (ε_s) yields more critical results. Thus, it was decided to adopt only this parameter as a damage index. In this way, it is possible to establish a relationship between the damage index (ε_s) and the intensity parameter expressed in terms of the peak ground acceleration (PGA) values at the seismic bedrock or permanent ground displacement (PGD) values at the slope area, for different building typologies and consequently to assign a median value of PGA/PGD to each limit state.

The next step is the definition of the limit states. For RC corroded buildings characterized by a low level of confinement, the limit steel strains needed to exceed post yield limit states should have lower values compared to adequately and properly confined structures (Crowley et al., 2004; Bird et al., 2005). As a consequence, lower limit state values were assumed to derive exceedance of moderate, extensive and complete damage for the corroded poorly confined buildings. The time-dependent limit state values finally adopted for the different limit states for the carbonation and chloride induced deterioration scenario are presented in Tables 8.5 and 8.6 respectively. Note that for carbonation induced corrosion the reduction in longitudinal reinforcing bar cross sectional area is less than 20% in time t=90 years (see Fig. 8.11a). Thus, a minor reduction on the limit strain values for the corroded structures is assigned as shown in Table 8.5. On the contrary, larger reduction in the longitudinal reinforcing bar cross sectional area is expected for the chloride induced corrosion (see Fig. 8.11b) resulting in significantly reduced values over time for the corresponding limit states.

Table 8.5. Definition of limit states for the buildings at different points in time for the carbonation induced deterioration scenario

		Limit strains		
Time (years)	Limit State 1	Limit State 2	Limit State 3	Limit State 4
0	Steel bar yielding	0.0125	0.040	0.060
40		0.0125	0.039	0.059
60		0.0117	0.037	0.057
90		0.0115	0.035	0.055

Table 8.6. Definition of limit states for the buildings at different points in time for the chloride induced deterioration scenario

		Limit strains		
Time (years)	Limit State 1	Limit State 2	Limit State 3	Limit State 4
0	Steel bar yielding	0.0125	0.040	0.060
20		0.0115	0.035	0.055
40		0.010	0.025	0.045
60		0.008	0.020	0.035
90		0.008	0.015	0.030

The overall fragility function of the buildings can be mathematically expressed as (e.g. Ghosh and Padgett, 2010):

$$P\left[LS \,/\, IM\right] = \Phi\left(\frac{In\left(IM\right) - In\left(m\left(t\right)\right)}{\beta\left(t\right)}\right) \tag{8.17}$$

where, IM is the intensity measure of the earthquake induced landslide expressed in terms of PGA at the "seismic bedrock" or PGD at the slope area, m(t) and β(t) are the median values (in units of *g* or *m* for PGA and PGD respectively) and logarithmic standard deviations of the structure's fragility at different points in time along the service life and LS is the limit state.

The median values of PGA (t) and PGD (t) that correspond to each limit state can be defined for the threshold values of the aforementioned damage indexes as the values that correspond to the 50% probability of exceeding each limit state. The time-dependent median of the buildings fragilities at each limit state can be adequately represented by a quadratic fit for both deterioration scenarios (see subsections §8.3.1.1 and §8.3.1.1 for the carbonation and chloride induced scenarios respectively). Similar models have also been adopted to demonstrate the increase in bridge fragility over time due to corrosion (e.g. Ghosh and Padgett, 2010). Such time-dependent models offer the advantage of estimating directly the fragility parameters at any point in time for the given building and corrosion parameters, once the initial non-degraded fragility of the building is known. The standard deviation values β(t) describe the total variability associated with each fragility curve for different points in time.

The Maximum Likelihood Method, as described in Chapter 4 (§4.4.2.2), is used herein to estimate the fragility parameters. The median and standard deviation values adopted are presented in Tables 8.7 and 8.9 for the carbonation induced corrosion for buildings with flexible and stiff foundations respectively and in Tables 8.11 and 8.13 for the chloride induced corrosion of the reinforcement for buildings with flexible and stiff foundations respectively. Tables 8.8 and 8.10 provide the percent (%) changes in fragility in terms of median PGA/PGD and dispersion β_{PGA}/ β_{PGD} with aging for the carbonation induced

corroded buildings with flexible and stiff foundation system respectively while Tables 8.12 and 8.14 present the corresponding changes for the chloride induced corroded buildings. Fragility curves in terms of PGA (outcrop conditions) and PGD for different limit states are analytically evaluated at different points in time along the service life of the studied buildings with flexible and stiff foundation system to assess the time-dependent effect of corrosion on their vulnerability for the given carbonation (§8.3.1.1) or chloride induced (§8.3.1.2) deterioration scenario. A 3D illustration of the fragility estimates over time (fragility surface) is also shown in order to obtain a better view of the evolution of vulnerability with time.

It is observed that the fragility of the structure generally increases over time due to corrosion. This increase is much more pronounced for the chloride induced corrosion scenario and for higher levels of damage. Greater increase in vulnerability is expected for the chloride induced corroded building with flexible foundation system, resulting to a maximum reduction of 56% and 78% in the median PGA and PGD predicted values respectively for the complete limit state after 90 years exposure to chlorides (see Tab. 8.11 and Figs. 8.25 and 8.26). There is also a change in the dispersion over time, generally indicating increased uncertainty in estimating the median PGA and PGD values. This trend is more evident for buildings with stiff foundation system subjected to chloride induced reinforcement corrosion (see Tab. 8.13).

8.3.3.1. Fragility functions for carbonation induced corrosion of reinforcement

Building with flexible foundation system

Table 8.7. Parameters of fragility functions over time as a function of PGA and PGD for buildings with flexible foundation system considering carbonation induced reinforcement corrosion

Time (years)	PGA (g)					PGD (m)				
	Median PGA (g)				Dispersion β_{PGA}	Median PGD (m)				Dispersion β_{PGD}
	LS_1	LS_2	LS_3	LS_4		LS_1	LS_2	LS_3	LS_4	
0	0.22	0.39	0.58	0.81	0.37	0.14	0.37	0.80	1.54	0.42
40	0.22	0.39	0.58	0.81	0.40	0.15	0.37	0.75	1.49	0.47
60	0.22	0.38	0.55	0.78	0.40	0.14	0.36	0.74	1.44	0.48
90	0.21	0.37	0.52	0.75	0.41	0.14	0.35	0.67	1.28	0.46

Table 8.8. Percent (%) changes in median PGA/PGD and dispersion β values with aging for buildings with flexible foundation system considering carbonation induced reinforcement corrosion

	Change (%) with aging									
Time (years)	**Median PGA (g)**				**Dispersion**	**Median PGD (m)**				**Dispersion**
	LS_1	**LS_2**	**LS_3**	**LS_4**	**β_{PGA}**	**LS_1**	**LS_2**	**LS_3**	**LS_4**	**β_{PGD}**
0	0.00	0.00	0.00	0.00	0.00	0.00	0.00	0.00	0.00	0.00
40	0.31	1.14	1.36	-0.32	-8.31	-1.88	-0.37	6.03	2.84	-11.68
60	-0.12	3.93	6.26	3.34	-9.95	-0.13	1.54	7.95	6.26	-14.59
90	3.01	5.85	11.29	7.15	-10.53	4.04	5.79	16.98	16.43	-9.22

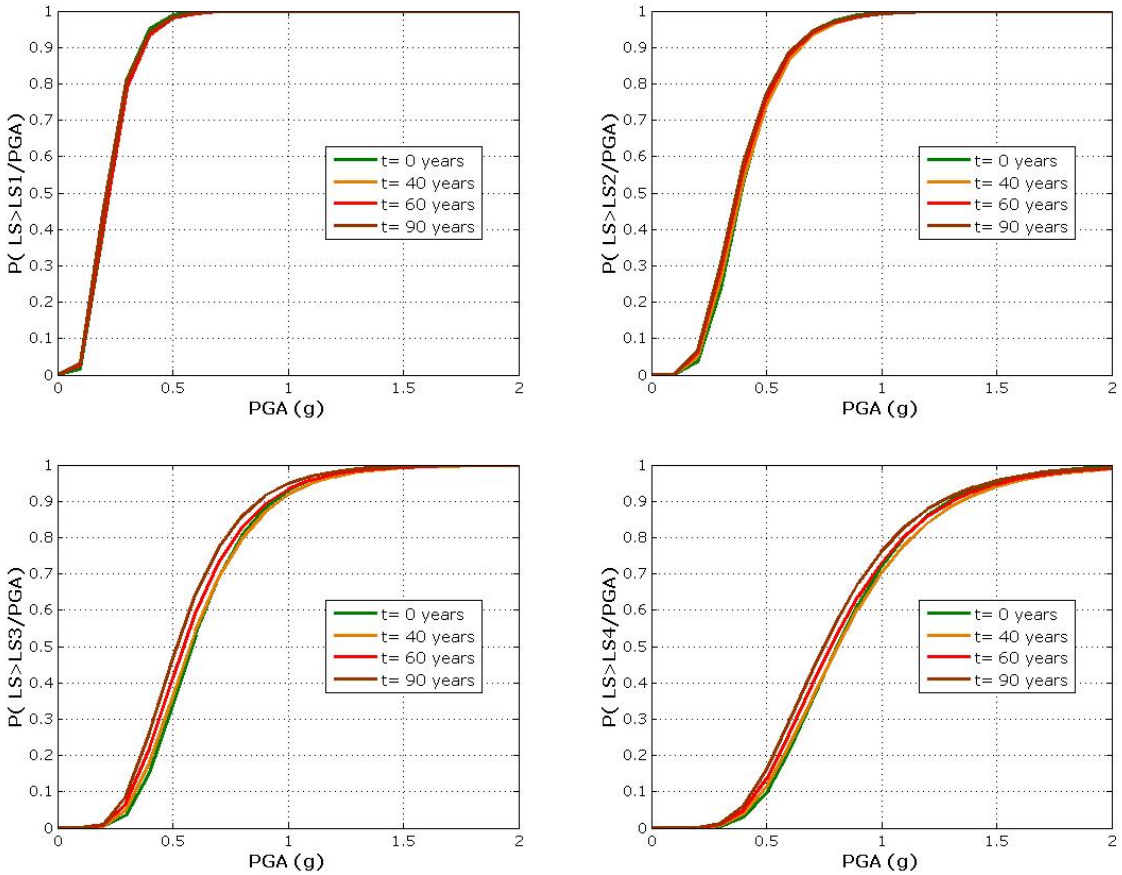


Figure 8.12. Fragility curves in terms of PGA for different points in time (0, 40, 60 and 90 years), for slight (LS_1), moderate (LS_2), extensive (LS_3) and complete (LS_4) limit states considering carbonation induced corroded buildings on flexible foundations.

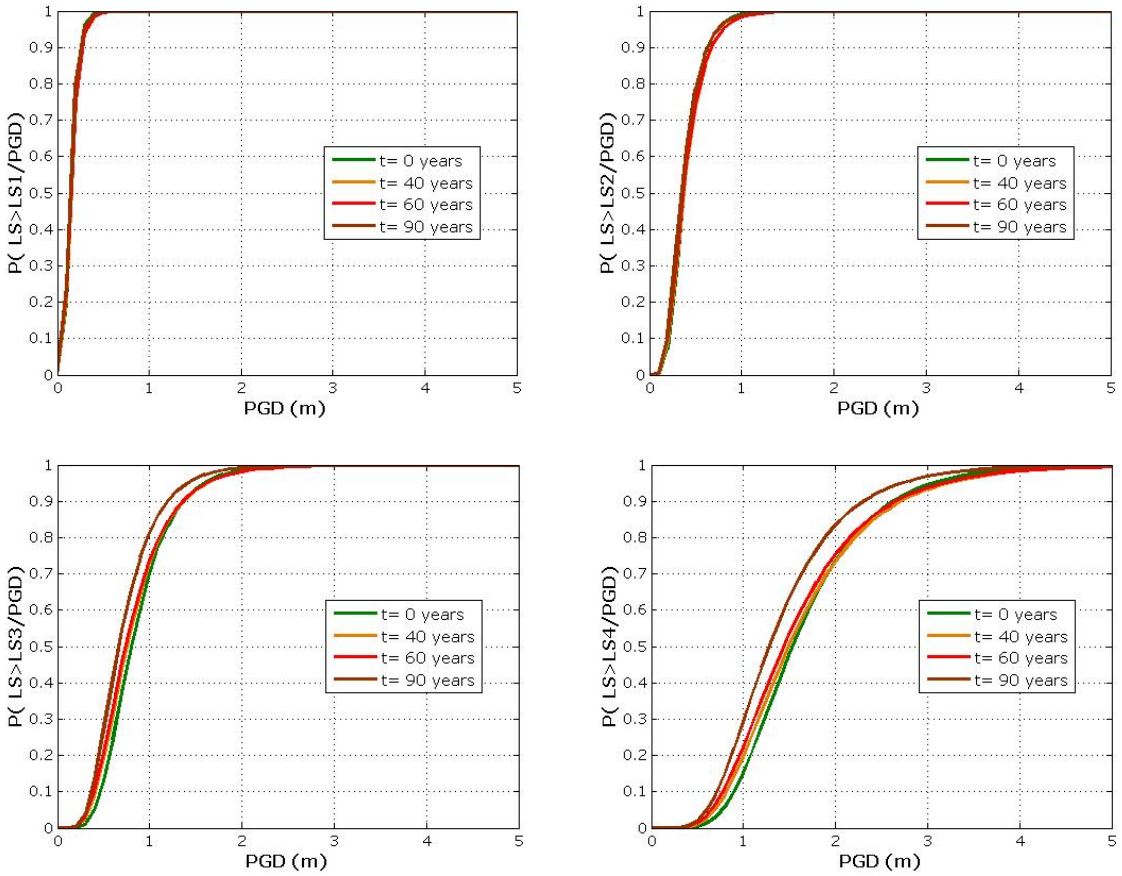
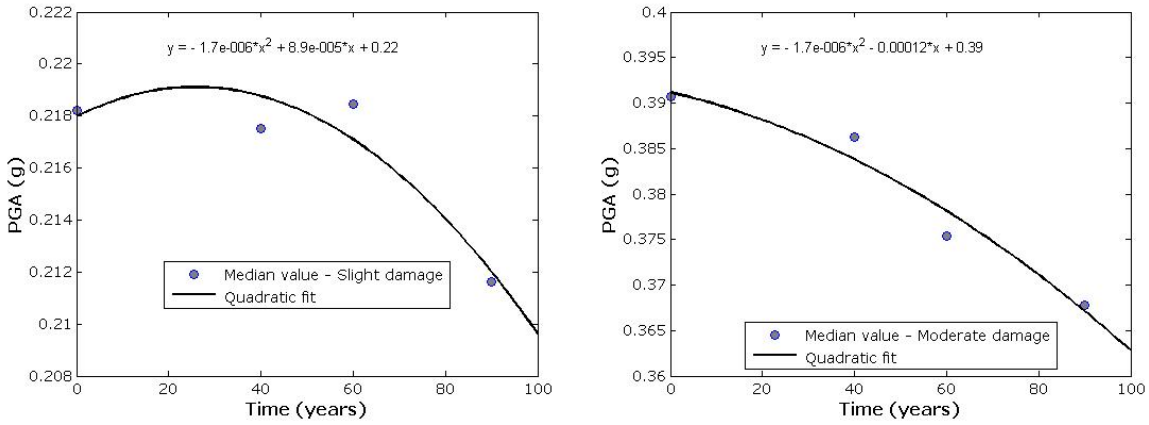


Figure 8.13. Fragility curves in terms of PGD for different points in time (0, 40, 60 and 90 years), for slight (LS_1), moderate (LS_2), extensive (LS_3) and complete (LS_4) limit states considering carbonation induced corroded buildings on flexible foundations.



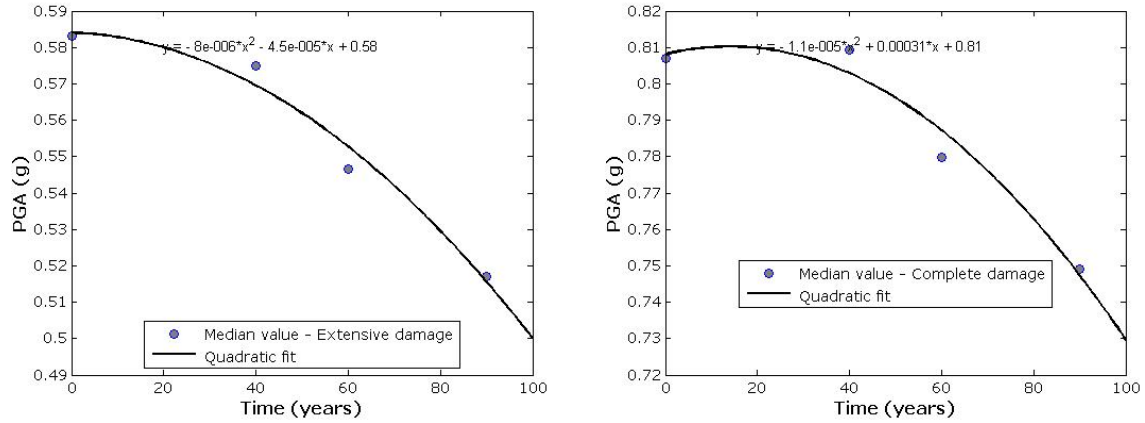


Figure 8.14. Time-dependent quadratic fit of median values of PGA for the slight, moderate, extensive and complete limit states considering carbonation induced corroded buildings on flexible foundations

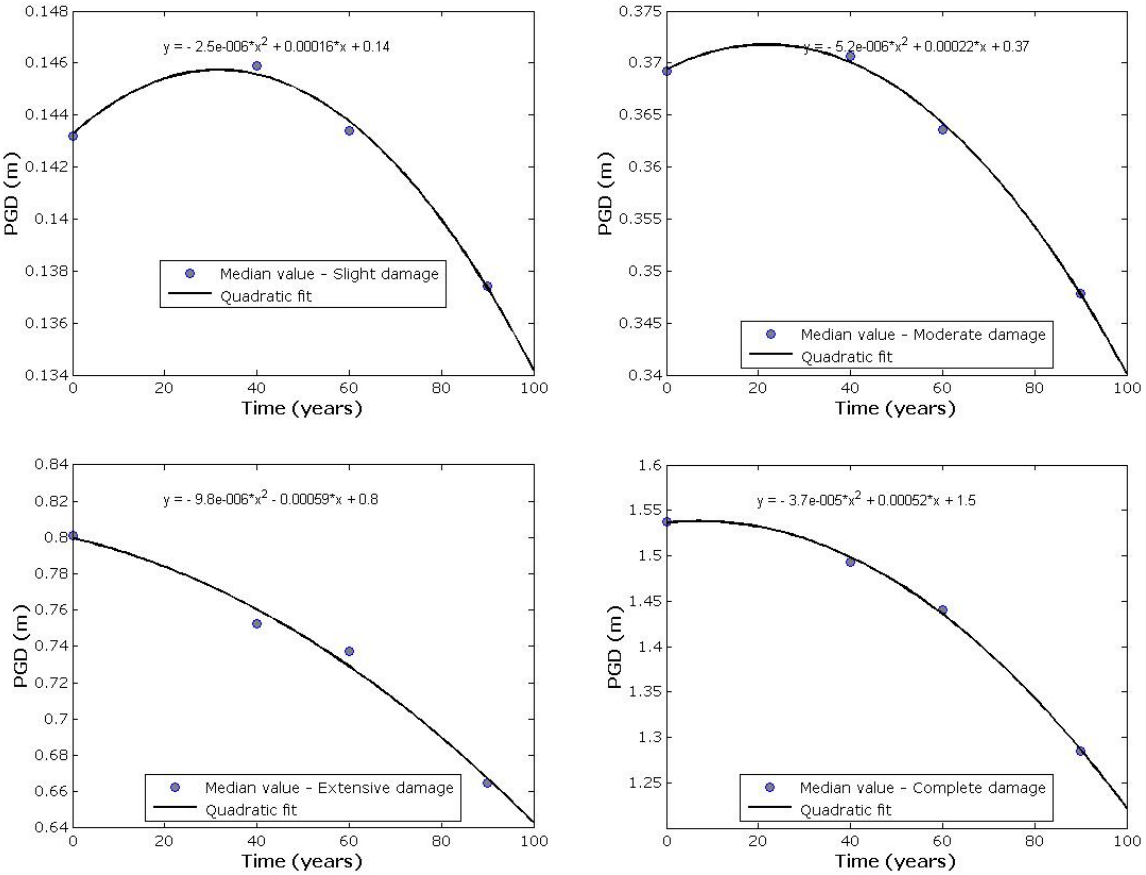


Figure 8.15. Time-dependent quadratic fit of median values of PGD for the slight, moderate, extensive and complete limit states considering carbonation induced corroded buildings on flexible foundations

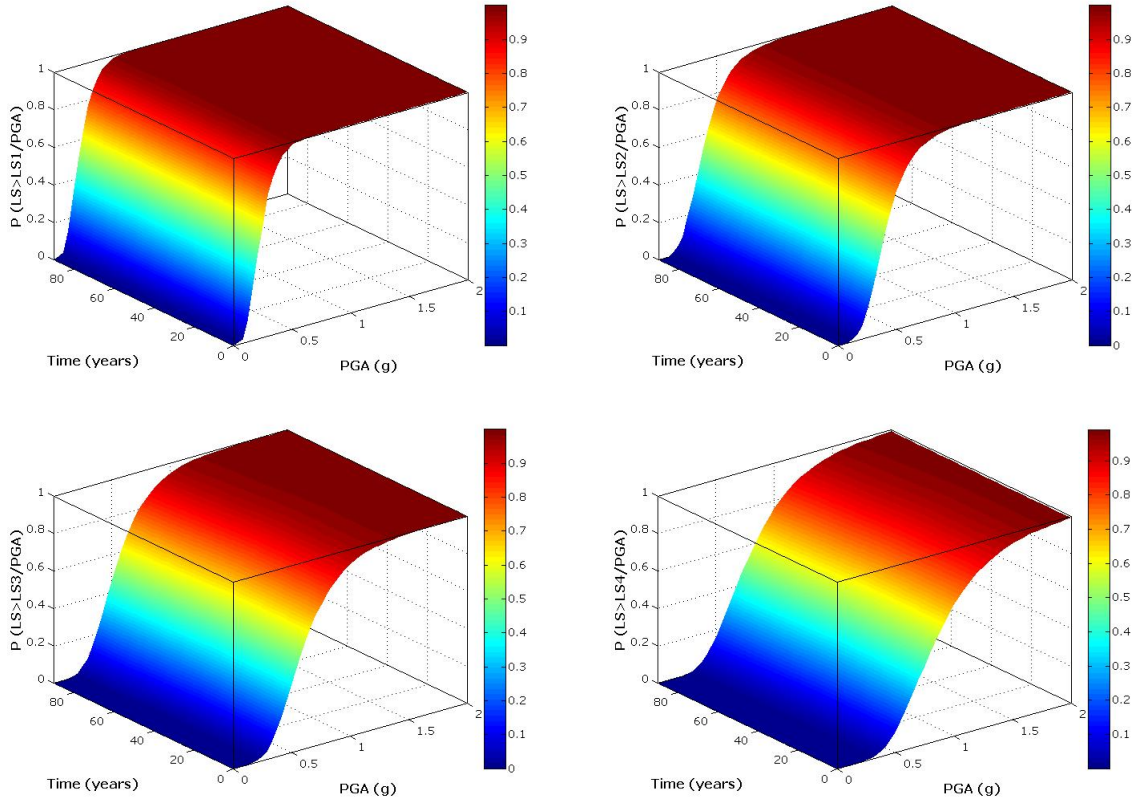
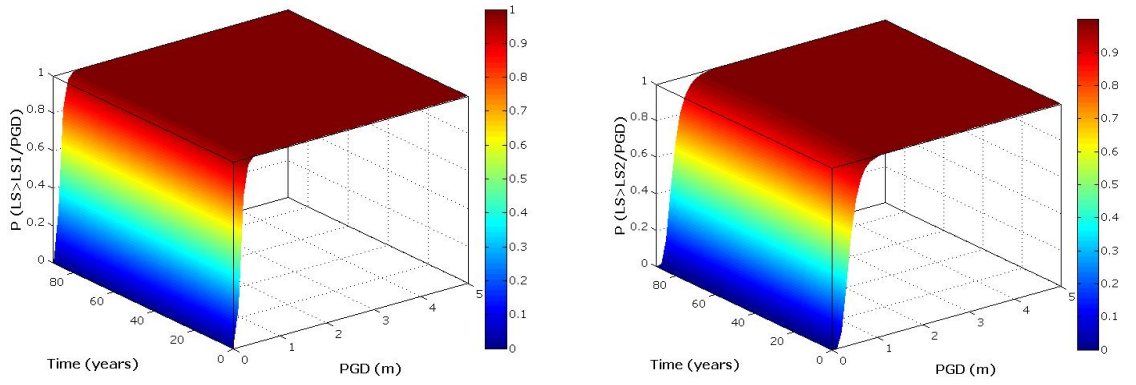


Figure 8.16. Fragility surfaces as a function of time and PGA for slight, moderate, extensive and complete limit states (fit: Interpolant) considering carbonation induced corroded buildings on flexible foundation



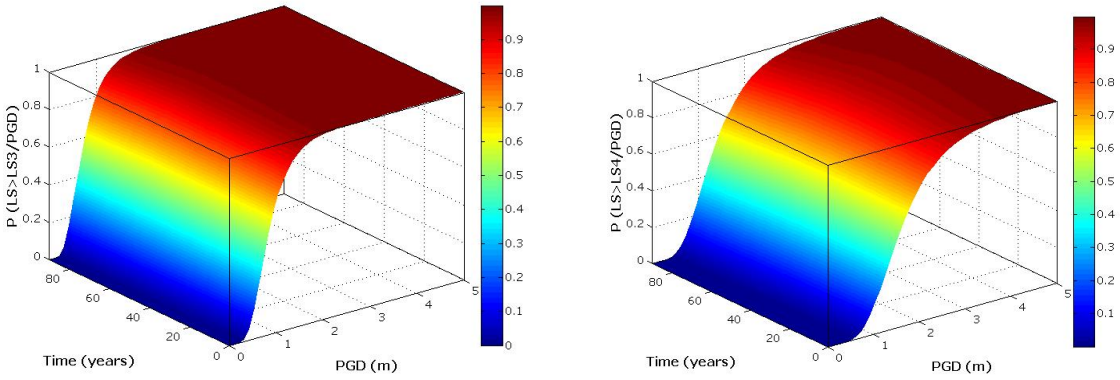


Figure 8.17. Fragility surfaces as a function of time and PGD for slight, moderate, extensive and complete limit states (fit: Interpolant) considering carbonation induced corroded buildings on flexible foundations

Building with stiff foundation system

Table 8.9. Parameters of fragility functions over time as a function of PGA and PGD for buildings with stiff foundation system considering carbonation induced reinforcement corrosion

Time (years)	PGA (g)					PGD (m)			
	Median PGA (g)				Dispersion β_{PGA}	Median PGD (m)			Dispersion β_{PGD}
	LS_1	LS_2	LS_3	LS_4		LS_1	LS_2	LS_3	
0	0.29	0.61	1.01	1.37	0.37	0.24	0.96	2.35	0.42
40	0.29	0.63	1.01	1.36	0.41	0.23	0.92	2.35	0.46
60	0.29	0.61	1.00	1.36	0.42	0.23	0.91	2.20	0.48
90	0.29	0.59	0.99	1.36	0.41	0.23	0.91	2.20	0.48

Table 8.10. Percent (%) changes in median PGA/PGD and dispersion β values with aging for buildings with stiff foundation system considering carbonation induced reinforcement corrosion

Time (years)	Change (%) with aging								
	Median PGA (g)				Dispersion β_{PGA}	Median PGD (m)			Dispersion β_{PGD}
	LS_1	LS_2	LS_3	LS_4		LS_1	LS_2	LS_3	
0	0.00	0.00	0.00	0.00	0.00	0.00	0.00	0.00	0.00
40	-0.08	-3.40	-0.20	0.87	-11.16	2.31	4.46	0.26	-11.17
60	1.04	0.67	1.17	0.78	-13.49	4.43	5.05	6.71	-13.89
90	1.58	2.89	2.08	0.98	-11.96	4.43	5.05	6.71	-13.89

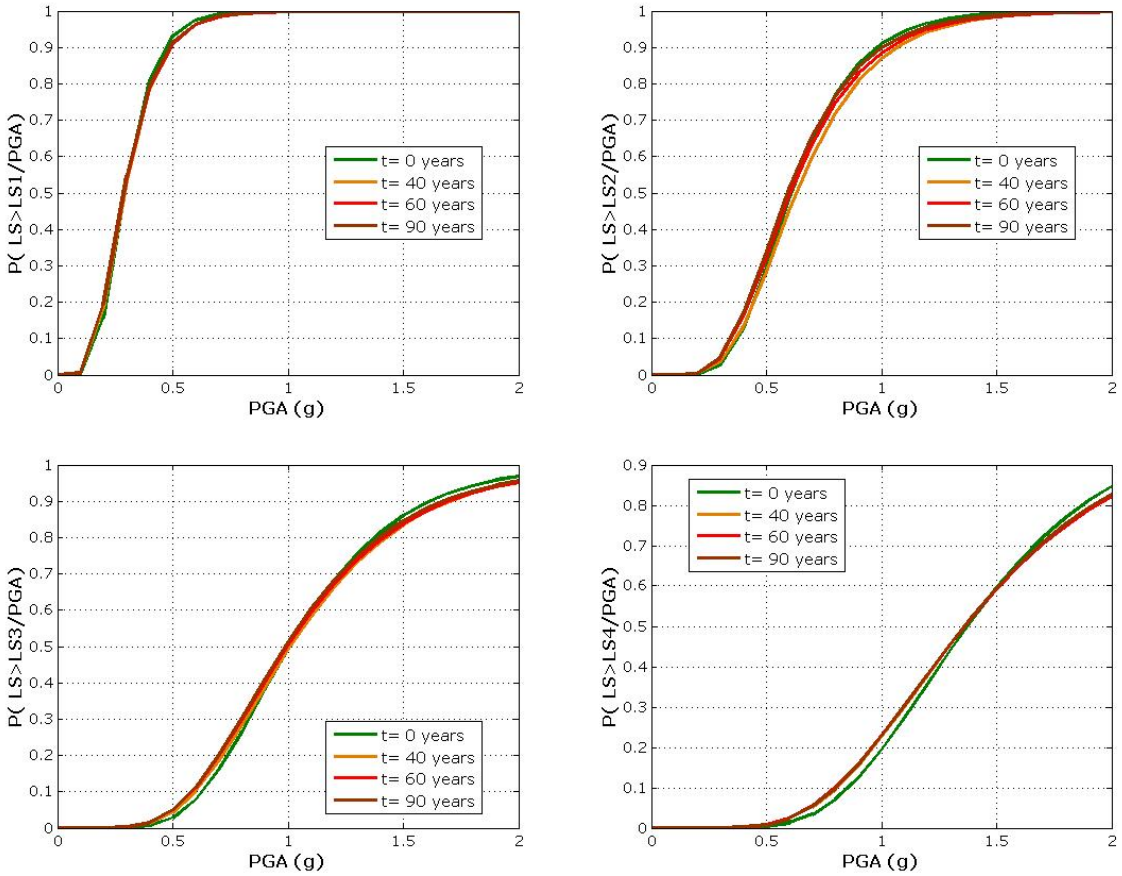
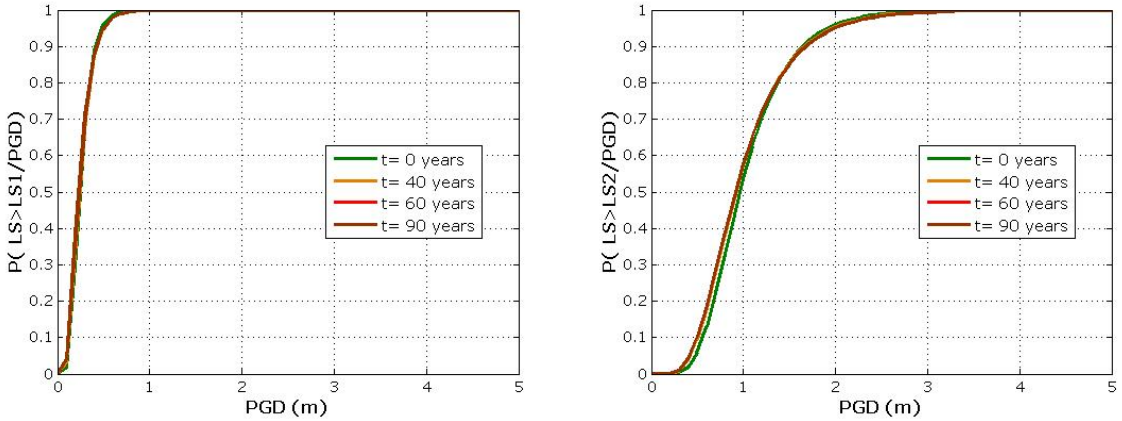


Figure 8.18. Fragility curves in terms of PGA for different points in time (0, 40, 60 and 90 years), for slight (LS_1), moderate (LS_2), extensive (LS_3) and complete (LS_4) limit states considering carbonation induced corroded buildings on stiff foundations.



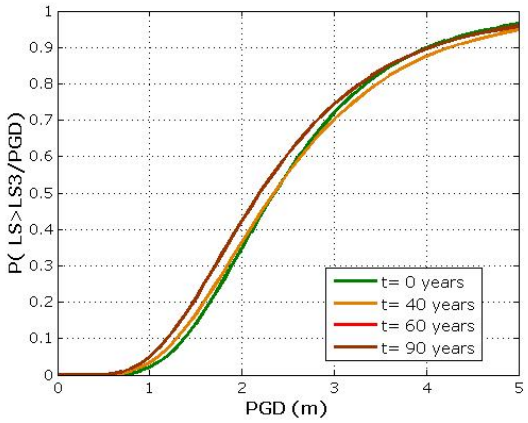


Figure 8.19. Fragility curves in terms of PGD for different points in time (0, 40, 60 and 90 years), for slight (LS_1), moderate (LS_2) and extensive (LS_3) limit states considering carbonation induced corroded buildings on stiff foundations.

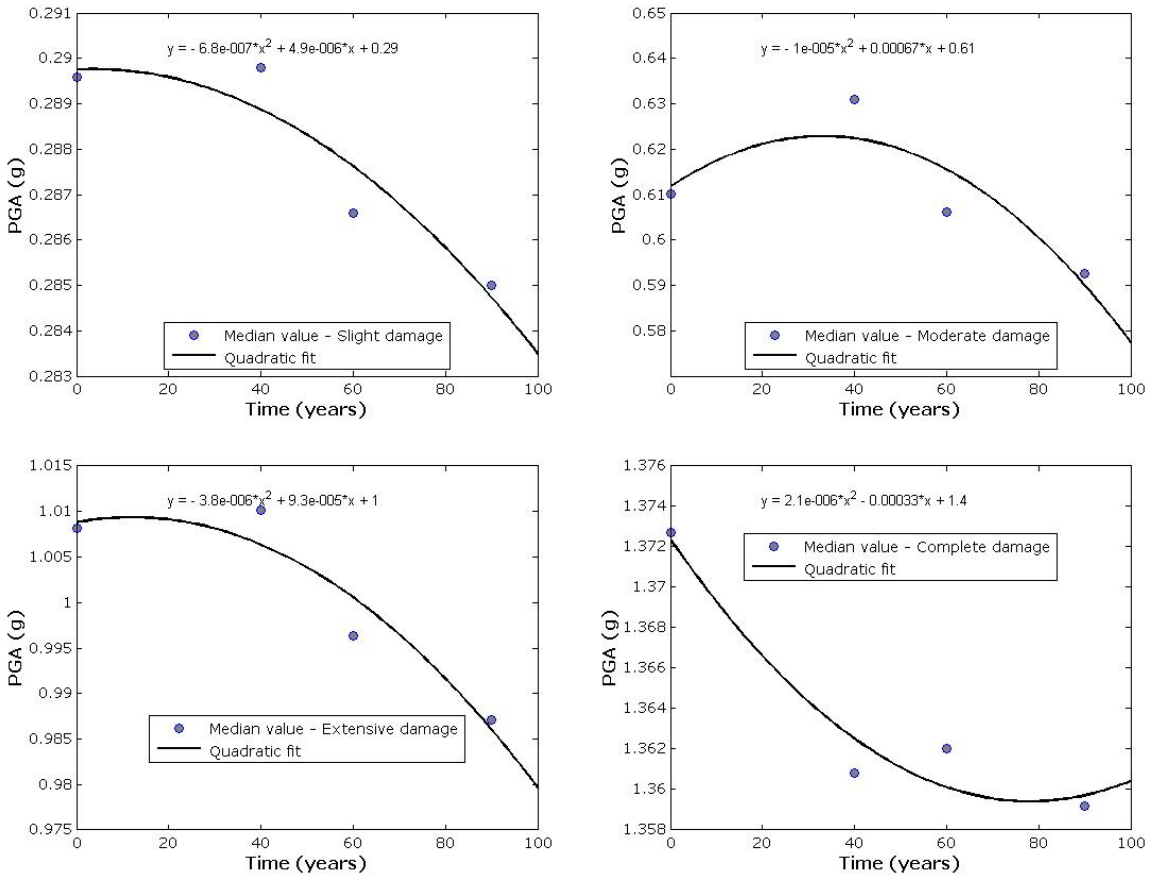


Figure 8.20. Time-dependent quadratic fit of median values of PGA for the slight, moderate, extensive and complete limit states considering carbonation induced corroded buildings on stiff foundations

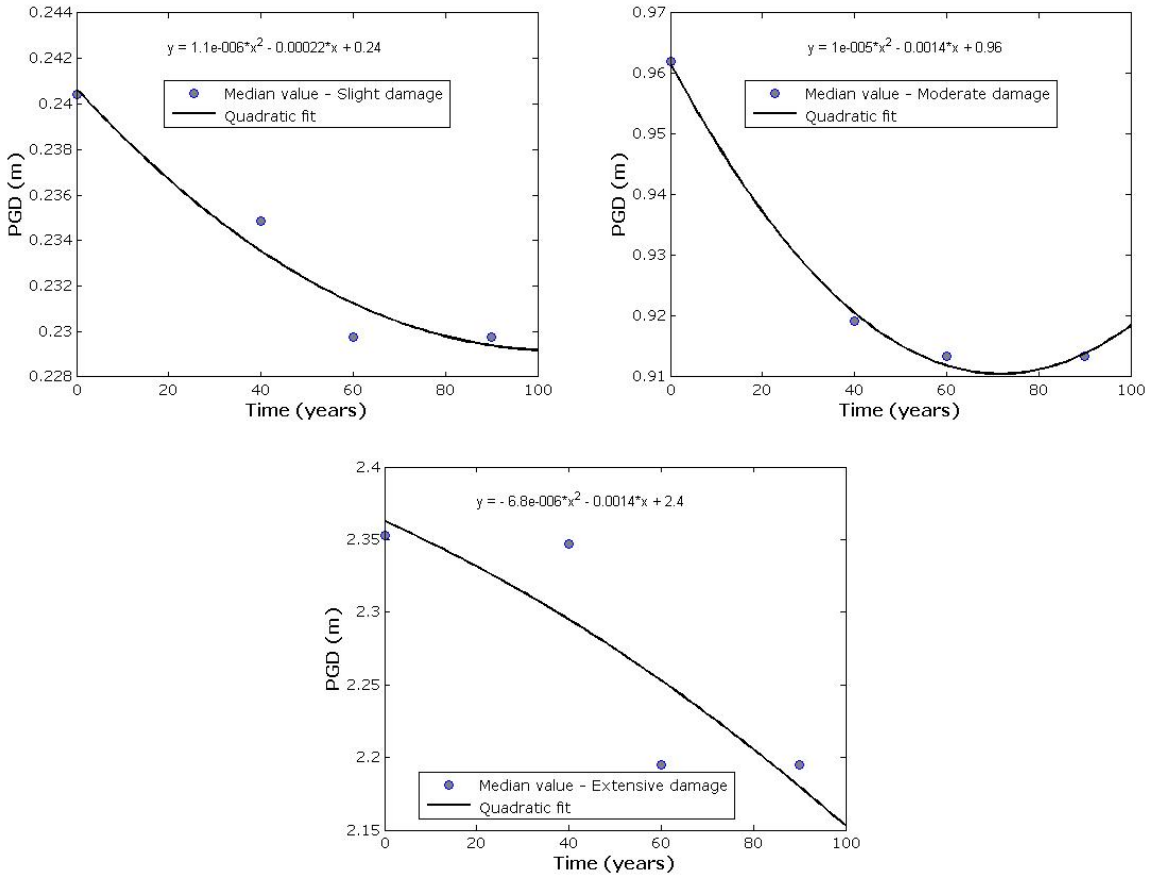
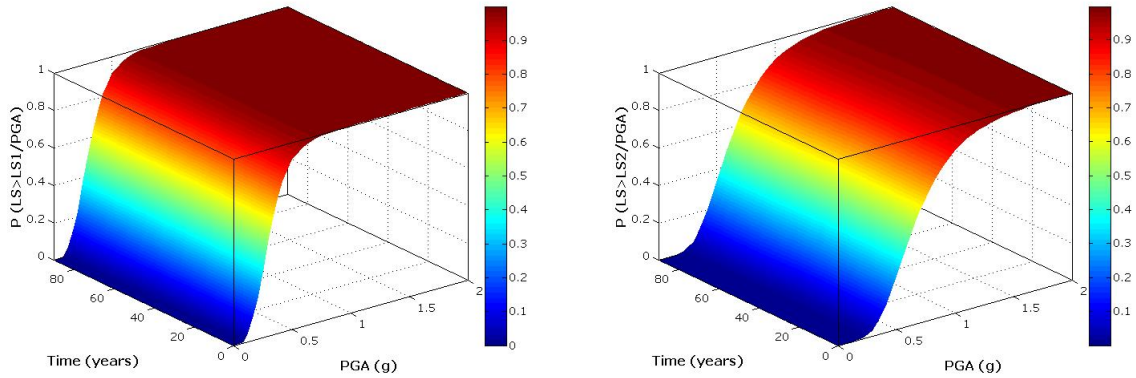


Figure 8.21. Time-dependent quadratic fit of median values of PGD for the slight, moderate, extensive and complete limit states considering carbonation induced corroded buildings on stiff foundations



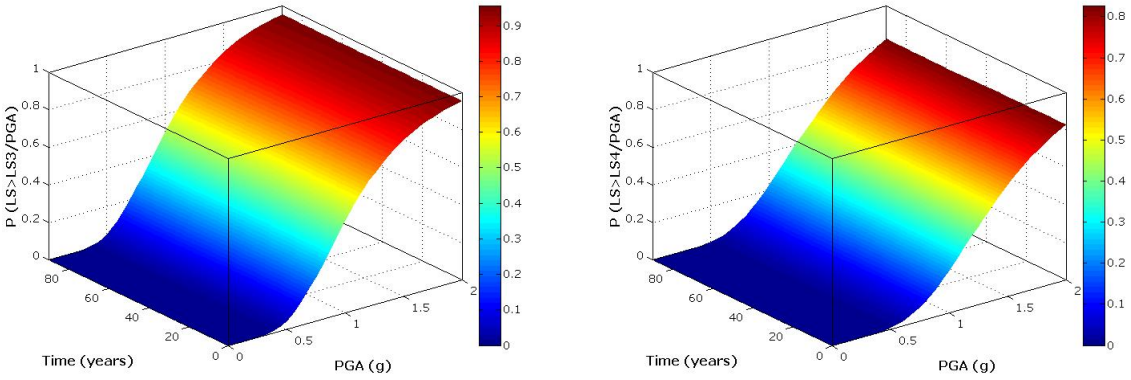


Figure 8.22. Fragility surfaces as a function of time and PGA for slight, moderate, extensive and complete limit states (fit: Interpolant) considering carbonation induced corroded buildings on stiff foundations

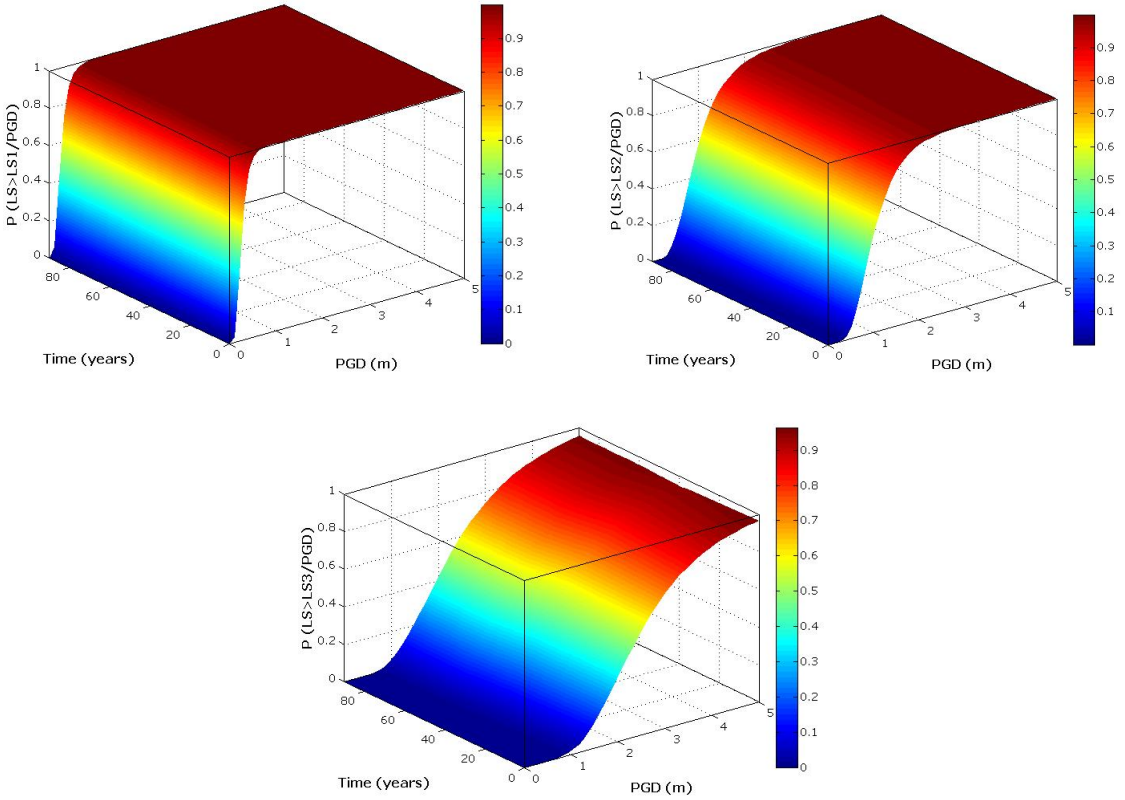


Figure 8.23. Fragility surfaces as a function of time and PGD for slight, moderate, extensive and complete limit states (fit: Interpolant) considering carbonation induced corroded buildings on stiff foundations

8.3.3.2. Fragility functions for chloride induced corrosion of reinforcement

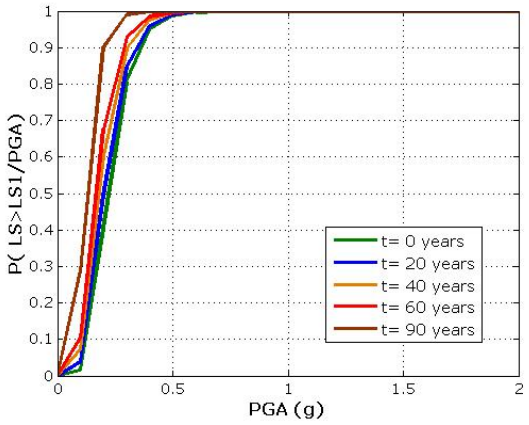
Building with flexible foundation system

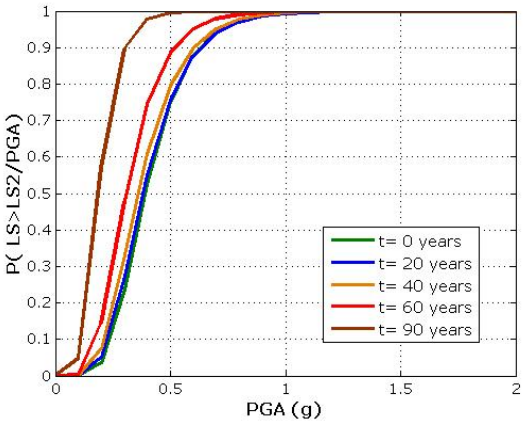
Table 8.11. Parameters of fragility functions over time as a function of PGA and PGD for buildings with flexible foundation system considering chloride induced reinforcement corrosion

Time (years)	PGA (g)					PGD (m)				
	Median PGA (g)				Dispersion	Median PGD (m)				Dispersion
	LS_1	LS_2	LS_3	LS_4	β_{PGA}	LS_1	LS_2	LS_3	LS_4	β_{PGD}
0	0.22	0.39	0.58	0.81	0.37	0.14	0.37	0.80	1.54	0.42
20	0.20	0.38	0.54	0.73	0.39	0.12	0.37	0.70	1.31	0.47
40	0.18	0.36	0.48	0.71	0.40	0.11	0.33	0.58	1.18	0.45
60	0.17	0.31	0.40	0.55	0.41	0.07	0.25	0.41	0.81	0.50
90	0.12	0.19	0.25	0.36	0.38	0.07	0.13	0.24	0.34	0.48

Table 8.12. Percent (%) changes in median PGA/PGD and dispersion β values with aging for buildings with flexible foundation system considering chloride induced reinforcement corrosion

Time (years)	Change (%) with aging									
	Median PGA (g)				Dispersion	Median PGD (m)				Dispersion
	LS_1	LS_2	LS_3	LS_4	β_{PGA}	LS_1	LS_2	LS_3	LS_4	β_{PGD}
0	0.00	0.00	0.00	0.00	0.00	0.00	0.00	0.00	0.00	0.00
20	8.02	2.62	8.21	9.75	-7.23	12.96	0.72	12.10	14.48	-11.64
40	17.49	8.39	18.08	12.43	-9.91	24.87	10.77	27.73	23.05	-8.25
60	23.89	21.58	31.13	31.33	-10.24	49.04	32.22	48.94	47.54	-19.44
90	43.53	52.14	56.47	55.75	-2.06	53.25	64.79	69.95	77.62	-15.90





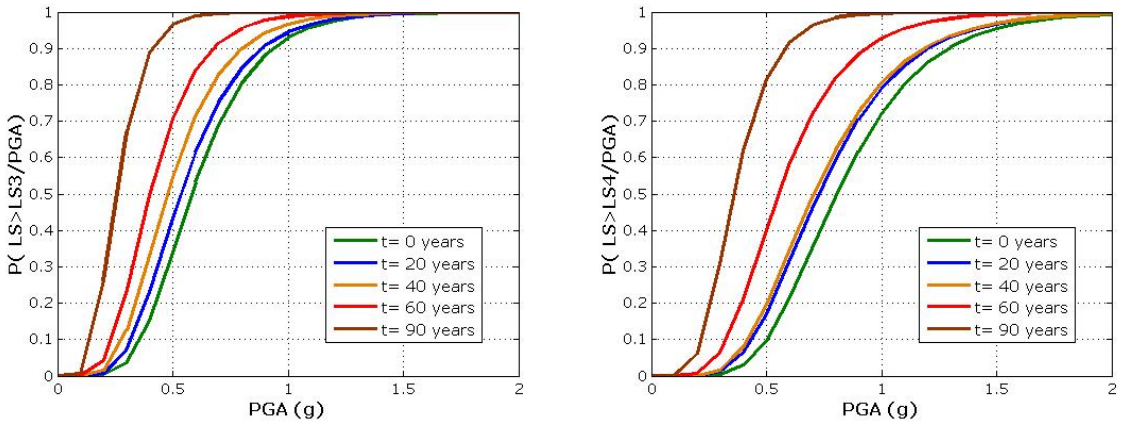


Figure 8.24. Fragility curves in terms of PGA for different points in time (0, 20, 40, 60 and 90 years), for slight (LS_1), moderate (LS_2), extensive (LS_3) and complete (LS_4) limit states considering chloride induced corroded buildings on flexible foundations.

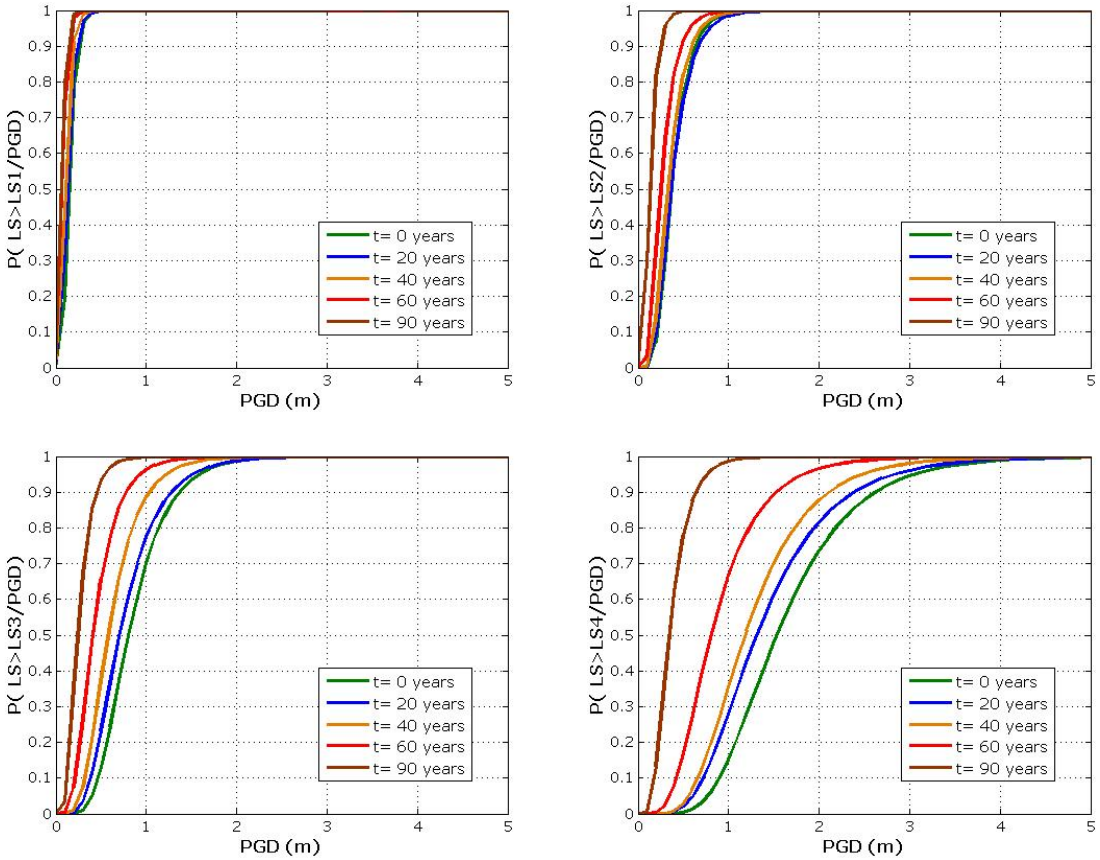


Figure 8.25. Fragility curves in terms of PGD for different points in time (0, 20, 40, 60 and 90 years), for slight (LS_1), moderate (LS_2), extensive (LS_3) and complete (LS_4) limit states considering chloride induced corroded buildings on flexible foundations.

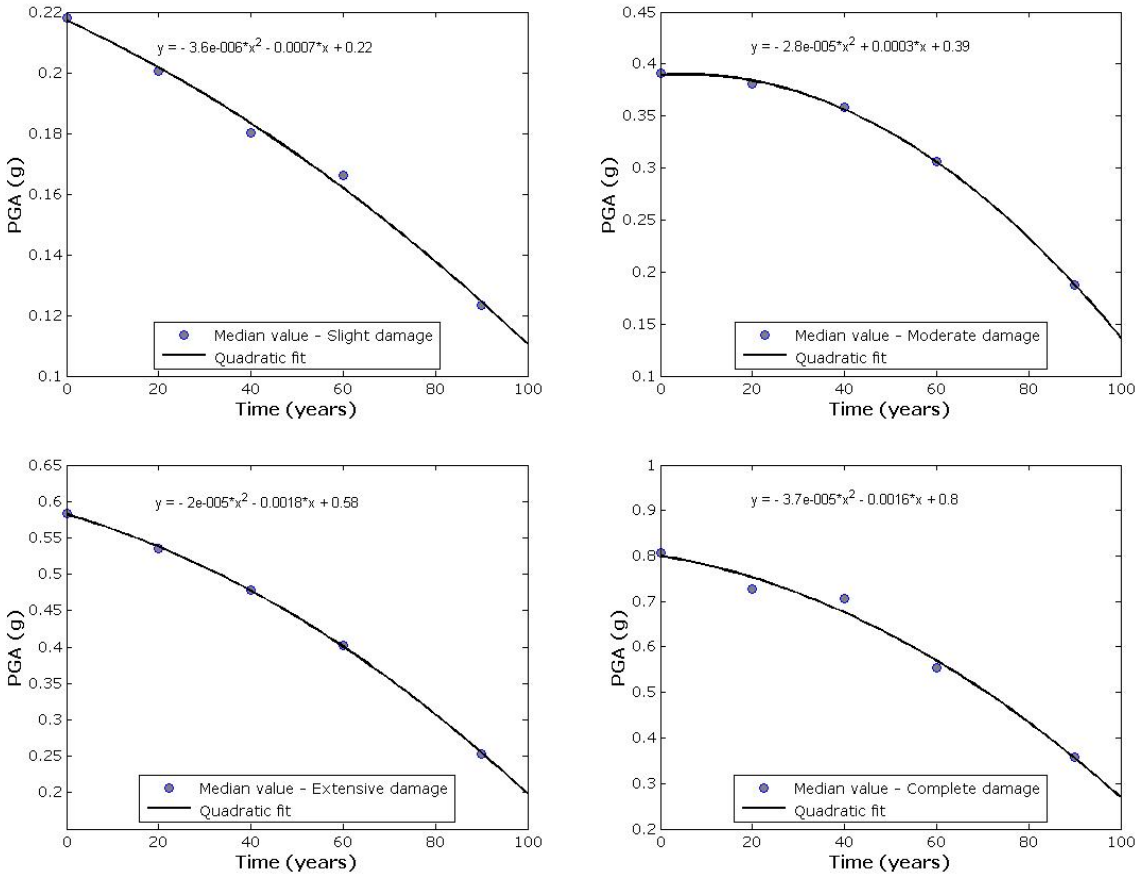
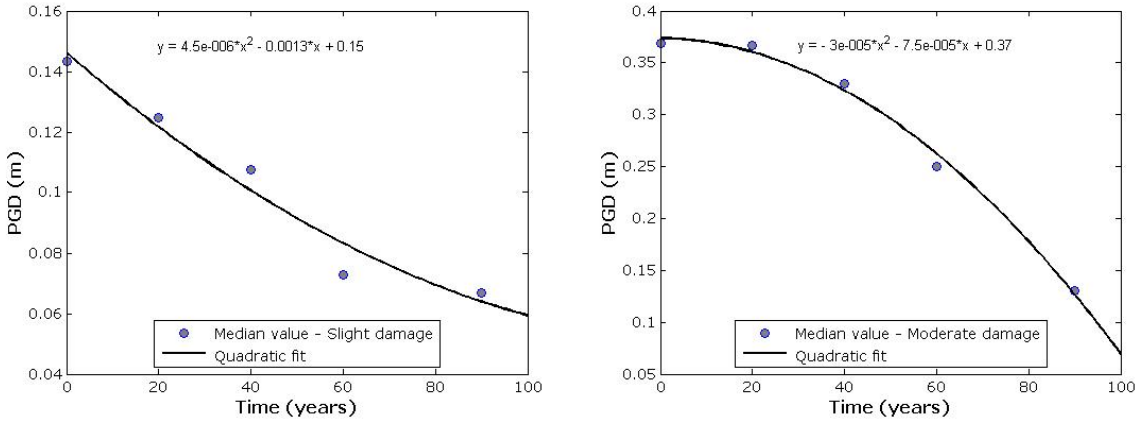


Figure 8.26. Time-dependent quadratic fit of median values of PGA for the slight, moderate, extensive and complete limit states considering chloride induced corroded buildings on flexible foundations



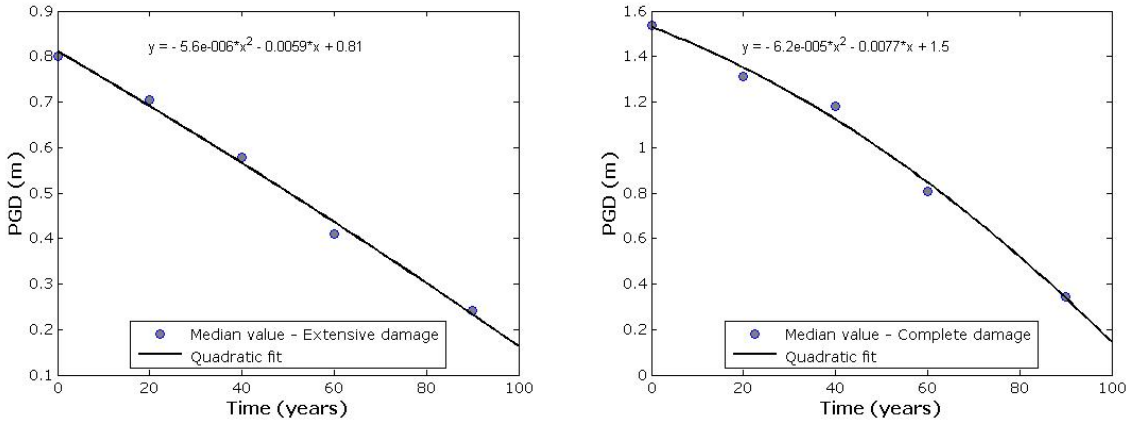


Figure 8.27. Time-dependent quadratic fit of median values of PGD for the slight, moderate, extensive and complete limit states considering chloride induced corroded buildings on flexible foundations

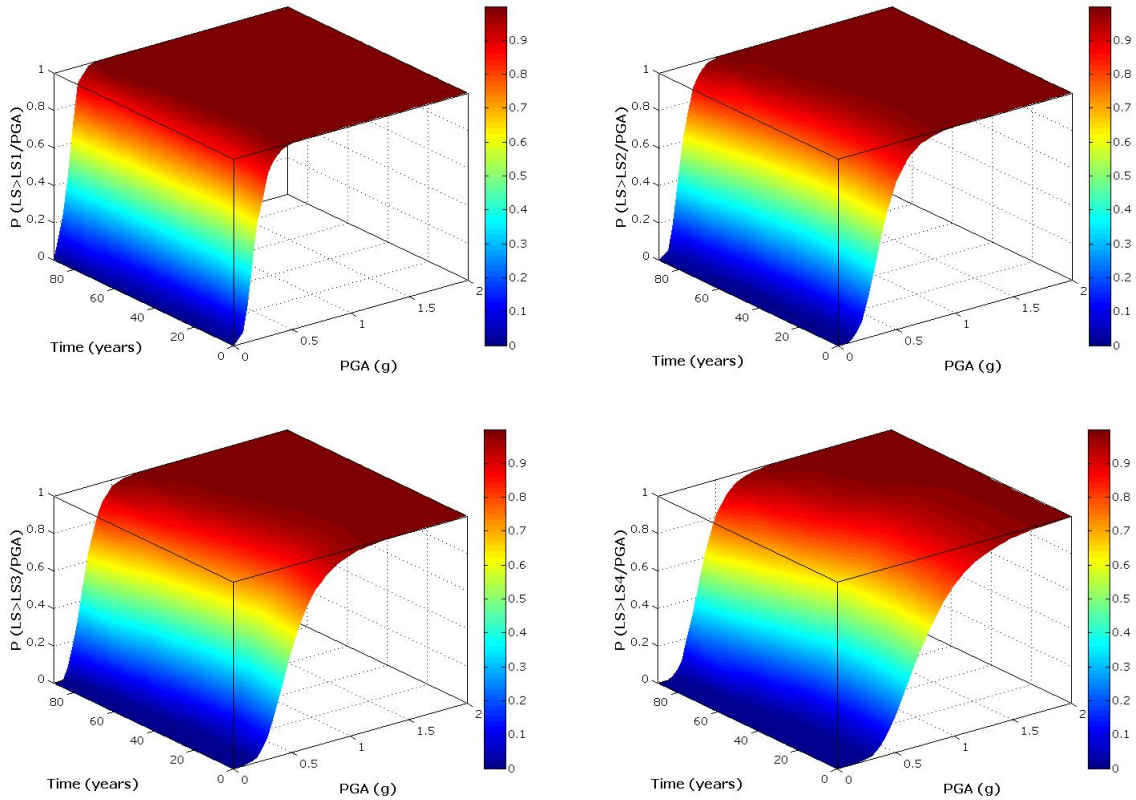


Figure 8.28. Fragility surfaces as a function of time and PGA for slight, moderate, extensive and complete limit states (fit: Interpolant) considering chloride induced corroded buildings on flexible foundations

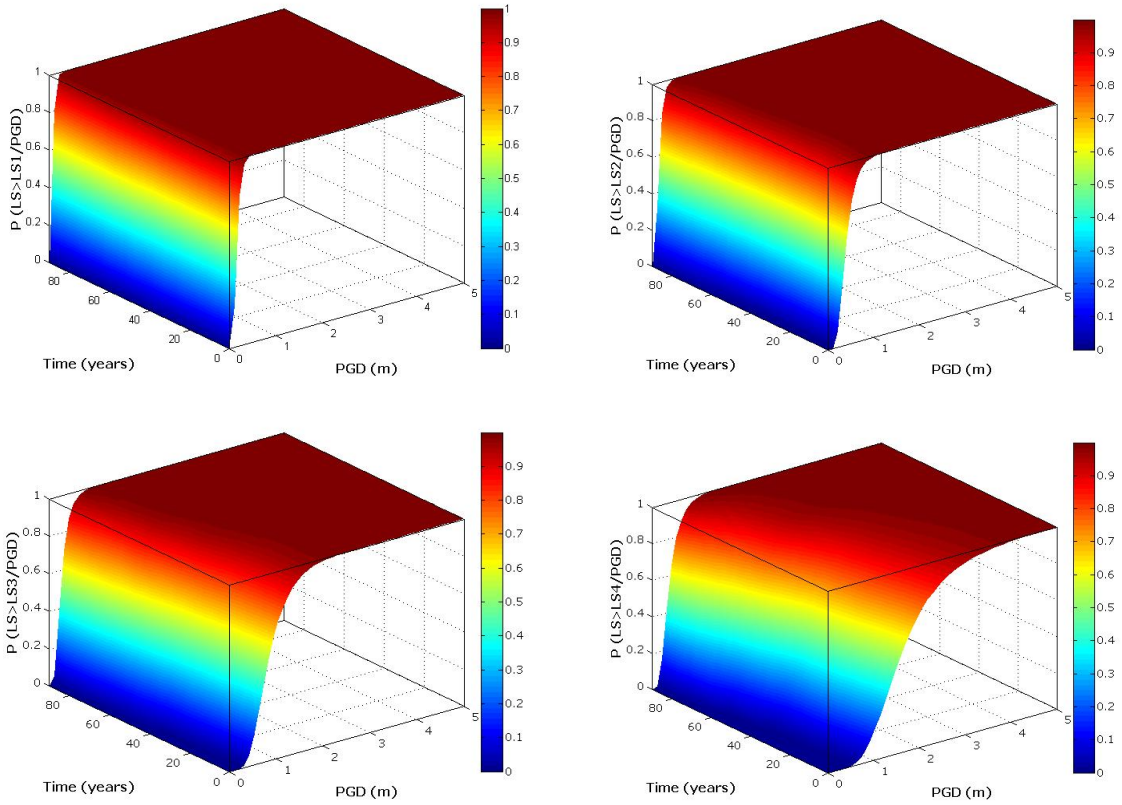


Figure 8.29. Fragility surfaces as a function of time and PGD for slight, moderate, extensive and complete limit states (fit: Interpolant) considering chloride induced corroded buildings on flexible foundations

Building with stiff foundation system

Table 8.13. Parameters of fragility functions over time as a function of PGA and PGD for buildings with stiff foundation system considering chloride induced reinforcement corrosion

Time (years)	PGA (g)					PGD (m)			
	Median PGA (g)				Dispersion β_{PGA}	Median PGD (m)			Dispersion β_{PGD}
	LS_1	LS_2	LS_3	LS_4		LS_1	LS_2	LS_3	
0	0.29	0.61	1.01	1.37	0.39	0.24	0.96	2.35	0.46
20	0.27	0.59	0.98	1.32	0.42	0.23	0.87	2.13	0.46
40	0.27	0.53	0.87	1.21	0.42	0.22	0.75	1.72	0.47
60	0.25	0.47	0.77	1.06	0.42	0.17	0.56	1.39	0.53
90	0.20	0.40	0.71	1.02	0.44	0.11	0.40	1.15	0.71

Table 8.14. Percent (%) changes in median PGA/PGD and dispersion β values with aging for buildings with stiff foundation system considering chloride induced reinforcement corrosion

Change (%) with aging									
Time (years)	Median PGA (g)				Dispersion	Median PGD (m)			Dispersion
	LS_1	LS_2	LS_3	LS_4	β_{PGA}	LS_1	LS_2	LS_3	β_{PGD}
0	0.00	0.00	0.00	0.00	0.00	0.00	0.00	0.00	0.00
20	5.05	2.52	2.83	4.01	-6.88	6.09	9.65	9.28	-1.19
40	8.43	13.35	13.21	11.97	-6.55	8.09	22.24	27.04	-3.48
60	12.90	22.75	24.00	22.58	-5.57	30.25	42.28	40.97	-16.61
90	31.74	34.48	29.65	25.72	-12.38	55.33	58.47	51.23	-54.61

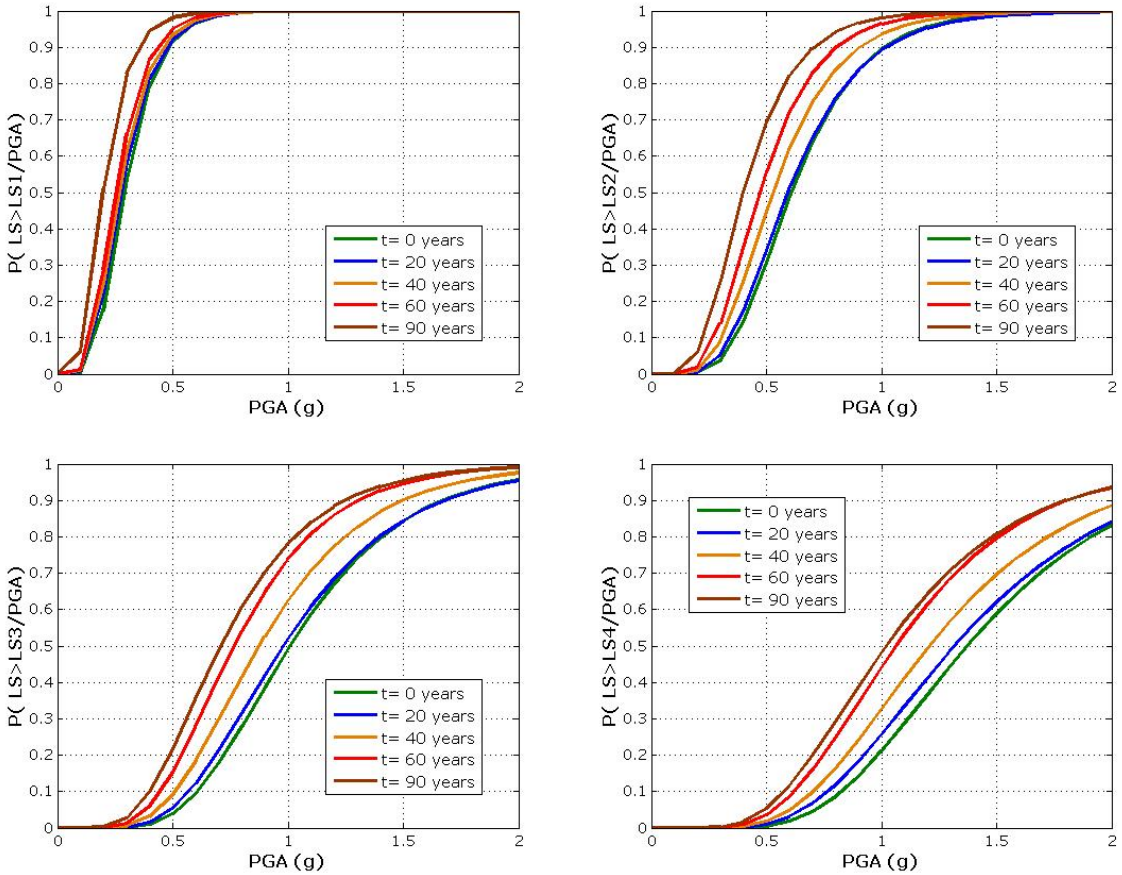


Figure 8.30. Fragility curves in terms of PGA for different points in time (0, 20, 40, 60 and 90 years), for slight (LS_1), moderate (LS_2), extensive (LS_3) and complete (LS_4) limit states considering chloride induced corroded buildings on stiff foundations.

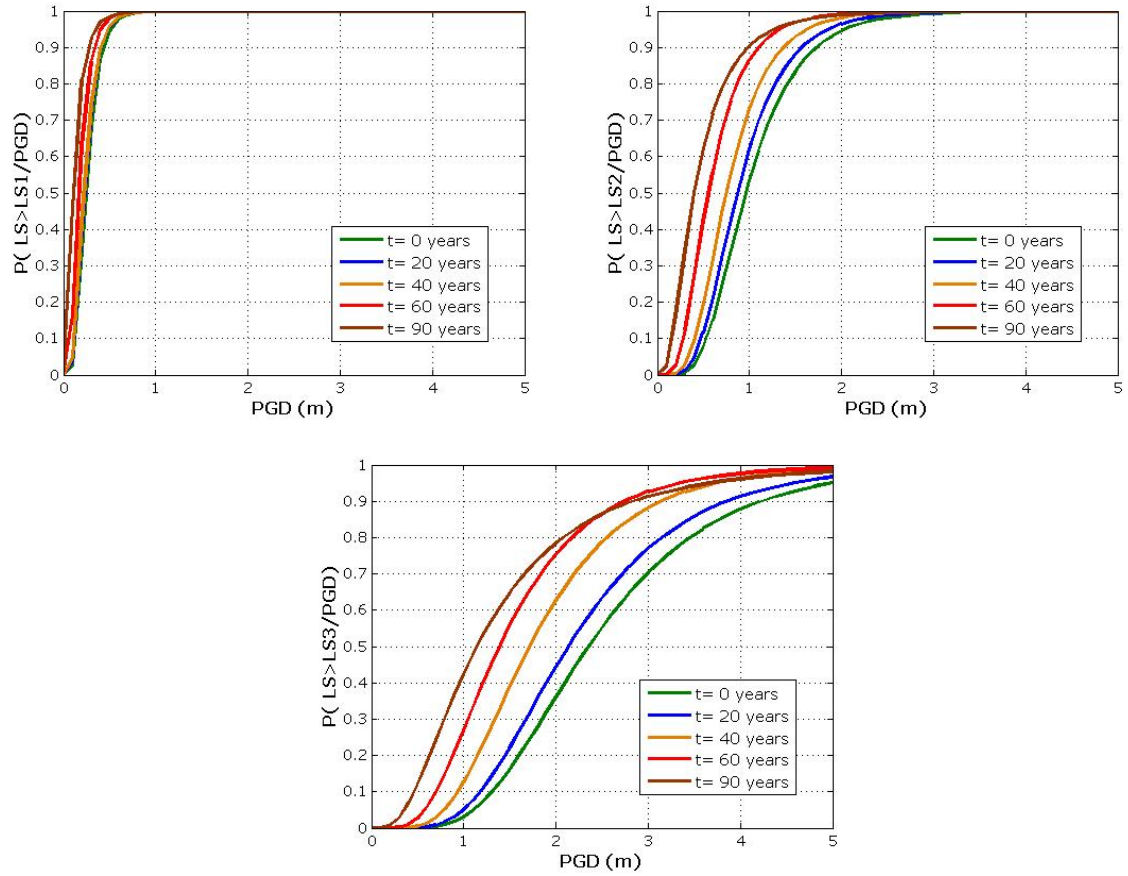
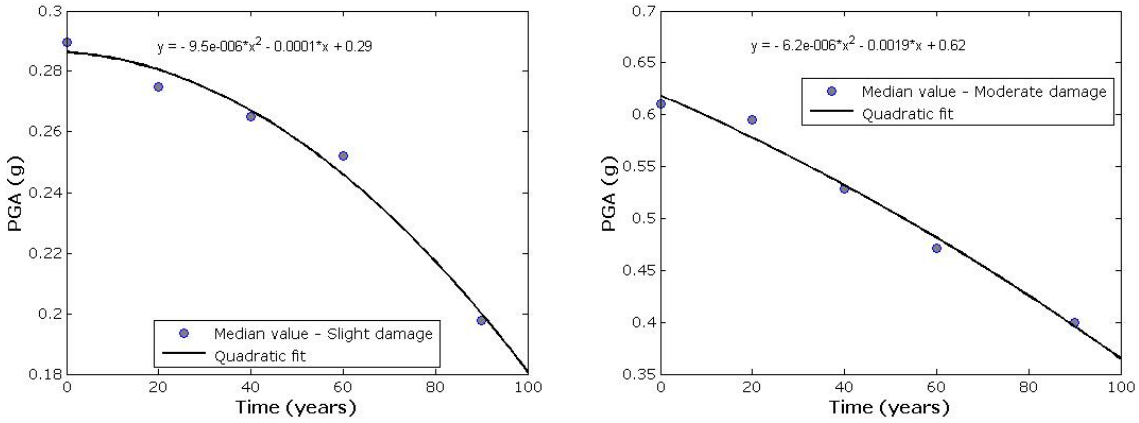


Figure 8.31. Fragility curves in terms of PGD for different points in time (0, 20, 40, 60 and 90 years), for slight (LS_1), moderate (LS_2) and extensive (LS_3) limit states considering chloride induced corroded buildings on stiff foundations.



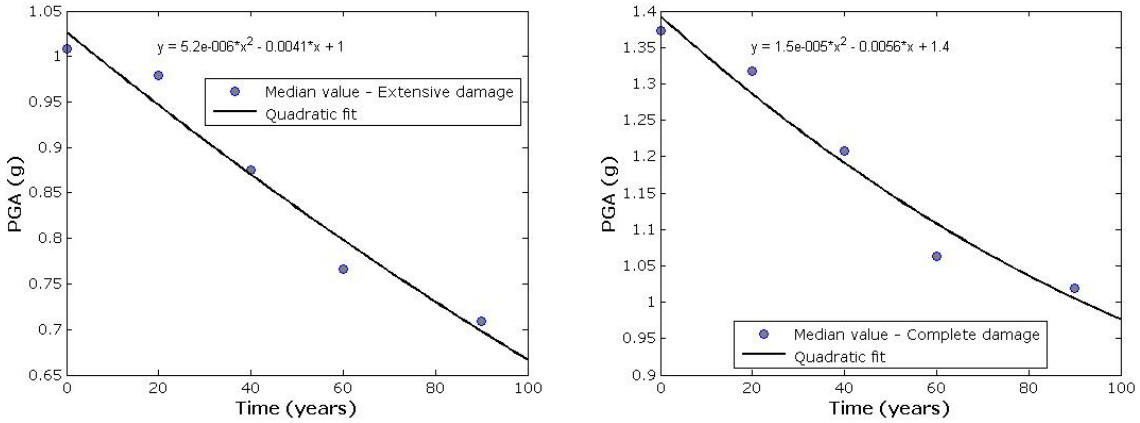


Figure 8.32. Time-dependent quadratic fit of median values of PGA for the slight, moderate, extensive and complete limit states considering chloride induced corroded buildings on stiff foundations

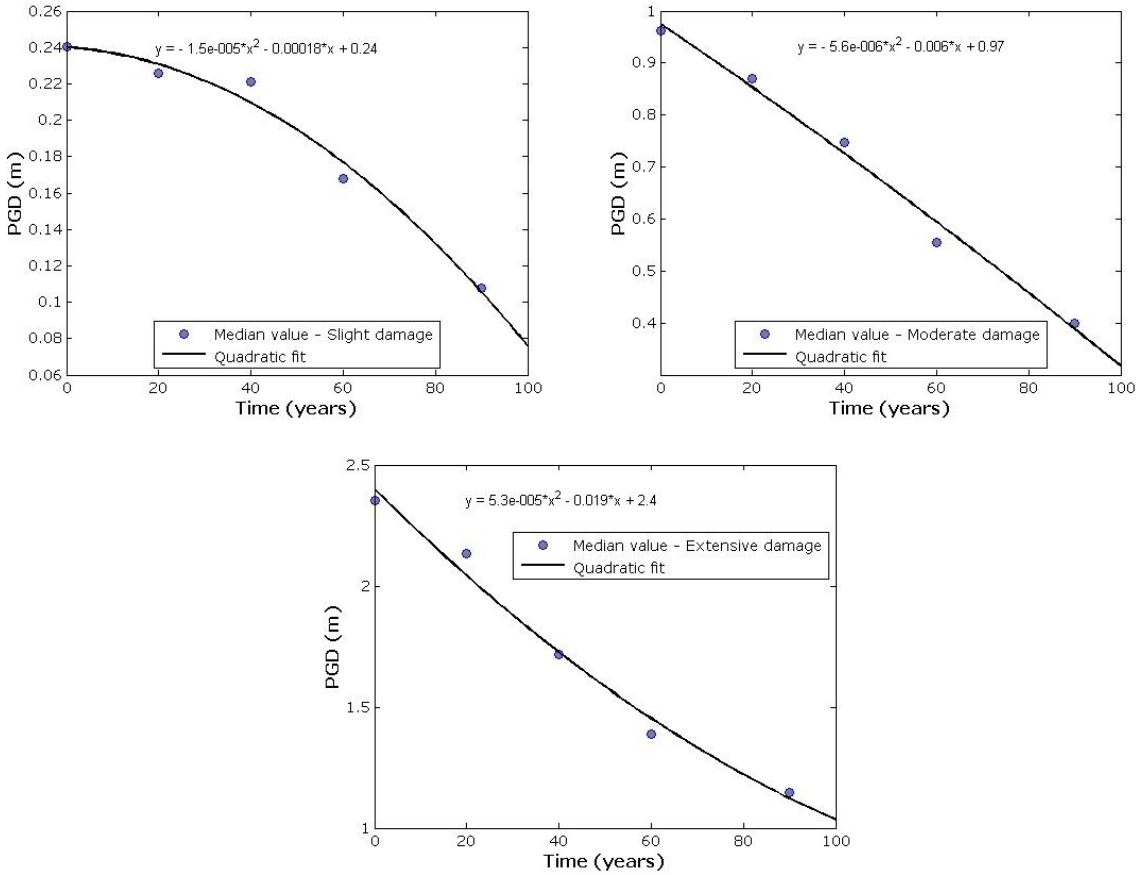


Figure 8.33. Time-dependent quadratic fit of median values of PGD for the slight, moderate, extensive and complete limit states considering chloride induced corroded buildings on stiff foundations

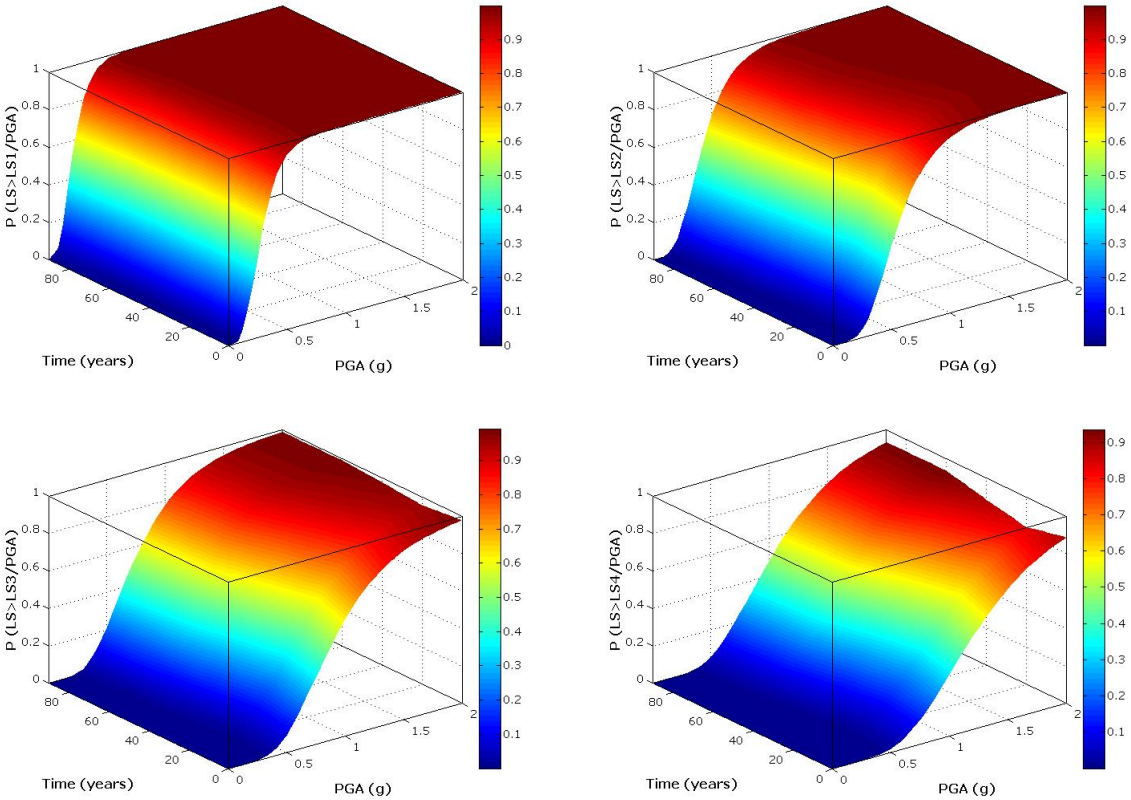
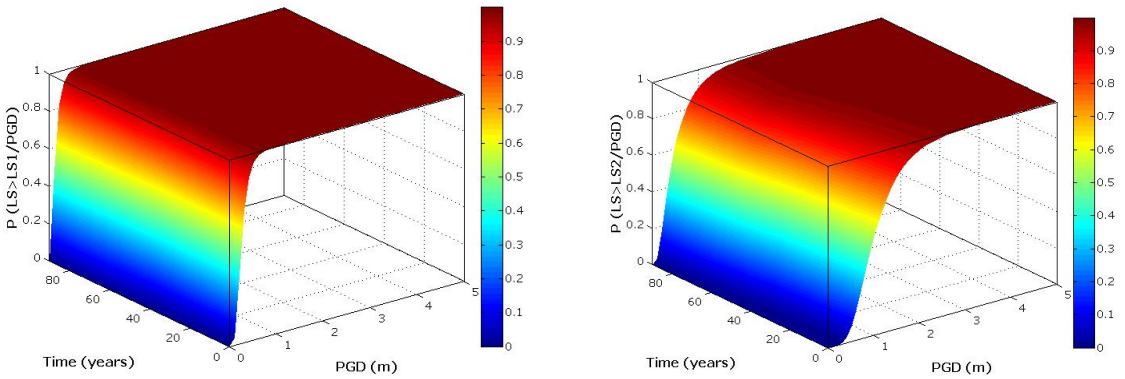


Figure 8.34. Fragility surfaces as a function of time and PGA for slight, moderate, extensive and complete limit states (fit: Interpolant) considering chloride induced corroded buildings on stiff foundations



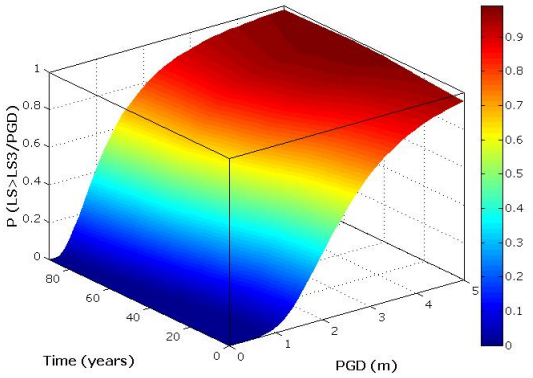


Figure 8.35. Fragility surfaces as a function of time and PGD for slight, moderate, extensive and complete limit states (fit: Interpolant) considering chloride induced corroded buildings on stiff foundations

8.4 Conclusions

An extension of the proposed vulnerability assessment framework to account for the time-dependent fragility analysis of corroded RC buildings impacted by co-seismic permanent landslide displacements has been presented. Two potential adverse corrosion scenarios are examined: chloride and carbonation induced corrosion of the steel reinforcement. The methodology is applied to reference low-rise RC frame buildings with varying strength and stiffness of the foundation system that are subjected to the combined effects of reinforcement corrosion and earthquake triggered landslide displacements. Fragility curves in terms of PGA (outcrop conditions) and PGD for different limit states are analytically evaluated at different points in time (0, 20, 40, 60, 90 years) to assess the time-dependent effect of corrosion on their vulnerability for the given carbonation or chloride induced deterioration scenario. It is observed that the fragility of the structures generally increases over time due to corrosion. This increase is more pronounced for the chloride induced corroded RC buildings founded on isolated footings.

Future work should aim at the validation of the proposed time-dependent model through comparison of the computed damages to experimental results and/or empirical data. Significant effort should also be devoted in the more refined definition of the time-dependent performance indicators and the corresponding limit states. Moreover, further research is needed to address time-dependent fragility of additional building types and geometries, different triggering mechanisms of the potential landslide mass (e.g. intense precipitation) and different hazard (e.g. earthquakes) as well as deterioration mechanisms.

CHAPTER 9

Conclusions-Limitations- Future work

9.1 Summary of findings and contributions

An efficient quantitative risk assessment (QRA) tool that allows for establishing risk management strategies and emergency planning in a cost-effective manner, requires the quantification of both hazard and vulnerability of the elements at risk. However, most of the existing risk assessment studies do not focus on assessing physical vulnerability to landslides comprehensively. Instead, they often provide empirical or expect judgment-based vulnerability values depending on the landslide type and the element at risk (e.g. Dai et al. 2002). This is principally due to its complex, dynamic and multidimensional nature and to the lack of reliable damage data from previous landslide events, which makes its quantitative evaluation within a risk assessment study an intrinsically difficult task. A better understanding on the type and extent of damage to various elements at risk (buildings, roads, population) produced by different landslide mechanisms (slow moving slides, debris flows, rock falls etc) is therefore essential to reduce the great deal of uncertainty associated with the landslide vulnerability modeling. The probabilistic treatment of these uncertainties through the use of the co-called fragility (or vulnerability) curves is also a further step towards the efficient integration of the physical vulnerability component into a QRA study.

Stemming from the general lack of methodologies to assess building vulnerability to slides (see **Chapter 3**), one of the most significant contributions of the present research was the proposition and quantification of an analytical methodology to estimate physical vulnerability of RC frame buildings subjected to earthquake triggered slow-moving slides (**Chapter 4**). Vulnerability was defined through probabilistic fragility curves which allow for direct implementation within a probabilistic risk assessment framework.

According to the suggested method, the damage caused by a slow-moving slide on a single building was attributed to the cumulative permanent (absolute or differential) displacement concentrated within the unstable or moving area. A low-rise RC frame

building located next to the crown of a potential unstable slope was considered subjected to forced differential displacement due to the earthquake triggered landslide and subsequently to structural distress and damage. The numerical analysis involved two consecutive steps and described through an idealized, yet realistic, example.

In the first step, the total and differential permanent displacements were estimated considering the actual stiffness and weight of the building and its foundation, using a non-linear finite difference dynamic finite slope model. A suite of seven gradually increasing acceleration time histories recorded on rock outcrop were applied at the base of the model to cover a wide range of seismic motions in terms of amplitude, frequency content and significant duration in order to provide the necessary response quantity statistics. The analyses were performed for single bay-single storey RC frame buildings on stiff and flexible foundations considering both sand and clayey surface slope layers. Additional analyses were also conducted for the free field case i.e. in the absence of any structure in the vicinity of the crest. It was shown that the presence of a structure next to the slope's crest may contribute in altering the free field response of the slope and the corresponding deformation demand for the building. The level of this differentiation varies with respect to the foundation type (flexible, stiff), the surface soil conditions (sand, clay) and the characteristics of the seismic motion.

The computed permanent displacements for the free field case at the slope area were validated through comparison with simplified Newmark-type displacement methods in **Chapter 5**. Three different displacement-based procedures were used to predict the permanent slope deformation: the conventional analytical Newmark rigid block model (Newmark 1965), the decoupled Rathje and Antonakos (2011) model and the coupled Bray and Travasarou (2007) sliding block model. Comparisons between the Newmark-type models were also conducted to demonstrate their relative degree of conservatism for different earthquake scenarios and compliance of the sliding surface. It was shown that Bray and Travasarou (2007) coupled model generally predicted larger displacements compared to conventional analytical Newmark rigid block and Rathje and Antonakos decoupled model. The difference in the displacement prediction was more pronounced for the considered flexible sliding masses.

It is concluded that permanent horizontal displacements along the unstable slope area derived by the proposed numerical approach were not inconsistent with the predicted Newmark-type displacements enhancing the reliability and robustness of the dynamic analysis results. More specifically, all three displacement-based models predicted displacements that were generally compatible with the numerical results for the sand stiff slope case. On the contrary, for the clay more flexible slope the correlation was not so good. In particular, Bray and Travasarou (2007) model predicted larger displacements

with respect to the dynamic analysis whereas Newmark rigid block and Rathje and Antonakos (2011) models underestimated the corresponding displacements. Among the three methods, Bray and Travasarou model was found to present the minimum average predictive error (%) in relation to the dynamic analysis whilst Newmark analytical approach showed the minimum dispersion of that error for both sand nearly rigid and clay relatively flexible slope cases. Overall, the differences in the displacement prediction between the models were larger for the more ductile clay slope. Thus, the compliance of the failure surface in relation to the frequency content of the input earthquake scenarios probably allowed for some bias to be introduced on the results.

In the second step, non-linear static time history analyses of the selected buildings were performed to assess the building's response to the permanent ground deformation induced by the landslide. The analyses were conducted for progressively increasing levels of differential displacements provided by the computed dynamic stress strain analysis for increasing amplitudes of input acceleration time histories. The derived differential displacements at the foundation level were imposed quasi-statically at one of the RC building supports (footings). The applied differential displacement vector was found to be principally governed by the horizontal component that controlled the deformation mode in buildings with flexible foundations whereas the corresponding displacements were practically vertical in buildings with stiff foundation system. Structural response data in terms of maximum material strain were then statistically correlated to the landslide intensity parameters to estimate structure's performance and fragility.

Damage limit states were defined with respect to the building classification and its structural characteristics in terms of threshold values of building's material strain based on the work of Crowley et al. (2004), Bird et al. (2005; 2006), Negulescu and Foerster (2010) and proper engineering judgment. Vulnerability was finally assessed through probabilistic fragility (or vulnerability) curves, which describe the probability of exceeding a certain limit state of the building exposed to the landslide hazard given the measure of the landslide intensity. The landslide intensity was expressed both in terms of peak horizontal ground acceleration (PGA) at the seismic bedrock (i.e the initial triggering force of the slow-moving slide) and permanent ground displacement (PGD) at the slope area (i.e. a product of PGA). The latter one was generally better correlated to structural deformation and damage and allowed for direct comparisons to non-earthquake related landslide damages to buildings.

Two different procedures were presented and applied to estimate the log-normally distributed fragility parameters (median and log-standard deviation) given the simulated damage data. The first one, was based on a regression analysis method (e.g. Nielson and DesRoches, 2007; Argyroudis and Pitilakis, 2012) whereas the second was based on a

purely statistical approach, i.e. the maximum likelihood method (e.g. Shinozuka et al., 2000; 2003). Various sources of uncertainty associated with the building capacity, the deformation demand and the definition of limit states were explicitly taken into account in the fragility analysis. The differences on the fragility curves when applying the two different approaches were due to the different assumptions adopted in each method and evidently displayed the influence of epistemic uncertainty on the fragility analysis. For the simulated dataset the maximum likelihood method was found to be more efficient (predicting lower log-standard deviation values) compared to the regression analysis method when considering PGA as an intensity parameter.

The derived fragility functions revealed that the foundation compliance and the slope soil type may greatly influence the structural response and damage. In particular, among the structures analyzed, the ones with flexible foundations located on sand slopes were the most vulnerable whereas the corresponding ones with stiff foundations located on clay slopes appeared to be the least susceptible to damage.

An abacus of fragility curves both in terms of PGA and PGD were developed in **Chapter 6** based on the suggested methodological framework via an extensive parametric investigation and sensitivity analysis of various slope geometries, soil properties and distances of the building with respect to the slope's crown. It is concluded that slope inclination in conjunction with the slope soil material were among the most influential features on the physical vulnerability of the building exposed to the seismically induced landslide. The slope height was also proved to greatly influence the building's fragility for the steep sand slope configurations. The above observations resulted to the proposition of seven sets of generalized fragility curves, considering the most unfavorable position of the building with respect to the slope's crest that was found to be different for sand and clay slopes.

To get further insight into the building's vulnerability to the permanent differential displacement due to landslide hazard several additional parameters were also studied. These included the water table level, the consideration of a strain softening landslide material, the flexibility of the foundation system, the number of bays and storeys of the building and the code design level. It was shown that the influence of each parameter may vary with respect to the slope soil material (e.g. for the water table) and the foundation compliance (e.g. for the building geometry). Overall, it was observed that their impact might be, under certain circumstances, crucial to the structure's fragility.

To gain confidence on the proposed methodological framework, representative developed fragility curves were compared with literature ones and recorded building damages from real past events in **Chapter 7**.

The validity the proposed method was first assessed through the comparison of representative suggested fragility curves with corresponding literature ones based on empirical damage data (Zhang and Ng, 2005), engineering judgement (NIBS, 2004) and on numerical simulations (Negulescu and Foerster, 2010). Taking into account the different assumptions associated with the proposed and the literature curves, the comparisons showed that the proposed curves were generally in good agreement with the literature ones for the case of the typical studied building on flexible foundations. On the contrary, it was found that the proposed curves underestimated the structure's fragility with respect to the literature ones for the corresponding building on stiff foundations.

Typical proposed fragility curves for low-rise RC buildings subjected to co-seismic permanent slope displacement were also correlated to fragility curves provided by various investigators for low-rise RC buildings subjected to ground shaking lying on an horizontally layered soil stratum. Overall, the comparisons allowed seeking an understanding of the relative extent of damage and the associated dominating failure mechanism for structures subjected to co-seismic slope deformation and ground shaking respectively. They revealed, however, the high aleatory and epistemic uncertainty associated with the different fragility curves found in the literature.

The proposed methodological framework and the corresponding fragility curves were also validated through its application to two real case histories: Kato Achaia slope in Peloponnese –Greece and the Corniglio village-Italy case study. The direct comparison of the recorded damage data on typical buildings with the corresponding damage predicted by the developed fragility functions proved that the proposed fragility curves could adequately capture the performance of the representative building affected by the slope co-seismic landslide differential displacement. In addition, to enhance the effective implementation of the proposed methodological framework within a probabilistic risk assessment study, more realistic fragility curves were developed for a representative building in Corniglio village based on numerical simulations. The reliability of the curves was verified through their comparison with the observed building damage data for the measured level of displacement.

Traditionally, the structural vulnerability implicitly refers to the intact, as-built structure assuming an optimum plan of maintenance. However, structures deteriorate due to various time-dependent mechanisms after they are put into service, without always subjected to the necessary interventions during their lifetime. These issues are becoming

even more crucial in presence of natural hazards striking the structure, such as landslides and/or earthquakes. A major contribution of the present research was thus the expansion of the proposed method to account for the changing patterns of building's vulnerability over time exposed to earthquake –induced landslide hazard (**Chapter 8)**. In particular, the progressive aging of typical RC buildings due to exposure to aggressive corrosive environment was investigated by including probabilistic models of corrosion deterioration of the RC elements within the vulnerability modeling framework. Two potential corrosion scenarios were examined: chloride and carbonation induced corrosion of the steel reinforcement. The proposed methodology was applied to reference low-rise RC frame buildings with varying strength and stiffness of the foundation system that are subjected to the combined effects of reinforcement corrosion and earthquake triggered landslide displacements. Time –dependent fragility curves in terms of PGA (outcrop conditions) and PGD for different damage states were analytically evaluated at different points in time (0, 20, 40, 60, 90 years) for the given carbonation or chloride induced deterioration scenario. It was shown that the fragility of the structures may increase over time due to corrosion. This increase was more evident for the chloride induced corroded RC buildings founded on flexible foundations.

9.2 Limitations and recommendations for future work

The work in the present study distinguishes certain limitations and should be extended through additional research in the following areas:

- The proposed vulnerability assessment method and the corresponding fragility curves are appropriate for predicting the structural damage of the building members implying a ductile failure of the structure. However, the total damage (structural and non-structural) will be quite different (certainly larger) in case of the building with the stiff foundation as a considerable amount of damage may be attributed to the rotation of the whole building as a rigid body. In the latter, the damage can only be defined using empirical criteria and proper engineering judgment (Bird et al., 2005).
- The complex issue of combined damages due to ground shaking and ground failure is not taken into account in the evaluation of building's vulnerability that is assessed only for the co-seismic permanent slope differential displacement. Thus, no strength or stiffness degradation to the building's structural members due to the effect of ground shaking is assumed to occur. Future work should be therefore oriented towards the study of the vulnerability of a typical building standing next

to the cliff exposed to the coupled effect of ground shaking and permanent ground deformation due to landslide.

- It is also suggested to increase the applicability band of the proposed methodological framework through the development of supplementary fragility curves for other structural typologies (e.g. for high-rise RC buildings), slope configurations and soil conditions. Various additional features such as the water table level should also be addressed more in depth.
- In addition, future research should aim at the validation of the proposed time-dependent vulnerability model via comparison of the damages predicted by the curves to experimental results and/or empirical data.
- Significant effort should also be devoted in the more refined definition of the time-dependent performance indicators and states. This is a very important and challenging issue which has not received much attention until very recently (REAKT, http://www.reaktproject.eu/)
- Finally, further research is needed to address time-dependent fragility of additional building types and geometries, different triggering mechanisms of the potential landslide mass (e.g. intense precipitation) as well as deterioration mechanisms.

REFERENCES

AGSO (2001). "Natural hazards and the risk they pose to South-East Queenland". AGSO-Geoscience Australia. Digital report on CD-ROM. 389 Pages.

AGS (2007). "Guideline for landslide susceptibility, hazard and risk zoning for land use management". Australian geomechanics society landslide taskforce landslide zoning working group. Australian Geomechanics 42 (1), 13–36.

Ahmad N., Crowley H., Pinho R. (2011). "Analytical fragility functions for reinforced concrete and masonry buildings and buildings aggregates of Euro-Mediterranean regions – UPAV methodology". Internal Report, Syner-G Project 2009/2012.

Akkar S., Sucuoglu H., Yakut A. (2005). "Displacement-based fragility functions for low- and mid-rise ordinary concrete buildings". Earthquake Spectra 21(4), 901-927.

Ambraseys N.N. (1988). "Engineering seismology". Int. J. Earthquake Eng. Struct. Dyn. 17, 1–105.

Ambraseys N.N., Menu J.M. (1988). "Earthquake-induced ground displacements". J. Earthquake Eng. 16, 985–1006.

Anastasopoulos I., Gazetas G., Bransby M.F., Davies M.C.R., El Nahas A. (2007). "Fault rupture propagation through sand: Finite element analysis and validation through centrifuge experiments". Journal of Geotechnical and Geoenvironmental Engineering 133(8), 943-958.

Antonakos G. (2009). "Models of dynamic response and decoupled displacements of earth slopes during earthquakes", M.S. Thesis, University of Texas at Austin, Austin, TX.

Argyroudis S. (2010). "Contribution to seismic vulnerability and risk of transportation networks in urban environment". PhD Thesis (in Greek), Dept. of Civil Engineering, Aristotle University of Thessaloniki, Greece.

Argyroudis S., Fotopoulou S., Pitilakis K. (2011). "Semi-empirical assessment of road vulnerability to seismically induced slides". 2nd World Landslide Forum, 3-8 October.

Argyroudis S., Pitilakis K. (2012). "Seismic fragility curves of shallow tunnels in alluvial deposits". Soil Dynamics and Earthquake Engineering 35, 1-12.

Ashford S.A., Sitar N., Lysmer J., Deng N., (1997). "Topographic effects on the seismic response of steep slopes". Bulletin of the Seismological Society of America 87, 701–709.

Assimaki D., Gazetas G. (2004). "Soil and topographic amplification on canyon banks and the 1999 Athens earthquake". Journal of Earthquake Engineering 8(1), 1–43.

Assimaki D., Kausel E., Gazetas G. (2005). "Wave propagation and soil–structure interaction on a cliff crest during the 1999 Athens Earthquake". Soil Dynamics and Earthquake Engineering 25(7-10), 513-527.

Assimaki D., Kausel E. (2007). "Modified topographic amplification factors for a single-faced slope due to kinematic soil-structure interaction". Journal of Geotechnical and Geoenvironmental Engineering 133, 1414–1431.

Association of Professional Engineers and Geoscientists of British Columbia (APEGBC) (2010). "Guidelines for legislated landslide assessments for proposed residential developments in BC". May 2010.

ATC-13 (1985). "Earthquake damage evaluation data for California". Applied Technology Council, Redwood City.

Ausilio E., Costanzo A., Silvestri F., Tropeano G. (2008). "Prediction of seismic slope displacements by dynamic stick-slip analyses". Seismic Engineering International Conference(MERCEA'08), Reggio Calabria and Messina, Italy, July 8–11.

Ausilio E., Costanzo A., Tropeano G., Silvestri F. (2009). "Evaluation of seismic displacements of a natural slope by simplified methods and dynamic analyses". Performance-Based Design in Earthquake Geotechnical Engineering – Kokusho, Tsukamoto & Yoshimine (eds)Taylor & Francis Group, London, ISBN 978-0-415-55614-9.

Barani S., Bazzurro P., Pelli F. (2010). "A probabilistic method for the prediction of earthquake induced slope displacements". Proceedings of 5th International Conference on recent advances in Geotechnical Earthquake Engineering and Soil dynamics and Symposium in Honor of professor I. M. Idriss, San Diego, May 24-29.

Beushausen, H., Alexander, M. (2010). "Concrete deterioration: causes, mechanisms, prevention". Concrete Technology for Structural Engineers, Workshop, May 2010.

Bird J.F., Crowley H., Pinho R., Bommer J.J. (2005). "Assessment of building response to liquefaction induced differential ground deformation". Bul of the New Zealand Society for Earthquake Engineering 38(4), 215-234.

Bird J.F., Bommer J.J., Crowley H., Pinho R. (2006). "Modelling liquefaction-induced building damage in earthquake loss estimation". Soil dynamics and Earthquake Engineering 26 (1), 15-30.

Bjerrum L. (1967). "Progressive failure in slopes of overconsolidated plastic clays and clay shales". J Mech Found Eng Div ASCE 93(5), 1–49.

Bjerrum L. (1963). "Allowable settlement of structures". Proceedings of the 3rd European Conf. on Soil Mech. and Found. Engng, Wiesbaden, 2, Brighton, England, 135–137.

Bommer J., Rodriguez C. (2002). "Earthquake-induced landslides in Central America". Engineering Geology 63(3-4), 189-220.

Bommer J.J., Alarcon J.E. (2006). "The prediction and use of peak ground velocity". Journal of Earthquake Engineering 10(1), 1-31.

Boone S.J. (1996). "Ground-movement-related building damage". J. Geotech. Eng.-ASCE, 122(11), 886–896.

Borzi B., Pinho R., Crowley H. (2007). "SP-BELA: un metodo meccanico per la definizione della vulnerabilità basato su analisi pushover semplificate". ANIDIS, Pisa, 2007 (in italian).

Boscardin M.D., Cording E.G. (1989). "Building response to excavation induced settlement". J. Geotech. Eng.-ASCE 115, 1–21.

Bouckovalas G.D., Gazetas G., Papadimitriou A.G. (1995). "Geotechnical aspects of the 1995 Aegion (Greece) earthquake". National Technical University of Athens, Greece.

Bouckovalas G.D., Kouretzis, G. (2001). "Review of soil and topography effects in the September 7,1999 Athens (Greece) earthquake". Proc. Forth International Conference on Recent Advances in Geotechnical Earthquake Engineering and Soil Dynamics and Symposium in Honor of Professor W.D. Liam Finn (S. Diego – California, 26-31/05/2001).

Bouckovalas G.D., Papadimitriou A.G. (2005). "Numerical evaluation of slope topography effects on seismic ground motion". Soil Dynamics and Earthquake Engineering 25(7-10), 547-558.

Bourdeau C., Havenith H.B., Fleurisson J.A., Grandjean, A.G. (2004). "Numerical modelling of seismic slope stability". Engineering Geology for Infrastructure Planning in Europe, Springer Berlin / Heidelberg 104, 671-684.

Bourdeau C., Havenith H.B. (2008). "Site effects modelling applied to the slope affected by the Suusamyr earthquake (Kyrgyzstan, 1992)". Engineering Geology 97(3-4), 126-145.

Bozzano F., Lenti L., Martino S., Paciello A., Scarascia Mugnozza G. (2008a). "Self-excitation process due to local seismic amplification responsible for the 31st October 2002 reactivation of the Salcito landslide (Italy)". J Geophys Res 113.

Bozzano F., Bretschneider A., Martino S. (2008b). "Stress–strain history from the geological evolution of the Orvieto and Radicofani cliff slopes (Italy)". Landslides 5(4), 351-366.

Bozzano F., Lenti L., Martino S., Paciello A., Scarascia Mugnozza, G. (2010). "Evidences of landslide earthquake triggering due to self-excitation process". International Journal of Earth Sciences 100(4), 861-879.

Bray J.D., Rathje E.M., Augello A. J., Merry S.M. (1998). "Simplified seismic design procedures for geosynthetic-lined, solid waste landfills". Geosynthet. Int. 5(1–2), 203–235.

Bray J.D., Rathje E.R. (1998). "Earthquake-induced displacements of solid-waste landfills". Journal of Geotechnical and Geoenvironmental Engineering, ACE 124(3), 242–253.

Bray J.D., Travasarou, T. (2007). "Simplified procedure for estimating earthquake-induced deviatoric slope displacements". Journal of Geotechnical and Geoenvironmental Engineering, ASCE, 133(4), 381-392.

Bray J.D. (2007). "Simplified seismic slope displacement procedures". Earthquake geotechnical engineering. K. D. Pitilakis Editor, 2007 Springer.

Bray J.D., Travasarou T. (2009). "Pseudostatic coefficient for use in simplified seismic slope stability evaluation". Journal of Geotechnical Engineering ASCE 135(9), 1336-1340.

BRGM (French Geological Survey) Software (1998). Cyberquake, version 1.1. User's guide.

Burland J.B., Broms B.B., De Mello V.F.B. (1977). "Behaviour of foundations and structures". SOA Report. Proc. 9th Int. Conf. SMFE, Tokyo, Vol. 2; pp 495-546.

Burland J.B. (1995). "Assessment of risk of damage to buildings due to tunneling and excavations". Invited special lecture, in: Proc. 1st Int. Conf. Earthquake Geotechnical Engineering, IS-Tokyo'95, pp. 1189-1201.

Burland, J. B. Wroth C. P. (1974). "Settlement of buildings and associated damage". Proceedings of the Conference on Settlement of Structures – Session V, Cambridge, England, pp. 611–654.

California Geological Survey (2008). "Guidelines for evaluating and mitigating seismic hazards in California". California Geological Survey Special Publication 117A, 98 pp.

Callerio A., Faccioli E., Kaynia A. (2007). Deliverable 121: Landslide risk assessment methods and applications (III) – Application to real active landslides – Phase II (68pp). LESSLOSS integrated project: Risk Mitigation for Earthquake and Landslides, Sub-Project 4 – Landslide risk scenarios and loss modelling.

Cascini L., Bonnard Ch., Corominas J., Jibson R., Montero-Olarte J. (2005). "Landslide hazard and risk zoning for urban planning and development". In: Hungr, O., Fell, R., Couture, R., Eberthardt, E. (Eds.), Landslide Risk Management. Taylor and Francis.

CEB-FIB Task Group 5.6 (2006). "Model code for service life design". Bulletin 31, fédération internationale du béton (fib).

CEN-European Committee for Standardization (2003). p.rENV 1998-1 – Eurocode 8: Design of structures for earthquake resistance. Part 1: General rules, seismic actions and rules for buildings, Draft No. 4, Brussels, Belgium.

Chang C.J., Chen W.F., Yao J.T.P., (1984). "Seismic displacements in slopes by limit analysis". Journal of Geotechnical Engineering 110, 860–874.

Chang K.J., Taboada A., Chan Y.C. (2005). "Geological and morphological study of the Jiufengershan landslide triggered by the Chi-Chi Taiwan earthquake". Geomorphology 71(3-4), 293-309.

Chatzipetros A., Valcaniotis S., Papathanassiou G., Sboras S., Neofotistos P., Mavrodis P., Paulidis S. (2008). "Quick report on the surface effects of the June 8, 2008 NW Peloponnese earthquake". Aristotle University of Thessaloniki, Greece.

Cheng Y. M., Lansivaara T., Wei W.B. (2007). "Two-dimensional slope stability analysis by limit equilibrium and strength reduction methods". Computers and Geotechnics 34(3), 137-150.

Choe, D.-E., Gardoni, P., Rosowsky, D. And Haukaas, T. (2009). "Seismic fragility estimates for reinforced concrete bridges subject to corrosion". Structural Safety 31, 275–283.

Choe, D.-E., Gardoni, P., Rosowsky, D. (2010). "Fragility increment functions for deteriorating reinforced concrete bridge columns". Journal of Engineering Mechanics 136(8), 969-978.

Chugh A. K., Stark T. D. (2006). "Permanent seismic deformation analysis of a landslide". Landslides 3(1), 2-12.

Conte E., Silvestri F., Troncone A. (2010)."Stability analysis of slopes in soils with strain-softening behavior", Computers and Geotechnics 37(5), 710-722.

Cornell C.A., Jalayer F., Hamburger R.O., Foutch D.A. (2002). "Probabilistic basis for 2000 SAC federal emergency management agency steel moment frame guidelines". Journal of Structural Engineering 128, 526-533.

Corominas J. Mavrouli O. (Eds.) (2011a). Deliverable 2.4: Guidelines for landslide susceptibility, hazard and risk assessment and zoning. Work Package 2.1 – Harmonization and development of procedures for quantifying landslide hazard.

SafeLand: Seventh Framework Programme for research and technological development (FP7) of the European Commission.

Corominas J. Mavrouli O. (Eds.) (2011b). Deliverable 2.11: QRA case studies at selected "hotspots". Synthesis of critical issues. Work Package 2.3 – Development of procedures for QRA at regional scale and European scale. SafeLand: Seventh Framework Programme for research and technological development (FP7) of the European Commission.

Crespellani T., Madiai C., Vannucchi G. (1998). "Earthquake destructiveness potential factor and slope stability". Geotechnique 48(3), 411–420.

Crosta G.B., Imposimato S., Roddeman D., Chiesa S., Moia F. (2005). "Small fast-moving flow-like landslides in volcanic deposits: The 2001 Las Colinas Landslide (El Salvador)". Engineering Geology 79(3-4), 185-214.

Crowley H., Pinho R., Bommer J.J. (2004). "A probabilistic displacement-based vulnerability assessment procedure for earthquake loss estimation". Bulletin of Earthquake Engineering 2(2),173-219.

Crowley et al. (2011). D3.1 - Fragility functions for common RC building types in Europe, in SYNER-G: Systemic Seismic Vulnerability and Risk Analysis for Buildings, Lifeline Networks and Infrastructures Safety Gain, WP3 – Fragility Functions of Elements at Risk.

Cruden D.M., Varnes D.J. (1996). "Landslides types and processes". In: Turner A.K. and Schuster R.L. (Eds.) Landslides: investigation and mitigation. Transportation Research Board Special Report 247. National Academy Press, Washington, DC, pp. 36–72.

Cundall P.A., Hansteen H., Lacasse S., Selnes P.B. (1980). "NESSI – soil structure interaction programme for dynamic and static problems". Report 51508-9, December, Norwegian Geotechnical Institute.

Dai F. C., Lee C. F., Ngai Y.Y. (2002). "Landslide risk assessment and management: an overview". Engineering Geology 64(1), 65-87.

Darendeli M. (2001). "Development of a new family of normalized modulus reduction and material damping curves". Ph.D. Dissertation, Univ. of Texas.

DARTS (2004). "Durable and reliable tunnel structures: Deterioration modelling". European Commission, Growths 2000, Contract G1RD-CT-2000-00467, Project GrD1-25633.

Das I., Kumar G., Stein A., Bagchi A., Dadhwal V.K. (2011). "Stochastic landslide vulnerability modeling in space and time in a part of the northern Himalayas, India". Environmental Monitoring and Assessment 178, 25–37.

Dawson E.M., Roth W.H. (1999). "Slope stability analysis with FLAC", in FLAC and Numerical Modeling in Geomechanics, Proceedings of the International FLAC Symposium on Numerical Modeling in Geomechanics, Minneapolis, Minnesota, September 1999, pp. 3-9.

Del Gaudio V., Wasowski J. (2011). "Advances and problems in understanding the seismic response of potentially unstable slopes". Engineering Geology, 122(1-2), 73-83.

Delgado, J., Garrido, J., López-Casado, C., Martino, S., Peláez, J. A. (2011). On far field occurrence of seismically induced landslides. Engineering Geology, 123(3), 204-213.

Densmore A.L., Hovius N., (2000). "Topographic fingerprints of bedrock landslides". Geology 28 (4), 371–374.

Ditlevsen O. (1984). "Probabilistic thinking: an imperative in engineering modeling". Danmarks Tekniske Hojskole, Lyngby, 1-23.

Dong J.J., Lee W.R., Lin M.L., Huang A.B., Lee Y.L. (2007). "Effects of seismic anisotropy and geological characteristics on the kinematics of the neighboring Jiufengershan and Hungtsaiping landslides during Chi-Chi earthquake". Tectonophysics 466(3-4), 438-457.

Dounias G.T., Potts D.M., Vaughan P.R. (1988). "Finite element analysis of progressive failure: two case studies". Comput. Geotech. 6, 155–175.

Dunning S., Mitchell W., Rosser N., Petley D. (2007). "The Hattian Bala rock avalanche and associated landslides triggered by the Kashmir Earthquake of 8 October 2005". Engineering Geology 93(3-4), 130-144.

DuraCrete (2000). "Probabilistic performance based durability design of concrete structures: Statistical quantification of the variables in the limit state functions". Report No.: BE 95-1347, pp. 62-63.

EAK2000 (2000). Greek Seismic Code, Organization of seismic planning and protection.

EC8 2004. Eurocode 8: Design of structures for earthquake resistance, Part 5: Foundations, retaining structures and geotechnical aspects. CEN-ENV, Brussels.

EERI, 2003. Special Earthquake Report. "Learning from earthquakes: Preliminary observations on the August 14, 2003, Lefkada island (Western Greece) earthquake". November 2003.

Erberik M.A. (2008). "Fragility-based assessment of typical mid-rise and low-rise RC buildings in Turkey". Engineering Structures 30(5), 1360-1374.

Federal Emergency Management Agency (FEMA), 2000. Prestandard and commentary for the seismic rehabilitation of buildings (FEMA 356), ASCE, Washington, DC.

Fell R., Bonnard C., Cascini L., Leroi E., Savage W. (2008). "Guidelines for landslide susceptibility, hazard and risk zoning for land-use planning". Engineering Geology 102, 99–111.

Fokaefs A., Papadopoulos G. (2007). "Testing the new INQUA intensity scale in Greek earthquakes". Quaternary International 173–174, 15–22.

Fotopoulou S., Anastasiadis A., Pitilakis K. (2011). "Building vulnerability to the 2008 Ilia- Achaia earthquake induced slides". 2nd World Landslide Forum, 3-8 October.

Fotopoulou S., Karapetrou S., Pitilakis K. (2012). "Seismic vulnerability of RC buildings considering SSI and aging effects". 15th World Conference on Earthquake Engineering, Lisbon, Portugal, 24-28 September.

Fotopoulou S., Pitilakis K. (2012). "Vulnerability assessment of reinforced concrete buildings subjected to seismically triggered slow-moving earth slides". Landslides (DOI: 10.1007/s10346-012-0345-5).

Galli M., Guzzetti F. (2007). "Vulnerability to landslides in Umbria, central Italy". Environmental Management 40, 649–664.

Ghobarah A. (2004). "On drift limits with different damage levels". Proceeding of International Workshop on Performance-based seismic design concepts and implementation, Bled, Slovenia, June 28th – July 1rd.

Ghosh J., Padgett J.E., (2010). "Aging Considerations in the Development of Time-Dependent Seismic Fragility Curves". Journal of Structural Engineering 136(12), 1497-1511.

Glade T. (2003). "Vulnerability assessment in landslide risk analysis". Beitr Erdsystemforschung 134(2), 123–146.

Glade T., Crozier M.J. (2005). "The nature of landslide hazard and impact". In: Glade T, Anderson MG, Crozier MJ (eds) Landslide hazard and risk. Wiley, Chichester, pp 43–74.

Griffiths D.V., Lane P.A. (1999). "Slope stability analysis by finite elements". Geotechnique 49(3), 387-403.

Han Y., Hart R. (2010). "Seismic analysis of the reservoir-earth dam-pore fluid system using an integrated numerical approach". Proceedings of 5th International Conference on recent advances in Geotechnical Earthquake Engineering and Soil dynamics and Symposium in Honor of professor I. M. Idriss, San Diego, May 24-29.

Hancox G.T., Perrin N.D., Dellow G.D. (2002). "Recent studies of historical earthquake-induced landsliding, ground damage, and MM intensity in New Zealand". Bulletin of the New Zealand Society for Earthquake Engineering 35(2), 59–94.

Hansen A., Franks C.A.M. (1991). "Characterisation and mapping of earthquake triggered landslides for seismic zonation". Proceedings of the Fourth International Conference on Seismic Zonation, Stanford, California, vol. 1, pp. 149–195.

Harp E.L., Jibson R.W. (1996). "Landslides triggered by the 1994 Northridge, California earthquake". Bulletin of the Seismological Society of America 86 (1B), S319–S332.

Hasegawa S., Dahal R. K., Nishimura T., Nonomura A., Yamanaka M. (2009). "DEM-based analysis of earthquake-induced shallow landslide susceptibility". Geotechnical and Geological Engineering 27(3), 419-430.

Heinimann H.R. (1999). "Risikoanalyse bei gravitativen Naturgefahren - Fallbeispiele und Daten". Umwelt-Materialen 107/I, Bern.

Hollenstein K. (2005). "Reconsidering the risk assessment concept: Standardizing the impact description as a building block for vulnerability assessment". Nat. Hazards Earth Syst. Sci. 5, 301–307.

Huang R., Li W. (2009). "Analysis of the geo-hazards triggered by the 12 May 2008 Wenchuan Earthquake, China". Bulletin of Engineering Geology and the Environment 68(3), 363-371.

Huang R., Li W. (2011). "Formation, distribution and risk control of landslides in China". Journal of Rock Mechanics and Geotechnical Engineering 3 (2), 97–116.

Hungr O. (1997). "Some methods of landslide hazard intensity mapping". In D. Cruden & R. Fell (editors). Landslide risk assessment. A.A. Balkema, Rotterdam. pp. 215-226

Hutchinson J.N. (1995). Keynote paper: "landslide hazard assessment". In: Bell, D.H. (Ed.), Landslides. Balkema, Rotterdam, pp. 1805– 1841.

International Code Council (2006). 2006 International Building Code (IBC-2006), United States.

Ishihara K., (1996). "Soil behaviour in earthquake geotechnics". Clarendon, London, 350 pp.

Itasca Consulting Group (2008). Inc. FLAC (Fast Lagrangian Analysis of Continua), ver. 6.0. Itasca Consulting Group, Inc., Minneapolis.

Itasca Consulting Group (2011). Inc. FLAC (Fast Lagrangian Analysis of Continua), ver. 7.0. Itasca Consulting Group, Inc., Minneapolis.

Itasca Consulting Group, Inc. (2004). UDEC, Universal Distinct Element Code, Ver. 4.0, Itasca Consulting Group, Inc., Minneapolis.

Japanese Geotechnical Society (2011). "Geo-Hazards during earthquake and mitigation measures – Lessons and recommendations from the 2011 Great East Japan Earthquake".

Jibson R.W. (2000). "A method for producing digital probabilistic seismic landslide hazard maps". Engineering Geology 58(3-4), 271-289.

Jibson R.W. (2007). "Regression models for estimating co seismic land- slide displacement". Eng. Geol. (Amsterdam) 91, 209–218.

Jibson R.W. (2011). "Methods for assessing the stability of slopes during earthquakes—A retrospective". Engineering Geology 122(1-1), 43-50.

Kakderi K. (2011). "Seismic vulnerability assessment and seismic risk management of complex transportation networks". Application to port facilities.PhD Thesis (in Greek), Dept. of Civil Engineering, Aristotle University of Thessaloniki, Greece.

Kappos A. Panagiotopoulos C., Panagopoulos G., Papadopoulos El. WP4 – Reinforced concrete buildings (Level 1 and Level 2 analysis). RISK-UE, 2003.

Kappos A.J., Panagopoulos G., Panagiotopoulos Ch., Penelis Gr. (2006). "A hybrid method for the vulnerability assessment of R/C and URM buildings". Bull. of Earthquake Engineering 4(4), 391-413.

Karakostas Ch., Makarios T., Lekidis V., Salonikios T., Sous I., Makra K, Anastasiadis A., Klimis N., Dimitriou P., Margaris B., Papaioannou Ch., Theodulidis N. and Savvaidis A., (2006). "The Kythira (Greece) earthquake of January 8, 2006: Preliminary report on strong motion data, geotechnical and structural damage". EERI Learning from Earthquakes report.

Kaynia A., Papathoma-Köhle M., Neuhaeuser B., Ratzinger K., Wenzel H., Medina-Cetina Z. (2008). "Probabilistic assessment of vulnerability to landslide: Application to the village of Lichtenstein, Baden-Württemberg, Germany". Engineering Geology 101, 33-48.

Keefer D.K. (1984). "Landslides caused by earthquakes". Geological Society of America Bulletin 95, 406- 421.

Keefer D.K., (2000). "Statistical analysis of an earthquake-induced landslide distribution – The 1989 Loma Prieta, California event". Engineering Geology 58, 231-249.

Keefer D.K. (2002). "Investigating landslides caused by earthquakes – A historical review". Surveys in Geophysics 23, 473-510.

Kokusho T., Ishizawa T., (2005). "Energy approach to slope failures and a case study during 2004 Niigata–ken Chuetsu earthquake". Proceedings of Geotechnical Earthquake Engineering Satellite Conference Osaka, Japan, ISSMGE, 255-262.

Kokusho T., Ishizawa T., Hara T., (2009). "Slope failures during the 2004 Niigataken Chuetsu earthquake in Japan". Earthquake geotechnical case histories for

performance-based design – Kokusho (ed), 2009 Taylor & Francis Group, London, ISBN 978-0-415-80484-4.

Konagai K., Orense R.P., Johansson J., (2009). "Las Colinas landslide caused by the 2001 El Salvador Earthquake". Earthquake geotechnical case histories for performance-based design –Kokusho (ed), 2009 Taylor & Francis Group, London, ISBN 978-0-415-80484-4.

Kourkoulis R., Anastasopoulos I., Gelagoti F., Gazetas G. (2010). "Interaction of foundation-structure systems with seismically precarious slopes: Numerical analysis with strain softening constitutive model". Soil Dynamics and Earthquake Engineering 30, 1430-1445.

Koutsourelakis P.S. (2010). "Assessing structural vulnerability against earthquakes using multi-dimensional fragility surfaces: A Bayesian framework". Probabilistic Engineering Mechanics 25, 49-60.

Kramer S.L. (1996). "Geotechnical earthquake engineering". Prentice Hall, Upper Saddle River, New Jersey, USA.

Kramer S.L., Stewart J.P. (2004). "Geotechnical aspects of seismic hazards". In: Earthquake Engineering: from engineering seismology to performance-based engineering, Y. Bozorgnia, V. Bertero (Eds.), CRC Press, Chapter 4, 85 pp.

Kramer S.L. (2011). "Performance-based earthquake design in geotechnical engineering practice". State-of-the art lecture, 5th International Conference on Earthquake Geotechnical Engineering, Santiago, Chile.

Ktenidou O.-J. (2010). "Theoretical and instrumental study of site and topographic effects on strong ground motion in Aegion". Ph.D. thesis, Aristotle University Thessaloniki, Greece.

Kwok A.O., Stewart J.P., Hashash Y.M.A., Matasovic N., Pyke R., Wang Z., Yang Z. (2007). "Use of exact solutions of wave propagation problems to guide implementation of nonlinear seismic ground response analysis procedures". J. Geotech. & Geoenv. Engrg. 133 (11), 1385-1398.

Kwon, O.-S. and Elnashai, A. S. (2007). "Probabilistic seismic assessment of structure foundation and soil interacting systems". NSEL Report Series, Report No. NSEL-004, Newmark Structural Engineering Laboratory, Department of Civil and Environmental Engineering, University of Illinois at Urbana-Champaign, Urbana, Illinois, USA.

Lagaros N.D., Tsompanakis Y., Psarropoulos P.N., Georgopoulos E.C. (2009). "Computationally efficient seismic fragility analysis of geostructures". Computers & Structures 87(19-20), 1195-1203.

Lenti L., Martino S. (2010). "The LEMA_DES approach for deriving dynamic equivalent signals: numerical modeling of input-slope interaction". Proc. 14ECEE Ohrid (Macedonia), pp. 1–9.

Lenti L., Martino S., (2012). "The interaction of seismic waves with step-like slopes and its influence on landslide movements". Engineering Geology 126, pp. 19–36.

Leone F., Aste J.P., Leroi E. (1996). "Vulnerability assessment of elements exposed to mass moving: working towards a better risk perception". In K. Senneset (Ed.), Landslides, Balkema, Rotterdam. pp. 263-269.

Leroueil S., Locat J., Vaunat J., Picarelli L., Lee H., Faure R. (1996). "Geotechnical characterization of slope movements". In: Senneset, K. (Ed.), Landslides. Balkema, Rotterdam, pp. 53–74.

Lessloss (2005). "The Corniglio landslide (Parma - Italy): Geological data". Studio Geotecnico Italiano, 28 April, Milan, 2005.

Li T.C., (1978). "Relation between earthquakes and landslides and prediction on earthquake induced landslides". (in Chinese). In: Chengdu Institute of Geography (ed) Earthquakes and landslides, pp 1–22.

Li Z., Nadim F., Huang H., Uzielli, M., Lacasse, S. (2010). "Quantitative vulnerability estimation for scenario-based landslide hazards". Landslides 7(2), 125-134.

Lin J.S., Whitman R. (1986). "Earthquake induced displacements of sliding blocks". J. Geotech. Engrg. 112(1), 44–59.

Lin C.W., Shieh C.L., Yuan B.D., Shieh, Y.C., Liu S.H., Lee S.Y. (2003). "Impact of Chi-Chi earthquake on the occurrence of landslides and debris flows: example from the Chenyulan River watershed, Nantou, Taiwan". Engineering Geology 71, 49–61.

Lysmer J., Kuhlemeyer R.L. (1969). "Finite dynamic model for infinite media". Journal of Engineering Mechanics 95, 859–877.

Makdisi F., Seed H., (1978). "Simplified procedure for estimating dam and embankment earthquake induced deformations". Journal of Geotechnical Engineering 104(7), 849–867.

Mander J.B., Priestley M.J.N., Park R. (1988). "Theoretical stress-strain model for confined concrete". Journal of Structural Engineering 114(8), 1804-1826.

Mansour M.F., Morgenstern N.I., Martin C.D. (2011). "Expected damage from displacement of slow-moving slides". Landslides 8(1), 117–131.

Marano K.D., Wald D. J., Allen T.I. (2010). "Global earthquake casualties due to secondary effects: a quantitative analysis for improving rapid loss analyses". Nat Hazards 52, 319–328.

Marchi F., Kaynia A., Gottardi G., Nadim F. (2011). "Role of numerical model and parameter variability on seismic response of slopes: the case of Las Colinas landslide". 5th International Conference on Earthquake Geotechnical Engineering January 2011, 10-13 Santiago, Chile.

Margaris B., Papaioannou C., Theodoulidis N., Savvaidis A., Klimis N., Makra K., Karakostas C., Lekidis V., Makarios T., Salonikios T., Demosthenus M., Athanasopoulos G., Mylonakis G., Papantonopoulos C., Efthymiadou V., Kloukinas P., Ordonez I., Vlachakis V., Stewart J.P. (2008). "Preliminary report on the principal seismological and engineering aspects of the Mw=6.5 Achaia-Ilia (Greece) earthquake on 8 June 2008". GEER Association Report No. GEER-013, http://research.eerc.berkeley.edu/projects/GEER/ Post_EQ_Reports.html (last accessed October 2008).

Margaris B., Athanasopoulos G., Mylonakis G., Papaioannou C., Klimis N., Theodoulidis N., Savvaidis A., Efthymiadou V., Stewart J.P. (2010). "Mw=6.4 Achaia-Elia (Greece) earthquake on 8 June 2008: Source characteristics, ground motions, and ground failure". Earthquake Spectra. 26(2), 399- 424.

Margottini C., Molin D., Serva L. (1992). "Intensity versus ground motion: A new approach using Italian data". Engineering Geology 33, 45-58.

Marques, P.F., Costa, A. (2010). "Service life of RC structures: Carbonation induced corrosion. Prescriptive vs. performance-based methodologies". Construction and Building Materials, vol. 24, pp.258–265.

Martino S., Scarascia Mugnozza G. (2005). "The role of the seismic trigger in the Calitri landslide (Italy): historical reconstruction and dynamic analysis". Soil Dynamics and Earthquake Engineering 25(12), 933-950.

Mavrouli O., Corominas J. (2010). "Vulnerability of simple reinforced concrete buildings in front of the rockfall impact". Landslides 7 (2), 169-180.

Mejia L.H., Dawson E.M. (2006). "Earthquake deconvolution for FLAC". Proc. 4th International FLAC Symposium, Madrid, Spain, 211-219.

Miles S.B., Keefer D.K. (2009). "Evaluation of CAMEL-comprehensive areal model of earthquake-induced landslides". Engineering Geology 104(1-2), 1-15.

Mohammed A.M., Almansour H.H., Martín-Pérez B. (2011). "Combined effect of reinforcement corrosion and seismic loads on RC bridge columns: modeling". 2nd International Engineering Mechanics and Materials Specialty Conference, Ottawa, Ontario, June 14-17, 2011, pp. 1-10.

Mousavi M.S., Omidvar B., Ghazban F., Feyzi R. (2011). "Quantitative risk analysis for earthquake-induced landslides—Emamzadeh Ali, Iran". Engineering Geology 122, 191–203.

National Institute of Building Sciences (2004). Direct physical damage—general building stock. HAZUS-MH Technical manual, Chapter 5. Federal Emergency Management Agency, Washington, D.C.

Negulescu C., Foerster E. (2010). "Parametric studies and quantitative assessment of the vulnerability of a RC frame building exposed to differential settlements". Natural Hazards and Earth System Sciences 10, 1781-1792.

Newmark N.M., (1965). "Effects of earthquakes on dams and embankments". Geotechnique 15 (2), 139–159.

Nielson B.G., DesRoches R. (2007). "Analytical seismic fragility curves for typical bridges in the central and southeastern United States". Earthquake Spectra 23(3), 615.

Nuti C., Vanzi I., Santini S. (1998). "Seismic risk of Italian hospitals", 11th European Conference on Earthquake Engineering.

Ohtsuka S., Isobe K., Takahara T. (2009). "Consideration on fill slope failure in Takamachi developed residential land in 2004 Niigata Chuetsu Earthquake". Proc. of International Conference on Performance- Based Design in Earthquake Geotechnical Engineering – from case history to practice (IS-Tokyo 2009).

Owen L.A., Kamp U., Khattak G.A., Harp E.L., Keefer D.K., Baueret M.A. (2008). "Landslides triggered by the 8 October 2005 Kashmir earthquake". Geomorphology 94(1-2), 1-9.

Ozmen H.B., Inel M., Meral E., Bucakli M. (2010). "Vulnerability of low and mid-rise reinforced concrete buildings in Turkey". 14ECEE, Ohrid.

Paolucci R., (2002). "Amplification of earthquake ground motion by steep topographic irregularities". Earthquake Engineering and Structural Dynamics 31 (10), 1831–1853.

Papadimitriou A.G., Chaloulos Y., 2010. "Aggravation of the peak seismic acceleration in the vicinity of 2D hills, canyons and slopes". Proc. Fifth International Conference on Recent Advances in Geotechnical Earthquake Engineering and Soil Dynamics (S. Diego – California, 24-29/05/2010). Paper n°3-26a, pp. 1–12.

Papadopoulos G.A., Plessa A. (2000). "Magnitude-distance relations for earthquake-induced landslides in Greece". Engineering Geology 58(3-4), 377-386.

Papadopoulos G.A., Drakatos G., Papanastassiou D., Kalogeras I., Stavrakakis G. (2000). "Preliminary results about the catastrophic earthquake of 7 September 1999 in Athens, Greece". Seismological Research Letters 71, 318–329.

Papathoma K., Neuhauser B., Ratzinger K., Wenzel H., Dominey-Howes D. (2007). "Elements at risk as a framework for assessing the vulnerability of communities to landslides". Natural Hazards and Earth System Sciences 7, 765–779.

Pavlides S.B., Papadopoulos G.A., Ganas A., Papathanassiou G., Karastathis V., Keramydas D., Fokaefs A. (2004). "The 14 August 2003 Lefkada (Ionian Sea) earthquake". Proceedings of the 5th International Symposium on Eastern Mediterranean Geology, Thessaloniki, Greece.

Pavlides S.B., Papadopoulos G.A., Ganas A. (2002). "The fault that caused the Athens September 1999 Ms ¼ 5.9 earthquake: field observations". Natural Hazards 27, 61–84.

Peng J., Stewart M.G. (2008). "Carbonation-induced corrosion damage and structural safety for concrete structures under enhanced greenhouse conditions". Research Report No. 270.11.2008.

Peng W.F., Wang C. L., Chen S.T., Lee S.T. (2009). "Incorporating the effects of topographic amplification and sliding areas in the modeling of earthquake-induced landslide hazards, using the cumulative displacement method". Computers and Geosciences 35(5), 946-966.

Pinto P.E. (editor) (2007). "Probabilistic methods for seismic assessment of existing structures". LESSLOSS Report No. 2007/06, Istituto Universitario di Studi Superiori di Pavia, IUSS Press, ISBN: 978-88-6198-010-5.

Pitilakis D. (2009). "Topographic irregularities and soil- foundation- structure interaction". Proceedings of 3rd Greece- Japan Workshop: Seismic Design, Observation, and Retrofit of Foundations. 22-23 September 2009. Santorini Greece.

Pitilakis D., Tsinaris A. (2010). "Soil-foundation-structure interaction close to natural slopes and topographic irregularities (In Greek)". In: Proc of the 6th National Conference of Geotechnical Engineering, Volos, Greece.

Pitilakis D., Moderessi-Farahmand-Razavi A., Clouteau D. (2012). "Equivalent-linear dynamic impedance functions of surface foundations". Journal of Geotechnical and Geoenvironmental Engineering (accepted for publication).

Pitilakis K.D., (2004). "Chapter 5: Site effects. Recent advances in earthquake geotechnical engineering & microzonation (A. Ansal, ed.)". Kluwer Publications.

Pitilakis K., Alexoudi M., Argyroudis S., Monge O., Martin C. (2006a). "Vulnerability and risk assessment of lifelines". Assessing and Managing Earthquake Risk 2, 185-211.

Pitilakis K., Alexoudi M., Argyroudis S., Monge O., Martin C. (2006b). "Earthquake risk assessment of lifelines". Bulletin of Earthquake Engineering 4(4), 365-390.

Pitilakis K.D., (2010). "Geotechnical earthquake engineering". Ziti publication (in Greek).

Polshin D.E., Tokar R.A. (1957). "Maximum allowable non-uniform settlement of structures". Proc. 4th Int. Conference Soil Mechanics and Foundation Engineering, London, Butterworths Scientific Publications, 402–405.

Porter K., Eeri M., Kennedy R., Bachman R. (2007). "Creating fragility functions for performance-based earthquake engineering". Background and objectives. Engineering 23(2), 471-489.

Potts D.M., Zdravkovi L. (1999). "Finite element analysis in geotechnical engineering: theory". Telford.

Pradel D., Smith P.M., Stewart J.P., Raad G. (2005). "Case history of landslide movement during the Northridge earthquake". Journal of Geotechnical and Geoenvironmental Engineering 131(11), 1360 –1369.

Ragozin A.L., Tikhvinsky I.O. (2000). "Landslide hazard, vulnerability and risk assessment". In: Bromhead E, Dixon N, Ibsen ML (eds) Proceedings of the 8th International Symposium on Landslides, Cardiff, pp 1257–1262.

Rathje E.M., Bray J.D. (1999). "An examination of simplified earthquake-induced displacement procedures for earth structures". Canadian Geotechnical Journal, 36, 72–87.

Rathje E.M., Bray J.D. (2000). "Nonlinear coupled seismic sliding analysis of earth structures". Journal of Geotechnical and Geoenvironmental Engineering 126(11), 1002–1014.

Rathje E.M., Saygili G. (2009). "Probabilistic assessment of earthquake-induced sliding displacements of natural slopes". Bull. of the New Zealand Society for Earthquake Engineering 42 (1), 18–27.

Rathje E.M., Antonakos G. (2011). "A unified model for predicting earthquake-induced sliding displacements of rigid and flexible slopes". Engineering Geology 122(1-2), 51-60.

Remondo J., Bonachea J., Cendrero A. (2008). "Quantitative landslide risk assessment and mapping on the basis of recent occurrences". Geomorphology 94, 496-507.

Rodriguez C.E., Bommer J.J., Chandler R.J. (1999). "Earthquake-induced landslides: 1980-1997". Soil Dynamics and Earthquake Engineering 18, 325-246.

Rossetto T., Elnashai A. (2003). "Derivation of vulnerability functions for European-type RC structures based on observational data". Engineering Structures 25(10), 1241-1263.

Saetta A., Simioni P., Berto L., Vitaliani R. (2008). "Seismic response of corroded r.c. structures". International fib Symposium 2008, May 19th - 22nd, Amsterdam, the Netherlands.

Sassa K. (2005). "Landslide disasters triggered by the 2004 Mid-Niigata Prefecture earthquake in Japan". Landslides 2(2), 135-142.

Sassa K., Fukuoka H., Wang F., Wang G. (2005). "Dynamic properties of earthquake-induced large-scale rapid landslides within past landslide masses". Landslides 2(2), 125-134.

Sato H.P., Harp E.L. (2007). "Interpretation of landslide distribution triggered by the 2005 Northern Pakistan earthquake using SPOT 5 imagery". Landslides 4(2), 113-122.

Saygili G., Rathje E.M. (2008). "Empirical Predictive Models for Earthquake-Induced Sliding Displacements of Slopes". Journal of Geotechnical and Geoenvironmental Engineering, 134(6), 790.

Schneider J.F. (2008). "Seismically reactivated Hattian slide in Kashmir, Northern Pakistan". Journal of Seismology 13(3), 387-398.

SEAOC (1995). "Vision 2000: performance based seismic engineering of buildings: conceptual framework". Structural Engineers Association of California, Sacramento.

Seed H.B. (1968). "Landslides During Earthquakes Due to Soil Liquefaction". American Society of Landslides for Seismic Zonation, Proceedings of the Fourth International Conference on Seismic Zonation Stanford, California, vol. 1, pp. 149–195.

Seed H.B., Idriss I.M. (1970). "Soil moduli and damping factors for dynamic response analyses". Univ. of California, Berkeley, California, Report No. EERC 70-10.

SeismoSoft, SeismoSignal (2011). A computer program for signal processing of strong-motion data. Available from URL: www.seismosoft.com.

SeismoSoft, SeismoStruct (2011). A computer program for static and dynamic nonlinear analysis of framed structures. Available from URL: www.seismosoft.com.

Shinozuka M., Feng M.Q., Lee J., Naganuma T. (2000). "Statistical analysis of fragility curves". J. Eng. Mech.-ASCE 126(12), 1224–1231.

Shinozuka M., Feng M.Q., Kim H.K., Uzawa T., Ueda T. (2003). "Statistical analysis of fragility curves". Technical Report MCEER-03-0002, State University of New York, Buffalo.

Shou K.J., Wang C.F. (2003). "Analysis of the Chiufengershan landslide triggered by the 1999 Chi-Chi earthquake in Taiwan". Engineering Geology 68(3-4), 237-250.

Siyahi B., Arslan H. (2008). "Nonlinear dynamic finite element simulation of Alibey earth dam". Environmental Geology 54(1), 77-85.

Skempton A.W., MacDonald D.H. (1956). "Allowable settlement of buildings". P. I. Civil Eng., 5, Part III, 727–768.

Smith J.T., Winter M.G., Fotopoulou S., Pitilakis K., Mavrouli O.-C., Corominas J., Agryroudis S. (2012). "The physical vulnerability of roads to debris flow: an expert judgement approach". 11th International & 2nd North American Symposium on Landslides, 3-8 June, Banff, Alberta, Canada.

Spencer E. (1967). "A method of analysis of the stability of embankments assuming parallel inter-slice forces". Geotechnique 17(1), 11-26.

Srivastava A., Babu S., Haldar S. (2010). "Influence of spatial variability of permeability property on steady state seepage flow and slope stability analysis". Engineering Geology 110, 93–101.

Standing J.R., Addenbrooke T.I. Burland J.B. (1999). "The assessment and building response to tunneling, risk of damage and structural monitoring". Proc. of International Congress on Urban Heritage and Building Maintenance: Foundations, L.G.W. Verhoef ed., Delft University of Technology.

Stead D., Eberhardt E., Coggan J. (2006). "Developments in the characterization of complex rock slope deformation and failure using numerical modelling techniques". Engineering Geology 83(1-3), 217-235.

Stewart M. (2004). "Spatial variability of pitting corrosion and its influence on structural fragility and reliability of RC beams in flexure". Structural Safety 26, 453–470.

Strenk (2010). "Evaluation of analytical procedures for estimating seismically induced permanent deformations in slopes". PhD thesis, Drexel University.

Sudret B., Defaux, G., Pendola, M. (2007). "Stochastic evaluation of the damage length in RC beams submitted to corrosion of reinforcing steel". Civil Engineering and Environmental Systems 24(2), 165–178.

Sun J.I., Golesorkhi R., Seed H.B. (1988). "Dynamic moduli and damping ratios for cohesive soils". Earthquake Engineering Research Center, University of California, Berkeley, Report No. UCB/EERC-88/15, p. 42.

Taiebat M., Kaynia A., Dafalias Y.F. (2011). "Application of an anisotropic constitutive model for structured clay to seismic slope stability". Journal of Geotechnical and Geoenvironmental Engineering 137(5), 492-504.

Terzaghi K. (1950). "Mechanics of landslides". Engineering geology (Berkley) volume. Geological Society of America.

Tika T. E., Vaughan P. R., Lemos L. J. (1996). ”Fast shearing of pre-existing shear zone in soil”. Geotechnique 46(2), p.97–233.

Travasarou T., Bray J.D. (2003). “Optimal ground motion intensity measures for assessment of seismic slope displacements”. 2003 Pacific Conf. on Earthquake Engineering, Christchurch, New Zealand.

Travasarou, T. (2003). “Optimal ground motion intensity measures for probabilistic assessment of seismic slope displacements”. Ph.D. Dissertation, U.C. Berkeley.

Troncone A. (2005). “Numerical analysis of a landslide in soils with strain-softening behavior”. Geotechnique 55(8), 585–96.

Tsionis G., Papailia A., Fardis M.N. (2011). “Analytical fragility functions for reinforced concrete buildings and buildings aggregates of Euro-Mediterranean regions – UPAT methodology”. Internal Report, Syner-G Project 2009/2012.

Tsukamoto Y., Ishihara K., (2005). “Residual strength of soils involved in earthquake–induced landslides”. Proceedings of Geotechnical Earthquake Engineering Satellite Conference, Osaka, Japan, 10 September 2005, Performance Based Design in Earthquake Geotechnical Engineering: Concepts and Research, ISSMGE, pp. 117-123.

Tuutti K. (1982). “Corrosion of steel in Concrete”. Report no 4, Swedish Cement and Concrete research Institute, Stockholm, Sweden.

UBC-97 (1997). Uniform Building Code. International conference of building officials, Vol.2.

Uzielli M., Nadim F., Lacasse S., Kaynia A.M. (2008). “A conceptual framework for quantitative estimation of physical vulnerability to landslides”. Eng. Geol. 102, 251–256.

Van Westen C.J., Van Asch T.W.J., Soeters R. (2006). “Landslide hazard and risk zonation—why is it still so difficult?”. Bull Eng Geol Env 65, 167–184.

Van Westen C.J., Castellanos E., Kuriakose S.L. (2008). "Spatial data for landslide susceptibility, hazard and vulnerability assessment: An overview". Engineering Geology 102(3-4), 112-131.

Varnes D.J. (1978). “Slope movement types and processes”. In: R.L. Schuster and R.J. Krizek, Editors, Landslide Analysis and Control Special Report 176, Transportation Research Board, N.R.C., National Academy of Sciences, Washington, DC , pp. 11–33 Chapter 2.

Varnes D.J. (1984). “Landslides hazard zonation: A review of principles and practice”. UNESCO, Paris.

Vucetic M., Dobry R. (1991). "Effect of soil plasticity on cyclic response". J. Geotech. Engrg. 117(1), 89–107.

Wang H., Wang G., Wang F., Sassa K., Chen Y. (2008). "Probabilistic modeling of seismically triggered landslides using Monte Carlo simulations". Landslides 5(4), 387-395.

Wasowski J., Del Gaudio V., Pierri P., Capolongo D. (2002). "Factors controlling seismic susceptibility of the Sele valley slopes: the case of the 1980 Irpinia earthquake re-examined". Surveys in Geophysics 23, 563-593.

Watson-Lamprey J., Abrahamson N. (2006). "Selection of ground motion time series and limits on scaling". Soil Dyn. Earthquake Eng. 26(5), 477–482.

Wen B., Wang S., Wang E., Zhang J. (2004). "Characteristics of rapid giant landslides in China". Landslides 1(4), 247-261.

Wilson R.C., Keefer D.K. (1983). "Dynamic analysis of a slope failure from the 6 August 1979 Coyote Lake, California, earthquake". Bulletin of Seismological Society of America 73, 863–877.

Yalciner H., Sensoy S., Eren O. (2012). "Time-dependent seismic performance assessment of a single-degree-of-freedom frame subject to corrosion". Engineering Failure Analysis 19, 109–122.

Yegian M., Marciano E., Ghahraman V. (1991). "Seismic risk analysis for earth dams". J. Geotech. Engrg. 117(1), 18–34.

Yenier E., Sandikkaya M.A., Akkar S. (2010). Report on the fundamental features of the extended strong motion databank prepared for the SHARE project (v1.0).

Yin Y., Wang F., Sun P. (2009). "Landslide hazards triggered by the 2008 Wenchuan earthquake, Sichuan, China". Landslides 6(2), 139-152.

Zêzere J.L., Garcia R.A.C., Oliveira S.C., Reis E. (2008). "Probabilistic landslide risk analysis considering direct costs in the area north of Lisbon (Portugal)". Geomorphology 94, 467–495.

Zhang L.M., Ng A.M.Y. (2005). "Probabilistic limiting tolerable displacements for serviceability limit state design of foundations". Geotechnique 55(2), 151–161.

Zhong J., Gardoni P., Rosowsky D. (2010). "Stiffness degradation and time to cracking of cover concrete in reinforced concrete structures subject to corrosion". Journal of Engineering Mechanics 136(2), 209-219.

ANNEX A

Slope Configurations

A.1 Slope geometries used for the parametric analysis

The main slope configurations used for the parametric analysis (Chapter 6) are schematically illustrated in Figures A.1 to A.6. For each geometry four different models are investigated by varying the relative location of the building to the crest and the soil geological settings.

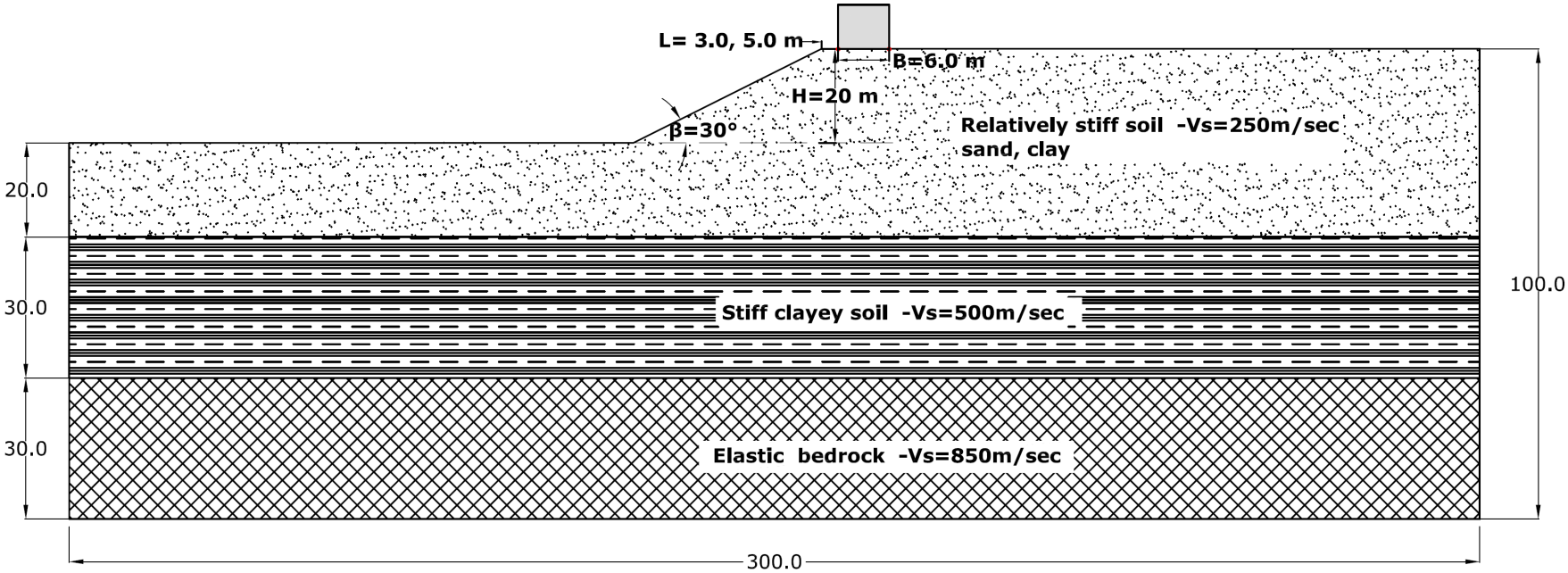


Figure A.1. Slope geometrical configuration 1- Models 1 to 4

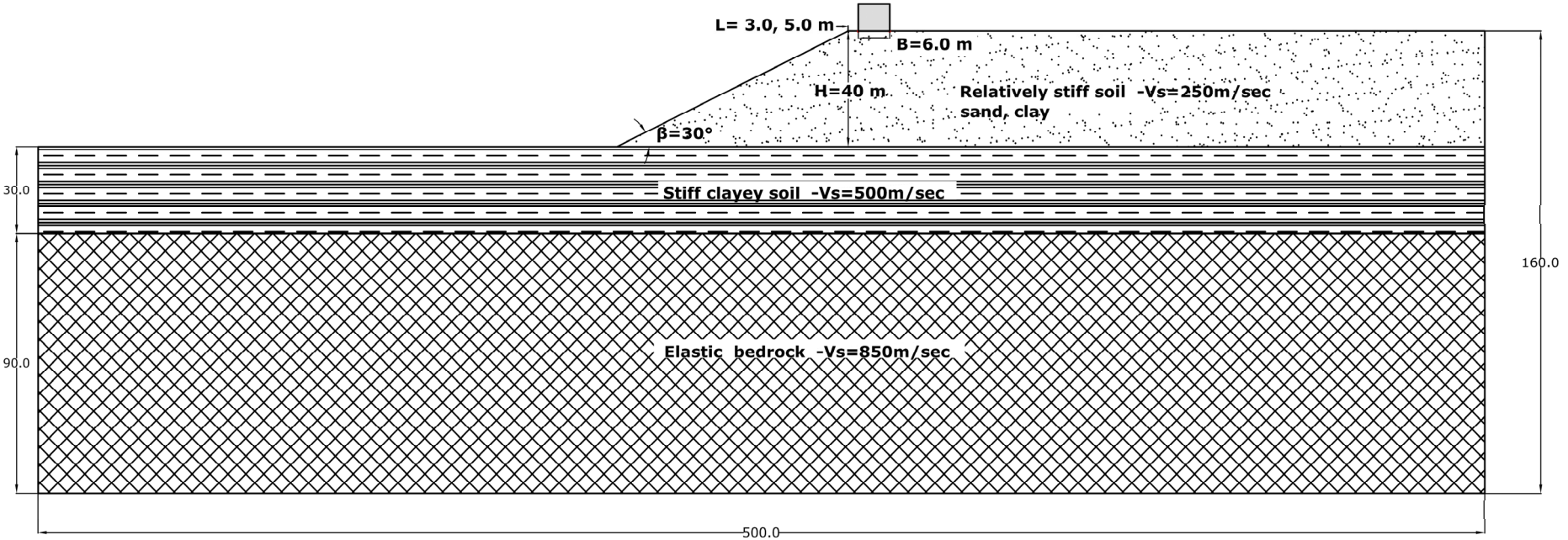


Figure A.2. Slope geometrical configuration 2- Models 5 to 9

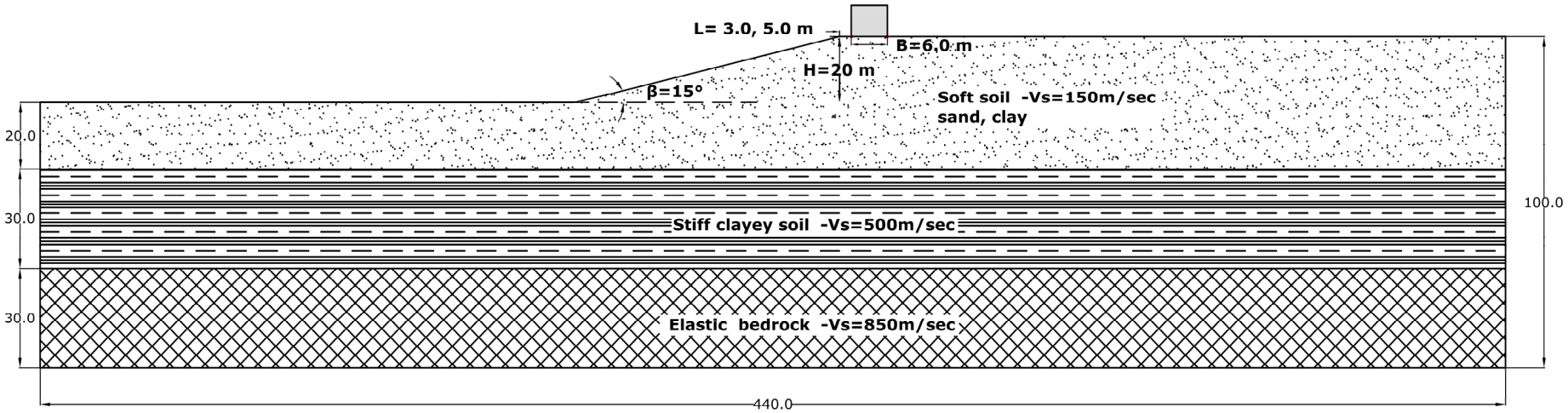


Figure A.3. Slope geometrical configuration 3- Models 9 to 12

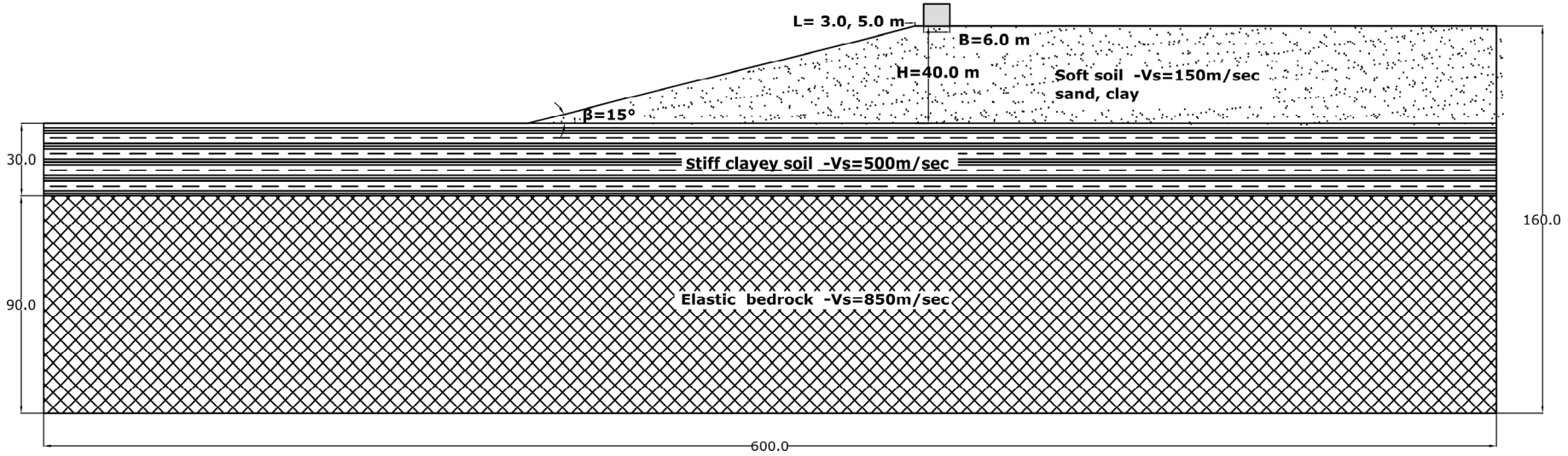


Figure A.4. Slope geometrical configuration 4- Models 13 to 16

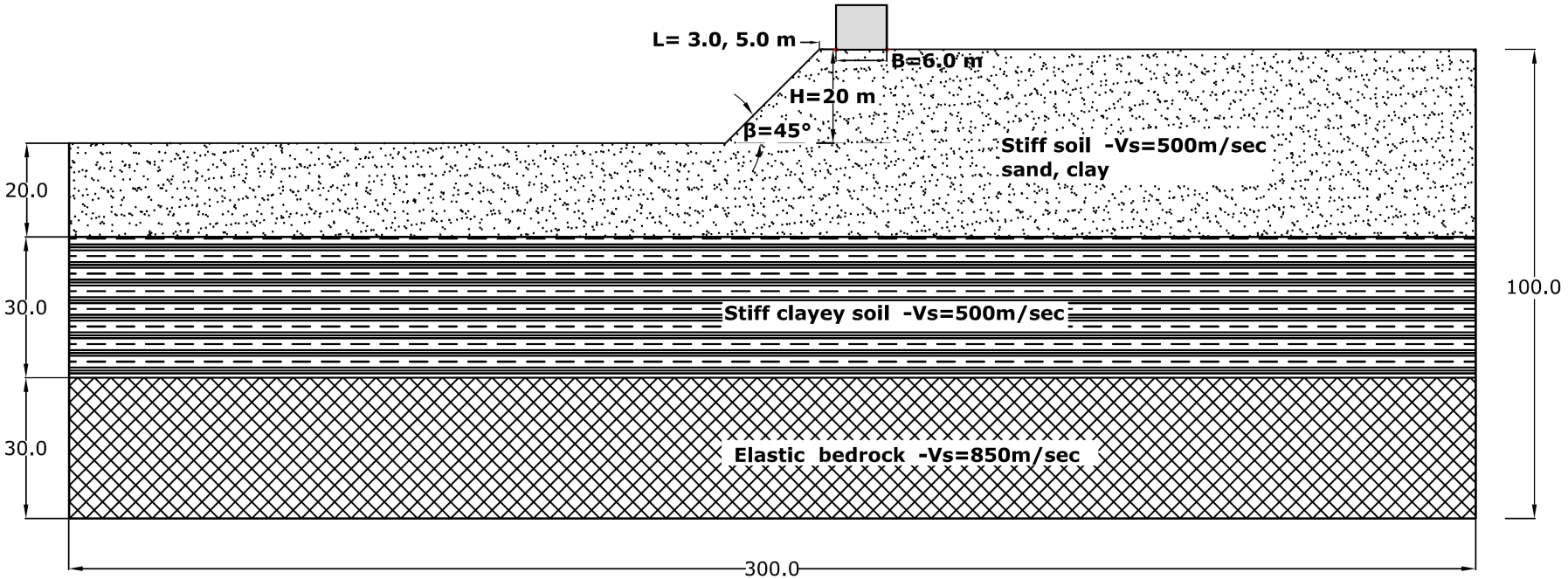


Figure A.5. Slope geometrical configuration 5- Models 17 to 20

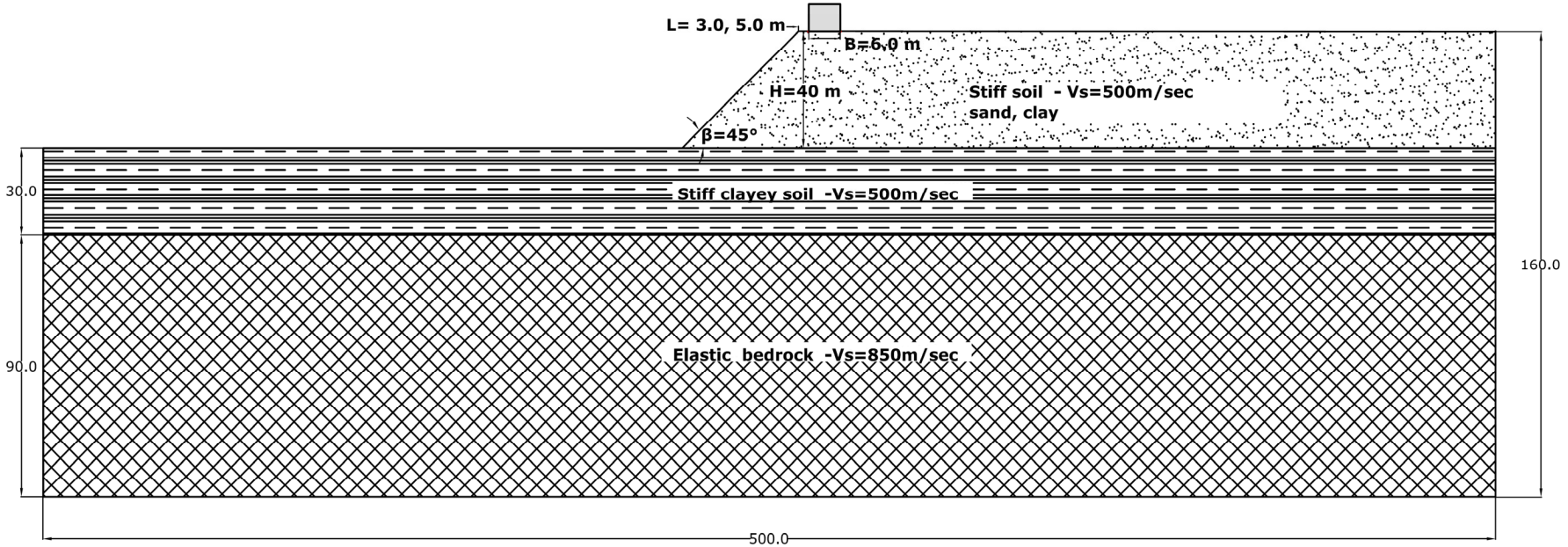


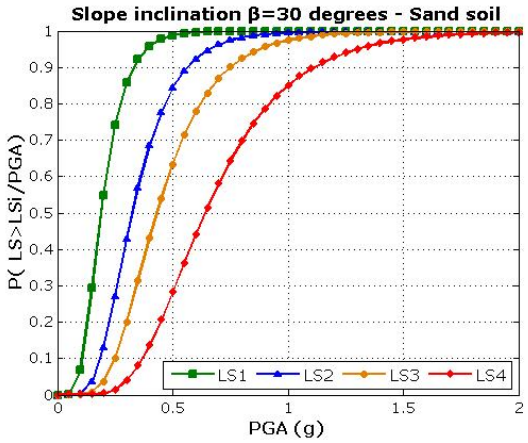
Figure A.6. Slope geometrical configuration 6- Models 21 to 24

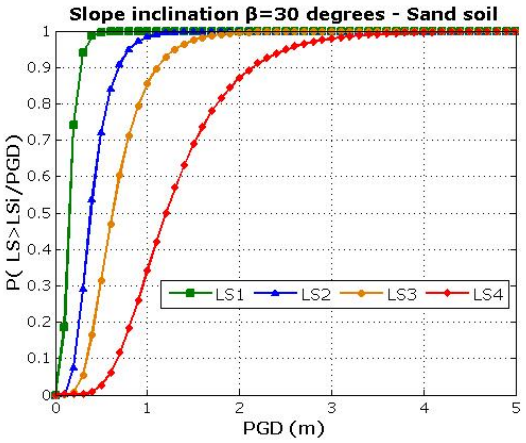
ANNEX B

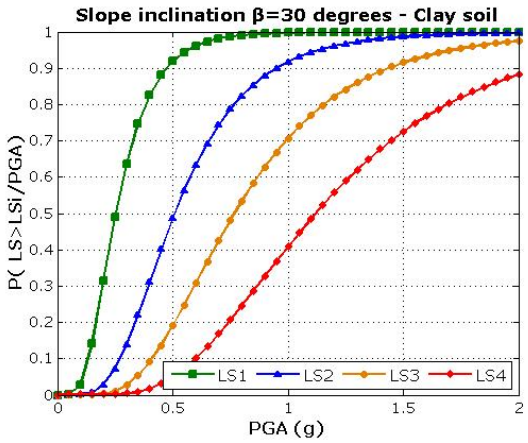
Fragility curves for "low-code" buildings

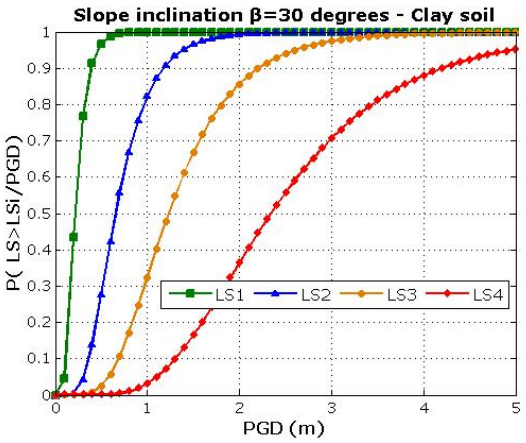
B.1 Proposed curves for "low-code" designed RC buildings

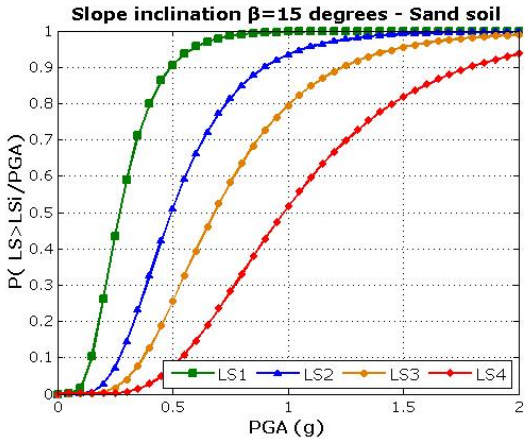
The suggested fragility curves for low-code designed, RC bare frame structures, characterized of a low level of confinement are presented herein (Fig. B.1) based on the analyzed features that proved to be the most influential in assessing the vulnerability of the building to the permanent landslide displacement (see Chapter 6). It is noted that lower limit state values were adopted for "low-code" frame RC building for the exceedance of extensive and complete damages (see Chapter 4, Table 4.6 and Chapter 6, § 6.3.5). Tables B.1 and B.2 present the median and dispersions of the suggested curves when using PGA and PGD as an intensity measure respectively. As expected, the suggested curves for "low-code" buildings are associated to lower median values of PGA and PGD for the exceedance of each limit state and to larger dispersion (represented by the β values) around the median estimates compared to the "high-code" buildings (see Chapter 6, § 6.2.2).

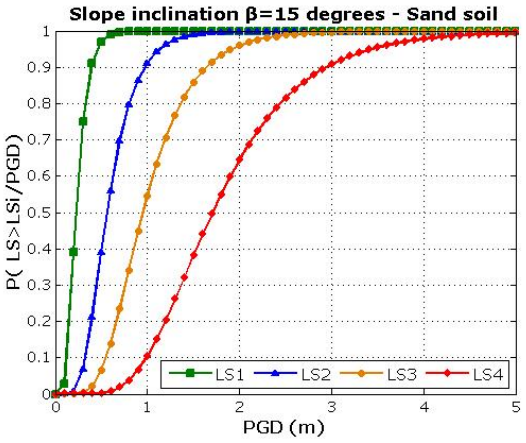

Slope inclination β=30 degrees - Sand soil
P(LS>LSi/PGA)
PGA (g)
LS1
LS2
LS3
LS4

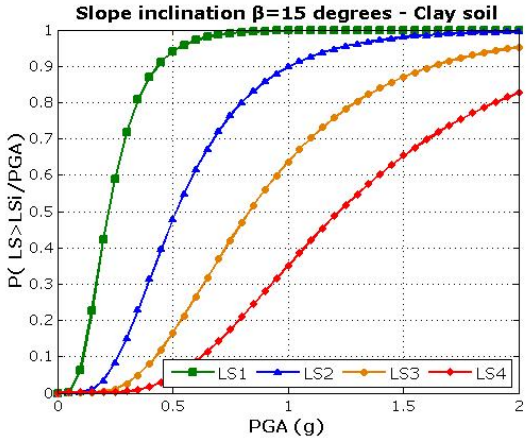

Slope inclination β=30 degrees - Sand soil
P(LS>LSi/PGD)
PGD (m)
LS1
LS2
LS3
LS4

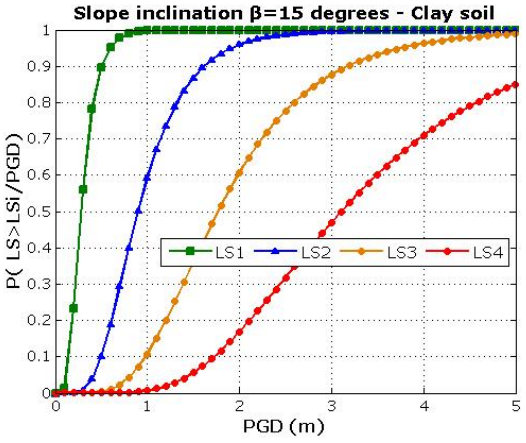

Slope inclination β=30 degrees - Clay soil
P(LS>LSi/PGA)
PGA (g)
LS1
LS2
LS3
LS4


Slope inclination β=30 degrees - Clay soil
P(LS>LSi/PGD)
PGD (m)
LS1
LS2
LS3
LS4


Slope inclination β=15 degrees - Sand soil
P(LS>LSi/PGA)
PGA (g)
LS1
LS2
LS3
LS4


Slope inclination β=15 degrees - Sand soil
P(LS>LSi/PGD)
PGD (m)
LS1
LS2
LS3
LS4


Slope inclination β=15 degrees - Clay soil
P(LS>LSi/PGA)
PGA (g)
LS1
LS2
LS3
LS4


Slope inclination β=15 degrees - Clay soil
P(LS>LSi/PGD)
PGD (m)
LS1
LS2
LS3
LS4

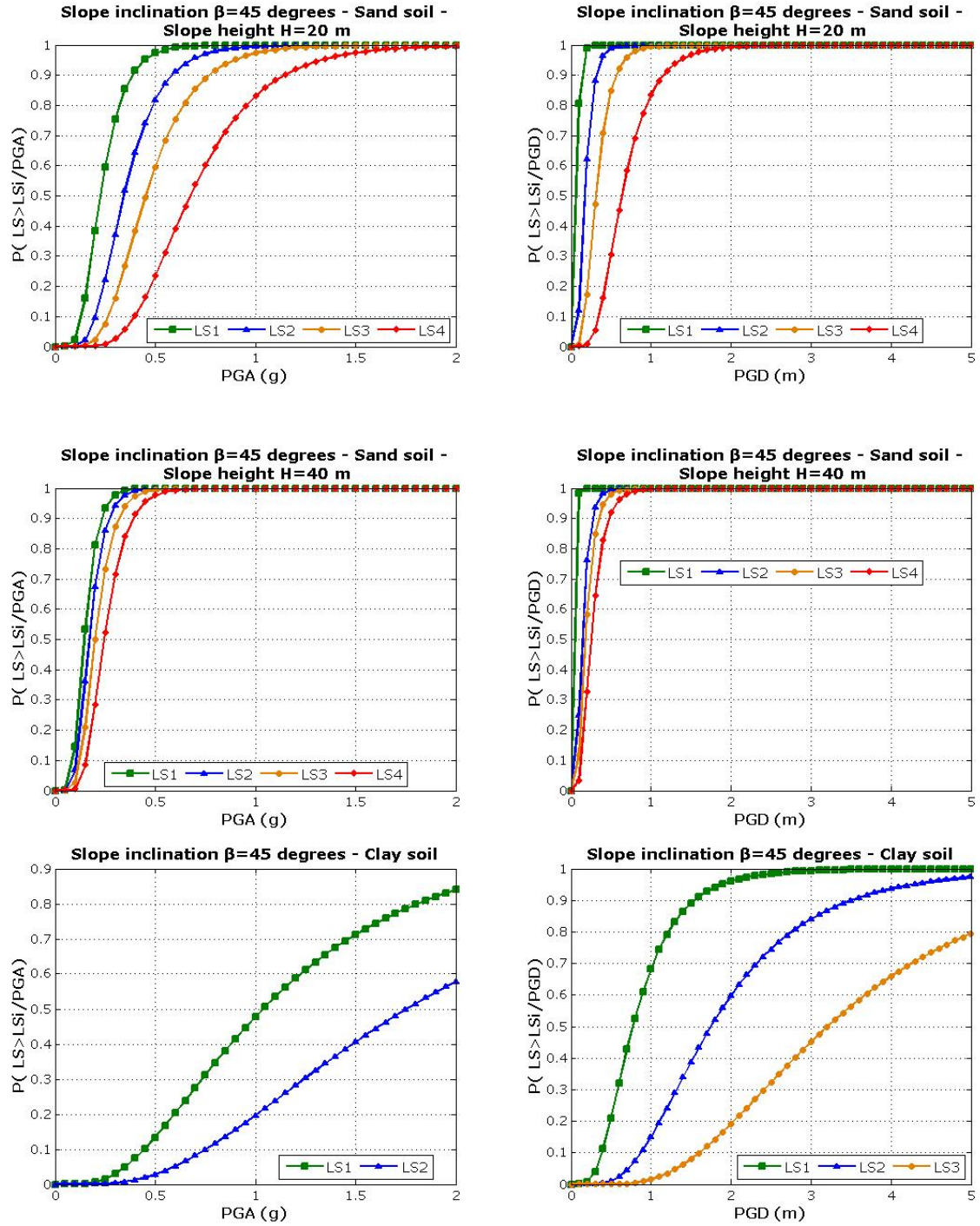


Figure B.1. Proposed fragility curves as a function of PGA (left) and PGD (right) for low-code, low-rise RC frame buildings subjected to permanent landslide displacements

Table B.1. Parameters of the proposed fragility functions using PGA as an intensity measure

Parametric models	Median PGA (g)				Dispersion β
	LS1 (g)	LS2 (g)	LS3 (g)	LS4 (g)	
sand_β30	0.19	0.32	0.43	0.64	0.43
clay_β30	0.25	0.51	0.77	1.12	0.49
sand_β15	0.27	0.49	0.68	0.98	0.47
clay_β15	0.22	0.52	0.83	1.22	0.52
sand_β45_h20	0.23	0.34	0.45	0.67	0.41
sand_β45_h40	0.15	0.17	0.20	0.25	0.36
clay_β45	1.04	1.76	-	-	0.66

Table B.2. Parameters of the proposed fragility functions using PGD as an intensity measure

Parametric models	Median PGD (m)				Dispersion β
	LS1 (m)	LS2 (m)	LS3 (m)	LS4 (m)	
sand_β30	0.15	0.38	0.62	1.20	0.45
clay_β30	0.22	0.66	1.23	2.34	0.43
sand_β15	0.22	0.56	0.95	1.71	0.43
clay_β15	0.28	0.90	1.77	3.11	0.46
sand_β45_h20	0.07	0.17	0.31	0.64	0.47
sand_β45_h40	0.04	0.14	0.18	0.25	0.50
clay_β45	0.77	1.75	3.21	-	0.54

ΕΚΤΕΝΗΣ ΠΕΡΙΛΗΨΗ

Ι.1 Εισαγωγή

Οι κατολισθήσεις που προκαλούνται από σεισμό αποτελούν μια κύριας μορφής απειλή για τον πληθυσμό και το δομημένο περιβάλλον στις περισσότερες ορεινές και ημιορεινές περιοχές του κόσμου. Οι Marano et al. (2010) παρατήρησαν ότι οι κατολισθήσεις αποτελούν την πιο διαδεδομένη και συνάμα την πιο φονική δευτερεύουσα συνέπεια των σεισμών καθώς θεωρούνται υπεύθυνες για το 71.1% των θανάτων από έμμεσες αιτίες πέραν της σεισμικής ταλάντωσης. Για παράδειγμα, ο ισχυρός σεισμός (M_s=8.0) που έλαβε χώρα στο Wenchuan της Κίνας στις 12 Μαΐου 2008 υπολογίζεται ότι ενεργοποίησε περισσότερες από 15000 κατολισθήσεις διαφόρων τύπων που κάλυπταν μια περιοχή 50000 km^2, προκαλώντας το θάνατο περίπου 20000 ανθρώπων και τεράστιες οικονομικές απώλειες (Yin et al., 2009). Υπάρχει επομένως μια αυξανόμενη απαίτηση από την κοινωνία και τους εμπλεκόμενους φορείς για την αποτελεσματική διαχείριση και μείωση της διακινδύνευσης που συνδέεται με τις σεισμικώς προκαλούμενες κατολισθήσεις.

Παρότι οι μέθοδοι ποσοτικής αποτίμησης της διακινδύνευσης είναι αρκετά διαδεδομένες για φυσικούς κινδύνους όπως οι σεισμοί και οι πλημμύρες, στην περίπτωση των κατολισθήσεων, οι μεθοδολογίες ποσοτικής αποτίμησης της διακινδύνευσης δεν έχουν αναπτυχθεί παρά μόνο πολύ πρόσφατα και δεν έχουν εφαρμοστεί ενδελεχώς από την επιστημονική κοινότητα και τους αρμόδιους φορείς. Το γεγονός αυτό μπορεί να αποδοθεί στο ότι διάφορες κρίσιμες συνιστώσες της διακινδύνευσης εμπεριέχουν σημαντικές αβεβαιότητες που καθιστούν δύσκολη την εκτίμησή τους (Corominas και Mavrouli, 2011b). Μεταξύ των συνιστωσών αυτών, η αποτίμηση της τρωτότητας των υπό διακινδύνευση στοιχείων επηρεάζεται από ποικίλες αβεβαιότητες, λόγω της πολυδιάστατης και δυναμικής της φύσης, που δυσχεραίνουν τον αντικειμενικό προσδιορισμό της και καθιστούν προβληματική την ενσωμάτωση της στην εξίσωση της διακινδύνευσης. Λαμβάνοντας υπόψη τα παραπάνω, κύριος στόχος της διδακτορικής διατριβής αποτελεί η πρόταση και ποσοτικοποίηση μιας αναλυτικής μεθοδολογίας για την αποτίμηση της τρωτότητας κτιρίων οπλισμένου σκυροδέματος (Ο/Σ) πλησίον σεισμικώς ασταθών

πρανών. Η αξιοπιστία του αριθμητικού προσομοιώματος επαληθεύεται μέσω της σύγκρισης των μετακινήσεων στην περιοχή του πρανούς που εξάγονται από τις αριθμητικές αναλύσεις με τις αντίστοιχες μετακινήσεις που υπολογίζονται από εμπειρικές μεθόδους εκτίμησης των μετακινήσεων τύπου Newmark. Στο πλαίσιο της διατριβής προτείνονται καμπύλες τρωτότητας για διάφορους τύπους κατασκευής, εδαφικές συνθήκες και γεωμετρίες πρανούς καθώς και αποστάσεις της θεωρούμενης κατασκευής από την πιθανή κατολίσθηση, οι οποίες μπορούν να βρουν άμεση εφαρμογή σε ένα πιθανοτικό πλαίσιο εκτίμησης της διακινδύνευσης λόγω των κατολισθήσεων. Η μεθοδολογία επιβεβαιώνεται μέσω της σύγκρισης αντιπροσωπευτικών αναπτυσσόμενων καμπυλών με σχετικές καμπύλες της βιβλιογραφίας και δεδομένα από βλάβες σε κτίρια λόγω κατολισθητικών φαινομένων στην Ελλάδα και την Ιταλία.

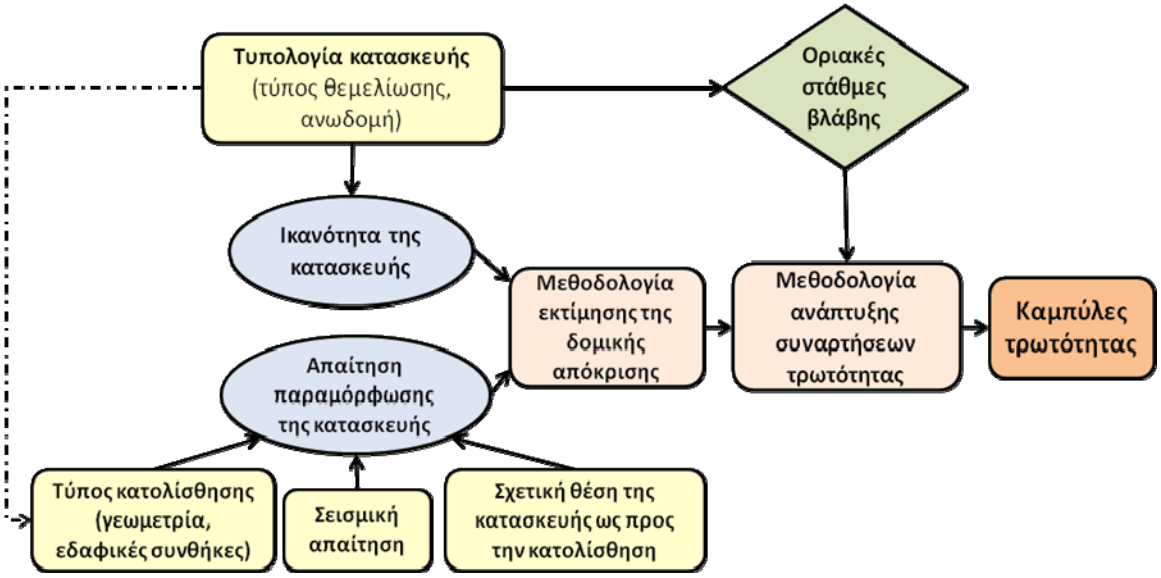
Παραδοσιακά, οι μελέτες αποτίμησης της τρωτότητας των κατασκευών λόγω κατολισθήσεων αλλά και άλλων φυσικών αιτιών αναφέρονται στην αρχική κατασκευή υποθέτοντας ότι αυτή υποβάλλεται σε μια ιδανική, συνεχή πρακτική συντήρησης. Παρόλα αυτά, η πραγματική, δυναμική τρωτότητα των κτιρίων μπορεί να επηρεαστεί σημαντικά από φαινόμενα γήρανσης των υλικών, ανθρωπογενείς δράσεις καθώς και τη συσσωρευτική βλάβη από προηγούμενες κατολισθήσεις ή άλλους φυσικούς κινδύνους. Για να γεφυρωθεί αυτό το κενό, η προτεινόμενη προσέγγιση επεκτείνεται ώστε να λάβει υπόψη της την εξέλιξη της τρωτότητας των κατασκευών στο χρόνο, προτείνοντας χρονικά εξαρτώμενες καμπύλες τρωτότητας για κτίρια Ο/Σ που εκτίθενται σε σεισμικώς προκαλούμενες κατολισθήσεις.

Ι.2 Μεθοδολογία αποτίμησης της τρωτότητας

Η διδακτορική διατριβή επικεντρώνεται στην πρόταση και ποσοτικοποίηση μιας καινοτόμου προσέγγισης για την αποτίμηση της τρωτότητας κτιρίων Ο/Σ που υπόκεινται σε σεισμικώς προκαλούμενες, σχετικά αργές, εδαφικές ολισθήσεις. Η τρωτότητα εκφράζεται μέσω αθροιστικών λογαριθμοκανονικών συναρτήσεων τρωτότητας που περιγράφουν την πιθανότητα υπέρβασης της κάθε οριζόμενης στάθμης βλάβης συναρτήσει μιας ή περισσοτέρων παραμέτρων που χαρακτηρίζουν την ένταση της πιθανής κατολίσθησης.

Το Σχήμα Ι.1 απεικονίζει το γενικό πλαίσιο της προτεινόμενης μεθοδολογίας. Η «ικανότητα» της κατασκευής ορίζεται από την τυπολογία του κτιρίου (τύπος θεμελίωσης και ανωδομής, γεωμετρία, αντοχή υλικών), ενώ η «απαίτηση» περιγράφεται από τη μόνιμη εδαφική παραμόρφωση, η οποία εξαρτάται από τον τύπο της κατολίσθησης (π.χ. αργή εδαφική ολίσθηση), τις εδαφικές συνθήκες και τη σχετική θέση του κτιρίου ως προς την πιθανή ολισθαίνουσα εδαφική μάζα. Σημειώνεται επίσης ότι η σχετική δυσκαμψία εδάφους-θεμελίωσης-ανωδομής μπορεί να επηρεάσει σημαντικά την απαίτηση

παραμόρφωσης για την κατασκευή. Οι δύο αυτές συνιστώσες (ικανότητα της κατασκευής και απαίτηση παραμόρφωσης) συνδυάζονται κατάλληλα ώστε να προκύψει η μεθοδολογία εκτίμησης της απόκρισης, η οποία αποτελεί την τρίτη κύρια συνιστώσα. Τα δεδομένα της απόκρισης σε επίπεδο παραμορφώσεων χρησιμοποιούνται στη συνέχεια για την ανάπτυξη των καμπυλών τρωτότητας. Είναι επίσης απαραίτητο να καθοριστούν οριακές στάθμες βλάβης με βάση την τυπολογία και τα δομικά χαρακτηριστικά της κατασκευής, εμπειρικά κριτήρια και την έμπειρη κρίση των ειδικών ώστε να είναι δυνατή η ανάπτυξη καμπυλών τρωτότητας για διαφορετικές στάθμες βλάβης. Τέλος, ακολουθεί η μεθοδολογία ανάπτυξης των πιθανοτικών συναρτήσεων τρωτότητας.



Σχήμα Ι.1. Διάγραμμα ροής της προτεινόμενης μεθοδολογίας για την εκτίμηση της τρωτότητας κτιρίων οπλισμένου σκυροδέματος

Στις επόμενες παραγράφους ακολουθεί μια πιο λεπτομερής περιγραφή των θεμελιωδών χαρακτηριστικών της προτεινόμενης μεθοδολογίας.

Ο τύπος της κατολίσθησης (καταπτώσεις βράχου, ροή φερτών, εδαφική ολίσθηση κτλ.) αποτελεί μια κρίσιμη παράμετρο της μεθοδολογίας, δεδομένου ότι κατολισθήσεις διαφορετικού τύπου και μεγέθους, απαιτούν συνήθως διαφορετικές και συμπληρωματικές μεθόδους για την εκτίμηση της τρωτότητας των υπό διακινδύνευση στοιχείων. Η βλάβη που προκαλείται από μια αργή εδαφική ολίσθηση σε ένα τυπικό κτίριο μπορεί να αποδοθεί κατά κύριο λόγο στην συσσωρευτική μόνιμη (ολική ή διαφορική) εδαφική μετακίνηση και εστιάζεται εντός της ασταθούς περιοχής του πρανούς (Mansour et al., 2011). Στην παρούσα εργασία μελετάται μια σχετικά αργή εδαφική ολίσθηση που παράγει καμπτικές ρηγματώσεις λόγω της διαφορικής μετακίνησης σε ένα κτίριο Ο/Σ που υπόκειται στον κίνδυνο κατολίσθησης.

Τα χαρακτηριστικά του σεισμού (πλάτος, συχνοτικό περιεχόμενο και διάρκεια) σε σχέση τα δυναμικά χαρακτηριστικά του εδάφους και τη στρωματογραφία μπορούν να επηρεάσουν σημαντικά την απαίτηση παραμόρφωσης της κατασκευής. Η μη-γραμμικότητα του εδάφους, η ικανότητα απόσβεσης του υλικού, η σχετική δυσκαμψία των εδαφικών αποθέσεων και του υποκείμενου υποβάθρου αποτελούν τους κύριους παράγοντες για ενίσχυση ή απομείωση της σεισμικής κίνησης (Kramer και Stewart, 2004; Pitilakis, 2010). Η πιθανότητα αστοχίας του πρανούς είναι γενικά μεγαλύτερη για χαμηλόσυχνους σεισμικούς κραδασμούς συνδυαζόμενους με φαινόμενα συντονισμού σε χαμηλές συχνότητες (Bourdeau et al., 2004).

Η θέση της κατασκευής σε σχέση με την κατολίσθηση είναι επίσης ένας καθοριστικός παράγοντας. Η επίδραση της τοπογραφίας μπορεί να μεταβάλλει το πλάτος και το συχνοτικό περιεχόμενο των ασκούμενων σεισμικών διεγέρσεων (Bouckovalas and Papadimitriou, 2005; Ktenidou, 2010). Επιπλέον, η αλληλεπίδραση εδάφους-κατασκευής λόγω της παρουσίας της κατασκευής κοντά στη στέψη του πρανούς μπορεί να συμβάλλει περαιτέρω στη μεταβολή της σεισμική απόκρισης πλησίον αυτού σε σχέση με την περίπτωση του ελευθέρου πεδίου (Assimaki and Kausel, 2007; D. Pitilakis and Tsinaris, 2010). Στην παρούσα εργασία μελετούνται κτίρια Ο/Σ διαφορετικής δυσκαμψίας τοποθετημένα κοντά στη στέψη του πρανούς, όπου η τοπογραφική επιρροή είναι γενικά ενισχυμένη.

Η τυπολογία της κατασκευής (π.χ. γεωμετρία, αριθμός των ορόφων, ιδιότητες των υλικών, το επίπεδο σχεδιασμού, τα χαρακτηριστικά της θεμελίωσης κλπ.) αποτελεί επίσης ένα βασικό παράγοντα. Η απόκριση στην διαφορική (και ολική) μόνιμη εδαφική μετακίνηση εξαρτάται πρωτίστως από τον τύπο της θεμελίωσης. Ένα κτίριο θεμελιωμένο σε πασσάλους είναι γενικά λιγότερο τρωτό σε σχέση με ένα κτίριο σε μια επιφανειακή θεμελίωση. Αναφορικά με τα επιφανειακά συστήματα θεμελίωσης, μια άκαμπτη θεμελίωση (π.χ. μια γενική κοιτόστρωση) παρουσιάζει μειωμένη τρωτότητα σε σχέση με μια εύκαμπτη (π.χ. μεμονωμένα πέδιλα). Όταν το σύστημα θεμελίωσης είναι άκαμπτο, το κτίριο αναμένεται να στραφεί ως στερεό σώμα και οι αναμενόμενες βλάβες μπορούν να αποδοθούν κυρίως σε απώλεια λειτουργικότητας. Οι στάθμες βλαβών ορίζονται εμπειρικά, καθότι υπάρχει περιορισμένη απαίτηση δομικής βλάβης στα μέλη του κτιρίου. Αντιθέτως, όταν το σύστημα θεμελίωσης είναι εύκαμπτο, η διαφορική μετακίνηση λόγω της κατολισθαίνουσας εδαφικής μάζας μπορεί να προκαλέσει δομική βλάβη στην κατασκευή (Bird et al., 2005; 2006). Οι στάθμες βλάβης μπορούν να κατηγοριοποιηθούν στην περίπτωση αυτή με τρόπο ανάλογο των σταθμών που χαρακτηρίζουν τις δομικές βλάβες, που οφείλονται σε σεισμική ταλάντωση.

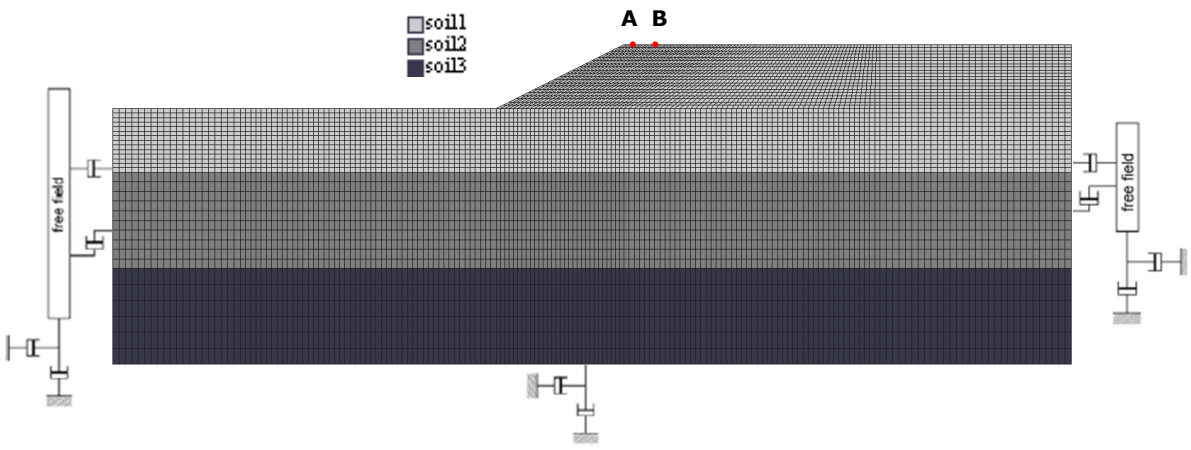
Η μεθοδολογία εκτίμησης της απόκρισης περιλαμβάνει δύο βήματα από πλευράς αριθμητικών αναλύσεων. Αρχικά, πραγματοποιείται ανελαστική σεισμική ανάλυση του

συστήματος πρανούς - θεμελίωσης κάνοντας μια απλοποιημένη θεώρηση για την ανωδομή, χρησιμοποιώντας τον κώδικα πεπερασμένων διαφορών FLAC2D (Itasca, 2008). Το έδαφος (αμμώδες ή αργιλικό) υπακούει σε ελαστοπλαστικό καταστατικό νόμο συμπεριφοράς με κριτήριο αστοχίας Mohr-Coulomb ενώ το «σεισμικό υπόβαθρο» ακολουθεί το νόμο της γραμμικής ελαστικότητας. Η προσομοίωση γίνεται με 4κόμβα στοιχεία επίπεδης παραμόρφωσης. Η διακριτοποίηση επιτρέπει τη διάδοση των σεισμικών κυμάτων έως τη συχνότητα των 10 Hz. Για την ελαχιστοποίηση των ανακλάσεων των κυμάτων στα πλευρικά όρια και στη βάση του προσομοιώματος χρησιμοποιούνται κατάλληλες συνοριακές συνθήκες «ελευθέρου πεδίου» (free field) και «διαφανών ορίων» (quiet boundaries) αντιστοίχως.

Η προσομοίωση της θεωρούμενης κατασκευής οπλισμένου σκυροδέματος πλησίον της στέψης του πρανούς εξαρτάται από τη δυσκαμψία της θεμελίωσης. Εξετάζονται δύο περιπτώσεις:

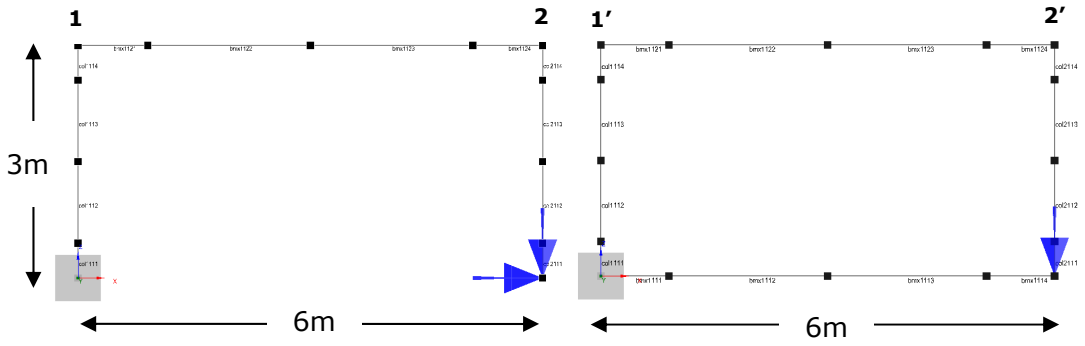
- μία εύκαμπτη θεμελίωση (π.χ. περίπτωση μεμονωμένων πεδίλων) όπου η προσομοίωση του συστήματος θεμελίωσης - ανωδομής επιτυγχάνεται μέσω της θεώρησης συγκεντρωμένων φορτίσεων στις απολήξεις των θεωρούμενων στύλων και

- μία δύσκαμπτη θεμελίωση που η προσομοίωση επιτυγχάνεται μέσω μιας συνεχούς παραμορφώσιμης ελαστικής δοκού υποβαλλόμενη σε ομοιόμορφα κατανεμημένη φόρτιση που συνδέεται με το υποκείμενο έδαφος με χρήση κατάλληλων στοιχείων διεπιφάνειας. Ένα τυπικό δισδιάστατο αριθμητικό προσομοίωμα δίδεται στο Σχήμα Ι.2. Κατάλληλα διορθωμένες, κλιμακούμενες σεισμικές διεγέρσεις ποικίλων χαρακτηριστικών (συχνοτικού περιεχομένου και διάρκειας) που έχουν καταγραφεί σε επιφανειακή εμφάνιση βράχου, εισάγονται στη βάση του αριθμητικού προσομοιώματος. Αποτέλεσμα της ανάλυσης αποτελεί η εκτίμηση της απαίτησης μόνιμης διαφορικής μετακίνησης στην κατασκευή, στο επίπεδο της θεμελίωσης, λόγω της σεισμικώς ασταθούς εδαφικής μάζας.



Σχήμα Ι.2. Τυπικό δισδιάστατο αριθμητικό προσομοίωμα που χρησιμοποιείται για την ανελαστική σεισμική ανάλυση

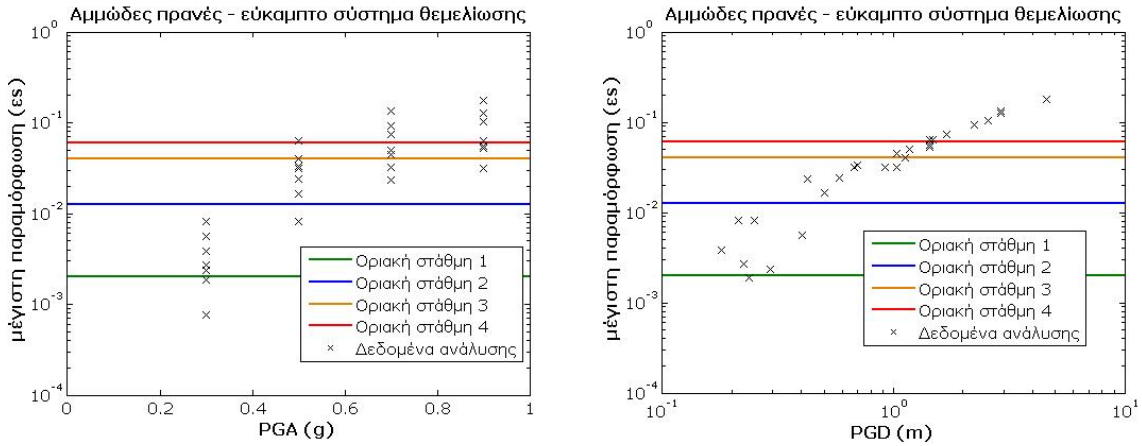
Στη συνέχεια, η προαναφερθείσα απαίτηση διαφορικής μετακίνησης συναρτήσει του χρόνου εισάγεται στη βάση ενός μη-γραμμικού προσομοιώματος της κατασκευής ως καταναγκασμός, ώστε να εκτιμηθεί η αναμενόμενη απόκρισή της. Διερευνώνται επαρκώς αντιπροσωπευτικά πλαισιακά κτίρια Ο/Σ χαμηλού ύψους χωρίς τοιχοπληρώσεις με εύκαμπτο και δύσκαμπτο σύστημα θεμελίωσης, για την ανάλυση των οποίων χρησιμοποιείται το πρόγραμμα πεπερασμένων στοιχείων Seismostruct (Seismostruct, Seismosoft 2011) (Σχ. Ι.3). Συγκεκριμένα, η ανάλυση που πραγματοποιείται είναι ψευδοστατική θεωρώντας ανελαστική τη συμπεριφορά των υλικών της κατασκευής υπό τη μορφή ινών (fibers). Για κάθε ανάλυση, εξάγεται τελικά η μέγιστη απόκριση της κατασκευής σε επίπεδο τοπικής παραμόρφωσης (που αποτελεί και το δείκτη βλάβης). Αξίζει να σημειωθεί ότι η συγκεκριμένη μέθοδος στηρίζεται στην υπόθεση ότι οι βλάβες στην κατασκευή είναι αποτέλεσμα μόνο της εδαφικής αστοχίας και όχι συνδυασμός αυτής με την εδαφική ανακυκλική φόρτιση. Έτσι, η κατασκευή δεν υποβάλλεται σε κάποια αρχική απομείωση της αντοχής ή της δυσκαμψίας της λόγω της επίδρασης της εδαφικής ταλάντωσης.



Σχήμα Ι.3. Αντιπροσωπευτικά πλαισιακά κτίρια Ο/Σ χαμηλού ύψους με εύκαμπτο και δύσκαμπτο σύστημα θεμελίωσης και περιγραφή της φόρτισης κινηματικού τύπου για τη διεξαγωγή της μη-γραμμικής, ψευδοστατικής ανάλυσης

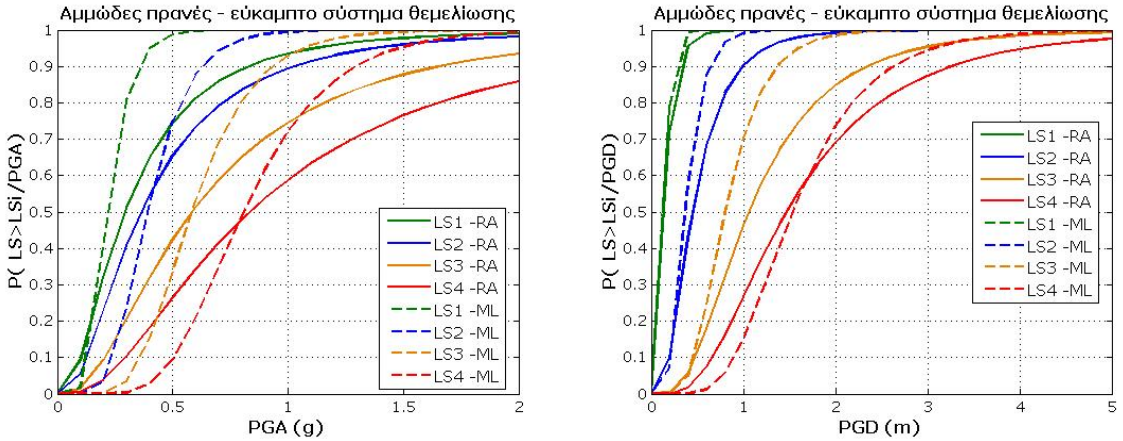
Οι οριακές στάθμες βλάβης για μικρές (Limit state 1), μέτριες (Limit state 2), εκτενείς (Limit state 3) βλάβες και ολική κατάρρευση (Limit state 4) ορίζονται με βάση οριακές τιμές παραμορφώσεων των υλικών του Ο/Σ (Crowley et al., 2004; Bird et al., 2005), ανάλογα με την ποιότητα και τα χαρακτηριστικά της κατασκευής. Στο Σχήμα Ι.4 παρουσιάζονται τυπικά διαγράμματα εξέλιξης της βλάβης σε όρους μέγιστης παραμόρφωσης συναρτήσει της μέγιστης εδαφικής επιτάχυνσης (PGA) και της μόνιμης εδαφικής μετακίνησης (PGD) αντιστοίχως για ένα πλαισιακό κτίριο Ο/Σ χαμηλού ύψους σχεδιασμένου βάσει σύγχρονου κανονισμού (ΕΑΚ, 2000) με εύκαμπτο σύστημα θεμελίωσης, τοποθετημένο πλησίον της στέψης ενός αμμώδους εν δυνάμει ασταθούς πρανούς. Στο σχήμα απεικονίζονται επίσης οι οριακές τιμές της παραμόρφωσης του χάλυβα του οπλισμού για κάθε στάθμη βλάβης. Τέλος, οι καμπύλες τρωτότητας συναρτήσει της μέγιστης εδαφικής επιτάχυνσης στο βράχο (PGA) ή της παραμένουσας

εδαφικής μετακίνησης (PGD) για τις διάφορες στάθμες βλάβης, παράγονται μετά από κατάλληλη μέθοδο στατιστικής επεξεργασίας της απόκρισης (σε επίπεδο τοπικών παραμορφώσεων), σε σχέση με την παράμετρο της έντασης της κατολίσθησης (PGA ή PGD) και τις οριζόμενες στάθμες βλάβης. Στην πιθανοτική προσέγγιση που προτείνεται, λαμβάνονται υπόψη διάφορες αβεβαιότητες που σχετίζονται με την ικανότητα της κατασκευής, τον ορισμό των σταθμών βλάβης και την απαίτηση παραμόρφωσης.



Σχήμα Ι.4. Μέγιστες τιμές αναπτυχθείσας παραμόρφωσης συναρτήσει της PGA (αριστερά) και PGD (δεξιά) για ένα πλαισιακό κτίριο Ο/Σ χαμηλού ύψους σχεδιασμένου βάσει σύγχρονου κανονισμού με εύκαμπτο σύστημα θεμελίωσης, τοποθετημένο εγγύς της στέψης ενός αμμώδους πρανούς

Δύο διαφορετικές μέθοδοι εφαρμόζονται για τον προσδιορισμό των λογαριθμοκανονικών παραμέτρων (διάμεσος και διασπορά) των καμπυλών τρωτότητας ώστε να διερευνηθεί η επιρροή της επιστημικής (epistemic) αβεβαιότητας στην εκτίμηση της τρωτότητας. Αυτές βασίζονται στη μέθοδο της παλινδρόμησης (regression analysis method) (e.g. Nielson και DesRoches, 2007; Argyroudis και Pitilakis, 2012) και στη μέθοδο της μέγιστης πιθανοφάνειας (maximum likelihood method) (e.g. Shinozuka et al., 2000; 2003).



Σχήμα Ι.5. Συγκριτική παρουσίαση τυπικών καμπυλών τρωτότητας συναρτήσει της PGA (αριστερά) και PGD (δεξιά) με βάση την μέθοδο της παλινδρόμησης (RA) και την μέθοδο της μέγιστης πιθανοφάνειας (ML)

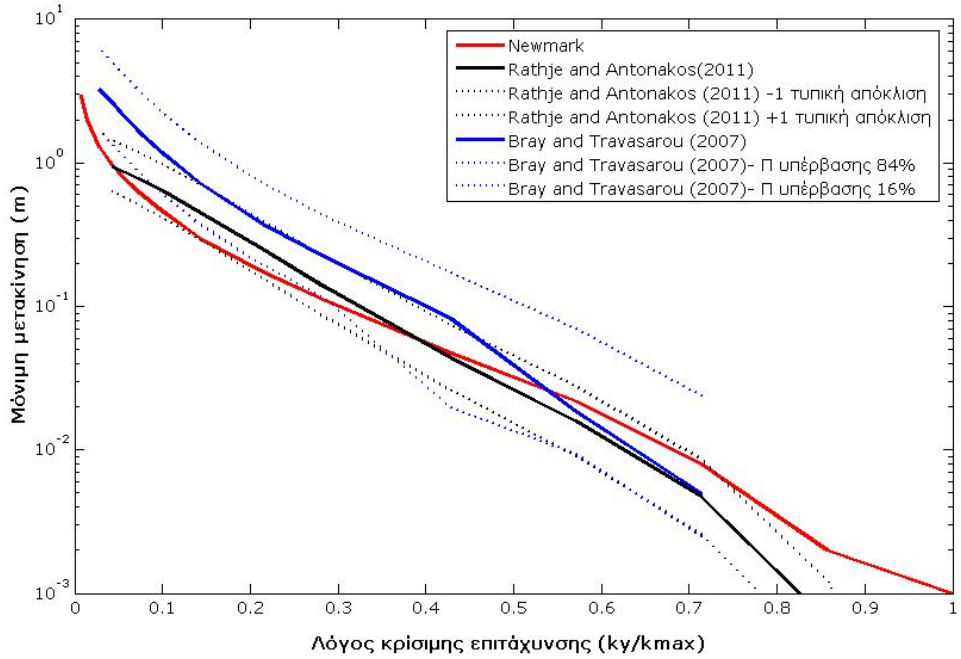
Στο σχήμα Ι.5 δίδονται τυπικές καμπύλες τρωτότητας συναρτήσει της PGA (αριστερά) και PGD (δεξιά) με βάση την μέθοδο της παλινδρόμησης (RA) και την μέθοδο της μέγιστης πιθανοφάνειας (ML). Οι δύο μέθοδοι εκτιμούν διάμεσες τιμές σε όρους PGA και PGD που βρίσκονται γενικά σε αρκετά καλή συμφωνία. Οι υπολογισθείσες τιμές της διασποράς β είναι συμβατές στις δύο μεθόδους όταν χρησιμοποιείται η PGD ως παράμετρος της έντασης της κατολίσθησης, ενώ είναι αρκετά διαφορετική όταν χρησιμοποιείται η PGA. Πιο συγκεκριμένα, διαπιστώνεται ότι η μέθοδος της μέγιστης πιθανοφάνειας εκτιμά σε γενικές γραμμές μικρότερη διασπορά β για το ίδιο δείγμα δεδομένων που προέκυψε από την αριθμητική ανάλυση.

Ι.3 Εμπειρικές μέθοδοι εκτίμησης των μόνιμων μετακινήσεων: Συγκρίσεις με τα αποτελέσματα των μη-γραμμικών, δυναμικών αναλύσεων

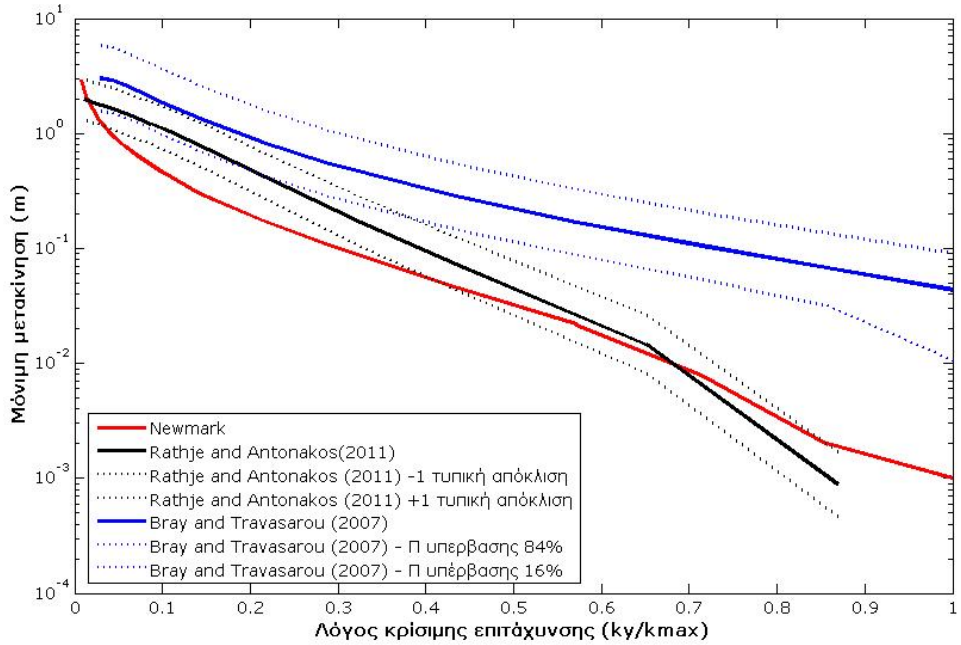
Σε μια μελέτη αποτίμησης της διακινδύνευσης λόγω πιθανής κατολίσθησης, η έκταση των παραμενουσών εδαφικών μετακινήσεων και όχι απλώς η εκτίμηση της πιθανότητας εμφάνισης της κατολίσθησης αποτελεί τον πρωταρχικό παράγοντα που ενδέχεται να οδηγήσει σε καταπόνηση και πιθανή βλάβη σε κτίρια και υποδομές. Στην παρούσα ενότητα αρχικά παρουσιάζονται και συγκρίνονται τρεις διαφορετικές εμπειρικές μέθοδοι εκτίμησης των μόνιμων σεισμικών μετατοπίσεων των φυσικών πρανών: το συμβατικό αναλυτικό μοντέλο άκαμπτου στερεού σώματος (rigid block) του Newmark (1965), το ασύζευκτο (decoupled) μοντέλο των Rathje και Antonakos (2011) και το συζευγμένο (coupled) μοντέλο των Bray και Travasarou (2007), έτσι ώστε να εκτιμηθεί η σχετική ικανότητά τους να προβλέπουν τις αναμενόμενες σεισμικές μετακινήσεις των πρανών για διαφορετικά σεισμικά σενάρια.

Τα αποτελέσματα επιδεικνύουν τον πολύ σημαντικό ρόλο του πλάτους και του συχνοτικού περιεχομένου του σεισμού καθώς και της ενδοσιμότητας της επιφάνειας ολίσθησης στην εκτίμηση των μετακινήσεων. Το μοντέλο των Bray και Travasarou εκτιμά μεγαλύτερες μετακινήσεις σε σχέση με αυτά του Newmark και των Rathje και Antonakos. Συγκεκριμένα, η διαφοροποίηση στην προβλεπόμενη μετακίνηση είναι πιο εμφανής για την περίπτωση της σχετικά εύκαμπτης (T_s=0.16sec) συγκρινόμενη με την σχεδόν άκαμπτη (T_s=0.032sec) ολισθαίνουσα εδαφική μάζα. Οι μετακινήσεις που υπολογίζονται χρησιμοποιώντας τις σχέσεις των Rathje και Antonakos είναι περισσότερο συμβατές με αυτές του Newmark ιδιαίτερα στην περίπτωση ενός χαμηλού πλάτους, υψίσυχνου σεισμικού κραδασμού. Στα Σχήματα Ι.6 και Ι.7 παρουσιάζονται ενδεικτικά συγκριτικά διαγράμματα όπου εκτιμώνται οι παραμένουσες σεισμικές μετακινήσεις των πρανών με τις τρεις μεθόδους για διάφορες τιμές του λόγου της κρίσιμης (k_y) προς τη μέγιστη

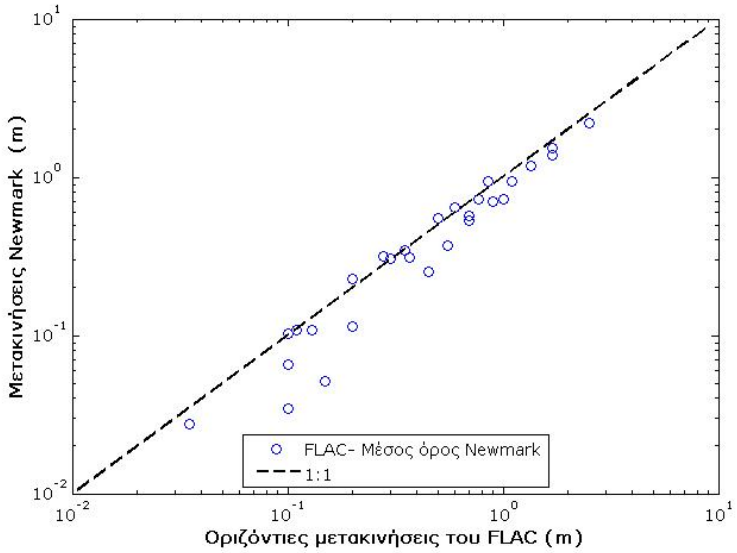
επιτάχυνση (k_{max}), για ένα δεδομένο σεισμικό σενάριο (σεισμός «Pacoima» κλιμακούμενος στα 0.7g), για την περίπτωση μιας παραμορφώσιμης (T_s=0.16sec) και μιας άκαμπτης (T_s=0.032sec) ολισθαίνουσας εδαφικής μάζας αντιστοίχως.

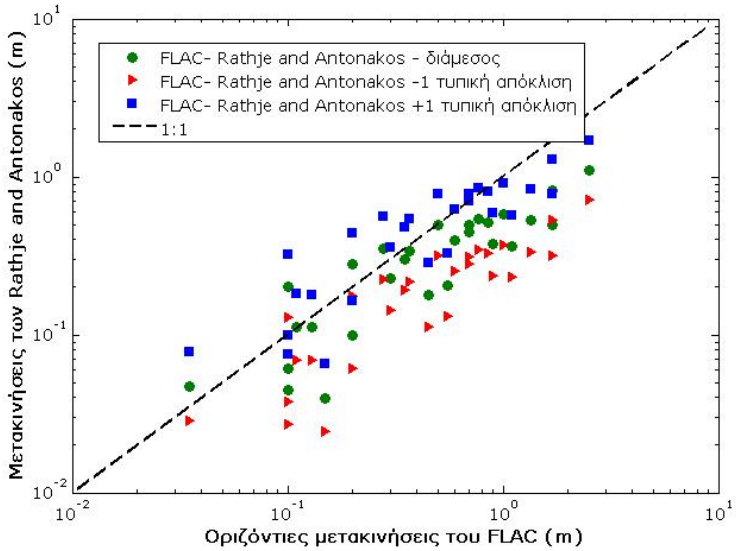


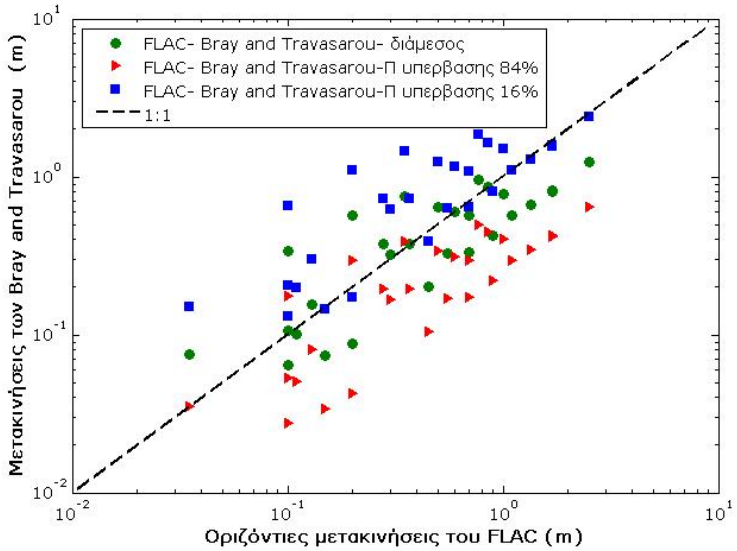
Σχήμα Ι.6. Συγκριτική παρουσίαση των διαφορετικών μοντέλων για την εκτίμηση των σεισμικών μετακινήσεων των πρανών θεωρώντας μια άκαμπτη ολισθαίνουσα εδαφική μάζα (T_s=0.032 sec)



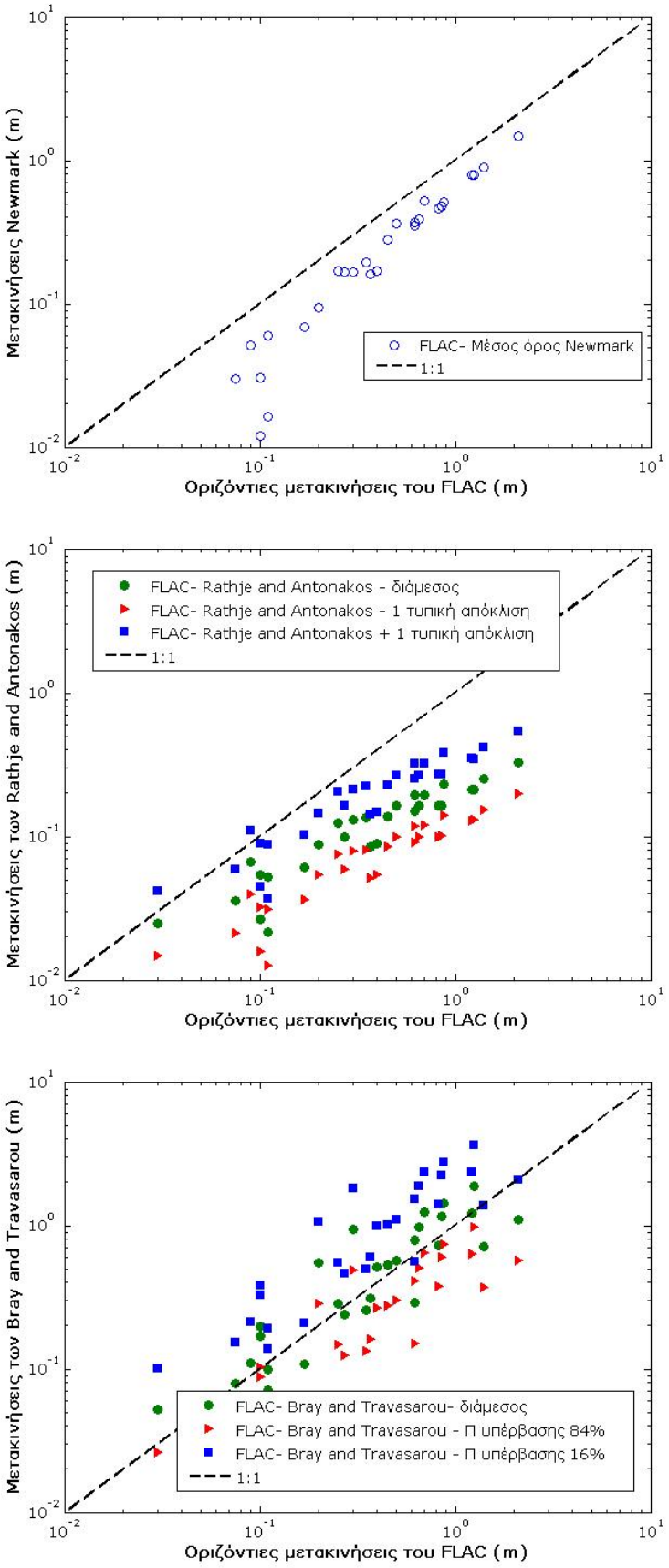
Σχήμα Ι.7. Συγκριτική παρουσίαση των διαφορετικών μοντέλων για την εκτίμηση των σεισμικών μετακινήσεων των πρανών θεωρώντας μια παραμορφώσιμη ολισθαίνουσα εδαφική μάζα (T_s=0.16 sec)







Σχήμα Ι.8. Σύγκριση των μετακινήσεων των Newmark's, Rathje και Antonakos (2011) και Bray και Travasarou (2007 με τις παραμένουσες σεισμικές μετακινήσεις των μη-γραμμικών δυναμικών αναλύσεων για την περίπτωση ενός δύσκαμπτου αμμώδους πρανούς



Σχήμα Ι.9. Σύγκριση των μετακινήσεων των Newmark's, Rathje και Antonakos (2011) και Bray και Travasarou (2007 με τις παραμένουσες σεισμικές μετακινήσεις των μη-γραμμικών δυναμικών αναλύσεων για την περίπτωση ενός εύκαμπτου αργιλώδους πρανούς

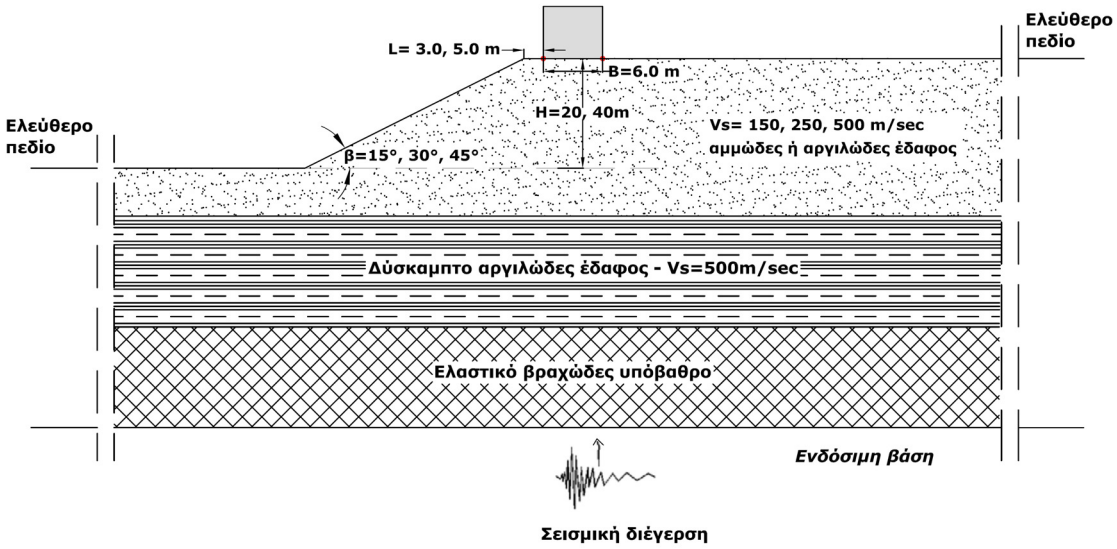
Επιπλέον, οι μετακινήσεις στην περιοχή του πρανούς για συνθήκες ελεύθερου πεδίου (δηλ. χωρίς την παρουσία κάποιας κατασκευής στην κορυφή του) που προέκυψαν από τις μη-γραμμικές, δυναμικές αναλύσεις στην προηγούμενη ενότητα συγκρίνονται με τις αντίστοιχες μετακινήσεις που υπολογίζονται από τα τρία εμπειρικά μοντέλα τύπου Newmark ώστε να ελεγχθεί η αξιοπιστία των αριθμητικών προσομοιωμάτων αλλά και να αξιολογηθεί η ικανότητα των τριών μοντέλων να εκτιμούν μόνιμες μετατοπίσεις πρανών σε σχέση με την αριθμητική ανάλυση. Τα αποτελέσματα των αριθμητικών αναλύσεων, εξαγόμενα σε όρους μόνιμων οριζόντιων μετακινήσεων στην θεωρούμενη επιφάνεια ολίσθησης, βρίσκονται γενικά σε καλή συμφωνία με αυτά των τριών εμπειρικών μοντέλων για την περίπτωση του εξετασθέντος αμμώδους πρανούς (Σχ. Ι.8). Αντιθέτως, η συσχέτιση δεν είναι ικανοποιητική για την περίπτωση του μελετηθέντος πιο εύκαμπτου πρανούς σε αργιλικό έδαφος (Σχ. Ι.9). Ειδικότερα, το μοντέλο των Bray και Travasarou (2007) τείνει να προβλέπει μεγαλύτερες τιμές μετακινήσεων σε σχέση με αυτές της αριθμητικής ανάλυσης ενώ τα μοντέλα του Newmark και των Rathje και Antonakos (2011) υποεκτιμούν τις αντίστοιχες μετακινήσεις. Μεταξύ των τριών μοντέλων, αυτό των Bray και Travasarou παρουσιάζει το ελάχιστο μέσο σφάλμα στην εκτίμηση των μετακινήσεων σε σχέση με τα αποτελέσματα της δυναμικής ανάλυσης και για τις δύο περιπτώσεις εδαφικών πρανών (σε αμμώδες και αργιλικό έδαφος). Η αναλυτική προσέγγιση του Newmark επιδεικνύει ωστόσο την μικρότερη διασπορά στο σφάλμα εκτίμησης των μετακινήσεων συγκρινόμενη με τις μεθόδους των Bray και Travasarou και των Rathje και Antonakos. Συνολικά, η διαφοροποίηση στην εκτίμηση των μετακινήσεων είναι μεγαλύτερη για τη πιο εύκαμπτη ολισθαίνουσα μάζα αποτελούμενη από αργιλικό έδαφος.

Ι.4 Καμπύλες τρωτότητας κτιρίων Ο/Σ σε κατολισθαίνοντα πρανή

Κύριος στόχος της παρούσας ενότητας αποτελεί η πρόταση γενικευμένων καμπυλών τρωτότητας για χαμηλού ύψους, πλαισιακά κτίρια Ο/Σ, τοποθετημένα πλησίον της στέψης σεισμικώς ασταθών πρανών σύμφωνα με τη μεθοδολογία που αναπτύχθηκε στην Ενότητα Ι.2. Οι καμπύλες αυτές μπορούν να έχουν εφαρμογή στην εκτίμηση της σεισμικής τρωτότητας και της σεισμικής διακινδύνευσης κτιρίων Ο/Σ σε κατολισθαίνοντα πρανή σε διάφορες μελέτες περίπτωσης για διάφορες κλίμακες.

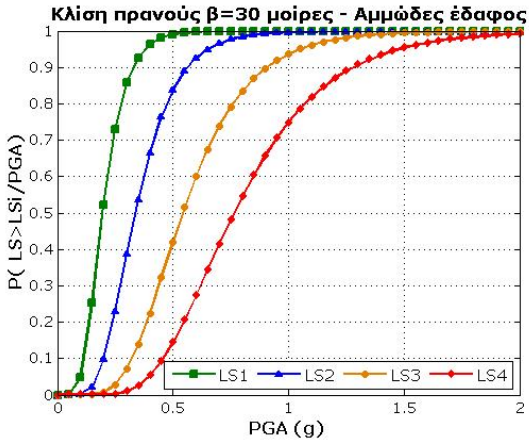
Εξετάζονται μονώροφα πλαισιακά κτίρια Ο/Σ θεμελιωμένα σε διαφορετικά εδάφη (αμμώδη, αργιλικά), για διάφορες κλίσεις (15^o, 30^o, 45^o) και ύψη (20m, 40m) πρανούς καθώς και αποστάσεις της κατασκευής από τη στέψη (3m, 5m) ώστε να διαπιστωθεί η επιρροή των διάφορων παραμέτρων στην απόκριση και τελικά στην τρωτότητα της κατασκευής. Στο Σχήμα Ι.10 παρουσιάζεται ένα σκαρίφημα του βασικού παραμετρικού μοντέλου. Σημειώνεται ότι οι ιδιότητες των εδαφών που εξετάστηκαν είναι συμβατές με τις

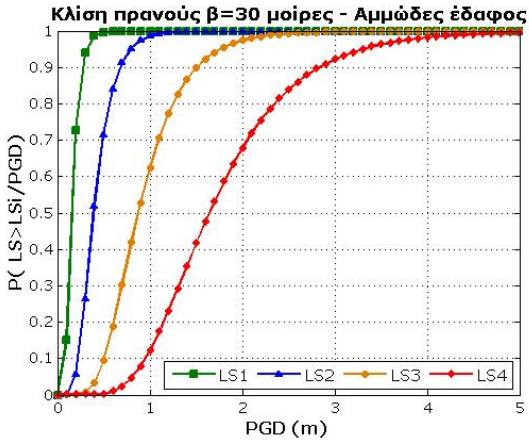
θεωρούμενες κλίσεις του πρανών ώστε να διασφαλίζεται η ευστάθειά τους υπό στατικές συνθήκες. Πρέπει επίσης να τονιστεί ότι μελετώνται μόνο οι περιπτώσεις που οδηγούν στην υψηλότερη επιδεκτικότητα των πρανών σε κατολίσθηση. Για παράδειγμα, πρανή με ήπιες κλίσεις (β=15^o) σε σκληρό έδαφος δεν αναλύονται καθώς η προκύπτουσα παραμένουσα παραμόρφωση και επομένως η αναμενόμενη δομική βλάβη θα ήταν αμελητέα και άρα εκτός του πεδίου μελέτης της παρούσας διατριβής. Τα 24 μοντέλα που τελικά προκύπτουν υποβάλλονται σε μια σειρά αριθμητικών αναλύσεων δύο βημάτων (συνολικά περίπου 1350 αναλύσεις) με βάση την προτεινόμενη μεθοδολογία. Αποτέλεσμα των αναλύσεων αποτελεί η αναμενόμενη απόκριση της κατασκευής λόγω της πιθανής κατολίσθησης και τελικά η τρωτότητά της για τις προκαθορισμένες στάθμες βλάβης.

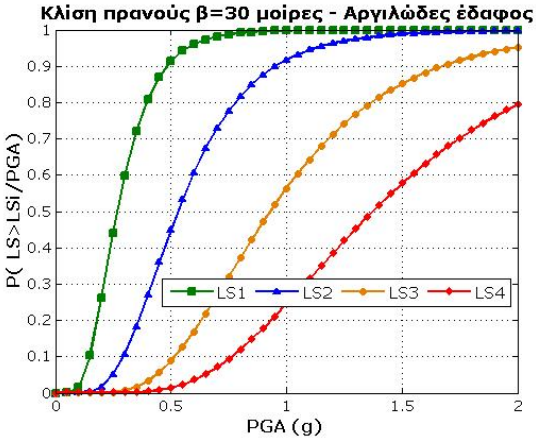


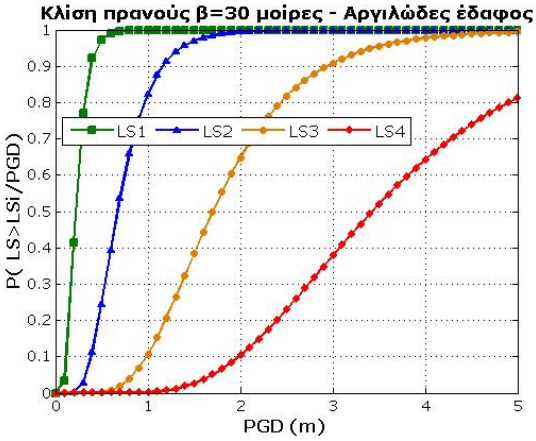
Σχήμα Ι.10. Το υπό μελέτη παραμετρικό μοντέλο

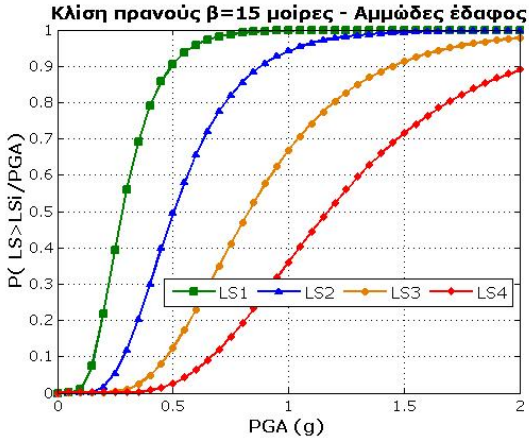
Με βάση τα αποτελέσματα της εκτενούς παραμετρικής διερεύνησης, προτείνονται τελικά επτά σετ καμπυλών τρωτότητας εξαρτώμενα από τις παραμέτρους που συμβάλλουν περισσότερο στον εκτιμώμενο βαθμό βλάβης της κατασκευής. Ύστερα από μια ανάλυση ευαισθησίας των αποτελεσμάτων προκύπτει ότι οι παράμετροι αυτές είναι η κλίση και το εδαφικό υλικό του πρανούς, τα οποία βρέθηκαν να είναι εντόνως αλληλοσυσχετιζόμενα. Το ύψος του πρανούς αποδεικνύεται επίσης μια σημαντική παράμετρος που συμβάλλει καθοριστικά στην τρωτότητα της κατασκευής για την περίπτωση απότομων αμμωδών πρανών. Έτσι, προτείνονται επιπλέον διαφορετικές καμπύλες τρωτότητας για αμμώδη πρανή 45^o ανάλογα με το ύψος τους. Σημειώνεται ότι οι προτεινόμενες καμπύλες κατασκευάζονται για την πιο δυσμενή θέση του κτιρίου ως προς την κατολίσθηση, η οποία είναι διαφορετική για την περίπτωση των αμμωδών και των αργιλωδών πρανών. Στο σχήμα Ι.11 δίδονται σχηματικά οι προτεινόμενες καμπύλες συναρτήσει της μέγιστης

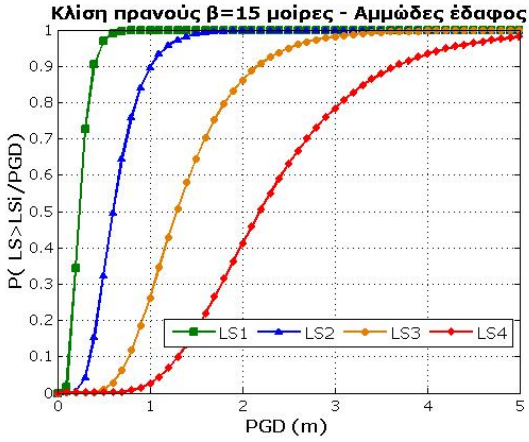

Κλίση πρανούς β=30 μοίρες - Αμμώδες έδαφος
P(LS>LSi/PGA)
PGA (g)
LS1 LS2 LS3 LS4

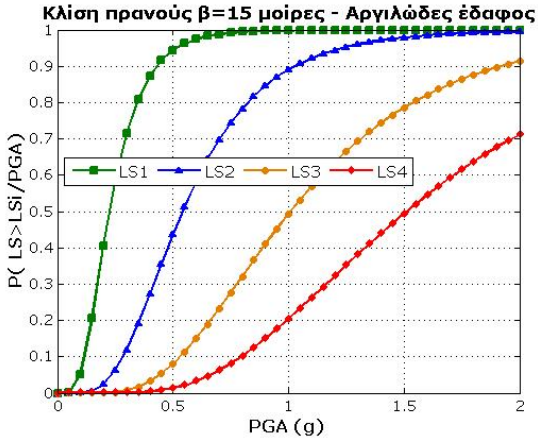

Κλίση πρανούς β=30 μοίρες - Αμμώδες έδαφος
P(LS>LSi/PGD)
PGD (m)
LS1 LS2 LS3 LS4

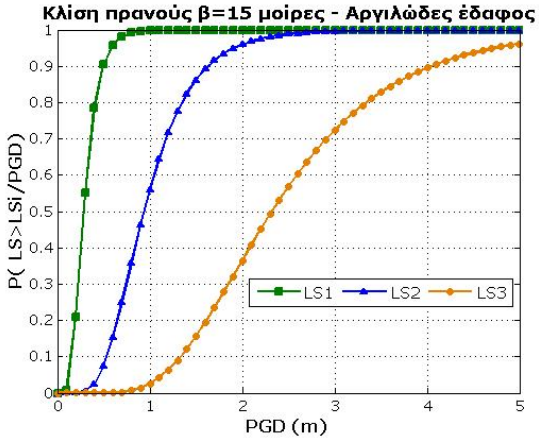

Κλίση πρανούς β=30 μοίρες - Αργιλώδες έδαφος
P(LS>LSi/PGA)
PGA (g)
LS1 LS2 LS3 LS4

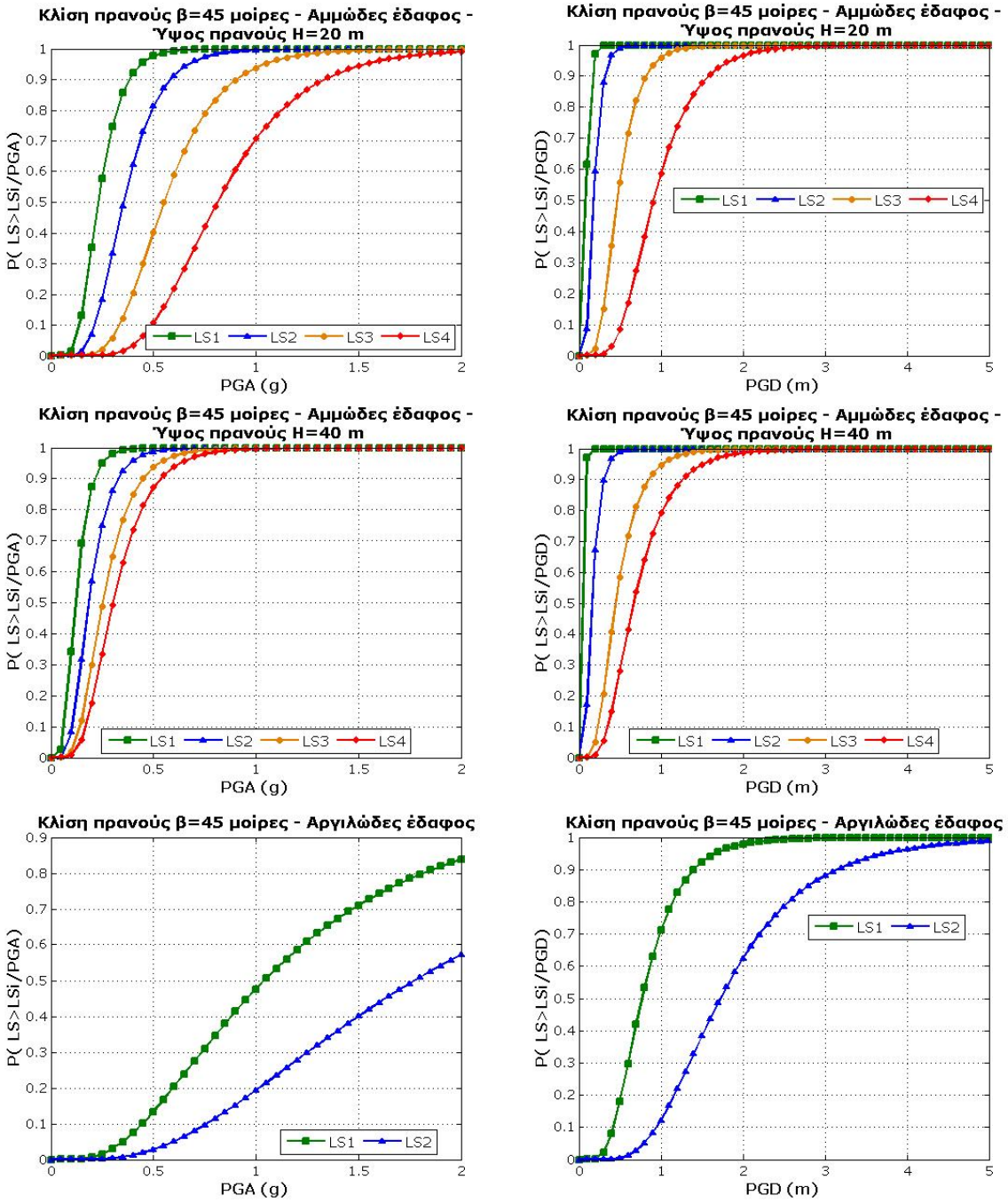

Κλίση πρανούς β=30 μοίρες - Αργιλώδες έδαφος
P(LS>LSi/PGD)
PGD (m)
LS1 LS2 LS3 LS4


Κλίση πρανούς β=15 μοίρες - Αμμώδες έδαφος
P(LS>LSi/PGA)
PGA (g)
LS1 LS2 LS3 LS4


Κλίση πρανούς β=15 μοίρες - Αμμώδες έδαφος
P(LS>LSi/PGD)
PGD (m)
LS1 LS2 LS3 LS4


Κλίση πρανούς β=15 μοίρες - Αργιλώδες έδαφος
P(LS>LSi/PGA)
PGA (g)
LS1 LS2 LS3 LS4


Κλίση πρανούς β=15 μοίρες - Αργιλώδες έδαφος
P(LS>LSi/PGD)
PGD (m)
LS1 LS2 LS3



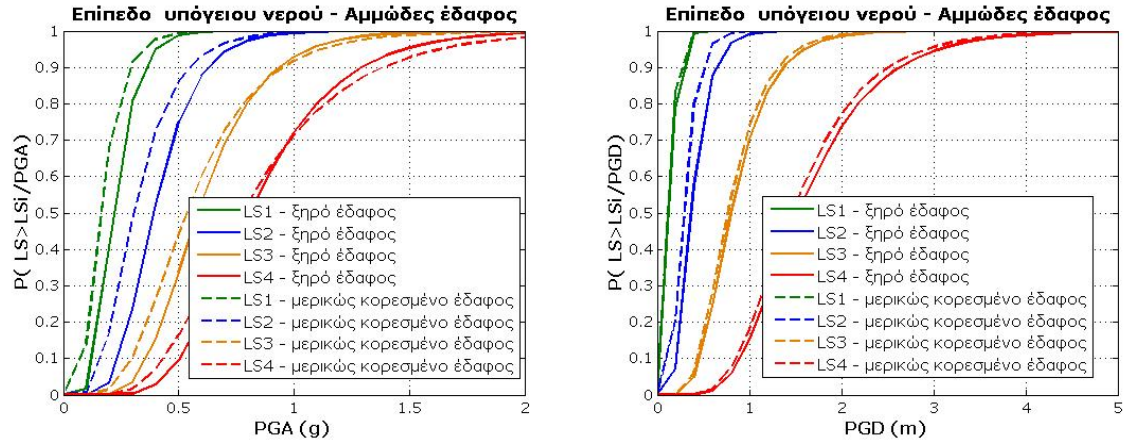
Σχήμα Ι.11. Προτεινόμενες καμπύλες τρωτότητας συναρτήσει της PGA (αριστερά) και της PGD (δεξιά) για τυπικά πλαισιακά κτίρια Ο/Σ χαμηλού ύψους σχεδιασμένα με συγχρόνους κανονισμούς που υπόκεινται σε παραμένουσες εδαφικές μετακινήσεις λόγω πιθανής κατολίσθησης

εδαφικής επιτάχυνσης (PGA) και της παραμένουσας εδαφικής μετακίνησης (PGD) για την περίπτωση ενός τυπικού πλαισιακού κτιρίου Ο/Σ χαμηλού ύψους, επαρκώς οπλισμένου και σχεδιασμένο με σύγχρονους κανονισμούς (π.χ. ΕΑΚ, 2000). Αντίστοιχες καμπύλες προτείνονται και για σχετικά κτίρια σχεδιασμένα με παλαιότερους κανονισμούς.

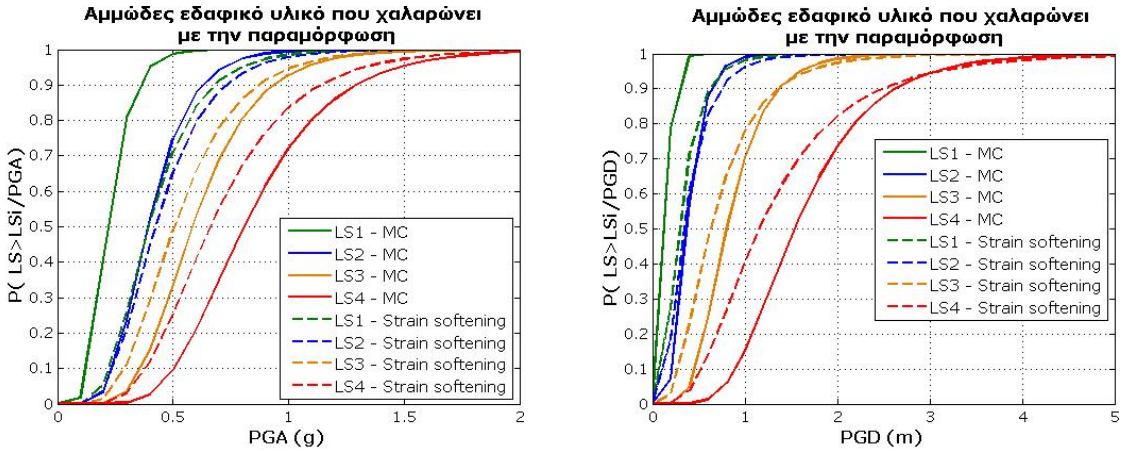
Το κτίριο που θεμελιώνεται σε αμμώδη πρανή αναμένεται να επιδείξει μεγαλύτερο βαθμό βλάβης σε σχέση με το αντίστοιχο σε αργιλώδη πρανή. Έτσι, οι καμπύλες τρωτότητας που αναφέρονται σε αμμώδη σε σύγκριση με τις αντίστοιχες για αργιλώδη πρανή είναι γενικά μετατοπισμένες προς τα αριστερά και ταυτόχρονα είναι συνυφασμένες με μια πιο γρήγορη

μετάβαση από τη στάθμη βλάβης που περιγράφει τις μικρές βλάβες προς αυτή που σχετίζεται με την ολική κατάρρευση. Οι διαφορές αυτές γίνονται εμφανέστερες καθώς η κλίση του πρανούς αυξάνει. Μεταξύ των περιπτώσεων που εξετάζονται, το 45° αμμώδες πρανές μεγαλύτερου ύψους και το 45° αργιλώδες πρανές προκαλούν τις μεγαλύτερες και μικρότερες βλάβες αντιστοίχως στην κατασκευή. Η διασπορά β των καμπυλών κυμαίνεται από 0.39 έως 0.66 και από 0.40 έως 0.50 όταν θεωρείται η PGA και η PGD αντιστοίχως ως μέτρο της έντασης της κατολίσθησης. Οι μεγαλύτερες τιμές της διασποράς β αναμένονται για τα πρανή με απότομη κλίση (45°) και για τα αργιλικά εδάφη.

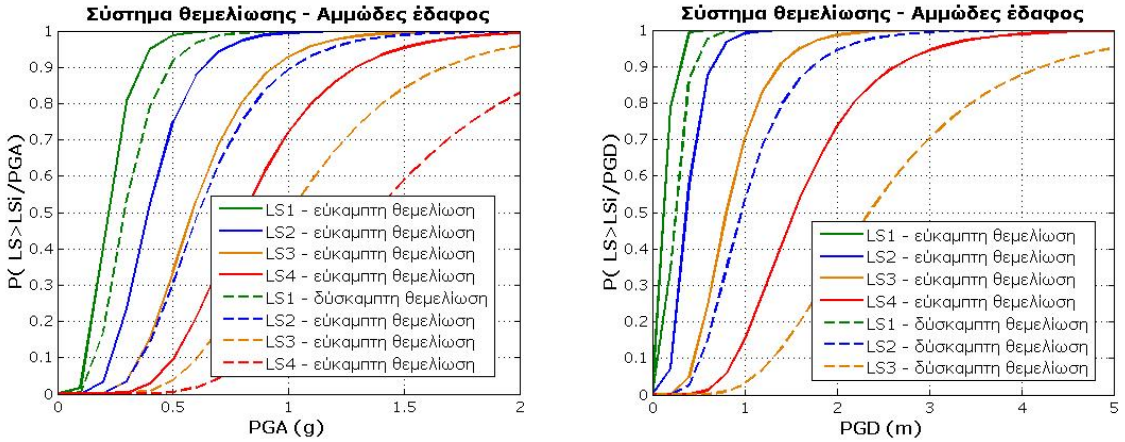
Επιπροσθέτως, εξετάστηκαν κάποιες επιπλέον παράμετροι όπως το επίπεδο του υπόγειου νερού, η θεώρηση υλικού κατολίσθησης που «χαλαρώνει» με την παραμόρφωση (strain softening material), η ενδοσιμότητα του συστήματος θεμελίωσης, η γεωμετρία της κατασκευής (ο αριθμός των ορόφων και των ανοιγμάτων) και το επίπεδο του σχεδιασμού της, με σκοπό να διερευνηθεί η σχετική επίδραση καθεμίας από αυτές στην τρωτότητα της κατασκευής. Η επιρροή της κάθε παραμέτρου μπορεί να διαφοροποιείται σε σχέση με το εδαφικό υλικό του πρανούς (π.χ. για την περίπτωση της θεώρησης υπόγειου νερού) και με την ενδοσιμότητα της θεμελίωσης (π.χ. για την περίπτωση όπου μεταβάλλεται η γεωμετρία της κατασκευής). Συνολικά, η επίδρασή τους μπορεί κάτω υπό ορισμένες συνθήκες να είναι καθοριστική για τον προβλεπόμενο βαθμό βλάβης της κατασκευής. Σημειώνεται, ωστόσο, ότι μια πιο διεξοδική ανάλυση καθεμιάς εκ των ανωτέρω παραμέτρων δικαιολογείται μόνο σε συγκεκριμένες μελέτες περίπτωσης όπου είναι διαθέσιμα επαρκή στοιχεία για τις ιδιότητες του εδάφους, τη γεωμετρία του πρανούς και την τυπολογία και τα υλικά των υπό διακινδύνευση κατασκευών. Στα Σχήματα Ι.12 έως Ι.17 δίνονται κάποια συγκριτικά αντιπροσωπευτικά αποτελέσματα υπό μορφή καμπυλών τρωτότητας όπου περιγράφεται η σχετική επιρροή της κάθε παραμέτρου για κατασκευές θεμελιωμένες σε αμμώδες έδαφος.



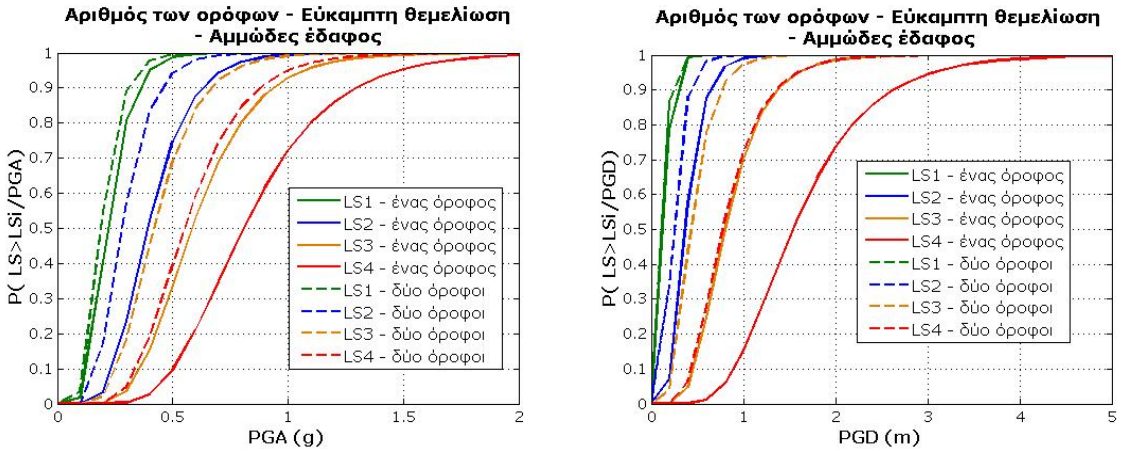
Σχήμα Ι.12 Καμπύλες τρωτότητας συναρτήσει της PGA (αριστερά) και της PGD (δεξιά) όταν μεταβάλλεται το επίπεδο του υπόγειου νερού (ξηρά ή μερικώς κορεσμένα εδαφικά υλικά)



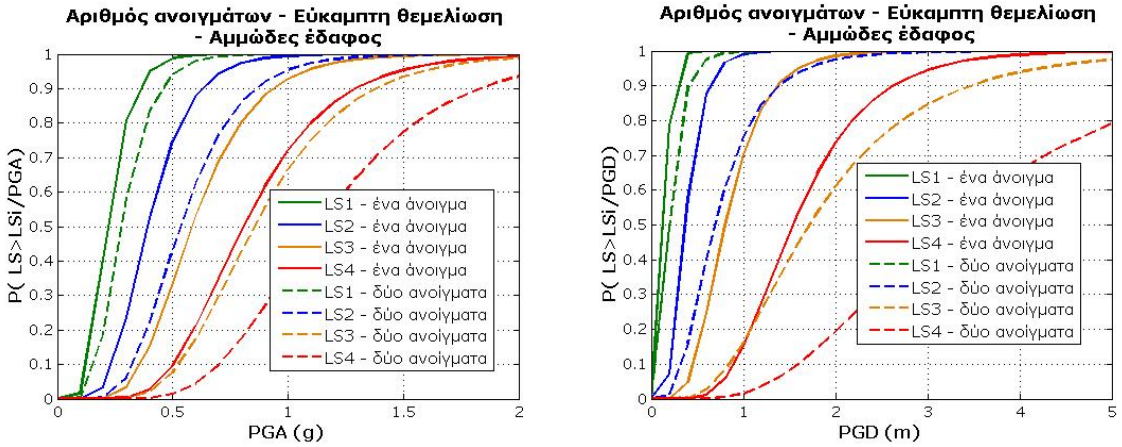
Σχήμα Ι.13. Καμπύλες τρωτότητας συναρτήσει της PGA (αριστερά) και της PGD (δεξιά) για θεωρούμενο (ή όχι) υλικό κατολίσθησης που «χαλαρώνει» με την παραμόρφωση (strain softening material)



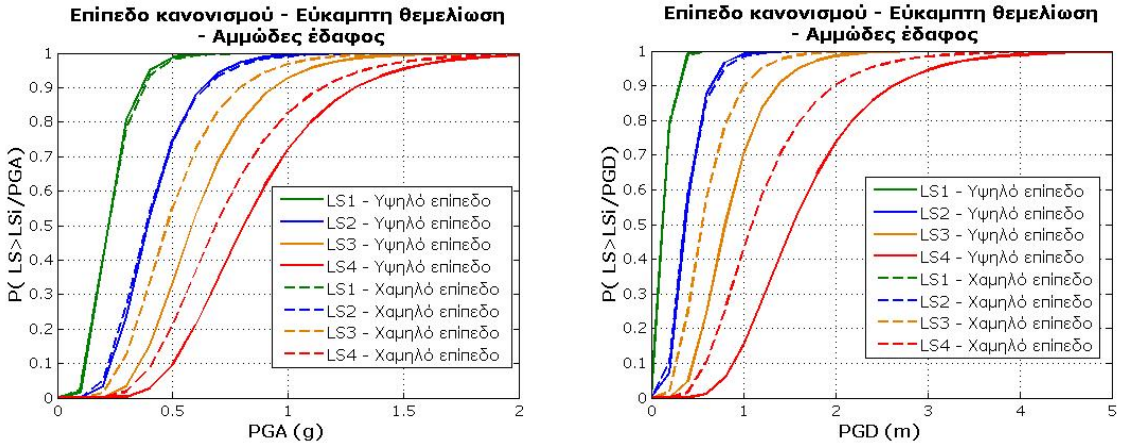
Σχήμα Ι.14. Καμπύλες τρωτότητας συναρτήσει της PGA (αριστερά) και της PGD (δεξιά) όταν μεταβάλλεται η ευκαμψία του συστήματος θεμελίωσης



Σχήμα Ι.15. Καμπύλες τρωτότητας συναρτήσει της PGA (αριστερά) και της PGD (δεξιά) για μονώροφα και διώροφα πλαισιακά κτίρια Ο/Σ ενός ανοίγματος



Σχήμα Ι.16. Καμπύλες τρωτότητας συναρτήσει της PGA (αριστερά) και της PGD (δεξιά) όταν για μονώροφα πλαισιακά κτίρια Ο/Σ ενός και δύο ανοιγμάτων



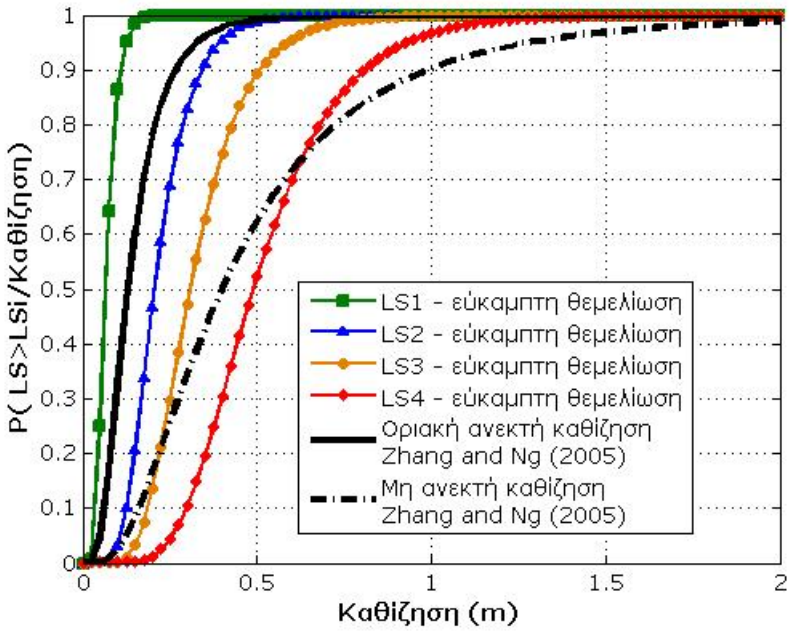
Σχήμα Ι.17. Καμπύλες τρωτότητας συναρτήσει της PGA (αριστερά) και της PGD (δεξιά) όταν μεταβάλλεται το επίπεδο σχεδιασμού της κατασκευής

Ι.5 Αξιολόγηση της προτεινόμενης μεθόδου

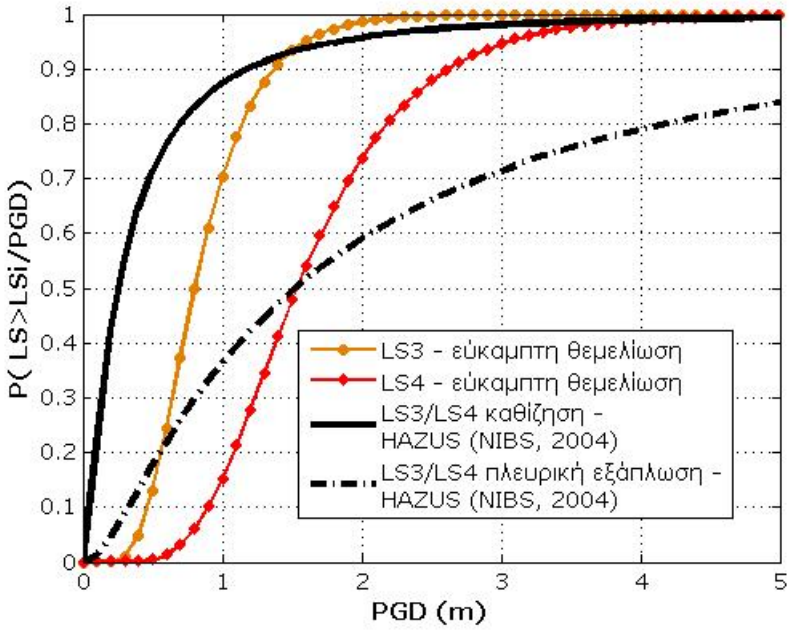
Η συγκεκριμένη ενότητα στοχεύει στην επαλήθευση της αξιοπιστίας της προτεινόμενης μεθοδολογίας και των σχετικών καμπυλών τρωτότητας.

Αρχικά η εγκυρότητα της μεθόδου εκτιμάται μέσω της σύγκρισης αντιπροσωπευτικών αναπτυχθέντων καμπυλών τρωτότητας για τυπικά πλαισιακά κτίρια Ο/Σ χαμηλού ύψους επί εύκαμπτης θεμελίωσης με αντίστοιχες καμπύλες της βιβλιογραφίας που προέκυψαν από διαφορετικές προσεγγίσεις. Ειδικότερα, καμπύλες τρωτότητας κτιρίων που βασίζονται σε εμπειρικά δεδομένα βλαβών (Zhang και Ng, 2005), την έμπειρη κρίση των ειδικών (NIBS, 2004) και σε αριθμητικές αναλύσεις (Negulescu και Foerster, 2010) χρησιμοποιήθηκαν γι' αυτή τη σύγκριση. Στα Σχήματα Ι.18 έως Ι.20 δίνονται κάποιες χαρακτηριστικές συγκρίσεις των προτεινόμενων καμπυλών τρωτότητας με τις αντίστοιχες καμπύλες των Zhang και Ng (2005), του HAZUS (NIBS, 2004) και των Negulescu και Foerster (2010). Πρέπει να σημειωθεί ότι οι προτεινόμενες καμπύλες που

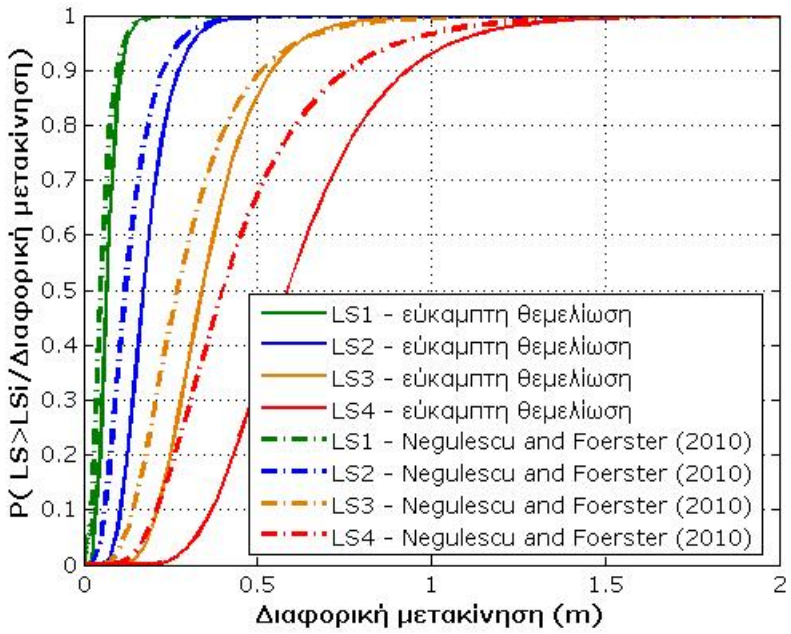
χρησιμοποιούνται για τις συγκρίσεις αντιστοιχούν σε μια μέση περίπτωση αναφορικά με τις αναμενόμενες βλάβες στην κατασκευή (για κλίση πρανούς 30° και αμμώδες έδαφος). Οι συγκρίσεις κρίνονται γενικά ικανοποιητικές δεδομένου των διαφορετικών υποθέσεων που σχετίζονται με τις προτεινόμενες καμπύλες και αυτές της βιβλιογραφίας.



Σχήμα Ι.18. Σύγκριση αντιπροσωπευτικών προτεινόμενων καμπυλών συναρτήσει της καθίζησης (ολικής κατακόρυφης μετακίνησης) με τις εμπειρικές καμπύλες των Zhang και Ng (2005)



Σχήμα Ι.19. Σύγκριση αντιπροσωπευτικών προτεινόμενων καμπυλών για εκτενείς βλάβες και ολική κατάρρευση συναρτήσει της παραμένουσας εδαφικής μετακίνησης (PGD) με τις καμπύλες του HAZUS (NIBS, 2004)



Σχήμα Ι.20. Σύγκριση αντιπροσωπευτικών προτεινόμενων καμπυλών συναρτήσει της διαφορικής μετακίνησης με τις αναλυτικές καμπύλες των Negulescu και Foerster (2010)

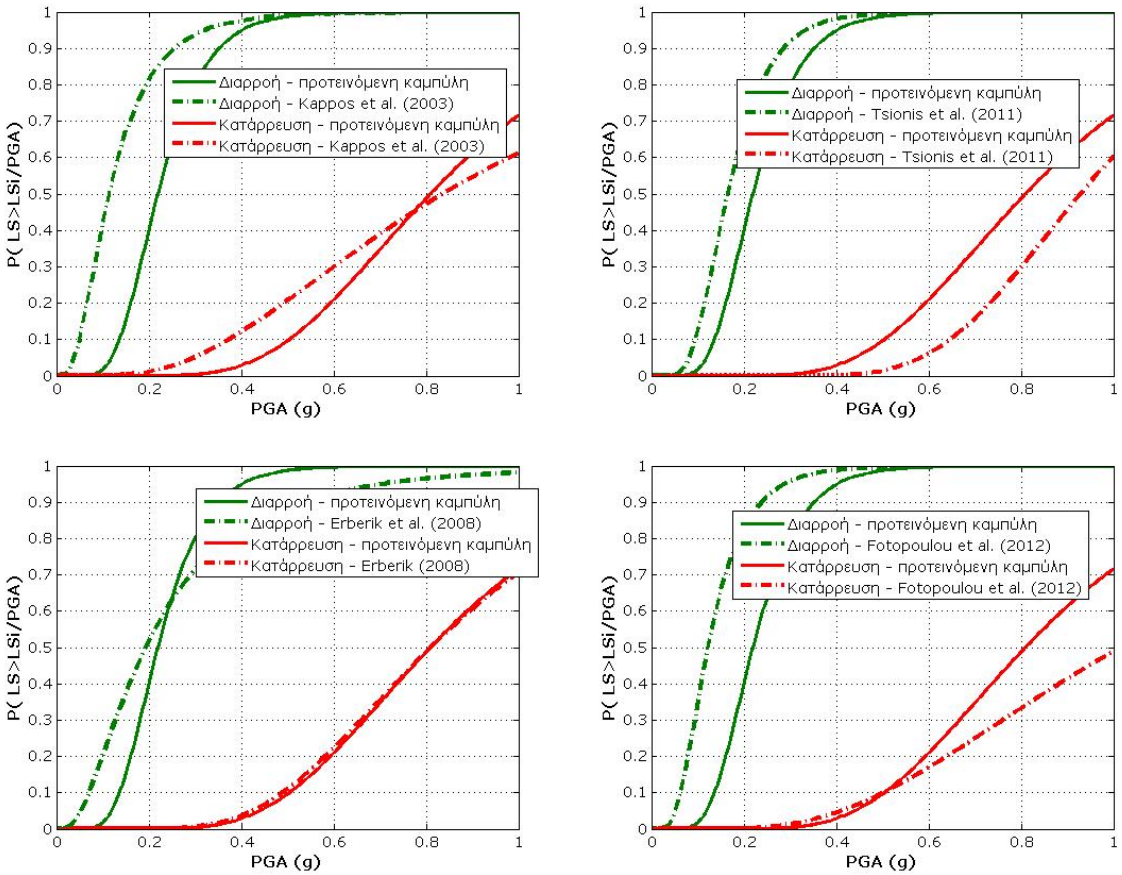
Ιδιαίτερο ενδιαφέρον παρουσιάζει επίσης η συσχέτιση των καμπυλών που προτείνονται στην συγκεκριμένη έρευνα για χαμηλού ύψους, πλαισιακά κτίρια Ο/Σ πλησίον της στέψης πρανών που εκτίθενται σε παραμένουσες σεισμικές μετακινήσεις λόγω πιθανής κατολίσθησης, με αντίστοιχες καμπύλες της βιβλιογραφίας για τις ίδιες τυπολογίες κτιρίων σε οριζόντια στρωματοποιημένες εδαφικές αποθέσεις (χωρίς την ύπαρξη οποιασδήποτε τοπογραφικής έξαρσης) που υποβάλλονται σε ανακυκλική φόρτιση λόγω ενός σεισμού.

Η εναρμόνιση όλων των καμπυλών ως προς το μέτρο της έντασης και τον αριθμό των σταθμών βλαβών αποτελεί απαραίτητη προϋπόθεση για να καταστεί δυνατή η προσεγγιστική σύγκριση των προτεινόμενων καμπυλών με αυτές της βιβλιογραφίας. Αυτή επιτυγχάνεται μέσω του εργαλείου Syner-G Fragility Function Manager (Crowley et al. 2011- SYNER-G project) που επιτρέπει την αποθήκευση, εναρμόνιση και σύγκριση διαφορετικών καμπυλών τρωτότητας. Συγκεκριμένα, η εναρμόνιση ως προς την ένταση επιτελείται θεωρώντας την μέγιστη εδαφική επιτάχυνση (PGA) στην επιφανειακή εμφάνιση βράχου ως μέτρο της έντασης και υιοθετώντας κατάλληλες σχέσης μετατροπής των αρχικών παραμέτρων έντασης σε PGA. Η εναρμόνιση ως προς τις στάθμες βλάβης διεξάγεται για δύο στάθμες βλαβών, αυτές που αντιστοιχούν στη διαρροή και στην ολική κατάρρευση της κατασκευής. Κάποια τυπικά συγκριτικά διαγράμματα των εναρμονισμένων προτεινόμενων καμπυλών με τις αντίστοιχες σεισμικές καμπύλες τρωτότητας της βιβλιογραφίας παρατίθενται στο Σχήμα Ι.21.

Διαπιστώνεται ότι για τη στάθμη βλάβης που αντιστοιχεί στη διαρροή οι περισσότερες εκ των καμπυλών τρωτότητας της βιβλιογραφίας προβλέπουν μεγαλύτερες βλάβες για την

κατασκευή σε σχέση με τις προτεινόμενες. Αυτό φαίνεται λογικό λαμβάνοντας υπόψη ότι η κατασκευή ενδέχεται γενικά να αναπτύξει κάποιες αρχικές (συνήθως μικρές) βλάβες λόγω της σεισμικής ταλάντωσης πριν την έναρξη της κατολίσθησης. Αντιθέτως, για την στάθμη βλάβης που αντιστοιχεί στην ολική κατάρρευση οι περισσότερες από τις καμπύλες της βιβλιογραφίας εκτιμούν μικρότερες βλάβες σε σχέση με τις προτεινόμενες. Έτσι, μετά την σεισμική ενεργοποίηση της κατολίσθησης, αυτή μπορεί, υπό προϋποθέσεις, να μετατραπεί στον κύριο μηχανισμό αστοχίας, οδηγώντας σε μεγαλύτερες βλάβες της κατασκευής κοντά στην κατάρρευση.

Συνολικά, οι προσεγγιστικές αυτές συγκρίσεις θεωρούνται αρκετά ικανοποιητικές. Φανερώνουν, ωστόσο, τη μεγάλη αβεβαιότητα που σχετίζεται με τις διαφορετικές καμπύλες τρωτότητας που συναντώνται στη βιβλιογραφία.



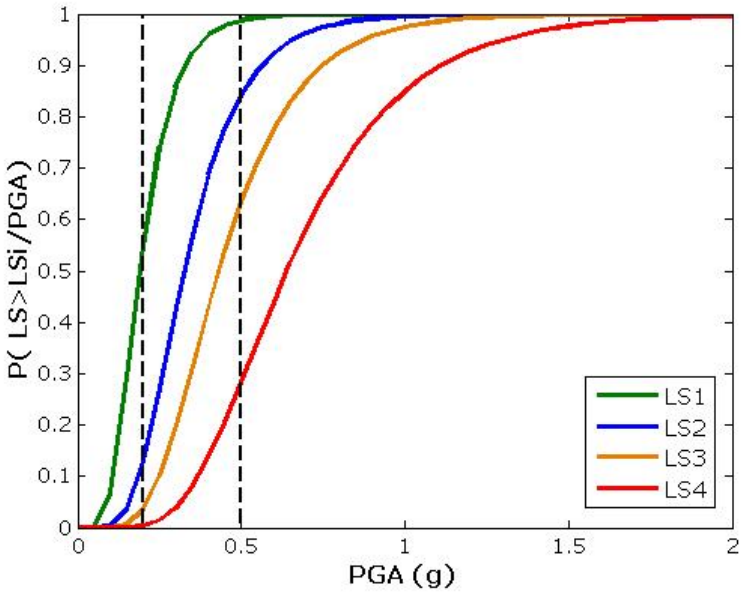
Σχήμα Ι.21. Συσχέτιση των εναρμονισμένων προτεινόμενων καμπυλών τρωτότητας συναρτήσει της PGA για χαμηλού ύψους, πλαισιακά κτίρια Ο/Σ σχεδιασμένων βάσει σύγχρονων κανονισμών που εκτίθενται σε παραμένουσες σεισμικές μετακινήσεις λόγω πιθανής κατολίσθησης με τις αντίστοιχες των Kappos et al. (2003), Tsionis et al. (2011), Erberik (2008) και Fotopoulou et al. (2012) για τις ίδιες τυπολογίες κτιρίων που υπόκεινται σε σεισμική ταλάντωση

Η αξιοπιστία της προτεινόμενης αναλυτικής προσέγγισης και των αντίστοιχων καμπυλών τρωτότητας εκτιμάται επίσης μέσω της εφαρμογής της σε δύο περιπτώσεις πραγματικών

κατασκευών: σε ένα τυπικό κτίριο τοποθετημένο πλησίον της στέψης ενός φυσικού πρανούς στην περιοχή της Κάτω Αχαΐας Πελοποννήσου στην Ελλάδα που υπέστη βλάβες στο σεισμό της Ηλείας - Αχαΐας το 2008 (M_w= 6.4) και σε ένα κτίριο που υποβλήθηκε σε μόνιμες μετακινήσεις λόγω κατολίσθησης στο χωριό Corniglio στην Ιταλία.

Πιο συγκεκριμένα, η προτεινόμενη μέθοδος εφαρμόζεται σε ένα αντιπροσωπευτικό κτίριο Ο/Σ τοποθετημένο κοντά στη στέψη ενός πρανούς στην περιοχή της Κάτω Αχαΐας, όπου παρατηρήθηκε συγκέντρωση των περισσότερων δομικών βλαβών σε κτίρια και υποδομές ως αποτέλεσμα του σεισμού της Ηλείας-Αχαιας (Mw= 6.4) στις 8 Ιουνίου του 2008. Τόσο το κτίριο όσο και το πρανές προσομοιώθηκαν κάνοντας χρήση μη-γραμμικών καταστατικών μοντέλων ώστε να εκτιμηθεί η τρωτότητα του τυπικού κτιρίου και να αποτιμηθεί η αξιοπιστία της αναπτυσσόμενης μεθοδολογίας και των αντίστοιχων συναρτήσεων τρωτότητας.

Η βασική συλλογιστική είναι αρχικά να επιβεβαιωθεί ότι για τον σεισμό της 8^{ης} Ιουνίου 2008 η συγκέντρωση των παρατηρηθεισών βλαβών στα κτίρια πλησίον της στέψης του πρανούς ήταν πρωτίστως αποτέλεσμα της ενίσχυσης της σεισμικής ταλάντωσης λόγω της τοπογραφίας. Στη συνέχεια, για ένα πιο ισχυρό σεισμικό σενάριο επιχειρείται η εκτίμηση των αναμενόμενων βλαβών σε ένα τυπικό κτίριο εγγύς της στέψης που υποβάλλεται σε παραμένουσες σεισμικές μετακινήσεις λόγω μιας πιθανής κατολίσθησης.



Σχήμα Ι.22. Προτεινόμενες καμπύλες τρωτότητας αντιπροσωπευτικές της περιοχής μελέτης και των χαρακτηριστικών των κατασκευών της περιοχής

Σύμφωνα με τα αποτελέσματα της αριθμητικής ανάλυσης, το τυπικό κτίριο αναμένεται να παρουσιάσει μικρές βλάβες για το επίπεδο επιβαλλόμενης σεισμικής φόρτισης που

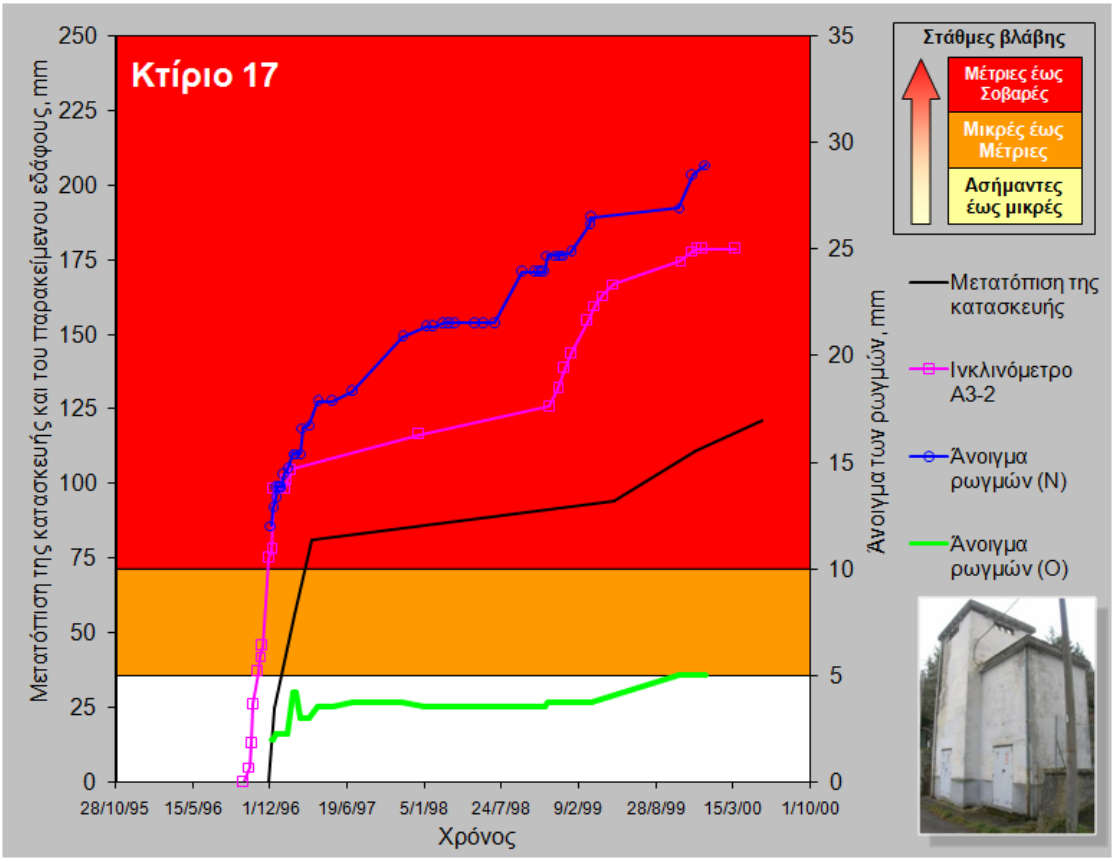
αντιστοιχεί κατά προσέγγιση στον κύριο σεισμό της 8ης Ιουνίου 2008 (PGA_{rock}=0.2g), οι οποίες βρίσκονται σε συμφωνία με τις παρατηρηθείσες, ενώ αναμένεται να υποστεί ολική κατάρρευση για το ισχυρότερο σεισμικό σενάριο (PGA_{rock}=0.5g). Η άμεση σύγκριση των βλαβών που προέκυψαν από την ανάλυση με τις αντίστοιχες βλάβες που προβλέπουν οι προτεινόμενες αντιπροσωπευτικές καμπύλες τρωτότητας (βλ. Σχ. Ι. 22) πιστοποιεί ότι οι καμπύλες που προτείνονται στη συγκεκριμένη διατριβή μπορούν να προβλέψουν επαρκώς την αναμενόμενη επίδοση αντιπροσωπευτικών κατασκευών Ο/Σ που εκτίθενται σε μόνιμες σεισμικές διαφορικές μετακινήσεις λόγω κατολίσθησης.

Ο στόχος της εφαρμογής της προτεινόμενης μεθοδολογίας σε ένα αντιπροσωπευτικό κτίριο στο χωριό Corniglio της Ιταλίας, το οποίο υπέστη μόνιμες μετακινήσεις λόγω της συνεχούς κατολισθητικής δραστηριότητας στην περιοχή, είναι διττός: πρώτον, να διερευνήσει την αξιοπιστία των καμπυλών τρωτότητας που αναπτύχθηκαν στην παρούσα διατριβή μέσω της σύγκρισης τους με την παρατηρηθείσα βλάβη στο κτίριο για το συγκεκριμένο επίπεδο μετακίνησης του εδάφους και της κατασκευής και δεύτερον, να επεκτείνει την εφαρμοσιμότητα της νέας προσέγγισης, προτείνοντας πιο ρεαλιστικές καμπύλες τρωτότητας για το υπό μελέτη κτίριο μέσω προηγμένων αριθμητικών αναλύσεων.

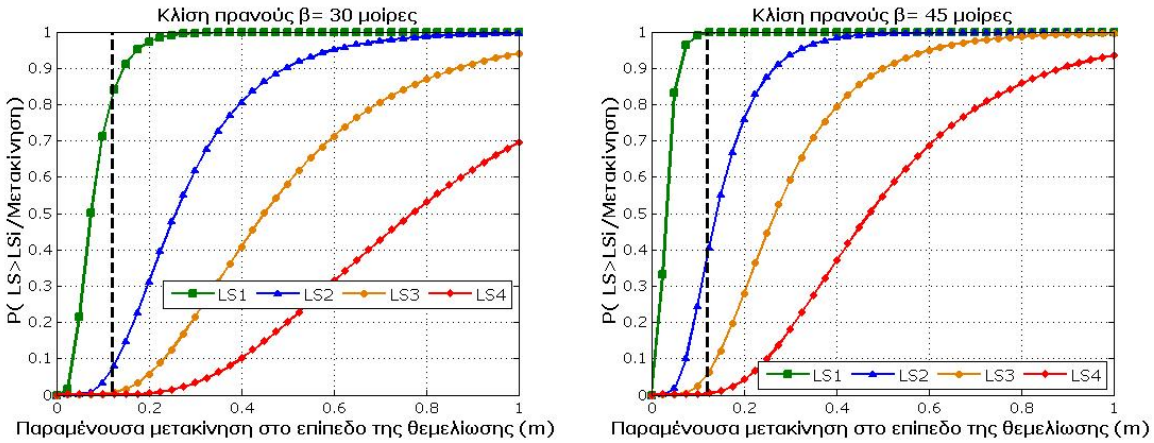
Ένας πολύτιμος όγκος δεδομένων (σε όρους παραμενουσών εδαφικών μετακινήσεων και μόνιμων μετατοπίσεων κτιρίων καθώς και καταγραφουσών βλαβών των κτιρίων λόγω της κατολίσθησης) κατέστη διαθέσιμος και επεξεργάστηκε (Callerio et al., 2007) για ένα πλήθος κτιρίων στο χωριό Corniglio, που τοποθετείται νοτιοδυτικά των Ιταλικών Appennines. Το Σχήμα Ι.23 απεικονίζει τυπικούς συσχετισμούς μεταξύ της μόνιμης μετατόπισης του υπό μελέτη κτιρίου από μετρήσεις γεωδαιτικής χωροστάθμησης (geodetic levelling), της παραμένουσας εδαφικής μετακίνησης από το κοντινότερο σε σχέση με τη θέση του κτιρίου ινκλινόμετρο καθώς και των μετρήσεων ανοίγματος των ρωγμών του κτιρίου. Στο σχήμα δίδεται επίσης η οριζόμενη κλίμακα εκτίμησης της βλάβης (συναρτήσει του ανοίγματος των ρωγμών), που επιτρέπει την αποτίμηση της αναμενόμενης βλάβης στην κατασκευή.

Αρχικά, επιλέχθηκαν δύο σετ καμπυλών τρωτότητας αντιπροσωπευτικών της περιοχής μελέτης που προέκυψαν από την παραμετρική διερεύνηση στην προηγούμενη ενότητα (Σχ. Ι.24). Αυτά συγκρίθηκαν με την παρατηρηθείσα βλάβη στο κτίριο, η οποία εκτιμήθηκε από *«μέτρια έως σοβαρή»* για το μετρηθέν επίπεδο μετακίνησης του κτιρίου (0,121 μ) (βλ. Σχ. Ι.23). Για το ίδιο επίπεδο μετακίνησης οι προτεινόμενες καμπύλες προβλέπουν *«μικρές έως μέτριες»* και *«μέτριες έως εκτενείς»* βλάβες που βρίσκονται σε σχετικά καλή συμφωνία με τις αντίστοιχες στάθμες βλάβης που ορίστηκαν με βάση την ενόργανη παρακολούθηση και την επί τόπου παρατήρηση. Σημειώνεται ότι οι

αναμενόμενες βλάβες που προκύπτουν από τις προτεινόμενες αντιπροσωπευτικές καμπύλες για κλίση πρανούς 45° είναι περισσότερο συμβατές με τις παρατηρηθείσες.

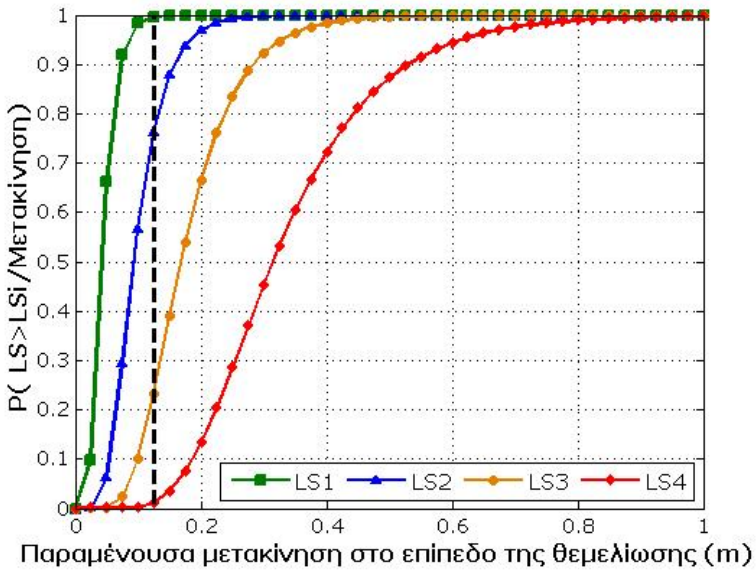


Σχήμα Ι.23. Συσχετίσεις μεταξύ της μόνιμης μετατόπισης του υπό μελέτη κτιρίου από μετρήσεις γεωδαιτικής χωροστάθμησης (geodetic levelling), της παραμένουσας εδαφικής μετακίνησης από το κοντινότερο σε σχέση με τη θέση του κτιρίου ινκλινόμετρο καθώς και των μετρήσεων ανοίγματος των ρωγμών του κτιρίου (συγκρινόμενα με τις οριζόμενες στάθμες βλάβης) συναρτήσει του χρόνου (Callerio et al., 2007)



Σχήμα Ι.24. Αντιπροσωπευτικές αναλυτικές καμπύλες τρωτότητας που προέκυψαν από την παραμετρική διερεύνηση για κλίση πρανούς β=30° (αριστερά) και β=45° (δεξιά)

Στη συνέχεια, προκειμένου να επεκταθεί το εύρος εφαρμογής της προτεινόμενης μεθοδολογίας, αναπτύχθηκαν περισσότερο ρεαλιστικές, αναλυτικές καμπύλες τρωτότητας για το υπό μελέτη κτίριο στο χωριό Corniglio μέσω μη-γραμμικών αριθμητικών αναλύσεων, με βάση τα διαθέσιμα δεδομένα της περιοχής (δυσδιάστατη γεωτεχνική τομή της περιοχής, καταγραφές του ινκλινόμετρου A3-2 που βρίσκεται πλησίον του υπό μελέτη κτιρίου, μετρήσεις μετατοπίσεων και ρωγμών στο κτίριο). Οι καμπύλες τρωτότητας που προτείνονται για το υπό μελέτη κτίριο (Σχ. I.25) εκτιμούν ότι αυτό αναμένεται να υποστεί *«μέτριες έως εκτενείς»* βλάβες για το μετρηθέν επίπεδο μετακίνησης. Αυτές βρίσκονται σε πολύ καλή συμφωνία με τις βλάβες που προέκυψαν από τις ενόργανες καταγραφές και την επί τόπου έρευνα, επιβεβαιώνοντας την εγκυρότητα της προτεινόμενης μεθοδολογίας και των αντίστοιχων καμπυλών για τη συγκεκριμένη εφαρμογή.



Σχήμα I.25. Καμπύλες τρωτότητας που προτείνονται για το υπό μελέτη κτίριο στην περιοχή του Corniglio

I.6 Εξέλιξη της τρωτότητας των κατασκευών στο χρόνο

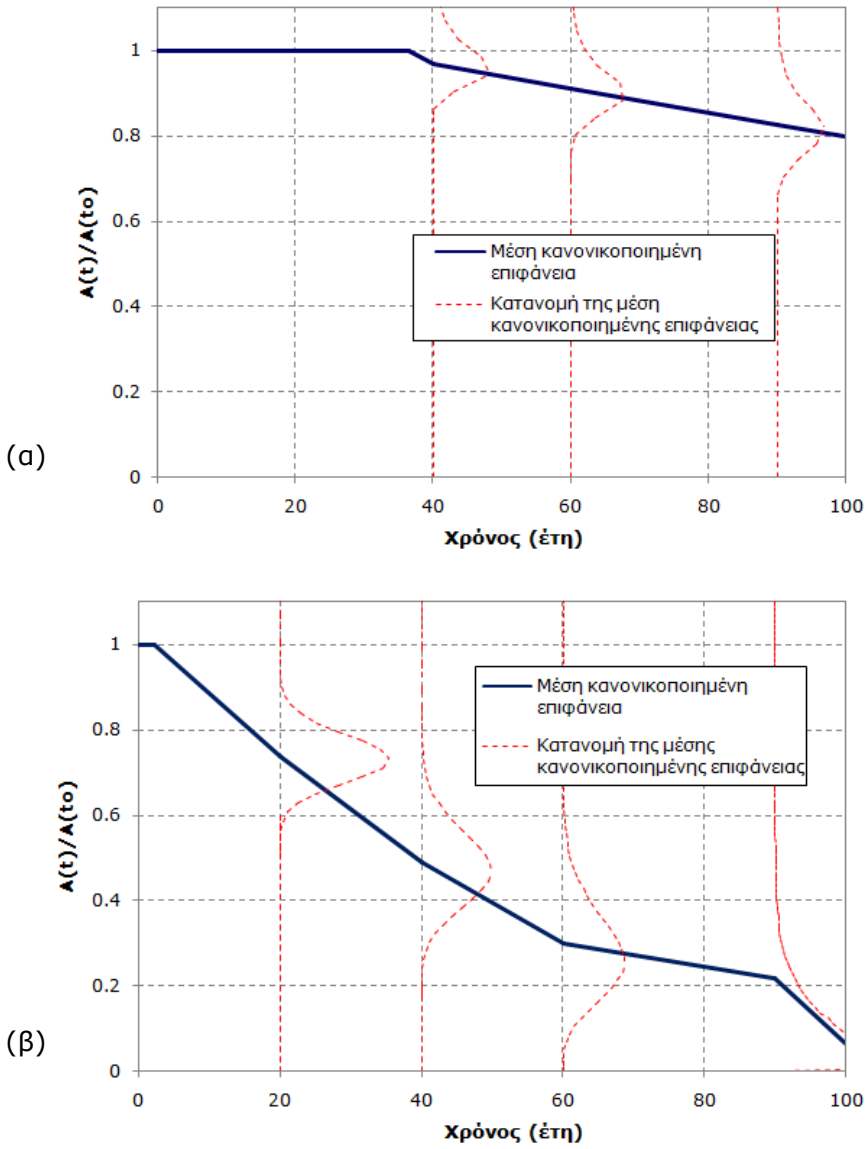
Οι περισσότερες μέθοδοι αποτίμησης θεωρούν τη φυσική τρωτότητα ως «αμετάβλητη» στο χρόνο. Ωστόσο, η πραγματική, δυναμική τρωτότητα των κατασκευών μπορεί να μεταβάλλεται στο χρόνο, επηρεαζόμενη από φαινόμενα γήρανσης των υλικών, ανθρωπογενείς δράσεις και συσσωρευτική βλάβη από προηγούμενες κατολισθήσεις ή άλλους φυσικούς κινδύνους. Παρά τις προσπάθειες κάποιων ερευνητών να συμπεριλάβουν τον χρόνο ως μια βασική συνιστώσα της τρωτότητας, η χρήση χρονικά εξαρτώμενων συναρτήσεων τρωτότητας δεν είναι αρκετά διαδεδομένη έως σήμερα.

Η παρούσα διατριβή φιλοδοξεί να καλύψει εν μέρει αυτό το κενό, επεκτείνοντας την προτεινόμενη προσέγγιση ώστε να λάβει υπόψη της την εξέλιξη της τρωτότητας των κτιρίων στο χρόνο. Συγκεκριμένα, η γήρανση των υλικών κτιρίων Ο/Σ λαμβάνεται υπόψη υιοθετώντας χρονικώς εξαρτώμενα, πιθανοτικά μοντέλα διάβρωσης του χάλυβα του οπλισμού στο μεθοδολογικό πλαίσιο αποτίμησης της τρωτότητας. Εξετάζονται δύο δυσμενή σενάρια διάβρωσης που σχετίζονται με την ενανθράκωση του χάλυβα του οπλισμού και τη διείσδυση χλωριόντων της ατμόσφαιρας. Η μεθοδολογία εφαρμόζεται σε τυπικά πλαισιακά κτίρια Ο/Σ χαμηλού ύψους, που εκτίθενται στη συνδυασμένη δράση της παραμένουσας σεισμικής διαφορικής μετακίνησης λόγω της κατολίσθησης και της διάβρωσης του οπλισμού. Εξετάζονται κτίρια με εύκαμπτο και δύσκαμπτο σύστημα θεμελίωσης, τοποθετημένα εγγύς της στέψης σεισμικώς εν δυνάμει ασταθών πρανών. Η ανάλυση που πραγματοποιείται είναι ψευδοστατική θεωρώντας ανελαστική τη συμπεριφορά των υλικών της κατασκευής υπό τη μορφή ινών (fibers). Η διαφορική μετακίνηση λόγω της κατολίσθησης συναρτήσει του χρόνου εισάγεται στη βάση του προσομοιώματος της κατασκευής ως φόρτιση κινηματικού τύπου.

Η κατανομή του χρόνου έναρξης της διάβρωσης εκτιμάται μέσω προσομοίωσης Monte Carlo κάνοντας χρήση κατάλληλων πιθανοκρατικών μοντέλων για τα δύο μελετηθέντα σενάρια διάβρωσης. Στη συνέχεια, η απώλεια της επιφάνειας του χάλυβα στο χρόνο λόγω της διάβρωσης προσομοιώνεται μέσω της απομείωσης της ενεργού διατομής των ράβδων του οπλισμού. Το Σχήμα Ι.26 απεικονίζει την πιθανοτική εκτίμηση της χρονικά-εξαρτώμενης απομειωμένης επιφάνειας διάβρωσης των ράβδων του οπλισμού στο χρόνο t, A(t), κανονικοποιημένης ως προς την αρχική επιφάνεια του οπλισμού, $A(t_0)$, για τα δύο σενάρια διάβρωσης που μελετώνται. Όπως αναμένονταν, η αβεβαιότητα στην εκτίμηση της απώλειας της επιφάνειας του οπλισμού τείνει να αυξάνει στο χρόνο, εξαρτώμενη από τη συζευγμένη αβεβαιότητα στην αρχική διάμετρο των ράβδων του οπλισμού, στο ρυθμό της διάβρωσης και στο χρόνο έναρξης της διάβρωσης.

Οι στάθμες βλάβης ορίζονται συναρτήσει οριακών τιμών τοπικών παραμορφώσεων του χάλυβα, οι οποίες επίσης μεταβάλλονται στο χρόνο.

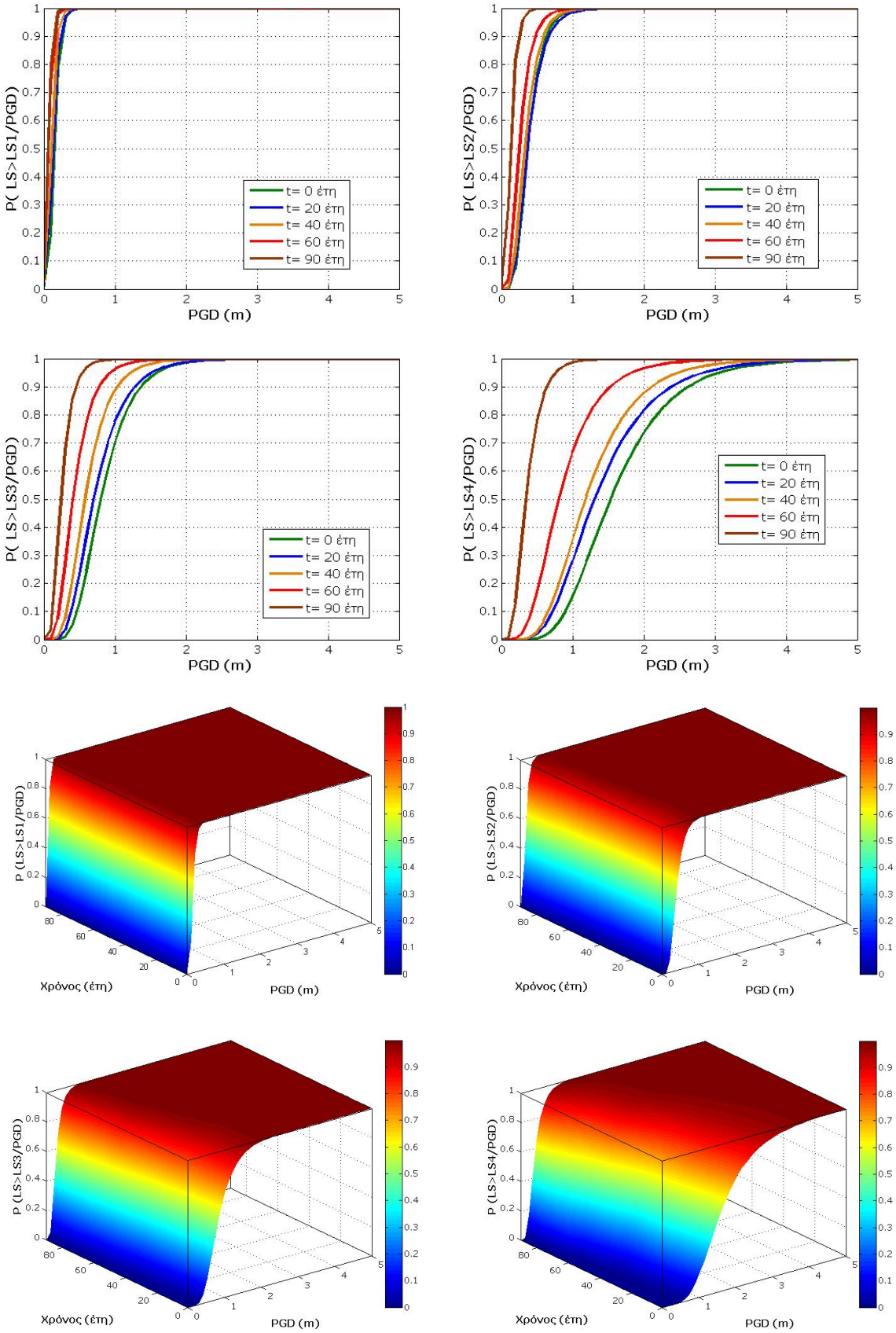
Η προτεινόμενη προσέγγιση καταλήγει στην ανάπτυξη χρονικά εξαρτώμενων λογαριθμοκανονικών καμπυλών και επιφανειών τρωτότητας συναρτήσει της PGA ή της PGD για κτίρια οπλισμένου σκυροδέματος, που εκτίθενται σε σεισμικώς προκαλούμενες κατολισθήσεις για τα δύο διαφορετικά σενάρια διάβρωσης (λόγω ενανθράκωσης του χάλυβα και λόγω διείσδυσης χλωριόντων). Στο Σχήματα Ι.27 δίνονται τυπικά αποτελέσματα υπό μορφή χρονικά μεταβαλλόμενων καμπυλών και επιφανειών τρωτότητας συναρτήσει της PGD για την περίπτωση του κτιρίου που εδράζεται σε εύκαμπτο σύστημα θεμελίωσης, για το σενάριο της διάβρωσης που σχετίζεται με τη διείσδυση χλωριόντων.



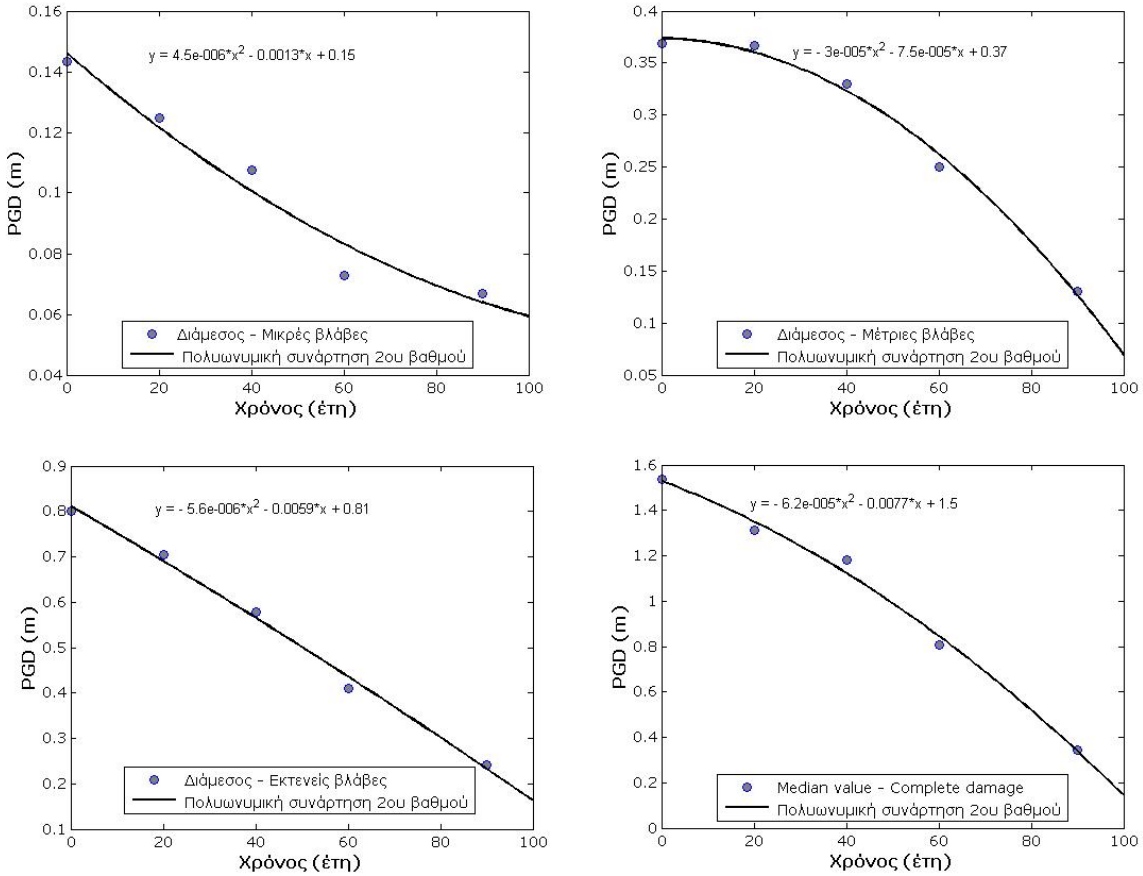
Σχήμα Ι.26. Μεταβολή της κανονικοποιημένης επιφάνειας του οπλισμού με το χρόνο λόγω του φαινομένου της διάβρωσης για τα σενάρια (α) της ενανθράκωσης του χάλυβα και (β) της επίδρασης χλωριόντων

Όπως φαίνεται στο Σχήμα Ι.29, η χρονικά εξαρτώμενη διάμεσος των καμπυλών μπορεί να αναπαρασταθεί επαρκώς με μια πολυωνυμική συνάρτηση 2^{ου} βαθμού. Τέτοια μοντέλα προσφέρουν το πλεονέκτημα της άμεσης εκτίμησης των διαμέσων των καμπυλών για το δεδομένο κτίριο και για το συγκεκριμένο σενάριο διάβρωσης για οποιαδήποτε στιγμή στο χρόνο, εφόσον είναι γνωστή η τρωτότητα της κατασκευής στην αρχική της κατάσταση.

Παρατηρείται ότι η τρωτότητα των κατασκευών αυξάνει στο χρόνο λόγω της διάβρωσης. Αυτή η αύξηση είναι περισσότερο εμφανής για την περίπτωση των κτιρίων Ο/Σ επί εύκαμπτης θεμελίωσης που επηρεάζονται από φαινόμενα διάβρωσης λόγω της διείσδυσης χλωριόντων.



Σχήμα Ι.27. Χρονικά εξαρτώμενες καμπύλες και επιφάνειες τρωτότητας συναρτήσει του PGD, για μικρές (LS_1), μέτριες (LS_2), εκτενείς (LS_3) βλάβες και ολική κατάρρευση (LS_4), για ένα τυπικό χαμηλού ύψους πλαισιακό κτίριο Ο/Σ επί εύκαμπτου συστήματος θεμελίωσης, για το σενάριο της διάβρωσης που σχετίζεται με τη διείσδυση χλωριόντων



Σχήμα Ι.28. Αναπαράσταση της χρονικά εξαρτώμενης διαμέσου (σε όρους PGD) των καμπυλών με πολυώνυμο 2^{ου} βαθμού για την περίπτωση των μικρών (LS_1), μέτριων (LS_2), εκτενών (LS_3) βλαβών και για ολική κατάρρευση (LS_4), για ένα τυπικό χαμηλού ύψους πλαισιακό κτίριο Ο/Σ επί εύκαμπτου συστήματος θεμελίωσης, για το σενάριο της διάβρωσης που σχετίζεται με τη διείσδυση χλωριόντων

Ι.7 Συμπεράσματα

Οι καταστρεπτικές συνέπειες των κατολισθήσεων που προκαλούνται από σεισμό σε κτίρια και υποδομές αλλά και σε ανθρώπινες ζωές, καθιστούν επιτακτική την ανάγκη ανάπτυξης νέων μεθόδων και πρακτικών για την αποτελεσματική αποτίμηση και μείωση της διακινδύνευσης. Ωστόσο, η ποσοτική εκτίμηση της διακινδύνευσης των διαφόρων τύπων κατολισθήσεων εμπεριέχει πλήθος αβεβαιοτήτων που παρεμποδίζουν τον αντικειμενικό προσδιορισμό της. Ένας πρωταρχικός παράγοντας αβεβαιότητας συνδέεται με την αποτίμηση της τρωτότητας των κατασκευών που υπόκεινται στον κίνδυνο κατολίσθησης λόγω της δυναμικής και πολυδιάστατης φύσης της αλλά και της γενικότερης έλλειψης αξιόπιστων στατιστικών στοιχείων βλαβών σε κτίρια και υποδομές λόγω των διαφόρων μηχανισμών κατολίσθησης. Σε αυτό το πλαίσιο, ένα εκ των βασικών επιτευγμάτων της συγκεκριμένης διδακτορικής διατριβής, αποτελεί η πρόταση μιας καινοτόμου αναλυτικής μεθοδολογίας για την αποτίμηση της τρωτότητας κτιρίων οπλισμένου σκυροδέματος πλησίον σεισμικώς ασταθών πρανών. Η αξιοπιστία του αριθμητικού προσομοιώματος

επιβεβαιώθηκε μέσω της σύγκρισης των μετακινήσεων στην περιοχή του πρανούς, που εξήχθησαν από τις αριθμητικές αναλύσεις με τις αντίστοιχες μετακινήσεις που υπολογίστηκαν από εμπειρικές μεθόδους εκτίμησης των μετακινήσεων τύπου Newmark. Στο πλαίσιο της διατριβής, προτείνονται καμπύλες τρωτότητας για διάφορους τύπους κατασκευής, εδαφικές συνθήκες και γεωμετρίες πρανούς καθώς και αποστάσεις της θεωρούμενης κατασκευής από την πιθανή κατολίσθηση μέσω μιας εκτενούς παραμετρικής διερεύνησης, οι οποίες μπορούν να βρουν άμεση εφαρμογή σε ένα πιθανοτικό πλαίσιο εκτίμησης της διακινδύνευσης λόγω των κατολισθήσεων. Η αξιοπιστία της προτεινόμενης μεθοδολογίας επαληθεύτηκε μέσω της σύγκρισης των αναπτυσσόμενων καμπυλών με σχετικές καμπύλες της βιβλιογραφίας και δεδομένα από βλάβες σε κτίρια λόγω κατολισθητικών φαινομένων στην Ελλάδα και την Ιταλία. Τέλος, σημαντική είναι η συμβολή της διδακτορικής διατριβής στη μελέτη του χρόνου ως βασικής συνιστώσας της τρωτότητας των κατασκευών. Συγκεκριμένα, η προτεινόμενη προσέγγιση επεκτάθηκε ώστε να λάβει υπόψη της την εξέλιξη της τρωτότητας των κατασκευών στο χρόνο, προτείνοντας χρονικά εξαρτώμενες καμπύλες και επιφάνειες τρωτότητας για κτίρια οπλισμένου σκυροδέματος που εκτίθενται σε κατολισθήσεις προκαλούμενων από σεισμό.

I.8 Βιβλιογραφικές αναφορές

Argyroudis S., Pitilakis K. (2012). "Seismic fragility curves of shallow tunnels in alluvial deposits". Soil Dynamics and Earthquake Engineering 35, 1-12.

Assimaki D., Kausel E. (2007). "Modified topographic amplification factors for a single-faced slope due to kinematic soil-structure interaction". J of Geotechnical and Geoenvironmental Engineering 133, 1414–1431.

Bird J.F., Crowley H., Pinho R., Bommer J.J. (2005). "Assessment of building response to liquefaction induced differential ground deformation". Bul of the New Zealand Society for Earthquake Engineering 38(4), 215-234.

Bird J.F., Bommer J.J., Crowley H., Pinho R. (2006). "Modelling liquefaction-induced building damage in earthquake loss estimation". Soil dynamics and Earthquake Engineering 26(1), 15-30.

Bouckovalas G.D., Papadimitriou A.G. (2005). "Numerical evaluation of slope topography effects on seismic ground motion". Soil Dynamics and Earthquake Engineering 25(7-10), 547-558.

Bourdeau C., Havenith H.-B., Fleurisson J.-A., Grandjean, A.G. (2004). "Numerical modelling of seismic slope stability". Engineering Geology for Infrastructure Planning in Europe, Springer Berlin / Heidelberg 104, 671-684.

Bray J.D., Travasarou, T. (2007). "Simplified procedure for estimating earthquake-induced deviatoric slope displacements". Journal of Geotechnical and Geoenvironmental Engineering 133(4), 381-392.

Callerio A., Faccioli E., Kaynia A. (2007). Deliverable 121: Landslide risk assessment methods and applications (III) – Application to real active landslides – Phase II (68pp), LESSLOSS integrated project: Risk Mitigation for Earthquake and Landslides, Sub-Project 4 – Landslide risk scenarios and loss modelling.

Corominas J. Mavrouli O. (Eds.) (2011b). Deliverable 2.11: QRA case studies at selected "hotspots". Synthesis of critical issues. Work Package 2.3 – Development of procedures for QRA at regional scale and European scale. SafeLand: Seventh Framework Programme for research and technological development (FP7) of the European Commission.

Crowley H., Pinho R., Bommer J.J. (2004). "A probabilistic displacement-based vulnerability assessment procedure for earthquake loss estimation". Bulletin of Earthquake Engineering 2(2),173-219.

Crowley et al. (2011). D3.1 - Fragility functions for common RC building types in Europe, in SYNER-G: Systemic Seismic Vulnerability and Risk Analysis for Buildings, Lifeline Networks and Infrastructures Safety Gain, WP3 – Fragility Functions of Elements at Risk.

EAK2000 (2000). Greek Seismic Code, Organization of seismic planning and protection.

Erberik M.A. (2008). "Fragility-based assessment of typical mid-rise and low-rise RC buildings in Turkey". Engineering Structures 30(5), 1360-1374.

Fotopoulou S., Karapetrou S., Pitilakis K. (2012). "Seismic vulnerability of RC buildings considering SSI and aging effects". 15th World Conference on Earthquake Engineering, Lisbon, Portugal, 24-28 September.

Ishihara K. (1996). "Soil behaviour in earthquake geotechnics". Clarendon, London, 350 pp.

Itasca Consulting Group (2008). Inc. FLAC (Fast Lagrangian Analysis of Continua), ver. 6.0. Itasca Consulting Group, Inc., Minneapolis.

Kappos A. Panagiotopoulos C., Panagopoulos G., Papadopoulos El. WP4 – Reinforced concrete buildings (Level 1 and Level 2 analysis). RISK-UE, 2003.

Kramer S.L., Stewart J.P. (2004). "Geotechnical aspects of seismic hazards". In: Earthquake Engineering: from Engineering Seismology to Performance-Based Engineering, Y. Bozorgnia, V. Bertero (Eds.), CRC Press, Chapter 4, 85 pp.

Ktenidou O.J. (2010). "Theoretical and instrumental study of site and topographic effects on strong ground motion in Aegion". Ph.D. thesis, Aristotle University Thessaloniki, Greece.

Mansour M.F., Morgenstern N.I., Martin C.D. (2011). "Expected damage from displacement of slow-moving slides". Landslides 8(1), 117–131.

Marano K.D., Wald D.J., Allen T.I. (2010). "Global earthquake casualties due to secondary effects: a quantitative analysis for improving rapid loss analyses". Nat Hazards 52, 319–328.

National Institute of Building Sciences (2004). Direct physical damage—general building stock. HAZUS-MH Technical manual, Chapter 5. Federal Emergency Management Agency, Washington, D.C.

Negulescu C., Foerster E. (2010). "Parametric studies and quantitative assessment of the vulnerability of a RC frame building exposed to differential settlements". Natural Hazards and Earth System Sciences 10, 1781-1792.

Newmark N.M. (1965). "Effects of earthquakes on dams and embankments". Geotechnique 15 (2), 139–159.

Nielson B.G., DesRoches R. (2007). "Analytical seismic fragility curves for typical bridges in the central and southeastern United States". Earthquake Spectra 23(3), 615.

Pitilakis D., Tsinaris A. (2010). "Soil-foundation-structure interaction close to natural slopes and topographic irregularities (In Greek)". In: Proc of the 6th National Conference of Geotechnical Engineering, Volos, Greece.

Pitilakis K.D. (2010). "Geotechnical earthquake engineering". Ziti publication (in Greek).

Rathje E.M., Antonakos G. (2011). "A unified model for predicting earthquake-induced sliding displacements of rigid and flexible slopes". Engineering Geology 122(1-2), 51-60.

SeismoSoft, SeismoStruct (2011). A computer program for static and dynamic nonlinear analysis of framed structures. Available from URL: www.seismosoft.com.

Shinozuka M., Feng M. Q., Lee J., Naganuma T. (2000). "Statistical analysis of fragility curves". J. Eng. Mech.-ASCE, 126(12), 1224– 1231.

Shinozuka M., Feng M.Q., Kim H.K., Uzawa T., Ueda T. (2003). "Statistical analysis of fragility curves". Technical Report MCEER-03-0002, State University of New York, Buffalo.

Tsionis G., Papailia A., Fardis M.N. (2011). "Analytical fragility functions for reinforced concrete buildings and buildings aggregates of Euro-Mediterranean regions – UPAT methodology". Internal Report, Syner-G Project 2009/2012.

Yin Y., Wang F., Sun P. (2009). "Landslide hazards triggered by the 2008 Wenchuan earthquake, Sichuan, China". Landslides 6(2), 139-152.

Zhang L.M., Ng A.M.Y. (2005). "Probabilistic limiting tolerable displacements for serviceability limit state design of foundations". Geotechnique 55(2), 151–161.